KEEPING IN TOUCH: THE ROLE OF ORGANELLE DYNAMICS AND CONTACTS IN HEALTH AND DISEASE

EDITED BY: Du Feng, Yusong Guo, Min Li, Laura Lackner, Liang Ge, Marta Giacomello, Nuno Raimundo and Timothy Wai

PUBLISHED IN: Frontiers in Cell and Developmental Biology and Frontiers in Cellular Neuroscience

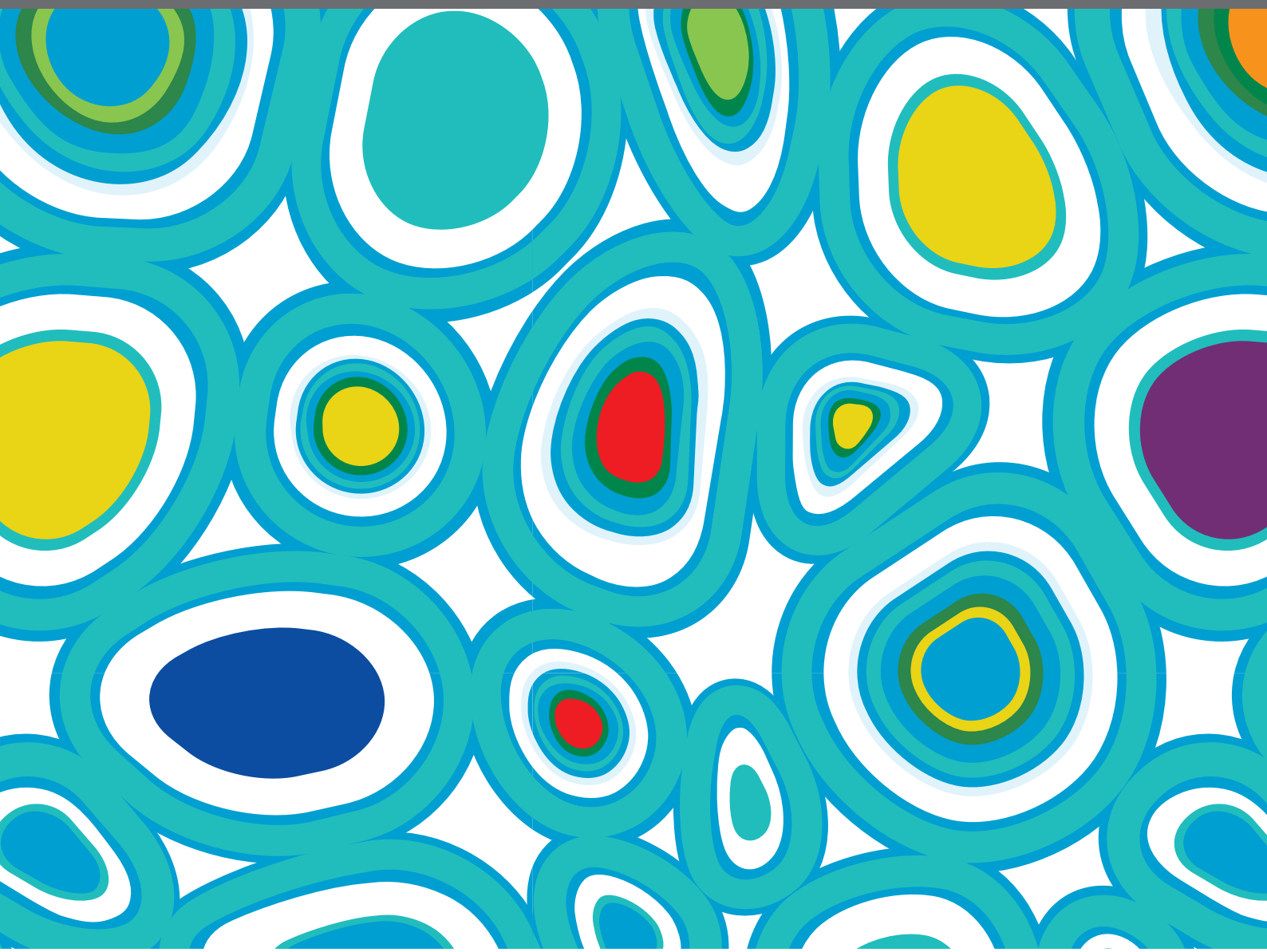

frontiers Research Topics

ISSN 1664-8714
ISBN 978-2-88971-342-4
DOI 10.3389/978-2-88971-342-4

About Frontiers

Frontiers is more than just an open-access publisher of scholarly articles: it is a pioneering approach to the world of academia, radically improving the way scholarly research is managed. The grand vision of Frontiers is a world where all people have an equal opportunity to seek, share and generate knowledge. Frontiers provides immediate and permanent online open access to all its publications, but this alone is not enough to realize our grand goals.

Frontiers Journal Series

The Frontiers Journal Series is a multi-tier and interdisciplinary set of open-access, online journals, promising a paradigm shift from the current review, selection and dissemination processes in academic publishing. All Frontiers journals are driven by researchers for researchers; therefore, they constitute a service to the scholarly community. At the same time, the Frontiers Journal Series operates on a revolutionary invention, the tiered publishing system, initially addressing specific communities of scholars, and gradually climbing up to broader public understanding, thus serving the interests of the lay society, too.

Dedication to Quality

Each Frontiers article is a landmark of the highest quality, thanks to genuinely collaborative interactions between authors and review editors, who include some of the world's best academicians. Research must be certified by peers before entering a stream of knowledge that may eventually reach the public - and shape society; therefore, Frontiers only applies the most rigorous and unbiased reviews.
Frontiers revolutionizes research publishing by freely delivering the most outstanding research, evaluated with no bias from both the academic and social point of view. By applying the most advanced information technologies, Frontiers is catapulting scholarly publishing into a new generation.

What are Frontiers Research Topics?

Frontiers Research Topics are very popular trademarks of the Frontiers Journals Series: they are collections of at least ten articles, all centered on a particular subject. With their unique mix of varied contributions from Original Research to Review Articles, Frontiers Research Topics unify the most influential researchers, the latest key findings and historical advances in a hot research area! Find out more on how to host your own Frontiers Research Topic or contribute to one as an author by contacting the Frontiers Editorial Office: frontiersin.org/about/contact

KEEPING IN TOUCH: THE ROLE OF ORGANELLE DYNAMICS AND CONTACTS IN HEALTH AND DISEASE

Topic Editors:
Du Feng, Guangzhou Medical University, China
Yusong Guo, Hong Kong University of Science and Technology, SAR China
Min Li, Sun Yat-sen University, China
Laura Lackner, Northwestern University, United States
Liang Ge, Tsinghua University, China
Marta Giacomello, University of Padua, Italy
Nuno Raimundo, The Pennsylvania State University, United States
Timothy Wai, Institut Pasteur, France

Citation: Feng, D., Guo, Y., Li, M., Lackner, L., Ge, L., Giacomello, M., Raimundo, N., Wai, T., eds. (2021). Keeping in Touch: The Role of Organelle Dynamics and Contacts in Health and Disease. Lausanne: Frontiers Media SA. doi: 10.3389/978-2-88971-342-4

Table of Contents

05 ***Blockage of Autophagic Flux and Induction of Mitochondria Fragmentation by Paroxetine Hydrochloride in Lung Cancer Cells Promotes Apoptosis via the ROS-MAPK Pathway***
Kun Wang, Qing Gong, Yujuan Zhan, Bonan Chen, Ting Yin, Yuhua Lu, Yilin Zhang, Huiqi Wang, Junzi Ke, Biaoyan Du, Xiaodong Liu and Jianyong Xiao

24 ***Endosome-to-TGN Trafficking: Organelle-Vesicle and Organelle-Organelle Interactions***
Yingfeng Tu, Lin Zhao, Daniel D. Billadeau and Da Jia

37 ***Current and Emerging Approaches for Studying Inter-Organelle Membrane Contact Sites***
Xue Huang, Chen Jiang, Lihua Yu and Aimin Yang

56 ***Mitochondrial Fusion Machinery Specifically Involved in Energy Deprivation-Induced Autophagy***
Choufei Wu, Weijing Yao, Wenwen Kai, Weikang Liu, Wenlve Wang, Shuzhen Li, Yingcong Chen, Xiaoyong Wu, Liefeng Wang, Ying Li, Jingjing Tong, Jing Qian, Liqin Zhang, Zhi Hong and Cong Yi

68 ***OPA1-Exon4b Binds to mtDNA D-Loop for Transcriptional and Metabolic Modulation, Independent of Mitochondrial Fusion***
Liang Yang, Haite Tang, Xiaobing Lin, Yi Wu, Sheng Zeng, Yongzhang Pan, Yukun Li, Ge Xiang, Yi-Fang Lin, Shi-Mei Zhuang, Zhiyin Song, Yiguo Jiang and Xingguo Liu

80 ***Autophagy Regulates Fungal Virulence and Sexual Reproduction in* Cryptococcus neoformans**
Su-Ting Jiang, An-Ni Chang, Lian-Tao Han, Jie-Shu Guo, Yuan-Hong Li and Tong-Bao Liu

96 ***Endoplasmic Reticulum Membrane and Contact Site Dynamics in Autophagy Regulation and Stress Response***
Etienne Morel

105 ***The Role of Mitochondrial Dynamics and Mitophagy in Carcinogenesis, Metastasis and Therapy***
Yigang Wang, Hui-Hui Liu, Yu-Ting Cao, Lei-Lei Zhang, Fang Huang and Cong Yi

117 ***Endoplasmic Reticulum–Mitochondria Contact Sites and Neurodegeneration***
Lingna Xu, Xi Wang and Chao Tong

129 ***Peroxisomal Membrane Contact Sites in Mammalian Cells***
Chao Chen, Jing Li, Xuhui Qin and Wei Wang

138 ***The Autophagy Machinery Contributes to E-cadherin Turnover in Breast Cancer***
Valentina Damiano, Paola Spessotto, Giulia Vanin, Tiziana Perin, Roberta Maestro and Manuela Santarosa

151 ***Casein Kinase 1 Family Member CK1δ/Hrr25 Is Required for Autophagosome Completion***
Yuting Li, Xuechai Chen, Qianqian Xiong, Yong Chen, Hongyu Zhao, Muhammad Tahir, Jingdong Song, Bing Zhou and Juan Wang

159 ***The Molecular Determinants of Mitochondrial Membrane Contact With ER, Lysosomes and Peroxisomes in Neuronal Physiology and Pathology***
Yajin Liao, Yuan Dong and Jinbo Cheng

169 ***Reweaving the Fabric of Mitochondrial Contact Sites in Astrocytes***
Matteo Bergami and Elisa Motori

177 ***Effects of Hyperoxia on Mitochondrial Homeostasis: Are Mitochondria the Hub for Bronchopulmonary Dysplasia?***
Yu Xuefei, Zhao Xinyi, Cai Qing, Zhang Dan, Liu Ziyun, Zheng Hejuan, Xue Xindong and Fu Jianhua

frontiers in Cell and Developmental Biology

ORIGINAL RESEARCH
published: 22 January 2020
doi: 10.3389/fcell.2019.00397

Blockage of Autophagic Flux and Induction of Mitochondria Fragmentation by Paroxetine Hydrochloride in Lung Cancer Cells Promotes Apoptosis via the ROS-MAPK Pathway

Kun Wang[1,2†], Qing Gong[3†], Yujuan Zhan[1,4†], Bonan Chen[1,4†], Ting Yin[4], Yuhua Lu[2], Yilin Zhang[2], Huiqi Wang[4], Junzi Ke[4], Biaoyan Du[2], Xiaodong Liu[5] and Jianyong Xiao[1,4]**

[1] Research Center of Integrative Medicine, School of Basic Medical Sciences, Guangzhou University of Chinese Medicine, Guangzhou, China, [2] Department of Pathology, Guangzhou University of Chinese Medicine, Guangzhou, China, [3] GMU-GIBH Joint School of Life Sciences, Guangzhou Medical University, Guangzhou, China, [4] Department of Biochemistry, Guangzhou University of Chinese Medicine, Guangzhou, China, [5] Department of Anaesthesia and Intensive Care, The Chinese University of Hong Kong, Shatin, Hong Kong

OPEN ACCESS

Edited by:
Min Li,
Sun Yat-sen University, China

Reviewed by:
Jin-Jian Lu,
University of Macau, China
Chung-Hang Leung,
University of Macau, China

***Correspondence:**
Xiaodong Liu
xdliu@cuhk.edu.hk
Jianyong Xiao
jianyongxiao@gzucm.edu.cn

[†] These authors have contributed equally to this work

Specialty section:
This article was submitted to Molecular Medicine, a section of the journal Frontiers in Cell and Developmental Biology

Received: 30 August 2019
Accepted: 31 December 2019
Published: 22 January 2020

Citation:
Wang K, Gong Q, Zhan Y, Chen B, Yin T, Lu Y, Zhang Y, Wang H, Ke J, Du B, Liu X and Xiao J (2020) Blockage of Autophagic Flux and Induction of Mitochondria Fragmentation by Paroxetine Hydrochloride in Lung Cancer Cells Promotes Apoptosis via the ROS-MAPK Pathway. Front. Cell Dev. Biol. 7:397. doi: 10.3389/fcell.2019.00397

Cancer cells are characterized by malignant proliferation and aberrant metabolism and are thereby liable to the depletion of nutrients and accumulation of metabolic waste. To maintain cellular homeostasis, cancer cells are prone to upregulating the canonical autophagy pathway. Here, we identified paroxetine hydrochloride (Paxil) as a late autophagy inhibitor and investigated its killing effect on lung cancer cells and with a xenograft mouse model *in vivo*. Upregulated LC3-II and p62 expression indicated that Paxil inhibited autophagy. Acid-sensitive dyes (e.g., LysoTracker and AO staining) indicated reduced lysosomal acidity following Paxil treatment; consequently, the maturation of the pH-dependent hydroxylases (e.g., cathepsin B and D) substantially declined. Paxil also induced the fragmentation of mitochondria and further intensified ROS overproduction. Since the autophagy pathway was blocked, ROS rapidly accumulated, which activated JNK and p38 kinase. Such activity promoted the localization of Bax, which led to increased mitochondrial outer membrane permeability. The release of Cytochrome c with the loss of the membrane potential triggered a caspase cascade, ultimately leading to apoptosis. In contrast, the clearance of ROS by its scavenger, NAC, rescued Paxil-induced apoptosis accompanied by reduced p38 and JNK activation. Thus, Paxil blocked the autophagic flux and induced the mitochondria-dependent apoptosis via the ROS-MAPK pathway.

Keywords: paroxetine hydrochloride, lung cancer, autophagy, ROS, apoptosis

INTRODUCTION

Autophagy is a highly conserved degradative process through which cells can recycle intracellular waste products to maintain cellular homeostasis (White, 2012). For cancer cells, malignant proliferation and abnormal metabolism leave cells depleted of nutrients and full of stressful waste products (e.g., dysfunctional mitochondria and its byproduct, reactive oxygen species [ROS]).

Theoretically, elevated levels of autophagy may protect cancer cells from programed cell death and thereby exhibit tumor-facilitating activity (White, 2012). Indeed, a high level of autophagy was observed in the tumor cells and believed to be a cell survival process that affected multiple processes, including anoikis, cell motility, and EMT (Mowers et al., 2017). Thus, the blockage of autophagic flux might be beneficial for the treatment of various cancers.

The blockage of autophagy may result in the accumulation of intracellular ROS, including peroxides, superoxides, and hydroxyl radicals. Compared with normal cells, cancer cells have a dominant number of dysfunctional mitochondria due to frequent fission and fusion events. Damaged mitochondria are the major sources of high levels of ROS production (Indo et al., 2007). Thus, with the blockage of the autophagy pathway, higher levels of ROS can possibly accumulate to a greater extent in cancer cells compared to normal cells. In most cases, excessive ROS is detrimental to the cells. For instance, ROS may activate JNK, leading to Bcl-2 or p53-dependent mitochondrial apoptosis (Shen and Liu, 2006; Shi et al., 2014; Redza-Dutordoir and verill-Bates, 2016); p38 MAPK can also be activated by ROS and cause apoptosis (Liu et al., 2014; Wu et al., 2017). Therefore, the present study sought to determine whether the inhibition of autophagy could preferentially kill cancer cells over normal cells. Collectively, autophagy inhibitors may cause the accumulation of ROS and exert cytotoxic activity toward cancer cells.

Lung cancer is the leading cause of cancer-related death globally, accounting for 18.4% of death to all cancers in 2018 (Bray et al., 2018). Despite therapeutic advances (e.g., radiation, chemotherapy, and targeted drugs), intolerable adverse effects and drug resistance is limited to the efficacy of these regimens. Novel compounds with anti-cancer activity, especially medications that have been regularly prescribed for non-cancer diseases, have the potential to become valuable alternatives to current therapies. We performed a preliminary screening of many small molecules provided by Gu et al. (2013) and discovered that Paxil exhibited considerable cancer suppressive capacity accompanied by its functions as an autophagy inhibitor. Paroxetine hydrochloride (Paxil), a phenylpiperidine derivative, is a selective serotonin reuptake inhibitor prescribed to treat mood disorders (e.g., depression, generalized anxiety disorders, and obsessive-compulsive disorder) (Germann et al., 2013). Based on the excellent medicinal characteristics of Paxil, in the present study, we sought to evaluate its anti-cancer activity both *in vitro* and *in vivo*, and further elucidate the associated underlying mechanisms in lung cancer cells.

RESULTS

Paxil Inhibits the Proliferation of NSCLC Cells

We first sought to determine whether Paxil had a potential anti-cancer effect on NSCLC using CCK8 assay. The data in **Figure 1A** showed that Paxil inhibited the cell viability of NSCLC cells in a dose-dependent fashion compared to vehicle control. The IC50 of Paxil on NCI-H1299 and NCI-H1650 cells was 16.4 and 18.75 μM, respectively. Intriguingly, Paxil induced a higher inhibition rate for NSCLC compared to a normal human lung epithelial cell line (BEAS-2B), which suggests that Paxil might preferentially kill cancer cells compared to normal cells (**Figure 1B**). To evaluate the cytotoxicity of Paxil, we also examined the cell viability of various types of cancer cells, and the IC50 of Paxil on A375, HepG2, MCF-7, and CNE1 cells for 24 h was 13.99, 15.86, 17.38, and 18.74 μM, respectively (**Supplementary Figure S1**). The inhibitory effect of Paxil on lung cancer cells was also confirmed by a colony formation assay. There was a reduced number of colonies that formed in the Paxil group compared with vehicle control (**Figure 1C**). At a concentration of 30 μM, Paxil completely blocked the colony-forming capability of both NCI-H1299 and NCI-H1650 cells (**Figure 1C**). Moreover, using CFDA-SE staining, we also monitored the proliferation rate of NSCLC following Paxil treatment. CFDA-SE is a fluorescent dye that is evenly distributed among dividing cells and the mean intensity of fluorescence decreases with each division. In contrast, in non-dividing cells, the fluorescence is sequestered, and the intensity is not attenuated. As demonstrated in **Figure 1D**, the mean fluorescent intensity in NSCLC cells was significantly higher in the Paxil group compared to that in the vehicle group, indicating that fewer cells underwent division following Paxil treatment. Compared to the vehicle, Paxil treatment also significantly reduced the incorporation of 5-ethynyl-20-deoxyuridine (EdU) into DNA, compared to vehicle control (**Figure 1E**). This result was in agreement with the CFDA-SE assay and demonstrated that DNA replication was inhibited by Paxil in a dose-dependent manner. Taken together, these data suggest that Paxil represents a novel inhibitor of NSCLC cell proliferation.

Paxil-Induces Damage of Mitochondria and Simultaneously Inhibits Autophagy in NSCLC Cells

Cellular viability or proliferation has a tight relationship with mitochondrial function. We observed the morphology of mitochondria stained with MitoTracker Red. The data showed a dramatic reduction in mitochondrial length following Paxil treatment (**Figure 2A**), which was indicative of fragmented mitochondria. Then we performed JC-1 assay to determine the effect of Paxil on mitochondrial membrane potential (MMP). As shown in **Figure 2B**, Paxil treatment caused a significant decrease of MMP in NCI-H1299 cells. The intracellular level of ROS as a byproduct of mitochondrial damage is likely to become elevated with an increase in damaged mitochondria. Indeed, Paxil upregulated the level of ROS in a dose-dependent manner in both cell lines, with as high as a four-fold elevation at the highest concentration (**Figures 2C,D**).

To maintain redox homeostasis and avert the detriment of ROS, cancer cells usually adapt to recycle the damaged mitochondria through the induction of autophagy (Ashrafi and Schwarz, 2013). Indeed, there was a substantial increase in the number of autophagosomes in NSCLC cells with exposure to Paxil, as evidenced by an elevated level of LC3-II (an autophagosome marker). As shown in **Figure 3A**, Paxil induced

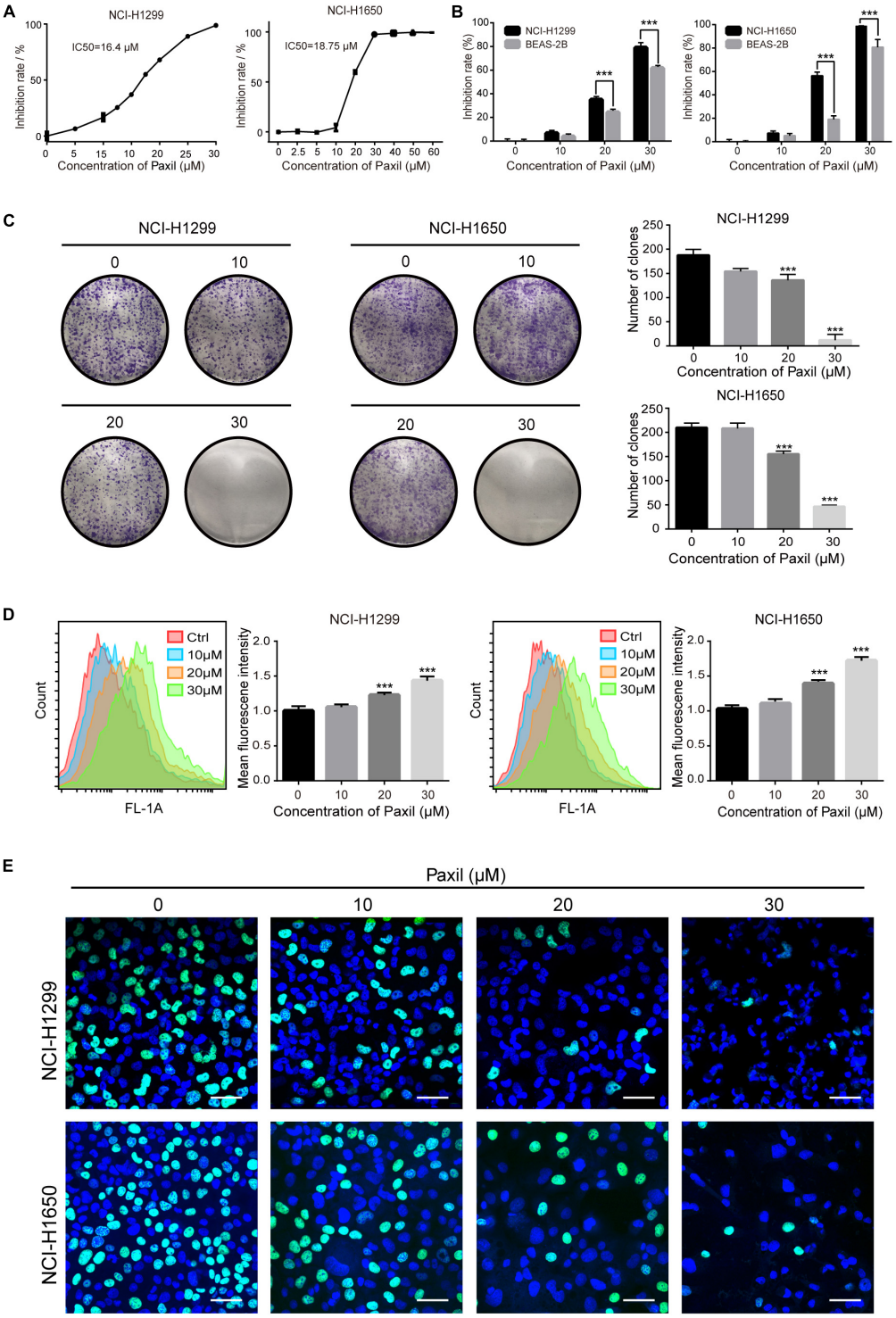

FIGURE 1 | Paxil inhibited the proliferation of human NSCLC cells. **(A)** NCI-H1299 and NCI-H1650 cells were treated with a gradient concentration of Paxil for 24 h, and cell viability was determined with a CCK8 assay and visualized with GraphPad software. The median inhibitory concentration (IC50) was estimated by log (inhibitor) vs. normalized response non-linear fit. **(B)** Inhibition rate of NSCLC cells vs. normal human lung epithelial cells (BEAS-2B) following Paxil treatment for 24 h determined by a CCK8 assay. **(C)** Paxil inhibited the colony formation of NSCLC cells. Cells were exposed to Paxil for seven days and then stained by crystal violet. **(D)** Cells were labeled with CFDA-SE and treated with Paxil for 24 h. The mean fluorescence intensity was inversely correlated with cell division was determined by flow cytometry. **(E)** Cells were treated with Paxil for 24 h. EdU-positive cells were marked in green. Blue represents nuclei labeled with Hoechst 33342. Images were obtained by a confocal laser scanning microscope. Scale bar: 20 μm. Error bars, means ± SD of three independent experiments; $^{***}p < 0.001$, compared to the control.

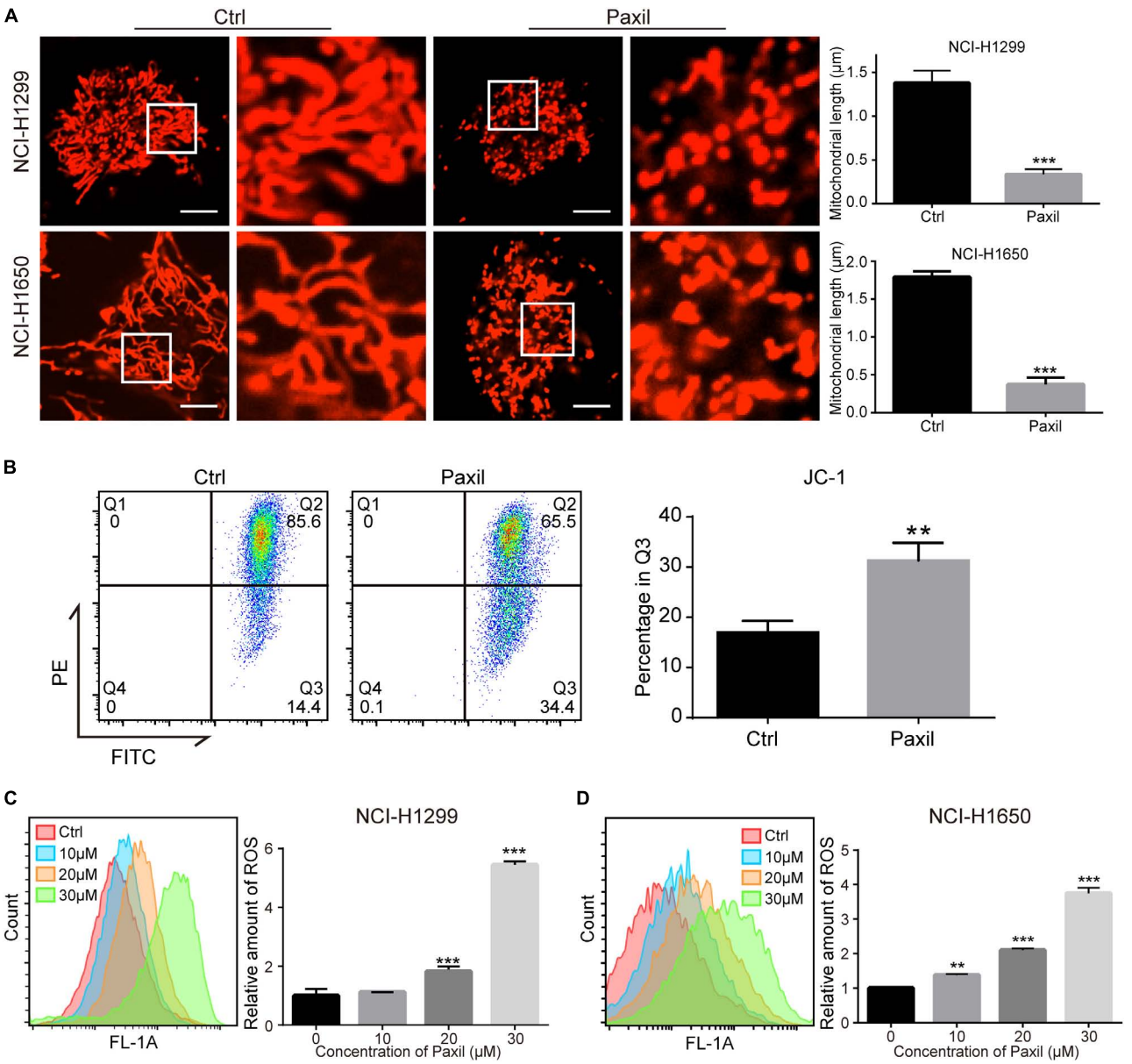

FIGURE 2 | Paxil induced fragmentation of mitochondria in NSCLC cells. **(A)** NCI-H1299 and NCI-H1650 cells were treated with either a vehicle or Paxil (20 μM) for 24 h. The mitochondria were stained by MitoTracker Red CMXRos. The length of the mitochondria was quantified in ImageJ. Scale bar: 5 μm; $^{***}p < 0.001$. **(B)** Paxil treatment caused a significant decrease of mitochondrial membrane potential (MMP). NCI-H1299 cells were treated with either a vehicle or Paxil (20 μM) for 24 h. The MMP was determined by JC-1 assay. $^{**}p < 0.01$. **(C,D)** Cells were treated with Paxil at the indicated concentrations and dyed with the green fluorescent dye DCFDA for labeling intracellular ROS. The green mean fluorescence intensity that indicated the relative amount of ROS was detected by flow cytometry. $^{**}p < 0.01$; $^{***}p < 0.001$.

the accumulation of green fluorescence in NSCLC cells stably overexpressing GFP-LC3. In addition, the immunoblotting results showed that compared to the vehicle control, the ratios of LC3-II/LC3-I and LC3-II/β-actin were gradually increased with exposure to Paxil in a dose- and time-dependent manner (**Figures 3B,C**). Of note, the increase in autophagosomes may result from either the induction of autophagy using Rapamycin (Rapa, 0.5 μM) or the blockage of the late autophagic flux, similar to that achieved following treatment with Bafilomycin A1 (Baf, 0.1 μM). Thus, the level of p62/SQSTM1 protein expression was assessed to differentiate autophagy induction or autophagic flux impairment. As demonstrated in **Figure 3D**, Paxil treatment induced a striking increase of p62 protein in both cell lines in a dose-dependent manner. With a concentration of 20 μM, Paxil induced p62 elevation as early as 2 h, which persisted for at least 24 h in both cell lines (**Figure 3E**). Since p62 is degraded through autophagy, its upregulation represented a blockage of the autophagy pathway. Compared with Baf, a canonical inhibitor

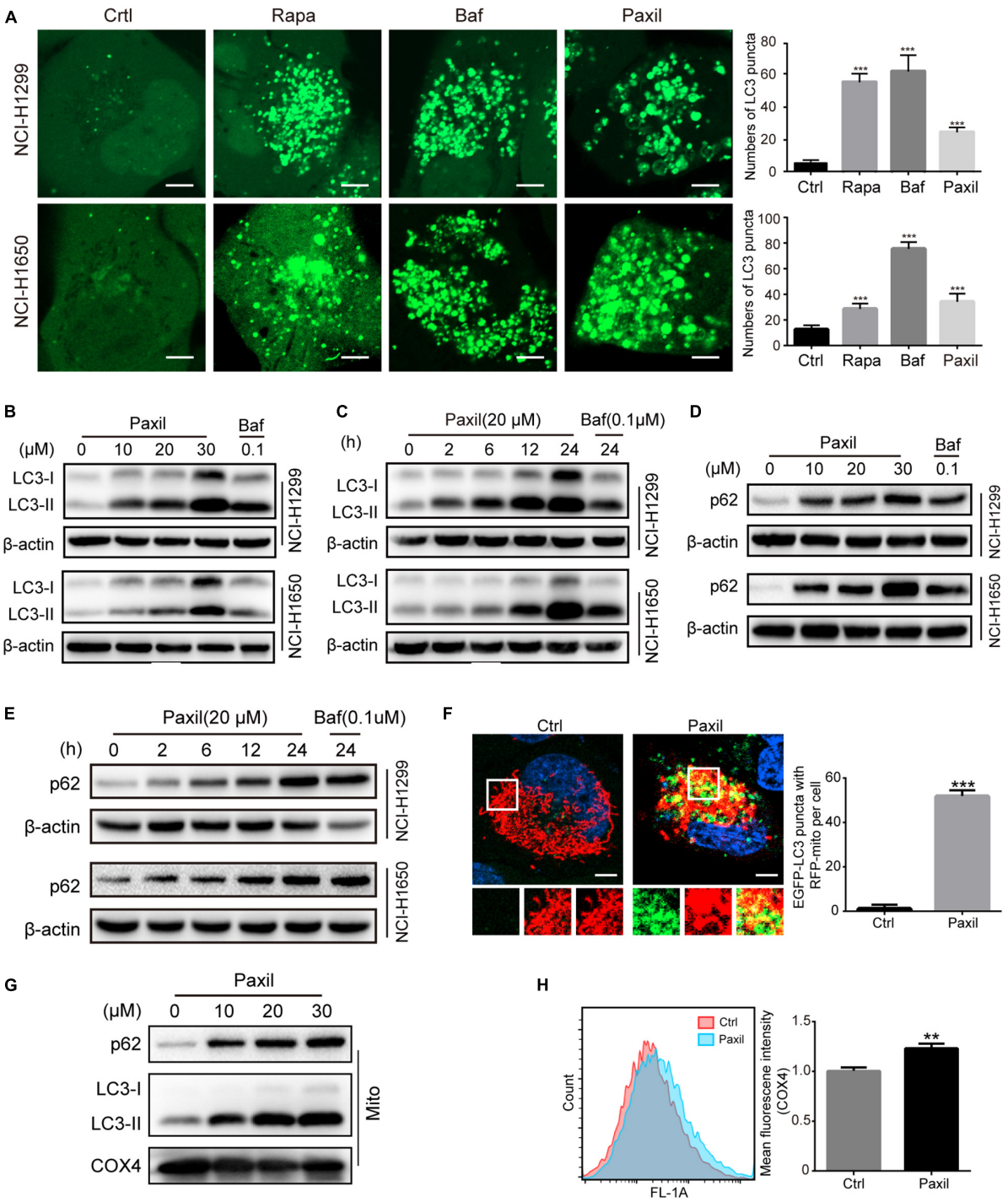

FIGURE 3 | Paxil inhibited autophagy in NSCLC cells. **(A)** The increased GFP-LC3 puncta with Paxil treatment. NSCLC cell lines (NCI-H1299 and NCI-H1650) that stably over-express GFP-LC3 were treated with a vehicle, rapamycin (Rapa, 0.5 μM), bafilomycin A1 (Baf, 0.1 μM), and Paxil (20 μM) for 24 h. Images were obtained with a confocal laser scanning microscope. Scale bar: 5 μm. **(B–E)** Cells were treated with Paxil or Baf at the concentration gradient for 24 h or at the indicated dose over a time course. The protein level was examined by western blot. **(F)** Colocalization of mitochondria and autophagosomes. An NCI-H1299$^{GFP-LC3}$ stable cell line was transiently transfected with a pDsRed$_2$-Mito plasmid and treated with either a vehicle or Paxil (20 μM) for 24 h. Green represents the autophagosomes labeled with GFP-LC3; red indicates the mitochondria labeled Red$_2$-Mito. Representative images are shown. Scale bar: 5 μm; $^{***}p < 0.001$. **(G)** The upregulation of p62 and LC3-II in mitochondrial fractions induced by Paxil. Following Paxil treatment for 24 h, the mitochondrial parts in NCI-H1299 cells were separately extracted from the total lysates. The protein level was examined by western blot. COX4 was used as an internal reference for the mitochondrial fractions. Mito, mitochondrial fractions. **(H)** NCI-H1299 cells were treated with either a vehicle or Paxil (20 μM) for 24 h, after which the cells were harvested and stained with an immunofluorescence assay. The mean fluorescence intensity of COX4, a mitochondrial marker, was detected by flow cytometry.

of autophagy, the modulation of LC3-II and p62 levels by Paxil implied that Paxil was a potent autophagy inhibitor.

These data suggest that Paxil induces mitochondrial damage in lung cancer cells. Such damaged mitochondria can be removed via the autophagy pathway. As demonstrated above, Paxil impaired autophagy flux by affecting the late stage of the autophagy pathway. Therefore, it is possible that mitophagy can be initialized but is arrested during the clearance stage. Compared with vehicle control, GFP-LC3 puncta were significantly induced and co-localized with mitochondria (red) after Paxil treatment (**Figure 3F**). The upregulation of LC3-II and p62 in the separated mitochondria following Paxil treatment corroborated the conclusion that mitophagy-associated compartments were formed and engulfed damaged mitochondria following Paxil treatment (**Figure 3G**). COX4, a mitochondrial marker, was quantified to determine the mitochondrial mass via flow cytometry. Although mitophagy was initialized, the mitochondrial mass was significantly increased in Paxil-treated cells compared with the vehicle-treated cells (**Figure 3H**).

Damaged Mitochondria Pack Into Autophagosomes Relying on a Ubiquitin Pathway

Now that the damaged mitochondria can be wrapped into the autophagosomes after Paxil treatment, next we dug into the mechanisms underly this process. Mitophagy was usually intermediated by ubiquitin-dependent pathways or receptor-mediated pathways (Harris et al., 2017). Knockdown of several major receptors localized in the mitochondria such as FUNDC1, BNIP3 and Nix by small interfering RNA did not reduce the extent of mitophagy, suggesting that the receptors are unlikely involved in mitophagy (**Figure 4A**).

In contrast, the elevated expression of PINK1 and phosphorylated ubiquitin (p-Ub) suggested that ubiqutination might be the mechanism that mediated the Paxil-induced mitophagy (**Figure 4B**). We also determined the co-localization of mitochondria and p-Ub. As shown in **Figure 4C**, p-Ub was mainly distributed on the mitochondria. Parkin, a key ubiquitin ligase in the ubiquitin-mediated mitophagy, however, seems not to participate in the ubiquitination process due to the downregulation of protein expression (**Figure 4B**). In order to prove the necessity of PINK1 for Paxil-induced mitophagy, we suppressed the expression of PINK1 by a small interfering RNA, and found that p-Ub and LC3-II upregulation induced by Paxil was indeed reversed (**Figure 4D**). Nonetheless, in the absence of Parkin, the basal ubiquitin of outer mitochondrial membrane followed by the phosphorylation by PINK1 is reported to be sufficient to mediate the mitophagy process, wherein Optineurin (OPTN) and NDP52 can be recruited to mitochondria (Stolz et al., 2014; Wong and Holzbaur, 2014; Michael, 2015), and bind to the phosphorylated basal ubiquitin (Nguyen et al., 2016). NDP52 and OPTN are important autophagy mediators which are thought to function primarily by bridging LC3 and ubiquitinated cargo (Svenning and Johansen, 2013; Stolz et al., 2014; Lazarou et al., 2015). In agreement with these reports, the protein level of OPTN and NDP52 did increase after Paxil induction in the mitochondrial fractions (**Figure 4E**) and both OPTN and NDP52 co-localized with LC3 (**Supplementary Figure S2**). **Figure 4F** showed that NDP52 and OPTN were also mainly distributed on the mitochondria which was similar to the distribution of p-Ub. Then we conducted small interfering RNA transfection assay to confirm the necessity of NDP52 and OPTN for Paxil-induced mitophagy and the data demonstrated that either NDP52 or OPTN knockdown could block Paxil-induced mitophagy (**Figure 4G**). Collectively, mitophagy induced by Paxil might be mediated through a ubiquitination process during which PINK1, NDP52, OPTN played important roles.

Paxil Blocks Autophagic Flux by Inhibiting Lysosomal Acidification Rather Than Interfering With Autophagosome and Lysosome Fusion

To further monitor the autophagic flux induced by Paxil, we transfected NSCLCL cells with GFP-mCherry-LC3 tandem plasmids (**Figure 5A**). HBSS treatment was used as a starvation mimic and promoted autophagic flux to produce a dominant number of autolysosomes. The GFP-mCherry-LC3 fusion protein was able to mark the autolysosomes by showing red fluorescence since the green fluorescence was quenched in an acidic environment. In contrast, Baf treatment ultimately resulted in an elevated pH in the autolysosomes due to its inhibition of lysosomal acidification. The GFP-mCherry-LC3 localized in the aberrant autolysosomes displayed both green and red fluorescence (i.e., yellow puncta). Similar to Baf, Paxil treatment also induced an increase in yellow puncta, which suggested that Paxil may inhibit lysosomal acidification. The co-localization of GFP and mCherry fluorescence was significantly increased in Paxil- or Baf-treated cells compared to the starvation group (HBSS treatment), as analyzed by a Pearson's correlation coefficient. These findings indicate that Paxil, similar to Baf, appeared to block the late stage of autophagic flux.

Of note, GFP-mCherry-LC3 can also label autophagosomes, in which green combined with red fluorescence manifests as yellow fluorescence. Therefore, the increase of yellow puncta in Paxil-induced NSCLC cells could also reflect an increase in autophagosomes due to a blockade of autophagosome-lysosome fusion. To exclude this possibility, NSCLC cells were transfected with GFP-LC3 as a marker of autophagosomes and subsequently treated with DMSO (vehicle), chloroquine (CQ), Rapa, or Paxil. The lysosomes were labeled by LysoBrite^{TM} red. In the vehicle-treated cells, signals for lysosomes (red) but not GFP-LC3 puncta, were present. Rapa strikingly induced the formation of GFP-LC3 puncta, a large number of which were also co-localized with the lysosomes. This observation was in agreement with the phenomena that Rapa promotes autophagy. Treatment with CQ, a well-known autophagy inhibitor, was used to interfere with autophagosome-lysosome fusion. CQ treatment induced the accumulation of GFP-LC3 puncta that only occasionally colocalized with the lysosomes. In contrast, although Paxil inhibited autophagy, Paxil did not affect the colocalization of

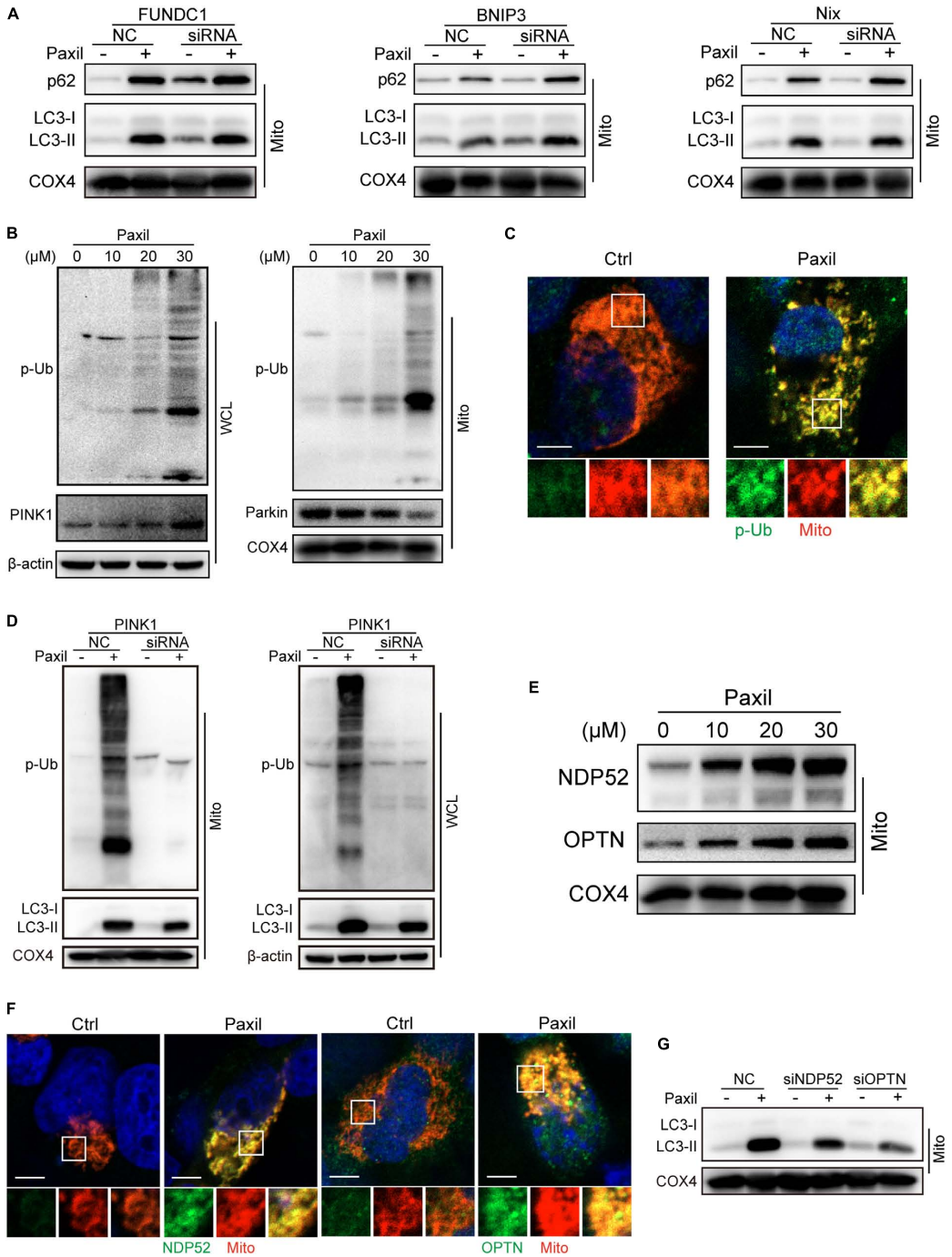

FIGURE 4 | Autophagosomes recognized and bound to the impaired mitochondria possibly relying on the ubiquitination process rather than receptor-mediated pathways. The mitochondrial parts in NCI-H1299 cells were separately extracted from the total lysates. The protein level was examined by western blot. **(A)** The expression of LC3-II and p62 in lung caner cells with the silence of FUNDC1, BNIP3 and Nix. NCI-H1299 cells were transfected with small interfering RNA and cultured for 24 h, subsequently treated with Paxil as indicated. **(B)** NCI-H1299 cells were treated with Paxil for 24 h, then the indicated proteins were detected by western blot assay. **(C)** Co-localization of mitochondria and phosphorylated ubiquitin. The mitochondria were marked as red by pDsRed2-mito plasmids transfection, then immunofluorescence experiments were performed to stain phosphorylated ubiquitin (p-Ub) as green. Scale bar, 5 μm. **(D)** PINK1 knockdown blocked mitophagy induced by Paxil treatment. NCI-H1299 cells were transfected with small interfering RNA and cultured for 24 h, subsequently treated with Paxil as indicated. Then the indicated proteins were detected by western blot assay. **(E)** The upregulation of Optineurin and NDP52 proteins in the mitochondrial fractions induced by Paxil. COX4 was used as an internal reference for the mitochondrial fractions. **(F)** Co-localization of mitochondria and NDP52 or OPTN. The mitochondria were marked as red by pDsRed2-mito plasmids transfection, then immunofluorescence experiments were performed to stain NDP52 or OPTN as green. Scale bar, 5 μm. **(G)** Either NDP52 or OPTN knockdown reversed Paxil-induced mitophagy. NCI-H1299 cells were transfected with small interfering RNA and cultured for 24 h, subsequently treated with Paxil as indicated. Then the indicated proteins were detected by western blot assay. WCL, whole-cell lysates; Mito, mitochondrial fractions.

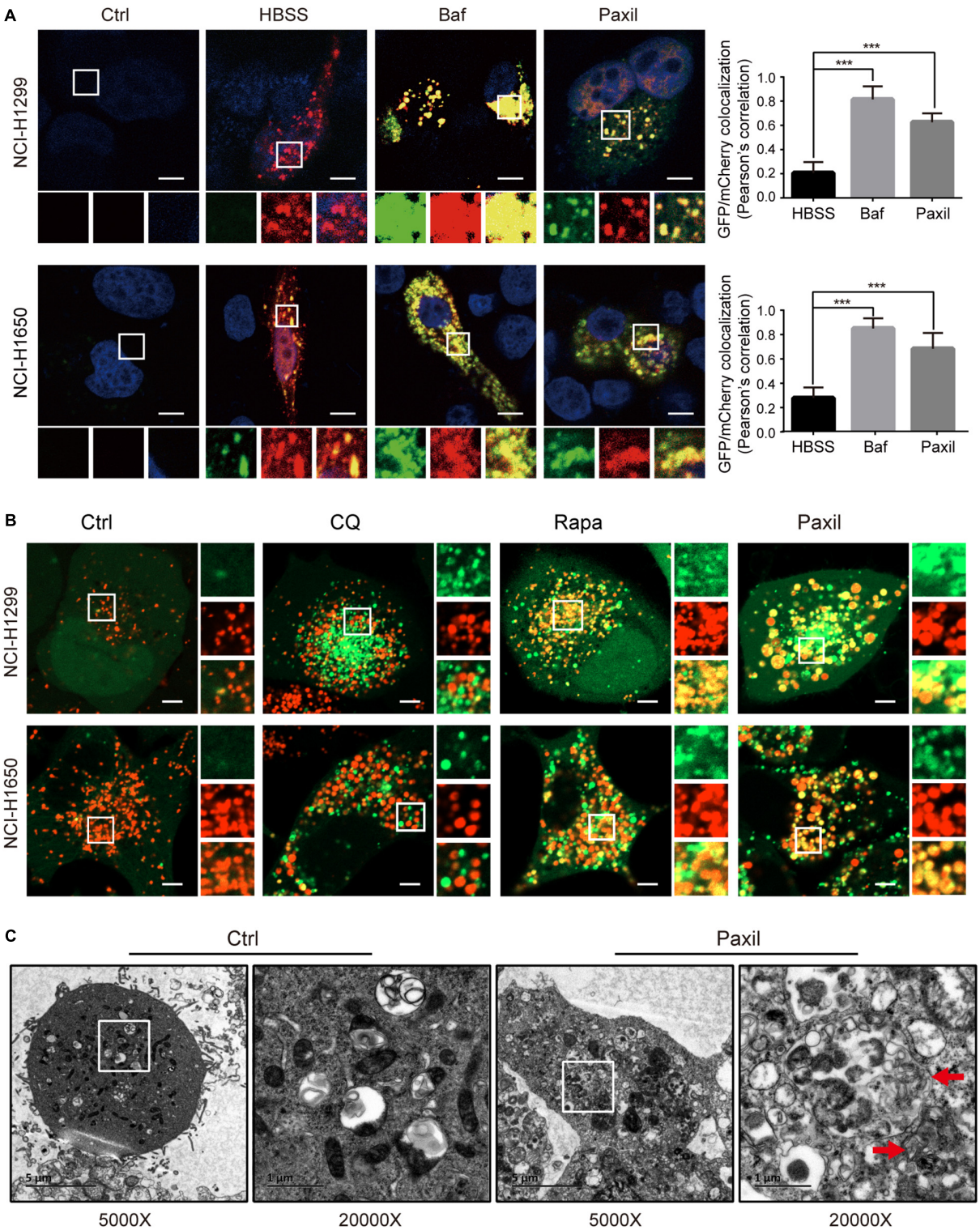

FIGURE 5 | Paxil did not block autophagic flux by interfering with autophagosome and lysosome fusion. **(A)** NCI-H1299 and NCI-H1650 cells were transiently transfected with mCherry-GFP-LC3 plasmids and treated with a vehicle, Paxil (20 μM), Baf (0.1 μM) for 24 h, or HBSS for 6 h. Representative images are shown. Scale bar: 5 μm. Error bars represent the means ± SD of three independent experiments; ***$p < 0.001$, compared to the control. **(B)** NCI-H1299 and NCI-H1650 cells stably expressing GFP-LC3, a canonical autophagosome marker with green fluorescence, were treated with a vehicle, chloroquine (CQ, 20 μM), Rapamycin (Rapa, 0.5 μM), or Paxil (20 μM) for 24 h. LysoBrite red dyes were used to label the lysosomes. Images were acquired with a confocal laser scanning microscope. Typical images are shown. Scale bar: 5 μm. **(C)** NCI-H1299 cells were treated by a vehicle or Paxil (20 μM) for 24 h. A transmission electron microscopy (TEM) assay was performed to observe the cellular structures. In each group, the image on the right is a partial enlargement of the image on the left. Red arrow, autolysosomes.

GFP-LC3 puncta and lysosomes (**Figure 5B**). Moreover, we observed the intracellular structures by transmission electron microscopy and discovered many autolysosomes (formed by autophagosome and lysosome fusion) in the cells treated with Paxil compared with the control group (**Figure 5C**). These results suggest that Paxil was unlikely to interfere with autophagosome-lysosome fusion.

Next, we investigated whether Paxil impaired autophagic flux via disrupting lysosomal acidification. LysoTracker and AO were applied, which emitted bright red fluorescence in the acidic vesicles. As expected, treatment with Baf, a well-known inhibitor of the lysosomal proton pump, completely abolished the LysoTracker (**Figure 6A**) and AO (**Figure 6B**)-related red fluorescence in both cell lines. To a lesser extent, treatment with Paxil for 6 h also significantly reduced the red fluorescence of both dyes compared to the vehicle control. Lysosomal cathepsins, such as cathepsin B (CatB) and cathepsin D (CatD), require an acidic environment for maturation. The ratio of mature to pro-forms of these cathepsins are widely used as indicators of an acidic lysosomal environment. As shown in **Figures 6C,D**, Paxil dose- and time-dependently reduced the mature forms of CatB and CatD in NCI-H1299 and NCI-H1650 cells, yet increased the levels of pro-CatB and pro-CatD. These data provide further evidence that Paxil may increase the pH of the acidic vesicles in NSCLC cells. Such effects, in turn, disrupted the processing of cathepsins in lysosomes, affected cargo degradation in the autolysosomes, and ultimately impaired autophagic flux.

Paxil-Induced ROS Accumulation Promotes Mitochondria-Dependent Apoptosis via Activation of the MAPK Pathway

Since Paxil induced the fragmentation of mitochondria and simultaneously blocked the clearance of damaged mitochondria, ROS accumulated in the cells (**Figures 2B,C**), which in turn was thought to activate the MAPK pathway. The immunoblotting results revealed that Paxil induced the upregulation of p-JNK and p-p38, the major kinases in the MAPK pathway, in

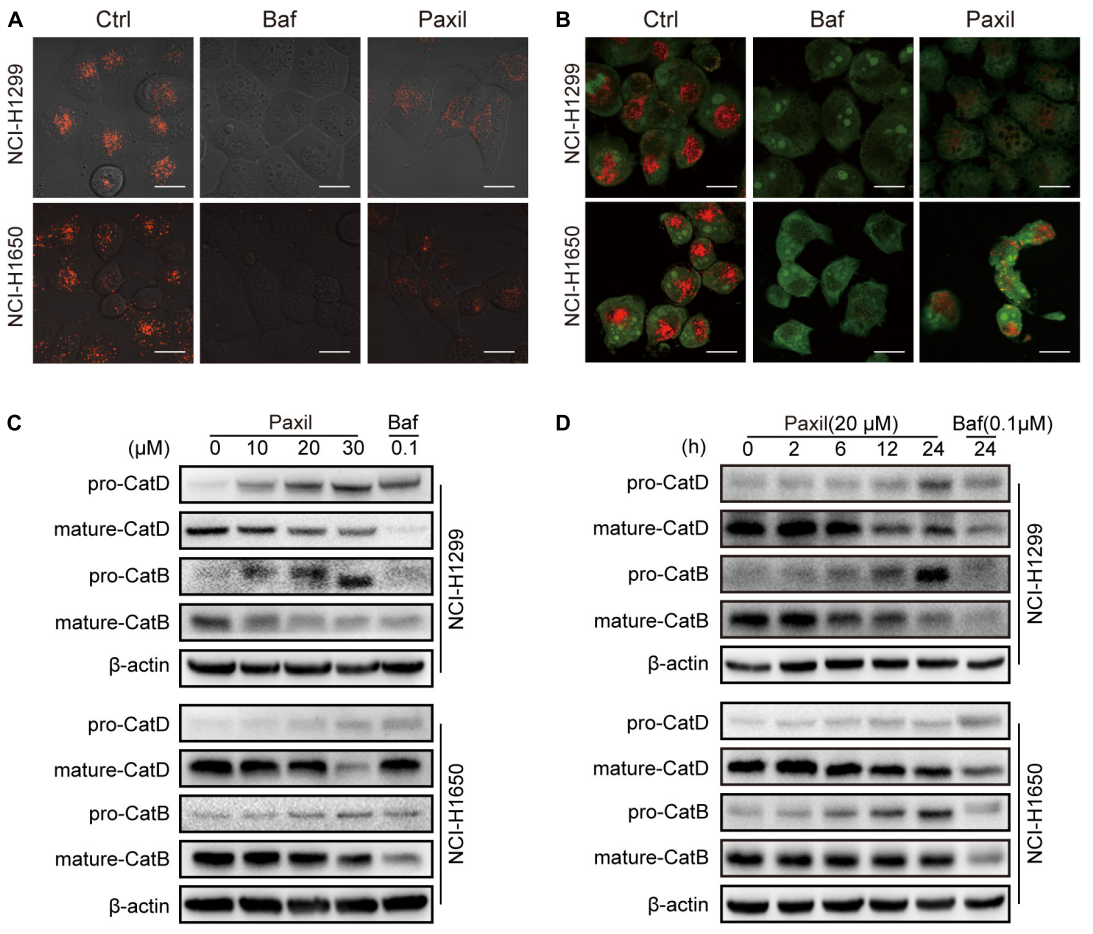

FIGURE 6 | Paxil blocked autophagic flux by inhibiting lysosomal acidification. **(A,B)** Cells were treated with a vehicle, Baf (0.1 μM) or Paxil (20 μM) for 24 h and stained with lysosome-philic fluorescent dyes, including acridine orange (AO) and LysoTracker Red DND-99. The dyes are sensitive to acidity, and therefore, the fluorescence weakened with increased pH value. Images were acquired by a confocal laser scanning microscope. Scale bar: 20 μm. **(C,D)** Mature forms of cathepsins decreased with exposure to Paxil in a time- and dose-dependent manner.

a dose-dependent manner (**Figure 7A**). MAPK is a well-known pathway that mediates the translocation of Bax, a pore-creating protein, from the cytoplasm to the mitochondria, which leads to mitochondrial outer membrane permeability (MOMP). To confirm this assumption, the mitochondria and cytosolic fractions were separated and analyzed by western blot (**Figure 7B**). After 24 h, Paxil dose-dependently induced the re-distribution of Bax to mitochondria fractions (Mito) and the accumulation of Cyto-c in the cytosolic fractions (Cyto). The occurrence of MOMP was typically accompanied by the loss of the mitochondrial membrane potential which had been confirmed in **Figure 2B**.

The release of cytochrome c is a crucial factor that triggers the caspase cascade leading to programed cell death, so we then confirmed that Paxil caused caspase 9 activation by western blot (**Figure 7C**). Thus, an Annexin V/PI staining assay was performed to determine the rate of apoptosis following Paxil treatment. Compared to vehicle control, different doses of Paxil significantly increased the apoptotic rates in both NSCLC cell lines (**Figure 7D**). It was found that as many as 50% of cancer cells underwent apoptosis following Paxil (30 μM) treatment for 24 h. Apoptotic markers were then assessed by a western blot. Compared to the vehicle control, the levels of cleaved-caspase 3 and cleaved-PARP protein were upregulated by Paxil treatment in a dose- and time-dependent manner (**Figures 7E,F**). These results suggest that Paxil can induce apoptosis in NSCLC cells.

Paxil Induces Apoptosis Through ROS-MAPK Signaling Pathways

To examine whether ROS plays an essential role in the Paxil-mediated cell response, we pre-treated cells with NAC, a ROS scavenger, followed by Paxil treatment. A CCK8 assay demonstrated that pre-treatment with NAC (2 mM) significantly reversed the cell growth-inhibiting activity of different doses of Paxil (**Figure 8A**). Coherently, NAC significantly suppressed Paxil-induced cancer cell apoptosis in an Annexin V/PI assay (**Figure 8B**; 34.0% vs. 49.4%, Paxil + NAC vs. Paxil, respectively). As expected, activation of the JNK and p38MAPK pathways by Paxil (20 or 30 μM) could also be attenuated in the presence of NAC (**Figure 8C**). To further confirm the essential roles of JNK and p38, we blocked the functions of JNK and p38 using JNK-IN-8 and SB203580, respectively. As evidenced in **Figure 8D**, the intervention of inhibitors to a great extent reversed Paxil-induced apoptosis, demonstrating JNK and p38 were indeed involved in the Paxil-induced anti-cancer effect. We also have examined ERK and p-ERK by western blot assay and p-ERK showed a dose-dependent upregulation after Paxil treatment (**Supplementary Figure S3A**). To verify whether p-ERK mediated the Paxil-induced apoptosis, we blocked the function of MEK1/2, the upstream kinase of ERK, using specific inhibitor (U0126-EtOH). As shown in **Supplementary Figure S3B**, with the addition of inhibitor, the level of p-ERK was reversed in a large part. However, the apoptosis rate of lung cancer cells was not rescued, or even worsened, suggesting ERK might not be involved in the Paxil-induced apoptosis (**Supplementary Figure S3C**).

Paxil Inhibits Tumor Growth in a NCI-H1299 Tumor Xenograft Model

The anticancer-like activity of Paxil was evaluated in nude mice with xenografted tumors. A total of 32 mice were subcutaneously injected with NCI-H1299 cells, and then randomly assigned to four groups: (1) control (normal saline); (2) Paxil-5 mg/kg; (3) Paxil-20 mg/kg; and (4) Cisplatin-1 mg/kg. After 16 days, the mice were sacrificed for tumor tissue collection (**Figure 9A**). Treatment with Paxil significantly reduced the weight of the xenografted tumors compared to the vehicle (**Figure 9B**). Consistently, the average tumor volume was significantly smaller from Day 4 to the end of the study in the Paxil-20 mg/kg group compared with the control group (**Figure 9C**). The mice weight was measured every day, and there was no significant decrease following the drug treatment (**Figure 9D**). Since Paxil induced apoptosis and inhibited autophagic flux *in vitro*, we wondered whether Paxil exerted similar activity in the xenografted tumors *in vivo*. As demonstrated in **Figure 9E**, a dose of 20 mg/kg Paxil significantly increased the level of cleaved-caspase 3 and cleaved-PARP compared to the vehicle control. Furthermore, the analysis of autophagy markers demonstrated consistent results with the *in vitro* studies. Compared to the vehicle control, Paxil (20 mg/kg) significantly induced an accumulation of p62, and increased the ratio of LC3-II to β-actin in the tumor tissues (**Figure 9F**), suggesting that Paxil may also impair autophagic flux *in vivo*.

DISCUSSION

Paxil, a widely used antidepressant, showed anti-cancer activity in various types of cancer cells such as colon cancer cells and breast cancer cells (Cho et al., 2019; Jang et al., 2019). The major kinases of MAPK pathways such as p38, JNK was proposed to mediate the drug-induced apoptosis. However, the underly mechanism whereby paroxetine activates MAPK pathways remains to answer. In addition, although the priming of autophagy pathways dependent on FKBP51 was linked to the potency of paroxetine (Gassen et al., 2014), how Paxil perturbed the autophagic flux is still elusive. In this study, we discovered that Paxil exhibited tumor-suppressive functions as demonstrated by both *in vitro* and *in vivo* evidence in lung cancer cells, and two biological processes were revealed to be involved in the anti-tumor effect of Paxil (**Figure 10**): (1) Paxil directly targeted mitochondria and induced mitochondrial fragmentation via the overproduction of ROS; and (2) Paxil disrupted the autophagic degradation pathway by inhibiting lysosomal acidification. These dual actions consequently induced the accumulation of ROS, a detrimental factor for cells. Moreover, the accumulated ROS was able to activate the MAPK pathway and responded as a positive feedback loop to induce mitochondrial damage (Scherz-Shouval and Elazar, 2007). The increase of MOMP with the loss of mitochondria membrane potential is an initial step for subsequent apoptosis via the activated caspase cascade. Since cancer cells feature a large number of damaged mitochondria with the overproduction of ROS, a blockage of autophagy might result in a greater amount of ROS in cancer cells compared to normal cells (Simon et al., 2000; Vyas et al., 2016).

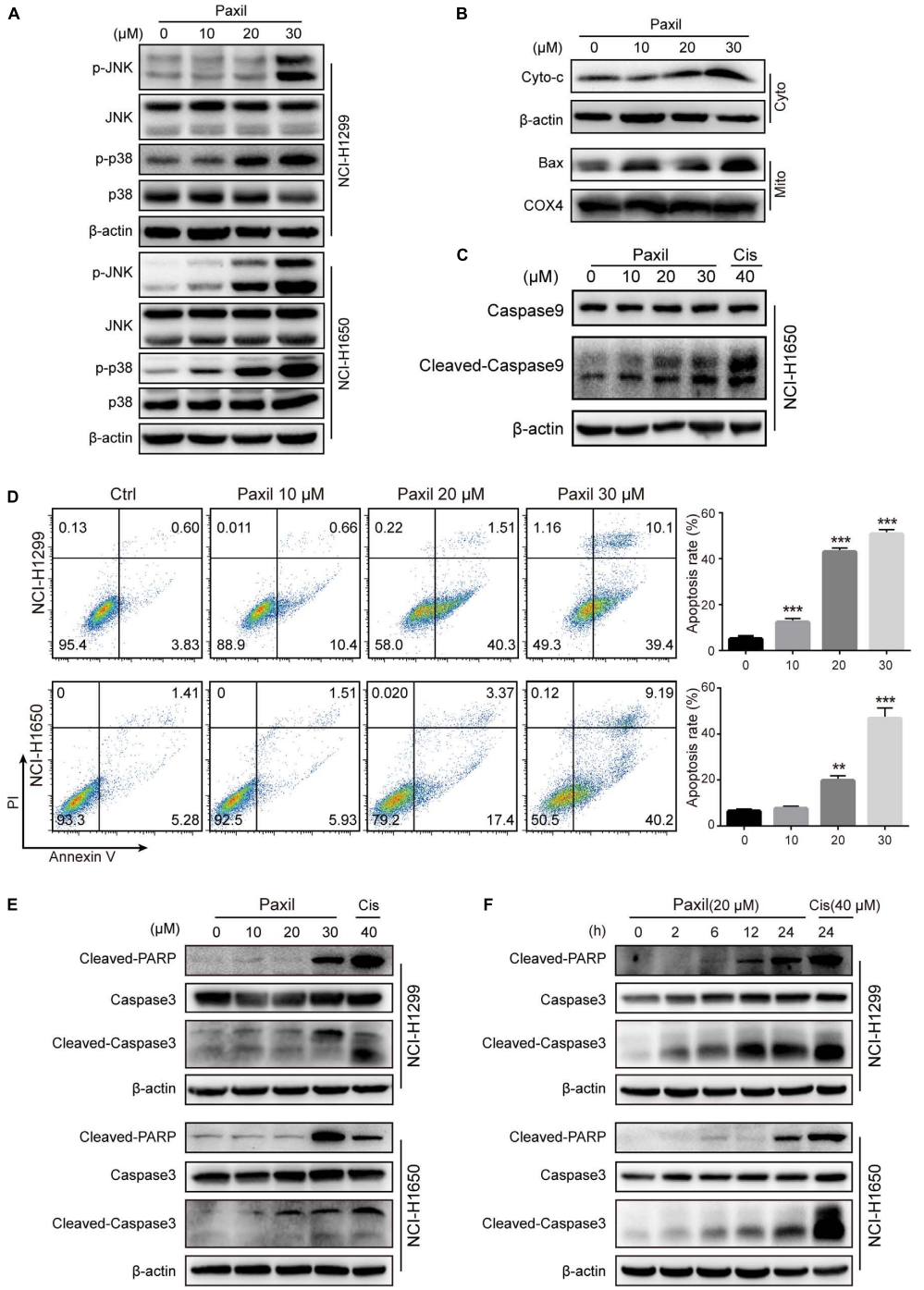

FIGURE 7 | Paxil-induced ROS accumulation promoted mitochondria-dependent apoptosis by activating the MAPK pathway. **(A)** The upregulation of p-JNK and p-p38 induced by Paxil. **(B)** The increase of cytosolic cytochrome c and Bax localized in the mitochondria. Following Paxil treatment for 24 h, the cytosolic fractions and the mitochondrial parts in NCI-H1299 cells were separately extracted from the total lysates. The protein level in each fraction was examined by western blot. β-actin was used as an internal reference for the cytosolic fraction. COX4 was used as an internal reference for the mitochondrial fractions. Cyto-c, cytochrome c; Cyto, cytosolic fractions; Mito, mitochondrial fractions. **(C)** Paxil caused caspase 9 activation in NCI-H1650 human lung cancer cells. Following Paxil treatment for 24 h, the whole cell lysates were extracted and the protein level was examined by western blot. **(D)** The increased apoptosis rate of NSCLC cells treated with increasing concentrations of Paxil for 24 h. The drug-treated cells were stained with Annexin V/PI followed by the analysis of flow cytometry. **(E,F)** Paxil dose-dependently upregulated the level of cleaved-caspase 3 and cleaved-PARP in NSCLC cells.

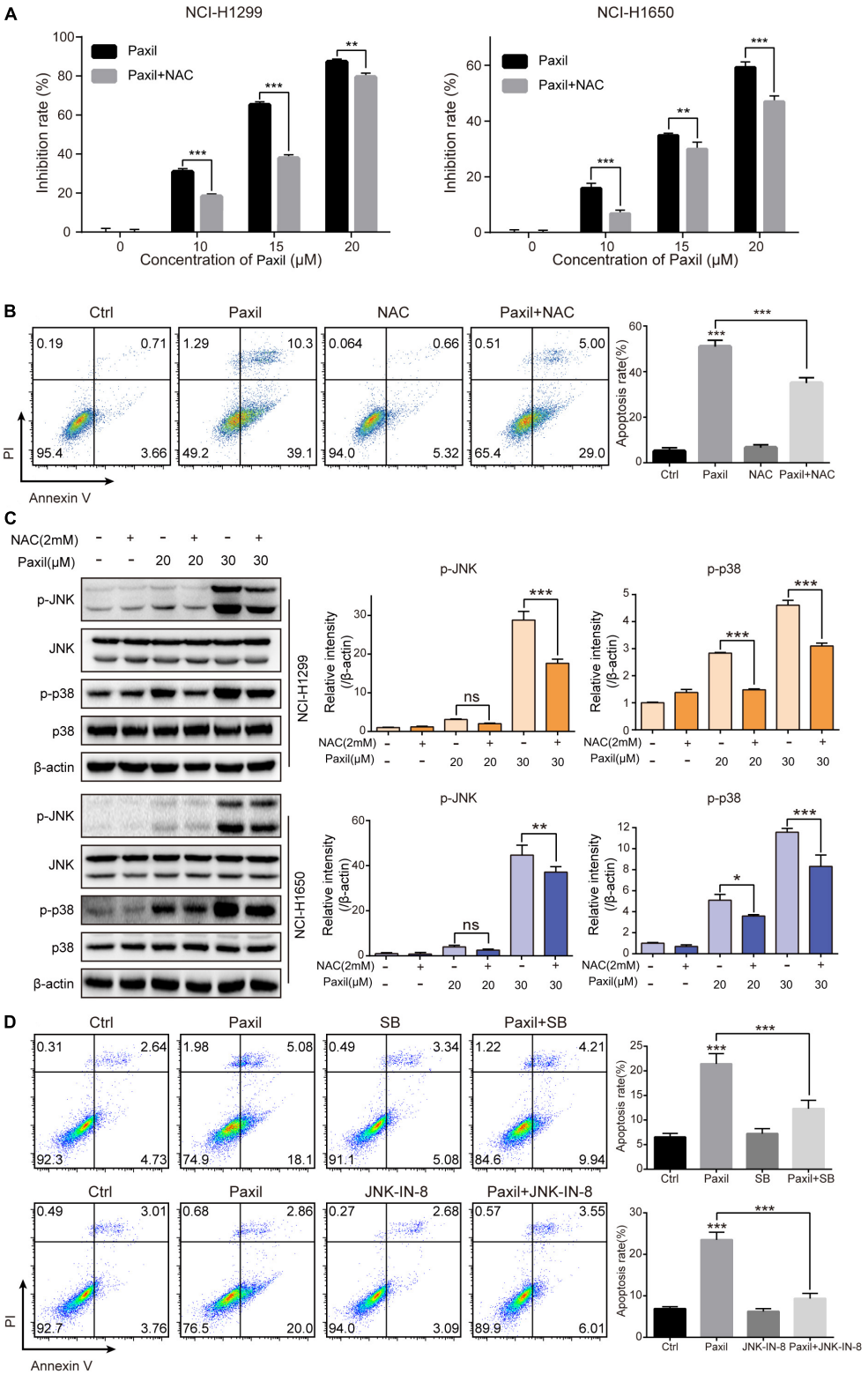

FIGURE 8 | Paxil induced apoptosis by activating ROS-MAPK pathways. **(A)** Cells were treated with different concentrations of Paxil with or without NAC (2 mM) for 24 h, and the cell viability was determined by a CCK8 assay. **(B)** NCI-H1299 cells were treated with Paxil (20 μM) and NAC (2 mM) alone or in combination for 24 h and stained with Annexin V/PI for apoptosis analysis. **(C)** Cells were subjected to drug treatment as described in **(B)**. The protein level was examined by western blot. **(D)** NCI-H1299 cells were treated with Paxil (20 μM), SB (SB203580, a p38 inhibitor, 10 μM) and JNK-IN-8 (a JNK inhibitor, 5 μM) alone or their combination for 24 h, and then stained with Annexin V/PI for apoptosis analysis. ns, no significance; $^{*}p < 0.05$; $^{**}p < 0.01$; $^{***}p < 0.001$.

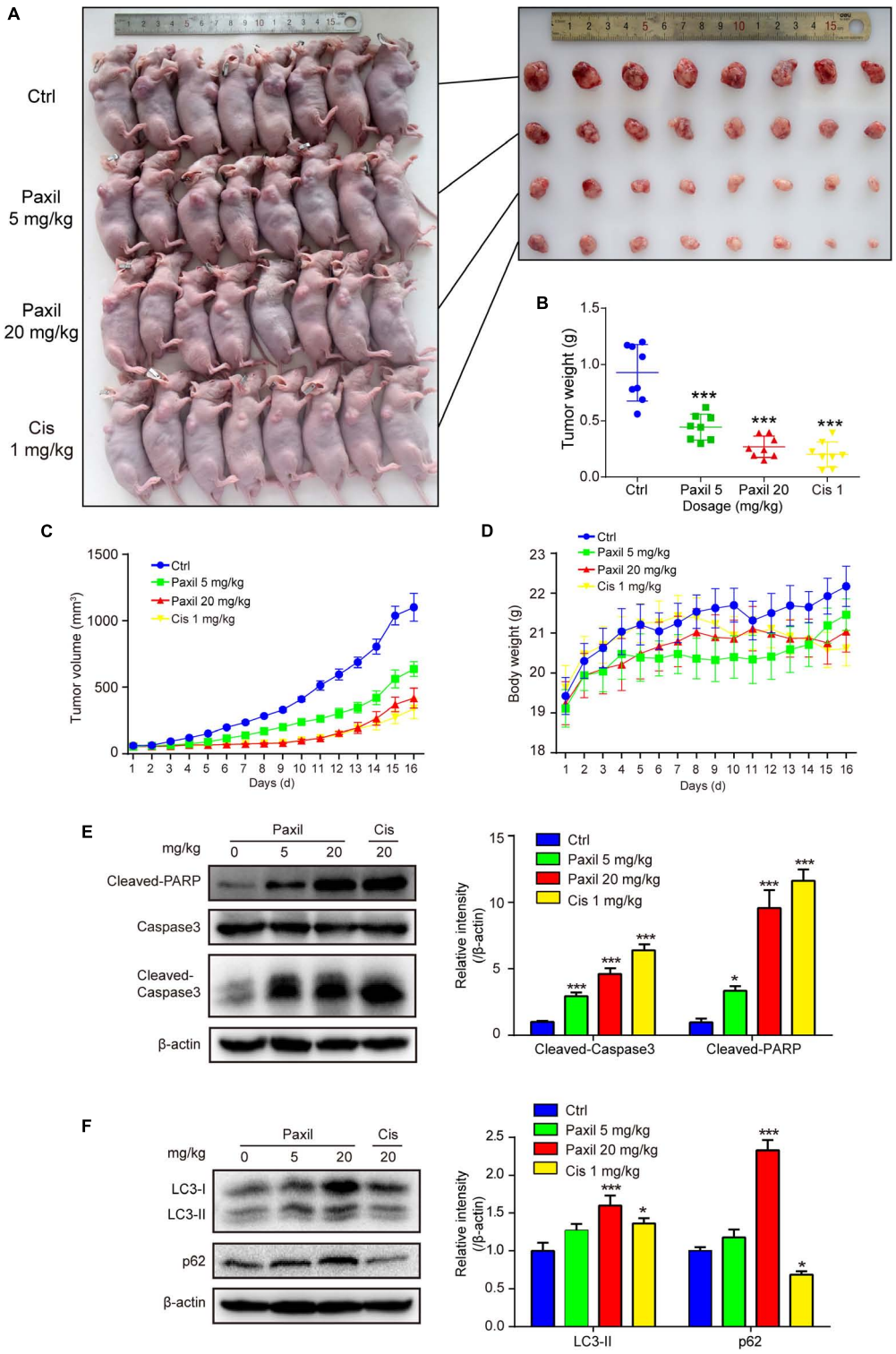

FIGURE 9 | Paxil inhibited tumor growth in NCI-H1299 tumor xenograft models. **(A)** The anticancer-like activity of Paxil was evaluated in nude mice with xenografted tumors. A total of 32 mice were subcutaneously injected with NCI-H1299 cells, and then randomly assigned to four groups: (1) control (treated with normal saline); (2) Paxil-5 mg/kg; and (3); Paxil-20 mg/kg and cisplatin-1 mg/kg. **(B)** After 16 days, the mice were sacrificed for tumor tissue collection and the tumors were weighted. **(C)** The tumor volume was measured daily. **(D)** The mice weight was measured every day, and there was no significant decrease following drug treatment. Error bars represent the mean ± SE. **(E,F)** The autophagic and apoptotic states were measured in lung cancer xenografts by analyzing the indicated proteins in mice treated with either Paxil or a vehicle. The relative level of the indicated proteins was shown. Error bars represent the mean ± SD; one-way analysis of variance: $^{*}p < 0.05$; $^{***}p < 0.001$. Cis, cisplatin.

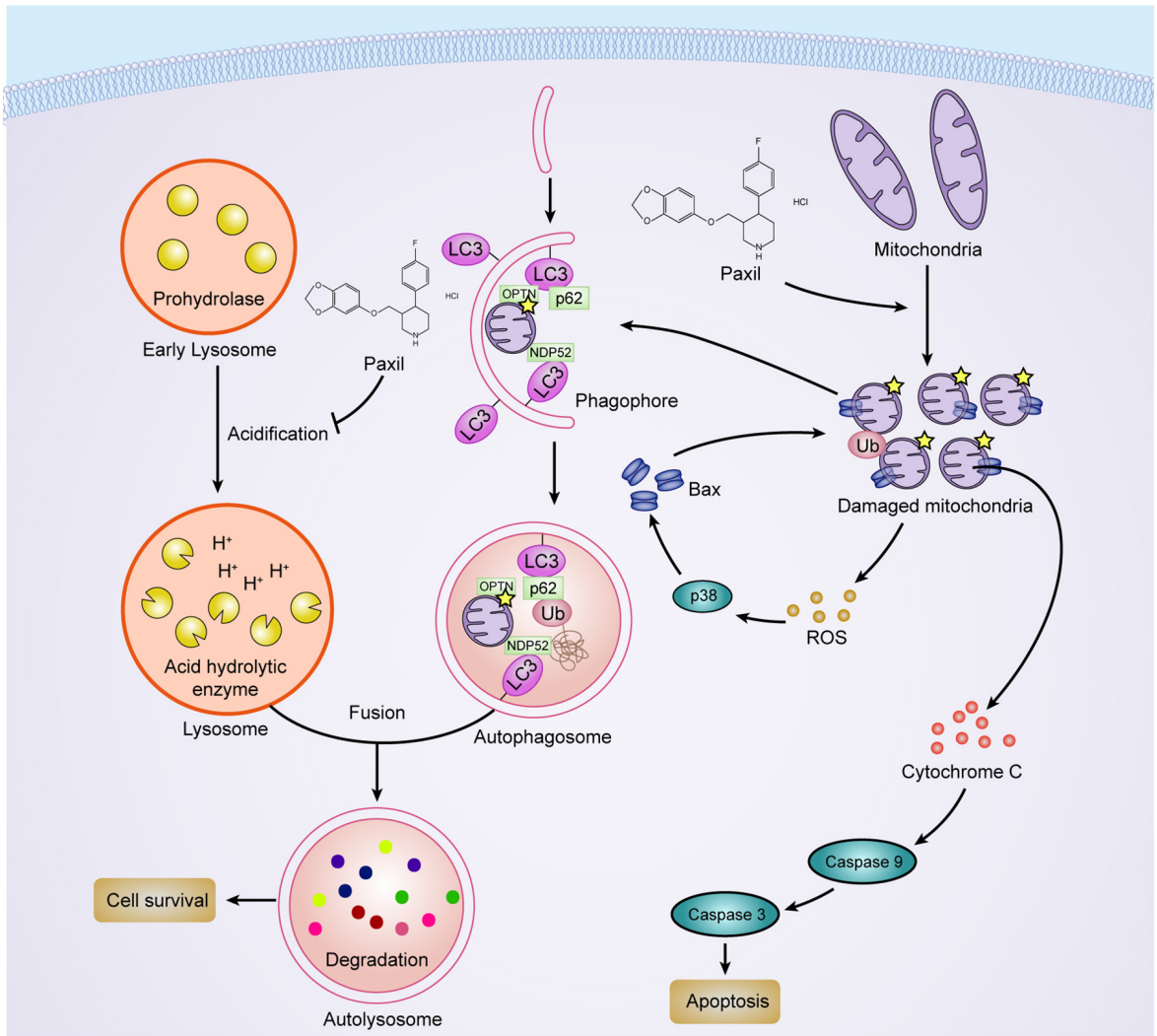

FIGURE 10 | The proposed mechanisms of Paxil-inhibited autophagy and Paxil-induced apoptosis.

Such metabolic differentiation may explain the prioritized killing effect of Paxil on cancer cells over normal cells.

Autophagy inhibition is considered to be a promising strategy for cancer therapy (Janku et al., 2011; Rubinsztein et al., 2012). Therefore, an increasing number of studies have focused on the identification of novel autophagy inhibitors; however, only a few inhibitors of autophagy (e.g., chloroquine and its derivative, hydroxychloroquine) are currently being evaluated in clinical trials aimed at assessing their efficacy (Mahalingam et al., 2014; Rangwala et al., 2014; Vogl et al., 2014). The main reason for this lack of clinical data is the unclear mechanism of the drug. In the present study, we demonstrated that Paxil blocked autophagic flux by inhibiting lysosomal acidification as follows: (1) Paxil inhibited the degradation of autophagosomes; (2) Paxil promoted substantial accumulation of autophagy substrates, such as LC3-II and p62; (3) Paxil quenched the fluorescence of lysosome-detecting probes (e.g., LysoTracker); and (4) Paxil attenuated the maturation of acid-sensitive lysosomal hydrolases (e.g., cathepsin B and D). Collectively, these findings indicate that Paxil interfered with the late stage of autophagic flux. Of note, since Paxil directly promoted mitochondrial damage, the initiation step of autophagy might be activated in cancer cells to promote survival. Compared with the vehicle, GFP-LC3 puncta were significantly induced and co-localized with mitochondria (red) following Paxil treatment (**Figure 3F**). This data demonstrates that mitophagy-relevant compartments were formed and engulfed the damaged mitochondria following Paxil treatment. Therefore, it is possible that mitophagy is initialized but arrested at the clearance stage. As such, the increased number of autophagosomes induced by Paxil might result from both the upregulation of the formation of autophagosomes and the inhibition of the downstream autophagic flux. Intracellular overloaded autophagosomes are per ser stress for cell survival. Several studies have reported that the accumulation of autophagosomes can result in tumor cell death, termed "autophagic cell death" (Zhou et al., 2015;

Feng et al., 2018). However, while we used 3-MA to inhibit autophagosome formation, it failed to attenuate Paxil-induced cell death (**Supplementary Figure S4**). Thus, the Paxil-induced cell death cannot be simply classified as "autophagic cell death." Since autophagy inhibition is considered as a promising strategy to synergize cancer chemotherapy (White, 2012), we also detected the killing effect of the combination of Paxil and cisplatin on NCI-H1299 cells. The result showed that the Paxil plus cisplatin combination treatment had a significantly increased rate of apoptosis as compared with cisplatin alone (**Supplementary Figure S5**).

When the autophagy pathway is obstructed, intracellular metabolic waste accumulates within the cell, and eventually disrupts cellular homeostasis (Yu et al., 2018). One typical source of cellular damage is ROS, an aging-promoting factor, which can also promote cellular apoptosis. Several studies have proposed that excessive ROS accumulation can activate the MAPK pathway and ultimately result in cell death. For example, palmitate was shown to induce H9c2 cell death through the activation of the ROS/MAPK signaling pathway (Liu et al., 2015). In addition, Isoliensinine was found to induce apoptosis in human breast cancer cells through ROS generation and p38/JNK activation (Zhang et al., 2015). Consistent with these findings, our present study demonstrates that the classical ROS-MAPK pathway mediates Paxil-induced apoptosis. We also determined that apoptosis induced by Paxil was mitochondria-dependent, based on the increase in MOMP followed by the release of cytochrome c and loss of membrane potential. However, it remains unknown which downstream effector of the MAPK pathway functions increase MOMP. Bax is a candidate since it can translocate to the mitochondria and create a pore if the guarding protein, BCL-2, becomes dysfunctional (Martinou and Youle, 2011). Moreover, there are several reports on the regulation of BCL-2 and Bax by MAPK. For example, Bax phosphorylation by JNK and p38 MAPK has been reported to initiate its activation and mitochondrial translocation (Kim et al., 2006). The JNK pathway also regulates mitochondrial apoptotic cell death via the modulation of Bcl-2 and Bax protein expression (Yamamoto et al., 1999; Schroeter et al., 2003; Asakura et al., 2008; Lee et al., 2008). As expected, our data indicate that treatment with Paxil induced the translocation of Bax to the mitochondria and the release of cytochrome c from mitochondria. To determine whether ROS plays an essential role in this process, we conducted a reverse assay in which ROS was neutralized by NAC, a ROS scavenger. The results showed the apoptosis was rescued and the key MAPK kinases (e.g., JNK and p38) were also deactivated. Collectively, our findings indicate that Paxil induces apoptosis in a mitochondria-dependent manner via the ROS-MAPK pathway.

MATERIALS AND METHODS

Chemicals and Antibodies

Paroxetine hydrochloride (Paxil, T1636) was purchased from TargetMol (Shanghai, China). DMEM, streptomycin, penicillin, HBSS, FBS, Prolong Diamond DAPI (P36966) were ordered from Thermo Fisher Scientific (Waltham, MA, United States). Bafilomycin A1 (Baf, B1793) were obtained from Sigma Biotechnology (St. Louis, MO, United States). U0126-EtOH (U0126, S1102) and 3-Methyladenine (3-MA, S2767) were obtained from Selleckchem (Houston, TX, United States). CCK-8 reagent (CK04) was obtained from Dojindo Laboratories, Kumamoto, Japan. A BCA protein assay kit (MA0082) was from Meilunbio (Dalian, China). FITC Annexin V Apoptosis Detection Kit (556547) was from BD Pharmingen (San Jose, CA, United States). The anti-p62 antibody (5114), anti-PARP antibody (9542), anti-LC3B antibody (12994S), anti-P-JNK antibody (9251), anti-JNK antibody (9252), anti-p-Ub antibody (62802), anti-PINK1 antibody (6946), anti-Parkin antibody (4211), anti-COX4 antibody (4850), anti-NDP52 antibody (60732), anti-Optineurin antibody (58981), anti-ERK antibody (9102), anti-p-ERK antibody (9101), anti-Cytochrome C antibody (11940), anti-Caspase 9 antibody (9502), cleaved-caspase 3 antibody (9662) and MitoTracker Red CMXRos (9082) were from Cell Signaling Technology (Boston, MA, United States). The anti-CatD antibody (sc-13985), anti-Optineurin antibody (sc-166576) and anti-NDP52 antibody (sc-376540) was obtained from Santa Cruz Biotechnology (Dallas, TX, United States). The siRNAs were synthesized by RiboBio (Guangzhou, China). Peroxidase-labeled antibody to rabbit IgG (AS014) and peroxidase-labeled antibody to mouse IgG (AS003) was from ABclonal (Wuhan, China).

Cell Culture

The human NSCLC cell lines, NCI-H1299 (ATCC® CRL-5803™) and NCI-H1650 (ATCC® CRL-5883™), were purchased from American Type Culture Collection (Rockville, MD, United States). All the cells were cultured in Dulbecco's modified Eagle's medium (DMEM) supplemented with 10% fetal bovine serum (FBS) and 100 U/mL penicillin/streptomycin at 37°C in a humidified atmosphere with 5% CO_2.

Cell Viability Assay

Cells were seeded onto 96-well plates at a density of 5×10^3 cells/well and treated with different compounds for 24 h. The medium was removed, and 100 μL CCK-8 reagent (10 times dilution with DMEM) was added into each well. The plates were incubated for 2 h at 37°C then measured at 450 nm. Cell viability in each well was assessed by comparing the readouts of vehicle-treated cells.

Colony Formation Assay

Cells were seeded into six-well plates at a density of 3000 cells/well and treated with Paxil at different concentrations. After 24 h, the medium was replaced with fresh complete DMEM. The cells were maintained for another seven days to allow the formation of colonies. Cell colonies were washed with PBS and fixed in 4% paraformaldehyde for 20 min. The colonies were stained with 0.01% (w/v) crystal violet in H_2O for 10 min, following by thoroughly wash with H_2O and air dried. The colonies were shot and counted by a researcher who was blinded for grouping information.

CFDA-SE Cell Tracer Assay

Cells were labeled with CFDA-SE (C0051, Beyotime, Shanghai, China) and seeded into six-well plates overnight. The cells were treated with different doses of Paxil. After 24 h, the cells were trypsinized, washed with PBS, and resuspended in HBSS. The fluorescence intensity of the cells was then measured on a BD Accuri^{TM} C6 flow cytometer (BD Pharmingen, San Diego, CA, United States).

5-Ethynyl-20-deoxyuridine (EdU) Staining

Cells were seeded into a confocal dish at a density of 3×10^6 cells/dish and treated with Paxil at different concentrations. After 24 h, the cells were administrated with EdU agent (C0071S, Beyotime, Shanghai, China) and cultured for an additional 8 h. The cells were then fixed in 4% paraformaldehyde for 20 min and washed with 3% BSA in PBS three times, followed by incubation with 0.3% TritonX-100 in PBS for 15 min and three washes of 3% BSA in PBS. The cells were incubated with 5 μg/mL Hoechst 33342 at room temperature for 10 min, washed with PBS, and mounted with Prolong Diamond (P36966, Karlsruhe, Germany). Images were obtained using a confocal microscope (LSM 800, Carl Zeiss, Jena, Germany).

Cell Apoptosis Assay

Cells were plated into six-well plates at a density of 3×10^5 cells/well and treated with different doses of Paxil for 24 h. The cells were trypsinized, washed with PBS, and resuspended with 600 μL annexin V binding buffer. The cells were mixed with 3 μL Annexin-V-FITC and incubated for 20 min at 37°C in the dark, followed by a PI (5 μL/sample) incubation for another 5 min in the dark. A total of 10,000 cells from each sample were analyzed with the FL1 channel and FL3 channel with a flow cytometer (BD Accuri C6, BD Pharmingen, San Diego, CA, United States).

Transmission Electron Microscopy (TEM)

NCI-H1299 cells were plated into 10 cm dishes at a density of 1.5×10^6 cells/dish and treated with either a vehicle or Paxil. After 24 h, the cells were collected and fixed with 2.5% glutaraldehyde for 12 h and incubated with osmium tetraoxide for 2 h at 4°C the specimens were embedded with epoxy resin. Sections 100 nm-thick were prepared and stained using uranyl acetate and lead citrate. Sections were imaged with a transmission electron microscope (HT7700, Hitachi, Tokyo, Japan).

Mitochondrial Mass Detection

The NCI-H1299 cells were seeded into a six-well plate at a cell density of 3×10^5 cells/well. The cells were treated with either a vehicle or Paxil for 24 h prior to fixing the cells with 4% paraformaldehyde for 15 min. After permeabilization in 95% methanol for 30 min, the cells were incubated in the antibody dilution buffer containing an anti-COX4 primary antibody (1:1000) for 2 h at room temperature and washed with PBS. After labeling the cells with an Alexa 488-conjugated secondary antibody, the fluorescence intensity of each group was examined with the FL1 channel of the flow cytometer.

Western Blot Analysis

The cells were lysed with 1 × loading buffer for protein extraction. The proteins were separated via 12% sodium dodecyl sulfate-polyacrylamide gel electrophoresis (SDS-PAGE) and transferred onto PVDF membranes. The membranes were blocked with 5% skim milk in TBST for 2 h and incubated with primary antibodies at 4°C overnight. The membrane was washed with TBST (0.05% Tween 20 in Tris-buffered saline) three times and incubated with the secondary antibodies (diluted 1:4000). The bands were visualized with enhanced chemiluminescence (ECL) using an ECL detection system. Then the band density was quantified using ImageJ software (US National Institutes of Health, Bethesda, MD, United States).

Plasmid Transfection Assay

Cells were seeded onto coverslips and cultured in 12-well plates for 24 h. Then, mCherry-GFP-LC3B plasmids were transfected using Lipofectamine 3000 reagent according to the manufacturer's instructions (Invitrogen, Carlsbad, CA, United States). After 6 h, the medium was replaced with complete DMEM and cultured for 24 h. The cells were then treated with different chemicals for 24 h, fixed with 4% paraformaldehyde for 20 min, and washed with PBS three times. The cells were stained with Hoechst 33342 (5 μg/mL) at room temperature for 10 min and mounted on a glass slide using Prolong Diamond. Images were obtained using a confocal microscope (LSM 800, Carl Zeiss, Jena, Germany).

Small Interfering RNA Transfection

The sequence of small interfering RNA for FUNDC1, BNIP3 and Nix were referred to the published articles (Bacon et al., 2007; Kuribayashi et al., 2011; Liu et al., 2012). NCI-H1299 cells seeded onto 15 cm dishes were transfected with small interfering RNA using riboFECT^{TM} CP Transfection Kit (R10035.4, RiboBio, Guangzhou, China) and cultured for 24 h followed by Paxil treatment. The mitochondrial parts in NCI-H1299 cells were separately extracted from the total lysates and then subjected to western blot. COX4 was used as an internal reference for the mitochondrial fractions.

Acridine Orange (AO) Staining

Cells were seeded onto glass slides in 12-well plates and treated with different chemicals for 24 h. The medium was removed and the cells were washed with PBS three times. The cells were stained with AO (5 μg/mL, A6014, Sigma, St. Louis, MO, United States) and incubated at 37°C with 5% CO_2 for 20 min. The samples were washed with PBS three times before imaging capture under a laser confocal scanning microscope equipped with an argon laser (excitation wavelength: 488 nm) and a 63 × objective lens. AO produces red fluorescence (emission filter: 620 nm long pass) in the acidic vesicles, whereas green fluorescence (emission between 520 and 560 nm) is emitted in the nuclear and cytosol compartments. The red and green fluorescence ratios were analyzed using ImageJ software.

Measurement of Mitochondrial Membrane Potential

Cells were seeded into six-well plates and treated with Paxil for 24 h. Cells were then harvested, washed with PBS, and stained with JC-1 (551302, BD Pharmingen, San Jose, CA, United States) for 15 min at 37°C in the dark. After staining, the cells were washed with PBS and suspended in HBSS. A total of 10,000 cells from each sample were recorded in the FITC and PE channels using a BD Fortessa flow cytometer.

Immunofluorescence Assay

Cells were seeded onto glass coverslips in a 12-well plate and treated with different chemicals for 24 h. After treatment, cells were fixed with 4% paraformaldehyde (PFA) for twenty minutes then rinsed for three times with PBS for five minutes. Then cells were blocked in antibody dilution buffer containing 10% FBS and 0.3% Triton X-100 in PBS for two hours at room temperature. Then cells were incubated with primary antibodies (1:500 dilution) overnight at 4°C. Then cells were washed with PBS for three times and blotted with fluorescent anti-rabbit secondary antibody (1:500 dilution) for 1 h at room temperature. Cells were rinsed in PBS three times before mounting by ProLong Diamond Antifade mounting medium with DAPI. Cells were imaged on a ZEISS LSM800 confocal laser scanning microscopy platform.

LysoTracker Red Staining

Cells were seeded onto glass slides in 12-well plates and treated with different chemicals for 24 h. Cells were then loaded with LysoTracker Red (50 nM, L7528, Thermo, Waltham, MA, United States). After 20 min, the cells were rinsed with PBS and observed under a laser confocal scanning microscope (excitation wavelength: 555 nm). Images were captured for analyzing the fluorescent intensity with ImageJ software.

MitoTracker Red CMXRos Staining

Cells were seeded onto glass slides in 12-well plates and treated with different compounds for 24 h. Cells were then stained with MitoTracker Red CMXRos (200 nM). After 20 min, the cells were rinsed with PBS and observed under a laser confocal scanning microscope equipped with a 63 × objective lens and an argon laser (excitation wavelength: 555 nm). Images were captured for analyzing fluorescent intensity with ImageJ software.

Mitochondrial and Cytosolic Fractionation

A mitochondrial protein extraction kit (BB-3171, BestBio, Shanghai, China) and cytosolic protein extraction kit (BB-3113, BestBio, Shanghai, China) were adopted to collect mitochondrial and cytosolic proteins, respectively. After treatment, the cells were washed with PBS and harvested. The cells were resuspended in 500 μL mitochondrial or cytoplasmic protein reagent and incubated on ice for 20 min with vertexing every 5 min. The mitochondrial protein was prepared by centrifugation at 11,000 × *g* for 20 min. The cytoplasmic protein was prepared by centrifugation at 16,000 × *g* for 5 min. The cytoplasmic and mitochondrial proteins were stored at −80°C until they were used in a western blot analysis.

Measurement of Intracellular ROS

Cells were seeded into six-well plates and treated with different chemicals for 24 h. Cells were then harvested, washed with PBS, and stained with 10 μM DCFH-DA (D399, Thermo, Waltham, MA, United States) for 15 min at 37°C in the dark. After staining, the cells were washed with PBS and suspended in HBSS. A total of 10,000 cells from each sample were recorded in the FL1 channel using a BD Accuri C6 flow cytometer.

Xenograft Tumor Model

Xenografts were established by subcutaneous inoculation of 5×10^6 cells into the right flank of nude mice. The xenograft tumor size was measured with a Vernier scale every five days. The mice began to receive different treatments (i.e., vehicle, Paxil [5 mg/kg], Paxil [20 mg/kg]) via an intraperitoneal injection when the tumor volume reached 0.1 mm^3. After 13 days, the mice were sacrificed with CO_2. The tumor tissues were harvested for weighting tumors, protein isolation, and western blot analysis.

Statistical Analysis

All experiments were repeated at least three times. Data were expressed as the mean ± standard deviation (SD). The statistical differences were evaluated using a one-way analysis of variance (ANOVA) followed by a *post hoc* test. $p < 0.05$ were considered statistically significant.

CONCLUSION

Our present study demonstrates that Paxil, a commonly used anti-depressant drug, functioned as a potent inhibitor of autophagy in lung cancer cells. Through impairing the acidic environment in lysosomes, Paxil can arrest late-stage autophagic flux. In addition, Paxil can induce the fragmentation of mitochondria. This dual function consequently caused an accumulation of ROS, which in turn activated MAPK to promote apoptosis in lung cancer cells. This anti-cancer effect of Paxil was also verified in an *in vivo* xenograft mouse model.

DATA AVAILABILITY STATEMENT

All datasets generated for this study are included in the article/**Supplementary Material**.

ETHICS STATEMENT

The experiments using nude mice were approved by the Animal Ethics Committee at Guangzhou University of Chinese Medicine.

AUTHOR CONTRIBUTIONS

JX and XL: conceptualization. KW, YJZ, and BC: methodology. TY, YJZ, and JK: software. QG and BD: validation. KW and

HW: formal analysis. KW, QG, and TY: investigation. YJZ and YL: resources. QG, YL, and YLZ: data curation. KW: writing – original draft preparation. XL and JX: writing – review and editing. KW, YLZ, and JK: visualization. XL: supervision. JX: project administration and funding acquisition.

FUNDING

This work was supported by the National Natural Science Foundation of China (Grant No. 81773953), the Guangdong Natural Science Foundation (Grant No. 2017A030313477), the Science and Technology Planning Project of Guangzhou (201904010067), the Education Department of Guangdong Province (2016KTSCX111), the Natural Science Foundation of Guangdong Province (2018A030313560), the Medical Scientific Research Foundation of Guangdong Province (A2018354), and the National Undergraduate Training Programs for Innovation and Entrepreneurship (Grant No. 201910572008).

ACKNOWLEDGMENTS

We would like to thank the native English speaking scientists of Elixigen Company (Huntington Beach, CA, United States) for editing our manuscript.

SUPPLEMENTARY MATERIAL

The Supplementary Material for this article can be found online at: https://www.frontiersin.org/articles/10.3389/fcell.2019.00397/full#supplementary-material

REFERENCES

Asakura, T., Maeda, K., Omi, H., Matsudaira, H., and Ohkawa, K. (2008). The association of deamidation of Bcl-xL and translocation of Bax to the mitochondria through activation of JNK in the induction of apoptosis by treatment with GSH-conjugated DXR. *Int. J. Oncol.* 33, 389–395.

Ashrafi, G., and Schwarz, T. (2013). The pathways of mitophagy for quality control and clearance of mitochondria. *Cell Death Diff.* 20, 31–42. doi: 10.1038/cdd.2012.81

Bacon, A., Fox, S., Turley, H., and Harris, A. (2007). Selective silencing of the hypoxia-inducible factor 1 target gene BNIP3 by histone deacetylation and methylation in colorectal cancer. *Oncogene* 26, 132–141. doi: 10.1038/sj.onc.1209761

Bray, F., Ferlay, J., Soerjomataram, I., Siegel, R. L., Torre, L. A., and Jemal, A. (2018). Global cancer statistics 2018: GLOBOCAN estimates of incidence and mortality worldwide for 36 cancers in 185 countries. *Cancer J. Clin.* 68, 394–424. doi: 10.3322/caac.21492

Cho, Y. W., Kim, E. J., Nyiramana, M. M., Shin, E. J., Jin, H., Ryu, J. H., et al. (2019). Paroxetine induces apoptosis of human breast cancer MCF-7 cells through Ca(2+)-and p38 MAP kinase-dependent ROS generation. *Cancers* 11:E64. doi: 10.3390/cancers11010064

Feng, X., Zhou, J., Li, J., Hou, X., Li, L., Chen, Y., et al. (2018). Tubeimoside I induces accumulation of impaired autophagolysosome against cervical cancer cells by both initiating autophagy and inhibiting lysosomal function. *Cell Death Dis.* 9:1117. doi: 10.1038/s41419-018-1151-3

Gassen, N. C., Hartmann, J., Zschocke, J., Stepan, J., Hafner, K., Zellner, A., et al. (2014). Association of FKBP51 with priming of autophagy pathways and mediation of antidepressant treatment response: evidence in cells, mice, and humans. *PLoS Med.* 11:e1001755. doi: 10.1371/journal.pmed.1001755

Germann, D., Ma, G., Han, F., and Tikhomirova, A. (2013). Paroxetine hydrochloride. *Profiles Drug Subst. Excip. Relat. Methodol.* 38, 367–406.

Gu, J., Gui, Y., Chen, L., Yuan, G., Lu, H.-Z., and Xu, X. (2013). Use of natural products as chemical library for drug discovery and network pharmacology. *PLoS One* 8:e62839. doi: 10.1371/journal.pone.0062839

Harris, J., Deen, N., Zamani, S., and Hasnat, M. A. (2017). Mitophagy and the release of inflammatory cytokines. *Mitochondrion* 41, 2–8. doi: 10.1016/j.mito.2017.10.009

Indo, H. P., Davidson, M., Yen, H.-C., Suenaga, S., Tomita, K., Nishii, T., et al. (2007). Evidence of ROS generation by mitochondria in cells with impaired electron transport chain and mitochondrial DNA damage. *Mitochondrion* 7, 106–118. doi: 10.1016/j.mito.2006.11.026

Jang, W. J., Jung, S. K., Vo, T. T. L., and Jeong, C. H. (2019). Anticancer activity of paroxetine in human colon cancer cells: involvement of MET and ERBB3. *J. Cell Mol. Med.* 23, 1106–1115. doi: 10.1111/jcmm.14011

Janku, F., McConkey, D. J., Hong, D. S., and Kurzrock, R. (2011). Autophagy as a target for anticancer therapy. *Nat. Rev. Clin. Oncol.* 8, 528–539. doi: 10.1038/nrclinonc.2011.71

Kim, B.-J., Ryu, S.-W., and Song, B.-J. (2006). JNK-and p38 kinase-mediated phosphorylation of Bax leads to its activation and mitochondrial translocation and to apoptosis of human hepatoma HepG2 cells. *J. Biol. Chem.* 281, 21256–21265. doi: 10.1074/jbc.m510644200

Kuribayashi, K., Finnberg, N. K., Jeffers, J. R., Zambetti, G. P., and El-Deiry, W. S. (2011). The relative contribution of pro-apoptotic p53-target genes in the triggering of apoptosis following DNA damage in vitro and in vivo. *Cell Cycle* 10, 2380–2389. doi: 10.4161/cc.10.14.16588

Lazarou, M., Sliter, D. A., Kane, L. A., Sarraf, S. A., Wang, C., Burman, J. L., et al. (2015). The ubiquitin kinase PINK1 recruits autophagy receptors to induce mitophagy. *Nature* 524, 309–314. doi: 10.1038/nature14893

Lee, S. J., Kim, M. S., Park, J. Y., Woo, J. S., and Kim, Y. K. (2008). 15-Deoxy-Δ12, 14-prostaglandin J2 induces apoptosis via JNK-mediated mitochondrial pathway in osteoblastic cells. *Toxicology* 248, 121–129. doi: 10.1016/j.tox.2008.03.014

Liu, J., Chang, F., Li, F., Fu, H., Wang, J., Zhang, S., et al. (2015). Palmitate promotes autophagy and apoptosis through ROS-dependent JNK and p38 MAPK. *Biochem. Biophys. Res. Commun.* 463, 262–267. doi: 10.1016/j.bbrc.2015.05.042

Liu, J., Wu, N., Ma, L.-N., Zhong, J.-T., Liu, G., Zheng, L.-H., et al. (2014). p38 MAPK signaling mediates mitochondrial apoptosis in cancer cells induced by oleanolic acid. *Asian Pac. J. Cancer Prevent.* 15, 4519–4525. doi: 10.7314/apjcp.2014.15.11.4519

Liu, L., Feng, D., Chen, G., Chen, M., Zheng, Q., Song, P., et al. (2012). Mitochondrial outer-membrane protein FUNDC1 mediates hypoxia-induced mitophagy in mammalian cells. *Nat. Cell Biol.* 14, 177–185. doi: 10.1038/ncb2422

Mahalingam, D., Mita, M., Sarantopoulos, J., Wood, L., Amaravadi, R. K., Davis, L. E., et al. (2014). Combined autophagy and HDAC inhibition: a phase I safety, tolerability, pharmacokinetic, and pharmacodynamic analysis of hydroxychloroquine in combination with the HDAC inhibitor vorinostat in patients with advanced solid tumors. *Autophagy* 10, 1403–1414. doi: 10.4161/auto.29231

Martinou, J.-C., and Youle, R. J. (2011). Mitochondria in apoptosis: Bcl-2 family members and mitochondrial dynamics. *Dev. Cell* 21, 92–101. doi: 10.1016/j.devcel.2011.06.017

Michael, L. (2015). Keeping the immune system in check: a role for mitophagy. *Immunol. Cell Biol.* 93, 3–10. doi: 10.1038/icb.2014.75

Mowers, E. E., Sharifi, M. N., and Macleod, K. F. (2017). Autophagy in cancer metastasis. *Oncogene* 36, 1619–1630. doi: 10.1038/onc.2016.333

Nguyen, T. N., Padman, B. S., and Lazarou, M. (2016). Deciphering the molecular signals of PINK1/parkin mitophagy. *Trends Cell Biol.* 26, 733–744. doi: 10.1016/j.tcb.2016.05.008

Rangwala, R., Chang, Y. C., Hu, J., Algazy, K. M., Evans, T. L., Fecher, L. A., et al. (2014). Combined MTOR and autophagy inhibition: phase I trial of hydroxychloroquine and temsirolimus in patients with advanced solid tumors and melanoma. *Autophagy* 10, 1391–1402. doi: 10.4161/auto.29119

Redza-Dutordoir, M., and verill-Bates, D. A. A. (2016). Activation of apoptosis signalling pathways by reactive oxygen species. *Biochim. Biophys. Acta Mol. Cell Res.* 1863, 2977–2992. doi: 10.1016/j.bbamcr.2016.09.012

Rubinsztein, D. C., Codogno, P., and Levine, B. (2012). Autophagy modulation as a potential therapeutic target for diverse diseases. *Nat. Rev. Drug Discov.* 11, 709–730. doi: 10.1038/nrd3802

Scherz-Shouval, R., and Elazar, Z. (2007). ROS, mitochondria and the regulation of autophagy. *Trends Cell Biol.* 17, 422–427. doi: 10.1016/j.tcb.2007.07.009

Schroeter, H., Ahmed, R., Spencer, J. P., Duncan, R. F., Catherine, R.-E., and Cadenas, E. (2003). c-Jun N-terminal kinase (JNK)-mediated modulation of brain mitochondria function: new target proteins for JNK signalling in mitochondrion-dependent apoptosis. *Biochem. J.* 372, 359–369. doi: 10.1042/bj20030201

Shen, H.-M., and Liu, Z.-G. (2006). JNK signaling pathway is a key modulator in cell death mediated by reactive oxygen and nitrogen species. *Free Radic. Biol. Med.* 40, 928–939. doi: 10.1016/j.freeradbiomed.2005.10.056

Shi, Y., Nikulenkov, F., Zawacka-Pankau, J., Li, H., Gabdoulline, R., Xu, J., et al. (2014). ROS-dependent activation of JNK converts p53 into an efficient inhibitor of oncogenes leading to robust apoptosis. *Cell Death Diff.* 21, 612–623. doi: 10.1038/cdd.2013.186

Simon, H.-U., Haj-Yehia, A., and Levi-Schaffer, F. (2000). Role of reactive oxygen species (ROS) in apoptosis induction. *Apoptosis* 5, 415–418.

Stolz, A., Ernst, A., and Dikic, I. (2014). Cargo recognition and trafficking in selective autophagy. *Nat. Cell Biol.* 16, 495–501. doi: 10.1038/ncb2979

Svenning, S., and Johansen, T. (2013). Selective autophagy. *Essays Biochem.* 55, 79–92. doi: 10.1042/bse0550079

Vogl, D. T., Stadtmauer, E. A., Tan, K.-S., Heitjan, D. F., Davis, L. E., Pontiggia, L., et al. (2014). Combined autophagy and proteasome inhibition: a phase 1 trial of hydroxychloroquine and bortezomib in patients with relapsed/refractory myeloma. *Autophagy* 10, 1380–1390. doi: 10.4161/auto.29264

Vyas, S., Zaganjor, E., and Haigis, M. C. (2016). Mitochondria and cancer. *Cell* 166, 555–566. doi: 10.1016/j.cell.2016.07.002

White, E. (2012). Deconvoluting the context-dependent role for autophagy in cancer. *Nat. Rev. Cancer* 12, 401–410. doi: 10.1038/nrc3262

Wong, Y. C., and Holzbaur, E. L. F. (2014). Optineurin is an autophagy receptor for damaged mitochondria in parkin-mediated mitophagy that is disrupted by an ALS-linked mutation. *Proc. Natl. Acad. Sci. U.S.A.* 111:E4439. doi: 10.1073/pnas.1405752111

Wu, J., Zhang, H., Xu, Y., Zhang, J., Zhu, W., Zhang, Y., et al. (2017). Juglone induces apoptosis of tumor stem-like cells through ROS-p38 pathway in glioblastoma. *BMC Neurol.* 17:70. doi: 10.1186/s12883-017-0843-0

Yamamoto, K., Ichijo, H., and Korsmeyer, S. J. (1999). BCL-2 is phosphorylated and inactivated by an ASK1/Jun N-terminal protein kinase pathway normally activated at G2/M. *Mol. Cell. Biol.* 19, 8469–8478. doi: 10.1128/mcb.19.12.8469

Yu, L., Chen, Y., and Tooze, S. A. (2018). Autophagy pathway: cellular and molecular mechanisms. *Autophagy* 14, 207–215. doi: 10.1080/15548627.2017.1378838

Zhang, X., Wang, X., Wu, T., Li, B., Liu, T., Wang, R., et al. (2015). Isoliensinine induces apoptosis in triple-negative human breast cancer cells through ROS generation and p38 MAPK/JNK activation. *Sci. Rep.* 5:12579. doi: 10.1038/srep12579

Zhou, J., Li, G., Zheng, Y., Shen, H.-M., Hu, X., Ming, Q.-L., et al. (2015). A novel autophagy/mitophagy inhibitor liensinine sensitizes breast cancer cells to chemotherapy through DNM1L-mediated mitochondrial fission. *Autophagy* 11, 1259–1279. doi: 10.1080/15548627.2015.1056970

Conflict of Interest: The authors declare that the research was conducted in the absence of any commercial or financial relationships that could be construed as a potential conflict of interest.

frontiers in Cell and Developmental Biology

REVIEW
published: 18 March 2020
doi: 10.3389/fcell.2020.00163

Endosome-to-TGN Trafficking: Organelle-Vesicle and Organelle-Organelle Interactions

Yingfeng Tu[1†], Lin Zhao[1†], Daniel D. Billadeau[2] and Da Jia[1]*

[1] *Key Laboratory of Birth Defects and Related Diseases of Women and Children, State Key Laboratory of Biotherapy, Department of Paediatrics, West China Second University Hospital, Sichuan University, Chengdu, China,* [2] *Division of Oncology Research, Schulze Center for Novel Therapeutics, Mayo Clinic, Rochester, MN, United States*

Retrograde transport from endosomes to the *trans*-Golgi network (TGN) diverts proteins and lipids away from lysosomal degradation. It is essential for maintaining cellular homeostasis and signaling. In recent years, significant advancements have been made in understanding this classical pathway, revealing new insights into multiple steps of vesicular trafficking as well as critical roles of ER-endosome contacts for endosomal trafficking. In this review, we summarize up-to-date knowledge about this trafficking pathway, in particular, mechanisms of cargo recognition at endosomes and vesicle tethering at the TGN, and contributions of ER-endosome contacts.

Keywords: endosome, TGN, human disease, membrane trafficking, membrane contact site, golgin, WASH complex, TBC1D23

OPEN ACCESS

Edited by:
Du Feng,
Guangzhou Medical University, China

Reviewed by:
Peter Schu,
University of Göttingen, Germany
Matthew Seaman,
University of Cambridge, United Kingdom
Sean Munro,
University of Cambridge, United Kingdom

***Correspondence:**
Da Jia
Jiada@scu.edu.cn

[†]These authors have contributed equally to this work

Specialty section:
This article was submitted to Molecular Medicine, a section of the journal Frontiers in Cell and Developmental Biology

Received: *12 January 2020*
Accepted: *28 February 2020*
Published: *18 March 2020*

Citation:
Tu Y, Zhao L, Billadeau DD and Jia D (2020) Endosome-to-TGN Trafficking: Organelle-Vesicle and Organelle-Organelle Interactions. Front. Cell Dev. Biol. 8:163. doi: 10.3389/fcell.2020.00163

INTRODUCTION

Endosomes are central collecting stations in cells where different trafficking pathways converge. Integral membrane proteins, together with their associated proteins and lipids, arrive at endosomes following internalization at the cell surface, and others are transported to endosomes from the *trans*-Golgi network (TGN) (Burd and Cullen, 2014). One of the major functions of endosomes is "sorting," a term referring to some endosomal proteins and lipids being delivered to the cell surface, via the recycling endosomes, or to the TGN, before reaching the degradative lysosomes (**Figure 1**). The former pathway is known as endosome-to-plasma membrane recycling, whereas the latter is referred to as endosome-to-TGN retrieval or retrograde transport. Endosomal sorting is crucial for maintaining cellular homeostasis and supporting organism development and growth. Accordingly, many human diseases, including neurological diseases, cancer, and diabetes, have been linked with defects in endosomal functions (Burd and Cullen, 2014; Lucas and Hierro, 2017; McMillan et al., 2017).

The endosome-to-TGN trafficking pathway diverts proteins and lipids away from lysosomal degradation. Mechanistically, this process can be divided into several interconnected steps (Lu and Hong, 2014; Cheung and Pfeffer, 2016; Saimani and Kim, 2017): (1) recognition of endosomal proteins, often in a sequence-dependent manner, by specific protein(s); (2) formation of cargo-enriched endosomal structures/subdomains; (3) endosomal fission leads to the formation of tubulo-vesicular transport carriers; (4) movement of these carriers toward TGN along cytoskeletal tracks; (5) carrier capturing by tethering proteins localized on the TGN; (6) carrier fusion with the Golgi membrane, mediated by the SNARE complex. Recent studies have provided important insights into these steps, including identification of new protein complexes mediating sequence-dependent cargo recognition,

identification and characterization of multiple regulatory protein complexes, and discovery of new tethering mechanisms at the TGN (McNally et al., 2017; Shin et al., 2017; Navarro Negredo et al., 2018; Simonetti et al., 2019; Singla et al., 2019).

Endosomes function via contacting and fusing with other endosomes or the incoming vesicles that arrive from the Golgi. In addition, non-fusogenic organelle-organelle interactions likely play a role in endosomal trafficking. Endosomes communicate with other organelles through membrane contact sites (MCSs). Most notably, tubules emanating from the endoplasmic reticulum (ER) contact endosomes within a distance of 30 nm or shorter. The ER-endosome MCSs function to regulate endosome fission, endosome positioning, and cholesterol and Ca^{2+} transfer (Raiborg et al., 2015). In this review, we summarize critical organelle-organelle and organelle-vesicle interactions in the endosome-to-TGN trafficking. We focus on recent advances in understanding recognition of cargo for retrieval, regulation of endosomal fission by ER-endosome contacts, and finally capturing of endosomal carriers at the TGN, in mammalian cells. We will also discuss the relevance of these processes for human development and disease. Due to space limitations, we are unable to cover every aspect of this trafficking pathway. Readers are invited to look through several recently published reviews that cover aspects not discussed here (Burd and Cullen, 2014; Lu and Hong, 2014; Raiborg et al., 2015; Liu, 2016; Lucas and Hierro, 2017; McMillan et al., 2017; Cullen and Steinberg, 2018).

CARGO RECOGNITION AT ENDOSOMES

The endosome-to-TGN trafficking pathway is one of two major routes that diverge from lysosomal degradation. Endosomal proteins are delivered to the TGN through two distinct itineraries: from either the early endosome/recycling endosome or the late endosome (Ghosh et al., 1998; Mallet and Maxfield, 1999). Proteins transiting this pathway include members of the Vps10 domain family cargo receptors (such as sortilin and SorLA/SorL1) (Nielsen et al., 2001; Willnow and Andersen, 2013), cation-dependent or cation-independent mannose-6-phosphate receptor (CD-MPR or CI-MPR) (Meyer et al., 2000; Schweizer et al., 2000; McKenzie et al., 2012), enzymes such as endoprotease furin and carboxypeptidase D (Varlamov and Fricker, 1998), and TGN38/46 (Ghosh et al., 1998). Furthermore, bacterial and plant toxins, such as Shiga toxin, Cholera toxin, and Ricin, hijack this pathway for their intracellular traveling before reaching the ER (Sandvig and van Deurs, 2002; Mukhopadhyay and Linstedt, 2012).

A number of proteins have been shown to mediate sequence-specific sorting to the TGN, including retromer (Seaman, 2018), SNX-BARs (Kvainickas et al., 2017a; Simonetti et al., 2017, 2019), clathrin and adaptors (Hirst et al., 2012, 2013), Rab9 GTPase and TIP45 (Carroll et al., 2001), and PACS-1 (Wan et al., 1998).

Retromer

Retromer was initially found to mediate endosome-to-TGN transport of Vps10 in yeast (Seaman et al., 1998; Nothwehr et al., 2000). Similarly, mammalian retromer (VPS35/VPS26/VPS29) has been shown by multiple groups to mediate the transport of CI-MPR, the functional equivalent of Vps10, and other cargo proteins, likely through a direct interaction (Arighi et al., 2004; Seaman, 2004). It is reported that a sequence comprising Trp-Leu-Met (WLM) present in the cytoplasmic tail of CI-MPR is required to associate with retromer and for the endosome-to-Golgi retrieval of CI-MPR (Seaman, 2007).

Multiple distinct cargo-recognizing mechanisms have been discovered. For instance, yeast Vps10 contains a bipartite signal that is recognized by the retromer subunit Vps35 and Vps26 (Suzuki et al., 2019). In mammals, the SNX3-retromer complex mediates the transport of wntless, DMT1 (divalent metal transporter 1), and CI-MPR, via recognizing the aromatic, hydrophobic motif in their cytoplasmic tails (Harterink et al., 2011; Zhang et al., 2011; Harrison et al., 2014; Lucas et al., 2016; Cui et al., 2019). Crystal structure of the quaternary VPS35-VPS26-SNX3-DMT1 tail complex revealed that VPS26 and SNX3 cooperate to mediate cargo recognition (Lucas et al., 2016). Cargo recognition is achieved through a different mechanism for another cargo protein, SorLA. It has been shown that VPS26 on its own binds to the FANSHY sorting motif presented in SorLA, although structural evidence remains to be established (Fjorback et al., 2012).

SNX-BAR Proteins

The SNX-BAR proteins belong to the PX (phox-homology) domain and SNX (sorting nexin) protein family (Teasdale and Collins, 2012). They contain a BAR (Bin/Amphiphysin/Rvs) domain, in addition to the PX domain. The retromer-related SNX-BAR proteins (referred to as SNX-BARs herein) function as a heterodimer, through the interaction between SNX1 or SNX2, and SNX5 or SNX6 or SNX32 (Carlton et al., 2004; Wassmer et al., 2007). Traditionally, SNX-BARs are regarded as a membrane-binding module to facilitate retromer-mediated cargo recognition and retrieval. The presence of two membrane-interacting domains in SNX–BARs enables coincidence detection of PI3P (phosphatidylinositol 3-phosphate), by the PX domain of SNX1/2, and membrane curvature, by the BAR domain (Teasdale and Collins, 2012). Recently, two independent studies reveled that SNX-BARs can directly associate with CI-MPR to mediate its retrieval (Kvainickas et al., 2017a; Simonetti et al., 2017). Moreover, these studies also showed that deletion of VPS35, unlike deletion of SNX-BARs, did not cause a pronounced defect in CI-MPR trafficking (Kvainickas et al., 2017a; Simonetti et al., 2017). Cargo proteins recognized and transported by SNX-BARs are not limited to CI-MPR, and now the list of cargoes includes IGF1R, SEMA4C, and dozens of other integral membrane proteins, which undergo either endosome-to-TGN or endosome-to-plasma membrane trafficking (Kvainickas et al., 2017a; Simonetti et al., 2017, 2019; Bareja et al., 2018).

The SNX-BAR proteins recognize a bipartite sorting signal [ΦXΩXΦ(X)nΦ, Φ, hydrophobic residues; X, any residue; Ω, aromatic residues] in cargo proteins (Simonetti et al., 2019). Interestingly, the WLM motif in the cytoplasmic tail of CI-MPR is part of the soring signal recognized by SNX-BARs. The PX domain of SNX5/SNX6/SNX32 contains a long

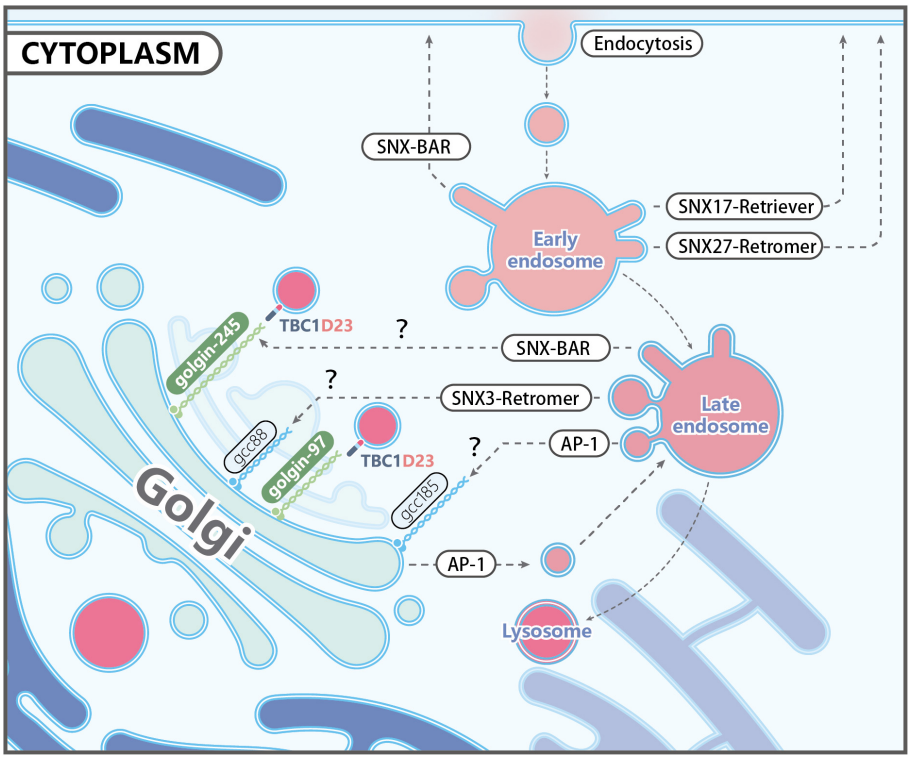

FIGURE 1 | Representative trafficking pathways of transmembrane proteins. Transmembrane receptors are internalized via endocytosis, and some of them are targeted to lysosomes as endosomes mature. Other receptors are recognized by specific coat proteins and sorted to the plasma membrane or the *trans*-Golgi network (TGN), thus evading degradation. Known protein complexes involved in endosome-to-plasma membrane trafficking include SNX17-retriver, SNX27-retromer, and SNX-BARs. Endosome-to-TGN transport depends on cargo recognition mediated by SNX3-retromer, SNX-BARs, or Clathrin/AP1. Other proteins mediating endosome-to-TGN trafficking, including other Adaptor Proteins, Rab9, TIP47, and PACS-1, are not shown for simplicity. The TGN-localized golgin proteins, such as golgin-97, golgin-245, GCC88, and GCC185, are capable of capturing distinct types of endosomal carriers, although the specificity and underlying mechanisms are largely unknown. TBC1D23 acts as an adapter by interacting with golgin-97 and golgin-245, and the WASH complex subunit FAM21 on endosomal vesicles. It should be noted that AP-1 is also found at the TGN, and mediates the bi-directional trafficking between endosomes and the TGN.

insertion relative to other PX domains, and does not bind to phosphoinositides, such as PI3P (Chandra et al., 2019). Instead, this insertion, together with a proximal β-strand, constitute the binding site for the sorting signal, which forms two antiparallel β-strands (Simonetti et al., 2019). Interestingly, structure of the sorting signal in the complex resembles that of the Chlamydia trachomatis effector protein IncE (Elwell et al., 2017; Paul et al., 2017; Sun et al., 2017).

Is CI-MPR a cargo of retromer, or SNX-BARs? Current evidence suggests two possible models. The first model suggests that retromer and SNX-BARs mediate two independent pathways for CI-MPR retrieval. Supporting this model is the observation that retromer and SNX3, and SNX-BARs, mediate CI-MPR transport in carriers that depend on different tether proteins on the TGN (see later) (Cui et al., 2019). The second model supports that SNX-BARs play a dominant role in CI-MPR trafficking, whereas retromer regulates CI-MPR trafficking through interacting with TBC1D5 and modulating the activity of Rab7 GTPase (Jia et al., 2016; Jimenez-Orgaz et al., 2018; Kvainickas et al., 2019). Consistent with this model, Steinberg et al. (2013) showed that deletion of VPS35, although not having a pronounced effect on the subcellular localization of CI-MPR, altered the transportation kinetics of endocytosed CI-MPR to the TGN (Kvainickas et al., 2017a). Distinguishing these two models represent an exciting direction in the field.

Clathrin and Adapters

In addition to retromer and SNX-BARs, clathrin and its adaptor proteins are also involved in endosome-to-TGN trafficking. Clathrin associates with two types of adaptor proteins: tetrameric and monomeric. The former includes five Adaptor Proteins: AP-1, AP-2, AP-3, AP-4, and AP-5. All of them, excepted for AP-2, participates in endosomal trafficking (Park and Guo, 2014). The monomeric adaptor proteins include epsinR and GGA (Golgi-localized, γ-adaptin ear-containing, Arf-binding). Among all the adaptor proteins associating with clathrin, AP-1 and epsinR have the most established roles in CI-MPR retrieval to the TGN. Unlike retromer, AP-1 and epsinR localize on both endosomes and the TGN (Meyer et al., 2000). Depletion of AP-1 or epsinR results in a dispersed MPR localization pattern, consisting with defects in endosome-to-TGN transport (Meyer et al., 2000; Hirst et al., 2004; Saint-Pol et al., 2004; Robinson et al., 2010). These results are further supported by rapid depletion of AP-1 by the "knocksideways" system, which reveals AP-1 affects a large

number of proteins, including lysosomal hydrolases and their receptors (MPR), various SNAREs, and many integral membrane proteins (Hirst et al., 2012). AP1 could directly bind cargos by interacting with YXXΦ and [DE]XXXL[LI] motifs in their cytosolic tails (Rapoport et al., 1998). In addition to AP-1, AP-5 is also implicated in the retrieval of CI-MPR (Hirst et al., 2013). Although retromer, SNX-BARs, and clathrin are all involved in the endosome-to-TGN trafficking, it remains obscure whether they function together or separately, and whether they function sequentially or concurrently.

ER-ENDOSOME CONTACT SITES AND ENDOSOME FISSION

ER-Endosome Contact Sites

The ER is a continuous network of tubules and cisternae that have versatile cellular functions, including protein synthesis and transport, lipid metabolism, calcium storage, and stress response. This network spreads throughout the cytoplasm, physically separated from other membrane compartments but functionally connected with organelles of the endocytic pathway, the nuclear membrane, and the plasma membrane (Wu et al., 2018). In addition to vesicular trafficking, MCSs have emerged as an alternative means of inter-organelle communication between the ER and other intracellular membranes. One developing theme is that each type of MCS has a unique molecular composition with unique functions (Raiborg et al., 2015; Wu et al., 2018).

ER-Endosome Contact Sites Regulate Endosome Fission

Endosome fission is the step whereby membrane carriers, including vesicles and tubules, bud and split from endosomes. It is critical for recycling of cargoes to the plasma membrane or TGN, and important for endosome maturation. ER tubules were initially found at the sites of mitochondria division (Friedman et al., 2011), and Rowland et al. demonstrated that ER-endosome contact sites are also required for endosome fission (Rowland et al., 2014). ER tubules make contact with the endosome, marked by the WASH complex subunit FAM21, just before the fission event (Rowland et al., 2014). Consistently, altered shape and dynamics of ER by overexpression of Reticulon 4a, which is known to generate ER tubules, results in a significantly decreased number of endosome buds undergoing fission (Shibata et al., 2008; Rowland et al., 2014).

Given the immediate establishment of ER-endosome contact sites prior to fission, these contact sites might be extremely transient, thus hampering the identification of its molecular composition. Using a proximity biotinylation assay in which FAM21 was tagged, Hoyer et al. identified the ER transmembrane protein TMCC1 as a critical protein mediating the ER-endosome contact (Hoyer et al., 2018). Depletion of TMCC1 specifically impairs fission of endosomal tubules and subsequent cargo sorting, but does not alter the formation of these tubules, emphasizing the importance of ER-endosome MCSs in endosome fission. Hoyer et al. further demonstrated that endosome-localized Coronin 1C is involved in ER-mediated endosome fission (Hoyer et al., 2018). Coronin 1C is an actin-binding protein that has been shown to accumulate at sites of Arp2/3-generated actin patches on endosomes (Puthenveedu et al., 2010). Interestingly, depletion of Coronin 1C prevented TMCC1 recruitment leading to a dramatic reduction in ER-endosome contacts and defective endosome fission of WASH-labeled endosomal buds (Hoyer et al., 2018; **Figure 2**). Since Coronin proteins are known to mediate F-actin disassembly by displacing Arp2/3 complexes, Coronin 1C might function to not only recruit TMCC1/ER MCSs, but to also simultaneously disassemble branched F-actin at the site of endosomal fission (**Figure 2**).

In addition to TMCC1 and Coronin 1C, the ER-endosome MCSs can be also mediated by ER protein VAP (vesicle-associated membrane protein-associated protein, including VAP-A and VAP-B) and two proteins localized on endosomes: SNX2 and OSBP (Oxysterol Binding Protein) (Dong et al., 2016). Loss of VAP or OSBP results in increased PI4P and actin levels on endosomes, and leads to defective endosome-to-Golgi traffic (Dong et al., 2016). It remains to be determined whether the loss of VAP or OSBP decreases endosome budding or subsequent bud fission.

From a mechanistic standpoint, it is unclear how ER-endosome MCSs contribute to scission of endosomal tubules. It is likely that some fission proteins are recruited to these sites to facilitate scission. Interesting candidates include Dynamin2 and the EHD (Eps15 homology domain) proteins, which could provide the mechanochemical force required for the fission. Dynamin2 has been reported to interact with the WASH complex, indicating a putative role for the scission of tubules (Derivery et al., 2009). The human genome encodes four EHD proteins, which share the conserved EHD domain. Structural studies of EHD2 reveals that the EHD domain forms ring-like oligomers around tubules, similar to the Dynamin GTPase (Daumke et al., 2007). It has been shown that EHD1 associates with retromer, and stabilizes the membrane tubules generated by SNX1 (Gokool et al., 2007; Zhang et al., 2012). Thus, Dynamin2 and EHD proteins may function together with the WASH complex to promote endosomal fission at the ER-endosome MCSs.

ER-Endosome MCSs and Human Diseases

Emphasizing the importance of ER-endosome MCSs for human health is the observation that mutations or aberrant expression of corresponding genes have been linked with many types of human diseases. Hereditary spastic paraplegia (HSP) is a group of inherited diseases characterized by progressive stiffness in the lower limbs. Among the over 60 genes that have been linked with HSP (Hensiek et al., 2015), many of them are implicated in the formation of ER-endosome MCSs, such as REEP1, WASH complex subunit strumpellin, ER protein protrudin, and spastin (Beetz et al., 2006, 2008; Mannan et al., 2006; Valdmanis et al., 2007). For instance, spastin is an

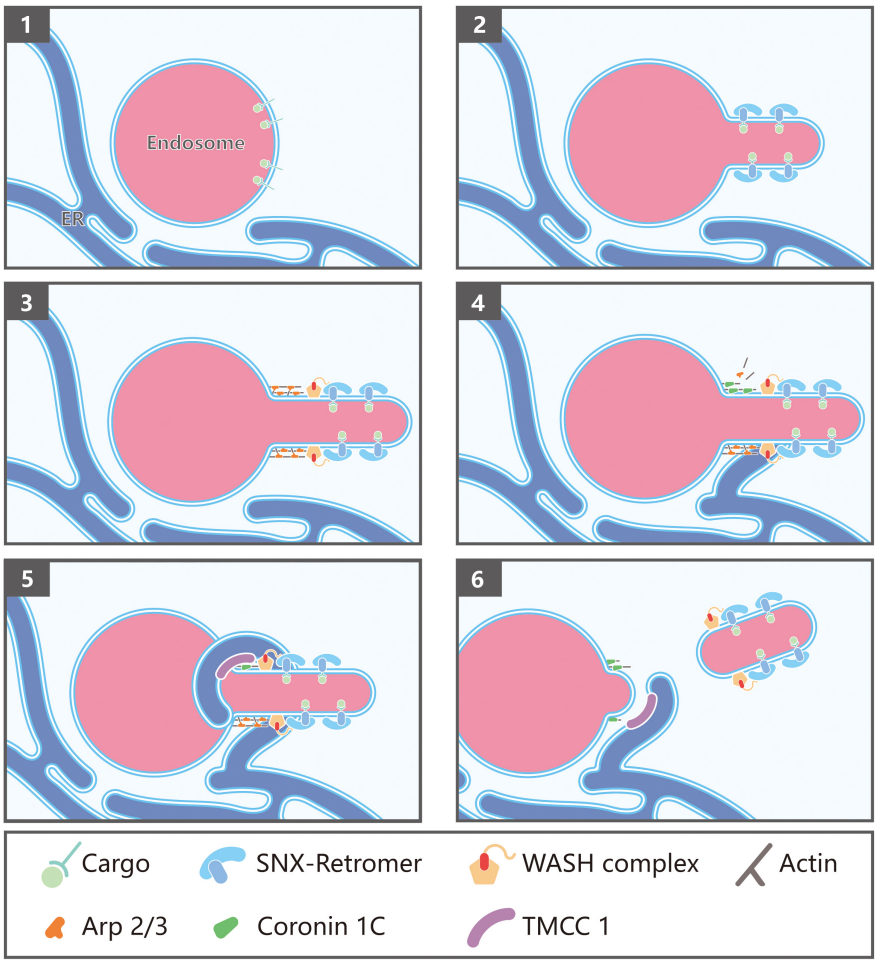

FIGURE 2 | Endoplasmic reticulum (ER)-endosome membrane contact sites in endosome fission: (1) Endosomes contain internalized transmembrane proteins or proteins delivered from the Golgi; (2) protein complexes, such as SNXs and retromer, recognize and concentrate specific cargo, and promote membrane remodeling; (3) retromer recruits the WASH complex via a direct interaction with the FAM21 subunit, which in turn promotes the assembly of branched actin via Arp2/3; (4) Coronin 1C associates with Arp2/3-mediated actin patches present on endosome buds; (5) Coronin 1C interacts with the ER membrane protein TMCC1 in order to recruit the ER to the Coronin 1C-labeled endosomal domains; (6) endosome fission occurs, likely via fission factors whose identity remains to be determined. Possible candidates include Dynamin2 and the EHD family proteins.

AAA family ATPase and functions as a microtubule severing protein (Roll-Mecak and Vale, 2008). The ER-localized spastin isoform mediates ER-endosome MCSs through interacting with the ESCRT-III protein IST1, which is critical for sorting of mannose 6-phosphate receptor and consequently lysosomal enzyme trafficking (Allison et al., 2017). Accordingly, abnormal lysosomal morphology has been observed in neurons and other types of cells that are depleted of not only spastin, but also REEP1 and strumpellin, suggesting that aberrant ER-endosome contacts likely contribute to the pathogenesis of HSP (Allison et al., 2017).

In addition to HSP, dysregulation of ER-endosome MCSs are implicated in other diseases. For instance, Niemann–Pick diseases are a group of metabolic diseases, in which large quantities of lipids accumulate in the spleen, liver, brain, and other parts of the body. Mutations of NPC1 (Niemann-Pick C1), which mediates the ER-late endosome contacts, and NPC2 (Niemann-Pick C2), result in failed cholesterol transport from the endosomal lumen and lead to Niemann–Pick disease (Carstea et al., 1997; Goldstein and Brown, 2001; Sleat et al., 2004).

CAPTURING ENDOSOMAL CARRIERS AT THE TGN

Transported vesicles destined for the Golgi are captured by tethering factors at a long distance (could extend for 100–400 nm), before subsequent vesicle docking and fusion mediated by the SNARE complex. Tethering factors localized on the Golgi can be divided into two classes: large oligomeric complexes including Golgi-associated retrograde protein (GARP) and conserved oligomeric Golgi (COG), and homodimeric golgin proteins (Whyte and Munro, 2002; Yu and Hughson, 2010).

GARP and COG

Both GARP and COG are recruited to the Golgi via interaction with small GTPases of the Rab and Arl families. COG is an octamer localized in all Golgi cisternae and plays a role in the retrieval of resident proteins between stacks (Zolov and Lupashin, 2005; Ungar et al., 2006). COG mutations have been linked with congenital disorders of glycosylation (CDG) (Zeevaert et al., 2008). The GARP complex (VPS51, VPS52, VPS53, and VPS54), mainly found at the TGN, is involved in transport of cargoes including the late-Golgi SNAREs and CI-MPR (Conibear et al., 2003; Perez-Victoria et al., 2008). This trafficking pathway is further stimulated by amino acids, requiring the small GTPase Arl5 and the Ragulator complex. Arl5 enhances the membrane recruitment of the GARP complex, and Ragulator may function as a guanine nucleotide exchange factor for Arl5 (Shi et al., 2018).

Golgins

Golgins represent another class of tethering proteins at the Golgi. Highly conserved among eukaryotes, golgins feature a long coiled-coil structure. The number of golgin-encoding genes has expanded during evolution, with 5 and more than 10 golgin-encoded genes in the *S. cerevisiae* and human genomes, respectively (Munro, 2011). The large number of golgin proteins is consistent with their diverse cellular functions. Using a mitochondrial re-location assay, Munro et al., found that golgin proteins could capture distinct sets of Golgi-bound transport vesicles (Wong and Munro, 2014). For instance, GM130 and GMAP-210 that localize in the *cis*-Golgi are capable of tethering vesicles arriving from the ER. The TGN-localized golgins, golgin-97, golgin-245, and GCC88, capture vesicles from endosomes; GCC185 did not capture vesicles in the assay (Wong and Munro, 2014). However, a separate study showed that GCC185 contains an AP-1 binding site and likely involves tethering of AP-1-decorated vesicles (Brown et al., 2011).

Different golgin proteins localize in different parts of the Golgi stack, and four mammalian golgins localize at the TGN: golgin-97, golgin-245, GCC88 and GCC185 (**Figure 1**). They share a conserved domain of about 80 residues at their carboxyl terminus, called the GRIP domain. The GRIP domain binds to the activated Arl1 GTPase localized at the TGN, which is critical for the Golgi-targeting of these golgins (Witkos and Lowe, 2015; Gillingham and Munro, 2016). In addition to Arl1 GTPase, these golgins also harbor binding sites for a variety of proteins, including AP-1, Rab GTPases, motor proteins and SNAREs (Derby et al., 2007; Burguete et al., 2008; Miller et al., 2009; Brown et al., 2011). These interactions allow golgins to capture specific transport vesicles from a long distance, as some golgins have a length of over 100 nm, and subsequently tether vesicles to the destination membrane.

One emerging concept in the field is that there are some degrees of crosstalk between the proteins involved in cargo recognition and carrier formation, and those involved in vesicle tethering (**Figure 1**). For instance, Cui et al. showed that SNX3- and retromer-dependent CI-MPR carriers are recognized and captured by GCC88, but not by golgin-97 or golgin-245 (Cui et al., 2019). On the other hand, SNX-BARs mediate CI-MPR trafficking in carriers that are captured by golgin-245 (Cui et al., 2019). It will be highly informative to determine how different types of carriers are recognized by different tethers.

TBC1D23

Three golgins mediate endosome-to-TGN transport: golgin-97, golgin-245, and GCC88 in the mitochondrial re-location assay (Wong and Munro, 2014). How these golgin proteins capture transport vesicles from endosomes remained unclear until recently. Earlier studies suggested that the N-termini of golgins are required to capture correct vesicles by interacting with vesicle-specific proteins or lipids (Wong and Munro, 2014). Using the mitochondrial re-location and proximity biotinylation assays, Shin et al. identified that the N-termini of golgin-97 and golgin-245, but not GCC88, interact with TBC1D23 (Shin et al., 2017). TBC1D23 also interacts with the WASH complex subunit FAM21, which is localized on vesicles derived from endosomes (Shin et al., 2017). Thus, TBC1D23 functions as an adapter to bridge endosomal vesicles with the TGN.

TBC1D23 is a member of the Tre2-Bub2-Cdc16 (TBC) family and can be found in most eukaryotic organisms, except for fungi and plants (Shin et al., 2017). The wide distribution and ubiquitous expression of TBC1D23 in various tissues and cells are consistent with its fundamental roles in biology and in development. Two human TBC1D23 isoforms are described so far, which differ by one exon (exon 15). As a result, the longer isoform including this exon encodes a protein with 699 residues, and the shorter one encodes 684 residues (Marin-Valencia et al., 2017). TBC1D23 contains three functional domains: an N-terminal TBC domain, a Rhodanese-like domain in the middle, and an C-terminal domain which is shown to be structurally similar to a Pleckstrin homology (PH) domain (**Figure 3A**; Wang et al., 2018; Huang et al., 2019). Its TBC domain interacts with the N-terminal 21 residues from golgin-97 or golgin-245 (Shin et al., 2017). Members of the TBC family often function as Rab GTPase-activating proteins (GAPs), and contain two conserved catalytic residues, Arg and Gln within their GAP domain (Pan et al., 2006). For instance, TBC1D5 is a GAP for both Rab7a and Rab7b, and functions to regulate retromer-dependent trafficking, and to regulate late endosomal and lysosomal functions (**Figure 3A**; Mukhopadhyay et al., 2007; Seaman et al., 2009; Jia et al., 2016; Borg Distefano et al., 2018; Jimenez-Orgaz et al., 2018; Kvainickas et al., 2019). In contrast, TBC1D23 lacks both essential catalytic residues, and is catalytically inactive (Marin-Valencia et al., 2017). Proteins with a rhodanese domain can possess sulphurtransferase (such as TSTD1) or phosphatase (such as CDC25) activity (Bordo and Bork, 2002). It remains to be determined whether the rhodanese domain of TBC1D23 possesses any enzymatic activities; if it does, how the enzymatic activities contribute to its functions in membrane trafficking remains to be determined. Finally, we recently solved the crystal structure of the TBC1D23 C-terminal domain, and showed that it selectively binds to phosphoinositides, including PI4P, and the FAM21 subunit of the WASH complex, using opposite surfaces (Huang et al., 2019). Whereas these observations are interesting, additional work is needed to address whether such interactions help to

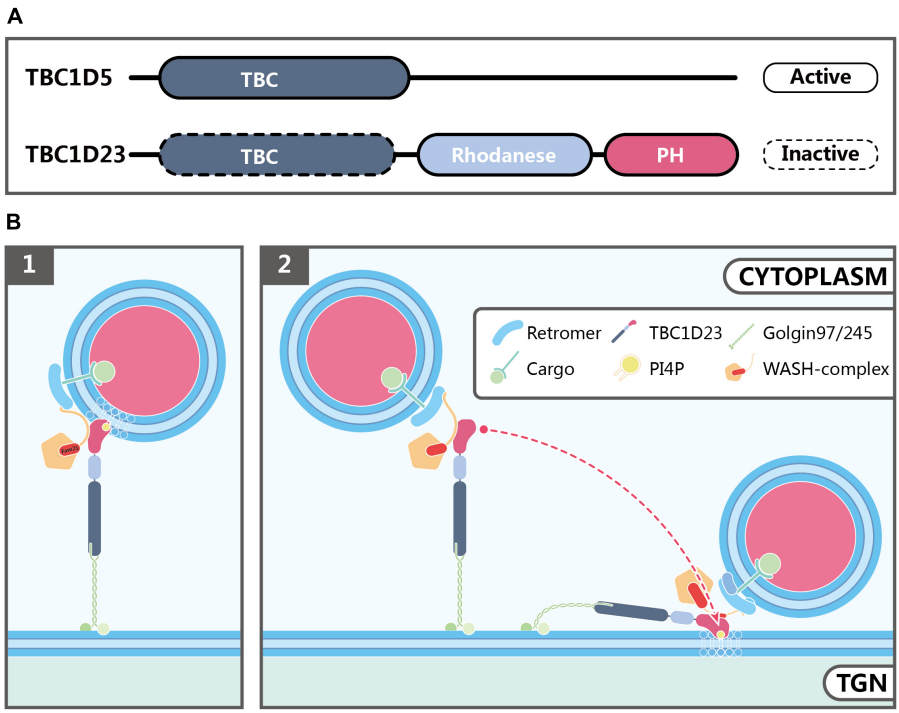

FIGURE 3 | Possible functions of TBC1D23 in endosome-to-TGN trafficking. **(A)** Domain structures of TBC1D5 and TBC1D23. Although both proteins possess a TBC domain, TBC1D5, but not TBC1D23, is an active GAP for Rab GTPases. In addition to the TBC domain, TBC1D23 also contains a rhodanese-like domain, and a C-terminal domain, which is structurally similar to phospholipid-binding PH domains despite bearing little sequence similarity. **(B)** Models showing how TBC1D23 regulates endosome-to-TGN trafficking by interacting with FAM21 and specific phosphoinositides, such as PI4P. FAM21 associates with WASH, TBC1D23 and retromer via its N-terminus, the middle region, and C-terminus, respectively. Whereas the C-terminal domain of TBC1D23 engages with PI4P, in addition to FAM21, future studies will be needed to address whether such interactions help to capture the PI4P-positive endosomal vesicles by TBC1D23 (1), or promote the tethering of TBC1D23-bound vesicles to the TGN (2).

capture the PI4P-positive endosomal vesicles by TBC1D23, or promote the tethering of TBC1D23 and bound vesicles by the TGN (**Figure 3B**).

Emphasizing the importance of TBC1D23 in human development, homozygous mutations of the TBC1D23 gene has recently been found in patients diagnosed with pontocerebellar hypoplasia (PCH) (Ivanova et al., 2017; Marin-Valencia et al., 2017; Harripaul et al., 2018). These mutations result in truncated proteins that are missing the C-terminal domain. PCH is a group of neurological disorders, characterized by the impaired development of the brain, especially the pons and the cerebellum. Other features of PCH patients include delayed development, microcephaly, movement problems, and intellectual disability. Interestingly, most of the genes linked with PCH are involved in RNA processing (Namavar et al., 2011; Rudnik-Schoneborn et al., 2014), unlike TBC1D23. Using cellular assays and zebrafish models, we demonstrated a strong correlation between cellular and zebrafish phenotypes caused by different TBC1D23 mutants, indicating that mis-regulation of cargo trafficking from endosomes, at least partially, contributes to the development of PCH (Huang et al., 2019). Future studies will be necessary to determine which cargo proteins are most severely affected by TBC1D23 deletion or mutations, which could provide fresh insights into the pathogenesis of certain types of PCH.

WDR11

In addition to goglin-97, golgin-245, and FAM21, TBC1D23 also interacts with a trimeric complex, consisting of WDR11, FAM91A, and C17orf75, through a region between the rhodanese and PH domains (Borner et al., 2014; Shin et al., 2017; Navarro Negredo et al., 2018). The WDR11 complex is proposed to function together with TBC1D23 and the clathrin adaptor, AP-1, to promote endosome-to-TGN trafficking (Navarro Negredo et al., 2018). One possibility is that WDR11 localizes on the TGN and functions to capture vesicles containing AP-1-dependent cargo; the other possibility is that WDR11 associates with the vesicle, and its interaction with TBC1D23 promotes vesicle tethering at the TGN (Navarro Negredo et al., 2018). Either scenario is consistent with some tethering roles of TBC1D23 and the WDR11 complex, although the exact mechanisms remain to be determined.

Intriguingly, mutations of WDR11 have been found in patients with congenital hypogonadotropic hypogonadism (CHH) and Kallmann syndrome (KS), developmental disorders characterized by delayed puberty and infertility (Kim et al., 2010). WDR11 is essential for normal ciliogenesis, by being involved in the Hedgehog (Hh) signaling pathway (Kim et al., 2018). However, it is unclear whether TBC1D23 is also involved in these processes.

WASH COMPLEX

One molecule recurring through many distinct processes of endosomal trafficking is the evolutionarily conserved WASH complex, which promotes endosomal branched actin polymerization (Derivery et al., 2009; Gomez and Billadeau, 2009; Jia et al., 2010). In cells, WASH forms a stable pentameric complex together with four other proteins, including FAM21 (WASHC2), CCDC53 (WASHC3), SWIP (Strumpellin and WASH1-interacting protein or WASHC4), and Strumpellin (WASHC5) (Derivery et al., 2009; Jia et al., 2010). The WASH complex predominantly localizes to endosomes and functions to regulate multiple endosomal trafficking pathways. Among them, the best-characterized function of WASH is to regulate retromer-dependent trafficking through an association with retromer, via a direct interaction between the retromer subunit VPS35 and FAM21 (Harbour et al., 2010; Jia et al., 2012). WASH modulates endosome-to-TGN or endosome-to-plasma membrane transport of many endosomal proteins, such as CI-MPR, the β2-adrenoceptor (β2AR), the glucose transporter GLUT1, and transferrin receptor (TfnR) (Derivery et al., 2009; Puthenveedu et al., 2010; Zech et al., 2011; Gomez et al., 2012; Piotrowski et al., 2013; Phillips-Krawczak et al., 2015). Recent studies demonstrate that the WASH complex also functions to orchestrate retromer-independent trafficking, by cooperating with retriever and the CCC complex (McNally et al., 2017). In addition to retromer, HRS (hepatocyte growth factor–regulated tyrosine kinase substrate) also plays a role in regulating endosomal localization of WASH, although it is unclear whether the interaction between WASH and HRS is direct (MacDonald et al., 2018). It is reported that WASH and HRS cooperate to regulate endosomal recycling of epidermal growth factor receptor and the matrix metalloproteinase MT1–MMP (MacDonald et al., 2018). The WASH complex also associates with BLOC-1 (biogenesis of lysosomal organelles complex-1), and may play a role in the formation of melanosomes (Monfregola et al., 2010; Ryder et al., 2013). In all of the above processes, WASH likely functions to promote actin polymerization and to provide the force required for the formation of endosomal recycling or retrieval subdomains, or for vesicle budding and scission. The WASH complex, especially FAM21, also likely serves as a recruiting hub for additional proteins involved in the trafficking of proteins to specific subcellular destinations (Seaman et al., 2013; Wang et al., 2018).

The WASH complex possesses additional functions. It has been shown that WASH defines endosome fission sites by locally activating the Arp2/3 complex to generate branched F-actin, and the subsequent recruitment of Coronin 1C, which facilitates interaction with TMCC1 leading to ER-endosome contact (Rowland et al., 2014; Hoyer et al., 2018). Finally, the interaction between endosomal-localized FAM21 and Golgi-localized TBC1D23 promotes vesicle tethering at the TGN (Shin et al., 2017; Huang et al., 2019). How can one protein complex possess so many diverse functions? Part of the answer lies in the fact that FAM21 is a large protein with over 1300 residues. Although slightly over 200 residues within the N-terminus of FAM21 are sufficient for assembly of the WASH pentameric complex, the C-terminal tail of FAM21 harbors 21 repeats of the LFa motif (L-F-[D/E]3-10-L-F), and is capable of engaging several proteins, including retromer, TBC1D23, CCC complex, CapZ, and FKBP15 among others (Hernandez-Valladares et al., 2010; Jia et al., 2010, 2012; Takeda et al., 2010; Harbour et al., 2011, 2012; Freeman et al., 2014; Phillips-Krawczak et al., 2015; Kvainickas et al., 2017b; Shin et al., 2017). Interestingly, although both retromer and TBC1D23 bind to LFa motifs within the FAM21 tail, their different sequence preference allows them to bind non-overlapping motifs (Huang et al., 2019).

Deletion of WASH in mice leads to embryonic lethality, emphasizing the indispensable role of the WASH complex in mammalian development (Gomez et al., 2012; Xia et al., 2013). Interestingly, WASH deletion in *Drosophila* does not result in lethality, likely due to a compensatory effect of related genes (Verboon et al., 2018). Furthermore, mutations in Strumpellin and SWIP have been linked with multiple neurological disorders, including intellectual disability, hereditary spastic paraplegia, and Ritscher-Schinzel/3C syndrome (Valdmanis et al., 2007; Ropers et al., 2011; Vardarajan et al., 2012; de Bot et al., 2013; Elliott et al., 2013). Finally, an early onset Parkinson's Disease (PD) mutation in VPS35 (D620N) was shown to compromise the interaction between the WASH complex and retromer, and to impair endosomal trafficking as well as autophagy (Vilarino-Guell et al., 2011; Zimprich et al., 2011; Follett et al., 2014; McGough et al., 2014; Miura et al., 2014; Zavodszky et al., 2014). Altogether, these studies highlight that regulation of endosomal trafficking via fine-tuning actin polymerization is essential for mammalian development, especially for neuronal development.

AN EVOLUTIONARY PERSPECTIVE

Although the endosome-to-TGN trafficking is absolutely conserved in eukaryotes, it is interesting to note the divergence of many important genes (**Table 1**). Whereas retromer, SNX3, SNX-BARs are conserved in the eukaryotic kingdom, many genes encoding proteins with regulatory functions, such as the WASH complex and EHD1, are missing in *S. cerevisiae* (Seaman, 2012). Similarly, whereas mammals have four golgin proteins localized at the TGN, yeast only has one, IMH1 (Munro, 2011). IMH1 is known to participate Ypt6-mediated, the yeast homolog of mammalian Rab6 GTPase, endosome-to-TGN transport (Chen et al., 2019). However, yeast does not have clear homologs of TBC1D23 or WDR11, suggesting that IMH1 exert its functions through a mechanism distinct from that of golgin-97 and golgin-245.

Furthermore, although retromer and SNX-BARs are conserved between yeast and mammals, they show marked differences in many aspects. First, yeast retromer is a stable pentameric complex, consisting of the Vps35-Vps26-Vps29 trimer and the SNX-BAR proteins Vps5 and Vps10 (Seaman et al., 1998). However, in mammals and other higher metazoans, the VPS35-VPS26-VPS29 trimer [referred to as retromer in metazoans (Burd and Cullen, 2014)] and the SNX-BAR dimer function as independent entities, and are only loosely connected with each other. Second, as separate entities, both mammalian

TABLE 1 | Conservation of selected genes involved in endosome-to-TGN trafficking.

		Homo sapiens	*Saccharomyces cerevisiae*
Coats and related proteins	Retromer	√	√
	TBC1D5	√	
	SNX-BAR	√ (SNX1/SNX2 + SNX5/SNX6/SNX32)	√ (Vps5 + Vps17)
	SNX3	√	√
	AP-1	√	√
Tethers and related proteins	Golgin-97	√	
	Golgin-245	√	Imh1
	GCC88	√	
	GCC185	√	
	TBC1D23	√	
	WDR11	√	
Other	WASH complex	√	
	EHD1	√	

VPS35-VPS26-VPS29 trimer and the SNX-BAR dimer have gained additional functions. For instance, mammalian VPS35-VPS26-VPS29 trimer associates with SNX3 or SNX27 to form functionally distinct entities, independent of SNX-BARs (Harterink et al., 2011; Temkin et al., 2011; Steinberg et al., 2013; Gallon et al., 2014). Similarly, mammalian SNX-BAR dimer, but not the yeast Vps5 and Vps10 dimer, are directly involved in sequence-dependent cargo recognition (Kvainickas et al., 2017a; Simonetti et al., 2017, 2019). Lastly, although yeast retromer is a known regulator of endosome-to-Golgi trafficking, both mammalian retromer and SNX-BARs play critical roles in both endosome-to-TGN and endosome-to-plasma membrane recycling. Thus, although yeast represents an excellent model to investigate the endosome-to-TGN trafficking, cautions must be taken when knowledge learned from different organisms are considered together.

CONCLUSION

The past a few years have witnessed great advances in the field of endosomal biology. First, multiple types of ER-endosome MCSs have been characterized, with each possessing unique molecular compositions and functions (Raiborg et al., 2015; Wu et al., 2018). ER-endosome contact sites are known to regulate many aspects of endosomal functions, ranging from endosome positioning and fission, to lipid and ion exchange. Second, several new protein complexes, including the SNX17-retriever complex and SNX-BARs, have been discovered to mediate sequence-dependent cargo retrieval and recycling (Kvainickas et al., 2017a; McNally et al., 2017; Simonetti et al., 2017, 2019). Third, the mechanisms by which endosomal vesicles are captured by the Golgi are emerging (Cheung et al., 2015; Shin et al., 2017; Navarro Negredo et al., 2018). These advances have greatly expanded our understanding of endosomal trafficking, and provided insight into mechanisms contributing to human disease.

The fast progress made in this field suggests that we can anticipate more exciting developments in the new decade. However, despite the huge leap forward in the field, we are still left with many important questions. For those studying ER-endosome contact, a big question is whether other types of contact sites exist, and what are their functions? How are the dynamics of ER-endosome contact sites regulated? How do ER-endosome MCSs promote endosome fission from a mechanistic standpoint? For those interested in vesicular trafficking, it remains to be determined the precise roles and relationship of different molecules involved in cargo recognition and carrier formation, such as retromer, SNX-BARs, and clathrin/AP-1. For most cases, it is still unclear how tethering proteins recognize specific vesicles. Whereas long tethering proteins can capture vesicles as far away as a few hundred nanometers, the SNARE complex mediates vesicle fusion at a much shorter distance (<10 nm). How does the vesicle tethering step connect with the fusion step? Lastly, as our knowledge increases regarding the molecular mechanisms by which dysregulation of endosomal functions contribute to human disease, the translation of these basic discoveries into the clinic are likely to be rapidly approaching.

AUTHOR CONTRIBUTIONS

All authors listed have made a substantial, direct and intellectual contribution to the work, and approved it for publication.

FUNDING

This research was supported by the National Natural Science Foundation of China (NSFC) grants (#91854121, #31871429, and #81901281), National Key Research and Development Program of China (2018YFC1005004), Sichuan Science and Technology Program (2018RZ0128), and US NIH grant (DK107733 to DB).

ACKNOWLEDGMENTS

We thank members of our laboratory for helpful discussions, and Mr. Chengxin Weng for help with making figures.

REFERENCES

Allison, R., Edgar, J. R., Pearson, G., Rizo, T., Newton, T., Gunther, S., et al. (2017). Defects in ER-endosome contacts impact lysosome function in hereditary spastic paraplegia. *J. Cell Biol.* 216, 1337–1355. doi: 10.1083/jcb.201609033

Arighi, C. N., Hartnell, L. M., Aguilar, R. C., Haft, C. R., and Bonifacino, J. S. (2004). Role of the mammalian retromer in sorting of the cation-independent mannose 6-phosphate receptor. *J. Cell Biol.* 165, 123–133. doi: 10.1083/jcb.200312055

Bareja, A., Hodgkinson, C. P., Soderblom, E., Waitt, G., and Dzau, V. J. (2018). The proximity-labeling technique BioID identifies sorting nexin 6 as a member of the insulin-like growth factor 1 (IGF1)-IGF1 receptor pathway. *J. Biol. Chem.* 293, 6449–6459. doi: 10.1074/jbc.RA118.002406

Beetz, C., Nygren, A. O., Schickel, J., Auer-Grumbach, M., Burk, K., Heide, G., et al. (2006). High frequency of partial SPAST deletions in autosomal dominant hereditary spastic paraplegia. *Neurology* 67, 1926–1930. doi: 10.1212/01.wnl.0000244413.49258.f5

Beetz, C., Schule, R., Deconinck, T., Tran-Viet, K. N., Zhu, H., Kremer, B. P., et al. (2008). REEP1 mutation spectrum and genotype/phenotype correlation in hereditary spastic paraplegia type 31. *Brain* 131(Pt 4), 1078–1086. doi: 10.1093/brain/awn026

Bordo, D., and Bork, P. (2002). The rhodanese/Cdc25 phosphatase superfamily. Sequence-structure-function relations. *EMBO Rep.* 3, 741–746. doi: 10.1093/embo-reports/kvf150

Borg Distefano, M., Hofstad Haugen, L., Wang, Y., Perdreau-Dahl, H., Kjos, I., Jia, D., et al. (2018). TBC1D5 controls the GTPase cycle of Rab7b. *J. Cell Sci.* 131:jcs216630. doi: 10.1242/jcs.216630

Borner, G. H., Hein, M. Y., Hirst, J., Edgar, J. R., Mann, M., and Robinson, M. S. (2014). Fractionation profiling: a fast and versatile approach for mapping vesicle proteomes and protein-protein interactions. *Mol. Biol. Cell* 25, 3178–3194. doi: 10.1091/mbc.E14-07-1198

Brown, F. C., Schindelhaim, C. H., and Pfeffer, S. R. (2011). GCC185 plays independent roles in Golgi structure maintenance and AP-1-mediated vesicle tethering. *J. Cell Biol.* 194, 779–787. doi: 10.1083/jcb.201104019

Burd, C., and Cullen, P. J. (2014). Retromer: a master conductor of endosome sorting. *Cold Spring Harb. Perspect. Biol.* 6:a016774. doi: 10.1101/cshperspect.a016774

Burguete, A. S., Fenn, T. D., Brunger, A. T., and Pfeffer, S. R. (2008). Rab and Arl GTPase family members cooperate in the localization of the Golgin GCC185. *Cell* 132, 286–298. doi: 10.1016/j.cell.2007.11.048

Carlton, J., Bujny, M., Peter, B. J., Oorschot, V. M., Rutherford, A., Mellor, H., et al. (2004). Sorting nexin-1 mediates tubular endosome-to-TGN transport through coincidence sensing of high- curvature membranes and 3-phosphoinositides. *Curr. Biol.* 14, 1791–1800. doi: 10.1016/j.cub.2004.09.077

Carroll, K. S., Hanna, J., Simon, I., Krise, J., Barbero, P., and Pfeffer, S. R. (2001). Role of Rab9 GTPase in facilitating receptor recruitment by TIP47. *Science* 292, 1373–1376. doi: 10.1126/science.1056791

Carstea, E. D., Morris, J. A., Coleman, K. G., Loftus, S. K., Zhang, D., Cummings, C., et al. (1997). Niemann-Pick C1 disease gene: homology to mediators of cholesterol homeostasis. *Science* 277, 228–231. doi: 10.1126/science.277.5323.228

Chandra, M., Chin, Y. K., Mas, C., Feathers, J. R., Paul, B., Datta, S., et al. (2019). Classification of the human phox homology (PX) domains based on their phosphoinositide binding specificities. *Nat. Commun.* 10:1528. doi: 10.1038/s41467-019-09355-y

Chen, Y. T., Wang, I. H., Wang, Y. H., Chiu, W. Y., Hu, J. H., Chen, W. H., et al. (2019). Action of Arl1 GTPase and golgin Imh1 in Ypt6-independent retrograde transport from endosomes to the trans-Golgi network. *Mol. Biol. Cell* 30, 1008–1019. doi: 10.1091/mbc.E18-09-0579

Cheung, P. Y., Limouse, C., Mabuchi, H., and Pfeffer, S. R. (2015). Protein flexibility is required for vesicle tethering at the Golgi. *eLife* 4:e12790. doi: 10.7554/eLife.12790

Cheung, P. Y., and Pfeffer, S. R. (2016). Transport vesicle tethering at the trans Golgi network: coiled coil proteins in action. *Front. Cell. Dev. Biol.* 4:18. doi: 10.3389/fcell.2016.00018

Conibear, E., Cleck, J. N., and Stevens, T. H. (2003). Vps51p mediates the association of the GARP (Vps52/53/54) complex with the late Golgi t-SNARE Tlg1p. *Mol. Biol. Cell* 14, 1610–1623. doi: 10.1091/mbc.e02-10-0654

Cui, Y., Carosi, J. M., Yang, Z., Ariotti, N., Kerr, M. C., Parton, R. G., et al. (2019). Retromer has a selective function in cargo sorting via endosome transport carriers. *J. Cell Biol.* 218, 615–631. doi: 10.1083/jcb.201806153

Cullen, P. J., and Steinberg, F. (2018). To degrade or not to degrade: mechanisms and significance of endocytic recycling. *Nat. Rev. Mol. Cell Biol.* 19, 679–696. doi: 10.1038/s41580-018-0053-7

Daumke, O., Lundmark, R., Vallis, Y., Martens, S., Butler, P. J., and McMahon, H. T. (2007). Architectural and mechanistic insights into an EHD ATPase involved in membrane remodelling. *Nature* 449, 923–927. doi: 10.1038/nature06173

de Bot, S. T., Vermeer, S., Buijsman, W., Heister, A., Voorendt, M., Verrips, A., et al. (2013). Pure adult-onset spastic paraplegia caused by a novel mutation in the KIAA0196 (SPG8) gene. *J. Neurol.* 260, 1765–1769. doi: 10.1007/s00415-013-6870-x

Derby, M. C., Lieu, Z. Z., Brown, D., Stow, J. L., Goud, B., and Gleeson, P. A. (2007). The trans-Golgi network golgin, GCC185, is required for endosome-to-Golgi transport and maintenance of Golgi structure. *Traffic* 8, 758–773. doi: 10.1111/j.1600-0854.2007.00563.x

Derivery, E., Sousa, C., Gautier, J. J., Lombard, B., Loew, D., and Gautreau, A. (2009). The Arp2/3 activator WASH controls the fission of endosomes through a large multiprotein complex. *Dev. Cell* 17, 712–723. doi: 10.1016/j.devcel.2009.09.010

Dong, R., Saheki, Y., Swarup, S., Lucast, L., Harper, J. W., and De Camilli, P. (2016). Endosome-ER contacts control actin nucleation and retromer function through VAP-dependent regulation of PI4P. *Cell* 166, 408–423. doi: 10.1016/j.cell.2016.06.037

Elliott, A. M., Simard, L. R., Coghlan, G., Chudley, A. E., Chodirker, B. N., Greenberg, C. R., et al. (2013). A novel mutation in KIAA0196: identification of a gene involved in Ritscher-Schinzel/3C syndrome in a First Nations cohort. *J. Med. Genet.* 50, 819–822. doi: 10.1136/jmedgenet-2013-101715

Elwell, C. A., Czudnochowski, N., von Dollen, J., Johnson, J. R., Nakagawa, R., Mirrashidi, K., et al. (2017). *Chlamydia* interfere with an interaction between the mannose-6-phosphate receptor and sorting nexins to counteract host restriction. *eLife* 6:e22709. doi: 10.7554/eLife.22709

Fjorback, A. W., Seaman, M., Gustafsen, C., Mehmedbasic, A., Gokool, S., Wu, C., et al. (2012). Retromer binds the FANSHY sorting motif in SorLA to regulate amyloid precursor protein sorting and processing. *J. Neurosci.* 32, 1467–1480. doi: 10.1523/JNEUROSCI.2272-11.2012

Follett, J., Norwood, S. J., Hamilton, N. A., Mohan, M., Kovtun, O., Tay, S., et al. (2014). The Vps35 D620N mutation linked to Parkinson's disease disrupts the cargo sorting function of retromer. *Traffic* 15, 230–244. doi: 10.1111/tra.12136

Freeman, C. L., Hesketh, G., and Seaman, M. N. (2014). RME-8 coordinates the activity of the WASH complex with the function of the retromer SNX dimer to control endosomal tubulation. *J. Cell Sci.* 127(Pt 9), 2053–2070. doi: 10.1242/jcs.144659

Friedman, J. R., Lackner, L. L., West, M., DiBenedetto, J. R., Nunnari, J., and Voeltz, G. K. (2011). ER tubules mark sites of mitochondrial division. *Science* 334, 358–362. doi: 10.1126/science.1207385

Gallon, M., Clairfeuille, T., Steinberg, F., Mas, C., Ghai, R., Sessions, R. B., et al. (2014). A unique PDZ domain and arrestin-like fold interaction reveals mechanistic details of endocytic recycling by SNX27-retromer. *Proc. Natl. Acad. Sci. U.S.A.* 111, E3604–E3613. doi: 10.1073/pnas.1410552111

Ghosh, R. N., Mallet, W. G., Soe, T. T., McGraw, T. E., and Maxfield, F. R. (1998). An endocytosed TGN38 chimeric protein is delivered to the TGN after trafficking through the endocytic recycling compartment in CHO cells. *J. Cell Biol.* 142, 923–936. doi: 10.1083/jcb.142.4.923

Gillingham, A. K., and Munro, S. (2016). Finding the Golgi: golgin coiled-coil proteins show the way. *Trends Cell Biol.* 26, 399–408. doi: 10.1016/j.tcb.2016.02.005

Gokool, S., Tattersall, D., and Seaman, M. N. (2007). EHD1 interacts with retromer to stabilize SNX1 tubules and facilitate endosome-to-Golgi retrieval. *Traffic* 8, 1873–1886. doi: 10.1111/j.1600-0854.2007.00652.x

Goldstein, J. L., and Brown, M. S. (2001). Molecular medicine. The cholesterol quartet. *Science* 292, 1310–1312. doi: 10.1126/science.1061815

Gomez, T. S., and Billadeau, D. D. (2009). A FAM21-containing WASH complex regulates retromer-dependent sorting. *Dev. Cell* 17, 699–711. doi: 10.1016/j.devcel.2009.09.009

Gomez, T. S., Gorman, J. A., de Narvajas, A. A., Koenig, A. O., and Billadeau, D. D. (2012). Trafficking defects in WASH-knockout fibroblasts originate from

collapsed endosomal and lysosomal networks. *Mol. Biol. Cell* 23, 3215–3228. doi: 10.1091/mbc.E12-02-0101

Harbour, M. E., Breusegem, S. Y., Antrobus, R., Freeman, C., Reid, E., and Seaman, M. N. (2010). The cargo-selective retromer complex is a recruiting hub for protein complexes that regulate endosomal tubule dynamics. *J. Cell Sci.* 123(Pt 21), 3703–3717. doi: 10.1242/jcs.071472

Harbour, M. E., Breusegem, S. Y., and Seaman, M. N. (2011). Recruitment of the endosomal WASH complex is mediated by the extended "tail" of Fam21 binding to the retromer protein VPS35. *Biochem. J.* 442, 209–220. doi: 10.1042/BJ20111761

Harbour, M. E., Breusegem, S. Y., and Seaman, M. N. (2012). Recruitment of the endosomal WASH complex is mediated by the extended 'tail' of Fam21 binding to the retromer protein Vps35. *Biochem. J.* 442, 209–220.

Harripaul, R., Vasli, N., Mikhailov, A., Rafiq, M. A., Mittal, K., Windpassinger, C., et al. (2018). Mapping autosomal recessive intellectual disability: combined microarray and exome sequencing identifies 26 novel candidate genes in 192 consanguineous families. *Mol. Psychiatry* 23, 973–984. doi: 10.1038/mp.2017.60

Harrison, M. S., Hung, C. S., Liu, T. T., Christiano, R., Walther, T. C., and Burd, C. G. (2014). A mechanism for retromer endosomal coat complex assembly with cargo. *Proc. Natl. Acad. Sci. U.S.A.* 111, 267–272. doi: 10.1073/pnas.1316482111

Harterink, M., Port, F., Lorenowicz, M. J., McGough, I. J., Silhankova, M., Betist, M. C., et al. (2011). A SNX3-dependent retromer pathway mediates retrograde transport of the Wnt sorting receptor Wntless and is required for Wnt secretion. *Nat. Cell Biol.* 13, 914–923. doi: 10.1038/ncb2281

Hensiek, A., Kirker, S., and Reid, E. (2015). Diagnosis, investigation and management of hereditary spastic paraplegias in the era of next-generation sequencing. *J. Neurol.* 262, 1601–1612. doi: 10.1007/s00415-014-7598-y

Hernandez-Valladares, M., Kim, T., Kannan, B., Tung, A., Aguda, A. H., Larsson, M., et al. (2010). Structural characterization of a capping protein interaction motif defines a family of actin filament regulators. *Nat. Struct. Mol. Biol.* 17, 497–503. doi: 10.1038/nsmb.1792

Hirst, J., Borner, G. H., Antrobus, R., Peden, A. A., Hodson, N. A., Sahlender, D. A., et al. (2012). Distinct and overlapping roles for AP-1 and GGAs revealed by the "knocksideways" system. *Curr. Biol.* 22, 1711–1716. doi: 10.1016/j.cub.2012.07.012

Hirst, J., Borner, G. H., Edgar, J., Hein, M. Y., Mann, M., Buchholz, F., et al. (2013). Interaction between AP-5 and the hereditary spastic paraplegia proteins SPG11 and SPG15. *Mol. Biol. Cell* 24, 2558–2569. doi: 10.1091/mbc.E13-03-0170

Hirst, J., Miller, S. E., Taylor, M. J., von Mollard, G. F., and Robinson, M. S. (2004). EpsinR is an adaptor for the SNARE protein Vti1b. *Mol. Biol. Cell* 15, 5593–5602. doi: 10.1091/mbc.e04-06-0468

Hoyer, M. J., Chitwood, P. J., Ebmeier, C. C., Striepen, J. F., Qi, R. Z., Old, W. M., et al. (2018). A novel class of ER membrane proteins regulates ER-associated endosome fission. *Cell* 175, 254–265.e14. doi: 10.1016/j.cell.2018.08.030

Huang, W., Liu, Z., Yang, F., Zhou, H., Yong, X., Yang, X., et al. (2019). Structural and functional studies of TBC1D23 C-terminal domain provide a link between endosomal trafficking and PCH. *Proc. Natl. Acad. Sci. U.S.A.* 116, 22598–22608. doi: 10.1073/pnas.1909316116

Ivanova, E. L., Mau-Them, F. T., Riazuddin, S., Kahrizi, K., Laugel, V., Schaefer, E., et al. (2017). Homozygous truncating variants in TBC1D23 cause pontocerebellar hypoplasia and alter cortical development. *Am. J. Hum. Genet.* 101, 428–440. doi: 10.1016/j.ajhg.2017.07.010

Jia, D., Gomez, T. S., Billadeau, D. D., and Rosen, M. K. (2012). Multiple repeat elements within the FAM21 tail link the WASH actin regulatory complex to the retromer. *Mol. Biol. Cell* 23, 2352–2361. doi: 10.1091/mbc.E11-12-1059

Jia, D., Gomez, T. S., Metlagel, Z., Umetani, J., Otwinowski, Z., Rosen, M. K., et al. (2010). WASH and WAVE actin regulators of the Wiskott-Aldrich syndrome protein (WASP) family are controlled by analogous structurally related complexes. *Proc. Natl. Acad. Sci. U.S.A.* 107, 10442–10447. doi: 10.1073/pnas.0913293107

Jia, D., Zhang, J. S., Li, F., Wang, J., Deng, Z., White, M. A., et al. (2016). Structural and mechanistic insights into regulation of the retromer coat by TBC1d5. *Nat. Commun.* 7:13305. doi: 10.1038/ncomms13305

Jimenez-Orgaz, A., Kvainickas, A., Nagele, H., Denner, J., Eimer, S., Dengjel, J., et al. (2018). Control of RAB7 activity and localization through the retromer-TBC1D5 complex enables RAB7-dependent mitophagy. *EMBO J.* 37, 235–254. doi: 10.15252/embj.201797128

Kim, H. G., Ahn, J. W., Kurth, I., Ullmann, R., Kim, H. T., Kulharya, A., et al. (2010). WDR11, a WD protein that interacts with transcription factor EMX1, is mutated in idiopathic hypogonadotropic hypogonadism and Kallmann syndrome. *Am. J. Hum. Genet.* 87, 465–479. doi: 10.1016/j.ajhg.2010.08.018

Kim, Y. J., Osborn, D. P., Lee, J. Y., Araki, M., Araki, K., Mohun, T., et al. (2018). WDR11-mediated Hedgehog signalling defects underlie a new ciliopathy related to Kallmann syndrome. *EMBO Rep.* 19, 269–289. doi: 10.15252/embr.201744632

Kvainickas, A., Jimenez-Orgaz, A., Nagele, H., Hu, Z., Dengjel, J., and Steinberg, F. (2017a). Cargo-selective SNX-BAR proteins mediate retromer trimer independent retrograde transport. *J. Cell Biol.* 216, 3677–3693. doi: 10.1083/jcb.201702137

Kvainickas, A., Nagele, H., Qi, W., Dokladal, L., Jimenez-Orgaz, A., Stehl, L., et al. (2019). Retromer and TBC1D5 maintain late endosomal RAB7 domains to enable amino acid-induced mTORC1 signaling. *J. Cell Biol.* 218, 3019–3038. doi: 10.1083/jcb.201812110

Kvainickas, A., Orgaz, A. J., Nagele, H., Diedrich, B., Heesom, K. J., Dengjel, J., et al. (2017b). Retromer- and WASH-dependent sorting of nutrient transporters requires a multivalent interaction network with ANKRD50. *J. Cell Sci.* 130, 382–395. doi: 10.1242/jcs.196758

Liu, J. J. (2016). Retromer-mediated protein sorting and vesicular trafficking. *J. Genet. Genomics* 43, 165–177. doi: 10.1016/j.jgg.2016.02.006

Lu, L., and Hong, W. (2014). From endosomes to the trans-Golgi network. *Semin. Cell Dev. Biol.* 31, 30–39. doi: 10.1016/j.semcdb.2014.04.024

Lucas, M., Gershlick, D. C., Vidaurrazaga, A., Rojas, A. L., Bonifacino, J. S., and Hierro, A. (2016). Structural mechanism for cargo recognition by the retromer complex. *Cell* 167, 1623–1635.e14. doi: 10.1016/j.cell.2016.10.056

Lucas, M., and Hierro, A. (2017). Retromer. *Curr. Biol.* 27, R687–R689. doi: 10.1016/j.cub.2017.05.072

MacDonald, E., Brown, L., Selvais, A., Liu, H., Waring, T., Newman, D., et al. (2018). HRS-WASH axis governs actin-mediated endosomal recycling and cell invasion. *J. Cell Biol.* 217, 2549–2564. doi: 10.1083/jcb.201710051

Mallet, W. G., and Maxfield, F. R. (1999). Chimeric forms of furin and TGN38 are transported with the plasma membrane in the trans-Golgi network via distinct endosomal pathways. *J. Cell Biol.* 146, 345–359.

Mannan, A. U., Krawen, P., Sauter, S. M., Boehm, J., Chronowska, A., Paulus, W., et al. (2006). ZFYVE27 (SPG33), a novel spastin-binding protein, is mutated in hereditary spastic paraplegia. *Am. J. Hum. Genet.* 79, 351–357. doi: 10.1086/504927

Marin-Valencia, I., Gerondopoulos, A., Zaki, M. S., Ben-Omran, T., Almureikhi, M., Demir, E., et al. (2017). Homozygous mutations in TBC1D23 lead to a non-degenerative form of pontocerebellar hypoplasia. *Am. J. Hum. Genet.* 101, 441–450. doi: 10.1016/j.ajhg.2017.07.015

McGough, I. J., Steinberg, F., Jia, D., Barbuti, P. A., McMillan, K. J., Heesom, K. J., et al. (2014). Retromer binding to FAM21 and the WASH complex is perturbed by the Parkinson disease-linked VPS35(D620N) mutation. *Curr. Biol.* 24, 1670–1676. doi: 10.1016/j.cub.2014.06.024

McKenzie, J. E., Raisley, B., Zhou, X., Naslavsky, N., Taguchi, T., Caplan, S., et al. (2012). Retromer guides STxB and CD8-M6PR from early to recycling endosomes, EHD1 guides STxB from recycling endosome to Golgi. *Traffic* 13, 1140–1159. doi: 10.1111/j.1600-0854.2012.01374.x

McMillan, K. J., Korswagen, H. C., and Cullen, P. J. (2017). The emerging role of retromer in neuroprotection. *Curr. Opin. Cell Biol.* 47, 72–82. doi: 10.1016/j.ceb.2017.02.004

McNally, K. E., Faulkner, R., Steinberg, F., Gallon, M., Ghai, R., Pim, D., et al. (2017). Retriever is a multiprotein complex for retromer-independent endosomal cargo recycling. *Nat. Cell Biol.* 19, 1214–1225. doi: 10.1038/ncb3610

Meyer, C., Zizioli, D., Lausmann, S., Eskelinen, E. L., Hamann, J., Saftig, P., et al. (2000). mu1A-adaptin-deficient mice: lethality, loss of AP-1 binding and rerouting of mannose 6-phosphate receptors. *EMBO J.* 19, 2193–2203. doi: 10.1093/emboj/19.10.2193

Miller, P. M., Folkmann, A. W., Maia, A. R., Efimova, N., Efimov, A., and Kaverina, I. (2009). Golgi-derived CLASP-dependent microtubules control Golgi organization and polarized trafficking in motile cells. *Nat. Cell Biol.* 11, 1069–1080. doi: 10.1038/ncb1920

Miura, E., Hasegawa, T., Konno, M., Suzuki, M., Sugeno, N., Fujikake, N., et al. (2014). VPS35 dysfunction impairs lysosomal degradation of alpha-synuclein

and exacerbates neurotoxicity in a *Drosophila* model of Parkinson's disease. *Neurobiol. Dis.* 71, 1–13. doi: 10.1016/j.nbd.2014.07.014

Monfregola, J., Napolitano, G., D'Urso, M., Lappalainen, P., and Ursini, M. V. (2010). Functional characterization of Wiskott-Aldrich syndrome protein and scar homolog (WASH), a bi-modular nucleation-promoting factor able to interact with biogenesis of lysosome-related organelle subunit 2 (BLOS2) and gamma-tubulin. *J. Biol. Chem.* 285, 16951–16957. doi: 10.1074/jbc.M109.078501

Mukhopadhyay, A., Pan, X., Lambright, D. G., and Tissenbaum, H. A. (2007). An endocytic pathway as a target of tubby for regulation of fat storage. *EMBO Rep.* 8, 931–938. doi: 10.1038/sj.embor.7401055

Mukhopadhyay, S., and Linstedt, A. D. (2012). Manganese blocks intracellular trafficking of Shiga toxin and protects against Shiga toxicosis. *Science* 335, 332–335. doi: 10.1126/science.1215930

Munro, S. (2011). The golgin coiled-coil proteins of the Golgi apparatus. *Cold Spring Harb. Perspect. Biol.* 3:a005256. doi: 10.1101/cshperspect.a005256

Namavar, Y., Barth, P. G., Poll-The, B. T., and Baas, F. (2011). Classification, diagnosis and potential mechanisms in pontocerebellar hypoplasia. *Orphanet. J. Rare Dis.* 6:50. doi: 10.1186/1750-1172-6-50

Navarro Negredo, P., Edgar, J. R., Manna, P. T., Antrobus, R., and Robinson, M. S. (2018). The WDR11 complex facilitates the tethering of AP-1-derived vesicles. *Nat. Commun.* 9:596. doi: 10.1038/s41467-018-02919-4

Nielsen, M. S., Madsen, P., Christensen, E. I., Nykjaer, A., Gliemann, J., Kasper, D., et al. (2001). The sortilin cytoplasmic tail conveys Golgi-endosome transport and binds the VHS domain of the GGA2 sorting protein. *EMBO J.* 20, 2180–2190. doi: 10.1093/emboj/20.9.2180

Nothwehr, S. F., Ha, S. A., and Bruinsma, P. (2000). Sorting of yeast membrane proteins into an endosome-to-Golgi pathway involves direct interaction of their cytosolic domains with Vps35p. *J. Cell Biol.* 151, 297–310. doi: 10.1083/jcb.151.2.297

Pan, X., Eathiraj, S., Munson, M., and Lambright, D. G. (2006). TBC-domain GAPs for Rab GTPases accelerate GTP hydrolysis by a dual-finger mechanism. *Nature* 442, 303–306. doi: 10.1038/nature04847

Park, S. Y., and Guo, X. (2014). Adaptor protein complexes and intracellular transport. *Biosci. Rep.* 34:e00123. doi: 10.1042/BSR20140069

Paul, B., Kim, H. S., Kerr, M. C., Huston, W. M., Teasdale, R. D., and Collins, B. M. (2017). Structural basis for the hijacking of endosomal sorting nexin proteins by *Chlamydia trachomatis*. *eLife* 6:e22311. doi: 10.7554/eLife.22311

Perez-Victoria, F. J., Mardones, G. A., and Bonifacino, J. S. (2008). Requirement of the human GARP complex for mannose 6-phosphate-receptor-dependent sorting of cathepsin D to lysosomes. *Mol. Biol. Cell* 19, 2350–2362. doi: 10.1091/mbc.E07-11-1189

Phillips-Krawczak, C. A., Singla, A., Starokadomskyy, P., Deng, Z., Osborne, D. G., Li, H., et al. (2015). COMMD1 is linked to the WASH complex and regulates endosomal trafficking of the copper transporter ATP7A. *Mol. Biol. Cell* 26, 91–103. doi: 10.1091/mbc.E14-06-1073

Piotrowski, J. T., Gomez, T. S., Schoon, R. A., Mangalam, A. K., and Billadeau, D. D. (2013). WASH knockout T cells demonstrate defective receptor trafficking, proliferation, and effector function. *Mol. Cell. Biol.* 33, 958–973. doi: 10.1128/MCB.01288-12

Puthenveedu, M. A., Lauffer, B., Temkin, P., Vistein, R., Carlton, P., Thorn, K., et al. (2010). Sequence-dependent sorting of recycling proteins by actin-stabilized endosomal microdomains. *Cell* 143, 761–773. doi: 10.1016/j.cell.2010.10.003

Raiborg, C., Wenzel, E. M., and Stenmark, H. (2015). ER-endosome contact sites: molecular compositions and functions. *EMBO J.* 34, 1848–1858. doi: 10.15252/embj.201591481

Rapoport, I., Chen, Y. C., Cupers, P., Shoelson, S. E., and Kirchhausen, T. (1998). Dileucine-based sorting signals bind to the beta chain of AP-1 at a site distinct and regulated differently from the tyrosine-based motif-binding site. *EMBO J.* 17, 2148–2155. doi: 10.1093/emboj/17.8.2148

Robinson, M. S., Sahlender, D. A., and Foster, S. D. (2010). Rapid inactivation of proteins by rapamycin-induced rerouting to mitochondria. *Dev. Cell* 18, 324–331. doi: 10.1016/j.devcel.2009.12.015

Roll-Mecak, A., and Vale, R. D. (2008). Structural basis of microtubule severing by the hereditary spastic paraplegia protein spastin. *Nature* 451, 363–367. doi: 10.1038/nature06482

Ropers, F., Derivery, E., Hu, H., Garshasbi, M., Karbasiyan, M., Herold, M., et al. (2011). Identification of a novel candidate gene for non-syndromic autosomal recessive intellectual disability: the WASH complex member SWIP. *Hum. Mol. Genet.* 20, 2585–2590. doi: 10.1093/hmg/ddr158

Rowland, A. A., Chitwood, P. J., Phillips, M. J., and Voeltz, G. K. (2014). ER contact sites define the position and timing of endosome fission. *Cell* 159, 1027–1041. doi: 10.1016/j.cell.2014.10.023

Rudnik-Schoneborn, S., Barth, P. G., and Zerres, K. (2014). Pontocerebellar hypoplasia. *Am. J. Med. Genet. C Semin. Med. Genet.* 166C, 173–183. doi: 10.1002/ajmg.c.31403

Ryder, P. V., Vistein, R., Gokhale, A., Seaman, M. N., Puthenveedu, M. A., and Faundez, V. (2013). The WASH complex, an endosomal Arp2/3 activator, interacts with the Hermansky-Pudlak syndrome complex BLOC-1 and its cargo phosphatidylinositol-4-kinase type IIalpha. *Mol. Biol. Cell* 24, 2269–2284. doi: 10.1091/mbc.E13-02-0088

Saimani, U., and Kim, K. (2017). Traffic from the endosome towards trans-Golgi network. *Eur. J. Cell Biol.* 96, 198–205. doi: 10.1016/j.ejcb.2017.02.005

Saint-Pol, A., Yélamos, B., Amessou, M., Mills, I. G., Dugast, M., Tenza, D., et al. (2004). Clathrin adaptor epsinR is required for retrograde sorting on early endosomal membranes. *Dev. Cell* 6, 525–538. doi: 10.1016/s1534-5807(04)00100-5

Sandvig, K., and van Deurs, B. (2002). Transport of protein toxins into cells: pathways used by ricin, cholera toxin and Shiga toxin. *FEBS Lett.* 529, 49–53. doi: 10.1016/s0014-5793(02)03182-4

Schweizer, A., Stahl, P. D., and Rohrer, J. (2000). A di-aromatic motif in the cytosolic tail of the mannose receptor mediates endosomal sorting. *J. Biol. Chem.* 275, 29694–29700. doi: 10.1074/jbc.m000571200

Seaman, M. N. (2004). Cargo-selective endosomal sorting for retrieval to the Golgi requires retromer. *J. Cell Biol.* 165, 111–122. doi: 10.1083/jcb.200312034

Seaman, M. N. (2007). Identification of a novel conserved sorting motif required for retromer-mediated endosome-to-TGN retrieval. *J. Cell Sci.* 120(Pt 14), 2378–2389. doi: 10.1242/jcs.009654

Seaman, M. N. (2012). The retromer complex - endosomal protein recycling and beyond. *J. Cell Sci.* 125(Pt 20), 4693–4702. doi: 10.1242/jcs.103440

Seaman, M. N., Gautreau, A., and Billadeau, D. D. (2013). Retromer-mediated endosomal protein sorting: all WASHed up! *Trends Cell Biol.* 23, 522–528. doi: 10.1016/j.tcb.2013.04.010

Seaman, M. N., Harbour, M. E., Tattersall, D., Read, E., and Bright, N. (2009). Membrane recruitment of the cargo-selective retromer subcomplex is catalysed by the small GTPase Rab7 and inhibited by the Rab-GAP TBC1D5. *J. Cell Sci.* 122(Pt 14), 2371–2382. doi: 10.1242/jcs.048686

Seaman, M. N., McCaffery, J. M., and Emr, S. D. (1998). A membrane coat complex essential for endosome-to-Golgi retrograde transport in yeast. *J. Cell Biol.* 142, 665–681. doi: 10.1083/jcb.142.3.665

Seaman, M. N. J. (2018). Retromer and the cation-independent mannose 6-phosphate receptor-Time for a trial separation? *Traffic* 19, 150–152. doi: 10.1111/tra.12542

Shi, M., Chen, B., Mahajan, D., Boh, B. K., Zhou, Y., Dutta, B., et al. (2018). Amino acids stimulate the endosome-to-Golgi trafficking through Ragulator and small GTPase Arl5. *Nat. Commun.* 9:4987. doi: 10.1038/s41467-018-07444-y

Shibata, Y., Voss, C., Rist, J. M., Hu, J., Rapoport, T. A., Prinz, W. A., et al. (2008). The reticulon and DP1/Yop1p proteins form immobile oligomers in the tubular endoplasmic reticulum. *J. Biol. Chem.* 283, 18892–18904. doi: 10.1074/jbc.M800986200

Shin, J. J. H., Gillingham, A. K., Begum, F., Chadwick, J., and Munro, S. (2017). TBC1D23 is a bridging factor for endosomal vesicle capture by golgins at the trans-Golgi. *Nat. Cell Biol.* 19, 1424–1432. doi: 10.1038/ncb3627

Simonetti, B., Danson, C. M., Heesom, K. J., and Cullen, P. J. (2017). Sequence-dependent cargo recognition by SNX-BARs mediates retromer-independent transport of CI-MPR. *J. Cell Biol.* 216, 3695–3712. doi: 10.1083/jcb.201703015

Simonetti, B., Paul, B., Chaudhari, K., Weeratunga, S., Steinberg, F., Gorla, M., et al. (2019). Molecular identification of a BAR domain-containing coat complex for endosomal recycling of transmembrane proteins. *Nat. Cell Biol.* 21, 1219–1233. doi: 10.1038/s41556-019-0393-3

Singla, A., Fedoseienko, A., Giridharan, S. S. P., Overlee, B. L., Lopez, A., Jia, D., et al. (2019). Endosomal PI(3)P regulation by the COMMD/CCDC22/CCDC93 (CCC) complex controls membrane protein recycling. *Nat. Commun.* 10:4271. doi: 10.1038/s41467-019-12221-6

Sleat, D. E., Wiseman, J. A., El-Banna, M., Price, S. M., Verot, L., Shen, M. M., et al. (2004). Genetic evidence for nonredundant functional cooperativity between

NPC1 and NPC2 in lipid transport. *Proc. Natl. Acad. Sci. U.S.A.* 101, 5886–5891. doi: 10.1073/pnas.0308456101

Steinberg, F., Gallon, M., Winfield, M., Thomas, E. C., Bell, A. J., Heesom, K. J., et al. (2013). A global analysis of SNX27-retromer assembly and cargo specificity reveals a function in glucose and metal ion transport. *Nat. Cell Biol.* 15, 461–471. doi: 10.1038/ncb2721

Sun, Q., Yong, X., Sun, X., Yang, F., Dai, Z., Gong, Y., et al. (2017). Structural and functional insights into sorting nexin 5/6 interaction with bacterial effector IncE. *Signal Transduct. Target. Ther.* 2:17030. doi: 10.1038/sigtrans.2017.30

Suzuki, S. W., Chuang, Y. S., Li, M., Seaman, M. N. J., and Emr, S. D. (2019). A bipartite sorting signal ensures specificity of retromer complex in membrane protein recycling. *J. Cell Biol.* 218, 2876–2886. doi: 10.1083/jcb.201901019

Takeda, S., Minakata, S., Koike, R., Kawahata, I., Narita, A., Kitazawa, M., et al. (2010). Two distinct mechanisms for actin capping protein regulation–steric and allosteric inhibition. *PLoS Biol.* 8:e1000416. doi: 10.1371/journal.pbio.1000416

Teasdale, R. D., and Collins, B. M. (2012). Insights into the PX (phox-homology) domain and SNX (sorting nexin) protein families: structures, functions and roles in disease. *Biochem. J.* 441, 39–59. doi: 10.1042/BJ20111226

Temkin, P., Lauffer, B., Jager, S., Cimermancic, P., Krogan, N. J., and von Zastrow, M. (2011). SNX27 mediates retromer tubule entry and endosome-to-plasma membrane trafficking of signalling receptors. *Nat. Cell Biol.* 13, 715–721. doi: 10.1038/ncb2252

Ungar, D., Oka, T., Krieger, M., and Hughson, F. M. (2006). Retrograde transport on the COG railway. *Trends Cell Biol.* 16, 113–120. doi: 10.1016/j.tcb.2005.12.004

Valdmanis, P. N., Meijer, I. A., Reynolds, A., Lei, A., MacLeod, P., Schlesinger, D., et al. (2007). Mutations in the KIAA0196 gene at the SPG8 locus cause hereditary spastic paraplegia. *Am. J. Hum. Genet.* 80, 152–161. doi: 10.1086/510782

Vardarajan, B. N., Bruesegem, S. Y., Harbour, M. E., Inzelberg, R., Friedland, R., St George-Hyslop, P., et al. (2012). Identification of Alzheimer disease-associated variants in genes that regulate retromer function. *Neurobiol. Aging* 33, 2231.e15–2231.e30. doi: 10.1016/j.neurobiolaging.2012.04.020

Varlamov, O., and Fricker, L. D. (1998). Intracellular trafficking of metallocarboxypeptidase D in AtT-20 cells: localization to the trans-Golgi network and recycling from the cell surface. *J. Cell Sci.* 111(Pt 7), 877–885.

Verboon, J. M., Decker, J. R., Nakamura, M., and Parkhurst, S. M. (2018). Wash exhibits context-dependent phenotypes and, along with the WASH regulatory complex, regulates *Drosophila* oogenesis. *J. Cell Sci.* 131:jcs211573. doi: 10.1242/jcs.211573

Vilarino-Guell, C., Wider, C., Ross, O. A., Dachsel, J. C., Kachergus, J. M., Lincoln, S. J., et al. (2011). VPS35 mutations in Parkinson disease. *Am. J. Hum. Genet.* 89, 162–167. doi: 10.1016/j.ajhg.2011.06.001

Wan, L., Molloy, S. S., Thomas, L., Liu, G., Xiang, Y., Rybak, S. L., et al. (1998). PACS-1 defines a novel gene family of cytosolic sorting proteins required for trans-Golgi network localization. *Cell* 94, 205–216. doi: 10.1016/s0092-8674(00)81420-8

Wang, J., Fedoseienko, A., Chen, B., Burstein, E., Jia, D., and Billadeau, D. D. (2018). Endosomal receptor trafficking: retromer and beyond. *Traffic* 19, 578–590. doi: 10.1111/tra.12574

Wassmer, T., Attar, N., Bujny, M. V., Oakley, J., Traer, C. J., and Cullen, P. J. (2007). A loss-of-function screen reveals SNX5 and SNX6 as potential components of the mammalian retromer. *J. Cell Sci.* 120(Pt 1), 45–54. doi: 10.1242/jcs.03302

Whyte, J. R., and Munro, S. (2002). Vesicle tethering complexes in membrane traffic. *J. Cell Sci.* 115(Pt 13), 2627–2637.

Willnow, T. E., and Andersen, O. M. (2013). Sorting receptor SORLA–a trafficking path to avoid Alzheimer disease. *J. Cell Sci.* 126(Pt 13), 2751–2760. doi: 10.1242/jcs.125393

Witkos, T. M., and Lowe, M. (2015). The Golgin family of coiled-coil tethering proteins. *Front. Cell. Dev. Biol.* 3:86. doi: 10.3389/fcell.2015.00086

Wong, M., and Munro, S. (2014). Membrane trafficking. The specificity of vesicle traffic to the Golgi is encoded in the golgin coiled-coil proteins. *Science* 346:1256898. doi: 10.1126/science.1256898

Wu, H., Carvalho, P., and Voeltz, G. K. (2018). Here, there, and everywhere: the importance of ER membrane contact sites. *Science* 361:eaan5835. doi: 10.1126/science.aan5835

Xia, P., Wang, S., Du, Y., Zhao, Z., Shi, L., Sun, L., et al. (2013). WASH inhibits autophagy through suppression of Beclin 1 ubiquitination. *EMBO J.* 32, 2685–2696. doi: 10.1038/emboj.2013.189

Yu, I. M., and Hughson, F. M. (2010). Tethering factors as organizers of intracellular vesicular traffic. *Annu. Rev. Cell Dev. Biol.* 26, 137–156. doi: 10.1146/annurev.cellbio.042308.113327

Zavodszky, E., Seaman, M. N., Moreau, K., Jimenez-Sanchez, M., Breusegem, S. Y., Harbour, M. E., et al. (2014). Mutation in VPS35 associated with Parkinson's disease impairs WASH complex association and inhibits autophagy. *Nat. Commun.* 5:3828. doi: 10.1038/ncomms4828

Zech, T., Calaminus, S. D., Caswell, P., Spence, H. J., Carnell, M., Insall, R. H., et al. (2011). The Arp2/3 activator WASH regulates alpha5beta1-integrin-mediated invasive migration. *J. Cell Sci.* 124(Pt 22), 3753–3759. doi: 10.1242/jcs.080986

Zeevaert, R., Foulquier, F., Jaeken, J., and Matthijs, G. (2008). Deficiencies in subunits of the conserved oligomeric Golgi (COG) complex define a novel group of congenital disorders of glycosylation. *Mol. Genet. Metab.* 93, 15–21. doi: 10.1016/j.ymgme.2007.08.118

Zhang, J., Reiling, C., Reinecke, J. B., Prislan, I., Marky, L. A., Sorgen, P. L., et al. (2012). Rabankyrin-5 interacts with EHD1 and Vps26 to regulate endocytic trafficking and retromer function. *Traffic* 13, 745–757. doi: 10.1111/j.1600-0854.2012.01334.x

Zhang, P., Wu, Y., Belenkaya, T. Y., and Lin, X. (2011). SNX3 controls Wingless/Wnt secretion through regulating retromer-dependent recycling of Wntless. *Cell Res.* 21, 1677–1690. doi: 10.1038/cr.2011.167

Zimprich, A., Benet-Pages, A., Struhal, W., Graf, E., Eck, S. H., Offman, M. N. A., et al. (2011). A mutation in VPS35, encoding a subunit of the retromer complex, causes late-onset Parkinson disease. *Am. J. Hum. Genet.* 89, 168–175. doi: 10.1016/j.ajhg.2011.06.008

Zolov, S. N., and Lupashin, V. V. (2005). Cog3p depletion blocks vesicle-mediated Golgi retrograde trafficking in HeLa cells. *J. Cell Biol.* 168, 747–759. doi: 10.1083/jcb.200412003

Conflict of Interest: The authors declare that the research was conducted in the absence of any commercial or financial relationships that could be construed as a potential conflict of interest.

frontiers in Cell and Developmental Biology

REVIEW
published: 27 March 2020
doi: 10.3389/fcell.2020.00195

Current and Emerging Approaches for Studying Inter-Organelle Membrane Contact Sites

*Xue Huang, Chen Jiang, Lihua Yu and Aimin Yang**

School of Life Sciences, Chongqing University, Chongqing, China

Inter-organelle membrane contact sites (MCSs) are classically defined as areas of close proximity between heterologous membranes and established by specific proteins (termed tethers). The interest on MCSs has rapidly increased in the last years, since MCSs play a crucial role in the transfer of cellular components between different organelles and have been involved in important cellular functions such as apoptosis, organelle division and biogenesis, and cell growth. Recently, an unprecedented depth and breadth in insights into the details of MCSs have been uncovered. On one hand, extensive MCSs (organelles interactome) are revealed by comprehensive analysis of organelle network with high temporal-spatial resolution at the system level. On the other hand, more and more tethers involving in MCSs are identified and further works are focusing on addressing the role of these tethers in regulating the function of MCSs at the molecular level. These enormous progresses largely depend on the powerful approaches, including several different types of microscopies and various biochemical techniques. These approaches have greatly accelerated recent advances in MCSs at the system and molecular level. In this review, we summarize the current and emerging approaches for studying MCSs, such as various microscopies, proximity-driven fluorescent signal generation and proximity-dependent biotinylation. In addition, we highlight the advantages and disadvantages of the techniques to provide a general guidance for the study of MCSs.

Keywords: membrane contact sites, electron microscopy, super-resolution microscopy, FRET, proximity ligation assay, bimolecular fluorescence complementation, BioID, APEX

OPEN ACCESS

Edited by:
Du Feng,
Guangzhou Medical University, China

Reviewed by:
Thomas Becker,
University of Freiburg, Germany
Carmen Faso,
University of Bern, Switzerland

***Correspondence:**
Aimin Yang
aimin.yang@cqu.edu.cn

Specialty section:
This article was submitted to Molecular Medicine, a section of the journal Frontiers in Cell and Developmental Biology

Received: *20 January 2020*
Accepted: *09 March 2020*
Published: *27 March 2020*

Citation:
Huang X, Jiang C, Yu L and Yang A (2020) Current and Emerging Approaches for Studying Inter-Organelle Membrane Contact Sites. Front. Cell Dev. Biol. 8:195. doi: 10.3389/fcell.2020.00195

INTRODUCTION

A defining characteristic of eukaryotic cells is the presence of membrane-bound organelles surrounded by plasma membrane (PM). Inter-organelle membrane contact sites (MCSs) are classically defined as areas of close proximity between heterologous membranes. At MCSs, specific proteins (termed tethers) hold two organelles together and mediate the transfer of cytoplasmic materials between two organelles (**Table 1**; Helle et al., 2013; Eisenberg-Bord et al., 2016). The interest on MCSs has rapidly increased in the last few years, since MCSs have been involved in important cellular functions such as apoptosis, cell growth, organelle division and biogenesis

(Cohen et al., 2018; Scorrano et al., 2019). Emerging evidence suggests that MCSs play a crucial role in the transfer of cellular components between different organelles, which controls exchange of cellular signaling and regulates organelle membrane dynamics (Friedman et al., 2011; Prinz, 2014; Lahiri et al., 2015; Stefan et al., 2017). For instance, ER-mitochondria MCS is responsible for Ca^{2+} exchange and non-vesicular transfer of phospholipid between mitochondria and ER (Hayashi et al., 2009; Naon and Scorrano, 2014; Krols et al., 2016). The ER-related MCSs, including ER-mitochondria MCS and ER-PM MCS, contribute to autophagosome biogenesis (Hamasaki et al., 2013; Bockler and Westermann, 2014; Garofalo et al., 2016; Nascimbeni et al., 2017). The lysosome-related MCSs in eukaryotic cells act as a dynamic network for nutrient uptake, metabolic control, macromolecule degradation and signaling (Mc Donald and Krainc, 2017; Lawrence and Zoncu, 2019). Therefore, MCSs exist widely in cell and ensure signaling exchange and materials transfer between two different organelles (**Table 1**).

The dysfunction of MCSs has been implicated in neurodegenerative disorders and cancer (Prinz et al., 2020). To date, most investigations into the roles of MCSs dysfunction in disease have focused on ER-mitochondria MCSs (Paillusson et al., 2016). The mutation of the tether Mnd, VAPB or REEP defects ER-mitochondria MCS and Ca^{2+} signaling transfer, and finally leads to neurodegenerative disease (Vance et al., 1997; Nishimura et al., 2004; Schon and Area-Gomez, 2013; Stoica et al., 2014; Bernard-Marissal et al., 2015; Lim et al., 2015). In addition, the mutation of the tether BAP31 dysregulates ER-Golgi crosstalk and impacts Golgi apparatus, and thereby causing the X-link phenotype with deafness, dystonia and central hypomyelination (Cacciagli et al., 2013).

Electron microscopy (EM) provides the first evidence for the existence of sites of physical interaction between ER and mitochondria in the 1950s (Bernhard and Rouiller, 1956; Copeland and Dalton, 1959). Since then, however, the research on MCSs has been proceeded slowly due to lack of suitable study tools. From the early of 21st century, an unprecedented depth and breadth in insights into the details of MCSs have been uncovered gradually. On one hand, extensive MCSs (organelles interactome) are revealed by comprehensive analysis of organelle network with high temporal-spatial resolution at the system level (**Figure 1**). On the other hand, more and more tethers involving in MCSs are identified and further works are focusing on addressing the role of these tethers in regulating the function of MCSs at the molecular level (**Table 1**; Jansen et al., 2011; Elbaz-Alon et al., 2015; Jing et al., 2015; Kim et al., 2015; Besprozvannaya et al., 2018). These enormous progresses largely depend on the powerful approaches, including several different types of microscopies and various biochemical techniques (**Figure 1**). These approaches have greatly accelerated recent advances in MCSs at the molecular and system level (**Figure 2**). In this review, the current and emerging approaches for studying MCSs are summarized. In addition, the advantages and disadvantages of the approaches are highlighted to provide a general guidance for tool selection and optimization for the study of MCSs.

AN OVERVIEW OF THE APPROACHES FOR STUDYING MCSs

Visualization is a prerequisite for study of MCSs. The "membrane contact" was originated from an observation that topographical proximity between mitochondria and ER in cells of the pseudobranch gland of a teleost by EM (Bernhard and Rouiller, 1956; Copeland and Dalton, 1959). EM of cell specimen at the nanometer scale make observation of subcellular structures and MCSs possible. Recently, EM and its variants, such as focused ion beam-scanning EM (FIB-SEM) and electron tomography (ET), are widely employed to observe MCSs. High resolution of three-dimensional (3D) structure at ER-PM MCS in COS-7 cells was obtained by cryo-ET (Fernandez-Busnadiego et al., 2015). Meanwhile, various light microscopies based on fluorescence were developed in living cells. Confocal microscopy is used to visualize subcellular localization of fluorescent fusion membrane proteins and has been employed to reconstruct 3D imaging of ER-mitochondria juxtaposition as sites of Ca^{2+} transfer between both organelles in HeLa cells (Rizzuto et al., 1998). Lattice light-sheet microscopy (LLSM) was developed by using ultrathin light sheets from two-dimensional optical lattices to reveal organelle interactome at the systems-level in COS-7, HEK293 and MEF cells (Valm et al., 2017; D'Eletto et al., 2018). Super-resolution fluorescence microscopy (SRM) offers a unique window with extreme high temporal and spatial resolution for MCSs (Sydor et al., 2015; Sezgin, 2017; Jing et al., 2019). Recently, grazing incidence structured illumination microscopy (GI-SIM), one of SRM, was developed and applied to visualize ER-mitochondria MCS in COS-7 and U2OS cells (Guo Y. et al., 2018). In brief, various microscopies provide a large of direct evidence for visualization of MCSs and greatly facilitate the development of the field.

In combination of confocal microscopy, a variety of biochemical techniques, including proximity ligation assay (PLA) (Soderberg et al., 2006), fluorescence resonance energy transfer (FRET) (Csordas et al., 2010), bimolecular fluorescence complementation (BiFC) (Cabantous et al., 2005; Magliery et al., 2005) and dimerization-dependent fluorescent proteins (ddFP) (Alford et al., 2012a) were designed to observe and identify MCSs. These biochemical techniques are dependent on proximity-driven signal generation and amplification. Briefly, two fragments or proteins, fused with tethers or membrane proteins of different organelles, are each no signal or low signal on their own but are reconstituted to give strong signal when driven together by close membrane-membrane proximity. These techniques are widely employed to visualize MCSs and identify tethers involving in MCSs. In recent years, many studies focused on identification of new tethers. To achieve this purpose, two novel tools, BioID and APEX based on proximity-driven biotinylation were engineered and applied to identify new tethers and even systematically map MCSs in COS-7 and HEK293 cells (Hua et al., 2015; Cho et al., 2017).

Overall, these approaches have greatly accelerated research progress in MCSs (**Table 1** and **Figure 2**). It is expected that new approaches, such as SRM and proximity-driven biotinylation

TABLE 1 | Summary of membrane contact sites (MCSs).

Contact site	Date Of Discovery	Organism	Proposed function	Used Tools for MCSs	*Identified tethers*
ER-PM	1957 (Porter and Palade, 1957)	Mammalian	lipid transfer; activation of store-operated Ca^{2+} entry; autophagosome biogenesis	EM, ET, Confocal, FM, TIRFM	E-Syts (Schauder et al., 2014), GRAMD2a (Besprozvannaya et al., 2018), VAP-B-Nir2 (Kim et al., 2015), VAP-ORPs (Jansen et al., 2011), JPs (Takeshima et al., 2000; Landstrom et al., 2007), STIM1-Orail-hTRPC1 (Liou et al., 2007; Jardin et al., 2008)
		Yeast	membrane complex formation and localization	EM, FM, Confocal, FRET	Scs2-Scs22 (Manford et al., 2012), Tcb1/2/3 (Manford et al., 2012), Osh2/3 (Levine and Munro, 2001), Ist2 (Manford et al., 2012)
ER-Mitochondria	1959 (Copeland and Dalton, 1959)	Mammalian	Ca^{2+} exchange; lipid exchange; scission of mitochondria; autophagosome biogenesis	EM, FM, Confocal, PLA, FRET, SR-FACT	IP3R-GRP75-VDAC (Rizzuto et al., 1993; Szabadkai et al., 2006; D'Eletto et al., 2018), GRP75-TG2 (D'Eletto et al., 2018), BAP31-FIS1 (Iwasawa et al., 2011), Mfn2-Mfn2/Mfn1-Mfn2 (Naon et al., 2016), VAP-PTPIP51 (De Vos et al., 2012), Lam6 (Elbaz-Alon et al., 2015)
		Yeast(ERMES)	lipid exchange; phospholipid synthesis and cell growth; sterols transport	EM, FM, Confocal, SIM, TIRFM	ERMES complex (Kornmann et al., 2009; Kawano et al., 2018), Gem1 (Kornmann et al., 2011), Mmmr1 (Swayne et al., 2011), TOM5 (Lahiri et al., 2014), Lam6 (Elbaz-Alon et al., 2015), Ltc1-TOM70/71 (Murley et al., 2015), Num1 (Lackner et al., 2013)
ER-Endosome	2009 (Rocha et al., 2009)	Mammalian	sterol sensing and endosome positioning; cholesterol transfer; endosomal tubule fission regulation	EM, FM, Confocal, 3D-SIM, PLA, FRET	VAP-A-STARD3/STARD3NL (Alpy et al., 2013), VAP-A-ORP1L (Rocha et al., 2009), ORP5-NPC1 (Du et al., 2011), Protrudin (Raiborg et al., 2015), PTP1B-EGFR (Eden et al., 2010), Rab5 (Hsu et al., 2018), Spastin-IST1 (Allison et al., 2017), VAP-OSBP-PI4P (Dong et al., 2016), TMCC1-Coronin1C (Hoyer et al., 2018), PTP1B-G-CSFR (Palande et al., 2011)
ER-Golgi	1988 (Schweizer et al., 1988)	Mammalian	lipid exchange	EM, FM, Cryo-EM, Confocal, FRET	VAP-PI4P-OSBP (Mesmin et al., 2013; Jamecna et al., 2019), VAP-CERT (Hanada et al., 2003), VAP-FAPP2 (D'Angelo et al., 2007), VAP-Nir2 (Litvak et al., 2005)
		Yeast	ceramides transfer	EM, FM, APEX2	Nvj2 (Liu et al., 2017)
ER-LD	2006 (Robenek et al., 2006)	Mammalian	LD growth regulation	Confocal, SIM, APEX	Rab18-NRZ (NAG-RINT1-ZW10) (Xu et al., 2018)
		C. elegans	LD expansion	EM, Confocal	FATP1-DGAT2 (Xu et al., 2012)
		Drosophila	LD growth regulation	EM, ET, Confocal, LLSM	Seipin (Wang et al., 2016)
ER-Peroxisome	1987 (Yamamoto and Fahimi, 1987)	Mammalian	peroxisome growth; lipid homeostasis	SIM	VAPs-ACBD4 (Costello et al., 2017), VAPs-ACBD5 (Hua et al., 2017)
		Yeast	peroxisome growth	Confocal	Pex3-Inp1-Pex3 (Knoblach et al., 2013), Pex30 (Joshi et al., 2018)
ER-Lysosome	2018 (Atakpa et al., 2018)	Mammalian	Ca^{2+} exchange	TIRFM, STORM, LLSM, FIB-SEM	unknown
ER-Autophagosome	2016 (Wijdeven et al., 2016)	Mammalian	lipid transfer	Cryo-EM, Confocal, FRET	LTP-ATG2, VAP-A-ORP1L (Wijdeven et al., 2016)
ER-Vacuole	2000 (Pan et al., 2000)	Yeast	selectively sterols transport	FM, BiFC	Ltc1-Vac8 (Murley et al., 2015; Kakimoto et al., 2018), Nvj3-Mdm1 (Henne et al., 2015)
ER-DB	2020 (Dong et al., 2020)	Mammalian	unknown	SR-FACT	unknown

(Continued)

TABLE 1 | Continued

Contact Site	Date Of Discovery	Organism	Proposed Function	Used Tools for MCSs	Identified Tethers
Mitochondria-Golgi	2007 (Ouasti et al., 2007)	Mammalian	apoptosis related	TEM, FM	Fas (CD95/Apo1) (Ouasti et al., 2007)
Mitochondria-Lysosome	2002 (Ponka et al., 2002)	Mammalian	unknown	EM, Confocal, SIM, FRET, SR-FACT	unknown
Mitochondria-Endosome	2002 (Ponka et al., 2002)	Mammalian	early endosomal-mitochondrial contacts and transferrin uptake regulation	EM, FM, SR-FACT	Rab5 (Hsu et al., 2018)
Mitochondria-Peroxisome	2007 (Schrader and Yoon, 2007)	Mammalian	unknown	LLSM, BiFC, Confocal, STEDM	unknown
Mitochondria-LD	2011 (Wang et al., 2011)	Mammalian	contact regulation	EM, SR-FACT	Perilipin-5 (Wang et al., 2011)
Mitochondria-Vacuole (vCLAMP)	2014 (Honscher et al., 2014)	Yeast	survival in starvation and stress	EM, BiFC	TOM40-Vps39, Mcp1-Vps13 (Gonzalez Montoro et al., 2018) (vCLAMP)
Mitochondria-DB	2020 (Dong et al., 2020)	Mammalian	mitochondrial fission	SR-FACT	unknown
Golgi-Autophagosome	2015 (Biazik et al., 2015)	Mammalian	autophagosome formation	EM, ET	unknown
Lysosome-Peroxisome	2015 (Chu et al., 2015)	Mammalian	cholesterol transfer	FM, LLSM	Syt7 (Chu et al., 2015; Valm et al., 2017)
Lysosome-Autophagosome	1992 (Lawrence and Brown, 1992)	Mammalian	autophagosome formation	EM, ET, FM	Rab7-HOPS related complex (Jiang et al., 2014)
		Yeast	autophagosome formation	EM, ET, FM	Ypt7-HOPS related complex (Kirisako et al., 1999)
Lysosome-Endosome	1999 (Ohashi et al., 1999)	Mammalian	proper lysosomal digestive functions	EM, FM	Vamp8-Syntaxin 7 (Mullock et al., 2000),
		Yeast	endosome fusion regulation	FM	Rab7-HOPS-Rab7 (Nordmann et al., 2010; Balderhaar and Ungermann, 2013)
Lysosome-LD	2014 (Dugail, 2014)	Mammalian	lipid homeostasis	EM, FM, LLSM	PLIN2-HSC70-LAMP2A (Olzmann and Carvalho, 2019)
Lysosome-Golgi	2018 (Hao et al., 2018)	Mammalian	amino acid supply response	FM, PLA	mTORC1-Rheb (Hao et al., 2018)
Peroxisome-LD	2006 (Binns et al., 2006)	Mammalian	fatty acid trafficking	FIB-SEM, Confocal, LLSM, BiFC	M1 Spastin-ABCD1-ESCRT-III (Prinz et al., 2020)
		Yeast	fatty acid trafficking	FIB-SEM, Confocal, LLSM, BiFC	M1 Spastin-ABCD1-ESCRT-III (Prinz et al., 2020)
Peroxisome-PM	2018 (Kakimoto et al., 2018)	Yeast	unknown	BiFC	unknown
Peroxisome-Vacuole	2018 (Kakimoto et al., 2018)	Yeast	unknown	BiFC	unknown
Nucleus-Vacuole	1976 (Severs et al., 1976)	Yeast	microautophagy related	BiFC	Nvj1p-Vac8p (Kvam and Goldfarb, 2006), Lam6-Vac8 (Elbaz-Alon et al., 2015)
Nucleus-DB	2020 (Dong et al., 2020)	Mammalian	nuclear membrane formation	SR-FACT	unknown
LD-PM	2018 (Kakimoto et al., 2018)	Yeast	unknown	BiFC	unknown
LD-Vacuole	2018 (Kakimoto et al., 2018)	Yeast	unknown	BiFC	unknown
Vacuole-PM	2018 (Kakimoto et al., 2018)	Yeast	unknown	BiFC	unknown

The table summarizes MCSs and related information in different organisms. PM, plasma membrane; LD, lipid droplet; DB, Dark-vacuole body; vCLAMP, vacuolar and mitochondrial patch; ERMES, ER-mitochondria encounter structure; EM, electron microscopy; TEM, transmission electron microscope; Cryo-EM, cryogenic electron microscopy; ET, electron tomography; FIB-SEM, focused ion beam-scanning EM; FM, fluorescence microscope; Confocal, confocal microscopy; SIM, structured illumination microscopy; 3D-SIM, three-dimensional structured illumination microscopy; TIRFM, total internal reflection fluorescence microscopy; SR-FACT, super-resolution fluorescence-assisted diffraction computational tomography; LLSM, lattice light-sheet microscopy; STORM, stochastic optical reconstruction microscopy; STEDM, stimulated emission depletion microscopy; PLA, proximity ligation assay; FRET, fluorescence resonance energy transfer; BiFC, bimolecular fluorescence complementation; APEX, engineered peroxidase; APEX2, engineered variant of soybean ascorbate peroxidase.

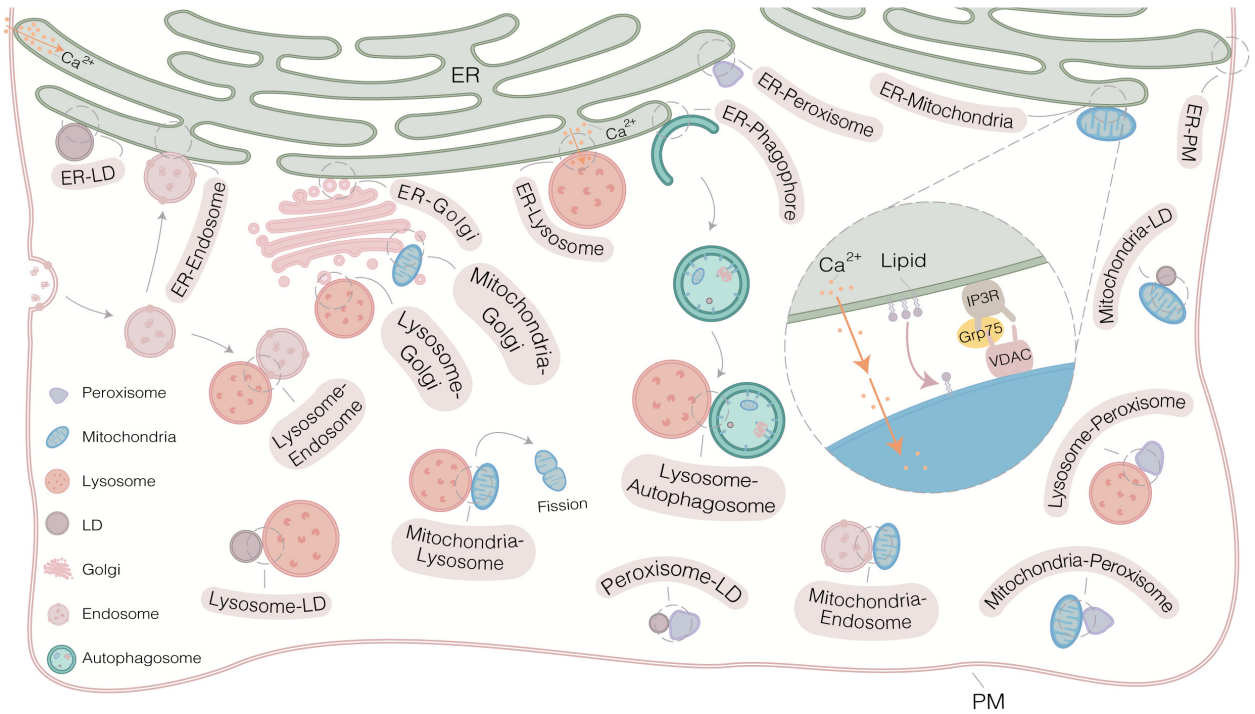

FIGURE 1 | Extensive membrane contact sites (MCSs) in mammalian cells. MCSs exist widely in cell and regulate exchanges signaling and regulates cellular functions. The common strategy for studying MCSs consists of various microscopies and biochemical approaches. Multiple canonical protein complexes have been reported to regulate MCSs, such as VDAC-IP3R-Grp 75 complex at ER-mitochondria MCS. Some MCSs, such as mitochondria-endosome MCS, Golgi-autophagosome MCS and lysosome-peroxisome MCS, are not shown due to limited space in this figure.

coupled with mass spectrometry (MS)-based proteomics, will facilitate the research of MCSs at the molecular and system level.

VISUALIZATION OF MCSs BY EM AND SRM

Electron microscopy provides the first evidence for ER-mitochondria MCS that improves the transfer of Ca^{2+} signal between both organelles in cells of the pseudobranch gland of a teleost (Copeland and Dalton, 1959; Rizzuto et al., 1998). Recently, EM and its variants, such as electron tomography (ET) and focused ion beam-scanning EM (FIB-SEM), are widely used to observe MCSs. High resolution structure of ER-mitochondria MCS was obtained by ET, an extension of traditional transmission EM (Csordas et al., 2006; de Brito and Scorrano, 2008). Two well-known structures, ER-mitochondria encounter structure (ERMES) and vacuolar and mitochondrial patch (vCLAMP) in yeast were directly observed by EM and ET (Kornmann et al., 2009; Honscher et al., 2014). The 3D ultrastructure of ER-PM MCS in COS-7 cells was visualized in close-to-native conditions by cryo-ET (Fernandez-Busnadiego et al., 2015; Fernandez-Busnadiego, 2016; Collado and Fernandez-Busnadiego, 2017). In FIB-SEM, a highly focused gallium ion beam ablates a thin layer of the sample after which the newly exposed surface is imaged with the scanning electron beam (Drobne, 2013; Fermie et al., 2018). FIB-SEM has recently been employed to systematically visualize ER MCSs with multiple other membranes including mitochondria and PM in neurons of mice (Wu et al., 2017). EM is regarded as the "gold standard" and exquisitely suited for investigation of MCSs, which provides fine architecture and spatial resolution of subcellular compartments. To some extent, EM has some drawbacks, such as fixation procedures, time-consuming and low through-put, restricting EM utility in living cells.

To enable visualization of MCSs in living cells, genetically encoded fluorescent proteins are tagged to resident proteins or tethers of different membranes so that MCSs become visible under multispectral fluorescence microscopy. Confocal microscopy is one of the most common methods to visualize subcellular localization of fluorescent membrane proteins. It has been employed to deconvolute and reconstruct 3D imaging of ER-mitochondria juxtaposition in living HeLa cells (Rizzuto et al., 1998) and of ERMES in yeast (Kornmann et al., 2009). To expand observation of dynamic multiple MCSs, lattice light-sheet microscopy (LLSM) was developed by using ultrathin light sheets from two-dimensional optical lattices (Chen et al., 2014). Multispectral imaging and computational analysis were introduced to visualize and quantify organelle interactome between six different organelles in COS-7 cells, such as ER, Golgi, lysosome, peroxisome, mitochondria and lipid droplet (LD) (Valm et al., 2017).

The dynamics and fine structure of MCSs require research tool with extreme high temporal and spatial resolution.

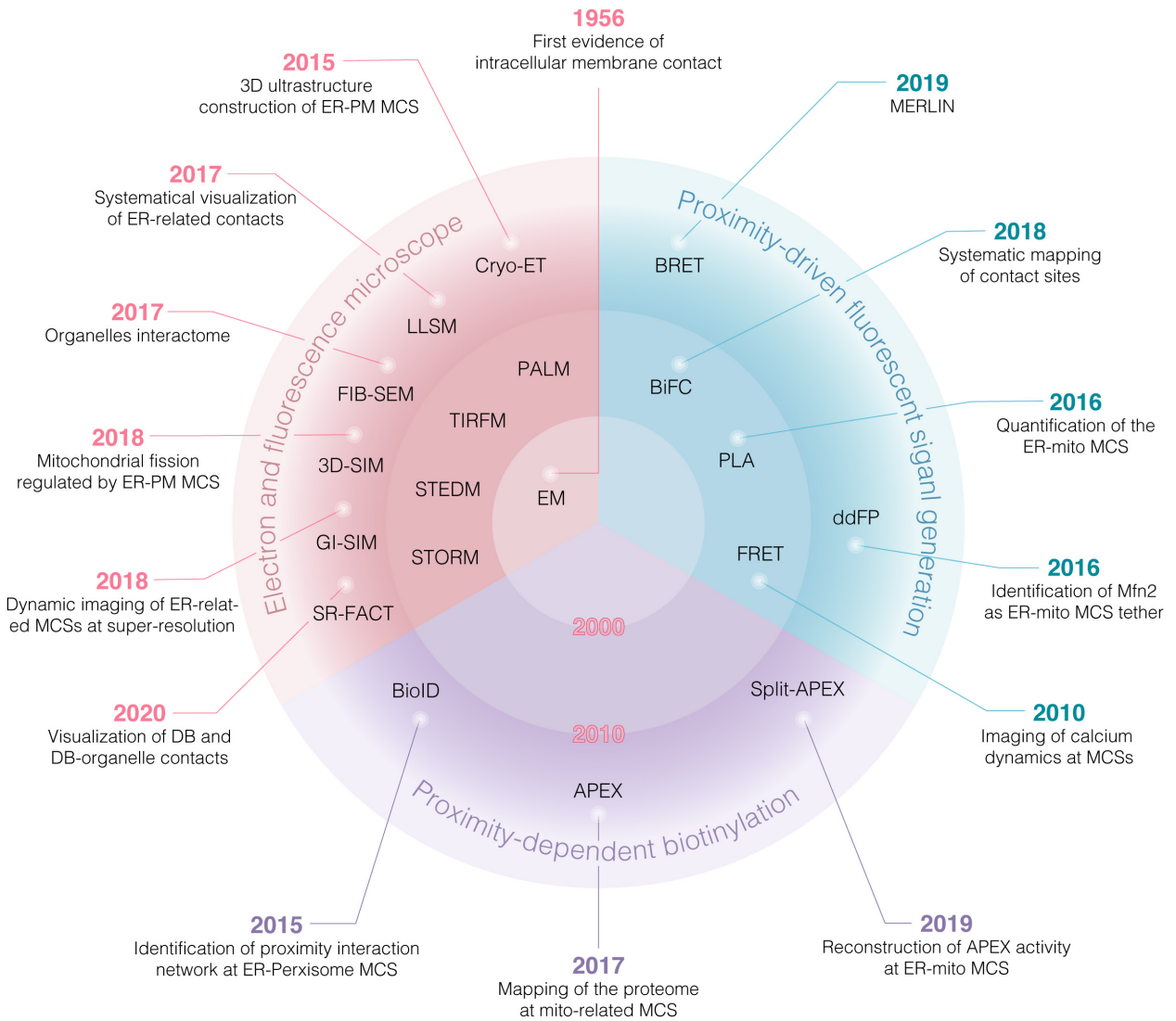

FIGURE 2 | Overview of various approaches for studying MCSs. Various approaches have greatly accelerated recent advances in MCSs at the system and molecular level. Before 2000, EM and confocal microscopy were most accessible tools. EM provided first evidence of intracellular membrane contact at nanoscale resolution, while confocal microscopy has been employed to reconstruct the 3D imaging of ER-mitochondria juxtaposition as sites of Ca^{2+} transfer between both organelles. Since 2010, super resolution microscopy (SRM) was increasingly used to visualize MCSs. Furthermore, proximity-driven fluorescent signal generation approaches, such as FRET, PLA, BiFC and ddFP were exploited to identify the potential MCSs. Notably, by combination with proteomic analysis, proximity-dependent biotinylation approaches mediated by BioID and APEX provide a promising strategy for global mapping MCSs and identification of tethers involving in MCSs, termed as "tether-omics." BRET, bioluminescence resonance energy transfer; BioID, proximity-dependent biotin identification; APEX, ascorbate peroxidase; MERLIN, mitochondria-ER length indicator nanosensor; FIB-SEM, focused ion beam-scanning EM; PALM, photoactivation localization microscopy; LLSM, lattice light-sheet microscopy; SR-FACT, super-resolution fluorescence-assisted diffraction computational tomography.

Super-resolution fluorescence microscopy (SRM) offers a unique window for the study of MCSs. Several SRMs, such as stimulated emission depletion microscopy (STEDM), photoactivation localization microscopy (PALM) and stochastic optical reconstruction microscopy (STORM), structured illumination microscopy (SIM), have been developed for imaging of nanoscale structural details and dynamics of MCSs, such as ER-PM MCS (Hsieh et al., 2017; Nascimbeni et al., 2017), ER-mitochondria MCS (Shim et al., 2012; Modi et al., 2019), ER-lysosome MCS (Shim et al., 2012), mitochondria-peroxisome MCS (Galiani et al., 2016). Among these SRMs, SIM is suitable for fast live-cell imaging and has been used to reveal numerous subcellular structures and dynamics (Li et al., 2015; Nixon-Abell et al., 2016; Zhanghao et al., 2019). Recently, ER-PM MCS in U2OS, Jurkat T and HEK293 cells was observed by SIM with total internal reflection fluorescence microscopy (TIRF-SIM) (Guo M. et al., 2018; Kang et al., 2019). The grazing incidence SIM (GI-SIM) was developed and applied to visualize ER-mitochondria, ER-late endosome and ER-lysosome MCSs in COS-7 and U2OS cells (Guo Y. et al., 2018). In addition, SIM based on Hessian matrixes

excels in extending the spatiotemporal resolution in live cells and is expected to apply for studying MCSs in COS-7 cells (Huang et al., 2018). More importantly, super-resolution fluorescence-assisted diffraction computational tomography (SR-FACT) was developed by combination of label-free three-dimensional optical diffraction tomography (ODT) with two-dimensional fluorescence Hessian structured illumination microscopy (Dong et al., 2020). The SR-FACT enable label-free visualization of various subcellular structures and complete division process of a COS-7 cell. By using SR-FACT, novel subcellular structures named dark-vacuole bodies (DB) were observed, and intensively contact with organelles such as mitochondria and nuclear membrane in COS-7 cells (Dong et al., 2020).

IDENTIFICATION OF MCSs BY PROXIMITY-DRIVEN FLUORESCENT SIGNAL GENERATION

Confocal microscopy is used to visualize subcellular localization of fluorescent membrane proteins, rather than suitable to study MCSs. On one hand, co-localization of resident proteins or tethers of different membranes observed by confocal microscopy, however, doesn't mean the existence of MCS. On the other hand, because of continuing organelles movement, dynamic MCSs are difficult to detect by confocal microscopy alone with low resolution. The proximity-driven fluorescent signal generation enable identification of MCSs with more reliability and easy operation. Briefly, two fragments or proteins fused with organelle markers or tethers, reside on outer membrane of different organelles, are each no signal or low signal on their own but are reconstituted to give strong fluorescent signal when driven together by membrane proximity. These approaches are widely used to visualize MCSs and identify important tethers involving in MCSs (**Figure 3** and **Table 1**).

PLA

Proximity ligation assay (PLA) is a unique method for protein detection. In PLA, single-stranded oligonucleotides are conjugated to affinity binders or antibody of proteins, followed by amplification of the signal by rolling-circle amplification (RCA) and detection of complementary fluorophore labeled oligonucleotides (Fredriksson et al., 2002; Schallmeiner et al., 2007; Soderberg et al., 2008). PLA has success to observe interaction of individual endogenous protein complexes *in situ* (Soderberg et al., 2006; Fredriksson et al., 2007), which validates protein-protein interactions in multiplexed proteins.

Recently, PLA has been employed to address MCSs. Dual binding by a pair of proximity probes (antibodies with attached DNA strands) to two membrane resident proteins or tethers serves to template the hybridization of circularization oligonucleotides, which is then joined by ligation into a circular DNA molecule (**Figure 3A**). ER-mitochondria MCS was visualized and quantified by using the close proximity between voltage-dependent anion channel 1 (VDAC1, localizes in outer mitochondrial membrane) and inositol 1,4,5-triphosphate receptor (IP3R, localizes in ER membrane) at the mitochondria-associated membranes (MAMs) interface in human HuH7 cells (Tubbs and Rieusset, 2016). The VDAC1-IP3R PLA system was used to reveal the role of ER-mitochondria tethering complex VAPB-PTPIP51 in regulating autophagy in HeLa and HEK293 cells (Gomez-Suaga et al., 2017). In addition, by using VDAC1-IP3R PLA system, Stoica et al. found that ALS/FTD-associated FUS activates GSK-3β to disrupt the VAPB-PTPIP51 interaction and ER-mitochondria associations in NSC-34 mouse motor neuron cells (Stoica et al., 2016), and Thomas et al. revealed that phenformin blocks MAMs that support autophagy in HEK293 cells (Thomas et al., 2018). ER-lysosome MCS was detected by PLA, and further experiment confirmed that the clusters of IP3R populate ER-lysosome MCS and facilitate local delivery of Ca^{2+} from the ER to lysosome (Atakpa et al., 2018).

FRET

Fluorescence resonance energy transfer is one of most accessible technologies that allow for detecting protein-protein interaction at super resolution. FRET was primally from Förster's theory, in which dipole-dipole interaction made the photon energy transfer from excited donor to acceptor between an energy donor-acceptor fluorescent pair when the distance between donor and acceptor was 1 to 10 nm. FRET is a non-destructive method of spectroscopy and therefore applied to observe the signal of MCSs in living cells (Zimmer, 2002; Pietraszewska-Bogiel and Gadella, 2011; Marx, 2017; **Figure 3B**). Fluorescent proteins were derived from 1980s when green fluorescent protein (GFP) of *Aequorea victoria* was exploited as a GFP-chimera targeted to specific organelles membrane and further optimized to the mutants, such as RFP and BFP (Rizzuto et al., 1996; Zimmer, 2002). Normally, fluorescent proteins fused with membrane proteins or tethers are used as donor/acceptor probes. The combination between fluorescent proteins and FRET brings a great progress for the great integration with targeted protein. FRET has been exploited to be a useful tool by combination with other technologies. Combination between fluorescence lifetime imaging (FLIM) and FRET offers direct evidence of temporal membrane proximity at high resolution (Bastiaens and Squire, 1999; Elangovan et al., 2002; Sekar and Periasamy, 2003). Photoswitching FRET (psFRET), a revised version of photobleaching FRET (pb FRET) of which detection of fluorescence signal required only imaging of donor before and after photobleaching of acceptor (Wouters et al., 1998). Improvement of psFRET make photobleach to be switched "off" and be re-detectable (Rainey and Patterson, 2019). Recent work systematically assessed the FRET from principle to screening of donor-acceptor pair (Algar et al., 2019).

Fluorescence resonance energy transfer is an indispensable experimental tool for the study of the MCSs (Jing et al., 2015; Subedi et al., 2018). Tandem GFP pairs allowed for detecting the alteration of intracellular Ca^{2+} level at mitochondria-ER MCS in HeLa and HEK293 cells, in which tandem expression of BFP-CBD (26-residue containing calmodulin-binding domain)-EGFP was sensitive to change of Ca^{2+} flux that causes a structural alteration of CBD and a destroyed FRET pair (Miyawaki et al., 1997; Romoser et al., 1997). Cooperation between FRET and total internal reflection microscopy (TIRFM) was designed to study

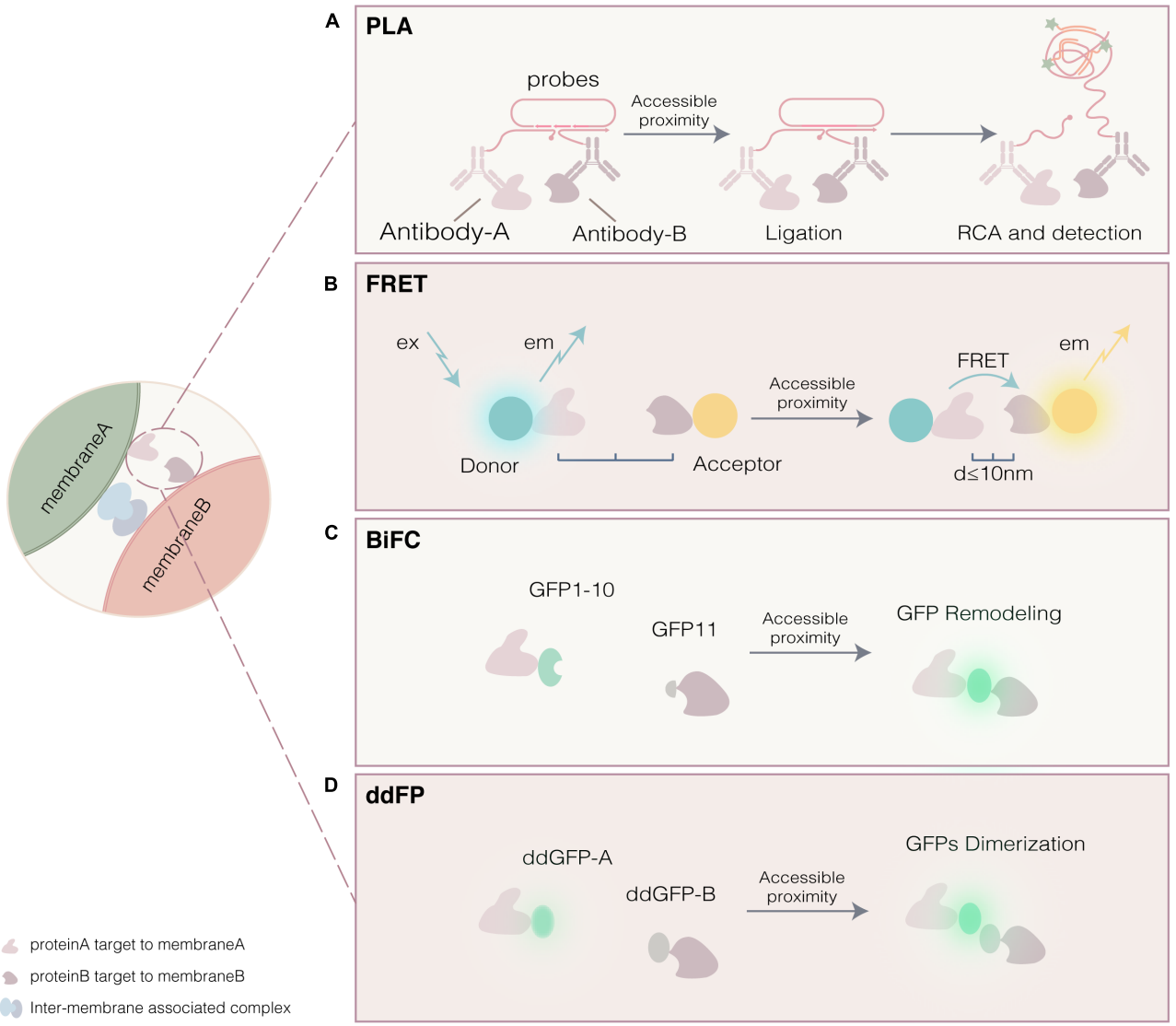

FIGURE 3 | Proximity-driven fluorescent signal generation approaches. **(A)** Proximity ligation assay (PLA). Single-stranded oligonucleotides are conjugated to antibody of proteins. Membrane proximity serves to template the hybridization of circularization oligonucleotides, which is then joined by ligation into a circular DNA molecule and followed by amplification of the signal by rolling-circle amplification (RCA). **(B)** Fluorescence resonance energy transfer (FRET). The photon energy transfers from excited donor to acceptor since the accessible proximity. **(C)** Bimolecular fluorescence complementation (BiFC). Accessible proximity made GFP1-10 and GFP11 remodel into a mature fluorescent protein. **(D)** Dimerization-dependent fluorescent proteins (ddFP). Two GFP monomer (ddGFP-A and ddGFP-B) with weak signal form a dimer with fluorescent strong signal since the accessible proximity.

ER-PM MCS in RBL-2H3 (mice) and HeLa cells (Poteser et al., 2016; Chen et al., 2017; Chang et al., 2018). FRET was applied to study lipid transfer regulated by oxysterol-binding protein (OSBP) at the MCSs between ER and other organelles in human RPE1 cells (Jamecna et al., 2019). Furthermore, another improved method is that FK506-binding protein 12 (FKBP 12) and FKBP 12-rapamycin binding domain (FRB) were anchored to different organelles by each resident membrane protein, respectively. As rapamycin induction, the closely spatial FKBP and FRB interact with each other, which activates FRET signal (Inoue et al., 2005). This method was applied to study ER-mitochondria MCS in rat H9C2 cardiomyoblast cells and basophilic leukemia (RBL)-2H3 cells (Csordas et al., 2010) and identify ER-mitochondria MCS tether Mfn2 in MEF cells (Naon et al., 2016). In another study, FRET venus-mTurquoise2 pair was fused to TOM20 and LAMP1 respectively, to study the regulation of mitochondria-lysosome MCS mediated by mitochondria fission via Rab7 GTP hydrolysis in HeLa cells (Wong et al., 2018).

A variant of FRET technique, bioluminescence resonance energy transfer (BRET) has been developed to study protein-protein interactions (Pfleger and Eidne, 2006). In BRET, the donor is luciferase enzyme which catalyzes a bioluminescent oxidation, and then the energy is transferred to the acceptor by resonance if the protein-protein interacts occurs. Compare with

FRET, BRET does not require sample illumination to excite the donor and has been emerged as a powerful tool for the study of protein-protein interactions (Perroy et al., 2004; De, 2011; Mo and Fu, 2016). Recently, a novel BRET-based biosensor with Renilla Luciferase 8 (RLuc) acting as a donor and mVenus as an acceptor, named MERLIN (mitochondria-ER length indicator nanosensor), was presented for the analysis of distances between ER and mitochondria in COS1 and HCT116 cells (Hertlein et al., 2020). In MERLIN, mVenus was targeted to mitochondria by the alpha-helical C-terminal domain of Bcl-xL (B33C) and RLuc was targeted to ER by a truncated non-functional variant of calnexin (sCal). The further experiments have demonstrated that MERLIN is a powerful and innovative tool for the investigation of ER-mitochondria MCS.

Bimolecular Fluorescence Complementation

Bimolecular complementation (BiC) system was successful applied in multiple proteins, such as ubiquitin (Johnsson and Varshavsky, 1994), β-lactamase (Galarneau et al., 2002), firefly (Luker et al., 2004) and fluorescent proteins. Bimolecular fluorescence complementation has emerged as a key technique to visualize protein-protein interactions in living cells. In BiFC system, split-fluorescent protein composes of two complementary protein residues, each no fluorescent signal on their own but are reassemble to give the bright fluorescence when driven together by protein interaction. In the earlier split-GFP system, GFP protein was divided into GFP-N (residues 1–157) and GFP-C (residues 158–230) with fused to leucine zipper, respectively. Leucine zipper interaction drive refold of GFP protein and the green fluorescence was recovered (Magliery et al., 2005). Because of low efficiency of fluorescence recovery, a more effective system, split super-folder GFP was engineered for efficient self-complementation without leucine zipper or other protein-protein interaction (Cabantous et al., 2005). In this method, GFP protein was divided into GFP1-10 (residues 1–214) fragment and GFP11 (residues 214–230) fragment, of which GFP 1-10 fragment contains three residues of the fluorophore. Only if GFP1-10 complement with the conserved residue E222 at GFP11, the fluorophore is reactive with brightest green fluorescence (Cabantous et al., 2005). For successful construction of split-fluorescent system, each individual protein residue cannot show any protein activity, and each individual protein residue cannot show a distinct fluorescent activity, instead a strong signal should be detected when reassembled (Magliery et al., 2005; Shekhawat and Ghosh, 2011). Notably, engineered GFP mutants were always considered due to the limited GFP fluorescent intensity (EGFP and Venus) (Wiens and Campbell, 2018). For the signal irreversibility, this method was commonly competent to detect transient protein-protein interaction (Magliery et al., 2005), instead of temporal information of protein-protein interaction.

Bimolecular fluorescence complementation is able to sensitively detect MCSs, where the contact signal always shows stable dots (**Figure 3C**). ER membrane protein Ifa38 and mitochondrial outer membrane protein TOM71 fused to GFP 1-10 and GFP11, respectively, highlight the signal of ER-mitochondria MCS as dots in yeast and HeLa cell. LD-peroxisome MCS can also be labeled with this split system mediated by LD protein Erg6 and peroxisome protein Pex3 in yeast (Kakimoto et al., 2018). The GFP variants, such as Venus, mCherry, and FusionRed, were also exploited to study MCSs (Toulmay and Prinz, 2012; Lahiri et al., 2014; Wiens and Campbell, 2018). Venus protein was derived from GFP and carries five amino acids mutation with improved brightness (Rekas et al., 2002). Similar with split GFP, split-Venus was developed and applied to detect MCSs such as ERMES, ER-LD MCS and vCLAMP in yeast (Shai et al., 2018). More importantly, split-Venus was employed to uncover new MCSs in yeast, such as vCOuPLE (vacuole-plasma membrane contact), pCLIP (plasma membrane-lipid droplet), PerPECs (peroxisome-plasma membrane) and PerVale (peroxisome-vacuole) (Shai et al., 2018). The split-Venus also was used to detect ER-mitochondria junctions, further experiment has demonstrated that ER membrane protein complex (EMC) tethers ER to mitochondria, which is required for phospholipid synthesis and cell growth in yeast (Lahiri et al., 2014). BiFC was employed to detect plastic remodeling of ER-mitochondria MCS and it is demonstrated that ER-mitochondria MCS is dynamic structure that undergoes active remodeling under different cellular needs in human osteosarcoma U2OS cells (Yang et al., 2018).

Recently, to expand BiFC toolset, direct engineering of self-complementing split fluorescent protein was developed by insertion a 32 amino acid spacer between the tenth and eleventh β-strands of GFP. The dual-color endogenous protein was tagged with sfCherry2 11 and GFP 11, revealing that the abundance of ER translocon complex Sec61B reduced in certain peripheral tubules. The new BiFC system offers multiple colors for imaging MCSs in HEK293T cells (Feng et al., 2017). In addition, a split GFP-based contact site sensor (SPLICS) was designed to detect the wide or narrow membrane contacts (narrow: 8–10 nm and wide: 40–50 nm) by the flexible spacer linked between GFP11 and ER targeting sequence. The ER-mitochondria MCS was allowed for detection and monitored by using this sensor in HeLa and HEK293 cells (Cieri et al., 2018).

ddFP

Dimerization-dependent fluorescent protein (ddFP) is a class of genetically encoded reporters based on the reversible binding of two dark fluorescent protein monomers to form a fluorescent heterodimeric complex, which can be used for detection of protein-protein interactions in living cells (Ding et al., 2015; Mitchell et al., 2018). The yellow or red fluorescent proteins are obligate tetrameric, however, is limited by its tetramerization disruption. To solve this problem, multiple monomeric fluorescence proteins were obtained through amino acid mutation, such as dTomato, mCherry and mStrawberry (Shaner et al., 2004). These monomeric proteins act as basic components to employ the ddFP tool. For earliest version of ddFP construction, a monomeric fluorescent dTomato variant (H162K and A164R) and a suitable "aptamer" (engineered another dTomato monomer) were screened. The "aptamer" allowed to constitute a heterodimer with the dTomato variant. Both two engineered dTomato monomer exhibited a weak red

fluorescence, however, the spatial proximity induced formation of the heterodimer through non-covalent interaction to exhibit a brighter fluorescent signal (Alford et al., 2012a). Furthermore, ddGFP was engineered with brighter fluorescent signal exhibited ∼60-fold increase in emission intensity upon heterodimerization. The protein-protein interaction can act as an indicator when two monomers are spatial proximity and thus an ideal tool for the study of MCSs. The advantage of ddFP is its reversibility, which is suitable to measure the dynamics of MCSs (**Figure 3D**).

By using ddGFP tool, a highly effective indicator of membrane proximity was generated to image MAM interface of ER and mitochondria by fusing two monomers of fluorescent protein to endoplasmic reticulum membrane (ERM) and outer mitochondrial membrane (OMM), respectively in HeLa cells (Alford et al., 2012b). When their spatial distance was less than 20 nm, a heterodimer was reconstructed by non-covalent interaction between monomers and then produce a stronger fluorescent signal. The ddGFP signal at ER-mitochondria MCS reduced when Mfn2, a crucial ER-mitochondria MCS tether, was deleted in MEF cells (Naon et al., 2016). The mutant TDP-43 did not impair mitochondrial bioenergetics by using ddGFP targeted to mitochondria and ER (TOM20-ddGFP and calN-ddGFP, respectively) in HeLa cells (Kawamata et al., 2017).

GLOBAL MAPPING MCSs BY PROXIMITY-DEPENDENT BIOTINYLATION

Inter-organelle membrane contact sites are established and maintained by tethers (**Table 1**). Although MCSs have been widely observed by EM and fluorescence techniques, tethers remained to be explored. Almost identified MCSs are mediated by multiple tethering proteins or protein complex, rather than only one tether. Some tethers were identified to mediate MCSs by traditional biochemical approaches, such as cell fractionation and pull-down. However, several considerable defects limit their application. Firstly, these approaches fail to catch the transient membrane contact; Secondly, the MCSs might be destroyed when detergent is added; Lastly, the dynamics of MCSs can't be monitored. The proximity biotinylation approaches such as proximity-based biotin identification (BioID) and ascorbate peroxidase (APEX) tagging are used to label neighboring proteins by generating a reactive biotin derivative (**Figure 4**). These proximity-dependent biotinylation approaches combined with proteomic analysis provide a promising strategy for global mapping MCSs.

BioID

Proximity-based biotin identification technology is dependent on BirA, a 35 kD DNA-binding biotin protein ligase that regulates the biotinylation of a subunit of acetyl-CoA carboxylase and inhibits biotin biosynthetic operon (Lane et al., 1964). For biotinylation, native biotin binds with ATP to constitute a biotinoyl-5′-AMP (BioAMP) prior to target to active site of BirA, biotin is then ligated to lysine residue when BAT sequence, a biotin acceptor tag, is recognized by BirA. Compared with BirA, BirA* (a R118G BirA mutant) with a lower affinity toward BioAMP causes promiscuous protein biotinylation. BioID enables to biotinylate potential proteins in proximity-dependent manner (Cronan, 2005; Gupta et al., 2015; Gingras et al., 2019). Cells expressing a bait resident protein fused to BirA* tag are incubated with biotin for several hours and then the biotinylated proteins are captured on a streptavidin affinity matrix for identification by LC-MS/MS (**Figures 4A,B**). BioID technology has proven to be a powerful method for identifying proximal proteins in cells.

The tethers involving in ER-peroxisome MCS were identified by BioID (Hua et al., 2017). PEX16 a key peroxisomal biogenesis protein and initially targets to the ER before the traffic to peroxisomes in COS-7 cells (Hua et al., 2015). By using BioID, a proximity interaction network (70 high-confidence proximal interactors) for PEX16 was mapped in human 293 T-REx Flp-In cells. The further experiment highlighted that ER-resident VAMP-associated proteins A and B (VAPA and VAPB) interact with peroxisomal membrane protein acyl-CoA binding domain containing 5 (ACBD5), which is required to tether two organelles together and thereby facilitates lipid exchange between the organelles in COS-7 cells. BioID was also used to investigate the role of tethers in ER-PM MCS. Unfolded protein response (UPR) PERK-BirA proximity interactome was obtained, and furthermore, actin-binding protein filamin A (FLNA) was identified as a key PERK interactor. The work revealed the role of PERK as a multimodal organizer of MCSs between ER and other vital organelles. As an apical sensor of ER-Ca^{2+} store alterations, PERK was able to tightly couple store depletion to facilitate the expansion of ER-PM MCS through interaction with FLNA and spatial organization of actin cytoskeleton in HEK293T cells (van Vliet et al., 2017).

In addition, as its effectiveness, split-BioID was exploited to uncover the PP1-interacting proteins (PIPs) targeted by protein phosphatase PP1 in HEK293T cells (De Munter et al., 2017). In split-BioID, BirA* was divided into BirA*-N and BirA*-C (at amino acid 140/141). The enzyme activity of BirA* is reconstructive after heterodimerization of BirA*-N and BirA*-C fragments.

APEX

Ascorbate peroxidase is an engineered ascorbate peroxidase. In the presence of hydrogen peroxide, APEX not only catalyzes 3,3′-diaminobenzidine (DAB) to generate an electron-dense product for visualization by EM (**Figure 4C**; Martell et al., 2012), but also converts a phenolic substrate (biotin-phenol) into a highly reactive radical and covalently tags proximal endogenous proteins (Rhee et al., 2013; Hung et al., 2014). Because the limited sensitivity of APEX precludes applications requiring low APEX expression, more active form APEX2 for intracellular specific protein imaging by EM and spatially-resolved proteomic mapping was obtained by yeast display evolution (Lam et al., 2015). In the presence of the APEX2 substrate biotin-phenol, a brief pulse of hydrogen peroxide (H_2O_2, < 1 min) results in the APEX2-catalyzed generation of short-lived, membrane impermeable biotin-phenoxyl radicals that form covalent adducts

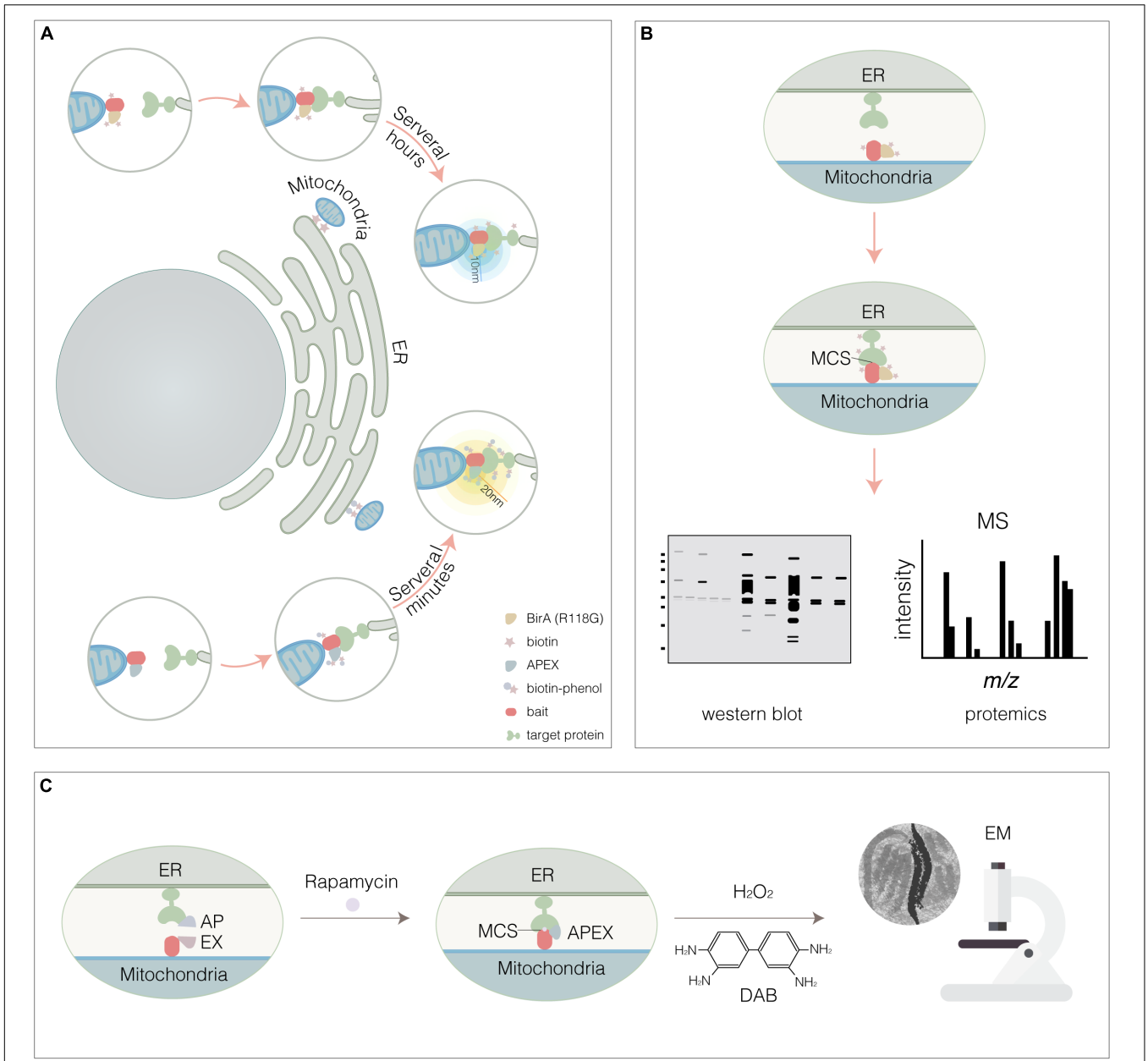

FIGURE 4 | Proximity-dependent biotinylation approaches. **(A)** BioID- or APEX-based proximity labeling. BirA* (Upper panel) or APEX (Lower panel) were fused to mitochondria membrane protein (bait). The potential target that be thought to interact with bait within the accessible proximity (10 nm for BirA*, 20 nm for APEX) would be biotinylated. For BirA*, endogenous biotin was accessible, instead APEX required the exogenous biotin-phenol and H_2O_2. **(B)** Cell expressing BirA*-bait or APEX-bait were lysed, then the biotinylated targets were captured by streptavidin-beads and identified by WESTERN BLOT and MS. **(C)** Reconstitution of split-APEX at ER- mitochondria MCS. By AP fused to $TOM20^{1-34}$ for targeting OMM and EX fused to $Cb5^{100-134}$ for targeting ERM, respectively, the split APEX enzyme activity was reconstituted and ER-mitochondria MCS was visualized at higher resolution by EM through the combination of the DAB staining.

with electron-rich amino acids in proteins located within a 10–20 nm radius, which enables to mark the potential proteins involving in MCSs (**Figures 4A,B**).

Ascorbate peroxidase has been successfully applied to localize mitochondria at proteomic level without mitochondria purification (Rhee et al., 2013), and also give insights into the composition and dynamics of LD proteomes in human osteosarcoma U2OS cells (Bersuker et al., 2018). The proteome at ER-mitochondria MCS was mapped by using APEX. The tethers localizing at the MCS between mitochondria and other organelles were identified and validated by combining biochemical subcellular fractionation. For instance, atlastin (ATL2) and reticulon (RTN1 and RTN3) are critical in forming ER-mitochondria MCS in HEK293 cells (Cho et al., 2017). Another work focused on ER-mitochondria MCS using APEX2 (Hung et al., 2017). By using APEX2-mediated proximity

biotinylation, endogenous proteins on the OMM and ERM of living human fibroblasts were captured and identified. By mining OMM and ERM proteomic data, it is reported that the tail-anchored OMM protein synaptojanin-2 binding protein SYNJ2BP was observed richly in both OMM- and ERM-targeted APEX2. The overexpression of SYNJ2BP dramatically increases ER-mitochondria MCSs mediated by RRBP1, SYNJ2BP's binding partner on the ER membrane.

To further advance the capabilities of APEX in protein-protein interactions and MCSs, split APEX2 was engineered. APEX2 was divided into N- and C-terminal fragments (at amino acid 201/202) for protein complementation assays (Xue et al., 2017). In addition, split APEX2 tool with more efficiency was engineered using directed evolution (Han et al., 2019). A total of 20 rounds of fluorescence activated cell sorting (FACS)-based selections from yeast displayed fragment libraries produced a 200-amino-acid N-terminal fragment (with 9 mutations relative to APEX2) called "AP" and a 50-amino-acid C-terminal fragment called "EX." AP and EX fragments were each inactive on their own but were reconstituted to give peroxidase activity when driven together by MCS. By AP fused to $TOM20^{1-34}$ for targeting OMM and EX fused to $Cb5^{100-134}$ for targeting ERM, respectively, the split APEX enzyme activity was reconstituted and ER-mitochondria MCS was visualized at higher resolution by EM through the combination of the DAB staining in HEK293T cells (**Figure 4C**; Han et al., 2019). Expectably, split-BioID and split APEX technologies that combine reporter-fragment complementation and proximity-dependent biotinylation will be promising tools to map MCSs and identify new tethers.

CONSIDERATIONS OF VARIOUS APPROACHES FOR STUDYING MCSs

In living cells, individual organelles are highly dynamic, so MCSs show a highly dynamic spatiotemporal pattern to response to various external stimuli. For example, ER enable enlarge its cytoplasmic volume from ∼35 to 97%, and mitochondria from ∼10 to 70% in 15 min in COS-7 cells (Valm et al., 2017), which drives transient alteration of MCSs. As described in previous chapters, although several different types of microscopies and various biochemical techniques are available for the study of MCSs, their principal drawbacks should be considered to avoid to gain the false positive or false negative results.

For the electron and light microscopy, spatiotemporal resolution and imaging condition have been supposed to be crucial for the study of MCSs. EM, FIB-SEM, and cyro-ET of cell specimen at the nanometer scale enable observation of subcellular structures of MCSs without fluorescence labeling. Although EM and FIB-SEM provide the fine structure details of MCSs with extreme spatial resolution, the fixation and dehydration procedures of EM tend to disrupt the intact architecture of intracellular organelles and MCSs. Cyro-ET allows thin samples to be imaged in 3D in a nearly native state by immobilizing samples in non-crystalline ice without fixation and dehydration procedures. However, like EM and FIB-SEM, cyro-ET is impossible to detect the dynamics of MCSs in living cells (**Figure 5A**). Light microscopy based on fluorescence was developed in living cells to overcome fixation procedures and low through-put of EM. Confocal microscopy is one of the most common methods to visualize the subcellular localization of fluorescent membrane resident proteins, however, confocal microscopy alone is not good choice to detect membrane contacts because of low spatiotemporal resolution. The combination of confocal microscopy and biochemical techniques (proximity-driven fluorescent signal generation) confers to powerful approaches for the study of MCSs. Super-resolution fluorescence microscopy (SRM), such as STEDM, PALM, STORM, and SIM, offers a unique window with super temporal and spatial resolution in living cells for MCSs. Especially, GI-SIM show extremely great advantage in the study of MCSs dynamics because of the extreme high temporal and spatial resolution. Compare to EM, fluorescence labeling of organelles is requisite to light microscopy. In addition, SRM imaging are mostly available in imaging facilities and a small number of laboratories due to its high cost, even some of them are not commercial (**Figure 5A**).

The reversible biochemical tools are required to catch the dynamics of MCSs. PLA is able to detect protein-protein interactions on endogenous levels and does not require a superior quantity of protein in comparison to traditional fluorescent fusion protein expression. More importantly, the quantitative analysis of MCSs can be accessed by PLA. However, some antibodies for endogenous proteins are not available. The fixation step is also necessary for PLA, which renders PLA to monitor the dynamic MCSs. FRET between donor- and acceptor-tagged membrane proteins is a quite suitable tool for dynamics of MCSs because FRET is dependent on non-interacted and distance-dependent fluorescence excitation. The optimization of FRET sensor and special microscopy set-up, however, are required. Notably, the equivalent expression of donor and acceptor are required in cell for the study of MCSs. BiFC gives the bright fluorescence when driven together by inter-organelle membrane proximity and is a widely used biochemical tool for the study of MCSs. BiFC allows to detect the transient organelles contact. The drawbacks of BiFC should be carefully considered. Irreversible binding of split FP fragments leads to accumulation of the fluorescent signal and stabilizes the MCSs, which could cause false-positive signals (Eisenberg-Bord et al., 2016). In brief, based on reversible dimerization, ddFP is a highly effective indicator of inter-organelle membrane proximity. In ddFP, low-fluorescence intensity of the probes could restrict its application. Except for PLA, the approaches based on proximity-driven fluorescent signal generation enable identification of MCSs in high confidence and high dynamic state in living cells. Therefore, the above biochemical techniques are widely used to study MCSs and their principal drawbacks should be considered (**Figure 5B**).

The proximity-dependent biotinylation approaches have been supposed to a promising tool to identify new tethers involving in MCSs. Because of dynamics of MCSs, labeling time is a crucial parameter when the proximity-dependent biotinylation approaches are employed to study MCSs in living cells. Generally, 12–24 h was required for biotinylation by BioID, and it take at least 3 h to finish labeling (Youn et al., 2018; Gingras et al., 2019). Instead, the biotinylation based on APEX2 required ∼30 min

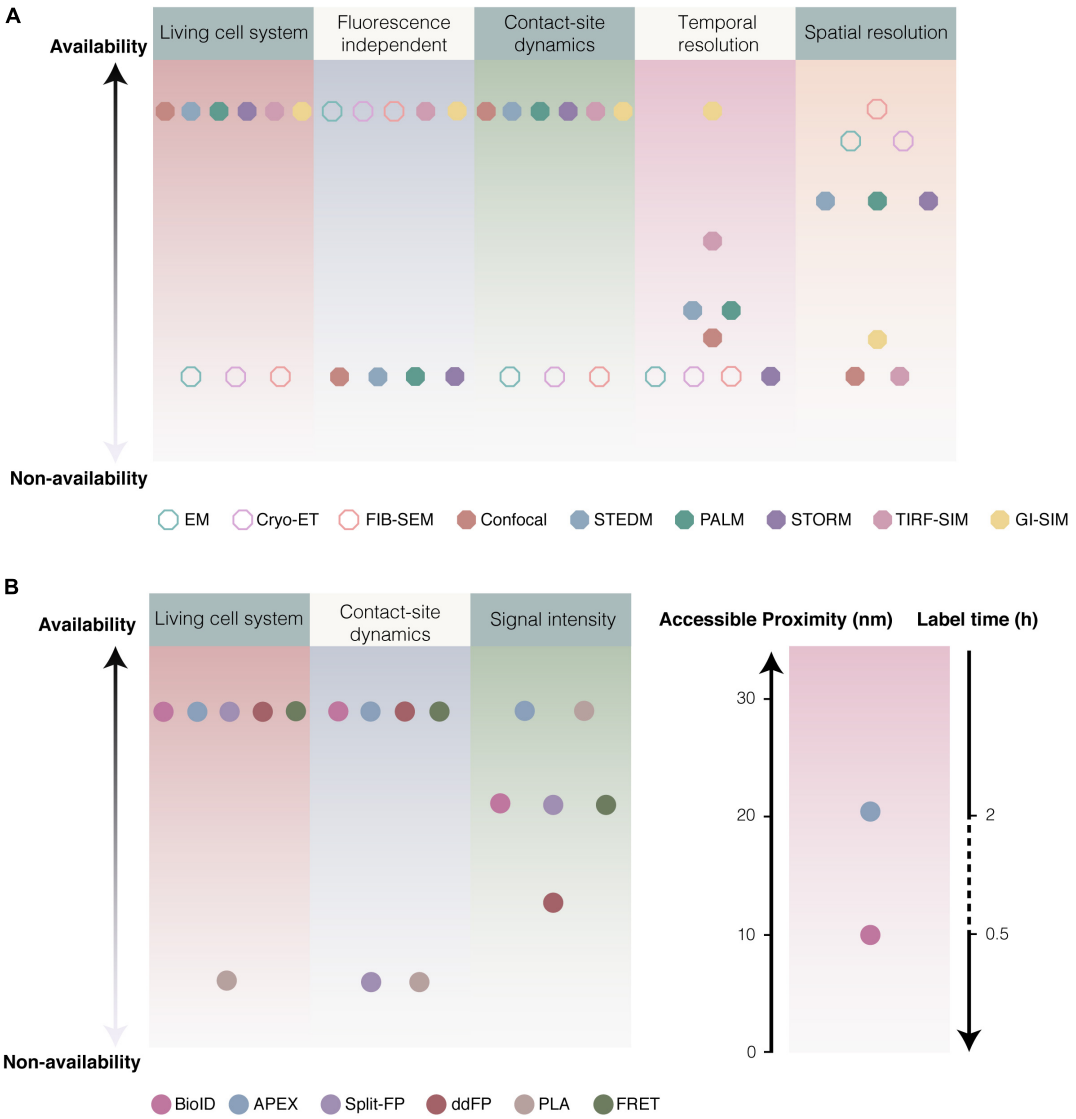

FIGURE 5 | Considerations of various approaches for studying MCSs. **(A)** Comparison of various microscopies. Imaging of EM, Cryo-ET and FIB-SEM are fluorescence independent with high resolution (1.8–4 nm), rather than suitable for the dynamics of MCSs in living cell. Comparison to confocal (<0.5 Hz, ∼200 nm) (Schulz et al., 2013), super resolution fluorescence microscopy like STEDM (Schneider et al., 2015), PALM (Betzig et al., 2006; Gould et al., 2009) and STORM (<10 Hz, ∼20 nm) (Rust et al., 2006), GI-SIM (266 Hz and 97 nm) (Guo Y. et al., 2018) as well as combination TIRF with SIM (TIRF-SIM: ∼11 Hz, 100 nm) (Kner et al., 2009) showed extreme high temporal and spatial resolution. **(B)** The availability of various biochemical techniques. Generally, 12–24 h was required for biotinylation by BioID, while biotinylation based on APEX2 required ∼30 min. BirA* enable to effectively label proteins at distance ∼10 nm, and APEX at ∼20 nm.

only, that is an obvious advantage of APEX2 compared with BioID (**Figure 5B**). In addition, BirA* is able to biotinylate the potential proteins using exogenous biotin as well as endogenous biotin. Whereas, APEX2 catalyzes the substrate biotin-phenol that is only from external supplement. If BirA* is anchored to membrane contact by transfection the fusion construct, it is possible to capture false positive proteins because of long labeling time and utilization of endogenous biotin. A new technology called TurboID or miniTurbo was reported to finish biotinylation in 10 min in HEK293 cells (Branon et al., 2018; Mair et al., 2019).

Inter-organelle membrane contact sites allow subdomains of organelle membranes to contact within 10–50 nm, in which membranes were considered to be spatial proximity and even exist lipids and signal (Ca^{2+}) transfer. For the biochemical techniques, it should be considered whether the distance reached by tools is suitable for the spatial proximity between inter-organelle membranes. PLA might lengthen its effective distance up to 30 nm (even more wider) as the adjustable length of nucleic acid arms and antibody affinity, which cause more false positive signals. FRET is able to detect a narrow contact with a typical range of roughly 1–10 nm (and up to 10 nm for atypical FRET pairs). Recently, split-GFP-based contact site sensor (SPLICS) was engineered to measure narrow (8–10 nm) and

wide (40–50 nm) juxtapositions between ER and mitochondria by increasing the length of the spacer of the probe and resident protein. In addition, labeling radius of BioID/APEX should be considered, BirA* enable to effectively label proteins at distance ∼10 nm (Kim et al., 2014), and APEX labeling ∼20 nm (Gingras et al., 2019). Therefore, the linker length between probe/enzyme and resident protein should be seriously considered when the proximity-driven fluorescent signal generation and proximity-dependent biotinylation are employed to study MCSs.

Given the diameter of general subcellular apparatus, BioID and APEX enable to ensure the signal reliability to uncover potential tethers (**Figure 3B**). However, some tethers involving in wide contacts could be missed because labeling radius of BioID/APEX does not reach the distance between the enzyme and candidate tethers. If the linker length between bait and BirA*/APEX is too long, it is easy to lead lots of false positives. To overcome this drawback, multiple baits or split-BirA*/APEX could be used to map MCSs. The remodeling of AP and EX in split-APEX be thought to maintain normal MCSs (Han et al., 2019). Instead, EGFP fusion overexpression always cause abnormal membrane contact (Snapp et al., 2003; Hung et al., 2017).

Overall, the drawbacks and limitations should be considered to keep in mind when these approaches are used to the study of the dynamic MCSs.

CONCLUSION AND PERSPECTIVES

The various microscopies, proximity-driven fluorescent signal generation and proximity-dependent biotinylation have greatly accelerated the recent advances of MCSs at the molecular and system level. The drawbacks of various approaches should be considered to keep in mind when these approaches are used for the study of dynamic MCSs. To overcome the limitations, the approaches combination would be a better choice for the study of MCSs.

In the near future, full scenario of MCSs will be presented using the current and emerging approaches. On one hand, the high temporal-spatial resolution microscopies will be used to draw the extensive MCSs (organelles interactome). On the other hand, biochemical techniques, especially proximity-driven biotinylation coupled with MS-based proteomics will be sharpest tools to map MCSs and identify new tethers involving in MCSs, termed as "tether-omics." In addition, cellular functions of MCSs and the role of MCSs in disease will be addressed.

AUTHOR CONTRIBUTIONS

All authors listed have made a substantial, direct and intellectual contribution to the work, and approved it for publication.

FUNDING

This work was supported by the National Natural Science Foundation of China (Nos. 91854101 and 31801166) and the Natural Science Foundation of Chongqing, China (No. cstc2019jcyj-msxmX0257) and the Fundamental Research Funds for the Central Universities (Nos. 2018CDQYSM0037 and 2019CDCGSM303).

REFERENCES

Alford, S. C., Abdelfattah, A. S., Ding, Y., and Campbell, R. E. (2012a). A fluorogenic red fluorescent protein heterodimer. *Chem. Biol.* 19, 353–360. doi: 10.1016/j.chembiol.2012.01.006

Alford, S. C., Ding, Y., Simmen, T., and Campbell, R. E. (2012b). Dimerization-dependent green and yellow fluorescent proteins. *ACS Synth. Biol.* 1, 569–575. doi: 10.1021/sb300050j

Algar, W. R., Hildebrandt, N., Vogel, S. S., and Medintz, I. L. (2019). FRET as a biomolecular research tool - understanding its potential while avoiding pitfalls. *Nat. Methods* 16, 815–829. doi: 10.1038/s41592-019-0530-8

Allison, R., Edgar, J. R., Pearson, G., Rizo, T., Newton, T., Gunther, S., et al. (2017). Defects in ER-endosome contacts impact lysosome function in hereditary spastic paraplegia. *J. Cell Biol.* 216, 1337–1355. doi: 10.1083/jcb.201609033

Alpy, F., Rousseau, A., Schwab, Y., Legueux, F., Stoll, I., Wendling, C., et al. (2013). STARD3 or STARD3NL and VAP form a novel molecular tether between late endosomes and the ER. *J. Cell Sci.* 126(Pt 23), 5500–5512. doi: 10.1242/jcs.139295

Atakpa, P., Thillaiappan, N. B., Mataragka, S., Prole, D. L., and Taylor, C. W. (2018). IP3 receptors preferentially associate with ER-lysosome contact sites and selectively deliver Ca^{2+} to lysosomes. *Cell Rep.* 25, 3180–3193.e7. doi: 10.1016/j.celrep.2018.11.064

Balderhaar, H. J., and Ungermann, C. (2013). CORVET and HOPS tethering complexes - coordinators of endosome and lysosome fusion. *J. Cell Sci.* 126(Pt 6), 1307–1316. doi: 10.1242/jcs.107805

Bastiaens, P. I., and Squire, A. (1999). Fluorescence lifetime imaging microscopy: spatial resolution of biochemical processes in the cell. *Trends Cell Biol.* 9, 48–52. doi: 10.1016/s0962-8924(98)01410-x

Bernard-Marissal, N., Medard, J. J., Azzedine, H., and Chrast, R. (2015). Dysfunction in endoplasmic reticulum-mitochondria crosstalk underlies SIGMAR1 loss of function mediated motor neuron degeneration. *Brain* 138(Pt 4), 875–890. doi: 10.1093/brain/awv008

Bernhard, W., and Rouiller, C. (1956). Close topographical relationship between mitochondria and ergastoplasm of liver cells in a definite phase of cellular activity. *J. Biophys. Biochem. Cytol.* 2 (4 Suppl.), 73–78. doi: 10.1083/jcb.2.4.73

Bersuker, K., Peterson, C. W. H., To, M., Sahl, S. J., Savikhin, V., Grossman, E. A., et al. (2018). A proximity labeling strategy provides insights into the composition and dynamics of lipid droplet proteomes. *Dev. Cell* 44, 97–112.e7. doi: 10.1016/j.devcel.2017.11.020

Besprozvannaya, M., Dickson, E., Li, H., Ginburg, K. S., Bers, D. M., Auwerx, J., et al. (2018). GRAM domain proteins specialize functionally distinct ER-PM contact sites in human cells. *eLife* 7:e31019. doi: 10.7554/eLife.31019

Betzig, E., Patterson, G. H., Sougrat, R., Lindwasser, O. W., Olenych, S., Bonifacino, J. S., et al. (2006). Imaging intracellular fluorescent proteins at nanometer resolution. *Science* 313, 1642–1645. doi: 10.1126/science.1127344

Biazik, J., Yla-Anttila, P., Vihinen, H., Jokitalo, E., and Eskelinen, E. L. (2015). Ultrastructural relationship of the phagophore with surrounding organelles. *Autophagy* 11, 439–451. doi: 10.1080/15548627.2015.1017178

Binns, D., Januszewski, T., Chen, Y., Hill, J., Markin, V. S., Zhao, Y., et al. (2006). An intimate collaboration between peroxisomes and lipid bodies. *J. Cell Biol.* 173, 719–731. doi: 10.1083/jcb.200511125

Bockler, S., and Westermann, B. (2014). ER-mitochondria contacts as sites of mitophagosome formation. *Autophagy* 10, 1346–1347. doi: 10.4161/auto.28981

Branon, T. C., Bosch, J. A., Sanchez, A. D., Udeshi, N. D., Svinkina, T., Carr, S. A., et al. (2018). Efficient proximity labeling in living cells and organisms with TurboID. *Nat. Biotechnol.* 36, 880–887. doi: 10.1038/nbt.4201

Cabantous, S., Terwilliger, T. C., and Waldo, G. S. (2005). Protein tagging and detection with engineered self-assembling fragments of green fluorescent protein. *Nat. Biotechnol.* 23, 102–107. doi: 10.1038/nbt1044

Cacciagli, P., Sutera-Sardo, J., Borges-Correia, A., Roux, J. C., Dorboz, I., Desvignes, J. P., et al. (2013). Mutations in BCAP31 cause a severe X-linked phenotype with deafness, dystonia, and central hypomyelination and disorganize the Golgi apparatus. *Am. J. Hum. Genet.* 93, 579–586. doi: 10.1016/j.ajhg.2013.07.023

Chang, C. L., Chen, Y. J., Quintanilla, C. G., Hsieh, T. S., and Liou, J. (2018). EB1 binding restricts STIM1 translocation to ER-PM junctions and regulates store-operated Ca^{2+} entry. *J. Cell Biol.* 217, 2047–2058. doi: 10.1083/jcb.201711151

Chen, B. C., Legant, W. R., Wang, K., Shao, L., Milkie, D. E., Davidson, M. W., et al. (2014). Lattice light-sheet microscopy: imaging molecules to embryos at high spatiotemporal resolution. *Science* 346:1257998. doi: 10.1126/science.1257998

Chen, Y. J., Chang, C. L., Lee, W. R., and Liou, J. (2017). RASSF4 controls SOCE and ER-PM junctions through regulation of PI(4,5)P2. *J. Cell Biol.* 216, 2011–2025. doi: 10.1083/jcb.201606047

Cho, I. T., Adelmant, G., Lim, Y., Marto, J. A., Cho, G., and Golden, J. A. (2017). Ascorbate peroxidase proximity labeling coupled with biochemical fractionation identifies promoters of endoplasmic reticulum-mitochondrial contacts. *J. Biol. Chem.* 292, 16382–16392. doi: 10.1074/jbc.M117.795286

Chu, B. B., Liao, Y. C., Qi, W., Xie, C., Du, X., Wang, J., et al. (2015). Cholesterol transport through lysosome-peroxisome membrane contacts. *Cell* 161, 291–306. doi: 10.1016/j.cell.2015.02.019

Cieri, D., Vicario, M., Giacomello, M., Vallese, F., Filadi, R., Wagner, T., et al. (2018). SPLICS: a split green fluorescent protein-based contact site sensor for narrow and wide heterotypic organelle juxtaposition. *Cell Death Differ.* 25, 1131–1145. doi: 10.1038/s41418-017-0033-z

Cohen, S., Valm, A. M., and Lippincott-Schwartz, J. (2018). Interacting organelles. *Curr. Opin. Cell Biol.* 53, 84–91. doi: 10.1016/j.ceb.2018.06.003

Collado, J., and Fernandez-Busnadiego, R. (2017). Deciphering the molecular architecture of membrane contact sites by cryo-electron tomography. *Biochim. Biophys. Acta Mol. Cell Res.* 1864, 1507–1512. doi: 10.1016/j.bbamcr.2017.03.009

Copeland, D. E., and Dalton, A. J. (1959). An association between mitochondria and the endoplasmic reticulum in cells of the pseudobranch gland of a teleost. *J. Biophys. Biochem. Cytol.* 5, 393–396. doi: 10.1083/jcb.5.3.393

Costello, J. L., Castro, I. G., Schrader, T. A., Islinger, M., and Schrader, M. (2017). Peroxisomal ACBD4 interacts with VAPB and promotes ER-peroxisome associations. *Cell Cycle* 16, 1039–1045. doi: 10.1080/15384101.2017.1314422

Cronan, J. E. (2005). Targeted and proximity-dependent promiscuous protein biotinylation by a mutant *Escherichia coli* biotin protein ligase. *J. Nutr. Biochem.* 16, 416–418. doi: 10.1016/j.jnutbio.2005.03.017

Csordas, G., Renken, C., Varnai, P., Walter, L., Weaver, D., Buttle, K. F., et al. (2006). Structural and functional features and significance of the physical linkage between ER and mitochondria. *J. Cell Biol.* 174, 915–921. doi: 10.1083/jcb.200604016

Csordas, G., Varnai, P., Golenar, T., Roy, S., Purkins, G., Schneider, T. G., et al. (2010). Imaging interorganelle contacts and local calcium dynamics at the ER-mitochondrial interface. *Mol Cell* 39, 121–132. doi: 10.1016/j.molcel.2010.06.029

D'Angelo, G., Polishchuk, E., Di Tullio, G., Santoro, M., Di Campli, A., Godi, A., et al. (2007). Glycosphingolipid synthesis requires FAPP2 transfer of glucosylceramide. *Nature* 449, 62–67. doi: 10.1038/nature06097

De, A. (2011). The new era of bioluminescence resonance energy transfer technology. *Curr. Pharm. Biotechnol.* 12, 558–568. doi: 10.2174/138920111795163922

de Brito, O. M., and Scorrano, L. (2008). Mitofusin 2 tethers endoplasmic reticulum to mitochondria. *Nature* 456, 605–610. doi: 10.1038/nature07534

De Munter, S., Gornemann, J., Derua, R., Lesage, B., Qian, J., Heroes, E., et al. (2017). Split-BioID: a proximity biotinylation assay for dimerization-dependent protein interactions. *FEBS Lett.* 591, 415–424. doi: 10.1002/1873-3468.12548

De Vos, K. J., Morotz, G. M., Stoica, R., Tudor, E. L., Lau, K. F., Ackerley, S., et al. (2012). VAPB interacts with the mitochondrial protein PTPIP51 to regulate calcium homeostasis. *Hum. Mol. Genet.* 21, 1299–1311. doi: 10.1093/hmg/ddr559

D'Eletto, M., Rossin, F., Occhigrossi, L., Farrace, M. G., Faccenda, D., Desai, R., et al. (2018). Transglutaminase type 2 regulates ER-mitochondria contact sites by interacting with GRP75. *Cell Rep.* 25, 3573.e–3581.e. doi: 10.1016/j.celrep.2018.11.094

Ding, Y., Li, J., Enterina, J. R., Shen, Y., Zhang, I., Tewson, P. H., et al. (2015). Ratiometric biosensors based on dimerization-dependent fluorescent protein exchange. *Nat. Methods* 12, 195–198. doi: 10.1038/nmeth.3261

Dong, D., Huang, X., Li, L., Mao, H., Mo, Y., Zhang, G., et al. (2020). Super-resolution fluorescence-assisted diffraction computational tomography reveals the three-dimensional landscape of the cellular organelle interactome. *Light Sci. Appl.* 9:11. doi: 10.1038/s41377-020-0249-4

Dong, R., Saheki, Y., Swarup, S., Lucast, L., Harper, J. W., and De Camilli, P. (2016). Endosome-ER contacts control actin nucleation and retromer function through VAP-dependent regulation of PI4P. *Cell* 166, 408–423. doi: 10.1016/j.cell.2016.06.037

Drobne, D. (2013). 3D imaging of cells and tissues by focused ion beam/scanning electron microscopy (FIB/SEM). *Methods Mol. Biol.* 950, 275–292. doi: 10.1007/978-1-62703-137-0_16

Du, X., Kumar, J., Ferguson, C., Schulz, T. A., Ong, Y. S., Hong, W., et al. (2011). A role for oxysterol-binding protein-related protein 5 in endosomal cholesterol trafficking. *J. Cell Biol.* 192, 121–135. doi: 10.1083/jcb.201004142

Dugail, I. (2014). Lysosome/lipid droplet interplay in metabolic diseases. *Biochimie* 96, 102–105. doi: 10.1016/j.biochi.2013.07.008

Eden, E. R., White, I. J., Tsapara, A., and Futter, C. E. (2010). Membrane contacts between endosomes and ER provide sites for PTP1B-epidermal growth factor receptor interaction. *Nat. Cell Biol.* 12, 267–272. doi: 10.1038/ncb2026

Eisenberg-Bord, M., Shai, N., Schuldiner, M., and Bohnert, M. (2016). A tether is a tether is a tether: tethering at membrane contact sites. *Dev. Cell* 39, 395–409. doi: 10.1016/j.devcel.2016.10.022

Elangovan, M., Day, R. N., and Periasamy, A. (2002). Nanosecond fluorescence resonance energy transfer-fluorescence lifetime imaging microscopy to localize the protein interactions in a single living cell. *J. Microsc.* 205(Pt 1), 3–14. doi: 10.1046/j.0022-2720.2001.00984.x

Elbaz-Alon, Y., Eisenberg-Bord, M., Shinder, V., Stiller, S. B., Shimoni, E., Wiedemann, N., et al. (2015). Lam6 regulates the extent of contacts between organelles. *Cell Rep.* 12, 7–14. doi: 10.1016/j.celrep.2015.06.022

Feng, S., Sekine, S., Pessino, V., Li, H., Leonetti, M. D., and Huang, B. (2017). Improved split fluorescent proteins for endogenous protein labeling. *Nat. Commun.* 8:370. doi: 10.1038/s41467-017-00494-8

Fermie, J., Liv, N., Ten Brink, C., van Donselaar, E. G., Muller, W. H., Schieber, N. L., et al. (2018). Single organelle dynamics linked to 3D structure by correlative live-cell imaging and 3D electron microscopy. *Traffic* 19, 354–369. doi: 10.1111/tra.12557

Fernandez-Busnadiego, R. (2016). Supramolecular architecture of endoplasmic reticulum-plasma membrane contact sites. *Biochem. Soc. Trans.* 44, 534–540. doi: 10.1042/BST20150279

Fernandez-Busnadiego, R., Saheki, Y., and De Camilli, P. (2015). Three-dimensional architecture of extended synaptotagmin-mediated endoplasmic reticulum-plasma membrane contact sites. *Proc. Natl. Acad. Sci. U.S.A.* 112, E2004–E2013. doi: 10.1073/pnas.1503191112

Fredriksson, S., Dixon, W., Ji, H., Koong, A. C., Mindrinos, M., and Davis, R. W. (2007). Multiplexed protein detection by proximity ligation for cancer biomarker validation. *Nat. Methods* 4, 327–329. doi: 10.1038/nmeth1020

Fredriksson, S., Gullberg, M., Jarvius, J., Olsson, C., Pietras, K., Gustafsdottir, S. M., et al. (2002). Protein detection using proximity-dependent DNA ligation assays. *Nat. Biotechnol.* 20, 473–477. doi: 10.1038/nbt0502-473

Friedman, J. R., Lackner, L. L., West, M., DiBenedetto, J. R., Nunnari, J., and Voeltz, G. K. (2011). ER tubules mark sites of mitochondrial division. *Science* 334, 358–362. doi: 10.1126/science.1207385

Galarneau, A., Primeau, M., Trudeau, L. E., and Michnick, S. W. (2002). Beta-lactamase protein fragment complementation assays as *in vivo* and *in vitro* sensors of protein protein interactions. *Nat. Biotechnol.* 20, 619–622. doi: 10.1038/nbt0602-619

Galiani, S., Waithe, D., Reglinski, K., Cruz-Zaragoza, L. D., Garcia, E., Clausen, M. P., et al. (2016). Super-resolution microscopy reveals compartmentalization of peroxisomal membrane proteins. *J. Biol. Chem.* 291, 16948–16962. doi: 10.1074/jbc.M116.734038

Garofalo, T., Matarrese, P., Manganelli, V., Marconi, M., Tinari, A., Gambardella, L., et al. (2016). Evidence for the involvement of lipid rafts localized at

the ER-mitochondria associated membranes in autophagosome formation. *Autophagy* 12, 917–935. doi: 10.1080/15548627.2016.1160971

Gingras, A. C., Abe, K. T., and Raught, B. (2019). Getting to know the neighborhood: using proximity-dependent biotinylation to characterize protein complexes and map organelles. *Curr. Opin. Chem. Biol.* 48, 44–54. doi: 10.1016/j.cbpa.2018.10.017

Gomez-Suaga, P., Paillusson, S., Stoica, R., Noble, W., Hanger, D. P., and Miller, C. C. J. (2017). The ER-mitochondria tethering complex VAPB-PTPIP51 regulates autophagy. *Curr. Biol.* 27, 371–385. doi: 10.1016/j.cub.2016.12.038

Gonzalez Montoro, A., Auffarth, K., Honscher, C., Bohnert, M., Becker, T., Warscheid, B., et al. (2018). Vps39 interacts with Tom40 to establish one of two functionally distinct vacuole-mitochondria contact sites. *Dev. Cell* 45, 621–636.e7. doi: 10.1016/j.devcel.2018.05.011

Gould, T. J., Verkhusha, V. V., and Hess, S. T. (2009). Imaging biological structures with fluorescence photoactivation localization microscopy. *Nat. Protoc.* 4, 291–308. doi: 10.1038/nprot.2008.246

Guo, M., Chandris, P., Giannini, J. P., Trexler, A. J., Fischer, R., Chen, J., et al. (2018). Single-shot super-resolution total internal reflection fluorescence microscopy. *Nat. Methods* 15, 425–428. doi: 10.1038/s41592-018-0004-4

Guo, Y., Li, D., Zhang, S., Yang, Y., Liu, J. J., Wang, X., et al. (2018). Visualizing intracellular organelle and cytoskeletal interactions at nanoscale resolution on millisecond timescales. *Cell* 175, 1430–1442.e17. doi: 10.1016/j.cell.2018.09.057

Gupta, G. D., Coyaud, E., Goncalves, J., Mojarad, B. A., Liu, Y., Wu, Q., et al. (2015). A dynamic protein interaction landscape of the human centrosome-cilium interface. *Cell* 163, 1484–1499. doi: 10.1016/j.cell.2015.10.065

Hamasaki, M., Furuta, N., Matsuda, A., Nezu, A., Yamamoto, A., Fujita, N., et al. (2013). Autophagosomes form at ER-mitochondria contact sites. *Nature* 495, 389–393. doi: 10.1038/nature11910

Han, Y., Branon, T. C., Martell, J. D., Boassa, D., Shechner, D., Ellisman, M. H., et al. (2019). Directed evolution of split APEX2 peroxidase. *ACS Chem. Biol.* 14, 619–635. doi: 10.1021/acschembio.8b00919

Hanada, K., Kumagai, K., Yasuda, S., Miura, Y., Kawano, M., Fukasawa, M., et al. (2003). Molecular machinery for non-vesicular trafficking of ceramide. *Nature* 426, 803–809. doi: 10.1038/nature02188

Hao, F., Kondo, K., Itoh, T., Ikari, S., Nada, S., Okada, M., et al. (2018). Rheb localized on the Golgi membrane activates lysosome-localized mTORC1 at the Golgi-lysosome contact site. *J. Cell Sci.* 131:jcs208017. doi: 10.1242/jcs.208017

Hayashi, T., Rizzuto, R., Hajnoczky, G., and Su, T. P. (2009). MAM: more than just a housekeeper. *Trends Cell Biol.* 19, 81–88. doi: 10.1016/j.tcb.2008.12.002

Helle, S. C., Kanfer, G., Kolar, K., Lang, A., Michel, A. H., and Kornmann, B. (2013). Organization and function of membrane contact sites. *Biochim. Biophys. Acta* 1833, 2526–2541. doi: 10.1016/j.bbamcr.2013.01.028

Henne, W. M., Zhu, L., Balogi, Z., Stefan, C., Pleiss, J. A., and Emr, S. D. (2015). Mdm1/Snx13 is a novel ER-endolysosomal interorganelle tethering protein. *J. Cell Biol.* 210, 541–551. doi: 10.1083/jcb.201503088

Hertlein, V., Flores-Romero, H., Das, K. K., Fischer, S., Heunemann, M., Calleja-Felipe, M., et al. (2020). MERLIN: a novel BRET-based proximity biosensor for studying mitochondria-ER contact sites. *Life Sci. Alliance* 3:e201900600. doi: 10.26508/lsa.201900600

Honscher, C., Mari, M., Auffarth, K., Bohnert, M., Griffith, J., Geerts, W., et al. (2014). Cellular metabolism regulates contact sites between vacuoles and mitochondria. *Dev. Cell* 30, 86–94. doi: 10.1016/j.devcel.2014.06.006

Hoyer, M. J., Chitwood, P. J., Ebmeier, C. C., Striepen, J. F., Qi, R. Z., Old, W. M., et al. (2018). A novel class of ER membrane proteins regulates ER-associated endosome fission. *Cell* 175, 254–265.e14. doi: 10.1016/j.cell.2018.08.030

Hsieh, T. S., Chen, Y. J., Chang, C. L., Lee, W. R., and Liou, J. (2017). Cortical actin contributes to spatial organization of ER-PM junctions. *Mol. Biol. Cell* 28, 3171–3180. doi: 10.1091/mbc.E17-06-0377

Hsu, F., Spannl, S., Ferguson, C., Hyman, A. A., Parton, R. G., and Zerial, M. (2018). Rab5 and Alsin regulate stress-activated cytoprotective signaling on mitochondria. *eLife* 7:e32282. doi: 10.7554/eLife.32282

Hua, R., Cheng, D., Coyaud, E., Freeman, S., Di Pietro, E., Wang, Y., et al. (2017). VAPs and ACBD5 tether peroxisomes to the ER for peroxisome maintenance and lipid homeostasis. *J. Cell Biol.* 216, 367–377. doi: 10.1083/jcb.201608128

Hua, R., Gidda, S. K., Aranovich, A., Mullen, R. T., and Kim, P. K. (2015). Multiple domains in PEX16 mediate its trafficking and recruitment of peroxisomal proteins to the ER. *Traffic* 16, 832–852. doi: 10.1111/tra.12292

Huang, X., Fan, J., Li, L., Liu, H., Wu, R., Wu, Y., et al. (2018). Fast, long-term, super-resolution imaging with Hessian structured illumination microscopy. *Nat. Biotechnol.* 36, 451–459. doi: 10.1038/nbt.4115

Hung, V., Lam, S. S., Udeshi, N. D., Svinkina, T., Guzman, G., Mootha, V. K., et al. (2017). Proteomic mapping of cytosol-facing outer mitochondrial and ER membranes in living human cells by proximity biotinylation. *eLife* 6:e24463. doi: 10.7554/eLife.24463

Hung, V., Zou, P., Rhee, H. W., Udeshi, N. D., Cracan, V., Svinkina, T., et al. (2014). Proteomic mapping of the human mitochondrial intermembrane space in live cells via ratiometric APEX tagging. *Mol. Cell* 55, 332–341. doi: 10.1016/j.molcel.2014.06.003

Inoue, T., Heo, W. D., Grimley, J. S., Wandless, T. J., and Meyer, T. (2005). An inducible translocation strategy to rapidly activate and inhibit small GTPase signaling pathways. *Nat. Methods* 2, 415–418. doi: 10.1038/nmeth763

Iwasawa, R., Mahul-Mellier, A. L., Datler, C., Pazarentzos, E., and Grimm, S. (2011). Fis1 and Bap31 bridge the mitochondria-ER interface to establish a platform for apoptosis induction. *EMBO J.* 30, 556–568. doi: 10.1038/emboj.2010.346

Jamecna, D., Polidori, J., Mesmin, B., Dezi, M., Levy, D., Bigay, J., et al. (2019). An intrinsically disordered region in OSBP acts as an entropic barrier to control protein dynamics and orientation at membrane contact sites. *Dev. Cell* 49, 220–234.e8. doi: 10.1016/j.devcel.2019.02.021

Jansen, M., Ohsaki, Y., Rega, L. R., Bittman, R., Olkkonen, V. M., and Ikonen, E. (2011). Role of ORPs in sterol transport from plasma membrane to ER and lipid droplets in mammalian cells. *Traffic* 12, 218–231. doi: 10.1111/j.1600-0854.2010.01142.x

Jardin, I., Lopez, J. J., Salido, G. M., and Rosado, J. A. (2008). Orai1 mediates the interaction between STIM1 and hTRPC1 and regulates the mode of activation of hTRPC1-forming Ca^{2+} channels. *J. Biol. Chem.* 283, 25296–25304. doi: 10.1074/jbc.M802904200

Jiang, P., Nishimura, T., Sakamaki, Y., Itakura, E., Hatta, T., Natsume, T., et al. (2014). The HOPS complex mediates autophagosome-lysosome fusion through interaction with syntaxin 17. *Mol. Biol. Cell* 25, 1327–1337. doi: 10.1091/mbc.E13-08-0447

Jing, J., He, L., Sun, A., Quintana, A., Ding, Y., Ma, G., et al. (2015). Proteomic mapping of ER-PM junctions identifies STIMATE as a regulator of Ca^{2+} influx. *Nat. Cell Biol.* 17, 1339–1347. doi: 10.1038/ncb3234

Jing, J., Liu, G., Huang, Y., and Zhou, Y. (2019). A molecular toolbox for interrogation of membrane contact sites. *J. Physiol.* doi: 10.1113/JP277761 [Epub ahead of print].

Johnsson, N., and Varshavsky, A. (1994). Split ubiquitin as a sensor of protein interactions *in vivo*. *Proc. Natl. Acad. Sci. U.S.A.* 91, 10340–10344. doi: 10.1073/pnas.91.22.10340

Joshi, A. S., Nebenfuehr, B., Choudhary, V., Satpute-Krishnan, P., Levine, T. P., Golden, A., et al. (2018). Lipid droplet and peroxisome biogenesis occur at the same ER subdomains. *Nat. Commun.* 9:2940. doi: 10.1038/s41467-018-05277-3

Kakimoto, Y., Tashiro, S., Kojima, R., Morozumi, Y., Endo, T., and Tamura, Y. (2018). Visualizing multiple inter-organelle contact sites using the organelle-targeted split-GFP system. *Sci. Rep.* 8:6175. doi: 10.1038/s41598-018-24466-0

Kang, F., Zhou, M., Huang, X., Fan, J., Wei, L., Boulanger, J., et al. (2019). E-syt1 Re-arranges STIM1 clusters to stabilize ring-shaped ER-PM contact sites and accelerate Ca^{2+} store replenishment. *Sci. Rep.* 9:3975. doi: 10.1038/s41598-019-40331-0

Kawamata, H., Peixoto, P., Konrad, C., Palomo, G., Bredvik, K., Gerges, M., et al. (2017). Mutant TDP-43 does not impair mitochondrial bioenergetics *in vitro* and *in vivo*. *Mol. Neurodegener.* 12:37. doi: 10.1186/s13024-017-0180-1

Kawano, S., Tamura, Y., Kojima, R., Bala, S., Asai, E., Michel, A. H., et al. (2018). Structure-function insights into direct lipid transfer between membranes by Mmm1-Mdm12 of ERMES. *J. Cell Biol.* 217, 959–974. doi: 10.1083/jcb.201704119

Kim, D. I., Birendra, K. C., Zhu, W., Motamedchaboki, K., Doye, V., and Roux, K. J. (2014). Probing nuclear pore complex architecture with proximity-dependent biotinylation. *Proc. Natl. Acad. Sci. U.S.A.* 111, E2453–E2461. doi: 10.1073/pnas.1406459111

Kim, Y. J., Guzman-Hernandez, M. L., Wisniewski, E., and Balla, T. (2015). Phosphatidylinositol-Phosphatidic acid exchange by Nir2 at ER-PM contact sites maintains phosphoinositide signaling competence. *Dev. Cell* 33, 549–561. doi: 10.1016/j.devcel.2015.04.028

Kirisako, T., Baba, M., Ishihara, N., Miyazawa, K., Ohsumi, M., Yoshimori, T., et al. (1999). Formation process of autophagosome is traced with Apg8/Aut7p in yeast. *J. Cell Biol.* 147, 435–446. doi: 10.1083/jcb.147.2.435

Kner, P., Chhun, B. B., Griffis, E. R., Winoto, L., and Gustafsson, M. G. (2009). Super-resolution video microscopy of live cells by structured illumination. *Nat. Methods* 6, 339–342. doi: 10.1038/nmeth.1324

Knoblach, B., Sun, X., Coquelle, N., Fagarasanu, A., Poirier, R. L., and Rachubinski, R. A. (2013). An ER-peroxisome tether exerts peroxisome population control in yeast. *EMBO J.* 32, 2439–2453. doi: 10.1038/emboj.2013.170

Kornmann, B., Currie, E., Collins, S. R., Schuldiner, M., Nunnari, J., Weissman, J. S., et al. (2009). An ER-mitochondria tethering complex revealed by a synthetic biology screen. *Science* 325, 477–481. doi: 10.1126/science.1175088

Kornmann, B., Osman, C., and Walter, P. (2011). The conserved GTPase Gem1 regulates endoplasmic reticulum-mitochondria connections. *Proc. Natl. Acad. Sci. U.S.A.* 108, 14151–14156. doi: 10.1073/pnas.1111314108

Krols, M., van Isterdael, G., Asselbergh, B., Kremer, A., Lippens, S., Timmerman, V., et al. (2016). Mitochondria-associated membranes as hubs for neurodegeneration. *Acta Neuropathol.* 131, 505–523. doi: 10.1007/s00401-015-1528-7

Kvam, E., and Goldfarb, D. S. (2006). Nucleus-vacuole junctions in yeast: anatomy of a membrane contact site. *Biochem. Soc. Trans.* 34(Pt 3), 340–342. doi: 10.1042/BST0340340

Lackner, L. L., Ping, H., Graef, M., Murley, A., and Nunnari, J. (2013). Endoplasmic reticulum-associated mitochondria-cortex tether functions in the distribution and inheritance of mitochondria. *Proc. Natl. Acad. Sci. U.S.A.* 110, E458–E467. doi: 10.1073/pnas.1215232110

Lahiri, S., Chao, J. T., Tavassoli, S., Wong, A. K., Choudhary, V., Young, B. P., et al. (2014). A conserved endoplasmic reticulum membrane protein complex (EMC) facilitates phospholipid transfer from the ER to mitochondria. *PLoS Biol.* 12:e1001969. doi: 10.1371/journal.pbio.1001969

Lahiri, S., Toulmay, A., and Prinz, W. A. (2015). Membrane contact sites, gateways for lipid homeostasis. *Curr. Opin. Cell Biol.* 33, 82–87. doi: 10.1016/j.ceb.2014.12.004

Lam, S. S., Martell, J. D., Kamer, K. J., Deerinck, T. J., Ellisman, M. H., Mootha, V. K., et al. (2015). Directed evolution of APEX2 for electron microscopy and proximity labeling. *Nat. Methods* 12, 51–54. doi: 10.1038/nmeth.3179

Landstrom, A. P., Weisleder, N., Batalden, K. B., Bos, J. M., Tester, D. J., Ommen, S. R., et al. (2007). Mutations in JPH2-encoded junctophilin-2 associated with hypertrophic cardiomyopathy in humans. *J. Mol. Cell. Cardiol.* 42, 1026–1035. doi: 10.1016/j.yjmcc.2007.04.006

Lane, M. D., Young, D. L., and Lynen, F. (1964). The enzymatic synthesis of holotranscarboxylase from apotranscarboxylase and (+)-Biotin. I. Purification of the apoenzyme and synthetase; characteristics of the reaction. *J. Biol. Chem.* 239, 2858–2864.

Lawrence, B. P., and Brown, W. J. (1992). Autophagic vacuoles rapidly fuse with pre-existing lysosomes in cultured hepatocytes. *J. Cell Sci.* 102(Pt 3), 515–526.

Lawrence, R. E., and Zoncu, R. (2019). The lysosome as a cellular centre for signalling, metabolism and quality control. *Nat. Cell Biol.* 21, 133–142. doi: 10.1038/s41556-018-0244-7

Levine, T. P., and Munro, S. (2001). Dual targeting of Osh1p, a yeast homologue of oxysterol-binding protein, to both the Golgi and the nucleus-vacuole junction. *Mol. Biol. Cell* 12, 1633–1644. doi: 10.1091/mbc.12.6.1633

Li, D., Shao, L., Chen, B. C., Zhang, X., Zhang, M., Moses, B., et al. (2015). Extended-resolution structured illumination imaging of endocytic and cytoskeletal dynamics. *Science* 349:aab3500. doi: 10.1126/science.aab3500

Lim, Y., Cho, I. T., Schoel, L. J., Cho, G., and Golden, J. A. (2015). Hereditary spastic paraplegia-linked REEP1 modulates endoplasmic reticulum/mitochondria contacts. *Ann. Neurol.* 78, 679–696. doi: 10.1002/ana.24488

Liou, J., Fivaz, M., Inoue, T., and Meyer, T. (2007). Live-cell imaging reveals sequential oligomerization and local plasma membrane targeting of stromal interaction molecule 1 after Ca^{2+} store depletion. *Proc. Natl. Acad. Sci. U.S.A.* 104, 9301–9306. doi: 10.1073/pnas.0702866104

Litvak, V., Dahan, N., Ramachandran, S., Sabanay, H., and Lev, S. (2005). Maintenance of the diacylglycerol level in the Golgi apparatus by the Nir2 protein is critical for Golgi secretory function. *Nat. Cell Biol.* 7, 225–234. doi: 10.1038/ncb1221

Liu, L. K., Choudhary, V., Toulmay, A., and Prinz, W. A. (2017). An inducible ER-Golgi tether facilitates ceramide transport to alleviate lipotoxicity. *J. Cell Biol.* 216, 131–147. doi: 10.1083/jcb.201606059

Luker, K. E., Smith, M. C., Luker, G. D., Gammon, S. T., Piwnica-Worms, H., and Piwnica-Worms, D. (2004). Kinetics of regulated protein-protein interactions revealed with firefly luciferase complementation imaging in cells and living animals. *Proc. Natl. Acad. Sci. U.S.A.* 101, 12288–12293. doi: 10.1073/pnas.0404041101

Magliery, T. J., Wilson, C. G., Pan, W., Mishler, D., Ghosh, I., Hamilton, A. D., et al. (2005). Detecting protein-protein interactions with a green fluorescent protein fragment reassembly trap: scope and mechanism. *J. Am. Chem. Soc.* 127, 146–157. doi: 10.1021/ja046699g

Mair, A., Xu, S. L., Branon, T. C., Ting, A. Y., and Bergmann, D. C. (2019). Proximity labeling of protein complexes and cell-type-specific organellar proteomes in Arabidopsis enabled by TurboID. *eLife* 8:e47864. doi: 10.7554/eLife.47864

Manford, A. G., Stefan, C. J., Yuan, H. L., Macgurn, J. A., and Emr, S. D. (2012). ER-to-plasma membrane tethering proteins regulate cell signaling and ER morphology. *Dev. Cell* 23, 1129–1140. doi: 10.1016/j.devcel.2012.11.004

Martell, J. D., Deerinck, T. J., Sancak, Y., Poulos, T. L., Mootha, V. K., Sosinsky, G. E., et al. (2012). Engineered ascorbate peroxidase as a genetically encoded reporter for electron microscopy. *Nat. Biotechnol.* 30, 1143–1148. doi: 10.1038/nbt.2375

Marx, V. (2017). Probes: FRET sensor design and optimization. *Nat. Methods* 14, 949–953. doi: 10.1038/nmeth.4434

Mc Donald, J. M., and Krainc, D. (2017). Lysosomal proteins as a therapeutic target in neurodegeneration. *Annu. Rev. Med.* 68, 445–458. doi: 10.1146/annurev-med-050715-104432

Mesmin, B., Bigay, J., Moser von Filseck, J., Lacas-Gervais, S., Drin, G., and Antonny, B. (2013). A four-step cycle driven by PI(4)P hydrolysis directs sterol/PI(4)P exchange by the ER-Golgi tether OSBP. *Cell* 155, 830–843. doi: 10.1016/j.cell.2013.09.056

Mitchell, A. C., Alford, S. C., Hunter, S. A., Kannan, D., Parra Sperberg, R. A., Chang, C. H., et al. (2018). Development of a protease biosensor based on a dimerization-dependent red fluorescent protein. *ACS Chem. Biol.* 13, 66–72. doi: 10.1021/acschembio.7b00715

Miyawaki, A., Llopis, J., Heim, R., McCaffery, J. M., Adams, J. A., Ikura, M., et al. (1997). Fluorescent indicators for Ca^{2+} based on green fluorescent proteins and calmodulin. *Nature* 388, 882–887. doi: 10.1038/42264

Mo, X. L., and Fu, H. (2016). BRET: nanoluc-based bioluminescence resonance energy transfer platform to monitor protein-protein interactions in live cells. *Methods Mol. Biol.* 1439, 263–271. doi: 10.1007/978-1-4939-3673-1_17

Modi, S., Lopez-Domenech, G., Halff, E. F., Covill-Cooke, C., Ivankovic, D., Melandri, D., et al. (2019). Miro clusters regulate ER-mitochondria contact sites and link cristae organization to the mitochondrial transport machinery. *Nat. Commun.* 10:4399. doi: 10.1038/s41467-019-12382-4

Mullock, B. M., Smith, C. W., Ihrke, G., Bright, N. A., Lindsay, M., Parkinson, E. J., et al. (2000). Syntaxin 7 is localized to late endosome compartments, associates with Vamp 8, and Is required for late endosome-lysosome fusion. *Mol. Biol. Cell* 11, 3137–3153. doi: 10.1091/mbc.11.9.3137

Murley, A., Sarsam, R. D., Toulmay, A., Yamada, J., Prinz, W. A., and Nunnari, J. (2015). Ltc1 is an ER-localized sterol transporter and a component of ER-mitochondria and ER-vacuole contacts. *J. Cell Biol.* 209, 539–548. doi: 10.1083/jcb.201502033

Naon, D., and Scorrano, L. (2014). At the right distance: ER-mitochondria juxtaposition in cell life and death. *Biochim. Biophys. Acta* 1843, 2184–2194. doi: 10.1016/j.bbamcr.2014.05.011

Naon, D., Zaninello, M., Giacomello, M., Varanita, T., Grespi, F., Lakshminaranayan, S., et al. (2016). Critical reappraisal confirms that Mitofusin 2 is an endoplasmic reticulum-mitochondria tether. *Proc. Natl. Acad. Sci. U.S.A.* 113, 11249–11254. doi: 10.1073/pnas.1606786113

Nascimbeni, A. C., Giordano, F., Dupont, N., Grasso, D., Vaccaro, M. I., Codogno, P., et al. (2017). ER-plasma membrane contact sites contribute to autophagosome biogenesis by regulation of local PI3P synthesis. *EMBO J.* 36, 2018–2033. doi: 10.15252/embj.201797006

Nishimura, A. L., Mitne-Neto, M., Silva, H. C., Richieri-Costa, A., Middleton, S., Cascio, D., et al. (2004). A mutation in the vesicle-trafficking protein VAPB

causes late-onset spinal muscular atrophy and amyotrophic lateral sclerosis. *Am. J. Hum. Genet.* 75, 822–831. doi: 10.1086/425287

Nixon-Abell, J., Obara, C. J., Weigel, A. V., Li, D., Legant, W. R., Xu, C. S., et al. (2016). Increased spatiotemporal resolution reveals highly dynamic dense tubular matrices in the peripheral ER. *Science* 354:aaf3928. doi: 10.1126/science.aaf3928

Nordmann, M., Cabrera, M., Perz, A., Brocker, C., Ostrowicz, C., Engelbrecht-Vandre, S., et al. (2010). The Mon1-Ccz1 complex is the GEF of the late endosomal Rab7 homolog Ypt7. *Curr. Biol.* 20, 1654–1659. doi: 10.1016/j.cub.2010.08.002

Ohashi, M., Miwako, I., Nakamura, K., Yamamoto, A., Murata, M., Ohnishi, S., et al. (1999). An arrested late endosome-lysosome intermediate aggregate observed in a Chinese hamster ovary cell mutant isolated by novel three-step screening. *J. Cell Sci.* 112(Pt 8), 1125–1138.

Olzmann, J. A., and Carvalho, P. (2019). Dynamics and functions of lipid droplets. *Nat. Rev. Mol. Cell Biol.* 20, 137–155. doi: 10.1038/s41580-018-0085-z

Ouasti, S., Matarrese, P., Paddon, R., Khosravi-Far, R., Sorice, M., Tinari, A., et al. (2007). Death receptor ligation triggers membrane scrambling between Golgi and mitochondria. *Cell Death Differ.* 14, 453–461. doi: 10.1038/sj.cdd.4402043

Paillusson, S., Stoica, R., Gomez-Suaga, P., Lau, D. H. W., Mueller, S., Miller, T., et al. (2016). There's Something Wrong with my MAM; the ER-Mitochondria Axis and Neurodegenerative Diseases. *Trends Neurosci.* 39, 146–157. doi: 10.1016/j.tins.2016.01.008

Palande, K., Roovers, O., Gits, J., Verwijmeren, C., Iuchi, Y., Fujii, J., et al. (2011). Peroxiredoxin-controlled G-CSF signalling at the endoplasmic reticulum-early endosome interface. *J. Cell Sci.* 124(Pt 21), 3695–3705. doi: 10.1242/jcs.089656

Pan, X., Roberts, P., Chen, Y., Kvam, E., Shulga, N., Huang, K., et al. (2000). Nucleus-vacuole junctions in Saccharomyces cerevisiae are formed through the direct interaction of Vac8p with Nvj1p. *Mol. Biol. Cell* 11, 2445–2457. doi: 10.1091/mbc.11.7.2445

Perroy, J., Pontier, S., Charest, P. G., Aubry, M., and Bouvier, M. (2004). Real-time monitoring of ubiquitination in living cells by BRET. *Nat. Methods* 1, 203–208. doi: 10.1038/nmeth722

Pfleger, K. D. G., and Eidne, K. A. (2006). Illuminating insights into protein-protein interactions using bioluminescence resonance energy transfer (BRET). *Nat. Methods* 3, 165–174. doi: 10.1038/nmeth841

Pietraszewska-Bogiel, A., and Gadella, T. W. (2011). FRET microscopy: from principle to routine technology in cell biology. *J. Microsc.* 241, 111–118. doi: 10.1111/j.1365-2818.2010.03437.x

Ponka, P., Sheftel, A. D., and Zhang, A. S. (2002). Iron targeting to mitochondria in erythroid cells. *Biochem. Soc. Trans.* 30, 735–738. doi: 10.1042/bst0300735

Porter, K. R., and Palade, G. E. (1957). Studies on the endoplasmic reticulum. III. Its form and distribution in striated muscle cells. *J. Biophys. Biochem. Cytol.* 3, 269–300. doi: 10.1083/jcb.3.2.269

Poteser, M., Leitinger, G., Pritz, E., Platzer, D., Frischauf, I., Romanin, C., et al. (2016). Live-cell imaging of ER-PM contact architecture by a novel TIRFM approach reveals extension of junctions in response to store-operated Ca^{2+}-entry. *Sci. Rep.* 6:35656. doi: 10.1038/srep35656

Prinz, W. A. (2014). Bridging the gap: membrane contact sites in signaling, metabolism, and organelle dynamics. *J. Cell Biol.* 205, 759–769. doi: 10.1083/jcb.201401126

Prinz, W. A., Toulmay, A., and Balla, T. (2020). The functional universe of membrane contact sites. *Nat. Rev. Mol. Cell Biol.* 21, 7–24. doi: 10.1038/s41580-019-0180-9

Raiborg, C., Wenzel, E. M., Pedersen, N. M., Olsvik, H., Schink, K. O., Schultz, S. W., et al. (2015). Repeated ER-endosome contacts promote endosome translocation and neurite outgrowth. *Nature* 520, 234–238. doi: 10.1038/nature14359

Rainey, K. H., and Patterson, G. H. (2019). Photoswitching FRET to monitor protein-protein interactions. *Proc. Natl. Acad. Sci. U.S.A.* 116, 864–873. doi: 10.1073/pnas.1805333116

Rekas, A., Alattia, J. R., Nagai, T., Miyawaki, A., and Ikura, M. (2002). Crystal structure of venus, a yellow fluorescent protein with improved maturation and reduced environmental sensitivity. *J. Biol. Chem.* 277, 50573–50578. doi: 10.1074/jbc.M209524200

Rhee, H. W., Zou, P., Udeshi, N. D., Martell, J. D., Mootha, V. K., Carr, S. A., et al. (2013). Proteomic mapping of mitochondria in living cells via spatially restricted enzymatic tagging. *Science* 339, 1328–1331. doi: 10.1126/science.1230593

Rizzuto, R., Brini, M., De Giorgi, F., Rossi, R., Heim, R., Tsien, R. Y., et al. (1996). Double labelling of subcellular structures with organelle-targeted GFP mutants in vivo. *Curr. Biol.* 6, 183–188. doi: 10.1016/s0960-9822(02)00451-7

Rizzuto, R., Brini, M., Murgia, M., and Pozzan, T. (1993). Microdomains with high Ca^{2+} close to IP3-sensitive channels that are sensed by neighboring mitochondria. *Science* 262, 744–747. doi: 10.1126/science.8235595

Rizzuto, R., Pinton, P., Carrington, W., Fay, F. S., Fogarty, K. E., Lifshitz, L. M., et al. (1998). Close contacts with the endoplasmic reticulum as determinants of mitochondrial Ca2+ responses. *Science* 280, 1763–1766. doi: 10.1126/science.280.5370.1763

Robenek, H., Hofnagel, O., Buers, I., Robenek, M. J., Troyer, D., and Severs, N. J. (2006). Adipophilin-enriched domains in the ER membrane are sites of lipid droplet biogenesis. *J. Cell Sci.* 119(Pt 20), 4215–4224. doi: 10.1242/jcs.03191

Rocha, N., Kuijl, C., van der Kant, R., Janssen, L., Houben, D., Janssen, H., et al. (2009). Cholesterol sensor ORP1L contacts the ER protein VAP to control Rab7-RILP-p150 Glued and late endosome positioning. *J. Cell Biol.* 185, 1209–1225. doi: 10.1083/jcb.200811005

Romoser, V. A., Hinkle, P. M., and Persechini, A. (1997). Detection in living cells of Ca^{2+}-dependent changes in the fluorescence emission of an indicator composed of two green fluorescent protein variants linked by a calmodulin-binding sequence. A new class of fluorescent indicators. *J. Biol. Chem.* 272, 13270–13274. doi: 10.1074/jbc.272.20.13270

Rust, M. J., Bates, M., and Zhuang, X. (2006). Sub-diffraction-limit imaging by stochastic optical reconstruction microscopy (STORM). *Nat. Methods* 3, 793–795. doi: 10.1038/nmeth929

Schallmeiner, E., Oksanen, E., Ericsson, O., Spangberg, L., Eriksson, S., Stenman, U. H., et al. (2007). Sensitive protein detection via triple-binder proximity ligation assays. *Nat. Methods* 4, 135–137. doi: 10.1038/nmeth974

Schauder, C. M., Wu, X., Saheki, Y., Narayanaswamy, P., Torta, F., Wenk, M. R., et al. (2014). Structure of a lipid-bound extended synaptotagmin indicates a role in lipid transfer. *Nature* 510, 552–555. doi: 10.1038/nature13269

Schneider, J., Zahn, J., Maglione, M., Sigrist, S. J., Marquard, J., Chojnacki, J., et al. (2015). Ultrafast, temporally stochastic STED nanoscopy of millisecond dynamics. *Nat. Methods* 12, 827–830. doi: 10.1038/nmeth.3481

Schon, E. A., and Area-Gomez, E. (2013). Mitochondria-associated ER membranes in Alzheimer disease. *Mol. Cell. Neurosci.* 55, 26–36. doi: 10.1016/j.mcn.2012.07.011

Schrader, M., and Yoon, Y. (2007). Mitochondria and peroxisomes: are the 'big brother' and the 'little sister' closer than assumed? *Bioessays* 29, 1105–1114. doi: 10.1002/bies.20659

Schulz, O., Pieper, C., Clever, M., Pfaff, J., Ruhlandt, A., Kehlenbach, R. H., et al. (2013). Resolution doubling in fluorescence microscopy with confocal spinning-disk image scanning microscopy. *Proc. Natl. Acad. Sci. U.S.A.* 110, 21000–21005. doi: 10.1073/pnas.1315858110

Schweizer, A., Fransen, J. A., Bachi, T., Ginsel, L., and Hauri, H. P. (1988). Identification, by a monoclonal antibody, of a 53-kD protein associated with a tubulo-vesicular compartment at the cis-side of the Golgi apparatus. *J. Cell Biol.* 107, 1643–1653. doi: 10.1083/jcb.107.5.1643

Scorrano, L., De Matteis, M. A., Emr, S., Giordano, F., Hajnoczky, G., Kornmann, B., et al. (2019). Coming together to define membrane contact sites. *Nat. Commun.* 10:1287. doi: 10.1038/s41467-019-09253-3

Sekar, R. B., and Periasamy, A. (2003). Fluorescence resonance energy transfer (FRET) microscopy imaging of live cell protein localizations. *J. Cell Biol.* 160, 629–633. doi: 10.1083/jcb.200210140

Severs, N. J., Jordan, E. G., and Williamson, D. H. (1976). Nuclear pore absence from areas of close association between nucleus and vacuole in synchronous yeast cultures. *J. Ultrastruct. Res.* 54, 374–387. doi: 10.1016/s0022-5320(76)80023-8

Sezgin, E. (2017). Super-resolution optical microscopy for studying membrane structure and dynamics. *J. Phys. Condens. Matter.* 29:273001. doi: 10.1088/1361-648X/aa7185

Shai, N., Yifrach, E., van Roermund, C. W. T., Cohen, N., Bibi, C., IJlst, L., et al. (2018). Systematic mapping of contact sites reveals tethers and a function for the peroxisome-mitochondria contact. *Nat. Commun.* 9:1761. doi: 10.1038/s41467-018-03957-8

Shaner, N. C., Campbell, R. E., Steinbach, P. A., Giepmans, B. N., Palmer, A. E., and Tsien, R. Y. (2004). Improved monomeric red, orange and yellow fluorescent proteins derived from Discosoma sp. red fluorescent protein. *Nat. Biotechnol.* 22, 1567–1572. doi: 10.1038/nbt1037

Shekhawat, S. S., and Ghosh, I. (2011). Split-protein systems: beyond binary protein-protein interactions. *Curr. Opin. Chem. Biol.* 15, 789–797. doi: 10.1016/j.cbpa.2011.10.014

Shim, S. H., Xia, C., Zhong, G., Babcock, H. P., Vaughan, J. C., Huang, B., et al. (2012). Super-resolution fluorescence imaging of organelles in live cells with photoswitchable membrane probes. *Proc. Natl. Acad. Sci. U.S.A.* 109, 13978–13983. doi: 10.1073/pnas.1201882109

Snapp, E. L., Hegde, R. S., Francolini, M., Lombardo, F., Colombo, S., Pedrazzini, E., et al. (2003). Formation of stacked ER cisternae by low affinity protein interactions. *J. Cell Biol.* 163, 257–269. doi: 10.1083/jcb.200306020

Soderberg, O., Gullberg, M., Jarvius, M., Ridderstrale, K., Leuchowius, K. J., Jarvius, J., et al. (2006). Direct observation of individual endogenous protein complexes in situ by proximity ligation. *Nat. Methods* 3, 995–1000. doi: 10.1038/nmeth947

Soderberg, O., Leuchowius, K. J., Gullberg, M., Jarvius, M., Weibrecht, I., Larsson, L. G., et al. (2008). Characterizing proteins and their interactions in cells and tissues using the in situ proximity ligation assay. *Methods* 45, 227–232. doi: 10.1016/j.ymeth.2008.06.014

Stefan, C. J., Trimble, W. S., Grinstein, S., Drin, G., Reinisch, K., De Camilli, P., et al. (2017). Membrane dynamics and organelle biogenesis-lipid pipelines and vesicular carriers. *BMC Biol.* 15:102. doi: 10.1186/s12915-017-0432-0

Stoica, R., De Vos, K. J., Paillusson, S., Mueller, S., Sancho, R. M., Lau, K. F., et al. (2014). ER-mitochondria associations are regulated by the VAPB-PTPIP51 interaction and are disrupted by ALS/FTD-associated TDP-43. *Nat. Commun.* 5:3996. doi: 10.1038/ncomms4996

Stoica, R., Paillusson, S., Gomez-Suaga, P., Mitchell, J. C., Lau, D. H., Gray, E. H., et al. (2016). ALS/FTD-associated FUS activates GSK-3beta to disrupt the VAPB-PTPIP51 interaction and ER-mitochondria associations. *EMBO Rep.* 17, 1326–1342. doi: 10.15252/embr.201541726

Subedi, K. P., Ong, H. L., Son, G. Y., Liu, X., and Ambudkar, I. S. (2018). STIM2 Induces Activated Conformation of STIM1 to Control Orai1 Function in ER-PM Junctions. *Cell Rep.* 23, 522–534. doi: 10.1016/j.celrep.2018.03.065

Swayne, T. C., Zhou, C., Boldogh, I. R., Charalel, J. K., McFaline-Figueroa, J. R., Thoms, S., et al. (2011). Role for cER and Mmr1p in anchorage of mitochondria at sites of polarized surface growth in budding yeast. *Curr. Biol.* 21, 1994–1999. doi: 10.1016/j.cub.2011.10.019

Sydor, A. M., Czymmek, K. J., Puchner, E. M., and Mennella, V. (2015). Super-resolution microscopy: from single molecules to supramolecular assemblies. *Trends Cell Biol.* 25, 730–748. doi: 10.1016/j.tcb.2015.10.004

Szabadkai, G., Bianchi, K., Varnai, P., De Stefani, D., Wieckowski, M. R., Cavagna, D., et al. (2006). Chaperone-mediated coupling of endoplasmic reticulum and mitochondrial Ca^{2+} channels. *J. Cell Biol.* 175, 901–911. doi: 10.1083/jcb.200608073

Takeshima, H., Komazaki, S., Nishi, M., Iino, M., and Kangawa, K. (2000). Junctophilins: a novel family of junctional membrane complex proteins. *Mol. Cell* 6, 11–22. doi: 10.1016/s1097-2765(00)00003-4

Thomas, H. E., Zhang, Y., Stefely, J. A., Veiga, S. R., Thomas, G., Kozma, S. C., et al. (2018). Mitochondrial complex I activity is required for maximal autophagy. *Cell Rep.* 24, 2404–2417.e8. doi: 10.1016/j.celrep.2018.07.101

Toulmay, A., and Prinz, W. A. (2012). A conserved membrane-binding domain targets proteins to organelle contact sites. *J. Cell. Sci.* 125(Pt 1), 49–58. doi: 10.1242/jcs.085118

Tubbs, E., and Rieusset, J. (2016). Study of endoplasmic reticulum and mitochondria interactions by *in situ* proximity ligation assay in fixed cells. *J. Vis. Exp.* 118:54899. doi: 10.3791/54899

Valm, A. M., Cohen, S., Legant, W. R., Melunis, J., Hershberg, U., Wait, E., et al. (2017). Applying systems-level spectral imaging and analysis to reveal the organelle interactome. *Nature* 546, 162–167. doi: 10.1038/nature22369

van Vliet, A. R., Giordano, F., Gerlo, S., Segura, I., Van Eygen, S., Molenberghs, G., et al. (2017). The ER Stress Sensor PERK Coordinates ER-Plasma Membrane Contact Site Formation through Interaction with Filamin-A and F-Actin Remodeling. *Mo. Cell* 65 88, 885–899.e6. doi: 10.1016/j.molcel.2017.01.020

Vance, J. E., Stone, S. J., and Faust, J. R. (1997). Abnormalities in mitochondria-associated membranes and phospholipid biosynthetic enzymes in the mnd/mnd mouse model of neuronal ceroid lipofuscinosis. *Biochim. Biophys. Acta* 1344, 286–299. doi: 10.1016/s0005-2760(96)00153-1

Wang, H., Becuwe, M., Housden, B. E., Chitraju, C., Porras, A. J., Graham, M. M., et al. (2016). Seipin is required for converting nascent to mature lipid droplets. *eLife* 5:e16582. doi: 10.7554/eLife.16582

Wang, H., Sreenivasan, U., Hu, H., Saladino, A., Polster, B. M., Lund, L. M., et al. (2011). Perilipin 5, a lipid droplet-associated protein, provides physical and metabolic linkage to mitochondria. *J. Lipid Res.* 52, 2159–2168. doi: 10.1194/jlr.M017939

Wiens, M. D., and Campbell, R. E. (2018). Surveying the landscape of optogenetic methods for detection of protein-protein interactions. *Wiley Interdiscip. Rev. Syst. Biol. Med.* 10:e1415. doi: 10.1002/wsbm.1415

Wijdeven, R. H., Janssen, H., Nahidiazar, L., Janssen, L., Jalink, K., Berlin, I., et al. (2016). Cholesterol and ORP1L-mediated ER contact sites control autophagosome transport and fusion with the endocytic pathway. *Nat. Commun.* 7:11808. doi: 10.1038/ncomms11808

Wong, Y. C., Ysselstein, D., and Krainc, D. (2018). Mitochondria-lysosome contacts regulate mitochondrial fission via RAB7 GTP hydrolysis. *Nature* 554, 382–386. doi: 10.1038/nature25486

Wouters, F. S., Bastiaens, P. I., Wirtz, K. W., and Jovin, T. M. (1998). FRET microscopy demonstrates molecular association of non-specific lipid transfer protein (nsL-TP) with fatty acid oxidation enzymes in peroxisomes. *EMBO J.* 17, 7179–7189. doi: 10.1093/emboj/17.24.7179

Wu, Y., Whiteus, C., Xu, C. S., Hayworth, K. J., Weinberg, R. J., Hess, H. F., et al. (2017). Contacts between the endoplasmic reticulum and other membranes in neurons. *Proc. Natl. Acad. Sci. U.S.A.* 114, E4859–E4867. doi: 10.1073/pnas.1701078114

Xu, D., Li, Y., Wu, L., Li, Y., Zhao, D., Yu, J., et al. (2018). Rab18 promotes lipid droplet (LD) growth by tethering the ER to LDs through SNARE and NRZ interactions. *J. Cell Biol.* 217, 975–995. doi: 10.1083/jcb.201704184

Xu, N., Zhang, S. O., Cole, R. A., McKinney, S. A., Guo, F., Haas, J. T., et al. (2012). The FATP1-DGAT2 complex facilitates lipid droplet expansion at the ER-lipid droplet interface. *J. Cell Biol.* 198, 895–911. doi: 10.1083/jcb.201201139

Xue, M., Hou, J., Wang, L., Cheng, D., Lu, J., Zheng, L., et al. (2017). Optimizing the fragment complementation of APEX2 for detection of specific protein-protein interactions in live cells. *Sci. Rep.* 7:12039. doi: 10.1038/s41598-017-12365-9

Yamamoto, K., and Fahimi, H. D. (1987). Three-dimensional reconstruction of a peroxisomal reticulum in regenerating rat liver: evidence of interconnections between heterogeneous segments. *J. Cell Biol.* 105, 713–722. doi: 10.1083/jcb.105.2.713

Yang, Z., Zhao, X., Xu, J., Shang, W., and Tong, C. (2018). A novel fluorescent reporter detects plastic remodeling of mitochondria-ER contact sites. *J. Cell Sci.* 131:jcs208686. doi: 10.1242/jcs.208686

Youn, J. Y., Dunham, W. H., Hong, S. J., Knight, J. D. R., Bashkurov, M., Chen, G. I., et al. (2018). High-density proximity mapping reveals the subcellular organization of mRNA-associated granules and bodies. *Mol. Cell* 69, 517–532.e11. doi: 10.1016/j.molcel.2017.12.020

Zhanghao, K., Chen, X., Liu, W., Li, M., Liu, Y., Wang, Y., et al. (2019). Super-resolution imaging of fluorescent dipoles via polarized structured illumination microscopy. *Nat. Commun.* 10:4694. doi: 10.1038/s41467-019-12681-w

Zimmer, M. (2002). Green fluorescent protein (GFP): applications, structure, and related photophysical behavior. *Chem. Rev.* 102, 759–781.

Conflict of Interest: The authors declare that the research was conducted in the absence of any commercial or financial relationships that could be construed as a potential conflict of interest.

frontiers in Cell and Developmental Biology

ORIGINAL RESEARCH
published: 07 April 2020
doi: 10.3389/fcell.2020.00221

Mitochondrial Fusion Machinery Specifically Involved in Energy Deprivation-Induced Autophagy

Choufei Wu[1†], Weijing Yao[2†], Wenwen Kai[1], Weikang Liu[2], Wenlve Wang[2], Shuzhen Li[2], Yingcong Chen[2], Xiaoyong Wu[2], Liefeng Wang[3], Ying Li[4], Jingjing Tong[5], Jing Qian[6], Liqin Zhang[1], Zhi Hong[7,8] and Cong Yi[2]**

[1] Key Laboratory of Vector Biology and Pathogen Control of Zhejiang Province, School of Life Sciences, Huzhou University, Huzhou, China, [2] Department of Biochemistry, Hepatobiliary and Pancreatic Surgery, The First Affiliated Hospital, Zhejiang University School of Medicine, Hangzhou, China, [3] Key Laboratory of Prevention and Treatment of Cardiovascular and Cerebrovascular Diseases, Ministry of Education, Gannan Medical University, Ganzhou, China, [4] School of Life Sciences, Tsinghua University-Peking University Joint Center for Life Sciences, Tsinghua University, Beijing, China, [5] School of Life Sciences, Central China Normal University, Wuhan, China, [6] Key Laboratory of Vector Biology and Pathogen Control of Zhejiang Province, School of Nursing and Medicine, Huzhou University, Huzhou, China, [7] Department of Breast Surgery, The Second Affiliated Hospital, Zhejiang University School of Medicine, Zhejiang University, Hangzhou, China, [8] ZJU-UoE Institute, Zhejiang University School of Medicine, International Campus, Zhejiang University, Haining, China*

OPEN ACCESS

Edited by:
Du Feng,
Guangzhou Medical University, China

Reviewed by:
Chunxin Wang,
National Institutes of Health (NIH), United States
Kang Dongchon,
Kyushu University, Japan
Takeshi Kaizuka,
RIKEN Brain Science Institute (BSI), Japan

***Correspondence:**
Zhi Hong
zhihong@intl.zju.edu.cn
Cong Yi
yiconglab@zju.edu.cn

[†]These authors share first authorship

Specialty section:
This article was submitted to Membrane Traffic, a section of the journal Frontiers in Cell and Developmental Biology

Received: *28 January 2020*
Accepted: *16 March 2020*
Published: *07 April 2020*

Citation:
Wu C, Yao W, Kai W, Liu W, Wang W, Li S, Chen Y, Wu X, Wang L, Li Y, Tong J, Qian J, Zhang L, Hong Z and Yi C (2020) Mitochondrial Fusion Machinery Specifically Involved in Energy Deprivation-Induced Autophagy. Front. Cell Dev. Biol. 8:221. doi: 10.3389/fcell.2020.00221

Mitochondria are highly dynamic organelles, which can form a network in cells through fusion, fission, and tubulation. Its morphology is closely related to the function of mitochondria. The damaged mitochondria can be removed by mitophagy. However, the relationship between mitochondrial morphology and non-selective autophagy is not fully understood. We found that mitochondrial fusion machinery, not fission or tubulation machinery, is essential for energy deprivation-induced autophagy. In response to glucose starvation, deletion of mitochondrial fusion proteins severely impaired the association of Atg1/ULK1 with Atg13, and then affected the recruitment of Atg1 and other autophagic proteins to PAS (phagophore assembly site). Furthermore, the deletion of fusion proteins blocks mitochondrial respiration, the binding of Snf1-Mec1, the phosphorylation of Mec1 by Snf1, and the dissociation of Mec1 from mitochondria under prolonged starvation. We propose that mitochondrial fusion machinery regulates energy deprivation-induced autophagy through maintaining mitochondrial respiration.

Keywords: mitochondrial morphology, fusion machinery, mitochondrial respiration, autophagy, glucose starvation

INTRODUCTION

Autophagy is a highly conserved material degradation pathway from yeast to human. It can degrade long-lived proteins, damaged organelles, aggregates, lipid droplets, and RNA, etc (Ohsumi, 2014). In the process of autophagy, a double-layer membrane structure envelops these substances to form autophagosome. Subsequently, autophagosome enters lysosomes/vacuoles through fusion. Finally, these substances are degraded by acid hydrolase in lysosomes/vacuoles (Shibutani and Yoshimori, 2014). Based on different degradation substrates, autophagy can be classified into non-selective autophagy and selective autophagy. Non-selective autophagy is usually also called as autophagy/macroautophagy, which has no selectivity for degradation substrates. Selective autophagy is mediated by specific autophagy receptors. Currently, selective autophagy includes

mitophagy, ER-phagy, pexophagy, and ribophagy, etc (Feng et al., 2014). Dysfunction of autophagy is closely related to the occurrence and development of many diseases that are harmful to human health (Zhao and Zhang, 2019).

Mitochondria are multifunctional organelles, which play a key role in cell activities and development, including ATP synthesis, iron and calcium homeostasis, programmed cell death, ROS generation, and fatty acid β-oxidation (Wu et al., 2016). These functions of mitochondria are closely related to the morphology of mitochondria. In eukaryotes, mitochondria form a dynamic tubular networks of continuous movement and interaction with other organelles. This dynamic network is mainly regulated by mitochondrial fusion, fission, and tubulation machinery (Okamoto and Shaw, 2005). In yeast, mitochondrial fusion machinery is composed of Fzo1, Ugo1, Mgm1, and Pcp1. Fzo1 is the evolutionary conserved GTPase, which locates in the outer membrane of mitochondria. Its N-terminus and C-terminus are both facing the cytoplasm, where N-terminus contains GTPase domain, and C-terminus interacts with Ugo1 protein. Mgm1, a second GTPase required for mitochondrial fusion, which locates in the inner membrane of mitochondria. Ugo1 protein acts as the adaptor to connect Mgm1 and Fzo1. When fusion is blocked, mitochondria are distributed as dots in cells (Westermann, 2008). Mitochondrial fission machinery is composed of Dnm1, Fis1, Caf4, and Mdv1. Dnm1 is also the conserved dynamin-related GTPase essential for mitochondrial fission and inheritance, which is localized on mitochondria by interacting with Mdv1 and Caf4. Fis1 mediates mitochondrial localization of Mdv1 on the outer membrane. When fission is blocked, mitochondria form interconnected networks (Schauss et al., 2006). Mitochondrial tubulation machinery is composed of Mmm1, Mmm2, Mdm10, Mdm12, Mdm20, Mdm31, and Mdm32, which plays an important role in the actin-mitochondria attachment, formation of tubular mitochondria and anchoring of mtDNA nucleoids. When tubulation pathway is impaired, mitochondria are changed to large spheres (Okamoto and Shaw, 2005). In addition, proteins like Mdm33 and Gem1, it is not known what their molecular mechanism is, but their deletion severely affected the morphology of mitochondria (Dimmer et al., 2002; Frederick et al., 2004). The change of mitochondrial morphology is closely related to aging, programmed cell death, autosomal dominant optic atrophy, charcot-marie-tooth neurophathy type 2A, and neuronal cell function (Alexander et al., 2000; Danial and Korsmeyer, 2004; Li et al., 2004; Kijima et al., 2005; Kauppila et al., 2017).

Recently, more and more attention has been paid to research on the relationship between autophagy and mitochondria. Mostly studied is the role and molecular mechanism of mitophagy in the process of mitochondrial quality control (Kanki and Klionsky, 2010; Montava-Garriga and Ganley, 2020). Mitochondrial damage and nitrogen starvation can induce mitophagy (Kanki et al., 2009; Okamoto et al., 2009). In yeast, Atg32, a receptor protein of mitophagy, mediates the removal of damaged mitochondria, and mitochondrial fission machinery facilitates mitophagy (Kanki et al., 2009; Okamoto et al., 2009). Nitrogen starvation-induced autophagy is involved in the determination of mtDNA copy number (Medeiros et al., 2018). Our previous study showed that mitochondrial oxidative respiratory chain participates in energy deficient-induced autophagy (Yi et al., 2017). In mammals, the mitophagy receptors FUNDC1, NIX, PINK1/Parkin, and BNIP3, directly interact with LC3 through different signaling pathways under different mitochondrial stress to transport damaged mitochondria to lysosomes for clearance (Wei et al., 2015). Mitochondria also supply membrane source for autophagosome formation during serum starvation; the disruption of mitochondria/ER can block autophagosome biogenesis (Hailey et al., 2010). However, the relationship of mitochondria morphology and non-selective autophagy is not well understood.

In this study, we found mitochondria fusion machinery is involved in initiation of glucose starvation-induced autophagy, by revealing the strong link between mitochondrial fusion machinery and mitochondrial respiration, the association of Snf1 with Mec1, the phosphorylation of Mec1 by Snf1, the recruitment of Atg1/ULK1 and other autophagic proteins to PAS, and the dissociation of Mec1 from mitochondria under glucose starvation condition. We propose mitochondrial fusion protein regulates energy deprivation-induced autophagy through maintaining mitochondrial respiration.

RESULTS

Mitochondrial Fusion Machinery Is Essential for Glucose Starvation-Induced Autophagy

To know whether mitochondrial fission, fusion, and tubulation machinery are required for autophagy, we knocked out fission/fusion/tubulation genes and analyzed GFP-Atg8 processing in glucose starvation medium (SD-G) and nitrogen starvation medium (SD-N). The principle of GFP-Atg8 assay is that GFP-Atg8 is encapsulated into autophagosome during autophagy process, and then autophagosome fused with vacuole. GFP-Atg8 is degraded by the acid hydrolase in the vacuole, as GFP is relatively stable in acid environment, the efficiency of autophagy can be judged by detecting the amount of free GFP (Sesaki and Jensen, 1999). As shown in **Figures 1A,B**, we knocked out mitochondrial fission machinery genes *FIS1*, *DNM1*, *CAF4*, and *MDV1*, respectively. Under either nitrogen starvation or glucose starvation, there is no significant difference in the cleavage of GFP-Atg8 compared with wild type, indicating that mitochondrial fission machinery is not involved in autophagy induced by nitrogen starvation and glucose starvation. Subsequently, we deleted the fusion machinery genes of mitochondria: *MGM1*, *PCP1*, *UGO1*, and *FZO1*, GFP-Atg8 processing assay showed that the fusion machinery of mitochondria doesn't affect the cleavage of GFP-Atg8 under nitrogen starvation, but completely blocked GFP-Atg8 processing under glucose starvation (**Figures 1C,D**). Furthermore, we knocked out *MDM33*, *GEM1,* and the tubulation machinery genes of mitochondria: *MDM20*, *MDM31*, and *MDM32*, same as mitochondria fission and fusion genes depleted cells, deletion of these genes did not affect nitrogen

starvation-induced autophagy. Under glucose starvation, deletion of *MDM32* and *MDM33* slightly impaired the cleavage of GFP-Atg8, while deletion of other genes has no effect on glucose starvation-induced autophagy (**Figures 1E,F**). Together, these results indicated that mitochondrial fusion machinery is specifically essential for glucose starvation-induced autophagy.

Mitochondrial Fusion Machinery Regulates the Recruitment of Atg1 and Other Autophagic Proteins to PAS and the Association of Atg1 With Atg13 Under Glucose Starvation

Next, to study which steps during autophagy is mitochondria fusion machinery involved upon glucose starvation, we knocked out *FZO1* and *UGO1* genes, respectively, in yeast strain co-expressing PAS marker Atg17-2XCherry and other autophagy-related proteins labeled with 2XGFP. In yeast cells, Atg17/FIP200, Atg31, and Atg29 proteins form a stable complex independent of nutritional status. Atg1, Atg11, and Atg13 form polymer complex with Atg17-Atg31-Atg29 as a platform for the recruitment of other ATG proteins (Araki et al., 2017). As shown in **Supplementary Figures S1A,B,** under nitrogen starvation and glucose starvation, Atg17 protein appears as puncta in the *fzo1*Δ and *ugo1*Δ yeast strain, indicating that mitochondrial fusion machinery is not involved in PAS formation. Consistently, Atg11 and Atg13 proteins form puncta and co-localize with Atg17 protein in *fzo1*Δ and *ugo1*Δ yeast strains upon glucose starvation (**Supplementary Figures S1A–E**). Next, we tested the localization of Atg1 protein. Image data showed that the localization of Atg1 protein dispersed well in the *fzo1*Δ and *ugo1*Δ yeast strains upon glucose starvation. In contrast, Atg1 proteins retained puncta formation despite of *FZO1* and *UGO1* knockout in response to nitrogen starvation (**Figures 2A–C**). Furthermore, immunoprecipitation experiments also showed glucose starvation did not increase the association of Atg1 with Atg13 in *fzo1*Δ and *ugo1*Δ yeast strains (**Figure 2D**). Using the same approach, Atg2 and Atg5 became diffused in the *fzo1*Δ and *ugo1*Δ yeast strains upon glucose starvation while remained unaltered upon nitrogen starvation (**Figures 2C,E–H**). Thus, we concluded that mitochondrial fusion machinery is involved in the recruitment of Atg1 protein to PAS, thus enhancing the recruitment of other proteins to PAS to initiate glucose starvation-induced autophagy.

Mitochondrial Fusion Proteins Are Required for Mitochondria Respiration and Snf1-Mec1 Association

Our previous report that mitochondrial oxidative respiratory chain-related gene depletion impairs the binding of Atg1–Atg13 through mediating phosphorylation of Mec1 by Snf1 under energy deficiency condition, prompts us to test whether mitochondrial fusion machinery is also involved in the regulation of mitochondrial respiration (Yi et al., 2017). We next performed in-depth bioenergetic studies of mitochondria using O2K for real-time monitoring of mitochondrial oxygen consumption in mitochondrion fusion, fission and tubulation machinery genes deleted yeast strains. As shown in **Figure 3A**, the aerobic respiration kept at a high level in wild-type yeast cells under full medium, while decreased but remained at a certain level upon nitrogen and glucose starvation. However, in *fzo1*Δ, *mgm1*Δ, *ugo1*Δ, and *pcp1*Δ yeast strains, which mitochondrial fusion is defected, the aerobic respiration decreased significantly under full medium, and almost completely abolished upon glucose starvation. In mitochondrial fission and tubulation-related genes deleted yeast strains, the oxygen consumption rate of mitochondria under full medium and nitrogen starvation condition had no significant change compared with wild type, while the oxygen consumption rate under glucose starvation decreased, but maintained a certain rate. These data suggested that mitochondrial fusion machinery is involved in the regulation of mitochondrial respiration.

To investigate whether the absence of fusion machinery leads to the loss of aerobic respiration by changing mitochondrial morphology, we made fission and fusion double mutant for analysis. Previous study reported that depletion of both fission and fusion genes can rescue the mitochondrial morphological changes caused by the deletion of fusion machinery genes (Sesaki and Jensen, 1999). Consistent with previous study, our image data showed that in the double knockout yeast strains, *dnm1*Δ *fzo1*Δ and *fis1*Δ *fzo1*Δ, mitochondria can be restored to a wild type-like morphology (**Supplementary Figure S2**). Subsequently, we analyzed mitochondrial oxygen consumption rate, and found that it was completely suppressed in *dnm1*Δ *fzo1*Δ and *fis1*Δ *fzo1*Δ mutants under glucose starvation (**Figure 3B**). We also tested whether glucose starvation-induced autophagy is affected in double knockout strains. As shown in **Figure 3C**, glucose starvation-induced autophagy was blocked in these mutants. Thus, we concluded that the inhibition of mitochondrial aerobic respiration is not due to the morphological changes of mitochondria caused by the absence of fusion machinery.

Next, we tested whether Snf1-phosphorylated Mec1 was affected by the absence of mitochondrial fusion machinery. The phosphorylation of Mec1 by Snf1 can be detected by anti-phospho-(Ser/Thr) AMPK substrate (P-S/T2-102) antibody (Yi et al., 2017). Consistent with our previous results, aerobic respiratory deficiency caused by the absence of mitochondrial fusion machinery resulted in the inability of Snf1 to phosphorylate Mec1 under glucose starvation (**Figure 3D**; Yi et al., 2017). To clarify the underlying molecular mechanism, Snf1 activity was detected under the condition of energy deficiency. As shown in **Figures 3E,F**, the same as wild type, phosphorylation level of Snf1 under glucose starvation was significantly increased in mitochondrial fusion machinery gene deleted yeast strains, indicating that upon glucose starvation, mitochondrial fusion machinery did not participate in the activation of Snf1. Subsequently, immunoprecipitation assay was carried out for testing Snf1-Mec1 association in full medium and SD-G, the results showed that the interaction between Snf1 and Mec1 significantly decreased in *fzo1*Δ, *ugo1*Δ, and *mgm1*Δ yeast strains in full medium (**Figure 3G**). Combined with the results above, we concluded that mitochondrial fusion machinery is required for the binding of Snf1 and Mec1 through participating

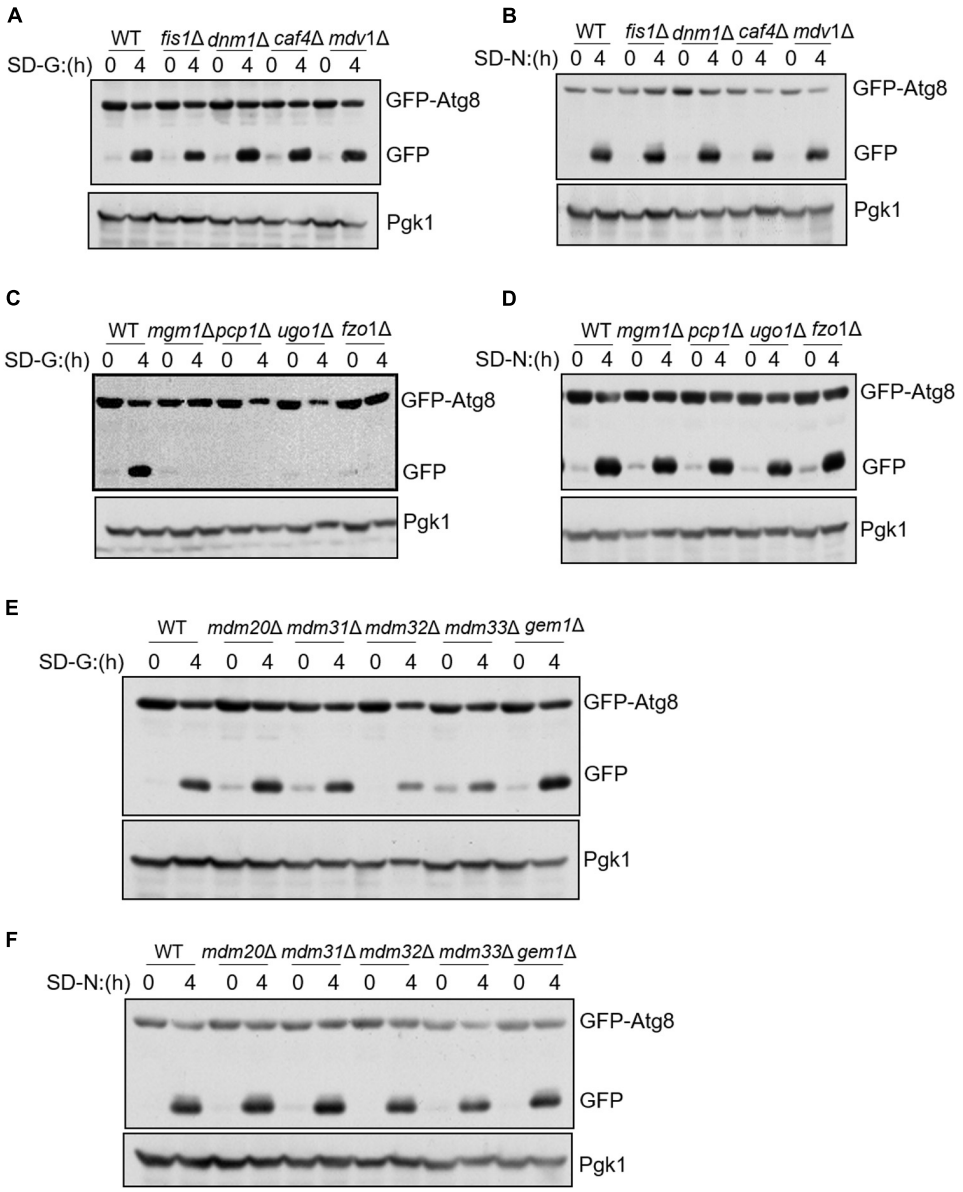

FIGURE 1 | Mitochondrial fusion machinery is specifically involved in glucose starvation-induced autophagy. GFP-Atg8 plasmids were expressed in yeast strains accordingly listed from **(A–F)**. Yeast cells were grown to the log-growth phase, then subjected to glucose starvation (SD-G) or nitrogen starvation (SD-N) for 4 h. Autophagic activity was detected by western blot using anti-GFP antibody.

in mitochondrial aerobic respiration, thus regulating the phosphorylation of Snf1 on Mec1, resulting in recruitment of Atg1 and other autophagic proteins to PAS to initiate autophagy under glucose starvation condition.

Mitochondrial Fusion Machinery Is Required for the Dissociation of Mec1 From Mitochondria During Prolonged Glucose Starvation

In the early stage of glucose starvation, recruitment of Mec1 to mitochondria is crucial for its phosphorylation by Snf1. And with prolonged starvation, Mec1 dissociates from mitochondria (Yi et al., 2017). To explore whether mitochondrial fusion machinery is involved in the dissociation of Mec1 from mitochondria, we knocked out fusion genes *FZO1*, *UGO1*, and fission gene *FIS1* in yeast cells co-expressing mitochondrial marker Om45-Cherry and GFP-Mec1, respectively. Image data showed that upon 4 h of glucose starvation, Mec1 dissociates from mitochondria in wild type and *fis1*Δ yeast cells (**Figure 4A** and **Supplementary Figure S3**). In contrast, knockout of *FZO1* and *UGO1* greatly inhibited the dissociation of Mec1 from mitochondria (**Figure 4A**). Statistical analysis indicated that Mec1 puncta was still

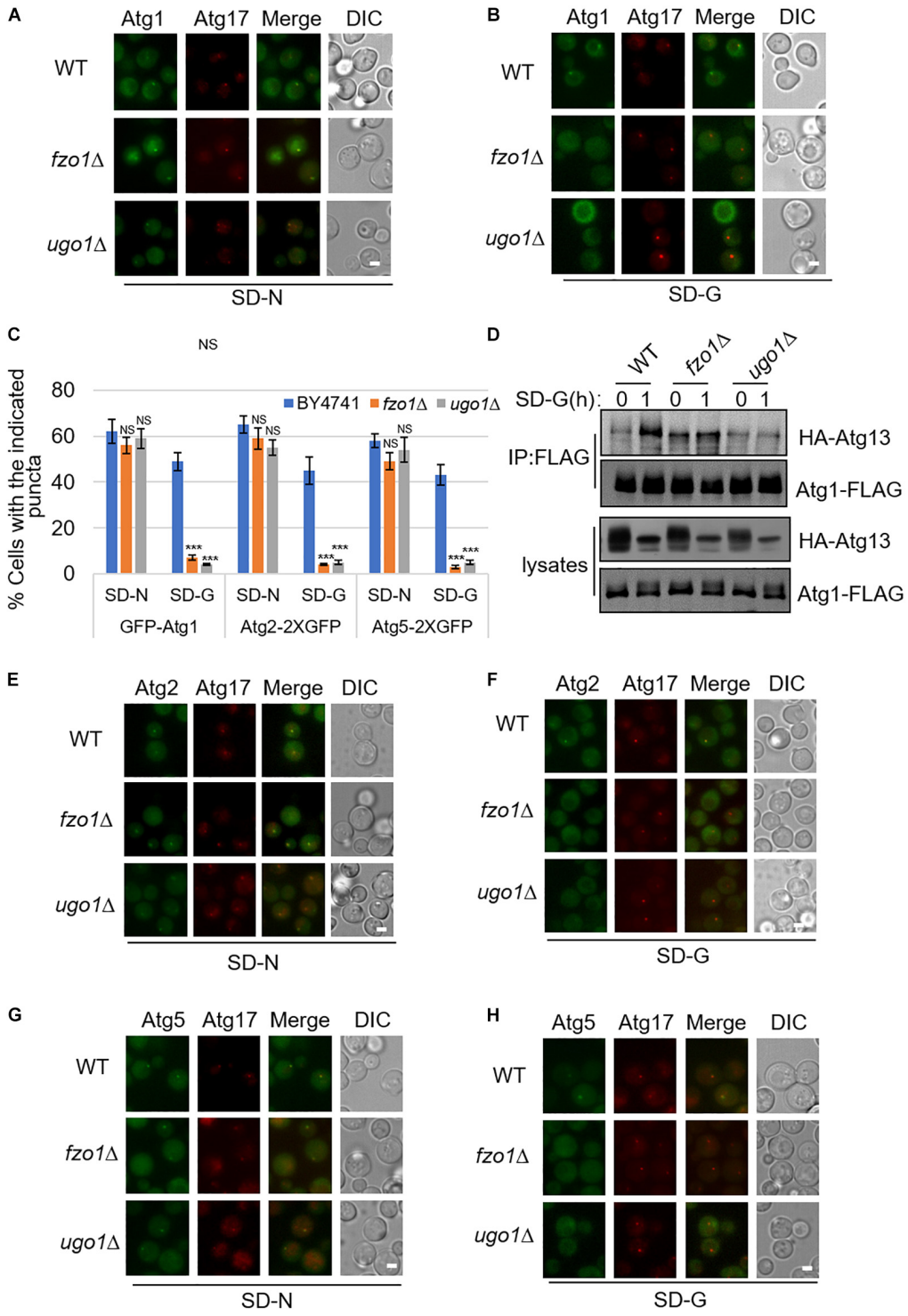

FIGURE 2 | The recruitment of Atg1, Atg2, and Atg5 to PAS is regulated by mitochondrial fusion machinery upon glucose starvation. **(A,B)** GFP-Atg1 and Atg17-2XCherry were co-expressed in wild type (WT), *fzo1*Δ, and *ugo1*Δ yeast strains. Yeast cells were grown to the log-growth phase, then subjected to SD-N and SD-G for 1 h. Cells were imaged by fluorescence inverted microscope. Scale bar, 2 μm. **(C)** Strains from **(A**,**B**,**E–H)** were analyzed for the number of cells with the indicated puncta. $n = 300$ cells pooled from three independent experiments. Data are presented as means ± SD. ***$p < 0.001$; NS, not significant; two-tailed Student's *t*-tests were used. **(D)** Wild type (WT), *fzo1*Δ, and *ugo1*Δ yeast cells co-expressing HA-Atg13 and Atg1-3XFLAG were subjected to SD-G for 0 and 1 h. Cell lysates were immunoprecipitated with anti-FLAG agarose beads and then analyzed by western blot using anti-HA antibody. **(E–H)** Atg2-2XGFP or Atg5-2XGFP and Atg17-2XCherry were co-expressed in the wild type (WT), *fzo1*Δ, and *ugo1*Δ yeast strains. Yeast cells were grown to the log-growth phase, then were starved in SD-N and SD-G medium for 1 h. Cells were viewed by fluorescence inverted microscope. Scale bar, 2 μm.

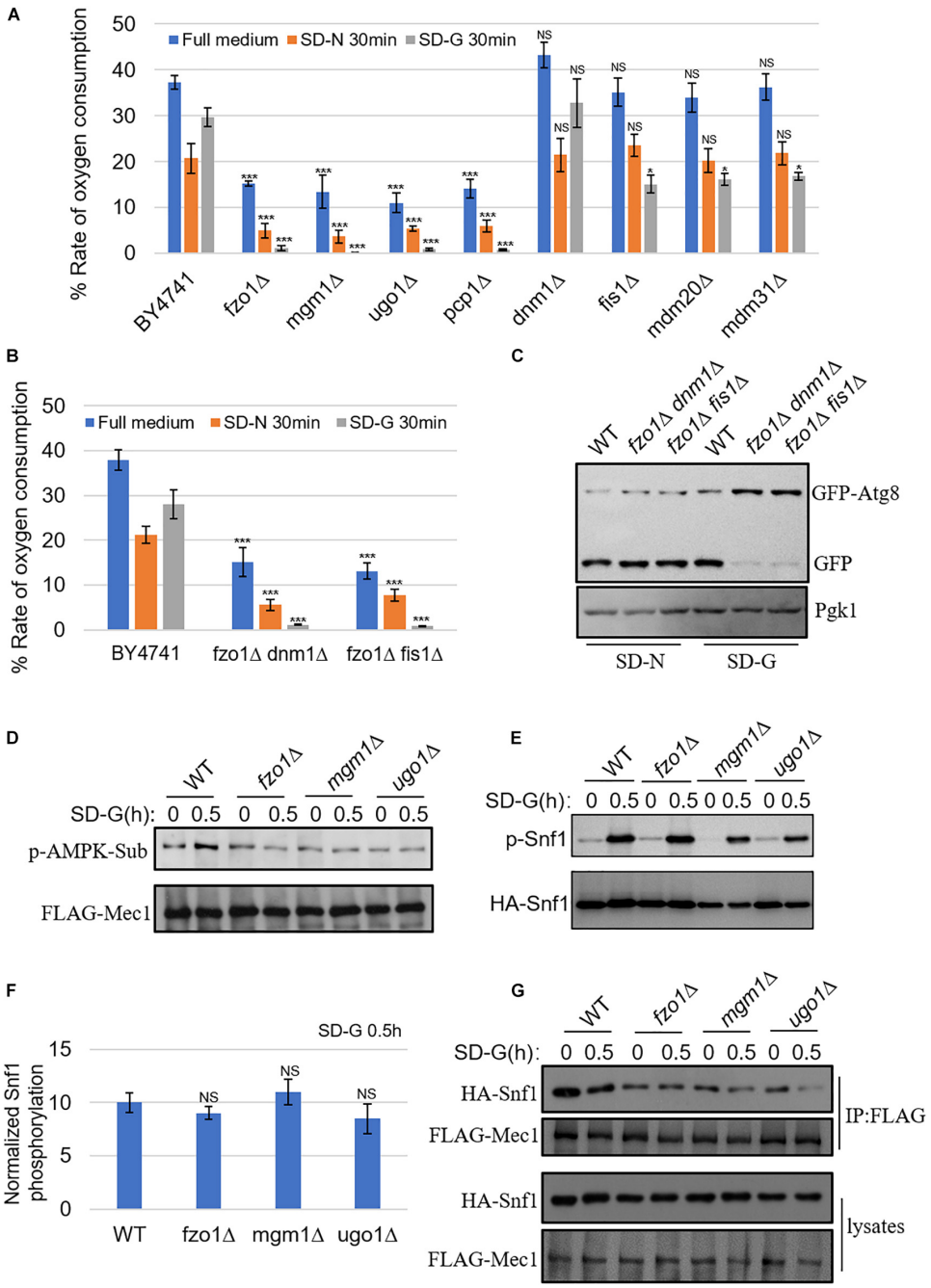

FIGURE 3 | Mitochondrial fusion machinery regulates aerobic respiration of mitochondria and the association of Mec1 with Snf1 upon glucose starvation. **(A)** WT (BY4741), *fzo1*Δ, *mgm1*Δ, *ugo1*Δ, *pcp1*Δ, *dnm1*Δ, *fis1*Δ, *mdm20*Δ, *and mdm31*Δ strains were cultured in SD-N or SD-G for 0 and 30 min. Cells were harvested and oxygen consumption was measured using O2K. $n = 3$ independent experiments were quantified. Data are presented as means ± SD. $^{***}p < 0.001$; $^{*}p < 0.05$; NS, not significant; two-tailed Student's *t*-tests were used. **(B)** WT (BY4741), *fzo1*Δ *dnm1*Δ, and *fzo1*Δ *fis1*Δ strains were starved in SD-N or SD-G for 0 and 30 min. Cells were harvested and oxygen consumption rate was measured using O2K. $n = 3$ independent experiments were quantified. Data are presented as means ± SD. $^{***}p < 0.001$; two-tailed Student's *t*-tests were used. **(C)** GFP-Atg8 plasmids were expressed in WT (BY4741), *fzo1*Δ *dnm1*Δ, and *fzo1*Δ *fis1*Δ strains. Cells were subjected to SD-G or SD-N for 4 h. Autophagic activity was detected by western blot using anti-GFP antibody. **(D)** FLAG-Mec1 was expressed in the yeast strains listed from Wild type (WT), *fzo1*Δ, *mgm1*Δ *and ugo1*Δ. Yeast cells were grown to the log-growth phase, then subjected to glucose starvation (SD-G) for 0 and 0.5 h. Phosphorylation of immunoprecipitated FLAG-Mec1 was detected by immunoblotting with phospho-(Ser/Thr) AMPK substrate antibody. **(E)** HA-Snf1 was expressed in Wild type (WT), *fzo1*Δ, *mgm1*Δ, and *ugo1*Δ yeast strains. Yeast cells were cultured in glucose starvation (SD-G) for 0 and 0.5 h. The kinase activity of Snf1 was detected by immunoblotting with anti-p-PRKAA/AMPKα (Thr172) antibody. **(F)** Quantification of the ratio of p-Snf1/HA-Snf1 from **(E)** by ImageJ software. NS, not significant; two-tailed Student's *t*-tests were used. **(G)** FLAG-Mec1 and HA-Snf1 were co-expressed in Wild type (WT), *fzo1*Δ, *mgm1*Δ and *ugo1*Δ yeast strains. Yeast cells were cultured in glucose starvation (SD-G) for 0 and 0.5 h. Cell lysates were immunoprecipitated with anti-FLAG agarose beads and then analyzed by western blot using the indicated antibody.

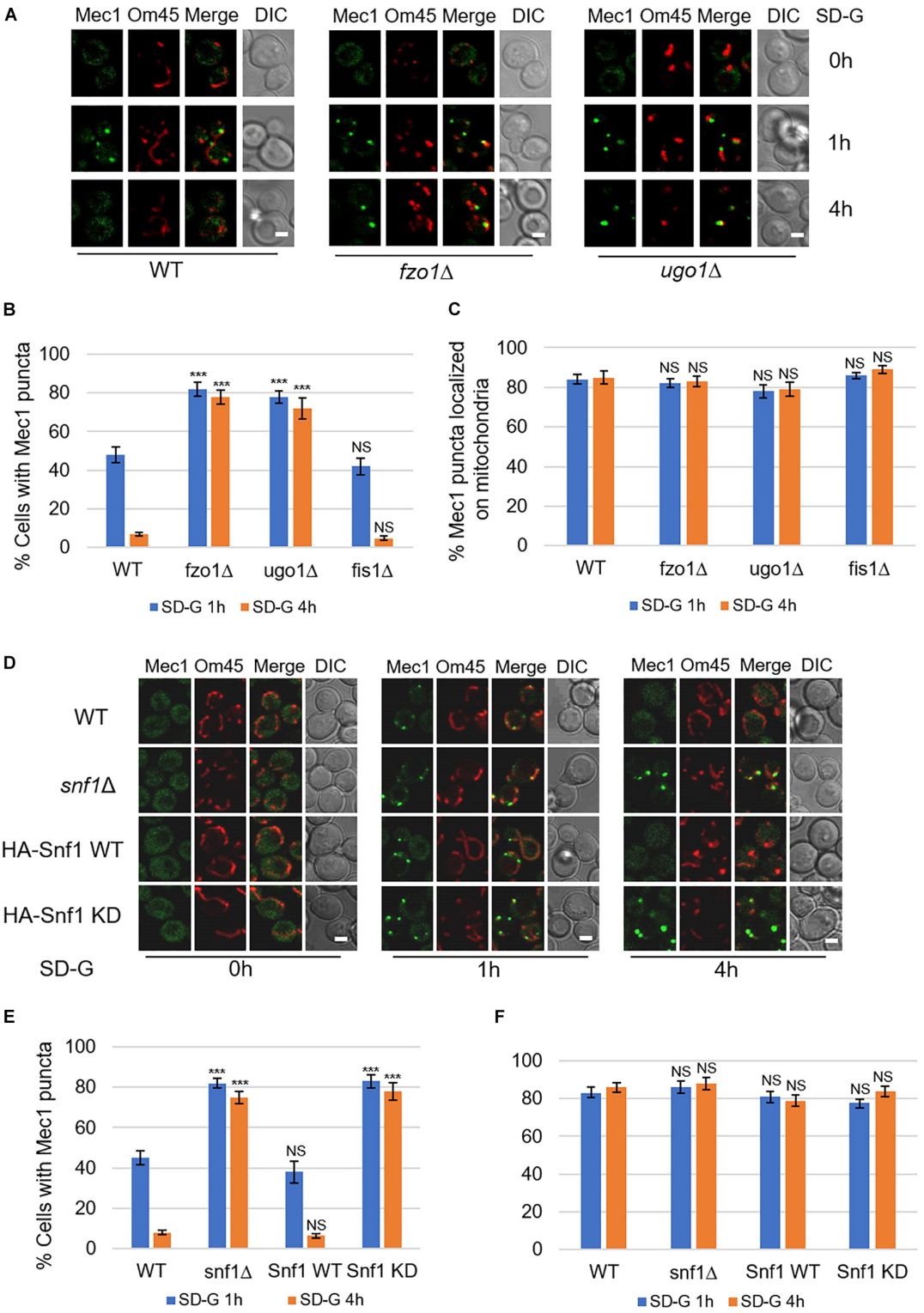

FIGURE 4 | Mitochondrial fusion machinery is required for the dissociation of Mec1 from mitochondria during prolonged starvation. **(A,D)** Co-expression of GFP-Mec1 and Om45-Cherry were expressed in the indicated yeast strains. Cells were cultured in SD-G medium for 0, 1, and 4 h, and then viewed by laser confocal microscopy. Scale bar, 2 μm. **(B,E)** Strains from **(A,D)** were analyzed for the number of cells with Mec1 puncta. $n = 300$ cells pooled from three independent experiments. Data are presented as means ± SD. $^{***}p < 0.001$; NS, not significant; two-tailed Student's *t*-tests were used. **(C,F)** Quantification of mitochondrial GFP-Mec1 puncta in cells from **(A,D)**. Mec1 puncta were examined in 300 cells pooled from three independent experiments. Data are presented as means ± SD. NS, not significant; two-tailed Student's *t*-tests were used.

mostly associated with mitochondria under prolonged glucose starvation (**Figures 4B,C**).

Based on the fact that mitochondrial fusion machinery is involved in the phosphorylation of Mec1 by Snf1, we speculated that the kinase activity of Snf1 is important in the dissociation of Mec1 from mitochondria. To test this possibility, we knocked out *SNF1* in the wild-type co-expressing Om45-Cherry and GFP-Mec1 yeast cells, and then re-introduced empty vector, Snf1 wild-type, Snf1 kinase dead plasmid into *snf1*Δ yeast cells. Image data showed that empty vector and Snf1 kinase-dead greatly inhibit the dissociation of Mec1 from mitochondria, while Snf1 wild-type plasmid rescued this phenotype (**Figures 4D–F**). Thus, the dissociation of Mec1 from mitochondria during prolonged glucose starvation is regulated by the kinase activity of Snf1 and mitochondria fusion machinery.

Glucose Starvation Does Not Induce Mitophagy

Next, to investigate autophagy level induced by energy deficiency, we compared autophagy under SD-N and SD-G by ALP assay (Araki et al., 2017). As shown in **Figure 5A**, the ALP activity under nitrogen starvation is about two times higher than that of under glucose starvation, indicating the intensity of autophagy induced by glucose starvation is weaker than that by nitrogen starvation. *ATG5* and *ATG17* knockout completely inhibited the increase of ALP activity, suggesting that Atg5 and Atg17 are essential for glucose starvation-induced autophagy. To clarify the existence of autophagosome in vacuole, electron microscopy experiments were carried out on *pep4*Δ yeast cells under glucose starvation condition (Epple et al., 2001; Kabeya et al., 2009). As shown in **Figures 5B,C**, there were more than 10 autophagosomes per vacuole after 4 h of glucose starvation, further suggesting that glucose starvation can indeed induce autophagy.

The fusion machinery of mitochondria specifically essential for energy deficiency -induced autophagy prompts us to test whether mitophagy can be induced upon energy deprivation. We selected three mitochondrial proteins: Atp5, mitochondrial inner membrane protein; Om45 and Alo1, mitochondrial outer membrane protein (Yaffe et al., 1989; Boyer, 1997; Sickmann et al., 2003). Image data showed that Om45, Atp5, and Alo1 did not enter the vacuole after 8 and 16 h of glucose starvation (**Figures 5D–F** and **Supplementary Figure S4A**). Subsequently, we knocked out autophagy essential genes *ATG1*, *ATG3*, *ATG12*, and mitophagy receptor gene *ATG32* to detect the degradation of endogenous mitochondrial protein Porin. Western blot results showed that in the wild type yeast strain, glucose starvation induces the cleavage of GFP-Atg8, but Porin is not degraded by autophagy at the indicated time point. Inhibition of autophagy and mitophagy did not lead to the accumulation of Porin (**Figure 5G** and **Supplementary Figure S4B**). Furthermore, we investigated two GFP-labeled mitochondrial proteins Idh1 and Idh2, which are usually used as the substrate of mitophagy in yeast (Wu and Tu, 2011). Western blot results showed that Idh1-GFP and Idh2-GFP can be cleavaged by nitrogen starvation, not by glucose starvation-induced autophagy (**Figure 5H**). Taken together, these results indicated that glucose starvation does not induce mitophagy, although mitochondria plays an important role in the initiation of energy deficiency-induced autophagy.

DISCUSSION

In this study, the relationship between mitochondrial fusion machinery and energy deficiency-induced autophagy has been fully elucidated. Our findings suggested that mitochondrial fusion machinery is essential for energy deficiency-induced autophagy. Deletion of mitochondrial fusion machinery genes significantly impaired the recruitment of autophagy proteins Atg1 and other autophagic proteins to PAS, mitochondrial aerobic respiration, the association of Snf1 with Mec1, phosphorylation of Mec1 by Snf1, and the disassociation of Mec1 from mitochondria. Despite mitochondrial fusion machinery is required for energy deficiency-induced autophagy, glucose starvation did not induce mitophagy. These results strongly suggested that autophagy induced by energy deficiency has its unique signaling pathway and molecular regulatory mechanism.

The fusion, fission and tubulation of mitochondria constitutes a highly dynamic network structure of mitochondria. The morphology of mitochondria is crucial for maintaining its own quality and quantity (Okamoto and Shaw, 2005). Our previous results showed that mitochondrial aerobic respiration is involved in the phosphorylation of Mec1 by Snf1, while phosphorylated Mec1 promoted the binding of Atg1 and Atg13 under glucose starvation (Yi et al., 2017). Oxygen consumption assay showed that only mitochondrial fusion machinery regulated mitochondrial aerobic respiration rate, and thus promotes the phosphorylation of Mec1 by Snf1. To elucidate how mitochondrial respiration regulates the phosphorylation of Mec1 by Snf1, the activation of Snf1 and the association of Mec1 with Snf1 in the absence of glucose was examined. Immunoprecipitation experiment results showed that the absence of mitochondrial fusion machinery genes led to significant decrease in the interaction between Snf1 and Mec1, which affected the phosphorylation of Mec1 by Snf1. In addition, mitochondrial respiration rate remained defective in fission and fusion double mutant albeit with restored mitochondrial morphology, indicating that aerobic respiratory deficiency is independent of mitochondrial morphological changes caused by mitochondrial fusion machinery deletion. These results showed that the mitochondrial fusion machinery involved in the autophagy induced by energy deficiency regulated the phosphorylation of Mec1 by Snf1 by affecting the association of Snf1 with Mec1.

With prolonged glucose starvation, Mec1 dissociated from mitochondria, while this dissociation of Mec1 was inhibited by mitochondrial fusion machinery genes knockout, suggesting Mec1 dissociation from mitochondria is regulated by fusion machinery. To understand the molecular mechanism of Mec1 dissociation, we knocked out *SNF1* gene, and then carried out *SNF1* gene replenishment experiments. The results showed that Mec1 remained associated with mitochondria in the absence of kinase activity of Snf1. As *SNF1* deletion and Snf1 KD

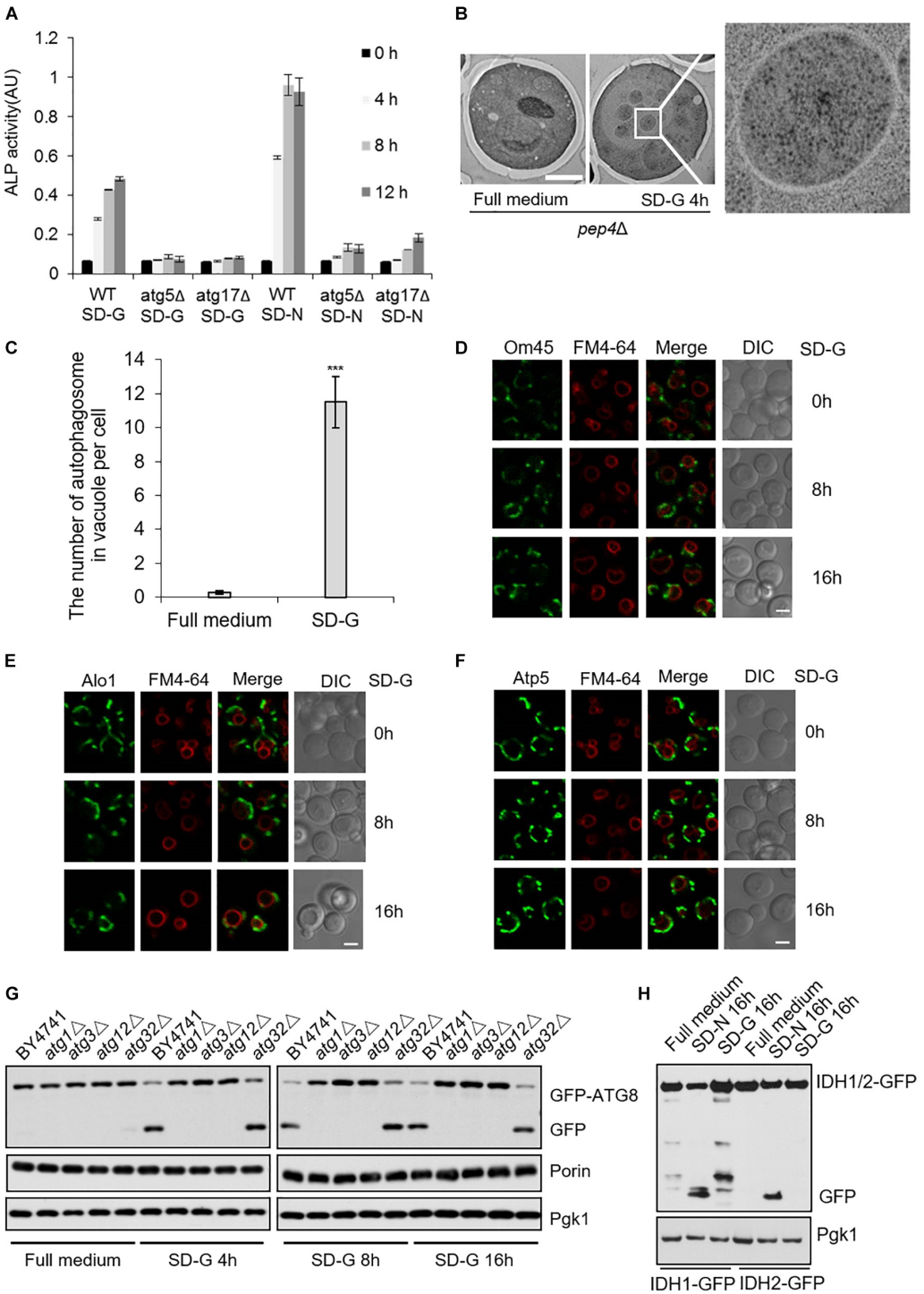

FIGURE 5 | Glucose starvation doesn't induce mitophagy. **(A)** ALP assay for autophagic activity. In wild type, *atg5*Δ, and *atg17*Δ cells, ALP activity was tested at the indicated time points under SD-G or SD-N conditions from $n = 3$ independent experiments. Error bars indicate standard deviation (SD). **(B)** EM analysis of autophagy in *pep4*Δ cells grown in full medium or SD-G. Scale bar, 2 μm. **(C)** 50 cells from **(B)** were analyzed for the number of autophagosomes inside the vacuole per cell from $n = 3$ independent experiments. Error bars indicate standard deviation (SD). ***$p < 0.001$; two-tailed Student's *t*-tests were used. **(D–F)** Cells expressing the GFP-tagged mitochondrial proteins Om45, Alo1, and Atp5 were glucose starved for 0, 8, and 16 h. Cells were viewed by laser confocal microscopy. Scale bar, 2 μm. FM4-64 is a vacuole membrane dye. **(G)** Wild type (BY4741), *atg1*Δ, *atg3*Δ, *atg12*Δ and *atg32*Δ cells expressing GFP-Atg8 were harvested at time point 0 (grown in full medium) and after 4, 8, and 16 h of glucose starvation. The cleavage of GFP-Atg8 and the status of Porin and Pgk1 were measured by western blot using the indicated antibodies. **(H)** Cells expressing the GFP-tagged mitochondrial proteins IDH1 and IDH2 were cultured in SD-G and SD-N for 16 h, respectively, the cleavage of IDH1-GFP and IDH2-GFP were detected by western blot using anti-GFP antibody.

inhibited aerobic respiration in glucose starvation (Yi et al., 2017), we speculated that mitochondrial aerobic respiration regulates the dissociation of Mec1 from mitochondria. In future, the phosphorylation substrate of Snf1 which regulated the dissociation of Mec1 from mitochondria need to be identified. In the early stage of glucose starvation, Mec1 was recruited onto mitochondria and then left mitochondria (Yi et al., 2017). In previous study, we found that Mec1 was recruited to mitochondria together with Atg1–Atg13. Based on this fact, we speculated that mitochondria might serve as a protein factor recruitment platform and a source of autophagosome membrane for autophagosome biogenesis under energy deprivation.

Since the fusion machinery of mitochondria is involved in the glucose starvation-induced autophagy, mitophagy was detected under glucose starvation condition. Image and western-blot data showed that glucose starvation does not induce mitophagy. So why energy deficiency does not induce mitophagy? Based on our data, we proposed a hypothesis that under glucose starvation, cells need to provide basic energy to maintain the necessary life activities for survival. As the factory for cells to generate energy, mitochondria need to maintain at certain quantity to provide energy for cell life activities, avoiding being damaged and removed by mitophagy. The phosphorylation modification of mitophagy receptor Atg32 by casein kinase 2 has been reported to be important for the initiation of mitophagy (Kanki et al., 2013). The next step is to test whether Atg32 can be phosphorylated by casein kinase 2 upon glucose starvation, which helps better understand the molecular mechanism of energy deficiency without inducing mitophagy. In summary, our study uncovers mitochondrial fusion machinery specifically essential for glucose starvation-induced autophagy, which provides a perspective for us to understand the biological significance of maintaining mitochondrial aerobic respiratory during energy deficiency.

MATERIALS AND METHODS

Yeast Strains, Constructs and Growth Conditions

All yeast strains and plasmids used in this study are listed in **Supplementary Table S1**. The related yeast strains were originated from wild type BY4741 and verified by western blot analysis with the indicated antibody or polymerase chain reaction (PCR) (Vazyme, P505-d1) (Janke et al., 2004). All mutant plasmids were sequenced and tested by western blot. Yeast cells were grown at 30°C in corresponding synthetic complete media (0.17% yeast nitrogen base without amino acids and ammonium sulfate, 0.5% ammonium sulfate, 2% dextrose, and 0.5% casamino acids) (rich medium). For autophagy induction, cells grown to mid-log phase in rich medium were subjected to nitrogen starvation medium (SD-N; 0.17% yeast nitrogen base without amino acids and ammonium sulfate, and 2% glucose) or glucose starvation medium (SD-G; 0.17% yeast nitrogen base without amino acids and ammonium sulfate, 0.5% ammonium sulfate, and 0.5% casamino acids) for 4 h at 30°C.

Antibodies

The company, product number and dilution ratio of antibody in this study are as follows: anti-GFP (Roche, 11814460001, 1:2500), anti-FLAG (Sigma, F1804, 1:2500), anti-HA (Abmart, M20003L, 1:3000), anti-phospho-AMPKα(Thr172) (Cell Signaling Technology, 2535S, 1:1000), anti-Phospho-(Ser/Thr) AMPK Substrate (Cell Signaling Technology, 5759, 1:1000), anti-Porin (Thermo Fisher Scientific, A6449, 1:10000), anti-PGK1 (Nordic Immunology, NE130/7S, 1:10000), Goat anti-Mouse IgG1, Human ads-HRP (SouthernBiotech, 1070-05, 1:10000), Goat anti-Rabbit, Human ads-HRP (SouthernBiotech, 4010-05, 1:10000).

Microscopy, Western Blots, and Immunoprecipitation

The yeast strains with different fluorescent tags grew to the log-growth phase, and then were treated with the indicated conditions. The cells were observed by fluorescence inversion microscope (IX83; Olympus) or laser confocal microscope (FV1000; Olympus) at the indicated time. Images were processed in ImageJ software and Adobe Photoshop. The images were not manipulated except brightness and contrast adjustments. Yeast protein extraction, western blotting and immunoprecipitation in this study were carried out according to the previously described methods (Yi et al., 2017).

Determination of Oxygen Consumption of Cells

Yeast cells were grown to log-growth phase, and then were subjected to glucose starvation or nitrogen starvation for 30 min. Oxygen consumption was measured using Oxygraph-2k (O2K, OROBOROS Instruments, Innsbruck, Austria) (Makrecka-Kuka et al., 2015).

Electron Microscopy

*pep4*Δ yeast strain was grown to log-growth phase, and then were subjected to glucose starvation for 0 and 4 h. Yeast was centrifuged using horizontal rotor centrifuge at 2,000 rpm for 2 min, then the supernatant was removed. Yeast was frozen by high-pressure freezer (Leica EM HPM100) with 100 μm deep carriers and 1-hexadecene as cryoprotect. Freeze substitution was performed by using a Leica EM AFS2 in dry acetone containing 5% ddH_2O, 1% OsO_4, and 0.1% uranyl acetate over a long period as follows: −90°C for 72 h, 2°C per hour increase for 15 h, −60°C for 8 h, 2°C per hour increase for 15 h, and −30°C for 8 h. After 1 h on ice, samples were then washed three times in pure acetone on ice, infiltrated in 1:1 (resin/acetone) 12 h, 2:1 12 h, 3:1 12 h, resin 12 h, resin 1 h Pon 812 resin and embedded. The polymerization was performed at 60°C for 48 h. Ultrathin sections were made using an ultramicrotome (Leica EM UC7), post-stained in uranyl acetate for 30 min and in lead citrate for 5 min. Grids were imaged with a transmission electron microscope (H-7650B; Hitachi) (Takeshige et al., 1992).

ALP Assay

The indicated yeast strains were grown to log-growth phase, and then were starved in nitrogen starvation and glucose starvation medium for 0, 4, 8, and 12 h. ALP assay was carried out as described previously (Araki et al., 2017).

Quantification and Statistical Analysis

For all quantitative and statistical analyses, the mean values are displayed together with the standard deviation (SD, shown as error bars). The phosphorylation level of Snf1 was quantified by Image J software. Student's two-tailed *t*-test was performed for *p*-value calculations according to all comparisons between control and experiment conditions.

DATA AVAILABILITY STATEMENT

The datasets generated for this study are available on request to the corresponding author.

AUTHOR CONTRIBUTIONS

CW, WY, ZH, and CY conceived the experiments. ZH and CY wrote the manuscript and supervised the project. CW, WY, WK, WL, WW, SL, YC, LW, YL, JT, and LZ carried out the experiments. All authors discussed the manuscript and contributed to preparing the manuscript.

FUNDING

This research was supported by the National Natural Science Foundation of China 91754107 and 31771528 to CY, and National Key R&D Program of China (Grant No:2018YFD0600201-02) to LZ.

ACKNOWLEDGMENTS

We are grateful to Prof. Y. Ohsumi, Prof. H. Nakatogawa, and Prof. Zhiping Xie for plasmids. We thank Dr. Hangjun Wu in the Center of Cryo-Electron Microscopy (CCEM), Zhejiang University for his technical assistance on Confocal Laser Scanning Microscopy, and the support by the Protein facility, Core facilities, Zhejiang University School of Medicine.

SUPPLEMENTARY MATERIAL

The Supplementary Material for this article can be found online at: https://www.frontiersin.org/articles/10.3389/fcell.2020.00221/full#supplementary-material

REFERENCES

Alexander, C., Votruba, M., Ulrike, E. A. P., Thiselton, D. L., Mayer, S., Moore, A., et al. (2000). OPA1, encoding a dynamin-related GTPase, is mutated in autosomal dominant optic atrophy linked to chromosome 3q28. *Nat. Genet.* 26, 211–215. doi: 10.1038/79944

Araki, Y., Kira, S., and Noda, T. (2017). Quantitative assay of macroautophagy using Pho8Δ60 assay and GFP-cleavage assay in yeast. *Methods Enzymol.* 588, 307–321. doi: 10.1016/bs.mie.2016.10.027

Boyer, P. D. (1997). The ATP synthase–a splendid molecular machine. *Annu. Rev. Biochem.* 66, 717–749. doi: 10.1146/annurev.biochem.66.1.717

Danial, N. N., and Korsmeyer, S. J. (2004). Cell death: critical control points. *Cell* 116, 205–219.

Dimmer, K. S., Fritz, S., Fuchs, F., Messerschmitt, M., Weinbach, N., Neupert, W., et al. (2002). Genetic basis of mitochondrial function and morphology in *Saccharomyces cerevisiae*. *Mol. Biol. Cell* 13, 847–853.

Epple, U. D., Suriapranata, I., Eskelinen, E. L., and Thumm, M. (2001). Aut5/Cvt17p, a putative lipase essential for disintegration of autophagic bodies inside the vacuole. *J. Bacteriol.* 183, 5942–5955. doi: 10.1128/jb.183.20.5942-5955.2001

Feng, Y., He, D., Yao, Z., and Klionsky, D. J. (2014). The machinery of macroautophagy. *Cell Res.* 24, 24–41. doi: 10.1038/cr.2013.168

Frederick, R. L., McCaffery, J. M., Cunningham, K. W., Okamoto, K., and Shaw, J. M. (2004). Yeast Miro GTPase, Gem1p, regulates mitochondrial morphology via a novel pathway. *J. Cell Biol.* 167, 87–98. doi: 10.1083/jcb.200405100

Hailey, D. W., Rambold, A. S., Satpute-Krishnan, P., Mitra, K., Sougrat, R., Kim, P. K., et al. (2010). Mitochondria supply membranes for autophagosome biogenesis during starvation. *Cell* 141, 656–667. doi: 10.1016/j.cell.2010.04.009

Janke, C., Magiera, M. M., Rathfelder, N., Taxis, C., Reber, S., Maekawa, H., et al. (2004). A versatile toolbox for PCR-based tagging of yeast genes: new fluorescent proteins, more markers and promoter substitution cassettes. *Yeast* 21, 947–962. doi: 10.1002/yea.1142

Kabeya, Y., Noda, N. N., Fujioka, Y., Suzuki, K., Inagaki, F., Ohsumi, Y., et al. (2009). Characterization of the Atg17-Atg29-Atg31 complex specifically required for starvation-induced autophagy in *Saccharomyces cerevisiae*. *Biochem. Biophys. Res. Commun.* 389, 612–615. doi: 10.1016/j.bbrc.2009.09.034

Kanki, T., and Klionsky, D. J. (2010). The molecular mechanism of mitochondria autophagy in yeast. *Mol. Microbiol.* 75, 795–800. doi: 10.1111/j.1365-2958.2009.07035.x

Kanki, T., Kurihara, Y., Jin, X., Goda, T., Ono, Y., Aihara, M., et al. (2013). Casein kinase 2 is essential for mitophagy. *EMBO Rep.* 14, 788–794. doi: 10.1038/embor.2013.114

Kanki, T., Wang, K., Cao, Y., Baba, M., and Klionsky, D. J. (2009). Atg32 is a mitochondrial protein that confers selectivity during mitophagy. *Dev. Cell* 17, 98–109. doi: 10.1016/j.devcel.2009.06.014

Kauppila, T. E. S., Kauppila, J. H. K., and Larsson, N. G. (2017). Mammalian mitochondria and aging: an update. *Cell Metab.* 25, 57–71. doi: 10.1016/j.cmet.2016.09.017

Kijima, K., Numakura, C., Izumino, H., Umetsu, K., Nezu, A., Shiiki, T., et al. (2005). Mitochondrial GTPase mitofusin 2 mutation in charcot-marie-tooth neuropathy type 2A. *Hum. Genet.* 116, 23–27. doi: 10.1007/s00439-004-1199-2

Li, Z., Okamoto, K., Hayashi, Y., and Sheng, M. (2004). The importance of dendritic mitochondria in the morphogenesis and plasticity of spines and synapses. *Cell* 119, 873–887. doi: 10.1016/j.cell.2004.11.003

Makrecka-Kuka, M., Krumschnabel, G., and Gnaiger, E. (2015). High-resolution respirometry for simultaneous measurement of oxygen and hydrogen peroxide fluxes in permeabilized cells, tissue homogenate and isolated mitochondria. *Biomolecules* 5, 1319–1338. doi: 10.3390/biom5031319

Medeiros, T. C., Thomas, R. L., Ghillebert, R., and Graef, M. (2018). Autophagy balances mtDNA synthesis and degradation by DNA polymerase POLG during starvation. *J. Cell Biol.* 217, 1601–1611. doi: 10.1083/jcb.201801168

Montava-Garriga, L., and Ganley, I. G. (2020). Outstanding questions in mitophagy: what we do and do not know. *J. Mol. Biol.* 432, 206–230. doi: 10.1016/j.jmb.2019.06.032

Ohsumi, Y. (2014). Historical landmarks of autophagy research. *Cell Res.* 24, 9–23. doi: 10.1038/cr.2013.169

Okamoto, K., Kondo-Okamoto, N., and Ohsumi, Y. (2009). Mitochondria-anchored receptor Atg32 mediates degradation of mitochondria via selective autophagy. *Dev. Cell* 17, 87–97. doi: 10.1016/j.devcel.2009.06.013

Okamoto, K., and Shaw, J. M. (2005). Mitochondrial morphology and dynamics in yeast and multicellular eukaryotes. *Annu. Rev. Genet.* 39, 503–536. doi: 10.1146/annurev.genet.38.072902.093019

Schauss, A. C., Bewersdorf, J., and Jakobs, S. (2006). Fis1p and Caf4p, but not Mdv1p, determine the polar localization of Dnm1p clusters on the mitochondrial surface. *J. Cell Sci.* 119, 3098–3106. doi: 10.1242/jcs.03026

Sesaki, H., and Jensen, R. E. (1999). Division versus fusion: Dnm1p and Fzo1p antagonistically regulate mitochondrial shape. *J. Cell Biol.* 147, 699–706. doi: 10.1083/jcb.147.4.699

Shibutani, S. T., and Yoshimori, T. (2014). A current perspective of autophagosome biogenesis. *Cell Res.* 24, 58–68. doi: 10.1038/cr.2013.159

Sickmann, A., Reinders, J., Reinders, Y., Schumbrutzki, C., Zahedi, R. P., Meyer, H., et al. (2003). The proteome of *Saccharomyces cerevisiae* mitochondria. *Proc. Natl. Acad. Sci. U.S.A.* 100, 13207–13212.

Takeshige, K., Baba, M., Tsuboi, S., Noda, T., and Ohsumi, Y. (1992). Autophagy in yeast demonstrated with proteinase-deficient mutants and conditions for its induction. *J. Cell Biol.* 119, 301–311. doi: 10.1083/jcb.119.2.301

Wei, H., Liu, L., and Chen, Q. (2015). Selective removal of mitochondria via mitophagy: distinct pathways for different mitochondrial stresses. *Biochim. Biophys. Acta* 1853, 2784–2790. doi: 10.1016/j.bbamcr.2015.03.013

Westermann, B. (2008). Molecular machinery of mitochondrial fusion and fission. *J. Biol. Chem.* 283, 13501–13505. doi: 10.1074/jbc.r800011200

Wu, H., Wei, H., Sehgal, S. A., Liu, L., and Chen, Q. (2016). Mitophagy receptors sense stress signals and couple mitochondrial dynamic machinery for mitochondrial quality control. *Free Radic. Biol. Med.* 100, 199–209. doi: 10.1016/j.freeradbiomed.2016.03.030

Wu, X., and Tu, B. P. (2011). Selective regulation of autophagy by the Iml1-Npr2-Npr3 complex in the absence of nitrogen starvation. *Mol. Biol. Cell* 22, 4124–4133. doi: 10.1091/mbc.E11-06-0525

Yaffe, M. P., Jensen, R. E., and Guido, E. C. (1989). The major 45-kDa protein of the yeast mitochondrial outer membrane is not essential for cell growth or mitochondrial function. *J. Biol. Chem.* 264, 21091–21096.

Yi, C., Tong, J., Lu, P., Wang, Y., Zhang, J., Sun, C., et al. (2017). Formation of a Snf1-Mec1-Atg1 module on mitochondria governs energy deprivation-induced autophagy by regulating mitochondrial respiration. *Dev. Cell* 41, 59–71.e4. doi: 10.1016/j.devcel.2017.03.007

Zhao, Y. G., and Zhang, H. (2019). Core autophagy genes and human diseases. *Curr. Opin. Cell Biol.* 61, 117–125. doi: 10.1016/j.ceb.2019.08.003

Conflict of Interest: The authors declare that the research was conducted in the absence of any commercial or financial relationships that could be construed as a potential conflict of interest.

frontiers in Cell and Developmental Biology

ORIGINAL RESEARCH
published: 09 April 2020
doi: 10.3389/fcell.2020.00180

OPA1-Exon4b Binds to mtDNA D-Loop for Transcriptional and Metabolic Modulation, Independent of Mitochondrial Fusion

Liang Yang[1,2†], Haite Tang[1,2†], Xiaobing Lin[1,2], Yi Wu[1,2], Sheng Zeng[3], Yongzhang Pan[1,2], Yukun Li[1,2], Ge Xiang[1,2], Yi-Fang Lin[4], Shi-Mei Zhuang[4], Zhiyin Song[5], Yiguo Jiang[6] and Xingguo Liu[1,2]*

[1] CAS Key Laboratory of Regenerative Biology, Joint School of Life Sciences, Hefei Institute of Stem Cell and Regenerative Medicine, Guangzhou Institutes of Biomedicine and Health, Chinese Academy of Sciences, Guangzhou Medical University, Guangzhou, China, [2] Guangzhou Regenerative Medicine and Health Guangdong Laboratory, Guangdong Provincial Key Laboratory of Stem Cell and Regenerative Medicine, South China Institute for Stem Cell Biology and Regenerative Medicine, Institute for Stem Cell and Regeneration, Guangzhou Institutes of Biomedicine and Health, University of Chinese Academy of Sciences, Chinese Academy of Sciences, Guangzhou, China, [3] State Key Laboratory of Respiratory Disease, Guangzhou Regenerative Medicine and Health Guangdong Laboratory, Guangzhou Institutes of Biomedicine and Health, Chinese Academy of Sciences, Guangzhou, China, [4] MOE Key Laboratory of Gene Function and Regulation, School of Life Sciences, Collaborative Innovation Center for Cancer Medicine, Sun Yat-sen University, Guangzhou, China, [5] Hubei Key Laboratory of Cell Homeostasis, College of Life Sciences, Wuhan University, Wuhan, China, [6] State Key Laboratory of Respiratory Disease, The First Affiliated Hospital of Guangzhou Medical University, Guangzhou, China

OPEN ACCESS

Edited by:
Laura Lackner, Northwestern University, United States

Reviewed by:
Ian Jame Holt, Biodonostia Health Research Institute (IIS Biodonostia), Spain
Ryan J. Mailloux, McGill University, Canada

***Correspondence:**
Xingguo Liu
liu_xingguo@gibh.ac.cn

† These authors have contributed equally to this work

Specialty section:
This article was submitted to Molecular Medicine, a section of the journal Frontiers in Cell and Developmental Biology

Received: *09 December 2019*
Accepted: *04 March 2020*
Published: *09 April 2020*

Citation:
Yang L, Tang H, Lin X, Wu Y, Zeng S, Pan Y, Li Y, Xiang G, Lin Y-F, Zhuang S-M, Song Z, Jiang Y and Liu X (2020) OPA1-Exon4b Binds to mtDNA D-Loop for Transcriptional and Metabolic Modulation, Independent of Mitochondrial Fusion. Front. Cell Dev. Biol. 8:180. doi: 10.3389/fcell.2020.00180

Optic Atrophy 1 (OPA1) has well-established roles in both mitochondrial fusion and apoptotic crista remodeling and is required for the maintenance and distribution of mitochondrial DNA (mtDNA), which are essential for energy metabolism. However, the relationship between OPA1 and mitochondrial metabolism and the underlying mechanisms remain unclear. Here, we show that OPA1-Exon4b modulates mitochondrial respiration and rescues inner mitochondrial membrane potential ($\Delta\psi m$), independent of mitochondrial fusion. OPA1-Exon4b is required for the maintenance of normal TFAM distribution and enhances mtDNA transcription by binding the D-loop of mtDNA. Finally, we show that mRNA levels of OPA1 isoforms containing Exon4b are specifically downregulated in hepatocellular carcinoma (HCC), leading to a reduction in $\Delta\psi m$. Thus, our study demonstrates a novel mitochondrial functional self-recovery pathway involving enhanced mtDNA transcription-mediated recovery of mitochondrial respiratory chain proteins. This mitochondrial fusion-independent pathway may contribute to mitochondrial multi-functional switches in tumorigenesis.

Keywords: Optic Atrophy 1 (OPA1), mitochondrial DNA, mitochondrial fusion, hepatocellular carcinoma, mtDNA D-loop

INTRODUCTION

Mitochondria contain their own DNA, which is organized in discrete structures called nucleoids and spread within the mitochondrial network (Amati-Bonneau et al., 2008; Bogenhagen et al., 2008). Nucleoid proteins include not only factors involved in replication and transcription but also structural proteins required for the maintenance of mitochondrial DNA (mtDNA)

(Brown et al., 2011). Nucleoids are reported to be tethered to the inner mitochondrial membrane (IMM) by a series of DNA–protein and protein–protein interactions (Chen et al., 2003; Chan, 2006). Super-resolution fluorescence microscopy techniques have been used to reveal the structure of nucleoids, which are closely associated with IMM and appear to be wrapped around the cristae or the crista-like inner membrane invaginations. Nucleoids differ greatly in size and shape, and exhibit in concave, split, or amorphous forms. Nucleoids co-localize with mitochondrial transcription factor A (TFAM) and mtDNA polymerase gamma (POLG) (Chen et al., 2007). Freely diffusible mitochondrial matrix proteins are found to be largely excluded from the nucleoid (Chen et al., 2010).

Maintenance and distribution of mtDNA are essential for mtDNA stability, energy metabolism, and mitochondrial lineage. Mounting evidence suggests that the mtDNA integrity can be affected by mitochondrial dynamics, including mitochondria fusion and fission. These mitochondrial dynamics also play a role in maintaining normal mitochondrial metabolic function, as well as the regulatory roles in cell signaling and differentiation (Coller et al., 2001; Delettre et al., 2001; Elachouri et al., 2011; Cui et al., 2013; Del Dotto et al., 2017; Farge and Falkenberg, 2019). Indeed, studies in neuronal (Frezza et al., 2006; Folmes et al., 2013) and muscular cells (Frilling et al., 2010) demonstrate that mitochondrial dynamics-related proteins, such as dynamin-related protein 1 (DRP1) and mitofusins (MFNs), contribute to the integrity and distribution of mtDNA. Optic Atrophy 1 (OPA1), a dynamin-related protein of IMM, functions in both IMM fusion and cristae maintenance (Gilkerson et al., 2008). *OPA1* mutations were reported to induce the accumulation of mtDNA deletions in skeletal muscle (Griparic et al., 2007; He et al., 2012). Furthermore, *OPA1* silencing led to mtDNA depletion, a phenomenon related to replication inhibition and distribution alteration of mtDNA (Chen et al., 2003). These findings lead to the hypothesis that OPA1 might contribute to the attachment of nucleoid to IMM.

OPA1 is encoded by a complicated set of at least eight mRNA variants that are specified by the presence of exons 4, 4b, or 5b (Holt et al., 2007; Hudson et al., 2008). OPA1 Exon4b is conserved throughout evolution and is involved in the maintenance of $\Delta\psi$m and mitochondrial fusion (Holt et al., 2007). OPA1 isoforms containing Exon4b such as OPA1 isoform 5 (OPA1-iso5) are cleaved into shorter isoforms by Yme1L, leading to an imbalance of long and short isoforms and thus to inhibition of mitochondrial fusion (Ishikawa et al., 2008; Kukat et al., 2015). Whether OPA1 is associated with mitochondrial metabolism and the underlying mechanisms are unclear.

Hepatocellular carcinoma (HCC) is one of the five most common cancers worldwide, and the 5-year survival rate of patients diagnosed with HCC is less than 10% (Lee et al., 2005). Western blotting evaluation of HCC samples and matched non-tumor tissue samples demonstrates that OPA1 expression is decreased in up to 40% of HCC patients (Legros et al., 2004), suggesting important roles for OPA1 in the development of HCC. In the present study, we demonstrate that Exon4b controls the transcription regulation of mtDNA and mitochondrial metabolic maintenance via maintaining TFAM distribution, a process conserved in HCC cells SK Hep1.

RESULTS

OPA1-Exon4b Rescues $\Delta\psi$m Independent of Mitochondrial Fusion

It has been known that bioenergetics of dysfunctional mitochondria can be restored by heteroplasmic mitochondrial fusion, leading to exchange of mtDNA nucleoids (Liu and Hajnoczky, 2011) or respiratory chain proteins (Liu et al., 2009). Given the regulatory role of OPA1 on IMM fusion, we first assessed the effect of OPA1-Exon4b on mitochondrial fusion. As the OPA1-iso5 differs from OPA1 isoform 1 (OPA1-iso1) only by its presence of OPA1-Exon4b, we investigated the roles of OPA1-Exon4b on mitochondrial fusion by complementing *Opa1* knockout (KO) mouse embryonic fibroblast (MEF) cells with either OPA1-iso5 or OPA1-iso1. After the OPA1 expression levels in wild type (WT) MEF cells expressing Flag and *Opa1* KO cells expressing Flag, OPA1-iso1, or OPA1-iso5 were confirmed by western blotting (**Supplementary Figure 1A**), we co-expressed mitochondrial matrix-targeted photoactivatable green fluorescent protein (mtPAGFP) and mtDsRed in WT cells expressing Flag and *Opa1* KO cells expressing Flag, OPA1-iso1-Flag, or OPA1-iso5-Flag. As reported previously (Coller et al., 2001), high-resolution time-lapse confocal microscopy with region-of-interest scanning was employed to selectively and irreversibly photoactivate subpopulations of mitochondria (**Figure 1A**). In this assay, fusion events were classified as either complete or kiss-and-run by monitoring mitochondrial dynamics after photoactivation (Coller et al., 2001). As expected, *Opa1* KO cells expressing Flag didn't show any fusion events. Expression of OPA1-iso1 restored both complete (p = 1.46398E-08) and kiss-and-run (p = 0.0002) fusion events. In stark contrast, expression of OPA1-iso5 failed to rescue the fusion defects of *Opa1* KO cells, indicating that the presence of Exon4b in OPA1-iso5 impedes mitochondrial fusion (**Figures 1A,B** and **Supplementary Figures 1B,C**).

Next, we measured $\Delta\psi$m in WT MEF cells expressing Flag and *Opa1* KO cells expressing Flag, OPA1-iso1-Flag, or OPA1-iso5-Flag by tetramethyl rhodamine methyl ester (TMRM, Invitrogen, United States) staining. We observed that, consistent with two previous reports (McBride et al., 2006; Liu et al., 2009), in *Opa1* KO cells but not WT cells, 42.5 $\pm$ 3.7% of mitochondria were depolarized, showing low $\Delta\psi$m (p = 0.0004), as judged by a TMRM FI ratio of less than 0.3, relative to normal mitochondria. As expected, expression of OPA1-iso1 reduced the percentage of mitochondrial with low $\Delta\psi$m (p = 0.0023), in agreement with its ability to rescue mitochondrial fusion (**Figures 1C,D**). OPA1-iso5 is constitutively cleaved into short isoforms by Yme1L and, as such, is not involved in IMM fusion (**Figure 1B**). Surprisingly, we observed that expression of OPA1-iso5 recovered $\Delta\psi$m to the same extent that OPA1-iso1 did (p = 0.0005) (**Figures 1C,D**). Then, we asked how the Exon4b-containing OPA1-iso5 could recover $\Delta\psi$m in the absence of IMM fusion. We first tested the possibility that OPA1-Exon4b

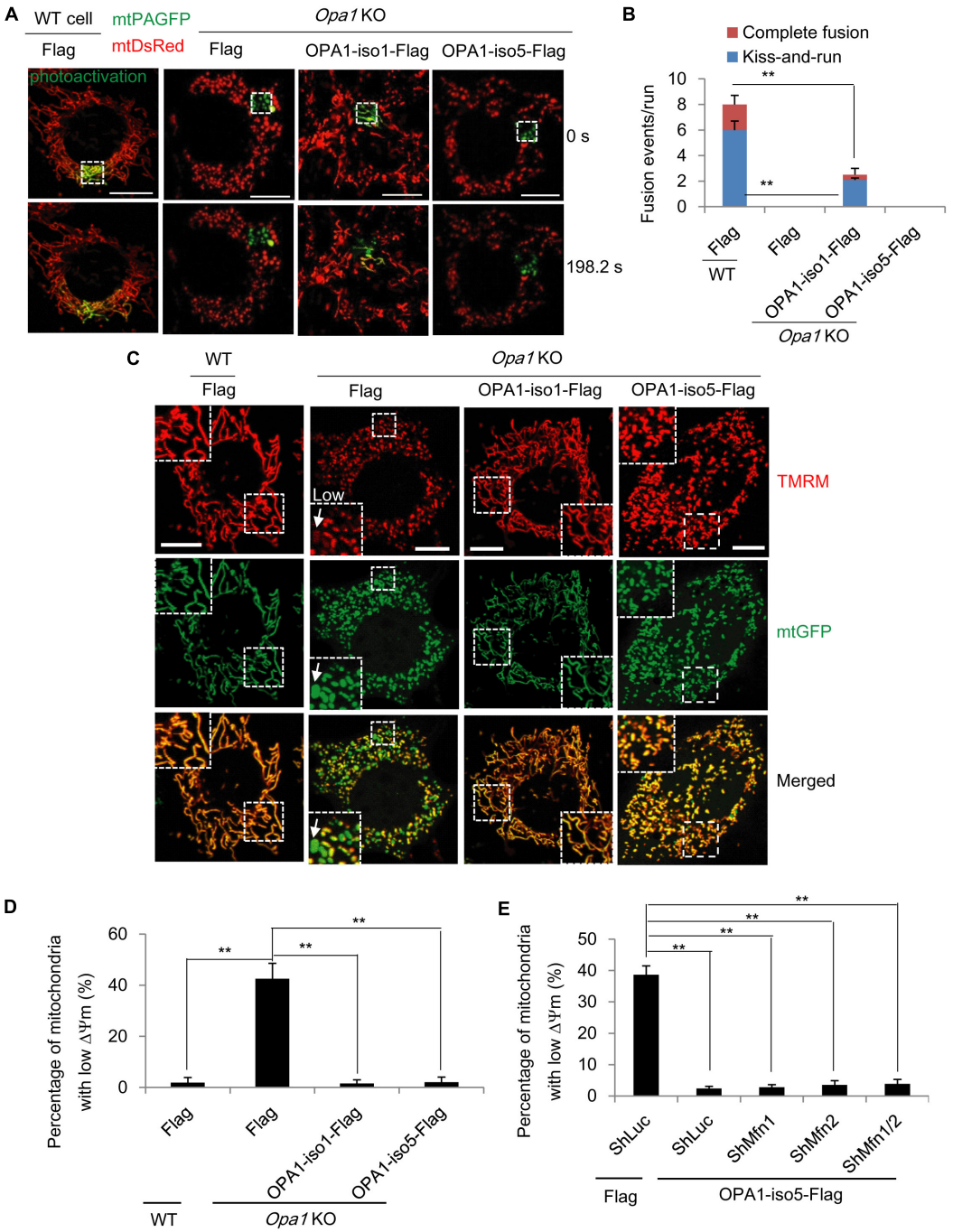

FIGURE 1 | OPA1-Exon4b is not required for mitochondrial fusion but ensues mitochondrial bioenergetic recovery. **(A)** Labeling of one subset of mitochondria by photoactivation of PAGFP in cells expressing both mtPAGFP and mtDsRed, as indicated on the top (scale bar: 10 μm). **(B)** Quantitation of mitochondrial fusion events, including kiss-and-run and complete fusion, per run (n = 10 runs). **(C)** Δψm of WT MEF cells expressing Flag and *Opa1* KO cells expressing Flag, OPA1-iso1-Flag, or OPA1-iso5-Flag. The mean TMRM FI of mitochondria in WT cells was normalized to 1. The TMRM FI per mitochondrion below 0.3 denoted low (white arrow). **(D)** Quantitation of percentage of mitochondria with low Δψm in WT MEF cells expressing Flag and *Opa1* KO cells expressing Flag, OPA1-iso1-Flag, or OPA1-iso5-Flag (≥20 cells for three biological replicates). **(E)** Quantitation of percentage of mitochondria with low Δψm in *Opa1* KO cells expressing ShLuc plus Flag and *Opa1* KO cells expressing OPA1-iso5-Flag plus ShLuc, Sh*Mfn*1, Sh*Mfn*2 or Sh*Mfn*1/2 (≥20 cells for three biological replicates). $^{**}p < 0.01$, one-way ANOVA.

recovered Δψm by mitochondrial outer membrane (OMM) fusion. We silenced the expression of *Mfn1* (p = 0.0067) and *Mfn2* (p = 0.0035) necessary for OMM fusion in *Opa*1 KO cells expressing OPA1-iso5-Flag (**Supplementary Figures 1D,E**). We observed that Δψm was maintained in *Opa1* KO MEF cells expressing OPA1-iso5 even after silencing *Mfn1*, *Mfn2*, or *Mfn1/2*

(**Figure 1E** and **Supplementary Figure 1F**). Therefore, OPA1-Exon4b recovered $\Delta\psi m$ not mainly dependent on OMM fusion.

OPA1-Exon4b Partly Rescues Mitochondrial Respiration

Besides $\Delta\psi m$, we asked how mitochondrial respiration activity is affected by OPA1-Exon4b. We measured oxygen consumption rate (OCR) and extracellular acidification rate (ECAR) in WT MEF cells expressing Flag and *Opa1* KO cells expressing Flag, OPA1-iso1-Flag, or OPA1-iso5-Flag. *Opa1* KO cells exhibited significantly lower basal OCR (p = 0.0176), with an increase in ECAR, compared to that of WT MEF cells. *Opa1* KO cells expressing either OPA1-iso1 or OPA1-iso5 displayed higher levels of basal OCR (p = 0.0124) and ATP production (p = 0.0422) than *Opa1* KO cells (**Figures 2A,B** and **Supplementary Figures 2A–C**), suggesting improved mitochondrial function. We further measured cellular and mitochondrial ATP production and found that *Opa1* KO cells expressing either OPA1-iso1 (p = 0.0039 for cellular ATP and p = 0.0501 for mitochondrial ATP) or OPA1-iso5 (p = 0.0003 for cellular ATP and p = 0.0059 for mitochondrial ATP) displayed higher levels of mitochondrial and cellular ATP than *Opa1* KO cells. *Opa1* KO cells expressing OPA1-iso5 displayed higher cellular (p = 0.0033) and mitochondrial ATP (p = 0.0402) levels and a lower ECAR than those expressing OPA1-iso1 (**Figure 2C**). Considering the possible impact of cell apoptosis and viability on ATP production, we measured cell apoptosis by flow cytometry and detected cell viability using CCK8 assay in WT MEF cells expressing Flag and *Opa1* KO cells expressing Flag, OPA1-iso1-Flag, or OPA1-iso5-Flag. The results showed that cell apoptosis and viability were not altered by OPA1 knockout or rescue (**Supplementary Figures 2D,E**). All these results indicate that OPA1-Exon4b partly rescues mitochondrial respiration. OPA1-iso5 overexpression also enhanced cellular ATP level in Hela (p = 0.0147) and 293T (p = 0.0090) cells (**Supplementary Figures 2G,H**).

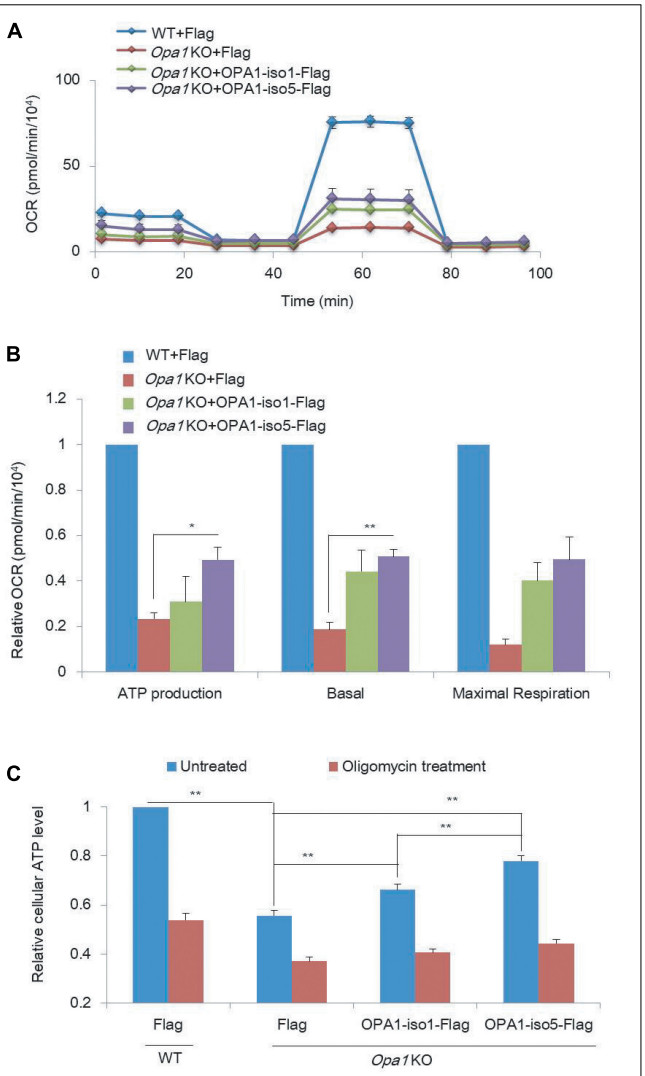

FIGURE 2 | OPA1 Exon-4b and Exon4 partially recover mitochondrial respiration activity. **(A)** OCR measurements in WT MEF cells expressing Flag and *Opa1* KO cells expressing Flag, OPA1-iso1-Flag, or OPA1-iso5-Flag. **(B)** Relative ATP production, basal, and maximal respiration using OCR measurements in WT MEF cells expressing Flag and *Opa1* KO cells expressing Flag, OPA1-iso1-Flag or OPA1-iso5-Flag (n = 2, biological replicates). WT MEF cells were used as control, whose ATP production, basal, and maximal respiration were normalized to 1. **(C)** Cellular ATP levels in WT MEF cells expressing Flag and *Opa1* KO cells expressing Flag, OPA1-iso1-Flag, or OPA1-iso5-Flag, with or without oligomycin treatment (n = 3, biological replicates). *p < 0.05, **p < 0.01, one-way ANOVA.

OPA1-Exon4b Maintains Normal TFAM Distribution

TFAM packs mtDNA into mitochondrial nucleoids that are required for mtDNA transcription and replication (Olichon et al., 2007; Parone et al., 2008), which is necessary for the maintenance of normal mitochondrial function (e.g., respiration and ATP production). Therefore, we investigated the effect of OPA1-Exon4b on TFAM distribution and the mtDNA nucleoid number. We applied TFAM-EYFP in combination with mtDsRed to visualize TFAM distribution by a Nikon structured illumination microscopy (N-SIM). While most mitochondria (98.0 ± 1.0%) in WT MEF cells showed normal punctate structures of TFAM, a large proportion of mitochondria (52.3 ± 2.5%) in *Opa1* KO cells showed diffuse TFAM. Notably, in cells expressing OPA1-iso5 but not OPA1-iso1, the proportion of mitochondria with diffuse TFAM was decreased to 7.3 ± 0.2% (p = 0.0106) (**Figures 3A,B** and **Supplementary Figure 3A**). We also detected the number of mtDNA nucleoids by Anti-DNA IF and mtDNA copy number by qPCR and found that *Opa1* KO cells expressing either OPA1-iso5 (p = 1.85742E-06 for mtDNA nucleoid number and p = 0.0034 for mtDNA copy number) or OPA1-iso1 (p = 0.0106 for mtDNA nucleoid number and p = 0.0141 for mtDNA copy number) had more mtDNA nucleoids and mtDNA copy number than *Opa1* KO cells expressing Flag (**Figures 3C,D** and **Supplementary Figure 3B**), while overexpression of OPA1-iso5 or OPA1-iso1 didn't increase mtDNA nucleoid number in Hela and 293T cells (**Supplementary Figures 3C,D**). These results indicate that, though both OPA1 iso1 and iso5 could rescue mtDNA nucleoid

number and mtDNA copy number, OPA1 iso5, but not iso1, maintains TFAM puncture structure, suggesting that Exon4b contributes largely to the normal TFAM distribution by its interaction with TFAM (Chen et al., 2003).

OPA1-Exon4b Binds mtDNA D-Loop Region and Increases mtDNA Transcription

The observation that OPA1-Exon4b maintained normal TFAM distribution (**Figures 2A,B**) led us to investigate its role in mtDNA transcription. Given the importance of D-loop in mtDNA transcription (Qiao et al., 2017), we first investigated whether OPA1-Exon4b could interact with the D-loop region of mtDNA. To this end, we performed anti-FLAG chromatin immunoprecipitation (ChIP) in *Opa1* KO cells expressing Flag, OPA1-iso1-Flag, or OPA1-iso5-Flag, and then detected the copy number of D-loop by quantitative PCR (qPCR). The results showed that OPA1-iso5, but not OPA1-iso1, interacted with the D-loop (p = 0.0083) (**Figure 4A**). To verify the specificity of the D-Loop binding of OPA1-Exon4b, we checked the binding of OPA1-iso5 with another region of mtDNA, i.e., the *Cox1* region. Importantly, OPA1-iso5 did not bind to the *Cox1* region (**Figure 4B**), supporting the specific binding of OPA1-Exon4b to the D-loop. N-terminal (NT)-Exon4/4b, a small hydrophobic 10-kDa peptide, generated by cleavage of OPA1-iso5 (Chen et al., 2003), was reported to interact with mtDNA nucleoids. We assessed whether NT-OPA1-Exon4/4b could interact with the D-loop using NT-OPA1-Exon4 as a control. We performed anti-Flag ChIP-qPCR in *Opa1* KO cells expressing NT-OPA1-Exon4-Flag, or NT-OPA1-Exon4/4b-Flag, and observed that NT-OPA1-Exon4/4b-Flag showed more interaction with the D-loop

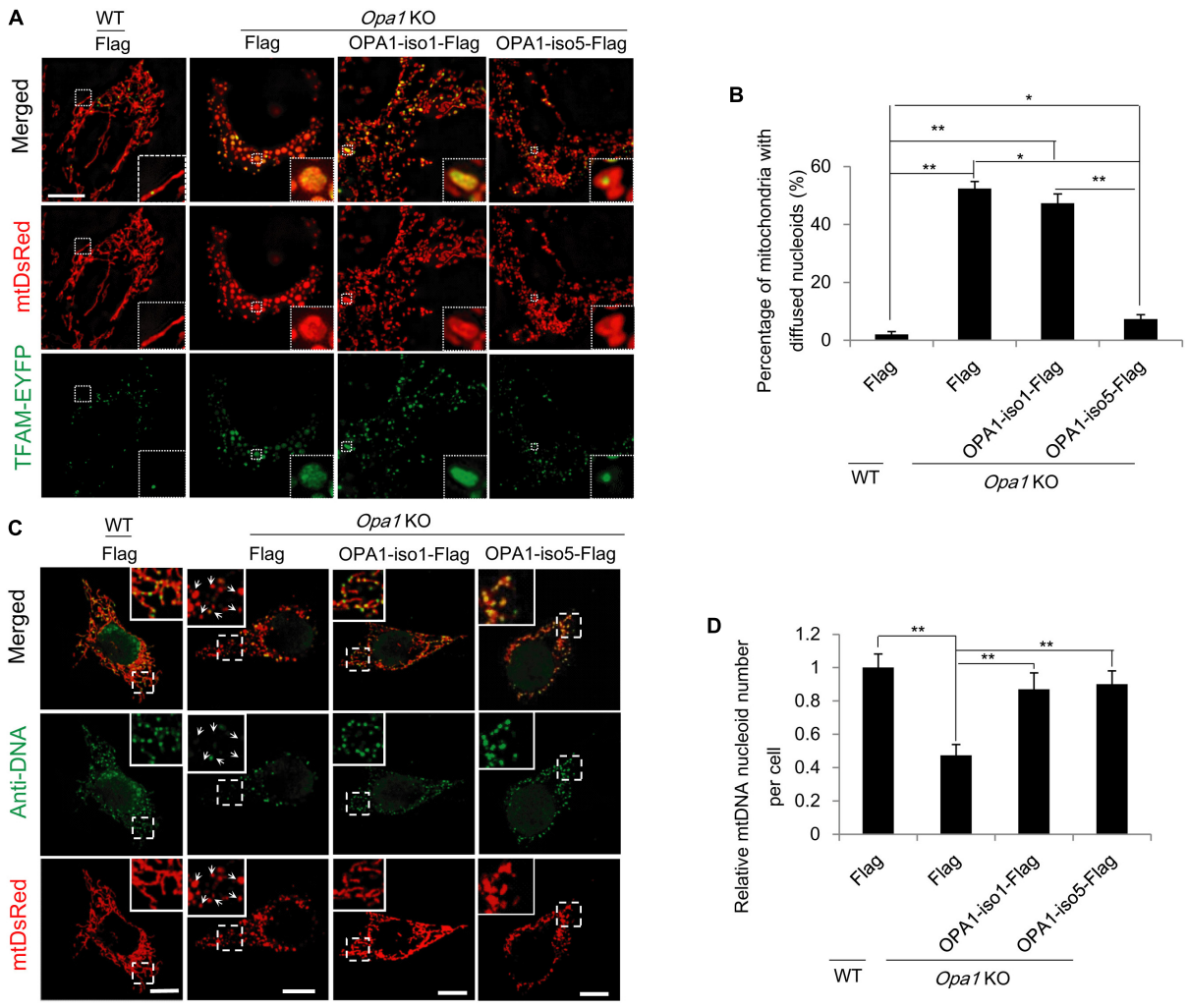

FIGURE 3 | OPA1-Exon4b maintains normal TFAM distribution. **(A)** N-SIM Images of TFAM distribution in WT MEF cells expressing Flag and *Opa1* KO cells expressing Flag, OPA1-iso1-Flag, or OPA1-iso5-Flag. **(B)** Quantification of the percentage of mitochondria with diffuse TFAM in panel **(A)** (≥15 cells for three biological replicates, scale bar: 10 μm). **(C)** Anti-DNA immunofluorescence in WT MEF cells expressing Flag and *Opa1* KO cells expressing Flag, OPA1-iso1-Flag, or OPA1-iso5-Flag (scale bar: 10 μm). **(D)** Quantification of mtDNA nucleoid number per cell in WT MEF cells expressing Flag and *Opa1* KO cells expressing Flag, OPA1-iso1-Flag, or OPA1-iso5-Flag (≥20 cells for three biological replicates). *$p < 0.05$, **$p < 0.01$, one-way ANOVA.

region than NT-OPA1-Exon4-Flag (p = 0.0118) (**Figure 4C**). Therefore, OPA1-Exon4b can bind to mtDNA D-loop region in a specific fashion.

The binding of OPA1-Exon4b to mtDNA D-loop led us to further assess the effect of Exon4b on mtDNA transcriptional regulation. We detected by qPCR transcriptional levels of nine mtDNA genes in WT MEF cells expressing Flag and *Opa1* KO cells expressing Flag, OPA1-iso1-Flag, or OPA1-iso5-Flag. All the tested genes showed significantly decreased expression in *Opa1* KO cells compared to the WT cells. Expression of both OPA1-iso1 and OPA1-iso5 restored the transcription of the tested genes in *Opa1* KO cells. Notably, OPA1-iso5 delivered a stronger effect than OPA1-iso1 (**Figure 4D**), indicating an important role for Exon4b in the regulation of mtDNA transcription. OPA1-iso5 also increased mtDNA transcription in Hela and 293T cells (**Supplementary Figures 4A,B**). We further analyzed transcription levels of three nuclear DNA-encoded respiratory chain subunits, such as *Sdha*. The expression of all the tested genes was reduced in *Opa1* KO cells, compared to that of WT cells. More importantly, expression of OPA1-iso1 or OPA1-iso5 failed to restore transcription of these nuclear genes in *Opa1* KO cells (**Figure 4E**). Finally, we assessed whether the effect on mtDNA transcription could alter the levels of proteins, we detected COX2 and SDHA by western blotting (**Figure 4F** and **Supplementary Figure 4C**). In agreement with the qPCR analysis, expression of both OPA1-iso5 (p = 0.0140) and OPA1-iso1 (p = 0.0253) increased the level of COX2, but not that of SDHA. Moreover, the effect of OPA1-iso5 was stronger than OPA1-iso1 (p = 0.0358). Taken together, OPA1-Exon4b binds the D-loop region and increases mtDNA transcription.

Downregulation of Exon4b-Containing OPA1 Isoforms in HCC

In cancer cells, energy is generated mainly through aerobic glycolysis, but not through mitochondrial respiration. Considering the essential roles of Exon4b on mitochondrial function including energetics, we tested whether the compromised mitochondrial respiration observed in some cancer cells could be associated with OPA1-Exon4b. We measured by qPCR the mRNA levels of Exon4b-containing OPA1 isoforms (i.e., isoforms 3, 5, 6, and 8) and those without Exon4b (i.e., isoforms 1, 2, 4, and 7) in 22 paired HCC and adjacent non-tumor liver tissues. We observed that both tissues expressed comparable levels of OPA1 isoforms without Exon4b (p = 0.4403). In contrast, the Exon4b-containing OPA1 isoforms were markedly decreased in tumor tissues (p = 0.0007, **Figures 5A,B**). This pointed to the correlation between the downregulation of OPA1-Exon4b and HCC tumorigenesis. Given this finding, we further tested the function of OPA1 Exon4b in human HCC cell line (SK-Hep1) by short hairpin RNA (shRNA)-mediated Exon4b silencing. After Exon4b silencing was validated by qPCR (p = 0.0009) and Western blotting (p = 0.0322) (**Supplementary Figures 5A,B**), we measured $\Delta\psi$m by TMRM staining and cellular ATP level by luciferase assay. We observed that silencing of Exon4b resulted in a significant decrease in $\Delta\psi$m (p = 0.0107) and cellular ATP (p = 0.0018) (**Figures 5C–D**). Hence, downregulation of OPA1 Exon4b is associated with compromised mitochondrial function in HCC.

DISCUSSION

We showed here that OPA1-Exon4b is required for the maintenance of normal TFAM distribution and enhances mtDNA transcription by binding the D-loop of mtDNA. Two non-coding regions (NCRs), i.e., the major and minor NCR, are present in mtDNA. The major NCR, also known as the D-loop, is a region of 900-bp fragment containing transcription promoters of the heavy/light strands and the origin of replication of the heavy strand. Thus, the D-loop is essential for mtDNA replication and transcription. Interestingly, Exon4b was found to interact with the D-loop region of mtDNA specifically, providing an alternative explanation for the regulatory role of Exon4b-containing OPA1-iso5 on mtDNA transcription.

Surprisingly, OPA1 Exon4b, without fusion activity, recovers mitochondrial bioenergetics in Opa1 KO cells. Thus, we demonstrated how OPA1 isoforms bidirectionally control mitochondrial metabolic recovery via fusion dependent and independent manner. OPA1 isoforms containing Exon4b were shown to be fully cleaved by i-AAA protease Yme1L into short forms (Kukat et al., 2015). A recent study showed that OPA1 short forms were shown to restore energetic efficiency (Reyes et al., 2011). Here, we found that OPA1 Exon4b could not only maintain TFAM distribution but also bind with mtDNA D-loop, conceivably leading to an enhanced expression of mtDNA-encoded respiratory proteins and thus the recovery of bioenergetics. Based on these, we propose a novel model of mitochondrial recovery involving the enhancement of mtDNA transcription (**Figure 5E**).

We also assessed the role of OPA1-Exon4b in mitochondrial bioenergetics of cancer cells. We found that the level of OPA1-Exon4b was downregulated in HCC tumor tissues and that Exon4b silencing compromised $\Delta\psi$m in an HCC cell line. These results suggest that the loss of function of Exon4b may be linked to the HCC tumorigenesis. Studies have demonstrated important roles for mitochondrial metabolism in tumorigenesis. For instance, the well-known Warburg effect describes that cancer cells derive their energy from glucose fermentation yielding lactate even in the presence of oxygen, despite the fact that they have higher energy needs. The Warburg effect is also characterized by the malfunction of mitochondria. Previous studies have shown that mtDNA point mutation and its content reduction may play a role in the regulation of mitochondrial function in various cancer cells including HCC (Song et al., 2007; Scarpulla, 2008; Suen et al., 2008; Tatsuta and Langer, 2008; Tondera et al., 2009). Based on our results, we identify in this study that the decreased expression of Exon4b, necessary for optimal mitochondrial function (**Figure 5E**), may also account for the malfunction of mitochondria and thus establishment of the Warburg effect in cancer cells.

In summary, we have revealed that Exon4b is essential for the maintenance of TFAM distribution and contributes

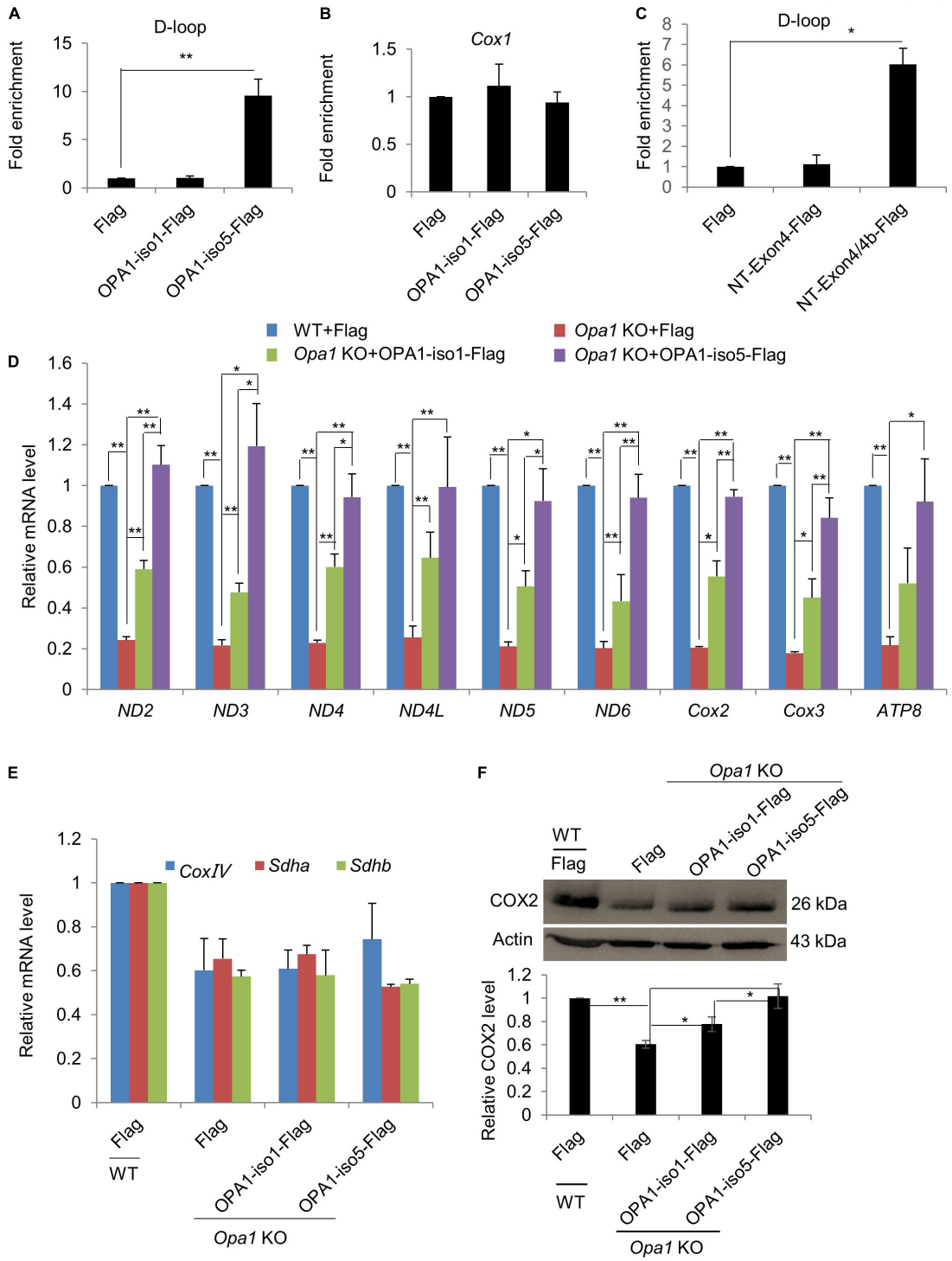

FIGURE 4 | OPA1-Exon4b modulates mtDNA transcription. **(A,B)** Anti-Flag ChIP was carried out using WT MEF cells expressing Flag and *Opa1* KO cells expressing Flag, OPA1-iso1-Flag, or OPA1-iso5-Flag. The precipitated DNA was analyzed by qPCR using primer pairs for the D-loop region **(A)** or *Cox1* **(B)**. $n = 3$, biological replicates. **(C)** Anti-Flag ChIP was carried out using WT MEF cells expressing Flag and *Opa1* KO cells expressing Flag, NT-Exon4-Flag, or NT-Exon4/4b-Flag. The precipitated DNA was analyzed by qPCR using primer pairs for the D-loop region. $n = 3$, biological replicates. **(D)** Relative mRNA levels of 9 mtDNA genes in WT MEF cells expressing Flag and *Opa1* KO cells expressing Flag, OPA1-iso1-Flag, or OPA1-iso5-Flag ($n = 3$, biological replicates). **(E)** Relative mRNA levels of three nuclear genes encoding respiratory subunits in WT MEF cells expressing Flag and *Opa1* KO cells expressing Flag, OPA1-iso1-Flag or OPA1-iso5-Flag ($n = 3$, biological replicates). **(F)** Western blotting analysis of mtDNA-encoded Cox2 in WT MEF cells expressing Flag and *Opa1* KO cells expressing Flag, OPA1-iso1-Flag or OPA1-iso5-Flag. Band densities were quantified using ImageJ, and relative band densities are shown on the bottom. $n = 3$, biological replicates. $^{*}p < 0.05$, $^{**}p < 0.01$, one-way ANOVA.

to mtDNA transcription through its binding with the D-loop region. In addition to the previous reported mitochondrial fusion-dependent pathway, we uncover here a novel fusion-independent mitochondrial function recovery pathway that is dependent on Exon4b (**Figure 5E**). The malfunction of this pathway may be linked to the establishment of the Warburg effect, which could play a role in tumorigenesis.

MATERIALS AND METHODS

Cells

Opa1 KO and control WT MEF cells were purchased from ATCC (Manassas, United States). Human HCC cells SK-Hep1 were obtained from Professor S-MZ (Sun Yat-sen University, China). Hela, 293T and Platinum-E cells were grown in Dulbecco's modified Eagle's medium (DMEM), supplemented with 10% fetal bovine serum (FBS), streptomycin (50 lg/ml), and penicillin (50 U/ml). All cultures were maintained at 37°C in a humidified incubator containing 5% CO_2. For imaging experiments, cells were plated on glass coverslips.

cDNA Samples of Human Tumor Tissue Specimens and Adjacent Non-tumor Tissues

cDNA samples of paired HCC and adjacent non-tumor liver tissues from patients undergoing HCC resection were obtained from the Cancer Center of Sun Yat-sen University in Guangzhou, China. None of the patients had received any local or systemic anticancer treatments before the surgery. Both tumor and non-tumor tissues were histologically confirmed. The protocol was approved by the Institute Research Ethics Committee at the Sun Yat−sen University Cancer Center (approval number: GZR2019-086) and informed consent was obtained from each patient. The patients were anonymously coded in accordance with local ethical guidelines, as instructed by the Declaration of Helsinki.

Plasmid Constructs

All mitochondrial matrix-targeting fluorescent protein (mtFP) vectors encoded the targeting sequence of cytochrome c oxidase subunit VIII to achieve mitochondrial matrix localization. TFAM-EYFP plasmid was constructed by replacing the sequence encoding the cytochrome c oxidase subunit VIII of mtEYFP with that of mTfam (NM_009360). mtDsRed, mtPAGFP, and TFAM-EYFP were sub-cloned into the retroviral vector pMXs-Flag. The pMSCV-puro vectors expressing eight isoforms of human OPA1 were gifts from Professor ZS (Wuhan University, China). All these OPA1 isoforms were then sub-cloned into the retroviral vector pMXs-Flag. NT-Exon4-Flag and NT-Exon4/4b-Flag were cloned with the primers by adding a C-terminus Flag sequence as described (Chen et al., 2003). The reported target sequence for Exon4b and Exon4 ShRNA as described (Chen et al., 2003) were used as shRNA and constructed into the pSUPER vector (oligoengine, VEC-PRT-0002), and then, cells infected with pSUPER were selected with puromycin (Genomeditech, GM-040401-2; 2 μg/mL) for 48 h prior to sampling.

Retrovirus Packaging

For virus production, 8×10^6 Platinum-E cells were plated in a 10-cm dish for 24 h, and then transfected with 10 μg pMXs-based plasmid/40 μg Polyethylenimine (PEI, Polyscience Co., United States) in 1 mL Opti-MEM (Invitrogen, United States). The culture medium was replaced 12 h after transfection, and the medium containing retrovirus was collected 36 h later. Retrovirus generated using pMXs-Flag vector were used as a control to equalize the total amount of retrovirus administered to cells.

Western Blotting

Equal amounts of total protein (∼20 μg) were resolved by 10% polyacrylamide/sodium dodecyl sulfate gel electrophoresis and then transferred onto polyvinylidene fluoride membranes. Membranes were then blocked for 1 h, followed by incubation with anti-SDHA (Abcam, 1:1,000), anti-Cox2 (Abcam, 1:1,000), anti-OPA1 (Abcam, 1:1,000), or anti-Actin (Santa Cruz, 1:2,000) antibodies. After incubation with the primary antibody, membranes were incubated with horseradish peroxidase-coupled secondary antibody and immunoreactivity was subsequently detected using Immobilon Western Chemiluminescent HRP Substrate (Millipore, United States).

Live Cell Oxygen Consumption

OCR and ECAR were measured with the XF24 extracellular flux analyzer (Seahorse Biosciences) as described (Wang et al., 2013). WT cells expressing Flag and *Opa*1 KO cells expressing Flag, OPA1-iso1-Flag, or OPA1-iso5-Flag were seeded at a density of 50,000 cells per well of a XF24 cell culture microplate and incubated overnight to ensure attachment. Before measurement, cells were equilibrated for 1 h in XF base assay medium supplemented with 25 mM glucose, 1 mM sodium pyruvate, and 2 mM L-glutamine in a non-CO_2 incubator. During the incubation time, we loaded 75 μL of 80 mM glucose, 9 μM oligomycin, and 1 M 2-deoxyglucose (for ECAR measurement) or 8 μM oligomycin, 9 μM FCCP, 10 μM rotenone, and 10 μM antimycin A (for OCR measurement), in XF assay media into the injection ports in the XF24 sensor cartridge. Each plotted value was normalized to total cells by counting cell number after measurements.

ATP Measurement

Cellular ATP levels were determined using the ENLITEN ATP Assay System (Promega Corp., Madison, WI, United States). Cell extraction was performed with 2.5% trichloroacetic acid, and the sample was neutralized and diluted in 10 mM Tris-acetate (pH 7.75). ATP levels were then measured using the Luciferase/Luciferin reagent according to the manufacturer's protocol. Mitochondrial ATP production was measured using a previous reported protocol (Yang L. et al., 2015) with a slight modification. Cells were treated with 10 μM oligomycin for 15 min before ATP levels were measured.

Live Cell Microscopic Imaging

Imaging was performed with a Leica DMIRE2 inverted microscope (Leica Microsystems, Montreal, Germany) using a

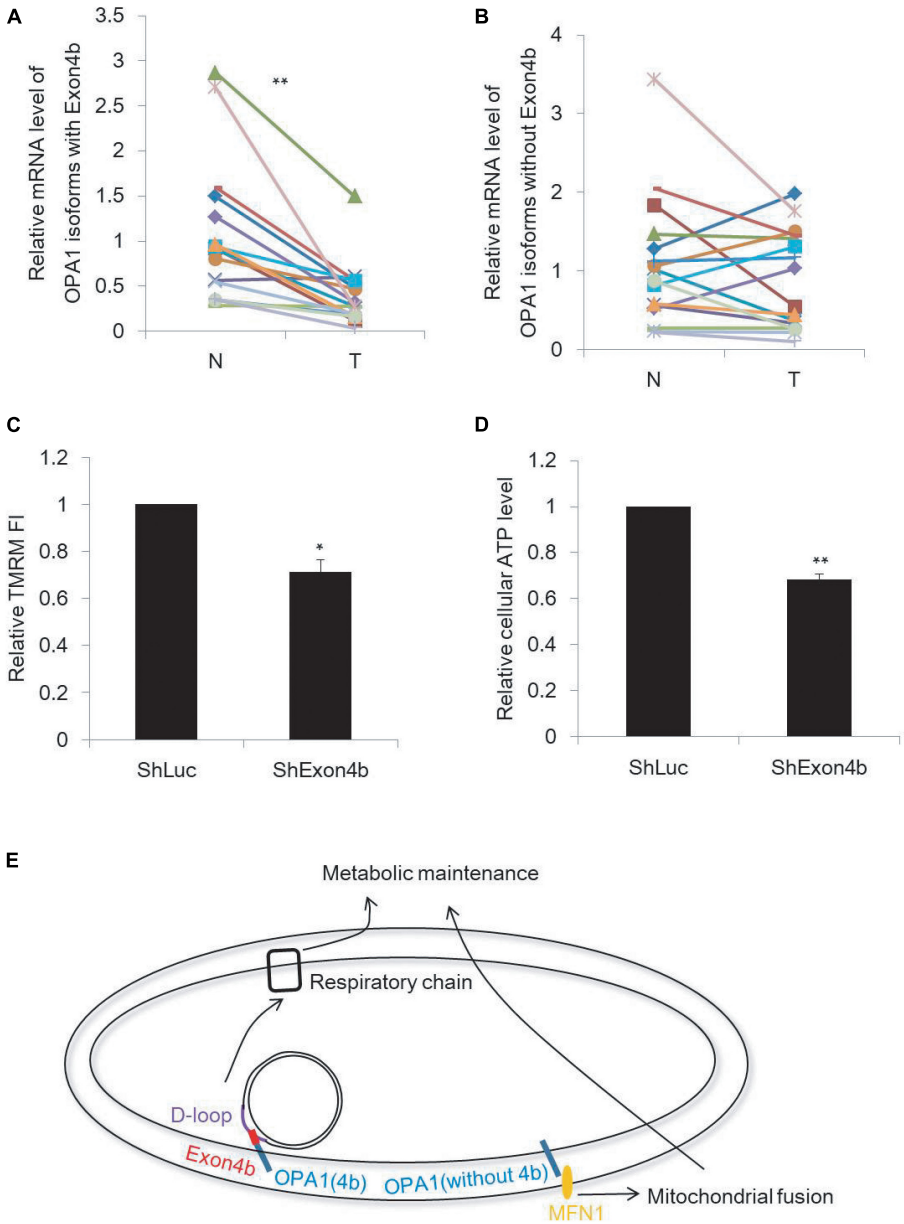

FIGURE 5 | Downregulation of Exon4b-containing OPA1 isoforms in HCC. **(A,B)** mRNA levels of OPA1 isoforms with Exon4b **(A)** and OPA1 isoforms without Exon4b **(B)** in 22 paired HCC (T) and adjacent non-tumor (N) liver tissues ($n = 22$, paired-samples t-test $^{**}p < 0.01$). **(C,D)** Relative TMRM fluorescence intensity (FI) (**C,** $n = 3$, biological replicates) and cellular ATP level (**D,** $n = 3$, biological replicates) in SK-Hep1 cells expressing ShExon4b compared to that in SK-Hep1 cells expressing ShLuc which is normalized to 1 (independent-samples t-test. $^{*}p < 0.05$, $^{**}p < 0.01$). **(E)** Model of the functions of OPA1 isoforms with or without Exon4b.

100 × oil lens (Uapo340, NA 1.40) recording 1,024 × 1,024-pixel image. The Ar/ArKr laser was used for photoactivation of PAGFP at 458-nm and imaging of GFP at 488-nm excitation. The HeNe laser source was used for imaging of DsRed or TMRM at 543-nm excitation. PAGFP was photoactivated using the region-of-interest (ROI) scanning option in the Leica LAS AF Lite software. One 25 μm^2 area was chosen per cell. 80 consecutive images were achieved every 5.83 s after photoactivation. Fusion events were classified as either complete fusion or kiss-and-run as described (Coller et al., 2001).

$\Delta\psi m$ was measured by TMRM staining. For TMRM staining, cells were treated with 25 nM TMRM for 30 min and then replaced with 5 nM TMRM for imaging using the same confocal parameters.

Apoptosis Assay

Cell apoptosis was analyzed using FITC Annexin V Apoptosis Detection Kit (BD Biosciences, 556547) according to the manufacturer's protocol. Cells were washed twice with cold PBS and then resuspended in 1 × binding buffer. Cells were incubated

with FITC Annexin V and PI for 15 min at room temperature in the dark. Then, cell suspension was treated with 1 × binding buffer and analyzed by flow cytometry using a BD Accuri C6 Plus flow cytometer (BD Biosciences) within 1 h, and data were analyzed by using FlowJo V10 software.

Cellular Viability Assay

Cell viability was detected and quantified using a CCK8 assay kit (Beyotime, China). For CCK8 assay, cells were seeded into 96-well culture plate at a density of 2×10^3 cells/well. After 6 h, 10 μL of CCK8 solution was added to each well and incubated for 1 h at 37°C. Then, the viability was recorded based on the optical density (OD) value detected at 450 nm.

mtDNA Nucleoids Imaging by SIM

Cells overexpressing mtDsRed and TFAM-EYFP were seeded on coverslips and cultured for 24 h. Then, cells were fixed and mounted in slides and imaged by N-SIM (Nikon, Japan). The images were taken with a dual-color (laser 488 nm and laser 561 nm) SIM mode, using a 100 × oil (NA 1.49) objective with autofocus maintained by the Nikon Perfect Focus system. All images were reconstructed to maximum projections using NIS-Elements AR software (Nikon, Japan).

Immunofluorescence

Cells were fixed with 4% paraformaldehyde for 15 min, washed, and permeabilized in 0.5% Triton X-100 for 15 min. Cells were then washed, blocked with 1% bovine serum albumen for 15 min, and incubated with primary antibody for 1 h. After washing, cells were then incubated with corresponding secondary antibody (Pierce, United States) for 1 h. All washes were with PBS and all procedures were performed at room temperature. Primary antibodies used were anti-DNA (Millipore, United States, 1:100).

ChIP-qPCR

ChIP-qPCR was done following a previously reported protocol (Yang R.F. et al., 2015) with some modifications. Cells were cross-linked with 1% formaldehyde for 10 min at room temperature, then washed once with ice-cold PBS, and then harvested by scraping with a spatula. Cells were lysed in SDS buffer [1% SDS, 50 mM Tris–HCl (pH 8.0), 10 mM EDTA, and protease inhibitor cocktail] for 10 min at 4°C and sheared into 200–500-bp DNA fragments by sonication. ChIP-grade anti-Flag and control mouse IgG were purchased from Santa Cruz. The primers (forward, 5′-TCAAATGCGTTATCGCCC-3′; reverse, 5′-TTTCATGCCTTGACGGCT-3′) were specific for the D-loop region of mouse mtDNA (GenBank: *AB033825.1*).

qPCR Analysis

Total RNA was extracted using Trizol reagent (Invitrogen, United States) according to the manufacturer's instructions, and cDNA was synthesized by reverse transcription of 1 μg total RNA per sample using the ReverTra Ace@ kit (Toyobo, Japan). qPCR was performed using a CFX-96 real-time PCR detection system (Bio-Rad, United States) in conjunction with SsoAdvanced Universal SYBR Green Supermix (Bio-Rad, United States) using the following conditions: an initial denaturation step of 95°C for 30 s, followed by 40 cycles of denaturation at 95°C for 5 s, and annealing-elongation at 60°C for 20 s. The primers for detecting *Opa1* mRNA and different variant abundances in human samples were used as described (Holt et al., 2007). The primers for detecting mice and human mtDNA genes were used as described (Zhao et al., 2013). Amplification of β-actin cDNA in the same samples was used as an internal control for all PCR amplification reactions, and the primers (forward, 5-TGACGTGGACATCCGCAAAG-3; reverse, 5-CTGGAAGGTGGACAGCGAGG-3) were used to detect β-actin. Gene expression values were calculated based on the comparative quantitative method (the DDCT method) and normalized to values obtained from the amplification of β-actin. For mtDNA copy number determination, total DNA was extracted by a TIANamp Genomic DNA Kit (Tiangen, DP304–03), and the primers for detecting ND5 were used to detect mtDNA copy number.

Statistics

The data were shown as mean ± standard deviation (SD), and all experiments were repeated at least three times. All statistical tests were two-sided and performed using SPSS software (SPSS/IBM Inc., Chicago, IL, United States). All data meet normal distribution and have uniform standard deviations. Paired-sample *t*-test (**Figures 5A,B**) and independent-sample *t*-test (**Figure 5C**) were used for comparisons between two groups. For three or more groups, one-way ANOVA (**Figures 1–4**) was used firstly to detect the difference among these groups; if the *P*-value was less than 0.05, and then multiple comparisons were performed using least significant difference (LSD) *t*-test to detect the difference between any two groups. *P*-value less than 0.05 is considered as significant, while value less than 0.01 is considered as highly significant.

DATA AVAILABILITY STATEMENT

All datasets generated for this study are included in the article/**Supplementary Material**.

ETHICS STATEMENT

The studies involving human participants were reviewed and approved by the Institute Research Ethics Committee at the Sun Yat−sen University Cancer Center (approval number: GZR2019-086). The patients/participants provided their written informed consent to participate in this study.

AUTHOR CONTRIBUTIONS

All authors listed have made a substantial, direct and intellectual contribution to the work, and approved it for publication.

FUNDING

Our work is funded by the National Key Research and Development Program of China (2018YFA0107100), the Strategic Priority Research Program of the Chinese Academy of Sciences (XDA16030505), the National Key Research and Development Program of China (2017YFA0106300, 2017YFA0102900, 2017YFC1001602, 2019YFA09004500, and 2016YFA0100300), the National Natural Science Foundation of China projects (U1601227, 31631163001, 31701281, 31701106, 31801168, 31900614, 31970709, and 81901275), the Key Research Program of Frontier Sciences, CAS (QYZDB-SSW-SMC001), CAS STS Program (KFJ-STS-QYZD-125), Guangzhou Health Care and Cooperative Innovation Major Project (201704020218), Guangdong Province Science and Technology Program (2017B020230005, 2017A020215056, 2017B030314056, 2018A030313825, 2018GZR110103002, 2020A1515011200, 2020A1515010919, and 2020A1515011410), Guangzhou Science and Technology Program (201707010178, 201807010067, and 201707020043), and grant from Yangtze River Scholar Bonus Schemes (XL) and Sun Yat-sen University MOE Key Laboratory of Gene Function and Regulation (LY).

ACKNOWLEDGMENTS

We thank the members in the lab of XL.

SUPPLEMENTARY MATERIAL

The Supplementary Material for this article can be found online at: https://www.frontiersin.org/articles/10.3389/fcell.2020.00180/full#supplementary-material

FIGURE S1 | OMM fusion is not required for $\Delta\psi$m recovery mediated by OPA1-Exon4b, related to **Figure 1**. **(A)** Western blotting analysis of OPA1 and Actin of WT MEF cells expressing Flag and Opa1 KO cells expressing Flag, OPA1-iso1-Flag, or OPA1-iso5-Flag. Band densities were quantified using ImageJ, and relative band densities are shown on the right. $n = 3$, biological replicates. **(B,C)** Time course of a typical mitochondrial kiss-and-run event **(B)** or complete fusion event **(C)**, as determined by photoactivation assay (Scale bar: 1 μm). **(D)** Detection of protein expression levels of *Mfn1* in WT MEF cells expressing ShMfn1 with ShLuc as control. $n = 3$, biological replicates. Band densities were quantified using ImageJ, and relative band densities are shown on the bottom. $n = 3$, biological replicates. **(E)** Detection of protein expression levels of *Mfn2* in WT MEF cells expressing ShMfn2 with ShLuc as control. $n = 3$, biological replicates. Band densities were quantified using ImageJ, and relative band densities are shown on the bottom. $n = 3$, biological replicates. (F) Measurement of $\Delta\psi$m of mitochondria with low $\Delta\psi$m in *Opa1* KO cells expressing OPA1-iso5-Flag plus ShLuc, ShMfn1, ShMfn2, or ShMfn1/2 and OPA1 KO cells expressing ShLuc plus Flag (≥10 cells for each group with three biological replicates). $^{*}p < 0.05$; $^{**}p < 0.01$, one-way ANOVA.

FIGURE S2 | OPA1 Exon-4b and Exon4 modulate mitochondrial respiration, related to **Figure 2**. **(A,B)** Basal and spare respiratory capacity **(A)**, proton leak, and ATP production **(B)** in WT MEF cells expressing Flag and *Opa1* KO cells expressing Flag, OPA1-iso1-Flag, or OPA1-iso5-Flag obtained from **Figure 2A**. **(C–E)** Glycolysis, glycolytic capacity, and glycolytic reserve calculated from ECAR measurements **(C)**, apoptotic cells by flow cytometry **(D)**, and cell viability by CCK-8 (**E**, $n = 3$, biological replicates) in WT MEF cells expressing Flag and *Opa1* KO cells expressing Flag, OPA1-iso1-Flag, or OPA1-iso5-Flag. OPA1 protein expression by western blotting **(F)** and relative cellular ATP level (**G**, $n = 3$, biological replicates) in Hela and 293T cells that expressed Flag, OPA1-iso1-Flag, or OPA1-iso5-Flag. $^{*}p < 0.05$, $^{**}p < 0.01$, one-way ANOVA.

FIGURE S3 | mtDNA nucleoid imaging in *Opa1* KO cells, Hela and 293T cells that overexpressed OPA1-iso1 or OPA1-iso5, related to **Figure 3**. **(A)** *N*-SIM images of diffuse TFAM in 3 *Opa1* KO cells expressing OPA1-iso1-Flag from **Figure 3A**. **(B)** Relative mtDNA copy number in WT MEF cells expressing Flag and Opa1 KO cells expressing Flag, OPA1-iso1-Flag, or OPA1-iso5-Flag ($n = 3$, biological replicates). **(C)** Anti-Tfam IF in Hela and 293T cells that overexpressed OPA1-iso1 or OPA1-iso5. **(D)** Quantification mtDNA nucleoid number of B (≥15 cells for three biological replicates).

FIGURE S4 | OPA1-iso5 increased mtDNA transcription, related to **Figure 4**. **(A,B)** Relative mRNA levels of mtDNA genes in Hela and 293T cells expressing Flag, OPA1-iso1-Flag, or OPA1-iso5-Flag ($n = 3$, biological replicates). **(C)** Western blotting analysis of nuclear-encoded SDHA in WT MEF cells expressing Flag and *Opa1* KO cells expressing Flag, OPA1-iso1-Flag or OPA1-iso5-Flag. Band densities were quantified using ImageJ, and relative band densities are shown on the bottom. $n = 3$, biological replicates. $^{*}p < 0.05$, $^{**}p < 0.01$, one-way ANOVA.

FIGURE S5 | Exon4b silencing in SK-Hep1 cells, related to **Figure 5**. Detection of mRNA levels of OPA1 isoforms with Exon4b **(A)** and protein level of OPA1 **(B)** in SK-Hep1 cells expressing ShExon4b with ShLuc as control. Band densities of B were quantified using ImageJ, and relative band densities are shown on the bottom. $n = 3$, biological replicates. $^{**}p < 0.01$, one-way ANOVA.

REFERENCES

Amati-Bonneau, P., Valentino, M. L., Reynier, P., Gallardo, M. E., Bornstein, B., Boissiere, A., et al. (2008). OPA1 mutations induce mitochondrial DNA instability and optic atrophy 'plus' phenotypes. *Brain* 131, 338–351. doi: 10.1093/brain/awm298

Bogenhagen, D. F., Rousseau, D., and Burke, S. (2008). The layered structure of human mitochondrial DNA nucleoids. *J. Biol. Chem.* 283, 3665–3675. doi: 10.1074/jbc.M708444200

Brown, T. A., Tkachuk, A. N., Shtengel, G., Kopek, B. G., Bogenhagen, D. F., Hess, H. F., et al. (2011). Superresolution fluorescence imaging of mitochondrial nucleoids reveals their spatial range, limits, and membrane interaction. *Mol. Cell. Biol.* 31, 4994–5010. doi: 10.1128/MCB.05694-11

Chan, D. C. (2006). Mitochondria: dynamic organelles in disease, aging, and development. *Cell* 125, 1241–1252. doi: 10.1016/j.cell.2006.06.010

Chen, H., Detmer, S. A., Ewald, A. J., Griffin, E. E., Fraser, S. E., and Chan, D. C. (2003). Mitofusins Mfn1 and Mfn2 coordinately regulate mitochondrial fusion and are essential for embryonic development. *J. Cell Biol.* 160, 189–200. doi: 10.1083/jcb.200211046

Chen, H., McCaffery, J. M., and Chan, D. C. (2007). Mitochondrial fusion protects against neurodegeneration in the cerebellum. *Cell* 130, 548–562. doi: 10.1016/j.cell.2007.06.026

Chen, H., Vermulst, M., Wang, Y. E., Chomyn, A., Prolla, T. A., McCaffery, J. M., et al. (2010). Mitochondrial fusion is required for mtDNA stability in skeletal muscle and tolerance of mtDNA mutations. *Cell* 141, 280–289. doi: 10.1016/j.cell.2010.02.026

Coller, H. A., Khrapko, K., Bodyak, N. D., Nekhaeva, E., Herrero-Jimenez, P., and Thilly, W. G. (2001). High frequency of homoplasmic mitochondrial DNA mutations in human tumors can be explained without selection. *Nat. Genet.* 28, 147–150. doi: 10.1038/88859

Cui, H., Huang, P., Wang, Z., Zhang, Y., Zhang, Z., Xu, W., et al. (2013). Association of decreased mitochondrial DNA content with the progression of colorectal cancer. *BMC Cancer* 13:110. doi: 10.1186/1471-2407-13-110

Del Dotto, V., Mishra, P., Vidoni, S., Fogazza, M., Maresca, A., Caporali, L., et al. (2017). OPA1 isoforms in the hierarchical organization of mitochondrial functions. *Cell Rep.* 19, 2557–2571. doi: 10.1016/j.celrep.2017.05.073

Delettre, C., Griffoin, J. M., Kaplan, J., Dollfus, H., Lorenz, B., Faivre, L., et al. (2001). Mutation spectrum and splicing variants in the OPA1 gene. *Hum. Genet.* 109, 584–591. doi: 10.1007/s00439-001-0633-y

Elachouri, G., Vidoni, S., Zanna, C., Pattyn, A., Boukhaddaoui, H., Gaget, K., et al. (2011). OPA1 links human mitochondrial genome maintenance to mtDNA replication and distribution. *Genome Res.* 21, 12–20. doi: 10.1101/gr.106896.110

Farge, G., and Falkenberg, M. (2019). Organization of DNA in mammalian mitochondria. *Int. J. Mol. Sci.* 20:2770. doi: 10.3390/ijms20112770

Folmes, C. D., Martinez-Fernandez, A., Perales-Clemente, E., Li, X., McDonald, A., Oglesbee, D., et al. (2013). Disease-causing mitochondrial heteroplasmy segregated within induced pluripotent stem cell clones derived from a patient with MELAS. *Stem Cells* 31, 1298–1308. doi: 10.1002/stem.1389

Frezza, C., Cipolat, S., Martins de Brito, O., Micaroni, M., Beznoussenko, G. V., Rudka, T., et al. (2006). OPA1 controls apoptotic cristae remodeling independently from mitochondrial fusion. *Cell* 126, 177–189. doi: 10.1016/j.cell.2006.06.025

Frilling, A., Malago, M., Testa, G., Schleyer, E., Grabellus, F., Kronenberger, R., et al. (2010). Liver transplantation for metastasized extragastrointestinal stromal tumor: a case report and an overview of literature. *Transplant Proc.* 42, 3843–3848. doi: 10.1016/j.transproceed.2010.06.016

Gilkerson, R. W., Schon, E. A., Hernandez, E., and Davidson, M. M. (2008). Mitochondrial nucleoids maintain genetic autonomy but allow for functional complementation. *J. Cell Biol.* 181, 1117–1128. doi: 10.1083/jcb.200712101

Griparic, L., Kanazawa, T., and van der Bliek, A. M. (2007). Regulation of the mitochondrial dynamin-like protein Opa1 by proteolytic cleavage. *J. Cell Biol.* 178, 757–764. doi: 10.1083/jcb.200704112

He, J., Cooper, H. M., Reyes, A., Di Re, M., Sembongi, H., Litwin, T. R., et al. (2012). Mitochondrial nucleoid interacting proteins support mitochondrial protein synthesis. *Nucleic Acids Res.* 40, 6109–6121. doi: 10.1093/nar/gks266

Holt, I. J., He, J., Mao, C. C., Boyd-Kirkup, J. D., Martinsson, P., Sembongi, H., et al. (2007). Mammalian mitochondrial nucleoids: organizing an independently minded genome. *Mitochondrion* 7, 311–321. doi: 10.1016/j.mito.2007.06.004

Hudson, G., Amati-Bonneau, P., Blakely, E. L., Stewart, J. D., He, L., Schaefer, A. M., et al. (2008). Mutation of OPA1 causes dominant optic atrophy with external ophthalmoplegia, ataxia, deafness and multiple mitochondrial DNA deletions: a novel disorder of mtDNA maintenance. *Brain* 131, 329–337. doi: 10.1093/brain/awm272

Ishikawa, K., Takenaga, K., Akimoto, M., Koshikawa, N., Yamaguchi, A., Imanishi, H., et al. (2008). ROS-generating mitochondrial DNA mutations can regulate tumor cell metastasis. *Science* 320, 661–664. doi: 10.1126/science.1156906

Kukat, C., Davies, K. M., Wurm, C. A., Spahr, H., Bonekamp, N. A., Kuhl, I., et al. (2015). Cross-strand binding of TFAM to a single mtDNA molecule forms the mitochondrial nucleoid. *Proc. Natl. Acad. Sci. U.S.A.* 112, 11288–11293. doi: 10.1073/pnas.1512131112

Lee, H. C., Yin, P. H., Lin, J. C., Wu, C. C., Chen, C. Y., Wu, C. W., et al. (2005). Mitochondrial genome instability and mtDNA depletion in human cancers. *Ann. N. Y. Acad. Sci.* 1042, 109–122. doi: 10.1196/annals.1338.011

Legros, F., Malka, F., Frachon, P., Lombes, A., and Rojo, M. (2004). Organization and dynamics of human mitochondrial DNA. *J. Cell Sci.* 117, 2653–2662. doi: 10.1242/jcs.01134

Liu, X., and Hajnoczky, G. (2011). Altered fusion dynamics underlie unique morphological changes in mitochondria during hypoxia-reoxygenation stress. *Cell Death. Differ.* 18, 1561–1572. doi: 10.1038/cdd.2011.13

Liu, X., Weaver, D., Shirihai, O., and Hajnoczky, G. (2009). Mitochondrial 'kiss-and-run': interplay between mitochondrial motility and fusion-fission dynamics. *EMBO J.* 28, 3074–3089. doi: 10.1038/emboj.2009.255

McBride, H. M., Neuspiel, M., and Wasiak, S. (2006). Mitochondria: more than just a powerhouse. *Curr. Biol.* 16, R551–R560. doi: 10.1016/j.cub.2006.06.054

Olichon, A., Elachouri, G., Baricault, L., Delettre, C., Belenguer, P., and Lenaers, G. (2007). OPA1 alternate splicing uncouples an evolutionary conserved function in mitochondrial fusion from a vertebrate restricted function in apoptosis. *Cell Death. Differ.* 14, 682–692. doi: 10.1038/sj.cdd.4402048

Parone, P. A., Da Cruz, S., Tondera, D., Mattenberger, Y., James, D. I., Maechler, P., et al. (2008). Preventing mitochondrial fission impairs mitochondrial function and leads to loss of mitochondrial DNA. *PLoS One* 3:e3257. doi: 10.1371/journal.pone.0003257

Qiao, L., Ru, G., Mao, Z., Wang, C., Nie, Z., Li, Q., et al. (2017). Mitochondrial DNA depletion, mitochondrial mutations and high TFAM expression in hepatocellular carcinoma. *Oncotarget* 8, 84373–84383. doi: 10.18632/oncotarget.21033

Reyes, A., He, J., Mao, C. C., Bailey, L. J., Di Re, M., Sembongi, H., et al. (2011). Actin and myosin contribute to mammalian mitochondrial DNA maintenance. *Nucleic Acids Res.* 39, 5098–5108. doi: 10.1093/nar/gkr052

Scarpulla, R. C. (2008). Transcriptional paradigms in mammalian mitochondrial biogenesis and function. *Physiol. Rev.* 88, 611–638. doi: 10.1152/physrev.00025.2007

Song, Z., Chen, H., Fiket, M., Alexander, C., and Chan, D. C. (2007). OPA1 processing controls mitochondrial fusion and is regulated by mRNA splicing, membrane potential, and Yme1L. *J. Cell Biol.* 178, 749–755. doi: 10.1083/jcb.200704110

Suen, D. F., Norris, K. L., and Youle, R. J. (2008). Mitochondrial dynamics and apoptosis. *Genes Dev.* 22, 1577–1590. doi: 10.1101/gad.1658508

Tatsuta, T., and Langer, T. (2008). Quality control of mitochondria: protection against neurodegeneration and ageing. *EMBO J.* 27, 306–314. doi: 10.1038/sj.emboj.7601972

Tondera, D., Grandemange, S., Jourdain, A., Karbowski, M., Mattenberger, Y., Herzig, S., et al. (2009). SLP-2 is required for stress-induced mitochondrial hyperfusion. *EMBO J.* 28, 1589–1600. doi: 10.1038/emboj.2009.89

Wang, Y. E., Marinov, G. K., Wold, B. J., and Chan, D. C. (2013). Genome-wide analysis reveals coating of the mitochondrial genome by TFAM. *PLoS One* 8:e74513. doi: 10.1371/journal.pone.0074513

Yang, L., Long, Q., Liu, J., Tang, H., Li, Y., and Bao, F. (2015). Mitochondrial fusion provides an 'initial metabolic complementation' controlled by mtDNA. *Cell. Mol. Life Sci.* 72, 2585–2598. doi: 10.1007/s00018-015-1863-9

Yang, R. F., Sun, L. H., Zhang, R., Zhang, Y., Luo, Y. X., Zheng, W., et al. (2015). Suppression of Mic60 compromises mitochondrial transcription and oxidative phosphorylation. *Sci. Rep.* 5:7990. doi: 10.1038/srep07990

Zhao, X., Tian, C., Puszyk, W. M., Ogunwobi, O. O., Cao, M., Wang, T., et al. (2013). OPA1 downregulation is involved in sorafenib-induced apoptosis in hepatocellular carcinoma. *Lab. Invest.* 93, 8–19. doi: 10.1038/labinvest.2012.144

Conflict of Interest: The authors declare that the research was conducted in the absence of any commercial or financial relationships that could be construed as a potential conflict of interest.

frontiers in Cell and Developmental Biology

ORIGINAL RESEARCH
published: 25 May 2020
doi: 10.3389/fcell.2020.00374

Autophagy Regulates Fungal Virulence and Sexual Reproduction in *Cryptococcus neoformans*

Su-Ting Jiang[1,2†], An-Ni Chang[1†], Lian-Tao Han[1,2], Jie-Shu Guo[1,2], Yuan-Hong Li[1,2] and Tong-Bao Liu[1,2]*

[1] State Key Laboratory of Silkworm Genome Biology, Southwest University, Chongqing, China, [2] Chongqing Key Laboratory of Microsporidia Infection and Control, Southwest University, Chongqing, China

Autophagy (macroautophagy) is an evolutionarily conserved degradation pathway involved in bulk degradation of cytoplasmic organelles, old protein, and other macromolecules and nutrient recycling during starvation. Extensive studies on functions of autophagy-related genes have revealed that autophagy plays a role in cell differentiation and pathogenesis of pathogenic fungi. In this study, we identified and characterized 14 core autophagy machinery genes (*ATG*s) in *C. neoformans*. To understand the function of autophagy in virulence and fungal development in *C. neoformans*, we knocked out the 14 *ATG*s in both α and **a** mating type strain backgrounds in *C. neoformans*, respectively, by using biolistic transformation and *in vivo* homologous recombination. Fungal virulence assay showed that virulence of each *atg*Δ mutants was attenuated in a murine inhalation systemic-infection model, although virulence factor production was not dramatically impaired *in vitro*. Fungal mating assays showed that all the 14 *ATG*s are essential for fungal sexual reproduction as basidiospore production was blocked in bilateral mating between each *atg*Δ mutants. Fungal nuclei development assay showed that nuclei in the bilateral mating of each *atg*Δ mutants failed to undergo meiosis after fusion, indicating autophagy is essential for regulating meiosis during mating. Overall, our study showed that autophagy is essential for fungal virulence and sexual reproduction in *C. neoformans*, which likely represents a conserved novel virulence and sexual reproduction control mechanism that involves the autophagy-mediated proteolysis pathway.

Keywords: *Cryptococcus neoformans*, autophagy, *ATG*s, virulence, sexual reproduction

OPEN ACCESS

Edited by:
Du Feng,
Guangzhou Medical University, China

Reviewed by:
Kwang-Woo Jung,
Korea Atomic Energy Research Institute (KAERI), South Korea
Changbin Chen,
Institut Pasteur of Shanghai (CAS), China

***Correspondence:**
Tong-Bao Liu
tongbaoliu@swu.edu.cn

† These authors have contributed equally to this work

Specialty section:
This article was submitted to Molecular Medicine, a section of the journal Frontiers in Cell and Developmental Biology

Received: *31 January 2020*
Accepted: *27 April 2020*
Published: *25 May 2020*

Citation:
Jiang S-T, Chang A-N, Han L-T, Guo J-S, Li Y-H and Liu T-B (2020) Autophagy Regulates Fungal Virulence and Sexual Reproduction in Cryptococcus neoformans. Front. Cell Dev. Biol. 8:374. doi: 10.3389/fcell.2020.00374

INTRODUCTION

Cryptococcus neoformans is ubiquitous encapsulated yeast pathogen causing life-threating meningoencephalitis predominantly in the immunocompromised population (Casadevall and Perfect, 1998). In recent decades, with the increase of the people having HIV/AIDS or who have received organ transplants and immunosuppressive therapy (Brown et al., 2012), *C. neoformans* infects more than one million people worldwide annually, and leading to in hundreds of thousands of people deaths per year (Park et al., 2009; Rajasingham et al., 2017). Being a human fungal pathogen, *C. neoformans* expresses several virulence factors, including the production

of polysaccharide capsule and melanin, and growth at 37°C, which favors the infection and the pathogenesis of *C. neoformans* (Kozel, 1995; Kronstad et al., 2008; Zaragoza, 2019). As a heterothallic basidiomycetous fungus, *C. neoformans* has two mating types, α and **a**, and can undergo a dimorphic transition to a filamentous growth by mating and monokaryotic fruiting. During mating in *C. neoformans*, haploid cells of α and **a** mating types fused to form dikaryotic hyphae leading to the formation of a basidium, and four chains of haploid basidiospores were eventually produced on top of the basidium following the completion of meiosis inside the basidium (**Figure 9**; Lin and Heitman, 2006; Zhao et al., 2019b). Cryptococcal cells of a single mating type, e.g., α, can also fuse and undergo monokaryotic fruiting to produce filaments and basidiospores under laboratory conditions (Zhao et al., 2019b).

Sexual reproduction favors fungal virulence in *C. neoformans* via producing infectious spores, in that α isolates can be more virulent than congenic **a** isolates (Nielsen et al., 2005). Spores and desiccated yeast cells are thought to be the initial infectious propagules to cause infection by *Cryptococcus* as they are small enough to fit down into the deep alveoli of the lung (Velagapudi et al., 2009). Sexual reproduction also enables the pathogenic fungi to proliferate and undergo genetic exchange in response to new environmental conditions such as stressful conditions, different host organisms, or changes in the host such as antimicrobial therapy. Further research on the sexual nature of pathogenic fungi will help to elucidate how fungi have evolved into successful pathogens.

Autophagy is an evolutionally conserved cellular degradation process in which the cytoplasmic components such as organelles, aggregated proteins, invading microorganisms, and other cytoplasmic materials are sequestered and transferred to vacuole or lysosome for degradation and recycling (Yorimitsu and Klionsky, 2005). Several types of autophagy have been described, including macroautophagy (Yorimitsu and Klionsky, 2005), microautophagy (Youle and Narendra, 2011), and chaperone-mediated autophagy (Arias and Cuervo, 2011). Macroautophagy (referred to hereafter as autophagy) is the main pathway that involves the delivery of cytosolic components to the vacuole/lysosome for degradation by double-membrane vesicles known as an autophagosome. In contrast, microautophagy involves direct engulfment of cytosolic material into the vacuole/lysosome. Chaperone mediated autophagy is a complicated and specific pathway for proteolysis of specific cytosolic proteins with the aid of chaperone molecules. In all types of autophagy, the formation of the sequestering vesicles, the autophagosome, is the hallmark morphological feature of this dynamic process (Xie and Klionsky, 2007). So far, there are at least 42 autophagy-related genes (*ATG*s) that have been identified in the model yeast *S. cerevisiae* by genetic screening, and many of them are conserved in fungi, plants, and mammals (Parzych et al., 2018). Among these *ATG*s, 15 of them are required for autophagosome formation, and their corresponding gene products are referred to as the core autophagy machinery. In *S. cerevisiae*, the core autophagy machinery proteins (Atgs) are as follows: Atg1-10, Atg12, Atg13, Atg14, Atg16, and Atg18 (Xie and Klionsky, 2007).

Autophagy plays an important role in protecting the organism against diverse pathologies, including infections, cancer, neurodegeneration, aging, and heart diseases (Levine and Kroemer, 2008). The role of autophagy has also been extensively studied and appears to play a critical role in growth, morphology, development, and pathogenicity in filamentous fungi (Pollack et al., 2009; Voigt and Poggeler, 2013; Liu et al., 2016). However, of the three fungal pathogens of most significant relevance to human health, autophagy is not required for the virulence of both *Candida albicans* and *Aspergillus fumigatus*. Only *C. neoformans* has been shown to require this process during infection (Palmer et al., 2008). In *A. fumigatus*, the serine-threonine kinase *Af* Atg1 was shown to be essential for normal conidiophore development and optimal conidiation under nutrient-limiting conditions, implying that autophagy is required to recycle internal resources to support fungal development (Richie et al., 2007). However, the A*fatg1*Δ mutant remained fully virulent in a mouse model of invasive aspergillosis despite its developmental defects under starvation-associated conditions (Richie and Askew, 2008a). In *C. albicans*, an autophagy-defective mutant Ca*atg9*Δ was generated through the deletion of an *ATG9* homolog. Fungal development and virulence assay of the Ca*atg9*Δ mutant proved that autophagy is not required for *C. albicans* differentiation, survival within or killing of a macrophage cell line, and fully virulent in an intravenous mouse model of disseminated candidiasis (Palmer et al., 2007, 2008).

The role of autophagy was also investigated in *C. neoformans*, and the evidence so far suggested that autophagy also plays an important role in virulence of *C. neoformans*. For instance, disruption of the phosphatidylinositol 3-kinase (PI3K) encoding gene resulted in virulence attenuation in a murine model of cryptococcosis (Hu et al., 2008). The role of autophagy during cryptococcal infection was also confirmed by RNAi suppression of *ATG8* in the same study, which attenuated virulence in both intranasal and intravenous infection models (Hu et al., 2008). Also, the *ATG7* gene has been shown to play roles in the virulence of *C. neoformans* (Oliveira et al., 2016). Recently, four *ATG* genes, *ATG1*, *ATG7*, *ATG8*, and *ATG9*, including the two (*ATG7* and *ATG8*) studied before, were functionally examined in *C. neoformans* and the results suggested that *ATG1*, *ATG7*, *ATG8*, and *ATG9* each make different contributions to *C. neoformans* virulence, indicating *Cryptococcus* virulence may not be utterly dependent on core autophagy functions (Ding et al., 2018). More recently, Zhao et al. constructed 22 autophagy-deficient strains in *C. neoformans* and found that 12 of them showed remarkable virulence attenuation in the invertebrate (*Galleria mellonella*) model of cryptococcosis (Zhao et al., 2019a).

The above studies provided insight into the contribution of *ATG* genes to virulence to *C. neoformans*. However, only four of the 15 *ATG*s have been tested for their role in fungal virulence in the murine model of systemic cryptococcosis. The remaining 11 *ATG*s have not been studied for their role in a mouse model of cryptococcosis to our knowledge and remain to be determined. Furthermore, besides its medical importance, *C. neoformans* has been developed as a model organism for fungal genetics study because of its defined sexual cycle. However, whether the autophagy pathway regulates the sexual reproduction of

C. neoformans and, if so, how does autophagy regulate the sexual reproduction of *C. neoformans* remains unknown.

In this study, we therefore systematically identified and characterized 14 core autophagy machinery proteins (Atgs) in *C. neoformans*. We found that each of the 14 Atgs was required for autophagy-related phenotypes. The outcome of fungal virulence study further suggested *C. neoformans* virulence may not be completely dependent on core autophagy functions as each *atg*Δ mutant displayed different levels of virulence and caused different disease progression profiles in infected mice in a murine inhalation model of cryptococcosis. Interestingly, when tested in a bilateral mating assay, all the *atg*Δ mutants failed to produce basidiospores, and the nuclei inside basidium failed to undergo meiosis after fusion, indicating Atgs are essential for regulating meiosis during mating. Overall, our study showed that autophagy is essential for fungal virulence and sexual reproduction in *C. neoformans*, which likely represents a conserved novel virulence and sexual reproduction control mechanism that involves the autophagy-mediated proteolysis pathway.

MATERIALS AND METHODS

Strains and Growth Media

Cryptococcus neoformans and its derived strains used in this study are listed in **Supplementary Table S1**. Strains were grown at 30°C on YPD agar medium. MS medium (Murashige and Skoog medium) and V8 used for mating and sporulation assays were prepared as described previously (Xue et al., 2007). SD-N medium was used for nitrogen starvation assay (Kim et al., 2002). Minimal medium (MM) was used to induce capsule formation (Vij et al., 2018). All other media were prepared as described previously (Fan et al., 2019).

Detection of *ATG*s Expression Under Starvation Condition

To test the expression of the *ATG*s under nitrogen starvation, we measured the *ATG*s at mRNA levels using quantitative real-time PCR (qRT-PCR) as previously described (Fan et al., 2019). Briefly, overnight cultures of the wild-type (WT) strain were washed three times with ddH_2O and resuspended in SD-N medium for starvation induction. The harvested cells were washed with ddH_2O, and the pellets were used for total RNA extraction and cDNA synthesis. Gene expression levels were normalized using *GAPDH* as the endogenous control gene, and the relative levels were determined using the comparative threshold cycle (C_T) method (Livak and Schmittgen, 2001). The specificity of the PCR was further verified by subjecting the amplification products to agarose gel electrophoresis and sequencing reaction.

Generation of *atg*Δ Mutants and Their Complemented Strains

Each of the 14 *atg*Δ mutants was generated in the WT H99 and KN99**a** strain backgrounds by using a split marker strategy with minor modification (Kim et al., 2009; Fan et al., 2019). The two overlap PCR fragments for homologous recombination were obtained after two rounds of PCR and then biolistically transformed into the cells of H99 or KN99**a** after combination and precipitation onto 10-μl of gold microcarrier beads (0.6 μm, BioRad). Stable transformants were selected on YPD plates containing 200 mg/L G418. The *ATG*s gene knockout mutants were first screened by diagnostic PCR using positive primers F4/R4 and negative primers F3/R3 (see **Supplementary Table S2**) and then further confirmed by Southern blotting.

To generate complemented strains of each *atg*Δ mutant, a genomic DNA fragment containing a 1.5-Kb upstream promoter region, the relevant *ATG* open reading frame (ORF), and its 500-bp downstream region was amplified in a PCR using primers Comp F1 and R1 (see **Supplementary Table S2**). This PCR fragment was cloned into the plasmid pTBL1, which contains the *NAT* selective marker gene to generate the complementation plasmid for each *atg*Δ mutant (see **Supplementary Table S1**). Each plasmid was linearized by the appropriate restriction endonuclease and biolistically transformed in both α and **a** mating-type *atg*Δ mutant strains. The mating assay was performed to identify transformants that complemented the *atg*Δ mutant phenotype.

Nitrogen Starvation Assay

To test whether the core autophagy genes we identified in *C. neoformans* are required for autophagosome formation, the 14 *atg*Δ mutants were first cultured overnight in YPD and then washed and switched to SD-N medium supplemented with 2 mM PMSF and further incubated for 4 or 5 h. The accumulation of autophagic bodies was observed under a microscope (Olympus BX53). To examine the survival of the cryptococcal strains under nitrogen starvation conditions, the cells of WT H99, *atg*Δ mutants, and their complemented strains were first grown overnight in YPD and then washed and resuspended in SD-N medium to an OD_{600} = 1.0. At indicated times, aliquots were removed and plated onto YPD plates in triplicate after appropriate dilution. Colony-forming units of cryptococcal strains survived in nitrogen starvation were counted after 2 days of incubation at 30°C. Meanwhile, a ten-fold serial dilution of the suspensions was also prepared, and 5 μl of the aliquots were grown on YPD plates for 48 h before photography.

Assays for Melanin, Capsule Production, and Mating

Melanin production of cryptococcal strains was performed on the Niger seed agar medium. 100 μl of each ddH_2O washed overnight culture was grown on Niger seed plates at 30°C or 37°C for 24 or 48 h, and the pigmentation of fungal colonies was assessed. To examine capsule production, a total of 10^6 cells from YPD overnight cultures of each strain were grown in MM medium at 30°C for 72 h. The capsule size was analyzed as described previously (Liu et al., 2011). In a mating assay, *C. neoformans* cell suspensions of opposite mating types (α or **a**) were mixed and cocultured on MS or V8 medium at 25°C in the dark. Mating filaments and basidiospore formation were examined and recorded by photography using the Olympus CX41 light microscope after incubation for 14 days.

Virulence Studies

Overnight cultures of each yeast strains were washed twice with PBS buffer and resuspended at a final concentration of 2×10^6 cells/ml. Groups of 10 female C57 BL/6 mice (Chongqing Medical University, China) were intranasally infected with 10^5 cells of each yeast strain as previously described (Cox et al., 2000). Animals that appeared moribund or in pain were sacrificed by CO_2 inhalation throughout the experiments. Survival data from the murine experiments were statistically analyzed between paired groups using the log-rank test, and statistical analysis of fungal burden was performed by non-parametric Mann-Whitney test with PRISM version 7.0 (GraphPad Software, San Diego, CA) (P values of <0.001 were considered significant).

Histopathology and Fungal Burdens in Infected Organs

Infected animals were sacrificed at the endpoint of the experiment according to Southwest University-approved animal protocol. For mice infected by the *atg6*Δ and *atg18*Δ mutants, the experiment was terminated at 80 days post-infection (DPI). To compare the fungal burdens, brains, lungs, and spleens from mice infected by H99, each *atg*Δ mutant, or the complemented strain of each *atg*Δ mutant were isolated at the end time point (ETP), fixed in 10% formalin solution, and sent to the Servicebio biological laboratory for section preparation (Servicebio, Wuhan, China). To evaluate the disease progression, mice infected by the WT, *atg6*Δ, *atg8*Δ, and *atg12*Δ mutants were sacrificed at 7, 14, 21 DPI, and the organs were also prepared for section and fungal burden examination. Tissue slides were stained with hematoxylin and eosin (H&E) and examined by light microscopy (Olympus BX53). Infected brains, lungs, and spleens were also isolated and homogenized using a homogenizer in PBS buffer. Resuspensions were diluted, 100 μl of each dilution was spread on YPD medium with ampicillin and chloramphenicol, and colonies were determined after 2 days of incubation at 30°C.

Ethics Statement

The animal studies conducted at Southwest University were in full compliance with "Guidelines on Ethical Treatment of Experimental Animals (2006, No. 398)" issued by the Ministry of Science and Technology of China and the "Regulation on the Management of Experimental Animals (2006, No. 195)" issued by Chongqing Municipal People's Government. The Animal Ethics Committee of Southwest University approved all of the vertebrate studies.

RESULTS

Identification of Core Autophagy Machinery Proteins (Atgs) in *C. neoformans*

To identify the orthologs of the Atgs in the H99 strain of *C. neoformans*, the 15 Atgs from *S. cerevisiae* S288c were used as quires for a BLASTp search. Meanwhile, reciprocal BLASTp was also used to ensure that the most similar sequence of each cryptococcal Atg candidate in *S. cerevisiae* was the same as that of the *S. cerevisiae* inquiry gene. Finally, we identified 14 orthologs out of the 15 *S. cerevisiae* Atgs in *C. neoformans* except for the Atg10 (**Table 1**).

To further ensure that the identified Atg candidates in *C. neoformans* are Atgs, we detected the expression of the *ATG* candidate gene in nitrogen starvation conditions by qRT-PCR. Our results showed that the expression levels of all the 14 candidate genes increased under nitrogen starvation conditions (**Figure 1**), implying that the 14 candidate genes are *ATG* genes in *C. neoformans*.

The *ATG*s Are Required for Autophagy in *C. neoformans*

To further investigate the roles of the *ATG* genes in *C. neoformans*, we generated the 14 single-gene deletion mutants in both H99 and KN99**a** strain backgrounds of *C. neoformans*. The 14 *ATG*s gene knockout mutants were first screened by diagnostic PCR using positive primers F4/R4 and negative primers F3/R3 (see **Supplementary Table S2**) and then further confirmed by Southern blotting (**Figure 2** and **Supplementary Figure S1**). The complemented strains of each *atg*Δ mutants were also obtained by introducing the corresponding complementation plasmid in both α and **a** mating-type *atg*Δ mutants (see **Supplementary Table S3** for a summary of the *ATG*-related strains).

First, we verified the formation of autophagosomes of each single deletion mutant under nitrogen starvation conditions (SD-N), and the results showed that all the single deletion mutants failed to produce autophagosomes in *C. neoformans*. At the same time, more than half of the WT cells had accumulated autophagosome-like vesicles in the vacuole in the present of 2 mM PMSF (**Figure 3A**). The autophagosomes formation levels of the mutants were restored to the WT level when each *ATG* gene was reintroduced into the respective mutants (**Figure 3A**). Besides, we tested the survival of every single mutant under nitrogen starvation conditions, and each single deletion mutant exhibited the expected autophagy phenotype of impaired survival upon nitrogen starvation (**Figures 3B,C**). After transfer from a nutrient-rich medium, e.g., YPD to a nitrogen-free medium, e.g., SD-N, the WT cells remained viable even after 15 days of starvation induction. In contrast, cells of all the *atg*Δ mutants showed survival defects during starvation (**Figure 3C**). The survival rate of the *atg*Δ mutants was restored to the WT level when each *ATG* gene was reintroduced into the respective mutants (**Figures 3B,C**).

Loss of Atgs Impairs Growth, Cell Membrane Integrity, and Capsule Production in *C. neoformans*

To investigate the roles of Atgs on cell growth and virulence in *C. neoformans*, we next examined the cell growth and the production of three major virulence factors of *atg*Δ mutants under various stress conditions. The *atg6*Δ, *atg7*Δ, and *atg18*Δ mutants had a slight growth defect on YPD

TABLE 1 | The core autophagy machinery proteins in *C. neoformans*.

Name	*S. cerevisae*	*C. neoformans*	Function	Identity (%)	Similarity (%)
Atg1	YGL180W	CNAG_05005	Protein serine/threonine kinase, regulates magnitude of autophagy	46	61
Atg2	YNL242W	CNAG_06732	Peripheral membrane protein, mediates the retrieval of Atg9 from the PAS back to peripheral sites	28	45
Atg3	YNR007C	CNAG_06892	E2-like conjugating enzyme, functions in the conjugation of Atg8-PE	35	48
Atg4	YNL223W	CNAG_02662	Cysteine protease, cleaves the C-terminal arginine residue from Atg8 or PE from Atg8-PE conjugate	33	47
Atg5	YPL149W	CNAG_06519	Conjugation target of Atg12, part of the Atg12-Atg5-Atg16 complex	17	33
Atg6	YPL120W	CNAG_01773	Subunit of class III PI3K complex I and II, functions in autophagy and the VPS pathway	32	47
Atg7	YHR171W	CNAG_04538	E1-like activating enzyme, functions in the conjugation of Atg12 and Atg5 or Atg8 and PE	37	52
Atg8	YBL078C	CNAG_00816	Ubiquitin-like protein, conjugated to PE, controls the phagophore expansion	78	90
Atg9	YDL149W	CNAG_01445	Transmembrane protein, cycles between the PAS and other cytosolic punctate structures	39	60
Atg12	YBR217W	CNAG_07645	Ubiquitin-like protein, conjugated to Atg5, part of the Atg12-Atg5-Atg16 complex	37	60
Atg13	YPR185W	CNAG_00778	Regulatory subunit of Atg1 complex, stimulates Atg1 activity and controls the magnitude of autophagy	36	60
Atg14	YBR128C	CNAG_03608	Autophagy-specific subunit of PI3K complex I, targets the complex I to the PAS	27	60
Atg16	YMR159C	CNAG_02576	Component of the Atg12-Atg5-Atg16 complex, mediates the oligomerization of the complex	35	62
Atg18	YFR021W	CNAG_02269	Phosphoinositide binding protein, binds PI3P and PI4P, interacts with Atg2 to mediate the retrieval of Atg9 from the PAS back to peripheral sites	35	52

plates at both 30°C and 37°C while other *atg*Δ mutants were not different from the WT strain H99 (**Figure 4A**). The *atg6*Δ, *atg7*Δ, *atg14*Δ, and *atg18*Δ mutants showed severe growth defects on YPD with 0.025% SDS and moderate growth defect on YPD with 1.5 M NaCl or KCl (**Figure 4A**), but not Congo red, indicating that Atg6, Atg7, Atg14, and Atg18 may regulate cell membrane integrity in *C. neoformans*. Additionally, *atg18*Δ mutant hardly grows on a nitrogen-deficient medium such as YNB or SD-N, implying that Atg18 is essential for nitrogen source utilization in *C. neoformans* (**Supplementary Figure S2**).

Besides the growth defect on YPD, the *atg18*Δ mutant produced less melanin than the WT strain after 24 or 48 h of incubation. However, the levels of melanin produced by the *atg18*Δ mutant at 48 h were comparable to those produced by the WT strain at 24 h (**Figure 4B**), suggesting that the less melanin production by *atg18*Δ mutant was due to impaired growth.

We next examined the capsule formation of the *atg*Δ mutants. Interestingly, we found a deletion of each *ATG* gene has different effects on cryptococcal capsule formation. The *atg4*Δ, *atg5*Δ, *atg12*Δ, and *atg13*Δ mutants were able to produce a capsule of a size similar to that of the WT strain. In contrast, deletion each of the *ATG1*, *ATG2*, *ATG3*, *ATG6*, *ATG8*, *ATG9*, and *ATG16* causes enlarged capsule, while disruption any of the *ATG7*, *ATG14*, and *ATG18* causes reduced capsule in *C. neoformans* (**Figures 4C,D**, $P < 0.0001$ for *ATG7* and $P < 0.0001$ for *ATG14* and *ATG18*), indicating that each of the *ATGs* has a different role in capsule formation in *C. neoformans* even though they are the Atgs.

All the defects showed in the *atg*Δ mutants were recovered when each gene was reintroduced into the respective mutants at the genomic safe haven locus (**Supplementary Figure S3**).

Roles of Atgs in Fungal Infection of *C. neoformans*

To evaluate the role of Atgs in fungal virulence in *C. neoformans*, we examined the virulence of all 14 *atg*Δ mutant strains in a murine inhalation model of systemic infection. Eight-week-old female C57 BL/6 mice (n = 10/group) were inoculated intranasally with 10^5 yeast cells of each *Cryptococcus* strain, and the animals were monitored twice a day. All the mice infected by the WT H99 strain died around 19 to 27 DPI. In contrast, the 14 *atg*Δ mutants showed significant differences in their ability to promote disease development in the murine inhalation model of cryptococcosis. Mice infected with the *atg2*Δ and *atg5*Δ mutant showed 100% mortality around 24 to 27 DPI and 22 to 30 DPI, respectively, with no statistical difference from the mice infected with the WT strains [$P > 0.9999$, Log-rank (Mantel-Cox) test] (**Figure 5A**). Mice infected by *atg3*Δ mutant survived between 27 and 36 DPI, which showed no significant difference compared with that of WT strain, even though 8 days later than WT-infected mice [$P > 0.9999$, Log-rank (Mantel-Cox) test] (**Figure 5A**). Meanwhile, severe organ damage with visible lesion development observed in brains, lungs, and spleens infected by *atg2*Δ, *atg3*Δ, and *atg5*Δ mutants (**Supplementary Figure S4**). The above results showed that loss of Atg2, Atg3, or Atg5 does not affect the virulence of *C. neoformans*. In contrast, mice infected by *atg6*Δ mutant, *atg14*Δ mutant or *atg18*Δ mutant had no illness or symptoms and continued gaining body weight until the end of the experiment (80 DPI) (**Figure 5A**), indicating that Atg6, Atg14, and Atg18 are essential for fungal virulence in *C. neoformans*.

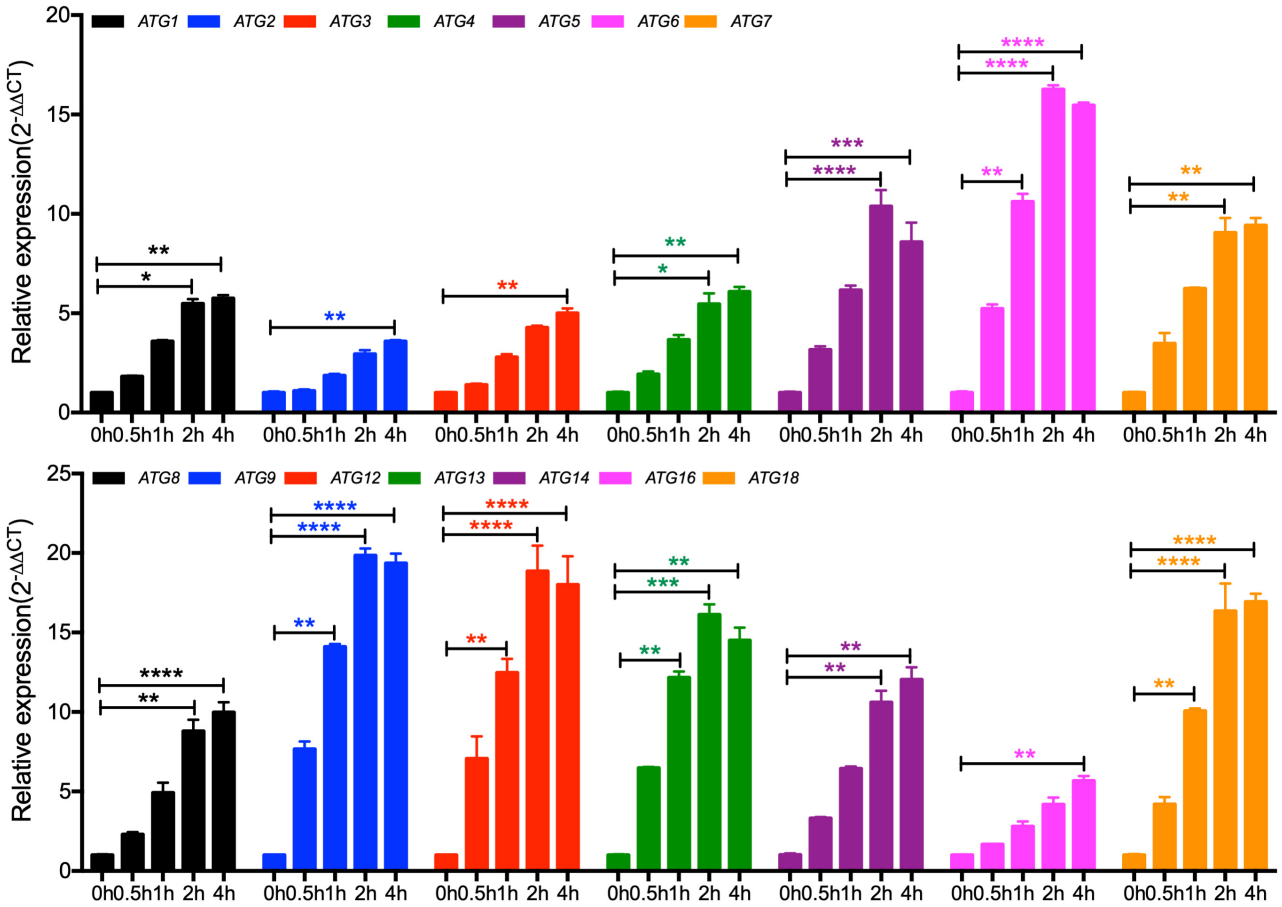

FIGURE 1 | Expression of the core autophagy machinery genes (*ATG*s) under nitrogen starvation in *C. neoformans*. The expression of *ATG*s under nitrogen starvation was measured by qRT-PCR. Overnight cultures of the WT H99 strain in YPD were washed three times with ddH_2O and resuspended in SD-N medium for the induction of nitrogen starvation. Cells were harvest after 0, 0.5, 1, 2, and 4 h induction, and RNAs were purified for cDNA synthesis and qRT-PCR analysis. The comparative C_T method was used for the relative quantification, and the *GAPDH* gene was used as an endogenous reference. Values are expressed as relative expression ($2^{-\Delta\Delta CT}$) of *ATG*s. Bars represent the mean ± the standard error of the mean. Statistical analysis of *ATG*s expression was done with the Kruskal-Wallis non-parametric test for multiple comparisons. *$P < 0.05$; **$P < 0.01$; ***$P < 0.001$; ****$P < 0.0001$ (for compared groups that showed statistically significant differences).

Fungal burden assay of the mouse organs at the endpoint of the infection showed that no yeast cells were recovered in *atg6*Δ-, *atg14*Δ-, or *atg18*Δ-infected lung, brain, and spleen (**Figures 5B–D**), indicating that *atg6*Δ mutant, *atg14*Δ mutant, and *atg18*Δ mutant cells were wholly cleared from the lung after inoculation.

The rest of the *atg*Δ mutants (*atg1*Δ, *atg4*Δ, *atg7*Δ, *atg8*Δ, *atg9*Δ, *atg12*Δ, *atg13*Δ, and *atg16*Δ) showed a similar ability to promote disease development in the murine model of cryptococcosis. Mice infected by the rest of the *atg*Δ mutants had a 40–80% mortality rate after 19–66 DPI, and the remaining 20–60% survived to the end of the experiment (80 dpi) (**Figure 5A**), which was significantly different from that of WT-infected mice [$P < 0.0001$, Log-rank (Mantel-Cox) test]. Fungal burdens in organs of the animals infected by the rest of the *atg*Δ mutants were also examined at the endpoint of the infection experiments and evaluated as yeast colony-forming unit (CFU) per gram fresh organ (See **Figures 5B–D**). Meanwhile, severe organ damage with visible lesion development observed in brains, lungs, and spleens of the mice died before 80 DPI (**Supplementary Figure S5**) while no detectable damage or lesion was detected in brains, lungs, and spleens of the mice survived at 80 DPI (**Supplementary Figure S6**). The complemented strains of each *atg*Δ mutant were also generated and killed the mice around 20 to 30 days after infection, confirming that the virulence attenuation phenotype in each *atg*Δ mutants is caused by the deletion of its corresponding *ATG* gene (**Figure 5A**).

To better understand the dynamics of the *atg*Δ mutants-host interaction during the infection process, three representative mutant strains, *atg6*Δ, *atg8*Δ, and *atg12*Δ, were used to infect the mice and fungal burdens in infected brains, lungs, and spleens were examined at 7, 14, and 21 DPI and ETP. Our results showed that in *atg6*Δ mutant-infected lungs, ∼10^3 CFU/gram fresh lung were recovered at 7 DPI and no yeast cells were recovered at 14, 21 DPI and ETP (**Figure 6B**), indicating that the yeast cells of *atg6*Δ mutant were gradually cleared away after inoculation. No yeast cells were recovered from the brains and spleens of the

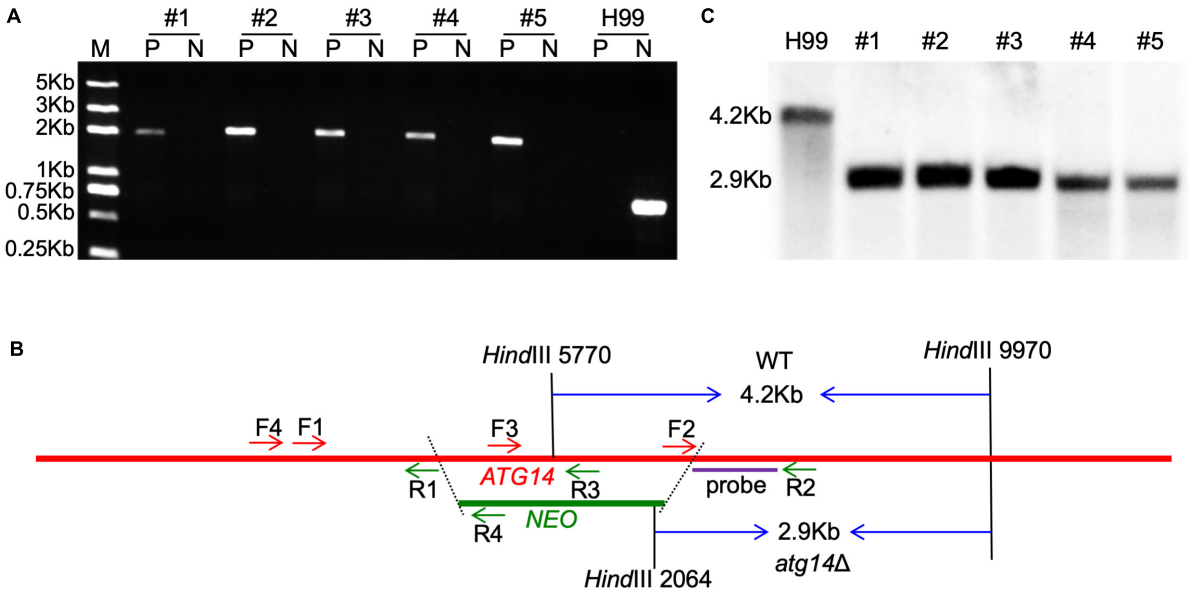

FIGURE 2 | Generation of *ATG14* deletion mutants. **(A)** PCR-based verification of the G418 resistant transformants. Number 1–5 are the five G418 resistant transformants used for PCR screening; P, positive primers, TL1134/TL59 (F4/R4 in 2B); N, negative primers, TL1132/TL1133 (F3/R3 in 2B). **(B)** Restriction enzymes used for digestion of the genomic DNAs for Southern blot. The TL1130/TL1131 (F2/R2) PCR products were used as a template to synthesize the probe. The WT H99 will generate a 4.2-Kb band while the *atg14*Δ mutants generate a 2.9-Kb band. **(C)** Southern blot analysis of the *ATG14* deletion transformants. All genomic DNAs were digested with *Hin*dIII, fractionated, and hybridized with a probe located in the downstream flanking sequence of *ATG14* shown in **Figure 2B**. As expected, a 4.2-Kb band was detected in the WT H99 in contrast with a 2.9-Kb band in *atg14*Δ mutants.

mice infected by *atg6*Δ mutant (**Figures 6A,C**). Fungal lesion development in the lung was also visualized in H&E-stained slides. As shown in **Figure 6D**, the WT strain H99 caused severe damage in infected brains, lungs, and spleens, with abundant yeast cells, as early as 7 DPI. In contrast, lungs infected by the *atg6*Δ mutant showed little damage, with very few yeast cells observed at different time points (**Figure 6E**). In *atg8*Δ and *atg12*Δ mutants infected mice, comparable yeast cells were recovered from brains at 21 DPI and ETP (**Figure 6A**), and from lungs at every time point (**Figure 6B**). Although no *atg8*Δ yeast cells were recovered from the spleens at 21 DPI, comparable yeast cells of *atg8*Δ mutant and *atg12*Δ mutant were recovered at the ETP (**Figures 6C,F,G**).

Taken together, our founding revealed that each *ATG* gene contributes differently to the virulence of *Cryptococcus* in C57 BL/6 mice. Our results also further suggest that, besides the roles of the genes in autophagy, non-autophagic functions associated with each *ATG* gene may contribute to the virulence of *Cryptococcus*.

The Atgs Are Essential for Sexual Reproduction

Cryptococcus neoformans is a basidiomycetous fungus having two mating types, α and **a**, and can undergo heterothallic sexual reproduction to generate dikaryotic mating hyphae and basidiospores. To evaluate the role of Atgs in fungal mating, we generated each of the 14 *atg*Δ mutants and its complemented strains in both H99 and KN99**a** strain backgrounds in *C. neoformans*, respectively. Both bilateral and unilateral matings in each *atg*Δ mutant were set up to examine the development of dikaryotic hyphae and basidiospores. Remarkably, when compared with the WT strains, all *atg*Δ mutants failed to produce basidiospores, even though they generate normal dikaryotic mating hyphae as the WT strains except *atg4*Δ and *atg18*Δ mutants in bilateral matings (**Figure 7**). The *atg4*Δ mutants showed a mating defect, and significant reduction of mating hyphal production and failure of basidiospore production were observed in the bilateral mating assays of *atg4*Δ mutants (**Figure 7**). No mating hyphae were produced by *atg18*Δ mutants in bilateral mating (**Figure 7**). The above results indicate that both Atg4 and Atg18 are required for α-**a** mating in *C. neoformans*. In contrast, mating hyphae and basidiospores were produced during unilateral matings in both *atg4*Δ and *atg18*Δ mutants, albeit at a slightly reduced level compared to matings between WT strains. Other *atg*Δ mutants produced normal mating hyphae and basidiospores as the WT strains in the unilateral matings (**Figure 7**).

Additionally, all the *atg*Δ mutants were recovered when each gene was reintroduced into the respective mutants at the genomic haven locus (**Figure 7**). These results clearly showed that the core autophagy machinery proteins are essential for sexual reproduction in *C. neoformans*.

The Atgs Are Involved in Meiosis and Nuclear Division

To investigate why *atg*Δ mutants fail to produce basidiospores, the nucleolar protein Nop1 tagged with mCherry at the C terminus (Lee and Heitman, 2012) was used to monitor the fungal

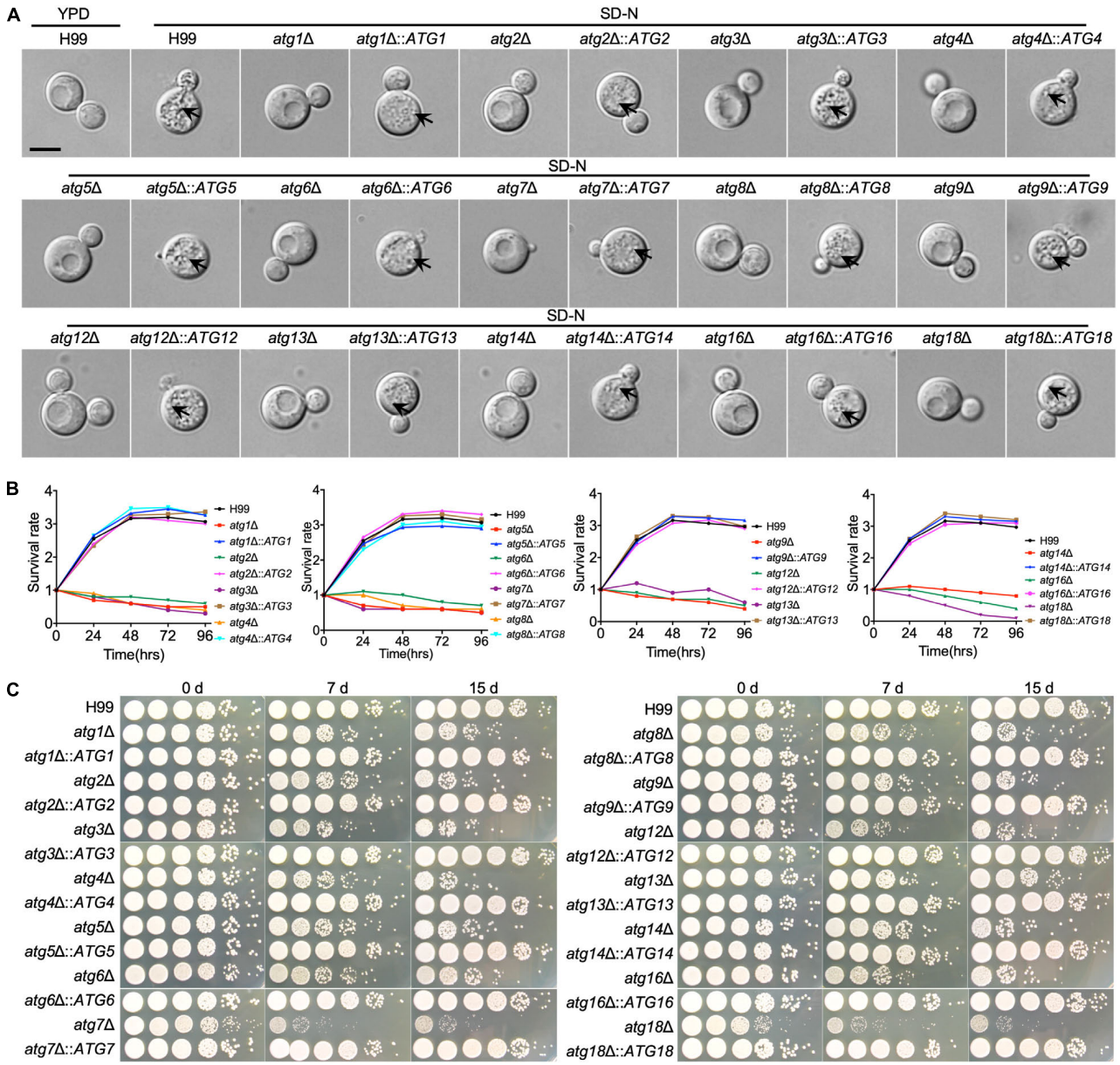

FIGURE 3 | The *ATG*s are required for autophagosome formation and survival under nitrogen starvation by *C. neoformans* **(A)**. WT and *atg*Δ cells were grown on YPD medium and then switched to SD-N medium with 2 mM PMSF for nitrogen starvation induction. Cells are collected after 4 h incubation and examined under microscopy. The vacuoles of the WT strain were filled with autophagic bodies, while no autophagic body was evident in the vacuoles of the *atg*Δ mutants. The name of WT strain, *atg*Δ mutants, and their complemented strains are indicated on the top. An autophagosome is indicated by the arrow. Bars, 5 μm. **(B)** Overnight cultures of the WT, *atg*Δ mutants and their complemented strains were washed three times with ddH_2O and diluted to an optical density at 600 nm (OD600) of 1.0 with SD-N medium. CFU was measured every 24 h and presented as relative CFU compared to that at 0 h. **(C)** Cultures of **(B)** induced in SD-N medium as indicative time were ten times diluted with ddH_2O, and 5 μl of each were plated on YPD. The plates were incubated at 30°C for 2 days. WT H99, *atg*Δ mutants, and their complemented strains are indicated on the left and the starvation induction time on the top.

nuclei development at different stages of mating in the living cells of *C. neoformans*. The *NOP1-mCherry* fusion construct was introduced into the native *NOP1* gene in both mating types of the WT and three selected *atg*Δ mutant strains (*atg5*Δ, *atg8*Δ, and *atg12*Δ) by biolistic transformation and homologous recombination (data not shown). The opposite mating strains of the WT or *atg*Δ mutants expressing Nop1-mCherry were crossed, respectively, and their nuclear positions were monitored using confocal fluorescence microscopy (Olympus, FV1200) during the mating process. A single nucleus in each yeast cell can be observed in both the WT and the *atg*Δ mutants cultures (**Figure 8**, first left panel), and two separated nuclei can be observed in dikaryotic hypha produced from bilateral matings after cell fusion (**Figure 8**, second left panel). Two separated

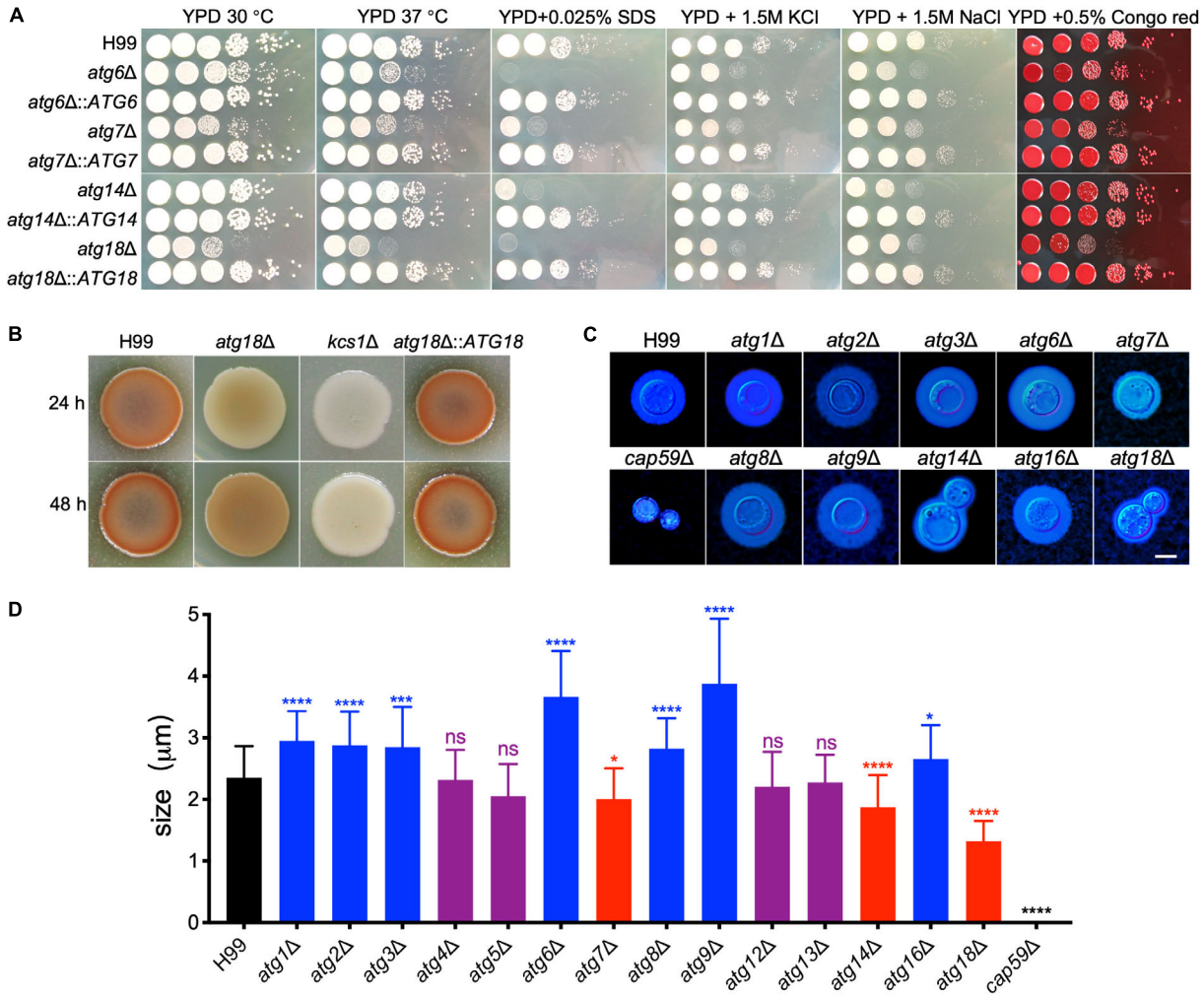

FIGURE 4 | Growth and virulence factors production by cryptococcal *atg*Δ mutants. **(A)** Overnight cultures in YPD were washed with ddH_2O three times and diluted to an optical density at 600 nm (OD600) of 2.0. Ten-fold serials were prepared in ddH_2O, and 5 μl of each was plated on YPD or YPD with different stresses. The plates were grown for 3 days at 30°C for the inhibitor plates and the indicated temperature for all others. The conditions are indicated on the top and cryptococcal strains on the left. **(B)** Melanin production of H99 and *atg18*Δ mutants were performed in Niger seed plates. Melanin levels produced by the strains were observed in photographs after incubation for 24 and 48 h at 37°C. **(C)** Capsule formation was assayed at 30°C on MM medium. Capsule formation was visualized by India ink staining after cells grown on MM for 3 days. Bar = 5 μm. **(D)** Statistical analysis of the capsule formation in *atg*Δ mutants. Quantitative measurement of capsule size was determined by measuring the distance from the cell wall to the capsule edge (India ink exclusion zone) in 106 cells. The experiment was repeated three times. Statistical analysis of capsule sizes was done with the Kruskal-Wallis non-parametric test for multiple comparisons. ns, not significant. $^{*}P < 0.05$; $^{***}P < 0.001$; $^{****}P < 0.0001$.

nuclei and a single fused nucleus could be observed in the young basidium, separately, of both the WT and *atg*Δ mutants, indicating that both kinds of strains can undergo standard nuclear fusion to produce basidia during mating (**Figure 8**, vertical middle panel).

Interestingly, the fused nuclei in the bilateral mating of all three *atg*Δ mutants failed to undergo meiosis, and only a single nucleus could be observed in each mature basidium even after14 days of incubation, while four nuclei were produced in all basidia from WT mating (**Figure 8B**, right panels). The above results indicated that autophagy is critical for regulating meiosis during mating, which could help explain why all the 14 *atg*Δ mutants failed to produce spores in the bilateral mating assay. However, all the 14 *atg*Δ mutants strains have a normal growth rate and also have normal nuclear division when grown in rich medium, suggesting that autophagy may not be involved in the cell cycle during mitotic division. Overall, our results reveal that autophagy may play a role only in regulating meiosis during the mating process.

DISCUSSION

Autophagy is a highly conserved degradation pathway involved in bulk degradation of cytoplasmic materials for nutrient recycling during starvation, playing a critical role in

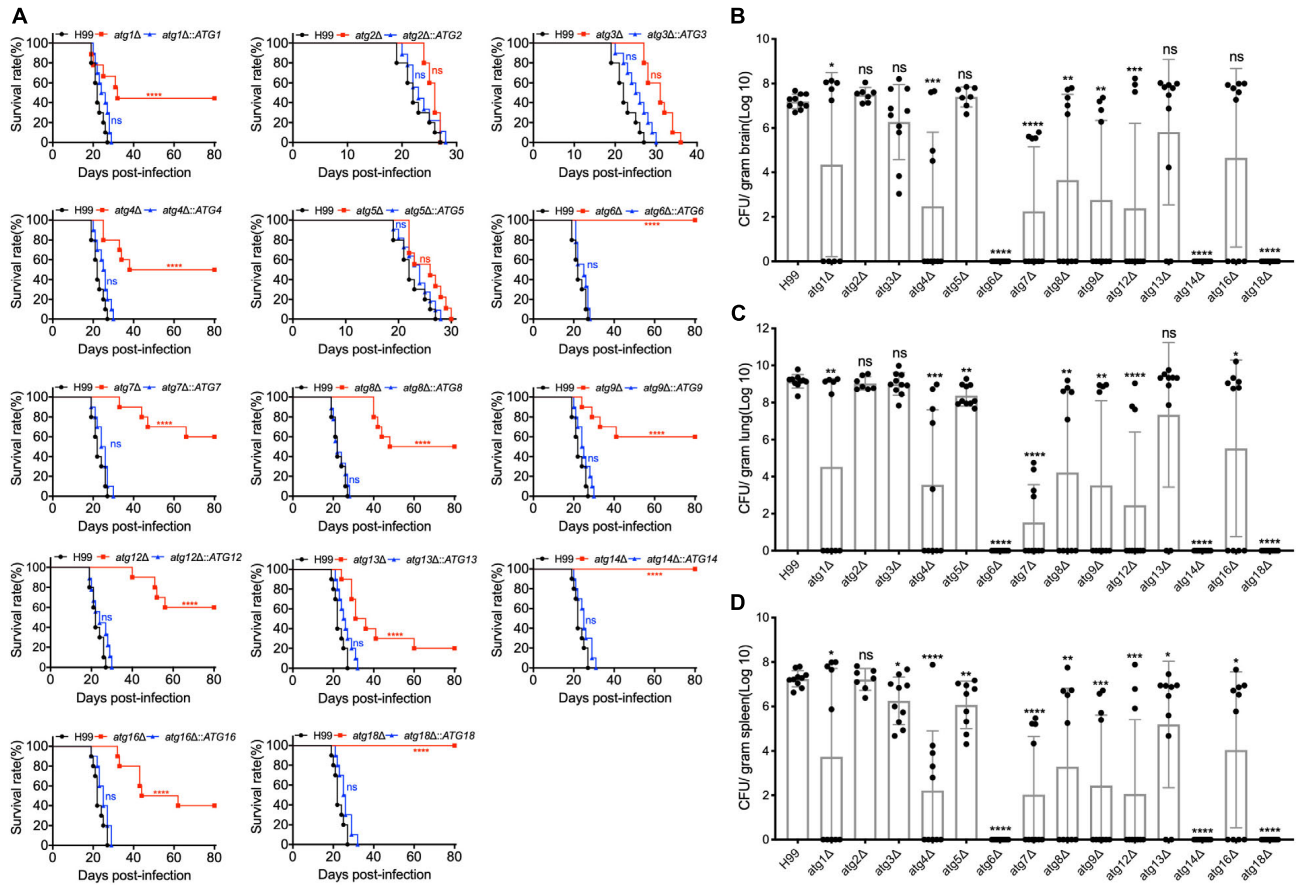

FIGURE 5 | Atgs regulate virulence of *C. neoformans* in a murine inhalation model. **(A)** C57 BL/6 mice were intranasally inoculated with 10^5 cells of H99, the 14 *atg*Δ mutants (*atg1*Δ, *atg2*Δ, *atg3*Δ, *atg4*Δ, *atg5*Δ, *atg6*Δ, *atg7*Δ, *atg8*Δ *atg9*Δ, *atg12*Δ, *atg14*Δ, *atg16*Δ, and *atg18*Δ), and their complemented strains (*atg1*Δ::*ATG1*, *atg2*Δ::*ATG2*, *atg3*Δ::*ATG3*, *atg4*Δ::*ATG4*, *atg5*Δ::*ATG5*, *atg6*Δ::*ATG6*, *atg7*Δ::*ATG7*, *atg8*Δ::*ATG8*, *atg9*Δ::*ATG9*, *atg12*Δ::*ATG12*, *atg14*Δ::*ATG14*, *atg16*Δ::*ATG16*, and *atg18*Δ::*ATG18*). The animals were monitored for clinical signs of cryptococcal infection and sacrificed at predetermined clinical endpoints that predict imminent mortality. All the *atg*Δ mutant strains except *atg2*Δ, *atg3*Δ, and *atg5*Δ are less virulent, and *atg6*Δ, *atg14*Δ, and *atg18*Δ are completely avirulent compared with the WT strain, H99. ns: not significant. $^{****}P < 0.0001$ [determined by log rank (Mantel-Cox) test]. **(B–D)** Brains, lungs, and spleens from ten mice infected with H99 and the 14 *atg*Δ mutant strains were isolated at the end time point of infection. The isolated organs were homogenized and spread on YPD plates containing ampicillin and chloramphenicol after dilution. CFU per gram of fresh organ was also measured in lung homogenates. Each data point and the error bar indicates the mean and standard error of the mean for values from five animals. $^{*}P < 0.05$; $^{**}P < 0.01$; $^{***}P < 0.001$; $^{****}P < 0.0001$; ns, not significant (determined by Mann-Whitney test).

cellular development and differentiation, tumor suppression, innate and adaptive immunity, and fighting against diverse pathologies (Yang and Klionsky, 2009). In this study, we systematically identified and characterized the 14 core autophagy machinery proteins required for autophagosome formation in *C. neoformans*. However, there are 15 core autophagy machinery proteins required for autophagosome formation in *S. cerevisiae*, and Atg10 is missing in *C. neoformans*. Atg10 is an E2-like conjugating enzyme and functions in the conjugation reaction between Atg12 and Atg5 in *S. cerevisiae* (Shintani et al., 1999). We used Atg10p as quires and did a BLASTp search against the *C. neoformans* H99 genome in FungiDB [(Basenko et al., 2018)] but no similar sequence was found. We also compared the sequence similarity of Atg10 and E2 conjugating enzymes in *C. neoformans* and found that the sequence similarity was very low (data not shown). Thus, there may be no Atg10 in *C. neoformans*, while other E2 conjugating enzymes perform the function of Atg10.

To investigate the role of the core autophagy machinery genes (*ATG*s), we knocked out all 14 *ATG* genes in *C. neoformans*. Each single deletion mutant showed the expected autophagy phenotype, such as impaired growth and survival upon nitrogen starvation, as previously reported by other groups (Hu et al., 2008; Oliveira et al., 2016; Gontijo et al., 2017; Ding et al., 2018; Zhao et al., 2019a; Roberto et al., 2020). However, our results suggested that autophagy-related genes may also be involved in other cellular functions, such as maintaining the integrity of cell membranes. In our study, the *atg6*Δ, *atg7*Δ, *atg14*Δ, and *atg18*Δ mutants showed severe growth defects on YPD with 0.025% SDS and moderate growth defect on YPD with 1.5 M NaCl or KCl, but not Congo red, which indicates that Atg6, Atg7, Atg14, and Atg18 may regulate cell

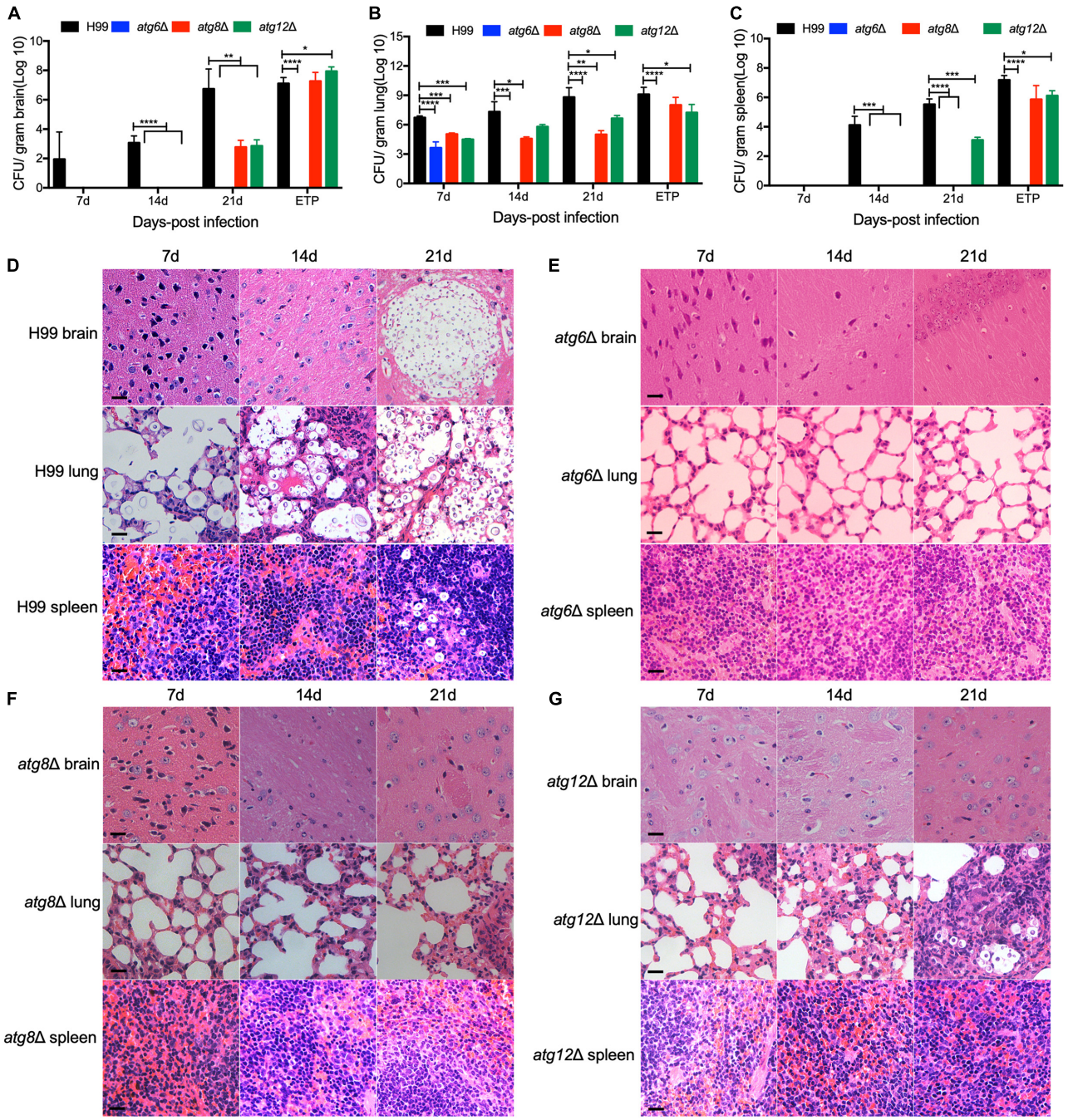

FIGURE 6 | Progression of *atg*Δ mutants infection *in vivo*. Brains, lungs, and spleens from the animals infected with H99, *atg6*Δ, *atg8*Δ, and *atg12*Δ mutants were isolated at 7, 14, and 21 DPI. Colony-forming units (CFU) were measured in the brain **(A)**, lung **(B)**, and spleen **(C)** homogenates. Each data point and the error bar indicates the standard error of the mean for values from ten mice. $^{*}P < 0.05$; $^{**}P < 0.01$; $^{***}P < 0.001$; $^{****}P < 0.0001$ (determined by Mann-Whitney test). **(D–G)** H&E-stained slides were also prepared from brain, lung, and spleen cross-sections and visualized by light microscopy. Bars, 20 μm.

membrane integrity in *C. neoformans* besides roles of the genes in autophagy. Other protein degradation pathways, such as the SCF E3 ubiquitin ligase-mediated ubiquitin-proteasome system (UPS), are also involved in the regulation of cell membrane integrity in *C. neoformans* (Liu et al., 2011; Liu and Xue, 2014). The UPS regulates cellular function by specifically degrading its ubiquitinated downstream target (Shabek and Ciechanover, 2010). It is now clear that autophagosomes can even recognize certain soluble proteins, such as ubiquitinated p62 and NBR1 (Kraft et al., 2010; Johansen and Lamark, 2011). Whether autophagy regulates cell membrane integrity by degrading the ubiquitinated substrates is still unknown and will be an exciting

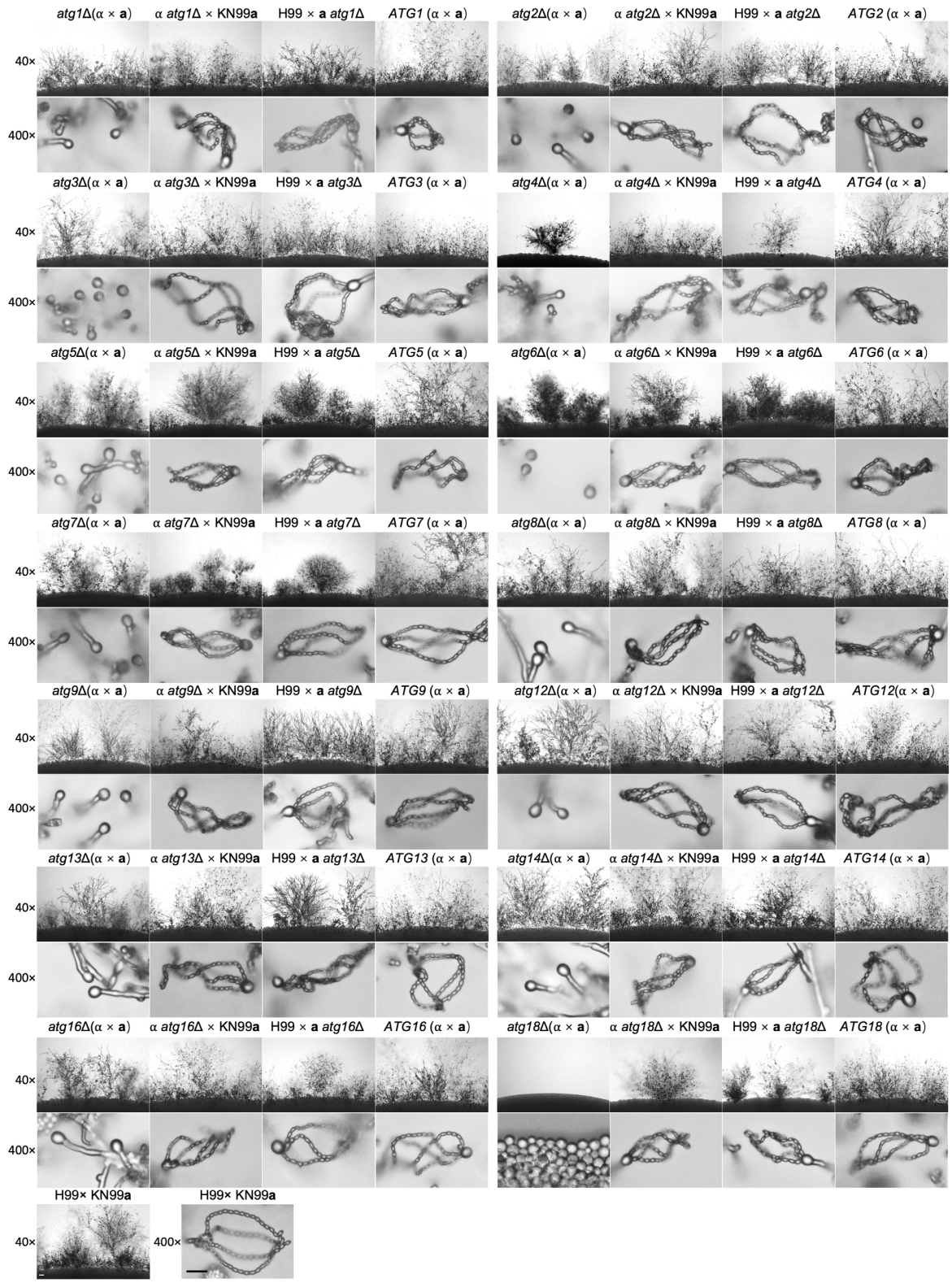

FIGURE 7 | Mating filaments production and sporulation on cryptococcal *atg*Δ mutants. Bilateral matings of the WT strains (H99 × KN99**a**), *atg*Δ mutants (α × **a**), and their complemented strains (*ATGs*, α × **a**) and unilateral matings of the *atg*Δ mutants (α *atg*Δ × KN99**a**, H99 × **a** *atg*Δ) were performed on MS medium. Mating structures at × 40 magnification (top, Bar = 100 μm) and ×400 magnification (bottom, Bar = 10 μm) were photographed after 14 days of incubation in the dark at 25°C.

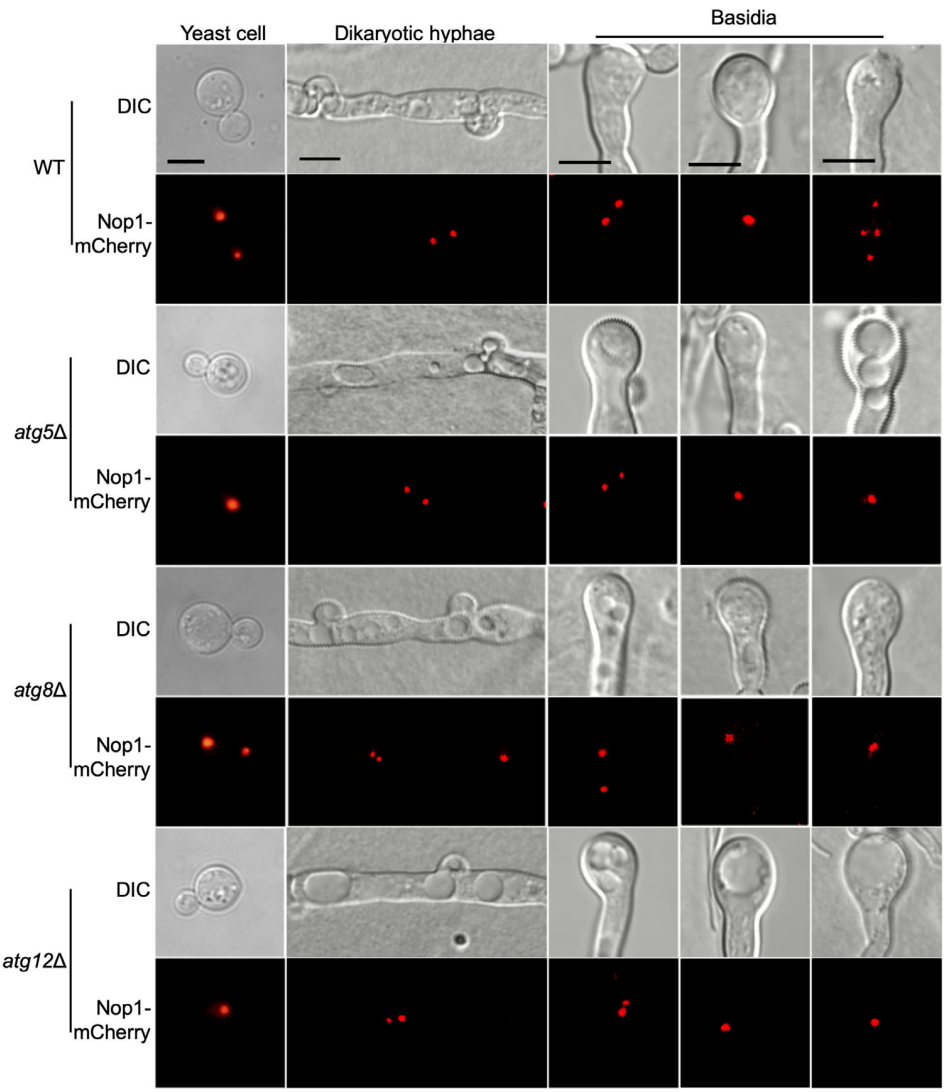

FIGURE 8 | Fungal nuclei development during mating in cryptococcal *atg*Δ mutants. Fungal nuclei development assay in yeast cells, mating hyphae and basidia of the WT, *atg5*Δ mutant, *atg8*Δ mutant, and *atg12*Δ mutant strains. Mating cultures were isolated from mating plates after incubation for 7 or 14 days on MS medium in the dark and visualized under Olympus inverted confocal laser scanning microscope. Bars, 5 μm.

topic for future research. Meanwhile, the *atg6*Δ, *atg7*Δ, and *atg18*Δ mutants also showed slight growth defects on YPD at 30 or 37°C, which is consistent with those of other groups (Ding et al., 2018; Zhao et al., 2019a).

Additionally, our results showed that the deletion of different *ATG* genes has a different effect on the capsule formation in *C. neoformans*. The deletion of *ATG1*, *ATG2*, *ATG3*, *ATG6*, *ATG8*, *ATG9*, and *ATG16* resulted in an enlarged capsule in *C. neoformans* while the deletion of *ATG7*, *ATG14*, and *ATG18* caused the capsule to become smaller *C. neoformans* in our study. However, the previous study showed that capsule formation was not affected by the deletion of the *ATG1*, *ATG7*, *ATG8*, or *ATG9* genes (Ding et al., 2018). In our opinion, the difference in the capsule formation may be caused by the difference of the capsule-induction medium. We used the minimum medium (Vij et al., 2018) in our study while other groups used low-iron capsule-inducing medium, which can increase the capsule more than threefold (Vartivarian et al., 1993). Therefore, it is worth trying to test the difference between the two media in the effect of capsule induction in the future. In a previous study, Ding et al. (2018) showed that the *atg1*Δ, *atg8*Δ, and *atg9*Δ mutants were not different from the WT in the production of melanin, which is consistent with our results. However, in another study, Zhao et al. (2019a) showed that the deletion of *ATG6* and *ATG14* affected melanin production in *C. neoformans*, which is different from our results. The first possible reason for this discrepancy is that we used different media for melanin production; we used the Niger seed medium while other groups used the L-DOPA medium, which may lead to different results. The second possible reason is that different autophagy genes may have different roles in the

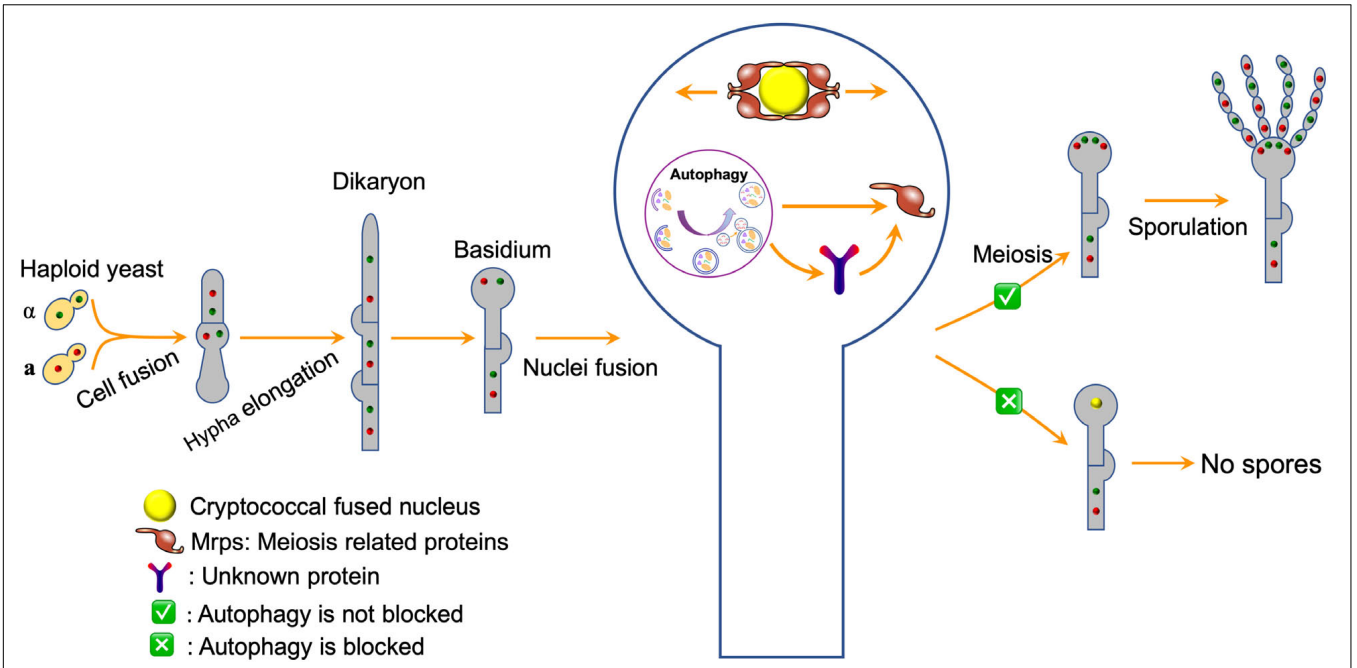

FIGURE 9 | A model for autophagy regulates sexual reproduction in *C. neoformans*. The model postulates that autophagy specifically recognizes the meiosis related proteins directly or indirectly and regulates their abundance, thus regulating the sexual sporulation process of *C. neoformans*.

melanin production in *C. neoformans*. Thus, it is also worthwhile to compare the difference between the two media in the induction of *Cryptococcus* melanin production in the future.

Moreover, the deletion of most *ATG* genes reduced the virulence of *Cryptococcus* strains in our study, although the virulence of individual *atg*Δ mutants (*atg2*Δ, *atg3*Δ, and *atg5*Δ) was not significantly different from that of WT strains. The most significant difference between our results and those of the other groups was the virulence of the *atg1*Δ mutant. Interestingly, the virulence of the *atg1*Δ mutant was reduced in our study but increased in that of the Ding et al. group (Ding et al., 2018), which may be caused by the use of different mice and different doses of inoculation for virulence study. In Ding et al. group, the female BALB/c mice were used for virulence study, and a suspension of 2×10^5 cells was inoculated into each mouse. In contrast, the C57 BL/6 mice were used for virulence study, and 1×10^5 cells were inoculated per mouse in our study. Another interesting thing is that the *atg4*Δ, *atg12*Δ, and *atg13*Δ mutants did show defects in fungal virulence but not involved regulation of any of the well-studied virulence factors such as capsule formation, melanin production, and growth at 37°C. This indicated that these three autophagy-related proteins might be involved in additional mechanisms or pathways of virulence regulation in *C. neoformans* except autophagy. What are mechanisms or pathways involved and whether autophagy-related proteins are related to these pathways remain to be further explored.

Previous studies showed that autophagy is required to recycle internal resources to support fungal development, such as conidiophore development and optimal conidiation in *A. fumigatus* (Richie et al., 2007; Richie and Askew, 2008b), conidiation and blastospore formation in *Beauveria bassiana* (Zhang et al., 2013; Ying et al., 2016; Chu et al., 2017), and conidiation in *Magnaporthe oryzae* (Liu et al., 2007, 2010, 2017). In the species mentioned above, blocking the autophagy pathway would affect mycelium growth and reduce conidium production, but would not result in complete loss of conidiation, indicating that autophagy is required to recycle internal resources to support fungal development. Interestingly, the deletion of the *ATG* genes blocks the basidiospore formation in *C. neoformans* but not affect the cell fusion, dikaryotic hyphae elongation, and basidium formation during the mating process except *ATG18* in our study. Fungal nuclei positioning showed that the two nuclei inside the basidium could fuse to form a nucleus but failed to undergo meiosis to form four nuclei. Based on these findings and the facts that autophagosomes can recognize certain soluble proteins, such as ubiquitinated p62 and NBR1 (Kraft et al., 2010; Johansen and Lamark, 2011), we proposed a model in which autophagy might regulate sexual reproduction of *C. neoformans* by specifically regulating meiosis related proteins (**Figure 9**). However, which meiosis-related protein regulates the basidiospore production of *C. neoformans*? Whether and how this meiosis-related protein is regulated by autophagy remains unknown. Thus, more data is needed to test this hypothesis.

Overall, this report described the identification and characterization of the core *ATG*s in *C. neoformans*. Our results demonstrated that the individual *ATG* genes in *C. neoformans* might contribute to virulence and sexual reproduction through participating in other cellular processes in addition to autophagy.

DATA AVAILABILITY STATEMENT

The original contributions presented in the study are included in the article/**Supplementary Material**, further inquiries can be directed to the corresponding author/s.

ETHICS STATEMENT

The animal studies conducted at Southwest University were in full compliance with "Guidelines on Ethical Treatment of Experimental Animals (2006, No. 398)" issued by the Ministry of Science and Technology of China and the "Regulation on the Management of Experimental Animals (2006, No. 195)" issued by Chongqing Municipal People's Government. The Animal Ethics Committee of Southwest University approved all of the vertebrate studies.

AUTHOR CONTRIBUTIONS

T-BL conceived and designed the experiments, and wrote the manuscript. T-BL, S-TJ, A-NC, and L-TH performed the experiments and acquired the data. J-SG and Y-HL contributed to the generation of cryptococcal strains. T-BL obtained the funding. All authors reviewed the manuscript and approved it for publication.

FUNDING

This work was supported by the National Natural Science Foundation of China (31970145 and 31400133), Chongqing Research Program of Basic Research and Frontier Technology (cstc2017jcyjBX0034), and the Venture & Innovation Support Program for Chongqing Overseas Returnees (cx2018084).

SUPPLEMENTARY MATERIAL

The Supplementary Material for this article can be found online at: https://www.frontiersin.org/articles/10.3389/fcell.2020.00374/full#supplementary-material

REFERENCES

Arias, E., and Cuervo, A. M. (2011). Chaperone-mediated autophagy in protein quality control. *Curr. Opin. Cell Biol.* 23, 184–189. doi: 10.1016/j.ceb.2010.10.009

Basenko, E. Y., Pulman, J. A., Shanmugasundram, A., Harb, O. S., Crouch, K., Starns, D., et al. (2018). FungiDB: an integrated bioinformatic resource for fungi and oomycetes. *J. Fungi* 4:39. doi: 10.3390/jof4010039

Brown, G. D., Denning, W. D., and Levitz, S. M. (2012). Tackling human fungal infections. *Science* 336:647. doi: 10.1126/science.1222236

Casadevall, A., and Perfect, J. R. (1998). *Cryptococcus Neoformans*. Washington, DC: ASM Press.

Chu, Z. J., Sun, H. H., Ying, S. H., and Feng, M. G. (2017). Discovery of a new intravacuolar protein required for the autophagy, development and virulence of *Beauveria bassiana*. *Environ. Microbiol.* 19, 2806–2818. doi: 10.1111/1462-2920.13803

Cox, G. M., Mukherjee, J., Cole, G. T., Casadevall, A., and Perfect, J. R. (2000). Urease as a virulence factor in experimental cryptococcosis. *Infect. Immun.* 68, 443–448. doi: 10.1128/iai.68.2.443-448.2000

Ding, H., Caza, M., Dong, Y., Arif, A. A., Horianopoulos, L. C., Hu, G., et al. (2018). ATG genes influence the virulence of *Cryptococcus neoformans* through contributions beyond core autophagy functions. *Infect. Immun.* 86:e069-18. doi: 10.1128/IAI.00069-18

Fan, C. L., Han, L. T., Jiang, S. T., Chang, A. N., Zhou, Z. Y., and Liu, T. B. (2019). The Cys2His2 zinc finger protein Zfp1 regulates sexual reproduction and virulence in *Cryptococcus neoformans*. *Fungal Genet. Biol.* 124, 59–72. doi: 10.1016/j.fgb.2019.01.002

Gontijo, F. A., de Melo, A. T., Pascon, R. C., Fernandes, L., Paes, H. C., Alspaugh, J. A., et al. (2017). The role of *Aspartyl aminopeptidase* (Ape4) in *Cryptococcus neoformans* virulence and authophagy. *PLoS One* 12:e0177461. doi: 10.1371/journal.pone.0177461

Hu, G. W., Hacham, M., Waterman, S. R., Panepinto, J., Shin, S., Liu, X., et al. (2008). PI3K signaling of autophagy is required for starvation tolerance and virulence of *Cryptocloccus neoformans*. *J. Clin. Invest.* 118, 1186–1197. doi: 10.1172/JCI32053

Johansen, T., and Lamark, T. (2011). Selective autophagy mediated by autophagic adapter proteins. *Autophagy* 7, 279–296. doi: 10.4161/auto.7.3.14487

Kim, J., Huang, W. P., Stromhaug, P. E., and Klionsky, D. J. (2002). Convergence of multiple autophagy and cytoplasm to vacuole targeting components to a perivacuolar membrane compartment prior to de novo vesicle formation. *J. Biol. Chem.* 277, 763–773. doi: 10.1074/jbc.M109134200

Kim, M. S., Kim, S. Y., Yoon, J. K., Lee, Y. W., and Bahn, Y. S. (2009). An efficient gene-disruption method in *Cryptococcus neoformans* by double-joint PCR with NAT-split markers. *Biochem. Biophys. Res. Commun.* 390, 983–988. doi: 10.1016/j.bbrc.2009.10.089

Kozel, T. R. (1995). Virulence factors of *Cryptococcus neoformans*. *Trends Microbiol.* 3, 295–299. doi: 10.1016/S0966-842X(00)88957-X

Kraft, C., Peter, M., and Hofmann, K. (2010). Selective autophagy: ubiquitin-mediated recognition and beyond. *Nat. Cell Biol.* 12, 836–841. doi: 10.1038/ncb0910-836

Kronstad, J., Jung, W. H., and Hu, G. (2008). Beyond the big three: systematic analysis of virulence factors in *Cryptococcus neoformans*. *Cell Host Microb.* 4, 308–310. doi: 10.1016/j.chom.2008.09.003

Lee, S. C., and Heitman, J. (2012). Function of *Cryptococcus neoformans* KAR7 (SEC66) in karyogamy during unisexual and opposite-sex mating. *Eukaryot. Cell* 11, 783–794. doi: 10.1128/EC.00066-12

Levine, B., and Kroemer, G. (2008). Autophagy in the pathogenesis of disease. *Cell* 132, 27–42. doi: 10.1016/j.cell.2007.12.018

Lin, X., and Heitman, J. (2006). The biology of the *Cryptococcus neoformans* species complex. *Annu. Rev. Microbiol.* 60, 69–105. doi: 10.1146/annurev.micro.60.080805.142102

Liu, T. B., Liu, X. H., Lu, J. P., Zhang, L., Min, H., and Lin, F. C. (2010). The cysteine protease MoAtg4 interacts with MoAtg8 and is required for differentiation and pathogenesis in *Magnaporthe oryzae*. *Autophagy* 6, 74–85. doi: 10.4161/auto.6.1.10438

Liu, T. B., Wang, Y., Stukes, S., Chen, Q., Casadevall, A., and Xue, C. (2011). The F-Box protein Fbp1 regulates sexual reproduction and virulence in *Cryptococcus neoformans*. *Eukaryot. Cell* 10, 791–802. doi: 10.1128/EC.00004-11

Liu, T. B., and Xue, C. (2014). Fbp1-mediated ubiquitin-proteasome pathway controls *Cryptococcus neoformans* virulence by regulating fungal intracellular growth in macrophages. *Infect. Immun.* 82, 557–568. doi: 10.1128/IAI.00994-13

Liu, X. H., Lu, J. P., Zhang, L., Dong, B., Min, H., and Lin, F. C. (2007). Involvement of a Magnaporthe grisea serine/threonine kinase gene, MgATG1, in appressorium turgor and pathogenesis. *Eukaryot. Cell* 6, 997–1005. doi: 10.1128/EC.00011-07

Liu, X. H., Xu, F., Snyder, J. H., Shi, H. B., Lu, J. P., and Lin, F. C. (2016). Autophagy in plant pathogenic fungi. *Semin. Cell Dev. Biol.* 57, 128–137. doi: 10.1016/j.semcdb.2016.03.022

Liu, X. H., Zhao, Y. H., Zhu, X. M., Zeng, X. Q., Huang, L. Y., Dong, B., et al. (2017). Autophagy-related protein MoAtg14 is involved in differentiation,

development and pathogenicity in the rice blast fungus *Magnaporthe oryzae*. *Sci. Rep.* 7:40018. doi: 10.1038/srep40018

Livak, K. J., and Schmittgen, T. D. (2001). Analysis of relative gene expression data using real-time quantitative PCR and the 2(T)(-Delta Delta C) method. *Methods* 25, 402–408. doi: 10.1006/meth.2001.1262

Nielsen, K., Cox, G. M., Litvintseva, A. P., Mylonakis, E., Malliaris, S. D., Benjamin, D. K. Jr., et al. (2005). *Cryptococcus neoformans* {alpha} strains preferentially disseminate to the central nervous system during coinfection. *Infect. Immun.* 73, 4922–4933. doi: 10.1128/IAI.73.8.4922-4933.2005

Oliveira, D. L., Fonseca, F. L., Zamith-Miranda, D., Nimrichter, L., Rodrigues, J., Pereira, M. D., et al. (2016). The putative autophagy regulator Atg7 affects the physiology and pathogenic mechanisms of *Cryptococcus neoformans*. *Future Microbiol.* 11, 1404–1419. doi: 10.2217/fmb-2016-0090

Palmer, G. E., Askew, D. S., and Williamson, P. R. (2008). The diverse roles of autophagy in medically important fungi. *Autophagy* 4, 982–988. doi: 10.4161/auto.7075

Palmer, G. E., Kelly, M. N., and Sturtevant, J. E. (2007). Autophagy in the pathogen *Candida albicans*. *Microbiology* 153, 51–58. doi: 10.1099/mic.0.2006/001610-0

Park, B. J., Wannemuehler, K. A., Marston, B. J., Govender, N., Pappas, P. G., and Chiller, T. M. (2009). Estimation of the current global burden of cryptococcal meningitis among persons living with HIV/AIDS. *AIDS* 23, 525–530. doi: 10.1097/QAD.0b013e328322ffac

Parzych, K. R., Ariosa, A., Mari, M., and Klionsky, D. J. (2018). A newly characterized vacuolar serine carboxypeptidase, Atg42/Ybr139w, is required for normal vacuole function and the terminal steps of autophagy in the yeast *Saccharomyces cerevisiae*. *Mol. Biol. Cell* 29, 1089–1099. doi: 10.1091/mbc.E17-08-0516

Pollack, J. K., Harris, S. D., and Marten, M. R. (2009). Autophagy in filamentous fungi. *Fungal Genet. Biol.* 46, 1–8. doi: 10.1016/j.fgb.2008.10.010

Rajasingham, R., Smith, R. M., Park, B. J., Jarvis, J. N., Govender, N. P., Chiller, T. M., et al. (2017). Global burden of disease of HIV-associated cryptococcal meningitis: an updated analysis. *Lancet Infect. Dis.* 17, 873–881. doi: 10.1016/S1473-3099(17)30243-8

Richie, D. L., and Askew, D. S. (2008a). Autophagy: a role in metal ion homeostasis? *Autophagy* 4, 115–117. doi: 10.4161/auto.5238

Richie, D. L., and Askew, D. S. (2008b). Autophagy in the filamentous fungus *Aspergillus fumigatus*. autophagy: lower eukaryotes and non-mammalian systems. *Methods Enzymol.* 451, 241–250. doi: 10.1016/S0076-6879(08)03217-5

Richie, D. L., Fuller, K. K., Fortwendel, J., Miley, M. D., McCarthy, J. W., Feldmesser, M., et al. (2007). Unexpected link between metal ion deficiency and autophagy in *Aspergillus fumigatus*. *Eukaryot. Cell* 6, 2437–2447. doi: 10.1128/EC.00224-07

Roberto, T. N., Lima, R. F., Pascon, R. C., Idnurm, A., and Vallim, M. A. (2020). Biological functions of the autophagy-related proteins Atg4 and Atg8 in *Cryptococcus neoformans*. *PLoS One* 15:e0230981. doi: 10.1371/journal.pone.0230981

Shabek, N., and Ciechanover, A. (2010). Degradation of ubiquitin: the fate of the cellular reaper. *Cell Cycle* 9, 523–530. doi: 10.4161/cc.9.3.11152

Shintani, T., Mizushima, N., Ogawa, Y., Matsuura, A., and Noda, T. (1999). Apg10p, a novel protein-conjugating enzyme essential for autophagy in yeast. *EMBO J.* 18, 5234–5241. doi: 10.1093/emboj/18.19.5234

Vartivarian, S. E., Anaissie, E. J., Cowart, R. E., Sprigg, H. A., Tingler, M. J., and Jacobson, E. S. (1993). Regulation of cryptococcal capsular polysaccharide by iron. *J. Infect. Dis.* 167, 186–190. doi: 10.1093/infdis/167.1.186

Velagapudi, R., Hsueh, Y. P., Geunes-Boyer, S., Wright, J. R., and Heitman, J. (2009). Spores as infectious propagules of *Cryptococcus neoformans*. *Infect. Immun.* 77, 4345–4355. doi: 10.1128/IAI.00542-09

Vij, R., Cordero, R. J. B., and Casadevall, A. (2018). The buoyancy of *Cryptococcus neoformans* is affected by capsule size. *mSphere* 3:e0534-18. doi: 10.1128/mSphere.00534-18

Voigt, O., and Poggeler, S. (2013). Self-eating to grow and kill: autophagy in filamentous ascomycetes. *Appl. Microbiol. Biotechnol.* 97, 9277–9290. doi: 10.1007/s00253-013-5221-2

Xie, Z., and Klionsky, D. J. (2007). Autophagosome formation: core machinery and adaptations. *Nat. Cell Biol.* 9, 1102–1109. doi: 10.1038/ncb1007-1102

Xue, C., Tada, Y., Dong, X., and Heitman, J. (2007). The human fungal pathogen *Cryptococcus* can complete its sexual cycle during a pathogenic association with plants. *Cell Host Microb.* 1, 263–273. doi: 10.1016/j.chom.2007.05.005

Yang, Z., and Klionsky, D. J. (2009). An overview of the molecular mechanism of autophagy. *Curr. Top. Microbiol. Immunol.* 335, 1–32. doi: 10.1007/978-3-642-00302-8_1

Ying, S. H., Liu, J., Chu, X. L., Xie, X. Q., and Feng, M. G. (2016). The autophagy-related genes BbATG1 and BbATG8 have different functions in differentiation, stress resistance and virulence of mycopathogen *Beauveria bassiana*. *Sci. Rep.* 6:26367. doi: 10.1038/srep26376

Yorimitsu, T., and Klionsky, D. J. (2005). Autophagy: molecular machinery for self-eating. *Cell Death Differ.* 12(Suppl. 2), 1542–1552. doi: 10.1038/sj.cdd.4401765

Youle, R. J., and Narendra, D. P. (2011). Mechanisms of mitophagy. *Nat. Rev. Mol. Cell Biol.* 12, 9–14. doi: 10.1038/nrm3028

Zaragoza, O. (2019). Basic principles of the virulence of *Cryptococcus*. *Virulence* 10, 490–501. doi: 10.1080/21505594.2019.1614383

Zhang, L., Wang, J., Xie, X. Q., Keyhani, N. O., Feng, M. G., and Ying, S. H. (2013). The autophagy gene BbATG5, involved in the formation of the autophagosome, contributes to cell differentiation and growth but is dispensable for pathogenesis in the entomopathogenic fungus *Beauveria bassiana*. *Microbiology* 159, 243–252. doi: 10.1099/mic.0.062646-0

Zhao, X., Feng, W., Zhu, X., Li, C., Ma, X., Li, X., et al. (2019a). Conserved autophagy pathway contributes to stress tolerance and virulence and differentially controls autophagic flux upon nutrient starvation in *Cryptococcus neoformans*. *Front. Microbiol.* 10:2690. doi: 10.3389/fmicb.2019.02690

Zhao, Y., Lin, J., Fan, Y., and Lin, X. (2019b). Life Cycle of *Cryptococcus neoformans*. *Annu. Rev. Microbiol.* 73, 17–42. doi: 10.1146/annurev-micro-020518-120210

Conflict of Interest: The authors declare that the research was conducted in the absence of any commercial or financial relationships that could be construed as a potential conflict of interest.

frontiers in Cell and Developmental Biology

REVIEW
published: 29 May 2020
doi: 10.3389/fcell.2020.00343

Endoplasmic Reticulum Membrane and Contact Site Dynamics in Autophagy Regulation and Stress Response

*Etienne Morel**

Cell Biology Department, Institut Necker-Enfants Malades (INEM), INSERM U1151-CNRS UMR 8253, Université de Paris, Paris, France

Autophagy mobilizes a variety of intracellular endomembranes to ensure a proper stress response and the maintenance of cellular homeostasis. While the process of *de novo* biogenesis of pre-autophagic structures is not yet fully characterized, the role of the endoplasmic reticulum (ER) appears to be crucial in early steps of autophagic process. Here, I review and discuss various aspects of ER and ER-driven membrane contact site requirements and effects on mammalian organelles and endomembrane biogenesis, in particular during the early steps of autophagy-related membrane dynamics.

Keywords: ER, autophogosome, membrane contact site, lipids, biogenesis

OPEN ACCESS

Edited by:
Liang Ge,
Tsinghua University, China

Reviewed by:
Yueguang Rong,
Huazhong University of Science and Technology, China
Alex R. Van Vliet,
The Francis Crick Institute, United Kingdom

***Correspondence:**
Etienne Morel
etienne.morel@inserm.fr

Specialty section:
This article was submitted to Membrane Traffic, a section of the journal Frontiers in Cell and Developmental Biology

Received: *25 February 2020*
Accepted: *20 April 2020*
Published: *29 May 2020*

Citation:
Morel E (2020) Endoplasmic Reticulum Membrane and Contact Site Dynamics in Autophagy Regulation and Stress Response. Front. Cell Dev. Biol. 8:343. doi: 10.3389/fcell.2020.00343

THE MOLECULAR MECHANISMS OF AUTOPHAGY AND AUTOPHAGOSOME BIOGENESIS

Macroautophagy (hereafter referred to as autophagy) is an evolutionarily conserved intracellular catabolic pathway that ensures degradation, turnover, and renewal of intracellular and cytosolic components. Autophagy necessitates the formation of a double-membrane organelle termed the autophagosome that ensures the capture and the transport of cargoes to the acidic lysosome (Boya et al., 2013). Autophagy functions in most mammalian cells at low levels, a condition commonly referred to as basal autophagy. However, a stimulated autophagy response can be induced in response to stress-related situations, such as nutrient(s) deprivation(s), infection, physical, or mechanical or chemical stresses. Because autophagic process is a crucial cell-survival mechanism and a pivotal cellular homeostasis regulator, it has been studied for decades in physiological conditions and disease (Yang and Klionsky, 2010). Defects in autophagy have been associated with a variety of human diseases such as cancer, inflammation, neurodegenerative diseases, and metabolic disorders (Boya et al., 2013).

The stimulated autophagic response, notably induced by nutrient deprivation, requires several key steps that will lead eventually to cytoplasmic material (such as protein aggregates, pathogens, or damaged organelles) sequestration by a newly formed autophagosome and delivery to the lysosome for degradation. This dynamic sequence of events first requires complex signalization that will allow the specific mobilization of dedicated proteins, lipids, and membranes to ensure

the formation and the maturation of the autophagosome; its transport inside the cytoplasm; and its fusion with lysosome. Autophagosome biogenesis starts with the assembly of a pre-autophagosomal cup-shaped membrane, the phagophore or isolation membrane, which captures autophagic cargoes and closes up to form a mature autophagosome (**Figure 1**). Most of these membrane-related events are regulated by autophagy-related genes (ATG) proteins, with non-ATG partners mostly required for intracellular signaling and membrane transportation on trafficking platforms (Walker and Ktistakis, 2019). The origin of the phagophore is still largely unknown (see section "The ER Membrane and ER Contact Sites in Autophagy Regulation"). It is suggested that this transient structure emanates from multiple origins, such as endosomal and Golgi vesicles, mitochondria, and the ER itself.

While there are several signaling pathways involved in autophagy, the mTORC1 and AMPK protein complexes appear to be crucial for the mobilization of the autophagic machinery (Molino et al., 2017b) in many stress situations. Inhibition of the mTORC1 signaling pathway leads to the activation of the ULK1 complex [composed of ULK1/2 kinases (ATG1/2), FIP200, ATG13, and ATG101]. The ULK1 complex will in turn activate the lipid kinase class III PI3K (formed by VPS34, Beclin1, VPS15, and ATG14L1) which generates the production of phosphatidylinositol-3-phosphate (PI3P) locally on ER subdomains, known as the pre-autophagosomal membrane(s) or omegasomes (**Figure 1**; Tooze, 2013).

The pre-autophagosomal membrane(s) are hallmarked by a dedicated pool of PI3P required for phagophore formation and expansion. PI3P allows the recruitment of several ATG proteins, including members of the WIPI family. WIPI2, which binds to PI3P via a proppins domain (Baskaran et al., 2012), recruits the ATG16L1–ATG5/12 conjugation system to the pre-autophagosome (Dooley et al., 2014), allowing in turn the membrane targeting of the LC3 protein (yeast ATG8 homolog), so far considered as the bona fide marker of autophagic organelles (**Figure 1**; Nishimura et al., 2013; Dooley et al., 2014; Wilson et al., 2014). Recently the autophagosome biogenesis key regulator ATG16L1 was shown to bind also to PI3P (Dudley et al., 2019), further stabilizing the conjugation complex. LC3 recruitment to the future autophagosome occurs via its lipidation (via the adjunction of a PE moiety, i.e., LC3-I to LC3-II) that also requires ATG proteins such as ATG4, ATG3, ATG7, and ATG10 (**Figure 1**; Mizushima, 2020). The local combination of PI3P presence and lipidated LC3-positive subdomains designate the membrane for autophagic activity initiation, heralding phagophore isolation, growth, and closure (Boya et al., 2013).

The membrane remodeling events leading to a dynamic transition from the omegasome to the phagophore are not yet fully deciphered. They probably require the coordination of multiple membrane sources to complete the *de novo* organelle biogenesis. In line with this hypothesis, membrane compartments such as endosomes, Golgi apparatus, ER exit sites, ERGIC vesicles, or plasma membrane have been shown to directly or indirectly participate in autophagosome biogenesis (Molino et al., 2017b). The involvement of ATG9-positive vesicles (which could originate from endosomal and Golgi associated structures) (Hurley and Young, 2017) corroborates the "multimembrane origins" of autophagosomes and suggests that heteromembranous structures are able to interact during phagophore assembly, which has to be tightly regulated in space, a situation that may be favored by the presence of ER membrane subdomains (see section "The ER Membrane and ER Contact Sites in Autophagy Regulation"). Moreover, crucial membrane trafficking regulators such as the recycling endosome-associated small GTPase Rab11 (Puri et al., 2018) are also required at this step, revealing the importance of membrane(s) and proteins classically associated with other trafficking stations in the cell during autophagosome biogenesis and maturation. Finally, the phagophore closes to form the double membrane autophagosome, which will fuse with the lysosome to ensure cargoes degradation and recycling. This fusion step requires regulators associated with the endo-lysosomal pathway, such as SNAREs (including STX proteins) and small Rab GTPases (Molino et al., 2017b).

THE ER AND ER CONTACT SITES IN ORGANELLE BIOGENESIS AND MEMBRANE DYNAMICS

The ER is a network of cisternae and tubule-based membrane network, physically connected with the nuclear envelope and the Golgi apparatus, which spreads all over the cytoplasm. One of the major functions of ER is to support membrane protein synthesis and quality control, via ribosomes, regulatory proteins, and proteasomes, as well as posttranslational modifications such as *N*-glycosylation. ER is also a major site of lipid synthesis, notably phospholipids and steroids, and actively participates in Ca^{2+} homeostasis. Besides its key role in protein and lipid synthesis and transport, the ER network is also a platform for *de novo* biogenesis and dynamics of several organelles and membrane structures (Joshi et al., 2017) such as peroxisomes, lipid droplets, and lipoproteins (**Figure 2**) and membraneless organelles such as P-bodies and stress granules (Lee et al., 2020). In the text that follows I shortly summarize the role of ER in the biogenesis of COPII vesicles, peroxisomes, lipid droplets, and lipoproteins.

ER AND COPII VESICLES

One of the major functions of the ER is to export newly synthesized proteins to the sorting part(s) of the Golgi apparatus to ensure proper vectorized transport of membrane-associated proteins toward the cell plasma membrane and organelles such as the endosomes. ER specialized subdomains, termed ERESs for "ER exit sites," are involved in the trafficking of protein cargoes en route to the Golgi, a step required for posttranslational modifications as further sorting occurs in Golgi saccules. This ER-to-Golgi vesicular transport is mediated by the small and round COPII vesicles that bud from ERESs in a Sar1 GTPase-mediated mechanism (Peotter et al., 2019). The biogenesis of these COPII vesicles could be regulated by lipids, such as

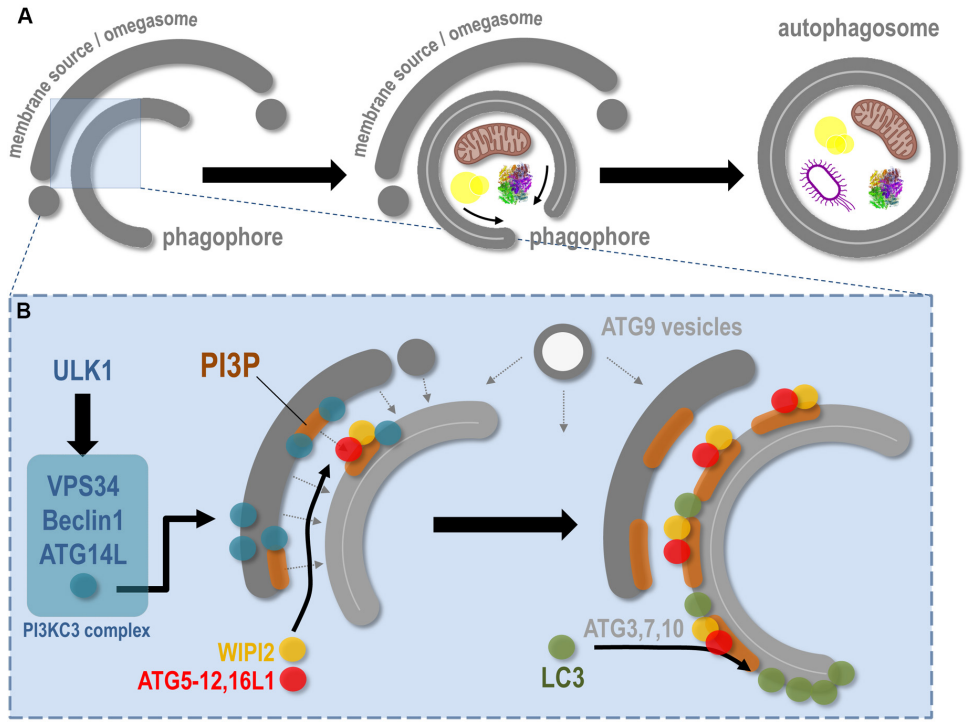

FIGURE 1

FIGURE 1 | Molecular aspects of phagophore biogenesis and autophagy initiation. This scheme summarizes in a simplified way the main steps associated with membrane remodeling events leading to phagophore assembly. **(A)** The *de novo* biogenesis of the pre-autophagosomal phagophore (also called the isolation membrane) occurs at the ER-associated omegasome and membrane(s) source(s) interface. The phagophore maturation implies cargoes (specific, such as mitochondria, lipid droplets, protein aggregates, bacteria, etc., and non-specific) capture, physical disassembly from the membrane source, and closure, through fission of limiting membrane, which leads to double membrane autophagosome formation. **(B)** At the omegasome and membrane source interface, the stress-induced ULK1 autophagic complex is locally recruited and in turn allows the direct activation and membrane binding of the PI3KC3 complex, notably composed of VPS34 (the lipid kinase), Beclin1, and ATG14L. Membrane fueling and *de novo* assembly initiate future phagophore biogenesis, via membrane(s) and lipid delivery (dashed arrows), including lipids from ATG9-positive vesicles. Concomitantly, the presence of VPS34 leads to PI3P local synthesis, a necessary step for membrane flagging and for major ATG recruitment to pre-autophagosomal membrane. Via interaction with the PI3P-binding WIPI2, and via a direct anchoring to PI3P-positive membranes, the ATG16L1 master regulator allows the targeting of the ATG5–12 complex to the membrane, which in turn, with the help of cytosolic ATGs, promotes the local lipidation of LC3 protein at the surface of the future phagophore.

PI4P (phosphatidylinositol-4-phosphate) and dedicated proteins, including the Sec16 oligomers (Joshi et al., 2017).

ER AND PEROXISOMES

Peroxisomes are small and transient organelles specialized in metabolism and present in every cell type. One of their key cellular functions is β-oxidation of long-chain fatty acids. The biogenesis and behavior of peroxisomes are directly connected to the cell metabolic state and needs (Smith and Aitchison, 2013). Several recent experimental data strongly suggest that peroxisomes—or pre-peroxysomal structures—originate *de novo* from the ER membrane (and maybe from the mitochondrial membrane as well) and acquire the set of material required for their metabolic functions later, once in the cytoplasm. The budding of pre-peroxysomal vesicles from the ER membrane (Hoepfner et al., 2005) requires several proteins of the Pex family, which might promote the physical formation and detachment of the vesicles, independently of the COP (COPII, COPI) ER and Golgi complexes (Smith and Aitchison, 2013). In a process that requires ubiquitination as well as ATP hydrolysis, Pex proteins cycle between cytosol, ER, and peroxisome membranes to allow their proper targeting and functions at peroxisome surface. Detailed information about peroxisome biogenesis and interplay with ER can be found in the recent review by Mast et al. (2020). Interestingly, peroxisomes are also reported to establish and maintain local tethering with ER membrane (Costello et al., 2017).

ER AND LIPID DROPLETS

In addition to the transport of cargo proteins and peroxisome biogenesis, ER subdomains contribute to neutral lipids storage and trafficking, mostly via the formation of lipid droplets (LDs), and lipoproteins in specialized cells handling important amounts of lipids (**Figure 2**). LDs are the main storage organelles for neutral lipids inside the eukaryote cytoplasm (Olzmann and Carvalho, 2019). They are composed of a core of triglycerides

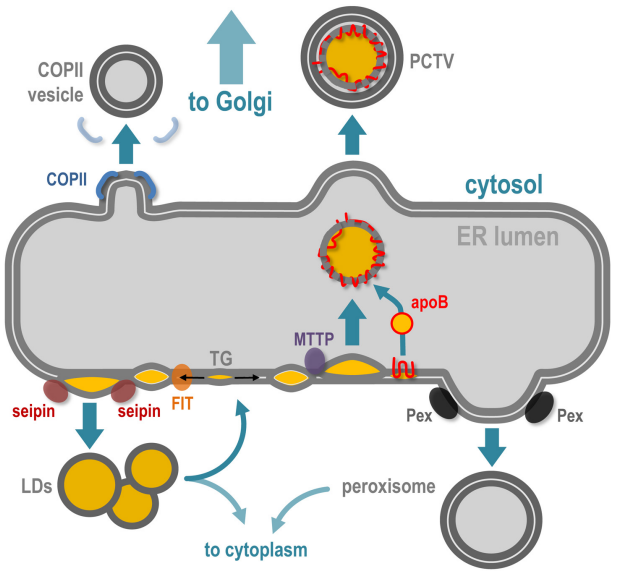

FIGURE 2 | The ER implication in *de novo* membrane-bound structures and organelles. The ER is the specific site of vesicles implied in ER-to-Golgi transport, which notably requires COPII coatomers to deform the ER membrane. Peroxisome biogenesis initiates at the ER membrane via the recruitment of Pex family proteins and the maturation of pre-peroxisome is finalized in the cytoplasm. Accumulation of neutral lipids [triglycerides (TGs)] in the bilayer of the ER leads to ER membrane deformation and release of lipid droplets (LDs) in the cytoplasm, via the coordinated action of FIT and seipin proteins. In specialized cells such as hepatocytes and enterocytes, the ER is also responsible for lipoproteins [chylomicrons in enterocytes and very low density lipoprotein (VLDL) in hepatocytes]. In parallel to LD biogenesis, the TG accumulation in the bilayer leads as well to ER intraluminal budding of neutral lipid structures, via the microsomal triglyceride transfer protein (MTTP), and this structure will be stabilized by fusion with lipidated apoliprotein B (apoB48 in enterocytes and apoB100 in hepatocytes), which leads to pre-lipoprotein synthesis inside the ER lumen. This particle is then transported via the prechylomicron transport vesicle (PCTV) along the secretory pathway via the Golgi apparatus.

(TGs) and esters of cholesterol surrounded by a monolayer of phospholipids, cholesterol and of a variety of proteins, including perilipins. Reflecting their key role in metabolism, LDs are present in every cell type and tissue and are dynamic structures able to interact with many intracellular compartments (Thiele and Spandl, 2008; Gao and Goodman, 2015). LDs can also remain associated with the ER membrane or travel back to it, probably to allow enzyme-mediated local metabolism at the LD–ER interface.

Biogenesis of LD is triggered by neutral lipid synthesis at ER, mostly TG and esters of cholesterol. Local presence of dedicated lipid enzymes, such as diglyceride acyltransferases (DGATs), is thus required for the initiation of LD formation. Neutral lipid hydrophobicity induces dispersion of lipids inside the ER membrane bilayer, and depending on a critical concentration, the neutral lipids will provoke a phase separation that induces the future LD isolation by surrounding phospholipid environment. The accumulation of newly synthesized TG between the two leaflets of the ER phospholipid bilayer is thus considered as the initial trigger (Chapman et al., 2019; Jackson, 2019) that will promote the formation of nascent LDs. The presence of a TG lens inside the ER bilayer promotes the latter deformation toward the cytoplasm side, initiating LD budding at specific sites of the ER membrane, in a surface tension manner (Ben M'barek et al., 2017). While the direct requirement of proteins in the biogenesis of LDs is not completely understood, the physical isolation of LDs from the ER membrane seems to be regulated by ER-associated proteins such as seipin oligomers, LDAF1, perilipins, and FIT proteins, illustrating the very close ER and LD relationship during the biogenesis of the latter (**Figure 2**). Detailed insights about LD biogenesis can be found in recent reviews (Olzmann and Carvalho, 2019; Renne et al., 2020).

ER AND LIPOPROTEINS SYNTHESIS

In cells managing massive amounts of neutral lipids of alimentary origin, such as enterocytes and hepatocytes, the ER is also a central player in cell protection via the specific biogenesis of lipoproteins, which are mostly composed of apolipoproteins stabilized by neutral lipids, cholesterol, phospholipids, and liposoluble vitamins. The primary lipoproteins synthesized at the ER are the chylomicrons in enterocytes (structurally organized by apob48 in humans) and very large density lipoproteins (VLDL) in hepatocytes (structurally organized by apoB100) (Mansbach and Siddiqi, 2010; Tiwari and Siddiqi, 2012). The apoB protein is synthesized at the ER membrane and, depending on the amount of TG present between the ER membrane leaflets, it will be either stabilized inside the lumen of the ER during its synthesis or retrotranslocated to the ER surface for proteasomal degradation. The process by which the neosynthesized apoB associates with TGs inside the ER lumen depends on the ER-associated proteins PDI and MTTP. The neutral lipids that will engage and stabilize the primordial apoB lipoprotein are of the same origin as LDs, making a strong and dynamic connection between ER membrane, LDs, and lipoproteins (**Figure 2**; Demignot et al., 2013). The central role of the ER in the management of neutral lipids in enterocytes (Singh et al., 2009; Singh and Cuervo, 2012) is illustrated by a specialized lipophagy (a specialized autophagy aimed toward lipid degradation) that takes place directly at surface of ER membranes in enterocytes facing massive loads of alimentary lipids. In this situation, the biogenesis of autophagosomes occurs concomitantly with the biogenesis of nascent LDs, at the same ER site, to ensure their immediate capture (Khaldoun et al., 2014).

THE ER MEMBRANE AND ER CONTACT SITES IN AUTOPHAGY REGULATION

One of the intriguing features of the organelles formed *de novo* at the ER membrane is that most of them—such as COPII vesicles, LDs, and peroxisomes—are short-lived organelles generated in response to a specific stress or stimulation, which is also true for autophagosome assembly. Thus, the role of the ER in autophagosome biogenesis is particularly interesting because the autophagic program is the major intracellular

pathway responding to cellular stress (see section "The Molecular Mechanisms of Autophagy and Autophagosome Biogenesis") and is thus a key regulator of cellular homeostasis. Indeed, despite the lack of understanding in the detailed steps leading to autophagosome biogenesis, it is now clearly established that ER subdomains are required to initiate the process, in particular omegasome [PI3P enriched ER membrane zone(s)] and ER-mediated contact sites, notably ER–mitochondria and ER–plasma membrane contact sites (MCSs) (Molino et al., 2017a; Prinz et al., 2020).

Membrane contact sites are sites of close apposition between endomembranes. They are considered as molecular hubs for organelle remodeling and membrane dynamics, as well as for metabolite and lipids exchanges and transfer from one compartment to another (Cohen et al., 2018; Scorrano et al., 2019; Prinz et al., 2020). The ER is the central player in MCSs formation and dynamics, as it spreads all through the cytoplasm and would virtually be able to touch all other membrane-bound structures inside the cellular space. ER establishes MCSs with mitochondria, which influences directly the mitochondrial fission/fusion cycles (Friedman et al., 2011), with plasma membrane, peroxisomes, endosomes, lysosomes, LDs, and Golgi (Friedman and Voeltz, 2011; De Matteis and Rega, 2015; Raiborg et al., 2015; Costello et al., 2017; Atakpa et al., 2018).

Interestingly, ER is also engaged in MCSs with several types of endomembranes at the same time, allowing local regulation of membrane-related processes between different organelles, as well as complex signal transduction regulation, particularly at ER–mitochondria MCSs. Complete and updated information about the molecular, physical, and biological features of MCSs are available in several recent detailed reviews (Cohen et al., 2018; Scorrano et al., 2019; Prinz et al., 2020).

The phagophore is the first autophagy-related organelle to be formed, prior to autophagosome, in response to a variety of stresses, including nutrient deprivation. The phagophore most probably grows via lipid acquisition and is hallmarked as "future autophagosome" on anchoring lipidated LC3 (see section "The Molecular Mechanisms of Autophagy and Autophagosome Biogenesis"). Despite the identification of most of the regulatory proteins involved in phagophore formation, closure, and maturation, the origin(s) of the membrane(s) that directly participate in its biogenesis is still unclear. In this context, a consensus suggests that the omegasome, an ER membrane transient subdomain, serves as an assembly platform to promote phagophore biogenesis (Ktistakis, 2020). In addition to the omegasome, many endomembranes have been linked directly or indirectly to the phagophore biogenesis: Golgi vesicles, endosomes and endosomal associated vesicles and tubules, mitochondria, lipid droplets, and plasma membrane. Several studies suggest that phagophore/autophagosome biogenesis directly requires ER-driven MCSs, notably ER-mitochondria MCSs, ER–LDs MCSs, and ER–plasma membrane MCSs (Molino et al., 2017a). This variety underlines a multiple and complex lipid sources crosstalk. It is tempting to speculate that the ER/omegasome promotes the necessary condition(s) for *de novo* phagophore assembly and fueling via vesicles (such as ATG9 vesicles) and membrane tubules from diverse origins and spatial localization (**Figure 3**).

The role of ER–mitochondria MCSs in autophagosome biogenesis in mammalian cells was the first demonstration of the importance of MCs in autophagy (Hamasaki et al., 2013). In a seminal study, the Yoshimori laboratory demonstrated that autophagosomes formed at ER–mitochondria MCSs in response to starvation. The authors showed that the PI3KC3 complex regulatory subunit ATG14L (a key partner of Beclin1 and VPS34 for autophagy-associated PI3P synthesis) relocalized to ER–mitochondria tethering domains together with Stx17, a protein required for membrane remodeling during phagophore and autophagosome biogenesis and maturation (Hamasaki et al., 2013). Other regulators of the PIK3C3 complex such as AMBRA1 are also stabilized at lipid rafts domains localized in the ER–mitochondria MCSs during autophagy (Garofalo et al., 2016). The effect of the ER–mitochondria interface on autophagosome biogenesis was also highlighted by the regulatory role of the VAPB–PTPIP51 tethering complex in autophagy initiation, at least in a non-starvation-induced autophagic program. More precisely, it was shown that the "tethering force" driven by the VAPB–PTPIP51 complex, which regulates membrane-to-membrane contact distance, influences the rate of autophagosome formation at least during non-starvation autophagy induction (Gomez-Suaga et al., 2017).

Recently, ER–plasma membrane tethering factors, and in particular stress responding extended synaptotagmins (E-Syts) (Giordano et al., 2013), were shown to actively participate in phagophore biogenesis in response to a variety of autophagy-associated stresses (Nascimbeni et al., 2017a,b). Membrane tether E-Syt2 interacts transiently with Beclin1 and the autophagy regulatory protein VMP1. This allows recruitment of the PI3KC3 complex at the ER–plasma membrane MCSs, which leads to local PI3P synthesis that initiates the formation of omegasomes harboring key pre-autophagic markers such as the PI3P-binding proteins DCFP1 and WIPI2 (Nascimbeni et al., 2017c).

Intriguingly, the ER seems to initiate (or maintain) a specific membrane tethering situation with the nascent phagophore itself, arguing for a complex membrane interconnection between preexisting ER membrane and newly formed autophagic membrane(s) in time and space. Recent studies show that *de novo* synthesized phospholipids can be directly transferred to the phagophore by fatty acid channeling in a very tight membrane environment (Schütter et al., 2020). ATG2, which might participate in autophagosome biogenesis on the ER–mitochondria interface (Velikkakath et al., 2012; Tang et al., 2019), was recently shown to directly contribute to lipid transfer from the ER membrane to the nascent autophagosome in both yeast and mammalian cells (Kotani et al., 2018; Valverde et al., 2019), in a PI3P-dependent manner (Maeda et al., 2019). ER membrane tethering proteins such as VAP A and VAP B were also suggested to promote phagophore assembly by enhancing and stabilizing local recruitment of the ULK1 signaling complex responsible for PI3KC3 activation, as well as the PI3P-associated WIPI2 targeting to phagophore membrane (Zhao et al., 2018). Whether the ER–phagophore transient tethering is for selective ER membrane degradation by autophagy

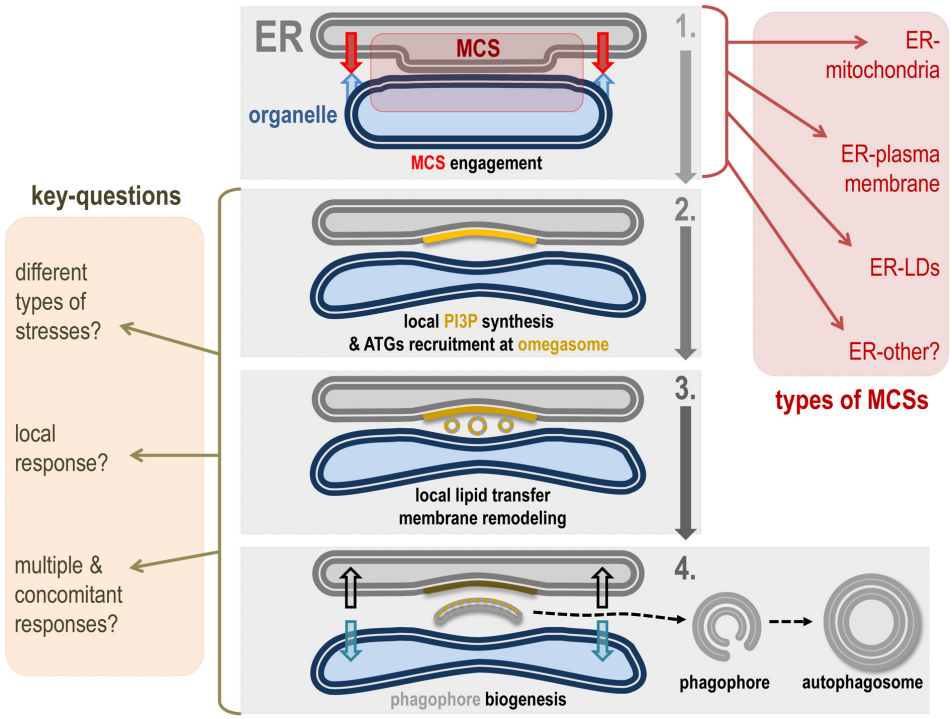

FIGURE 3 | Hypothetical model of ER contact site role in phagophore biogenesis. This scheme represents a hypothetical model of how ER-driven MCSs can be involved in phagophore biogenesis membrane dynamics. Step 1: Under appropriate conditions, the ER membrane mobilizes tethers to ensure the establishment of a MCS with a given membrane. Types of ER-driven MCSs known to participate in autophagosome formation and maturation are listed in the red square (right). Step 2: The specific area created by the ER-engaged MCS allows autophagic machinery mobilization and local PI3P synthesis on the ER subdomain called the omegasome. In turn, the omegasome is considered as a hub for autophagy-associated signaling and membrane dynamics–associated protein interplay. Notably, the PI3P-positive membrane promotes recruitment of PI3P binding proteins directly involved in phagophore assembly. Step 3: The presence of PI3P and associated autophagic membrane modulators as well as the peculiar cytoplasmic properties generated by the MCS space between ER and the engaged organelle allow the *de novo* biogenesis of membrane structures (by direct or indirect lipid transfer and/or capture), which will be necessary for phagophore assembly. Step 4: Newly formed vesicles and/or membrane-bound structures fuse together in the "cradle-like" intermembrane space delineated by the omegasome and this leads to phagophore isolation. At this stage one can imagine that MCS has to be disengaged or turn down to allow the physical disassembly of the phagophore, which will acquire cargoes and specific molecular complexes responsible for its maturation into a closed double membrane autophagosome. The key questions about the role(s) of MCS in autophagosome biogenesis are listed on the yellow square (left).

(a process referred to as ER-phagy) (Khaminets et al., 2015; Dikic, 2018) or for autophagy of ER content such as for pro-collagen degradation (Forrester et al., 2019) is not clear. This underlines the close interplay between membranes that will participate in autophagosome biogenesis and membranes that will be degraded by autophagy.

Interestingly, but making sense with *de novo* phagophore biogenesis from omegasome ER domain, ER and ER–MCS lipid supply associated machineries seem to be central in the initiation of autophagosome biogenesis. While the role of LDs was nicely demonstrated in the early steps of autophagy, notably via delivery of neutral lipids to nascent autophagosomes (Dupont et al., 2014), the ER–LD MCSs can be mobilized to transfer triglycerides and cholesterol esters to the phagophore (Shpilka et al., 2015). A hallmark of the role of MCSs in autophagosome biogenesis is the local PI3P synthesis at these specialized ER domains, both at ER–mitochondria (Hamasaki et al., 2013) and ER–plasma membrane MCSs (Nascimbeni et al., 2017c). Phosphoinositide metabolism is further involved in autophagy through the recruitment of a phosphatidylinositol synthase (Nishimura et al., 2017) on phagophore-forming ER domains, suggesting that local PI synthesis will positively regulate autophagic processes by providing a specific pool of PI ready to be phosphorylated by the PI3KC3 complex. Finally the PI3KC3 partner and autophagic regulator VMP1 (Molejon et al., 2013), which is associated with most of the MCSs in mammalian cells (Tábara and Escalante, 2016), could play a role in the space (i.e., ER-driven MCSs) and time regulation of MCS PI3P-associated synthesis during the autophagic response, as it was recently shown to negatively regulate physical disassociation of phagophores from omegasomes via the Ca^{2+}-ATPase SERCA complex (Zhao et al., 2017), demonstrating the importance of Ca^{2+} import from cytosol to ER during autophagy triggering. This highlights the importance of membrane tethering in phagophore assembly, as the absence of MCSs would probably lead to the failure of pre-autophagic machinery recruitment to the ER membrane, while a permanent membrane-to-membrane binding would slow down or abolish the physical separation of the newly formed phagophore from its MCS-associated membrane cradle.

CONCLUDING REMARKS: THE ER AS A CENTRAL NETWORK IN THE CELLULAR STRESS RESPONSE?

ER is not only devoted to protein and lipid biogenesis, but also participates in the regulation of stress(es) sensing signalization hubs (Spang, 2018). This is illustrated by the role of ER–mitochondria MCSs in defense processes such as inflammasome regulation and complex antiviral mechanisms (Namgaladze et al., 2019) that contribute directly to the global cellular stress response and protection. Moreover, ER–mitochondria MCSs have been shown to respond to ER stress, via the unfolded protein response (UPR), PERK signaling, and Ca^{2+}/IRE1α signaling (Bravo et al., 2011; van Vliet et al., 2017; Carreras-Sureda et al., 2019) and ER–plasma membrane MCSs are stabilized by several autophagy-inducing stress situations (Nascimbeni et al., 2017c).

The autophagic pathway is a stress response mechanism that undoubtedly mobilizes an important amount of proteins and lipids to maintain cellular homeostasis. *De novo* biogenesis of autophagosomes requires specialized membrane-bound structures assembly and space-and-time coordination for the proper regulation of phagophore formation. ER could be considered as an "organellar and moving scaffold" within the cell, virtually touching every endomembrane in the cytoplasm area, and thus acting as a master regulator of membrane coordination via a wide variety of MCSs. Thus, an important topic of interest for future research on autophagosome biogenesis at ER-driven MCSs will be the analysis of the physical and chemical properties of the cytoplasmic areas of MCSs in comparison with the "classical" cytosol properties, as ATG proteins can organize themselves as liquid-phase condensates to promote pre-autophagosome assembly in yeast (Fujioka et al., 2020). Indeed, MCSs have been associated with non-vesicular lipid transfer (Stefan et al., 2013). This specialized cytosolic microenvironment might promote the conditions required for *de novo* phagophore biogenesis (fusion? exchanges? membrane budding? membrane pinching?). Moreover, the local phosphoinositide metabolism occurring at MCSs (Stefan et al., 2013; Prinz et al., 2020) makes a strong connection with pre-autophagic machinery and membranes mobilization, notably through PI3P and PI4P, two lipids directly associated with autophagic processes and membrane dynamics (Wang et al., 2015; Nascimbeni et al., 2017b,c; Judith et al., 2019).

One of the most intriguing questions on autophagosome biogenesis and ER-driven MCSs concerns the nature of the autophagosomes formed at different MCSs. Are these autophagic structures capturing specific cargoes? Are they responding preferentially to specialized stresses? Are MCSs spatial coordinators (to promote autophagosome biogenesis in a given area of the cell) or "opportunistic" platforms that are randomly mobilized during autophagic processes?

Finally, the identification of other ER MCSs and specific ER MCS-associated tethers (as suggested for VMP1 protein, which plays as well a key function in autophagosome biogenesis regulation) will be one of the challenges in future research on ER membrane mobilization during autophagosome biogenesis.

AUTHOR CONTRIBUTIONS

EM wrote the manuscript and prepared the figures.

FUNDING

This work in my laboratory is supported by grants from Inserm, CNRS, and ANR.

ACKNOWLEDGMENTS

I thank my team colleagues for fruitful discussions and constant support, and I warmly thank Dr. Zeina Chamoun for critical reading of the manuscript.

REFERENCES

Atakpa, P., Thillaiappan, N. B., Mataragka, S., Prole, D. L., and Taylor, C. W. (2018). IP3 receptors preferentially associate with ER-lysosome contact sites and selectively deliver Ca2+ to lysosomes. *Cell Rep.* 25, 3180–3193.e7. doi: 10.1016/j.celrep.2018.11.064

Baskaran, S., Ragusa, M. J., Boura, E., and Hurley, J. H. (2012). Two-site recognition of phosphatidylinositol 3-Phosphate by PROPPINs in autophagy. *Mol. Cell* 47, 339–348. doi: 10.1016/j.molcel.2012.05.027

Ben M'barek, K., Ajjaji, D., Chorlay, A., Vanni, S., Forêt, L., and Thiam, A. R. (2017). ER membrane phospholipids and surface tension control cellular lipid droplet formation. *Dev. Cell* 41, 591–604.e7. doi: 10.1016/j.devcel.2017.05.012

Boya, P., Reggiori, F., and Codogno, P. (2013). Emerging regulation and functions of autophagy. *Nat. Cell Biol.* 15, 713–720. doi: 10.1038/ncb2788

Bravo, R., Vicencio, J. M., Parra, V., Troncoso, R., Munoz, J. P., Bui, M., et al. (2011). Increased ER-mitochondrial coupling promotes mitochondrial respiration and bioenergetics during early phases of ER stress. *J. Cell Sci.* 124, 2143–2152. doi: 10.1242/jcs.080762

Carreras-Sureda, A., Jaña, F., Urra, H., Durand, S., Mortenson, D. E., Sagredo, A., et al. (2019). Non-canonical function of IRE1α determines mitochondria-associated endoplasmic reticulum composition to control calcium transfer and bioenergetics. *Nat. Cell Biol.* 21, 755–767. doi: 10.1038/s41556-019-0329-y

Chapman, K. D., Aziz, M., Dyer, J. M., and Mullen, R. T. (2019). Mechanisms of lipid droplet biogenesis. *Biochem. J.* 476, 1929–1942. doi: 10.1042/BCJ20180021

Cohen, S., Valm, A. M., and Lippincott-Schwartz, J. (2018). Interacting organelles. *Curr. Opin. Cell Biol.* 53, 84–91. doi: 10.1016/j.ceb.2018.06.003

Costello, J. L., Castro, I. G., Hacker, C., Schrader, T. A., Metz, J., Zeuschner, D., et al. (2017). ACBD5 and VAPB mediate membrane associations between peroxisomes and the ER. *J. Cell Biol.* 216, 331–342. doi: 10.1083/jcb.201607055

De Matteis, M. A., and Rega, L. R. (2015). Endoplasmic reticulum–Golgi complex membrane contact sites. *Curr. Opin. Cell Biol.* 35, 43–50. doi: 10.1016/j.ceb.2015.04.001

Demignot, S., Beilstein, F., and Morel, E. (2013). Triglyceride-rich lipoproteins and cytosolic lipid droplets in enterocytes: key players in intestinal physiology and metabolic disorders. *Biochimie* 96, 48–55. doi: 10.1016/j.biochi.2013.07.009

Dikic, I. (2018). Open questions: why should we care about ER-phagy and ER remodelling? *BMC Biol.* 16:131. doi: 10.1186/s12915-018-0603-607

Dooley, H. C., Razi, M., Polson, H. E. J., Girardin, S. E., Wilson, M. I., and Tooze, S. A. (2014). WIPI2 links LC3 conjugation with PI3P, autophagosome

formation, and pathogen clearance by recruiting Atg12-5-16L1. *Mol. Cell* 55, 238–252. doi: 10.1016/j.molcel.2014.05.021

Dudley, L. J., Cabodevilla, A. G., Makar, A. N., Sztacho, M., Michelberger, T., Marsh, J. A., et al. (2019). Intrinsic lipid binding activity of ATG16L1 supports efficient membrane anchoring and autophagy. *EMBO J.* 38:e100554. doi: 10.15252/embj.2018100554

Dupont, N., Chauhan, S., Arko-Mensah, J., Castillo, E. F., Masedunskas, A., Weigert, R., et al. (2014). Neutral lipid stores and lipase PNPLA5 contribute to autophagosome biogenesis. *Curr. Biol.* 24, 609–620. doi: 10.1016/j.cub.2014.02.008

Forrester, A., De Leonibus, C., Grumati, P., Fasana, E., Piemontese, M., Staiano, L., et al. (2019). A selective ER -phagy exerts procollagen quality control via a Calnexin- FAM 134B complex. *EMBO J.* 38:e99847. doi: 10.15252/embj.201899847

Friedman, J. R., Lackner, L. L., West, M., DiBenedetto, J. R., Nunnari, J., and Voeltz, G. K. (2011). ER tubules mark sites of mitochondrial division. *Science* 334, 358–362. doi: 10.1126/science.1207385

Friedman, J. R., and Voeltz, G. K. (2011). The ER in 3D: a multifunctional dynamic membrane network. *Trends Cell Biol.* 21, 709–717. doi: 10.1016/j.tcb.2011.07.004

Fujioka, Y., Alam, J. M., Noshiro, D., Mouri, K., Ando, T., Okada, Y., et al. (2020). Phase separation organizes the site of autophagosome formation. *Nature* 578, 301–305. doi: 10.1038/s41586-020-1977-1976

Gao, Q., and Goodman, J. M. (2015). The lipid droplet–a well-connected organelle. *Front. Cell Dev. Biol.* 3:49. doi: 10.3389/fcell.2015.00049

Garofalo, T., Matarrese, P., Manganelli, V., Marconi, M., Tinari, A., Gambardella, L., et al. (2016). Evidence for the involvement of lipid rafts localized at the ER-mitochondria associated membranes in autophagosome formation. *Autophagy* 12, 917–935. doi: 10.1080/15548627.2016.1160971

Giordano, F., Saheki, Y., Idevall-Hagren, O., Colombo, S. F., Pirruccello, M., Milosevic, I., et al. (2013). PI(4,5)P(2)-dependent and Ca(2+)-regulated ER-PM interactions mediated by the extended synaptotagmins. *Cell* 153, 1494–1509. doi: 10.1016/j.cell.2013.05.026

Gomez-Suaga, P., Paillusson, S., Stoica, R., Noble, W., Hanger, D. P., and Miller, C. C. J. (2017). The ER-Mitochondria tethering complex VAPB-PTPIP51 regulates autophagy. *Curr. Biol.* 27, 371–385. doi: 10.1016/j.cub.2016.12.038

Hamasaki, M., Furuta, N., Matsuda, A., Nezu, A., Yamamoto, A., Fujita, N., et al. (2013). Autophagosomes form at ER-mitochondria contact sites. *Nature* 495, 389–393. doi: 10.1038/nature11910

Hoepfner, D., Schildknegt, D., Braakman, I., Philippsen, P., and Tabak, H. F. (2005). Contribution of the endoplasmic reticulum to peroxisome formation. *Cell* 122, 85–95. doi: 10.1016/j.cell.2005.04.025

Hurley, J. H., and Young, L. N. (2017). Mechanisms of autophagy initiation. *Annu. Rev. Biochem.* 86, 225–244. doi: 10.1146/annurev-biochem-061516-44820

Jackson, C. L. (2019). Lipid droplet biogenesis. *Curr. Opin. Cell Biol.* 59, 88–96. doi: 10.1016/j.ceb.2019.03.018

Joshi, A. S., Zhang, H., and Prinz, W. A. (2017). Organelle biogenesis in the endoplasmic reticulum. *Nat. Cell Biol.* 19, 876–882. doi: 10.1038/ncb3579

Judith, D., Jefferies, H. B. J., Boeing, S., Frith, D., Snijders, A. P., and Tooze, S. A. (2019). ATG9A shapes the forming autophagosome through Arfaptin 2 and phosphatidylinositol 4-kinase IIIβ. *J. Cell Biol.* 218, 1634–1652. doi: 10.1083/jcb.201901115

Khaldoun, S. A., Emond-Boisjoly, M.-A., Chateau, D., Carrière, V., Lacasa, M., Rousset, M., et al. (2014). Autophagosomes contribute to intracellular lipid distribution in enterocytes. *Mol. Biol. Cell* 25, 118–132. doi: 10.1091/mbc.E13-06-0324

Khaminets, A., Heinrich, T., Mari, M., Grumati, P., Huebner, A. K., Akutsu, M., et al. (2015). Regulation of endoplasmic reticulum turnover by selective autophagy. *Nature* 522, 354–358. doi: 10.1038/nature14498

Kotani, T., Kirisako, H., Koizumi, M., Ohsumi, Y., and Nakatogawa, H. (2018). The Atg2-Atg18 complex tethers pre-autophagosomal membranes to the endoplasmic reticulum for autophagosome formation. *Proc. Natl. Acad. Sci. U.S.A.* 115, 10363–10368. doi: 10.1073/pnas.1806727115

Ktistakis, N. T. (2020). ER platforms mediating autophagosome generation. *Biochim. Biophys. Acta Mol. Cell Biol. Lipids* 1865:158433. doi: 10.1016/j.bbalip.2019.03.005

Lee, J. E., Cathey, P. I., Wu, H., Parker, R., and Voeltz, G. K. (2020). Endoplasmic reticulum contact sites regulate the dynamics of membraneless organelles. *Science* 367:eaay7108. doi: 10.1126/science.aay7108

Maeda, S., Otomo, C., and Otomo, T. (2019). The autophagic membrane tether ATG2A transfers lipids between membranes. *eLife* 8:e45777. doi: 10.7554/eLife.45777

Mansbach, C. M., and Siddiqi, S. A. (2010). The biogenesis of chylomicrons. *Annu. Rev. Physiol.* 72, 315–333. doi: 10.1146/annurev-physiol-021909-135801

Mast, F. D., Rachubinski, R. A., and Aitchison, J. D. (2020). Peroxisome prognostications: exploring the birth, life, and death of an organelle. *J. Cell Biol.* 219:e201912100. doi: 10.1083/jcb.201912100

Mizushima, N. (2020). The ATG conjugation systems in autophagy. *Curr. Opin. Cell Biol.* 63, 1–10. doi: 10.1016/j.ceb.2019.12.001

Molejon, M. I., Ropolo, A., Lo Re, A., Boggio, V., and Vaccaro, M. I. (2013). The VMP1-Beclin 1 interaction regulates autophagy induction. *Sci. Rep.* 3:1055. doi: 10.1038/srep01055

Molino, D., Nascimbeni, A. C., Giordano, F., Codogno, P., and Morel, E. (2017a). ER-driven membrane contact sites: evolutionary conserved machineries for stress response and autophagy regulation? *Commun. Integr. Biol.* 10:e1401699. doi: 10.1080/19420889.2017.1401699

Molino, D., Zemirli, N., Codogno, P., and Morel, E. (2017b). The journey of the autophagosome through mammalian cell organelles and membranes. *J. Mol. Biol.* 429, 497–514. doi: 10.1016/j.jmb.2016.12.013

Namgaladze, D., Khodzhaeva, V., and Brüne, B. (2019). ER-Mitochondria communication in cells of the innate immune system. *Cell* 8:1088. doi: 10.3390/cells8091088

Nascimbeni, A. C., Codogno, P., and Morel, E. (2017a). Autophagosomal membranes assemble at ER-plasma membrane contact sites. *Mol. Cell. Oncol.* 4:e1356431. doi: 10.1080/23723556.2017.1356431

Nascimbeni, A. C., Codogno, P., and Morel, E. (2017b). Phosphatidylinositol-3-phosphate in the regulation of autophagy membrane dynamics. *FEBS J.* 284, 1267–1278. doi: 10.1111/febs.13987

Nascimbeni, A. C., Giordano, F., Dupont, N., Grasso, D., Vaccaro, M. I., Codogno, P., et al. (2017c). ER-plasma membrane contact sites contribute to autophagosome biogenesis by regulation of local PI3P synthesis. *EMBO J.* 36, 2018–2033. doi: 10.15252/embj.201797006

Nishimura, T., Kaizuka, T., Cadwell, K., Sahani, M. H., Saitoh, T., Akira, S., et al. (2013). FIP200 regulates targeting of Atg16L1 to the isolation membrane. *EMBO Rep.* 14, 284–291. doi: 10.1038/embor.2013.6

Nishimura, T., Tamura, N., Kono, N., Shimanaka, Y., Arai, H., Yamamoto, H., et al. (2017). Autophagosome formation is initiated at phosphatidylinositol synthase-enriched ER subdomains. *EMBO J.* 36, 1719–1735. doi: 10.15252/embj.201695189

Olzmann, J. A., and Carvalho, P. (2019). Dynamics and functions of lipid droplets. *Nat. Rev. Mol. Cell Biol.* 20, 137–155. doi: 10.1038/s41580-018-0085-z

Peotter, J., Kasberg, W., Pustova, I., and Audhya, A. (2019). COPII-mediated trafficking at the ER/ERGIC interface. *Traffic* 20, 491–503. doi: 10.1111/tra.12654

Prinz, W. A., Toulmay, A., and Balla, T. (2020). The functional universe of membrane contact sites. *Nat. Rev. Mol. Cell Biol.* 21, 7–24. doi: 10.1038/s41580-019-0180-189

Puri, C., Vicinanza, M., Ashkenazi, A., Gratian, M. J., Zhang, Q., Bento, C. F., et al. (2018). The RAB11A-positive compartment is a primary platform for autophagosome assembly mediated by WIPI2 recognition of PI3P-RAB11A. *Dev. Cell* 45, 114–131.e8. doi: 10.1016/j.devcel.2018.03.008

Raiborg, C., Wenzel, E. M., and Stenmark, H. (2015). ER – endosome contact sites?: molecular compositions and functions. *EMBO J.* 34, 1848–1858. doi: 10.15252/embj.201591481

Renne, M. F., Klug, Y. A., and Carvalho, P. (2020). Lipid droplet biogenesis: a mystery "unmixing"? *Semin. Cell Dev. Biol.* doi: 10.1016/j.semcdb.2020.03.001

Schütter, M., Giavalisco, P., Brodesser, S., and Graef, M. (2020). Local fatty acid channeling into phospholipid synthesis drives phagophore expansion during autophagy. *Cell* 180, 135–149.e14. doi: 10.1016/j.cell.2019.12.005

Scorrano, L., De Matteis, M. A., Emr, S., Giordano, F., Hajnóczky, G., Kornmann, B., et al. (2019). Coming together to define membrane contact sites. *Nat. Commun.* 10:1287. doi: 10.1038/s41467-019-09253-9253

Shpilka, T., Welter, E., Borovsky, N., Amar, N., Mari, M., Reggiori, F., et al. (2015). Lipid droplets and their component triglycerides and steryl esters

regulate autophagosome biogenesis. *EMBO J.* 34, 2117–2131. doi: 10.15252/embj.201490315

Singh, R., and Cuervo, A. M. (2012). Lipophagy: connecting autophagy and lipid metabolism. *Int. J. Cell. Biol.* 2012:282041. doi: 10.1155/2012/282041

Singh, R., Kaushik, S., Wang, Y., Xiang, Y., Novak, I., Komatsu, M., et al. (2009). Autophagy regulates lipid metabolism. *Nature* 458, 1131–1135. doi: 10.1038/nature07976

Smith, J. J., and Aitchison, J. D. (2013). Peroxisomes take shape. *Nat. Rev. Mol. Cell Biol.* 14, 803–817. doi: 10.1038/nrm3700

Spang, A. (2018). The endoplasmic reticulum-the caring mother of the cell. *Curr. Opin. Cell Biol.* 53, 92–96. doi: 10.1016/j.ceb.2018.06.004

Stefan, C. J., Manford, A. G., and Emr, S. D. (2013). ER-PM connections: sites of information transfer and inter-organelle communication. *Curr. Opin. Cell Biol.* 25, 434–442. doi: 10.1016/j.ceb.2013.02.020

Tábara, L.-C., and Escalante, R. (2016). VMP1 establishes ER-Microdomains that regulate membrane contact sites and autophagy. *PLoS One* 11:e0166499. doi: 10.1371/journal.pone.0166499

Tang, Z., Takahashi, Y., and Wang, H.-G. (2019). ATG2 regulation of phagophore expansion at mitochondria-associated ER membranes. *Autophagy* 15, 2165–2166. doi: 10.1080/15548627.2019.1666594

Thiele, C., and Spandl, J. (2008). Cell biology of lipid droplets. *Curr. Opin. Cell Biol.* 20, 378–385. doi: 10.1016/j.ceb.2008.05.009

Tiwari, S., and Siddiqi, S. A. (2012). Intracellular trafficking and secretion of VLDL. *Arterioscler. Thromb. Vasc. Biol.* 32, 1079–1086. doi: 10.1161/ATVBAHA.111.241471

Tooze, S. A. (2013). Current views on the source of the autophagosome membrane. *Essays Biochem.* 55, 29–38. doi: 10.1042/bse0550029

Valverde, D. P., Yu, S., Boggavarapu, V., Kumar, N., Lees, J. A., Walz, T., et al. (2019). ATG2 transports lipids to promote autophagosome biogenesis. *J. Cell Biol.* 218, 1787–1798. doi: 10.1083/jcb.201811139

van Vliet, A. R., Giordano, F., Gerlo, S., Segura, I., Van Eygen, S., Molenberghs, G., et al. (2017). The ER stress sensor PERK coordinates ER-plasma membrane contact site formation through interaction with Filamin-A and F-Actin remodeling. *Mol. Cell* 65, 885–899.e6. doi: 10.1016/j.molcel.2017.01.020

Velikkakath, A. K., Nishimura, T., Oita, E., Ishihara, N., and Mizushima, N. (2012). Mammalian Atg2 proteins are essential for autophagosome formation and important for regulation of size and distribution of lipid droplets. *Mol. Biol. Cell* 23, 896–909. doi: 10.1091/mbc.E11-09-0785

Walker, S. A., and Ktistakis, N. T. (2019). Autophagosome biogenesis machinery. *J. Mol. Biol.* 432, 2449–2461. doi: 10.1016/j.jmb.2019.10.027

Wang, H., Sun, H.-Q., Zhu, X., Zhang, L., Albanesi, J., Levine, B., et al. (2015). GABARAPs regulate PI4P-dependent autophagosome:lysosome fusion. *Proc. Natl. Acad. Sci. U.S.A.* 112, 7015–7020. doi: 10.1073/pnas.1507263112

Wilson, M. I. I., Dooley, H. C. C., and Tooze, S. A. A. (2014). WIPI2b and Atg16L1: setting the stage for autophagosome formation. *Biochem. Soc. Trans.* 42, 1327–1334. doi: 10.1042/BST20140177

Yang, Z., and Klionsky, D. J. (2010). Eaten alive: a history of macroautophagy. *Nat. Cell Biol.* 12, 814–822. doi: 10.1038/ncb0910-814

Zhao, Y. G., Chen, Y., Miao, G., Zhao, H., Qu, W., Li, D., et al. (2017). The ER-localized transmembrane protein EPG-3/VMP1 regulates SERCA activity to control ER-isolation membrane contacts for autophagosome formation. *Mol. Cell* 67, 974–989.e6. doi: 10.1016/j.molcel.2017.08.005

Zhao, Y. G., Liu, N., Miao, G., Chen, Y., Zhao, H., and Zhang, H. (2018). The ER contact proteins VAPA/B interact with multiple autophagy proteins to modulate autophagosome biogenesis. *Curr. Biol.* 28, 1234–1245.e4. doi: 10.1016/j.cub.2018.03.002

Conflict of Interest: The author declares that the research was conducted in the absence of any commercial or financial relationships that could be construed as a potential conflict of interest.

frontiers in Cell and Developmental Biology

REVIEW
published: 10 June 2020
doi: 10.3389/fcell.2020.00413

The Role of Mitochondrial Dynamics and Mitophagy in Carcinogenesis, Metastasis and Therapy

Yigang Wang[1], Hui-Hui Liu[1], Yu-Ting Cao[1], Lei-Lei Zhang[1], Fang Huang[2] and Cong Yi[3]**

[1] Xinyuan Institute of Medicine and Biotechnology, School of Life Sciences and Medicine, Zhejiang Sci-Tech University, Hangzhou, China, [2] Department of Pathology, Zhejiang Provincial People's Hospital, People's Hospital of Hangzhou Medical College, Hangzhou, China, [3] Department of Biochemistry, Hepatobiliary and Pancreatic Surgery, The First Affiliated Hospital, Zhejiang University School of Medicine, Hangzhou, China

Mitochondria are key cellular organelles and play vital roles in energy metabolism, apoptosis regulation and cellular homeostasis. Mitochondrial dynamics refers to the varying balance between mitochondrial fission and mitochondrial fusion that plays an important part in maintaining mitochondrial homeostasis and quality. Mitochondrial malfunction is involved in aging, metabolic disease, neurodegenerative disorders, and cancers. Mitophagy, a selective autophagy of mitochondria, can efficiently degrade, remove and recycle the malfunctioning or damaged mitochondria, and is crucial for quality control. In past decades, numerous studies have identified a series of factors that regulate mitophagy and are also involved in carcinogenesis, cancer cell migration and death. Therefore, it has become critically important to analyze signal pathways that regulate mitophagy to identify potential therapeutic targets. Here, we review recent progresses in mitochondrial dynamics, the mechanisms of mitophagy regulation, and the implications for understanding carcinogenesis, metastasis, treatment, and drug resistance.

Keywords: mitochondria, mitochondrial dynamics, mitophagy, carcinogenesis, therapy

OPEN ACCESS

Edited by:
Du Feng,
Guangzhou Medical University, China

Reviewed by:
Paolo Remondelli,
University of Salerno, Italy
Lei Liu,
Institute of Zoology (CAS), China

****Correspondence:***
Fang Huang
huangfang0794@163.com
Cong Yi
yiconglab@zju.edu.cn

Specialty section:
This article was submitted to Membrane Traffic, a section of the journal Frontiers in Cell and Developmental Biology

Received: *07 February 2020*
Accepted: *04 May 2020*
Published: *10 June 2020*

Citation:
Wang Y, Liu H-H, Cao Y-T, Zhang L-L, Huang F and Yi C (2020) The Role of Mitochondrial Dynamics and Mitophagy in Carcinogenesis, Metastasis and Therapy. Front. Cell Dev. Biol. 8:413. doi: 10.3389/fcell.2020.00413

Abbreviations: ABCB1, *P*-glycoprotein; ADAM17, A disintegrin and metalloproteinase; Ambra1, Autophagy and Beclin 1 Regulator 1; ARIH1, Ariadne RBR E3 Ubiquitin Protein Ligase 1; AT 101, (-)-gossypol; Atg, autophagy-related protein; ATP, adenosine triphosphate; Bcl2L13, BCL2 Like 13; BNIP3, BCL2/adenovirus E1B 19 kDa protein-interacting protein 3; BNIP3L/NIX, BNIP3-like; CDK 1, cyclin dependent kinase 1; CDKN2A, cyclin-dependent kinase inhibitor 2A; CSC, cancer stem cell; CTLA4, cytotoxic T lymphocyte-associated antigen-4; Cvt, cytoplasm to vacuole targeting; DCIS, ductal carcinoma *in situ;* DNM1L, dynamin-1-like protein; Drp1, dynamin-related protein 1; ESCC, esophageal squamous cell carcinoma; Fis1, fission, mitochondrial 1; FKBP8, FK506-binding protein 8; FOX03, Forkhead Box O3; FUNDC1, FUN14 domain-containing protein 1; GTP, guanosine triphosphate; GTPases, guanosine triphosphatase; HCT8, Human Colon Tumor (HCT8) Cell Line; HNSCC, head and neck squamous cell carcinoma; JNK, c-Jun N-terminal kinase; KRAS, Kirsten Rat Sarcoma Viral Oncogene; LC3, microtubule-associated proteins 1A/1B light chain 3A; LIR, LC3-interacting domain; MAPK, mitogen-activated protein kinase; MARCH5, membrane-associated RING finger protein 5; Mdivi-1, mitochondrial division inhibitor 1; MID49, mitochondrial dynamics protein of 49 kDa; MID51, mitochondrial dynamics protein of 51 kDa; MIRO1, Mitochondrial Rho GTPase 1; Mito-CP, 3-carboxyl proxyl (CP) nitroxide; mTOR, mammalian target of rapamycin; NBR1, neighbor of BRCA1 gene protein; NDP52, nuclear dot protein 52; NF-κβ, nuclear factor kappa beta; NLRX1, NLR (Nucleotide-binding domain and leucine-rich repeat-containing receptors) family member X1; NOS, nitric oxide synthase; OPA1, optic atrophy 1; OPTN, optineurin; OSCC, oral squamous cell carcinoma; OXPHOS, oxidative phosphorylation; PARK2, gene encoding Parkin; PARL, presenilin-associated rhomboid-like; PD-L1, Programmed Cell Death 1 Ligand 1; PGAM5, hosphoglycerate mutase-5; PHB2, Prohibitin 2; PINK1, mitochondrial PTEN-induced kinase 1; PUMA, p53 upregulated modulator of apoptosis; Ras, Rat Sarcoma protein, Small GTP Binding Protein; RB, retinoblastoma; Rheb, Ras homolog enriched in brain protein; ROS, reactive oxygen species; TAX1BP1, TAX1 binding protein 1; TNBC, triple negative breast cancer; TR3, orphan nuclear receptor; ULK1, Unc-51 Like Autophagy Activating Kinase 1; VDAC, Voltage Dependent Anion Channel 1; Yme1L, YME1-Like Protein 1.

INTRODUCTION

Mitochondria are the energy-producing cellular compartment, also known as the cell's "power house," and act as the primary site for aerobic respiration (Giampazolias and Tait, 2016). Mitochondria not only have this core bioenergy function, but they also provide basic materials for tumor anabolism, tumor cell redox and calcium homeostasis control, transcription regulation and cell death control (Chen and Mellman, 2017). The effects of the host immune system on tumor development, progression, and response to therapy are similarly dependent on tumor mitochondrial metabolism (Wallace, 2012; Vyas et al., 2016). Consequently, mitochondria are expected to be an excellent target to exploit for new anticancer drugs (Porporato et al., 2018).

Mitophagy, the specific autophagy of mitochondria, plays a pivotal role in mitochondrial quality control by clearing damaged mitochondria. Severe defects in mitophagy, are associated with complete impairment of mitochondrial functions, oncogenesis and tumor progression in multiple tumors (Guo et al., 2013; Rosenfeldt et al., 2013; Rao et al., 2014). Hence, the study of mitophagy regulatory mechanisms in cancer-related events is of great significance. Mitochondria are highly dynamic structures. The coordinated cycle of mitochondrial division and fusion ("mitochondrial dynamics"; Tilokani et al., 2018) provides fast morphological adaptation of mitochondria and plays an important role in the regulation of the cell cycle, cellular immunity, apoptosis, and mitochondrial mass (Wai and Langer, 2016). Mitochondrial dynamic dysfunction can directly damage cells through inadequate ATP supply or high production of ROS and NOS. This in turn can lead to abnormalities, such as neurodegenerative diseases, cancer and autoimmune diseases (Vásquez-Trincado et al., 2016). Many human diseases are associated with mutations in mitochondrial core mechanical components and flaws in mitochondrial dynamics (Mishra and Chan, 2016; Chan, 2020).

This review covers the latest progress in mitochondrial dynamics and mechanisms of mitophagy regulation in the context of carcinogenesis, metastasis, cancer therapy and drug resistance, and proposes future directions for developing novel cancer therapy strategies focused on mitochondria.

MITOCHONDRIAL DYNAMICS

Mitochondrial dynamics is the process of mitochondrial fusion and fission, and determines the shape, quality and quantity of mitochondria (Chan, 2012; Pernas and Scorrano, 2016). Mitochondrial dynamics is closely linked to mitochondrial functions, such as cell proliferation, cell metabolism, and cell migration (Chan, 2006) and is tightly regulated by a variety of proteins.

Mitochondrial Fission and Fusion

The mitochondrial fission process (mitofission) is mainly mediated by Drp1. Drp1 belongs to a class of GTP-binding proteins and can be recruited from cytoplasm to the mitochondrial membrane with the assistance of mitochondrial receptor proteins Fis1, MFF, MID49, and MID51 (Losón et al., 2013). Then Drp1 located on the mitochondrial membrane can form a ring structure that closely surrounds the mitochondrion (Ingerman et al., 2005), and induces a breakage of the mitochondrial membrane requiring hydrolysis of GTP (Ji et al., 2015). The phosphorylation, ubiquitination and sumoylation of Drp1 can regulate mitofission by influencing Drp1 stability and recruitment (Chang and Blackstone, 2010). Phosphorylation of Drp1 on Ser585 catalyzed by CDK 1/Cyclin B promotes mitofission in mitotic cells (Taguchi et al., 2007), while phosphorylation of Drp1 on Ser637 can inhibit mitofission.

The mitochondrial fusion process (mitofusion) can be divided into outer mitochondrial membrane (OMM) fusion mediated by mitofusin 1 (Mfn1) and mitofusin 2 (Mfn2) and inner mitochondrial membrane (IMM) fusion mediated by OPA1 (Ni et al., 2015). Mfn and OPA1 are dynamin-related GTPases. Mfn1 and Mfn2 expressed on the OMM can interact to mediate fusion between adjacent OMM (Cao et al., 2017). OPA1 located in the IMM together with Mfn1 mediates the fusion of IMM (Cipolat et al., 2004). At present, the exact mechanism of IMM fusion is not clear, but OPA1 has been proved to be necessary. Fusion-related proteins are regulated by posttranslational modifications that effect their abundance and activity (Senft and Ronai, 2016); Mfn1 and Mfn2 activities can be modified by specific phosphorylations, and ubiquitination of the proteins may lead to their degradation.

The Roles of Mitochondrial Dynamics in Cancer

Mitochondrial dynamics are closely related to the occurrence and metastasis of tumors. Environmental alterations around a cell lead to mitochondrial dynamics change, which is also a mechanism for cancer adaption. There are disorders of mitochondrial dynamics in many cancers; up-regulation of fission-related proteins and down-regulation of fusion-related proteins is found in many types of cancer (Rehman et al., 2012; Zhao et al., 2013; Huang et al., 2017). For example, there is an increase of mitochondrial fragmentation and phosphorylation activation of Drp1 in brain tumor initiation cells (Xie et al., 2015). Additionally, the expression of Mfn2 in lung cancer is lower than that in normal tissues, and overexpression of Drp1/Mfn2 can affect mitochondrial dynamics and inhibit the proliferation of lung cancer cells (Rehman et al., 2012). The findings imply that Drp1/Mfn2 exerts different effects in different cancers.

Targeting therapy based on mitochondrial dynamic-related factors is becoming a potential method for cancer therapy. For instance, hypoxia increases the expression of Drp1 and mitofission in glioblastoma cells, enhances tumor migration, and treatment with Mdivi-1 (DRP1 inhibitor) reduces hypoxia-induced migration (Wan et al., 2014). Mdivi-1 is the best drug to use to characterize mitochondrial dynamics (Cassidy-Stone et al., 2008). It can induce proliferation arrest and apoptosis of tumor cells (Rehman et al., 2012; Wang et al., 2015), but it has some cytotoxicity to normal cells. The chemosensitivity of cancer cells can be improved by mitofission. By down-regulating the phosphorylation of Drp1 at Ser637, Piperlongumine can induce

TABLE 1 | Compounds targeting mitochondria in the treatment of cancer.

Compound	Cancer type	Effect	References
Mdivi-1	Lung cancer	Inhibitor of Drp1 and proapoptotic effects	Rehman et al., 2012
Piperlongumine	Ovarian cancer	Activate Drp1 and induce both fission and apoptosis	Farrand et al., 2013
Lectin	Ovarian cancer	Activate AKT signal pathways and de-phosphorylates Drp1	Chowdhury et al., 2017
DHE	Lung cancer	Induce mitochondrial dysfunction, mitophagy and apoptosis	Chang et al., 2016
Nanomicelle	Non-small cell lung carcinoma	Trigger excessive mitophagy /autophagy and energy depletion	Zhu et al., 2020
CerS1/C18 pyridinium ceramide	Hypopharyngeal cancer	Target autophagosomes to mitochondria and induce lethal mitophagy	Sentelle et al., 2012
AT 101	Glioma	Induce mitochondrial dysfunction and mitophagy	Meyer et al., 2018
Sodium selenite	Glioma	Induce mitochondrial damage and subsequent mitophagy	Kim et al., 2007
LCL-461	Acute myeloid leukemia	Induce lethal mitophagy	Dany et al., 2016
Liensinine	Breast cancer	Sensitize cancer cells to chemotherapy through DNM1L-mediated mitofission	Zhou et al., 2015
Isoliensinine	Breast cancer	Induce cancer cell apoptosis through ROS and p38 MAPK/JNK activation	Zhang et al., 2015
Mito-CP	Colon cancer	Induce changes in mitochondrial bioenergetics, block mTOR-mediated proliferation and induce mitophagy	Boyle et al., 2018
Mito-Metformin			
Abrus agglutinin	Glioblastoma	Trigger ceramide production, induce ER stress and ROS to promote mitophagy	Panda et al., 2018
BAY 87-2243	Melanoma	Inhibit mitochondrial complex I, trigger mitophagy	Basit et al., 2017
B5G1	Liver cancer	Inhibit PINK1-Parkin dependent mitophagy	Yao et al., 2019

the apoptosis of cisplatin-resistant ovarian cancer cells (Farrand et al., 2013; **Table 1**). Moreover, treatment with a lectin, *Sambucus nigra* agglutinin, induces mitofission-mediated apoptosis by stimulating Drp1 translocation (Chowdhury et al., 2017). However, there is a reverse action for Drp1 in cancer treatment. The inhibition of Drp1-mediated mitochondrial fission results in the sensitization of ovarian cancer cells to cisplatin (Yang et al., 2017). Thus, the mechanisms of mitochondrial dynamics can rationally be used as a potential target for cancer therapy.

MOLECULAR MECHANISMS OF MITOPHAGY REGULATION

Mitophagy can selectively remove damaged or redundant mitochondria. Mitophagy is an essential part of mitochondrial stress response and homeostasis regulation, also playing a regulatory role in mitochondrial quality control (Abeliovich et al., 2013). Thus, when the mechanism of mitophagy is impaired, mitochondrial function is reduced or mitochondrial redundancy is caused, which will affect cell homeostasis and lead to the occurrence of related diseases.

Principally, mitophagy pathway can be divided into two types: ubiquitin-mediated mitophagy and receptor-mediated mitophagy. The well-studied pathways are PINK1-Parkin mediated ubiquitin pathway and FUNDC1 receptor-mediated pathway, respectively (**Figure 1**).

Mechanisms of the Ubiquitin Type Mitophagy Pathway

The PINK1-Parkin mediated regulation of mitophagy is characterized by the ubiquitylation of some key mitochondrial proteins. Parkin, as an E3 ubiquitin ligase, and PINK1, as a serine/threonine kinase, were initially found to be closely related to Parkinson's disease (Kitada et al., 1998). In normal cells, the PINK1 protein synthesized in the cytoplasm is firstly translocated into the mitochondrial inner membrane, in which is cleaved by PARL protease and degraded by the ubiquitin mediated proteasome pathway (Sekine and Youle, 2018). However, upon mitochondrial impairment or depolarization of mitochondrial membrane potential, the lysis of PINK1 is inhibited, which causes the selective accumulation of PINK1 in OMM (Kondapalli et al., 2012). PINK1 can be activated by autophosphorylation and then phosphorylate Ub at Ser65. Phosphorylated Ub can bind and recruit Parkin from cytoplasm to OMM where PINK1 phosphorylates Parkin at Ser65 and activates its ubiquitin ligase activity (Schubert et al., 2017). Parkin can ubiquitylate a few outer mitochondrial membrane proteins, such as Mfn1, Mfn2, VDAC, MIRO1 (Chan et al., 2011). Ubiquitylated protein such as VDAC can be recognized by LC3 junction proteins in the cytoplasm, including SQSTM1/P62, OPTN, NDP52, TAX1BP1, and NBR1, can bind with this ubiquitinated protein and induce mitophagy by recognizing and binding to LC3 on the autophagy membrane (Lazarou et al., 2015). During this process, Ambra1 is thought to be an interaction protein of Parkin, and its main function is to stimulate cellular autophagy and mitochondrial clearance by motivating the formation of new phagophore (Fimia et al., 2007). Thus, Ambra1 plays the crucial role in cell autophagy and mitophagy.

Mechanisms of the Receptor-Mediated Pathway

The main feature of the mitophagy pathway is that it is receptor-mediated, via not only protein receptors, but also some lipid

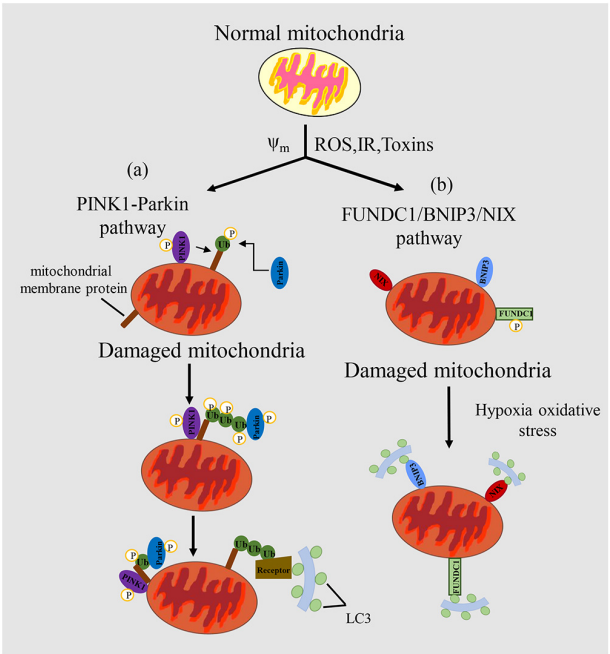

FIGURE 1 | Mechanism of mitophagy regulation in mammals. **(a)** In the PINK/PARKIN pathway, upon mitochondrial impairment or loss of mitochondrial potential, PINK1 can phosphorylate various target proteins, such as ubiquitin. Then, PINK1 recruits Parkin, and Parkin can amplify the signal through ubiquitination of miyochondrial surface receptor proteins. Receptor proteins can recognize the ubiquitinated proteins, which promotes mitochondria to form autophagosomes and eventually degrade them. **(b)** In the FUNDC1/BNIP3/NIX pathway, LC3 can be recognized by receptor proteins of mitochondria to promote the complementation of phagophores, thus targeting the mitochondrion for mitophagy. Mitochondrial outer membrane proteins FUNDC1, BNIP3 or NIX bind to LC3-II through their cytoplasmic LIR motifs to promote selective clearance of mitochondria. $\Delta\psi_m$, mitochondrial potential; ROS, reactive oxygen species; IR, ischemia/reperfusion; Toxins, poisons produced naturally by organisms.

molecules (Bingol et al., 2014). ATG32 (Kanki et al., 2009; Okamoto et al., 2009) in yeast and NIX (Novak et al., 2010), BNIP3 (Zhu et al., 2013), FUNDC1 (Liu et al., 2012), FKBP8 (Bhujabal et al., 2017), Bcl2L13 (Murakawa et al., 2015; Otsu et al., 2015), Ambra1 (Strappazzon et al., 2015), PHB2 (Wei et al., 2017), and NLRX1 (Zhang et al., 2019) in mammalian systems have been identified. The common characteristic of these receptor proteins is that they contain a conserved LC3-interacting receptor (LIR) domain, a key domain that binds directly to Atg8/LC3 and other proteins in the family.

Under the starvation conditions, mitophagy occurs in yeast cells. The occurrence may be related to the accumulation of mitochondrial oxidative damage (Farré et al., 2009). Yeast mitophagy is mainly mediated by Atg32, the first receptor that was found to mediate mitophagy (Kanki et al., 2009; Okamoto et al., 2009). Atg32 is a single transmembrane protein with the N-terminal and C-terminal exposed to cytoplasm and mitochondrial stroma respectively (Kondo-Okamoto et al., 2012). After mitochondrial damage, Protein kinase 2 can promote the phosphorylation of Atg32 in Ser114 and Ser119. Phosphorylated Atg32 forms a complex with Atg11, which is the first step of mitochondrial degradation (Hirota et al., 2012) and essential for the initiation of mitophagy in a pre-autophagosomal structure (PAS). Then Atg11 interacts with Atg8 which enables mitochondrial recognition by autophagy elements and recruitment into autophagy precursors. Atg32 can also directly interact with Atg8, to promote the engulfment of the mitochondria by the phagocytosis membrane. The interaction of Atg32 with Atg8 and Atg11 promotes the formation a mitophagy-initiating polymeric body (Kanki et al., 2011). Under nitrogen starvation conditions, the effect of Atg32-Atg11 is enhanced (Kanki et al., 2011). The knockout of Atg32 does not affect the non-selective autophagy, the cytosol-to-vacuole targeting (Cvt) pathway or the occurrence of peroxidase autophagy, but completely inhibits mitophagy. Atg11 is a binding protein in selective mitophagy that recognizes localized receptor proteins on autophagosomes. Atg8 is implicated in the expansion of phagocytic bubbles. LC3 is the Atg8 homologue in mammals, and is involved in the identification process between autophagosome membrane and target (Kabeya et al., 2000). When Atg32 is absent, cells grow normally and intracellular ROS levels remain unchanged when using non-fermentable carbon as a carbon source (Ashrafi and Schwarz, 2013), suggesting that there is another mitophagy pathway independent of Atg32.

BNIP3 and BNIP3L/NIX are both OMM proteins that can trigger mitophagy under hypoxia through binding of their LIR sequences with LC3. NIX-mediated mitophagy was firstly found in the maturation process of red blood cells (Sandoval et al., 2008). The dimerization of BNIP3 is necessary for its interaction with LC3 that is promoted by the phosphorylation of two serine sites (Ser17 and Ser24) in BNIP3 promotes the interaction with LC3. BNIP3 and Nix have different tissue specificity. Nix is mainly expressed in hematopoietic tissue (Diwan et al., 2007), while BNIP3 is widely distributed in heart, liver and muscle. BNIP3 is regulated by RB, NF-κβ, FOX03, Ras and p53, while p53 can also regulate Nix (Mammucari et al., 2007). Hypoxia activates hypoxia inducible factor 1α (HIF1α), which can increases the expression of BNIP3 (Subarsky and Hill, 2003). Additionally, BNIP3 knockout can up-regulate the expression of NIX, but this upregulation cannot make up for the decrease of mitochondrial autophagy caused by BNIP3 knockout (Shi et al., 2014). Hypoxia-induced mitophagy can also be mediated by the outer mitochondrial membrane (OMM) protein termed FUN14 domain-containing protein 1 (FUNDC1) (Liu et al., 2012). FUNDC1 induces mitophagy in a manner independent of the Parkinson's disease-associated E3 ubiquitin ligase Parkin and does so through the direct binding of its LIR motif to LC3. Phosphorylation or ubiquitin modification of FUNDC1 can affect mitophagy. PGAM5 and ULK1 catalyze de-phosphorylation and phosphorylation of FUNDC1 on Ser13 and Ser17 respectively, which transduces hypoxia signals and induces FUNDC1-mediated mitophagy (Chen et al., 2014). In addition, MARCH5 promotes the degradation of FUNDC1 by ubiquitin modification, and ultimately inhibits the occurrence of mitophagy (Chen Z. et al., 2017).

THE ROLES OF MITOPHAGY IN CANCER

Mitochondria play important roles in cellular metabolism. Mitophagy maintains mitochondrial homeostasis and normal physiological function, while abnormal mitophagy will cause multiple diseases, such as heart disease, neurodegenerative disease and muscle disease. However, the role of mitophagy in tumor development and progression needs further study. More and more studies have found that there are different levels of mitophagy in diverse cancers including liver cancer, rectal cancer, breast cancer, lung cancer, which reflects the close relationship between mitophagy and cancer (Chourasia et al., 2015a). The changes in the complex functions of mitochondria have important impacts on the growth and progression of cancer (Panigrahi et al., 2019). The roles of mitophagy in cancer are shown in **Figure 2**.

Mitophagy and Carcinogenesis

Dysfunction in mitophagy has a close connection with tumorigenesis and tumor development (Chang et al., 2017). The role of mitophagy differs in different stages of tumor development. In the early stage of tumorigenesis, mitophagy maintains normal cell metabolism and inhibits tumorigenesis, while in the later stage of tumor development, the occurrence of mitophagy improves cell tolerance and promotes the development of the tumor.

The loss, mutation or functional change in diverse pivotal genes results in the accumulation of damaged mitochondria and suppression of mitophagy, which eventually stimulates tumorigenesis (Panigrahi et al., 2019). PINK1/Parkin pathway is known as the key pathway of mitophagy (Youle and Narendra, 2011). The loss of function of Parkin can inhibit mitophagy and promote carcinogenesis in various cancer models. The inhibition of mitophagy further results in an upsurge of reactive oxygen species which influence on the function of cells, tissues, organs and even whole systems. An early study found that mice with Parkin knock-out are more susceptible to spontaneous development of hepatocellular carcinoma (HCC) than the mock mice (Fujiwara et al., 2008). Moreover, the result also showed that Parkin-deficient hepatocytes continue to proliferate and exert an antiapoptotic effect by upregulating endogenous follistatin, which eventually promotes cancer progress.

PARK2 gene which is located on human chromosome 6 (FRA6E, 6q26), encodes Parkin protein and is very sensitive to gene mutation (Burrell et al., 2013). Parkin mutations are often detected in various tumors such as lung cancer (D'Amico et al., 2015), glioma (Maugeri et al., 2015), and colon cancer (Poulogiannis et al., 2010). The appearance of mutated forms of PARK2 gene is distinct in different cancers (Bernardini et al., 2017). For example, PARK2 amplification is common in sarcomas and uterine cancers, but damaging mutations of PARK2 such as deletion or loss of function often occur in other tumors. It was reported that up-regulation of Parkin expression can inhibit cancer cell growth in hepatocarcinoma, colon cancer, breast cancer and glioblastoma (Wang et al., 2004; Poulogiannis et al., 2010; Tay et al., 2010; Veeriah et al., 2010), while

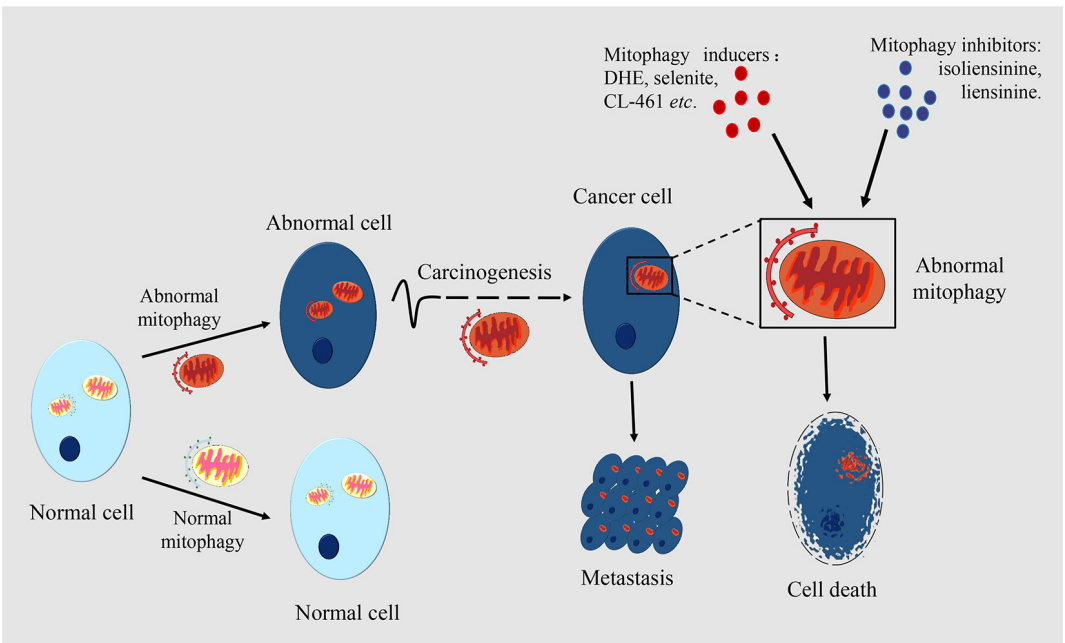

FIGURE 2 | The roles of mitophagy in cancer. Mitophagy occurs in many types of cell. Mitophagic levels are usually enhanced or inhibited in cancer cells, which is different from normal cells. Mitophagy is associated with the occurrence and metastasis of cancers. In certain periods of tumorigenesis, limited mitophagy promotes the development of the tumor, while in established tumors, mitophagy can help the survival of tumor cells. Mitophagy also plays an important role in cancer metastasis. By making mitophagy as the target, inducers or inhibitors of mitophagy can have an anticancer effect through regulating the level of mitophagy. Damaged mitochondria in cancer cells are rapidly cleared through mitophagy which mediates the drug resistance of cancer cells.

down-regulation of Parkin expression promotes cell proliferation and tumorigenesis in pancreatic cancer (Sun et al., 2013). When PARK2 knock-out mice were hybridized with colorectal cancer adenomatous polyposis mice, the development of intestinal adenoma in neonatal mice accelerated rapidly, and the diversity of polyps increased (Poulogiannis et al., 2010), indicating that PARK2 is a tumor suppressor gene.

Mitophagy has gradually become recognized as a critical adaptation in response to hypoxia. Just as cells can reduce the number of mitochondria and not only limit the production of reactive oxygen clusters, they can also maximize the use of available oxygen. Under hypoxic condition, BNIP3 and its ligand Nix are two main receptors in mitophagy. Like Parkin, Nix also can play an important role in tumorigenesis. Under hypoxia conditions, HIF-1 induces up-regulation of Nix and BNIP3 expression in tumor tissues (Sowter et al., 2001). Nix is highly expressed in hypoxic tumor cells, and Nix-mediated mitophagy promotes glioblastoma survival. The silencing of Nix impairs the clearance of ROS, cancer stem cell maintenance, and inhibits the survival of tumor cells (Jung et al., 2019). Oncogenic KRAS induces NIX-mediated mitophagy, and promotes pancreatic carcinogenesis, but the loss of NIX leads to the restoration of mitochondrial function, which significantly delays pancreatic cancer progression (Humpton et al., 2019). However, another report showed that up-regulated expression of NIX induced by p53 under hypoxia promotes tumor cells apoptosis, while knockout of Nix gene accelerates tumor growth (Fei et al., 2004).

Another mitophagy-related protein FUNDC1 also plays a vital role in carcinogenesis. In early-stage cervical cancer patients, it was found that FUNDC1 has a higher expression level than adjacent normal cells (Hou et al., 2017). Moreover, the deletion of FUNDC1 in tumor cells obviously inhibited cell proliferation, triggered cell apoptosis and increased the sensibility of tumor cell to chemo-radiotherapy such as cisplatin and ionizing radiation. FUNDC1 accumulates in most human HCC. In hepatocytes, FUNDC1 knock-out promotes the initiation and development of diethylnitrosamine (DEN)-induced primary HCC; in contrast when FUNDC1 is transferred into hepatocytes it inhibits hepatocarcinogenesis (Li et al., 2019). In this context, specific deletion of FUNDC1 in hepatocytes leads to the accumulation of dysfunctional mitochondria, and further stimulates a series of events including the activation of inflammasome and JAK/STAT signaling. This suggests that mitophagy can inhibit the occurrence and development of HCC by inhibiting the activation of inflammatory bodies.

Mitophagy and Cancer Metastasis

During cancer progression, some cancer cells convert the aerobic respiration of mitochondria into glycolysis to maintain cancer cell's energy needs. This is called the Warburg effect (Bensinger and Christofk, 2012). Cancer cells are typically characterized by a Warburg effect, abnormal quality control of mitochondria, production of ROS, regulation of cell redox state, and lack of apoptosis signals (Panigrahi et al., 2019). By eliminating dysfunctional mitochondria, mitophagy can promote tumor cell survival as an adaptation to stress. In the process of mitophagy, Parkin increases the level of oxidative metabolism and inhibits the Warburg effect downstream of the p53 tumor suppressor, which is likely to be achieved by enhancing the integrity of mitochondrion (Zhang et al., 2011). Thus, as a p53 target gene, Parkin may exhibit tumor suppressive activity. Another study further confirmed that in breast cancer, Parkin inhibited tumor migration and invasion through targeting HIF-1α for ubiquitination and degradation (Deng et al., 2017). When the Parkin gene was transferred into breast cancer cells with a deleted Parkin gene the progression of breast cancer and the rate of metastasis were significantly decreased. Notably, there is also emerging evidence that Parkin may promote cancer metastasis. Compared with normal dermatic tissues, pathological analysis showed that the expression of Parkin and cancer metastasis was obviously enhanced in melanoma (Lee et al., 2018). Further results indicated that the loss of Parkin inhibited tumor formation and metastasis of melanoma by suppressing Mfn2 ubiquitination (Lee et al., 2018). The cause of the opposite result for Parkin's role in cancer metastasis could be due to different mechanisms for metastasis in several tumor types.

BNIP3 as a pro-apoptotic protein, can inhibit the fusion of damaged mitochondria and enhance mitophagy (Gustafsson, 2011). However, the role of BNIP3 in cancer metastasis is varied in different cancers. It is frequently found that the high expression of BNIP3 that occurs in many kinds of malignancies, such as salivary gland adenoid cystic carcinoma (Chen et al., 2015), endometrial cancer (Giatromanolaki et al., 2008), DCIS of breast and cervical cancer (Leo et al., 2006) is associated with the aggressiveness of the tumor and poor prognosis. The loss of BNIP3 makes mitophagy proceed abnormally and increases mitochondrial ROS levels, which is related with tumor metastasis in TNBC (Chourasia et al., 2015b). In DCIS, the expression of BNIP3 and Nix are increased, while BNIP3 is not expressed in invasive carcinoma, which is related to tumor cell proliferation index and lymph node metastasis (Sowter et al., 2003). It is also suggested that the higher expression of BNIP3 mediates excessive mitophagy, which inhibits HCC metastasis (Shi et al., 2018). As a small GTPase, Rheb can not only interact with BNIP3 and NIX, but also effectively acts on the upstream region of mTOR pathway to promote cell growth (Li et al., 2007). The inhibition of BNIP3 by Rheb under the interaction of Rheb and BNIP3 decreases the activity of mTOR signal, and suppresses cell growth, which corresponds to the role of BNIP3 in tumor inhibition (Ray et al., 2000).

However, similarly to PINK1/PARKIN, BNIP3 can not only serve as a tumor suppressor, but can also exert oncogenic activity. The epigenetic silencing of BNIP3 could enhance the aggressiveness and metastasis of pancreatic cancer cells, and contribute to resistance to hypoxia-induced cell death in pancreatic cancer (Okami et al., 2004). Besides, up-regulation of BNIP3 has also been reported to accelerate cancer cell migration and invasion (Maes et al., 2014; Wu H. et al., 2015). The dual roles of BNIP3 in cancer progress and metastasis could be due to different interact with different factors through its Bcl-2 homology 3 (BH3) domain, also to the heterogeneity of different tumors.

Mitophagy and Cancer Therapy

It is clear that mitophagy is beneficial in maintaining normal healthy physiological processes. Mitophagy shares common regulatory pathways with carcinogenesis and cancer cell death which converge at mitochondria (Lu et al., 2013). Thus, it provides therapeutic targets for removing cancer cells and inducing cancer cell apoptosis; therapies can aim at the crosstalk signals between the processes of mitophagy and cancer progression. Concurrently, mitochondria have a function on cell apoptosis and the ability to inhibit apoptosis and resist cell death is one of the well-established hallmarks of cancer (Hanahan and Weinberg, 2011), which implies the potential for mitochondria-mediated apoptosis in cancer therapy.

In a similar way to macroautophagy, mitophagy also plays dual roles in cancer therapy, including the induction of cell death and promotion of cell survival (Panigrahi et al., 2019). Generally, chemotherapy induces mitochondrial dysfunction and oxidative stress to generate the cytotoxic effects on cancer cells which result in the generation of mitophagy (Cao et al., 2019). Excessive mitophagy causes the loss of functional mitochondria, and further destruction of cellular energy requirement, leading to a form of cancer cell death called mitophagic cell death. However, another role of mitophagy in cancer is that of improving the cell internal environment by clearing abnormal mitochondria, which can result in better fitness in the aggressive environments (Araki et al., 2019).

Some compounds that activate mitophagy are gradually being identified as chemotherapeutic drugs. Dihydroergotamine tartrate (DHE) is a common drug for migraine. A study has reported that DHE induces lung cancer cell death by mitophagy and mitochondria-dependent cell apoptosis (Chang et al., 2016). Mechanistically, DHE could induce PINK1/PARKIN activation, ROS production and cell apoptosis, and reduce membrane permeability and destroy ATP synthesis, finally activating mitophagic cell death. This suggests that DHE might be a promising anticancer medicine for lung cancer. More recently, Zhu et al. (2020) reported a novel anticancer strategy based on excessive mitophagy. They used a novel nanomicelle that targets mitochondria to selectively damage mitochondria in tumor cells, thereby further activating excessive mitophagy pathway-driven lethal energy depletion and phototherapy. An *in vivo* study showed that CerS1/C18 pyridinium ceramide efficiently induces lethal mitophagy and abrogates growth of tumor xenograft in various solid cancers (Sentelle et al., 2012). In glioma cells, a novel BH3-mimetic AT101 (Meyer et al., 2018) and sodium selenite (Kim et al., 2007) induced an excessive mitophagic cell death that suggests lethal mitophagy as the tumor-suppressor mechanism. Similarly, LCL-461, a mitochondria-targeted ceramide analog, could also kill crenolanib-resistant acute myeloid leukemia (AML) cells through lethal mitophagy (Dany et al., 2016). However, other studies revealed that some compounds that inhibit mitophagy exert antitumor effects in breast cancer. Liensinine, a new inhibitor of autophagy and/or mitophagy, could enhance the sensitivity of breast cancer cells to chemotherapy via mitochondrial fission mediated by DNM1L (Zhou et al., 2015). Isoliensinine could induce cell apoptosis in TNBC by the production of ROS and the activation of p38 MAPK/JNK and improve anti-breast cancer effects by inhibiting mitophagy (Zhang et al., 2015).

In addition to the use of mitophagy-associated compounds, the most prominent approach for mitophagy-mediated cell death is by targeting regulation of mitophagy associated proteins by a selective reduction in mitochondrial compartments (Zhou et al., 2015; Panigrahi et al., 2019). Several mitophagy-related proteins PINK1, Parkin, BNIP3, CDKN2A, PUMA, ULK1, and TR3 could induce mitochondrial damage and activate mitophagy, and ultimately lead to cell death. Activated TR3 receptor could result in irreversible mitophagic cell death and excessive clearance of mitochondria in the melanoma cells to TR3-specific compounds (Wang et al., 2014). Mitochondria-targeting drugs (Mito-CP and Mito-Metformin) trigger mitophagy and inhibit the proliferation of colon cancer cell through an AMPK-mTOR-ULK1-dependent pathway (Boyle et al., 2018). Moreover, lethal mitophagy also happens through activation of ceramide stress in human cancer cells (Sentelle et al., 2012), and PUMA-mediated mitophagy by Abrus agglutinin promotes cell apoptosis by the generation of C18 ceramide or the overexpression of CerS1 (Panda et al., 2018).

Inhibition of the tumor promotion role of mitophagy is another promising strategy for cancer therapy. Many studies reported that mitophagy-associated molecules PINK1, Parkin, BNIP3, FUNDC1 promote tumor development, and provide targets for therapeutic inhibition in multiple cancers (Tan et al., 2007; D'Amico et al., 2015; Liu et al., 2018; Hui et al., 2019). For example, the silencing of PINK1 can not only inhibit the proliferation and migration of lung cancer cells, but can also induce cell apoptosis (Liu et al., 2018). Furthermore, high expression of PINK1 in ESCC patients receiving neoadjuvant therapy is related to low chemotherapy effects and poor prognosis (Yamashita et al., 2017). PINK1-mediated excessive mitophagy promotes survival of cancer cells resistant to chemotherapy, implying that suppression of mitophagy can restore the chemo-sensitivity of ESCC cells (Yamashita et al., 2017). Moreover, overexpression of FUNDC1 promotes growth of cervical cancer cells, and inhibition of expression enhances the sensitivity to cisplatin treatment and ionizing radiation (Hou et al., 2017). This shows that the regulation of mitophagy-associated molecules could affect the outcome of cancer therapy.

Mitophagy and Drug Resistance

Tumor resistance raises complex questions involving multiple steps and factors. Recent study has shown that both the efficacy of tumor chemotherapy and the degree of drug resistance are influenced by mitophagy, probably because cancer cells rapidly sweep away damaged mitochondria through mitophagy to mediate their own drug resistance (Yamashita et al., 2017). Consistent with this, the toxicity of most chemotherapeutics is at least partly due to the induction of mitochondrial dysfunction and oxidative stress (Hockenbery, 2010).

The common chemotherapeutic drugs such as cisplatin, paclitaxel, doxorubicin (Dox) and 5-fluorouracil (5-FU) can kill cancer cells in early treatment of multiple solid cancers. However, the occurrence of drug resistance often leads to treatment failure due to autophagy or mitophagy (Oun et al., 2018). For

instance, activation of autophagy triggered by overexpression of galectin-1 leads to chemotherapy resistance of epithelial ovarian cancer to cisplatin (Chen L. et al., 2017) and a similar result has been observed in liver cancer (Su et al., 2016). In addition, hypoxia-induced mitophagy accounts for lung cancer cells resisting cisplatin in an HIF1α- and HIF2α-dependent manner (Wu H. et al., 2015). Notably, an E3 ubiquitin ligase ARIH1 highly expressed in cancer cells could trigger mitophagy in a PINK1-dependent and Parkin-defective way; this countered the chemotherapy-induced cell death in breast cancer and lung adenocarcinomas, eventually resulting in cancer cell resistance (Villa et al., 2017).

However, the desired anticancer results can be achieved through regulation of autophagy or mitophagy. On one hand, suppression of autophagy by *Atg* gene knockdown could activate the BNIP3-mediated cancer cell death pathway after treatment with cisplatin (Wu H. et al., 2015). Similarly, enhanced sensitivity of multidrug-resistant cancer cells to betulinic acid analog B5G1 that was induced by the inhibition of PINK1-Parkin dependent mitophagy resulted in liver cancer cell death (Yao et al., 2019). On the other hand, inducement of mitophagy could improve drug sensitivity of cancer cells. A recent study found that mitophagy-dependent necrosis and ferroptosis can be induced through the suppression of mitochondrial respiratory chain by BAY 87-2243 in melanoma cells (Basit et al., 2017). In addition, through DNM1L-mediated mitochondrial fusion, mitophagy can enhance the sensitivity of breast cancer cells to liensinine (Zhou et al., 2015). These results implicate mitophagy in drug resistance call for further exploration in different cancers.

CSCs are usually resistant to chemotherapy. Interestingly, mitophagy participates in CSCs-mediated drug resistance. In OSCC, the $CD44^{+}$/$ABCB1^{+}$/$ADAM17^{+}$cells behave with the characteristics of CSCs and exhibit chemo-resistance through the modulation of mitophagy (Naik et al., 2018). BNIP3/NIX-mediated mitophagy contributes to the dox-resistance to CSCs in colorectal cancer and the silencing of BNIP3L both prevents mitophagy and increases the sensitivity to doxorubicin therapy (Yan et al., 2017), which suggests the importance of mitophagy in drug resistance for cancer therapy targeting CSCs.

Furthermore, drug resistance regulated by mitophagy also restricts the efficiency of radiotherapy. A recent study has shown that mitophagy induced by p53/BNIP3 exerts an important effect on the viability of HNSCC cancer cells following radiotherapy by maintaining the integrity of mitochondrial (Chang et al., 2019). BNIP3-dependent mitophagy in the radio-resistant cancer cells relies on wild type p53 status to limit glycolytic remodeling, highlighting the potential use of drugs targeting glycolysis as an alternative strategy for overcoming radio-resistant cancers.

CONCLUSION AND PERSPECTIVE

Mitophagy appears to be a pivotal cellular event that disposes of dysfunctional mitochondria by autophagic degradation. Although significant advances have been made in delineating mitophagy regulation and the role of mitophagy in carcinogenesis and cancer therapeutics, it is still an intractable problem to understand how mitophagy acts either as a suppressor or an inducer in cancer therapy. Moreover, the homeostasis and regulation of mitochondrial dynamics and mitophagy retain a complexity that requires more exploration. For example, what is the relationship of mitochondrial dysfunction to the maintenance of CSCs self-renewal in tumor progression? What are the molecular crosstalks and interactions between mitophagy and key oncogenic signaling pathways? Can the regulation of mitophagy can be beneficial to molecular targeting in cancer therapy, for example with checkpoint inhibitors (anti-PD-1, PD-L1, and CTLA4), oncolytic virotherapy, molecular immunotherapy? How might we adjust cancer cell mitophagy behavior in relation to specific oncometabolites in various cellular stresses, including hypoxia, nutrient deficiency, and elevated ROS level? How might we best exploit the targeting therapy strategies based on mitochondria and mitophagy by enhancing drug uptake into cancer cells? How does mitophagy further orchestrate the crosstalk that constitutes the metabolic regulation system of cancer cells, which is the key step for maintaining the balance between glycolysis and OXPHOS? In consideration of such questions, further studies will undoubtedly focus on the exploration of the molecular mechanisms of mitophagy in cancer events, the identification of novel mitophagic modulators and the development of promising mitophagy-based cancer treatments.

AUTHOR CONTRIBUTIONS

YW, Y-TC, H-HL, and L-LZ performed the literature searches and wrote the manuscript. FH received a grant for this project, conceived the idea, and reviewed the drafts. YW contributed to the conceptual idea and supervised the writing process. CY gave suggestions and significantly refined the manuscript.

FUNDING

This work was supported by the Zhejiang Provincial Natural Science Foundation (No. LY18C070002), the National Natural Science Foundation of China (No. 81803069), Zhejiang Medical and Health Science and Technology project (No. 2019337459) and the Grant for 521 talent project of ZSTU to YW, and National Natural Science Foundation of China (Nos. 91754107 and 31771528) to CY.

REFERENCES

Abeliovich, H., Zarei, M., Rigbolt, K. T. G., Youle, R. J., and Dengjel, J. (2013). Involvement of mitochondrial dynamics in the segregation of mitochondrial matrix proteins during stationary phase mitophagy. *Nat. Commun.* 4:2789. doi: 10.1038/ncomms3789

Araki, K., Kawauchi, K., Sugimoto, W., Tsuda, D., Oda, H., Yoshida, R., et al. (2019). Mitochondrial protein E2F3d, a distinctive E2F3 product, mediates

hypoxia-induced mitophagy in cancer cells. *Commun. Biol.* 2:3. doi: 10.1038/s42003-018-0246-9

Ashrafi, G., and Schwarz, T. L. (2013). The pathways of mitophagy for quality control and clearance of mitochondria. *Cell Death Differ.* 20, 31–42. doi: 10.1038/cdd.2012.81

Basit, F., Van Oppen, L. M., Schöckel, L., Bossenbroek, H. M., Van Emst-De Vries, S. E., Hermeling, J. C., et al. (2017). Mitochondrial complex I inhibition triggers a mitophagy-dependent ROS increase leading to necroptosis and ferroptosis in melanoma cells. *Cell Death Dis.* 8:e2716. doi: 10.1038/cddis.2017.133

Bensinger, S. J., and Christofk, H. R. (2012). New aspects of the Warburg effect in cancer cell biology. *Semin. Cell Dev. Biol.* 23, 352–361. doi: 10.1016/j.semcdb.2012.02.003

Bernardini, J. P., Lazarou, M., and Dewson, G. (2017). Parkin and mitophagy in cancer. *Oncogene* 36, 1315–1327. doi: 10.1038/onc.2016.302

Bhujabal, Z., Birgisdottir, ÅB., Sjøttem, E., Brenne, H. B., Øvervatn, A., Habisov, S., et al. (2017). FKBP8 recruits LC3A to mediate Parkin-independent mitophagy. *EMBO Rep.* 18, 947–961. doi: 10.15252/embr.201643147

Bingol, B., Tea, J. S., Phu, L., Reichelt, M., Bakalarski, C. E., Song, Q., et al. (2014). The mitochondrial deubiquitinase USP30 opposes parkin-mediated mitophagy. *Nature* 510, 370–375. doi: 10.1038/nature13418

Boyle, K. A., Van Wickle, J., Hill, R. B., Marchese, A., Kalyanaraman, B., and Dwinell, M. B. (2018). Mitochondria-targeted drugs stimulate mitophagy and abrogate colon cancer cell proliferation. *J. Biol. Chem.* 293, 14891–14904. doi: 10.1074/jbc.RA117.001469

Burrell, R. A., Mcclelland, S. E., Endesfelder, D., Groth, P., Weller, M.-C., Shaikh, N., et al. (2013). Replication stress links structural and numerical cancer chromosomal instability. *Nature* 494, 492–496. doi: 10.1038/nature11935

Cao, S., Shen, Z., Wang, C., Zhang, Q., Hong, Q., He, Y., et al. (2019). Resveratrol improves intestinal barrier function, alleviates mitochondrial dysfunction and induces mitophagy in diquat challenged piglets. *Food Funct.* 10, 344–354. doi: 10.1039/c8fo02091d

Cao, Y.-L., Meng, S., Chen, Y., Feng, J.-X., Gu, D.-D., Yu, B., et al. (2017). MFN1 structures reveal nucleotide-triggered dimerization critical for mitochondrial fusion. *Nature* 542, 372–376. doi: 10.1038/nature21077

Cassidy-Stone, A., Chipuk, J. E., Ingerman, E., Song, C., Yoo, C., Kuwana, T., et al. (2008). Chemical inhibition of the mitochondrial division dynamin reveals its role in Bax/Bak-dependent mitochondrial outer membrane permeabilization. *Dev. Cell* 14, 193–204. doi: 10.1016/j.devcel.2007.11.019

Chan, D. C. (2006). Mitochondrial fusion and fission in mammals. *Annu. Rev. Cell Dev. Biol.* 22, 79–99. doi: 10.1146/annurev.cellbio.22.010305.104638

Chan, D. C. (2012). Fusion and fission: interlinked processes critical for mitochondrial health. *Annu. Rev. Genet.* 46, 265–287. doi: 10.1146/annurev-genet-110410-132529

Chan, D. C. (2020). Mitochondrial dynamics and its involvement in disease. *Annu. Rev. Pathol.* 15, 235–259. doi: 10.1146/annurev-pathmechdis-012419-032711

Chan, N. C., Salazar, A. M., Pham, A. H., Sweredoski, M. J., Kolawa, N. J., Graham, R. L. J., et al. (2011). Broad activation of the ubiquitin-proteasome system by Parkin is critical for mitophagy. *Hum. Mol. Genet.* 20, 1726–1737. doi: 10.1093/hmg/ddr048

Chang, C.-R., and Blackstone, C. (2010). Dynamic regulation of mitochondrial fission through modification of the dynamin-related protein Drp1. *Ann. N. Y. Acad. Sci.* 1201, 34–39. doi: 10.1111/j.1749-6632.2010.05629.x

Chang, H. W., Kim, M. R., Lee, H. J., Lee, H. M., Kim, G. C., Lee, Y. S., et al. (2019). p53/BNIP3-dependent mitophagy limits glycolytic shift in radioresistant cancer. *Oncogene* 38, 3729–3742. doi: 10.1038/s41388-019-0697-6

Chang, J. Y., Yi, H.-S., Kim, H.-W., and Shong, M. (2017). Dysregulation of mitophagy in carcinogenesis and tumor progression. *Biochim. Biophys. Acta. Bioenerg.* 1858, 633–640. doi: 10.1016/j.bbabio.2016.12.008

Chang, S.-H., Lee, A. Y., Yu, K.-N., Park, J., Kim, K. P., and Cho, M.-H. (2016). Dihydroergotamine tartrate induces lung cancer cell death through apoptosis and mitophagy. *Chemotherapy* 61, 304–312. doi: 10.1159/000445044

Chen, D. S., and Mellman, I. (2017). Elements of cancer immunity and the cancer-immune set point. *Nature* 541, 321–330. doi: 10.1038/nature21349

Chen, G., Han, Z., Feng, D., Chen, Y., Chen, L., Wu, H., et al. (2014). A regulatory signaling loop comprising the PGAM5 phosphatase and CK2 controls receptor-mediated mitophagy. *Mol. Cell* 54, 362–377. doi: 10.1016/j.molcel.2014.02.034

Chen, L., Yao, Y., Sun, L., and Tang, J. (2017). Galectin-1 promotes tumor progression via NF-κB signaling pathway in epithelial ovarian cancer. *J. Cancer* 8, 3733–3741. doi: 10.7150/jca.20814

Chen, Z., Liu, L., Cheng, Q., Li, Y., Wu, H., Zhang, W., et al. (2017). Mitochondrial E3 ligase MARCH5 regulates FUNDC1 to fine-tune hypoxic mitophagy. *EMBO Rep.* 18, 495–509. doi: 10.15252/embr.201643309

Chen, Z., Wu, H., Huang, S., Li, W., Zhang, S., Zheng, P., et al. (2015). Expression of BNIP3 and its correlations to hypoxia-induced autophagy and clinicopathological features in salivary adenoid cystic carcinoma. *Cancer Biomark.* 15, 467–475. doi: 10.3233/CBM-150474

Chourasia, A. H., Boland, M. L., and Macleod, K. F. (2015a). Mitophagy and cancer. *Cancer Metab.* 3:4. doi: 10.1186/s40170-015-0130-8

Chourasia, A. H., Tracy, K., Frankenberger, C., Boland, M. L., Sharifi, M. N., Drake, L. E., et al. (2015b). Mitophagy defects arising from BNip3 loss promote mammary tumor progression to metastasis. *EMBO Rep.* 16, 1145–1163. doi: 10.15252/embr.201540759

Chowdhury, S. R., Ray, U., Chatterjee, B. P., and Roy, S. S. (2017). Targeted apoptosis in ovarian cancer cells through mitochondrial dysfunction in response to *Sambucus nigra* agglutinin. *Cell Death Dis.* 8:e2762. doi: 10.1038/cddis.2017.77

Cipolat, S., Martins De Brito, O., Dal Zilio, B., and Scorrano, L. (2004). OPA1 requires mitofusin 1 to promote mitochondrial fusion. *Proc. Natl. Acad. Sci. U.S.A.* 101, 15927–15932. doi: 10.1073/pnas.0407043101

D'Amico, A. G., Maugeri, G., Magro, G., Salvatorelli, L., Drago, F., and D'agata, V. (2015). Expression pattern of parkin isoforms in lung adenocarcinomas. *Tumour Biol.* 36, 5133–5141. doi: 10.1007/s13277-015-3166-z

Dany, M., Gencer, S., Nganga, R., Thomas, R. J., Oleinik, N., Baron, K. D., et al. (2016). Targeting FLT3-ITD signaling mediates ceramide-dependent mitophagy and attenuates drug resistance in AML. *Blood* 128, 1944–1958. doi: 10.1182/blood-2016-04-708750

Deng, Y., Wu, W., Guo, S., Chen, Y., Liu, C., Gao, X., et al. (2017). Altered mTOR and Beclin-1 mediated autophagic activation during right ventricular remodeling in monocrotaline-induced pulmonary hypertension. *Respir Res.* 18:53. doi: 10.1186/s12931-017-0536-7

Diwan, A., Koesters, A. G., Odley, A. M., Pushkaran, S., Baines, C. P., Spike, B. T., et al. (2007). Unrestrained erythroblast development in Nix-/- mice reveals a mechanism for apoptotic modulation of erythropoiesis. *Proc. Natl. Acad. Sci. U.S.A.* 104, 6794–6799. doi: 10.1073/pnas.0610666104

Farrand, L., Kim, J. Y., Im-Aram, A., Suh, J.-Y., Lee, H. J., and Tsang, B. K. (2013). An improved quantitative approach for the assessment of mitochondrial fragmentation in chemoresistant ovarian cancer cells. *PLoS One* 8:e74008. doi: 10.1371/journal.pone.0074008

Farré, J.-C., Krick, R., Subramani, S., and Thumm, M. (2009). Turnover of organelles by autophagy in yeast. *Curr. Opin. Cell Biol.* 21, 522–530. doi: 10.1016/j.ceb.2009.04.015

Fei, P., Wang, W., Kim, S.-H., Wang, S., Burns, T. F., Sax, J. K., et al. (2004). Bnip3L is induced by p53 under hypoxia, and its knockdown promotes tumor growth. *Cancer Cell* 6, 597–609. doi: 10.1016/j.ccr.2004.10.012

Fimia, G. M., Stoykova, A., Romagnoli, A., Giunta, L., Di Bartolomeo, S., Nardacci, R., et al. (2007). Ambra1 regulates autophagy and development of the nervous system. *Nature* 447, 1121–1125. doi: 10.1038/nature05925

Fujiwara, M., Marusawa, H., Wang, H. Q., Iwai, A., Ikeuchi, K., Imai, Y., et al. (2008). Parkin as a tumor suppressor gene for hepatocellular carcinoma. *Oncogene* 27, 6002–6011. doi: 10.1038/onc.2008.199

Giampazolias, E., and Tait, S. W. G. (2016). Mitochondria and the hallmarks of cancer. *FEBS J.* 283, 803–814. doi: 10.1111/febs.13603

Giatromanolaki, A., Koukourakis, M. I., Gatter, K. C., Harris, A. L., and Sivridis, E. (2008). BNIP3 expression in endometrial cancer relates to active hypoxia inducible factor 1alpha pathway and prognosis. *J. Clin. Pathol.* 61, 217–220. doi: 10.1136/jcp.2007.046680

Guo, J. Y., Karsli-Uzunbas, G., Mathew, R., Aisner, S. C., Kamphorst, J. J., Strohecker, A. M., et al. (2013). Autophagy suppresses progression of K-ras-induced lung tumors to oncocytomas and maintains lipid homeostasis. *Genes Dev.* 27, 1447–1461. doi: 10.1101/gad.219642.113

Gustafsson, A. B. (2011). Bnip3 as a dual regulator of mitochondrial turnover and cell death in the myocardium. *Pediatr. Cardiol.* 32, 267–274. doi: 10.1007/s00246-010-9876-5

Hanahan, D., and Weinberg, R. A. (2011). Hallmarks of cancer: the next generation. *Cell* 144, 646–674.

Hirota, Y., Kang, D., and Kanki, T. (2012). The physiological role of mitophagy: new insights into phosphorylation events. *Int. J. Cell Biol.* 2012:354914. doi: 10.1155/2012/354914

Hockenbery, D. M. (2010). Targeting mitochondria for cancer therapy. *Environ. Mol. Mutagen.* 51, 476–489. doi: 10.1002/em.20552

Hou, H., Er, P., Cheng, J., Chen, X., Ding, X., Wang, Y., et al. (2017). High expression of FUNDC1 predicts poor prognostic outcomes and is a promising target to improve chemoradiotherapy effects in patients with cervical cancer. *Cancer Med.* 6, 1871–1881. doi: 10.1002/cam4.1112

Huang, Q., Cao, H., Zhan, L., Sun, X., Wang, G., Li, J., et al. (2017). Mitochondrial fission forms a positive feedback loop with cytosolic calcium signaling pathway to promote autophagy in hepatocellular carcinoma cells. *Cancer Lett.* 403, 108–118. doi: 10.1016/j.canlet.2017.05.034

Hui, L., Wu, H., Wang, T. W., Yang, N., Guo, X., and Jang, X. J. (2019). Hydrogen peroxide-induced mitophagy contributes to laryngeal cancer cells survival via the upregulation of FUNDC1. *Clin. Transl. Oncol.* 21, 596–606. doi: 10.1007/s12094-018-1958-5

Humpton, T. J., Alagesan, B., Denicola, G. M., Lu, D., Yordanov, G. N., Leonhardt, C. S., et al. (2019). Oncogenic KRAS induces NIX-mediated mitophagy to promote pancreatic cancer. *Cancer Discov.* 9, 1268–1287. doi: 10.1158/2159-8290.CD-18-1409

Ingerman, E., Perkins, E. M., Marino, M., Mears, J. A., Mccaffery, J. M., Hinshaw, J. E., et al. (2005). Dnm1 forms spirals that are structurally tailored to fit mitochondria. *J. Cell Biol.* 170, 1021–1027. doi: 10.1083/jcb.200506078

Ji, W.-K., Hatch, A. L., Merrill, R. A., Strack, S., and Higgs, H. N. (2015). Actin filaments target the oligomeric maturation of the dynamin GTPase Drp1 to mitochondrial fission sites. *eLife* 4:e11553. doi: 10.7554/eLife.11553

Jung, J., Zhang, Y., Celiku, O., Zhang, W., Song, H., Williams, B. J., et al. (2019). Mitochondrial NIX promotes tumor survival in the hypoxic niche of glioblastoma. *Cancer Res.* 79, 5218–5232. doi: 10.1158/0008-5472.CAN-19-0198

Kabeya, Y., Mizushima, N., Ueno, T., Yamamoto, A., Kirisako, T., Noda, T., et al. (2000). LC3, a mammalian homologue of yeast Apg8p, is localized in autophagosome membranes after processing. *EMBO J.* 19, 5720–5728. doi: 10.1093/emboj/19.21.5720

Kanki, T., Klionsky, D. J., and Okamoto, K. (2011). Mitochondria autophagy in yeast. *Antioxid. Redox Signal.* 14, 1989–2001.

Kanki, T., Wang, K., Cao, Y., Baba, M., and Klionsky, D. J. (2009). Atg32 is a mitochondrial protein that confers selectivity during mitophagy. *Dev. Cell* 17, 98–109. doi: 10.1016/j.devcel.2009.06.014

Kim, E. H., Sohn, S., Kwon, H. J., Kim, S. U., Kim, M.-J., Lee, S.-J., et al. (2007). Sodium selenite induces superoxide-mediated mitochondrial damage and subsequent autophagic cell death in malignant glioma cells. *Cancer Res.* 67, 6314–6324. doi: 10.1158/0008-5472.CAN-06-4217

Kitada, T., Asakawa, S., Hattori, N., Matsumine, H., Yamamura, Y., Minoshima, S., et al. (1998). Mutations in the parkin gene cause autosomal recessive juvenile parkinsonism. *Nature* 392, 605–608. doi: 10.1038/33416

Kondapalli, C., Kazlauskaite, A., Zhang, N., Woodroof, H. I., Campbell, D. G., Gourlay, R., et al. (2012). PINK1 is activated by mitochondrial membrane potential depolarization and stimulates Parkin E3 ligase activity by phosphorylating Serine 65. *Open Biol.* 2:120080. doi: 10.1098/rsob.120080

Kondo-Okamoto, N., Noda, N. N., Suzuki, S. W., Nakatogawa, H., Takahashi, I., Matsunami, M., et al. (2012). Autophagy-related protein 32 acts as autophagic degron and directly initiates mitophagy. *J. Biol. Chem.* 287, 10631–10638. doi: 10.1074/jbc.M111.299917

Lazarou, M., Sliter, D. A., Kane, L. A., Sarraf, S. A., Wang, C., Burman, J. L., et al. (2015). The ubiquitin kinase PINK1 recruits autophagy receptors to induce mitophagy. *Nature* 524, 309–314. doi: 10.1038/nature14893

Lee, Y. S., Jung, Y. Y., Park, M. H., Yeo, I. J., Im, H. S., Nam, K. T., et al. (2018). Deficiency of parkin suppresses melanoma tumor development and metastasis through inhibition of MFN2 ubiquitination. *Cancer Lett.* 433, 156–164. doi: 10.1016/j.canlet.2018.07.007

Leo, C., Horn, L. C., and Höckel, M. (2006). Hypoxia and expression of the proapoptotic regulator BNIP3 in cervical cancer. *Int. J. Gynecol. Cancer* 16, 1314–1320. doi: 10.1111/j.1525-1438.2006.00394.x

Li, W., Li, Y., Siraj, S., Jin, H., Fan, Y., Yang, X., et al. (2019). FUN14 domain-containing 1-mediated mitophagy suppresses hepatocarcinogenesis by inhibition of inflammasome activation in mice. *Hepatology (Baltimore, Md.)* 69, 604–621. doi: 10.1002/hep.30191

Li, Y., Wang, Y., Kim, E., Beemiller, P., Wang, C.-Y., Swanson, J., et al. (2007). Bnip3 mediates the hypoxia-induced inhibition on mammalian target of rapamycin by interacting with Rheb. *J. Biol. Chem.* 282, 35803–35813. doi: 10.1074/jbc.M705231200

Liu, L., Feng, D., Chen, G., Chen, M., Zheng, Q., Song, P., et al. (2012). Mitochondrial outer-membrane protein FUNDC1 mediates hypoxia-induced mitophagy in mammalian cells. *Nat. Cell Biol.* 14, 177–185. doi: 10.1038/ncb2422

Liu, L., Zuo, Z., Lu, S., Wang, L., Liu, A., and Liu, X. (2018). Silencing of PINK1 represses cell growth, migration and induces apoptosis of lung cancer cells. *Biomed. Pharmacother.* 106, 333–341. doi: 10.1016/j.biopha.2018.06.128

Losón, O. C., Song, Z., Chen, H., and Chan, D. C. (2013). Fis1, Mff, MiD49, and MiD51 mediate Drp1 recruitment in mitochondrial fission. *Mol. Biol. Cell* 24, 659–667. doi: 10.1091/mbc.E12-10-0721

Lu, H., Li, G., Liu, L., Feng, L., Wang, X., and Jin, H. (2013). Regulation and function of mitophagy in development and cancer. *Autophagy* 9, 1720–1736. doi: 10.4161/auto.26550

Maes, H., Van Eygen, S., Krysko, D. V., Vandenabeele, P., Nys, K., Rillaerts, K., et al. (2014). BNIP3 supports melanoma cell migration and vasculogenic mimicry by orchestrating the actin cytoskeleton. *Cell Death Dis.* 5:e1127. doi: 10.1038/cddis.2014.94

Mammucari, C., Milan, G., Romanello, V., Masiero, E., Rudolf, R., Del Piccolo, P., et al. (2007). FoxO3 controls autophagy in skeletal muscle in vivo. *Cell Metab.* 6, 458–471. doi: 10.1016/j.cmet.2007.11.001

Maugeri, G., D'amico, A. G., Magro, G., Salvatorelli, L., Barbagallo, G. M. V., Saccone, S., et al. (2015). Expression profile of parkin isoforms in human gliomas. *Int. J. Oncol.* 47, 1282–1292. doi: 10.3892/ijo.2015.3105

Meyer, N., Zielke, S., Michaelis, J. B., Linder, B., Warnsmann, V., Rakel, S., et al. (2018). AT 101 induces early mitochondrial dysfunction and HMOX1 (heme oxygenase 1) to trigger mitophagic cell death in glioma cells. *Autophagy* 14, 1693–1709. doi: 10.1080/15548627.2018.1476812

Mishra, P., and Chan, D. C. (2016). Metabolic regulation of mitochondrial dynamics. *J. Cell Biol.* 212, 379–387. doi: 10.1083/jcb.201511036

Murakawa, T., Yamaguchi, O., Hashimoto, A., Hikoso, S., Takeda, T., Oka, T., et al. (2015). Bcl-2-like protein 13 is a mammalian Atg32 homologue that mediates mitophagy and mitochondrial fragmentation. *Nat. Commun.* 6:7527. doi: 10.1038/ncomms8527

Naik, P. P., Mukhopadhyay, S., Panda, P. K., Sinha, N., Das, C. K., Mishra, R., et al. (2018). Autophagy regulates cisplatin-induced stemness and chemoresistance via the upregulation of CD44, ABCB1 and ADAM17 in oral squamous cell carcinoma. *Cell Prolif.* 51:e12411. doi: 10.1111/cpr.12411

Ni, H.-M., Williams, J. A., and Ding, W.-X. (2015). Mitochondrial dynamics and mitochondrial quality control. *Redox Biol.* 4, 6–13. doi: 10.1016/j.redox.2014.11.006

Novak, I., Kirkin, V., Mcewan, D. G., Zhang, J., Wild, P., Rozenknop, A., et al. (2010). Nix is a selective autophagy receptor for mitochondrial clearance. *EMBO Rep.* 11, 45–51. doi: 10.1038/embor.2009.256

Okami, J., Simeone, D. M., and Logsdon, C. D. (2004). Silencing of the hypoxia-inducible cell death protein BNIP3 in pancreatic cancer. *Cancer Res.* 64, 5338–5346. doi: 10.1158/0008-5472.CAN-04-0089

Okamoto, K., Kondo-Okamoto, N., and Ohsumi, Y. (2009). Mitochondria-anchored receptor Atg32 mediates degradation of mitochondria via selective autophagy. *Dev. Cell* 17, 87–97. doi: 10.1016/j.devcel.2009.06.013

Otsu, K., Murakawa, T., and Yamaguchi, O. (2015). BCL2L13 is a mammalian homolog of the yeast mitophagy receptor Atg32. *Autophagy* 11, 1932–1933. doi: 10.1080/15548627.2015.1084459

Oun, R., Moussa, Y. E., and Wheate, N. J. (2018). The side effects of platinum-based chemotherapy drugs: a review for chemists. *Dalton Trans.* 47, 6645–6653. doi: 10.1039/c8dt90088d

Panda, P. K., Naik, P. P., Meher, B. R., Das, D. N., Mukhopadhyay, S., Praharaj, P. P., et al. (2018). PUMA dependent mitophagy by *Abrus agglutinin* contributes to apoptosis through ceramide generation. *Biochim. Biophys. Acta. Mol. Cell Res.* 1865, 480–495. doi: 10.1016/j.bbamcr.2017.12.002

Panigrahi, D. P., Praharaj, P. P., Bhol, C. S., Mahapatra, K. K., Patra, S., Behera, B. P., et al. (2019). The emerging, multifaceted role of mitophagy in cancer and cancer therapeutics. *Semin. Cancer Biol.* doi: 10.1016/j.semcancer.2019.07.015 [Epub ahead of print].

Pernas, L., and Scorrano, L. (2016). Mito-morphosis: mitochondrial fusion, fission, and cristae remodeling as key mediators of cellular function. *Annu. Rev. Phys.* 78, 505–531. doi: 10.1146/annurev-physiol-021115-105011

Porporato, P. E., Filigheddu, N., Pedro, J. M. B.-S., Kroemer, G., and Galluzzi, L. (2018). Mitochondrial metabolism and cancer. *Cell Res.* 28, 265–280. doi: 10.1038/cr.2017.155

Poulogiannis, G., Mcintyre, R. E., Dimitriadi, M., Apps, J. R., Wilson, C. H., Ichimura, K., et al. (2010). PARK2 deletions occur frequently in sporadic colorectal cancer and accelerate adenoma development in Apc mutant mice. *Proc. Natl. Acad. Sci. U.S.A.* 107, 15145–15150. doi: 10.1073/pnas.1009941107

Rao, S., Tortola, L., Perlot, T., Wirnsberger, G., Novatchkova, M., Nitsch, R., et al. (2014). A dual role for autophagy in a murine model of lung cancer. *Nat. Commun.* 5:3056. doi: 10.1038/ncomms4056

Ray, R., Chen, G., Vande Velde, C., Cizeau, J., Park, J. H., Reed, J. C., et al. (2000). BNIP3 heterodimerizes with Bcl-2/Bcl-X(L) and induces cell death independent of a Bcl-2 homology 3 (BH3) domain at both mitochondrial and nonmitochondrial sites. *J. Biol. Chem.* 275, 1439–1448. doi: 10.1074/jbc.275.2.1439

Rehman, J., Zhang, H. J., Toth, P. T., Zhang, Y., Marsboom, G., Hong, Z., et al. (2012). Inhibition of mitochondrial fission prevents cell cycle progression in lung cancer. *FASEB J.* 26, 2175–2186. doi: 10.1096/fj.11-196543

Rosenfeldt, M. T., O'prey, J., Morton, J. P., Nixon, C., Mackay, G., Mrowinska, A., et al. (2013). p53 status determines the role of autophagy in pancreatic tumour development. *Nature* 504, 296–300. doi: 10.1038/nature12865

Sandoval, H., Thiagarajan, P., Dasgupta, S. K., Schumacher, A., Prchal, J. T., Chen, M., et al. (2008). Essential role for Nix in autophagic maturation of erythroid cells. *Nature* 454, 232–235. doi: 10.1038/nature07006

Schubert, A. F., Gladkova, C., Pardon, E., Wagstaff, J. L., Freund, S. M. V., Steyaert, J., et al. (2017). Structure of PINK1 in complex with its substrate ubiquitin. *Nature* 552, 51–56. doi: 10.1038/nature24645

Sekine, S., and Youle, R. J. (2018). PINK1 import regulation; a fine system to convey mitochondrial stress to the cytosol. *BMC Biol.* 16:2. doi: 10.1186/s12915-017-0470-7

Senft, D., and Ronai, Z. E. A. (2016). Regulators of mitochondrial dynamics in cancer. *Curr. Opin. Cell Biol.* 39, 43–52. doi: 10.1016/j.ceb.2016.02.001

Sentelle, R. D., Senkal, C. E., Jiang, W., Ponnusamy, S., Gencer, S., Selvam, S. P., et al. (2012). Ceramide targets autophagosomes to mitochondria and induces lethal mitophagy. *Nat. Chem. Biol.* 8, 831–838. doi: 10.4161/auto.22739

Shi, C., Cai, Y., Li, Y., Li, Y., Hu, N., Ma, S., et al. (2018). Yap promotes hepatocellular carcinoma metastasis and mobilization via governing cofilin/F-actin/lamellipodium axis by regulation of JNK/Bnip3/SERCA/CaMKII pathways. *Redox Biol.* 14, 59–71. doi: 10.1016/j.redox.2017.08.013

Shi, R.-Y., Zhu, S.-H., Li, V., Gibson, S. B., Xu, X.-S., and Kong, J.-M. (2014). BNIP3 interacting with LC3 triggers excessive mitophagy in delayed neuronal death in stroke. *CNS Neurosci. Ther.* 20, 1045–1055. doi: 10.1111/cns.12325

Sowter, H. M., Ferguson, M., Pym, C., Watson, P., Fox, S. B., Han, C., et al. (2003). Expression of the cell death genes BNip3 and NIX in ductal carcinoma in situ of the breast; correlation of BNip3 levels with necrosis and grade. *J. Pathol.* 201, 573–580. doi: 10.1002/path.1486

Sowter, H. M., Ratcliffe, P. J., Watson, P., Greenberg, A. H., and Harris, A. L. (2001). HIF-1-dependent regulation of hypoxic induction of the cell death factors BNIP3 and NIX in human tumors. *Cancer Res.* 61, 6669–6673.

Strappazzon, F., Nazio, F., Corrado, M., Cianfanelli, V., Romagnoli, A., Fimia, G. M., et al. (2015). AMBRA1 is able to induce mitophagy via LC3 binding, regardless of PARKIN and p62/SQSTM1. *Cell Death Differ.* 22, 419–432. doi: 10.1038/cdd.2014.139

Su, Y.-C., Davuluri, G. V. N., Chen, C.-H., Shiau, D.-C., Chen, C.-C., Chen, C.-L., et al. (2016). Galectin-1-induced autophagy facilitates cisplatin resistance of hepatocellular carcinoma. *PLoS One* 11:e0148408. doi: 10.1371/journal.pone.0148408

Subarsky, P., and Hill, R. P. (2003). The hypoxic tumour microenvironment and metastatic progression. *Clin. Exp. Metastasis* 20, 237–250. doi: 10.1023/a:1022939318102

Sun, X., Liu, M., Hao, J., Li, D., Luo, Y., Wang, X., et al. (2013). Parkin deficiency contributes to pancreatic tumorigenesis by inducing spindle multipolarity and misorientation. *Cell Cycle* 12, 1133–1141. doi: 10.4161/cc.24215

Taguchi, N., Ishihara, N., Jofuku, A., Oka, T., and Mihara, K. (2007). Mitotic phosphorylation of dynamin-related GTPase Drp1 participates in mitochondrial fission. *J. Biol. Chem.* 282, 11521–11529. doi: 10.1074/jbc.M607279200

Tan, E. Y., Campo, L., Han, C., Turley, H., Pezzella, F., Gatter, K. C., et al. (2007). BNIP3 as a progression marker in primary human breast cancer; opposing functions in in situ versus invasive cancer. *Clin. Cancer Res.* 13, 467–474. doi: 10.1158/1078-0432.CCR-06-1466

Tay, S.-P., Yeo, C. W. S., Chai, C., Chua, P.-J., Tan, H.-M., Ang, A. X. Y., et al. (2010). Parkin enhances the expression of cyclin-dependent kinase 6 and negatively regulates the proliferation of breast cancer cells. *J. Biol. Chem.* 285, 29231–29238. doi: 10.1074/jbc.M110.108241

Tilokani, L., Nagashima, S., Paupe, V., and Prudent, J. (2018). Mitochondrial dynamics: overview of molecular mechanisms. *Essays Biochem.* 62, 341–360. doi: 10.1042/EBC20170104

Vásquez-Trincado, C., García-Carvajal, I., Pennanen, C., Parra, V., Hill, J. A., Rothermel, B. A., et al. (2016). Mitochondrial dynamics, mitophagy and cardiovascular disease. *J. Physiol.* 594, 509–525. doi: 10.1113/JP271301

Veeriah, S., Taylor, B. S., Meng, S., Fang, F., Yilmaz, E., Vivanco, I., et al. (2010). Somatic mutations of the Parkinson's disease-associated gene PARK2 in glioblastoma and other human malignancies. *Nat. Genet.* 42, 77–82. doi: 10.1038/ng.491

Villa, E., Proïcs, E., Rubio-Patiño, C., Obba, S., Zunino, B., Bossowski, J. P., et al. (2017). Parkin-independent mitophagy controls chemotherapeutic response in cancer cells. *Cell Rep.* 20, 2846–2859. doi: 10.1016/j.celrep.2017.08.087

Vyas, S., Zaganjor, E., and Haigis, M. C. (2016). Mitochondria and Cancer. *Cell* 166, 555–566. doi: 10.1016/j.cell.2016.07.002

Wai, T., and Langer, T. (2016). Mitochondrial Dynamics and Metabolic Regulation. *Trends Endocrinol. Metab.* 27, 105–117. doi: 10.1016/j.tem.2015.12.001

Wallace, D. C. (2012). Mitochondria and cancer. *Nat. Rev. Cancer* 12, 685–698. doi: 10.1038/nrc3365

Wan, Y.-Y., Zhang, J.-F., Yang, Z.-J., Jiang, L.-P., Wei, Y.-F., Lai, Q.-N., et al. (2014). Involvement of Drp1 in hypoxia-induced migration of human glioblastoma U251 cells. *Oncol. Rep.* 32, 619–626. doi: 10.3892/or.2014.3235

Wang, F., Denison, S., Lai, J.-P., Philips, L. A., Montoya, D., Kock, N., et al. (2004). Parkin gene alterations in hepatocellular carcinoma. *Genes Chromosomes Cancer* 40, 85–96. doi: 10.1002/gcc.20020

Wang, J., Li, J., Santana-Santos, L., Shuda, M., Sobol, R. W., Van Houten, B., et al. (2015). A novel strategy for targeted killing of tumor cells: induction of multipolar acentrosomal mitotic spindles with a quinazolinone derivative mdivi-1. *Mol. Oncol.* 9, 488–502. doi: 10.1016/j.molonc.2014.10.002

Wang, W.-J., Wang, Y., Chen, H.-Z., Xing, Y.-Z., Li, F.-W., Zhang, Q., et al. (2014). Orphan nuclear receptor TR3 acts in autophagic cell death via mitochondrial signaling pathway. *Nat. Chem. Biol.* 10, 133–140. doi: 10.1038/nchembio.1406

Wei, Y., Chiang, W.-C., Sumpter, R., Mishra, P., and Levine, B. (2017). Prohibitin 2 is an inner mitochondrial membrane mitophagy receptor. *Cell* 168, 224–238.e10. doi: 10.1016/j.cell.2016.11.042

Wu, H., Huang, S., Chen, Z., Liu, W., Zhou, X., and Zhang, D. (2015). Hypoxia-induced autophagy contributes to the invasion of salivary adenoid cystic carcinoma through the HIF-1α/BNIP3 signaling pathway. *Mol. Med. Rep.* 12, 6467–6474. doi: 10.3892/mmr.2015.4255

Wu, H.-M., Jiang, Z.-F., Ding, P.-S., Shao, L.-J., and Liu, R.-Y. (2015). Hypoxia-induced autophagy mediates cisplatin resistance in lung cancer cells. *Sci. Rep.* 5:12291. doi: 10.1038/srep12291

Xie, Q., Wu, Q., Horbinski, C. M., Flavahan, W. A., Yang, K., Zhou, W., et al. (2015). Mitochondrial control by DRP1 in brain tumor initiating cells. *Nature Neurosci.* 18, 501–510. doi: 10.1038/nn.3960

Yamashita, K., Miyata, H., Makino, T., Masuike, Y., Furukawa, H., Tanaka, K., et al. (2017). High expression of the mitophagy-related protein pink1 is associated with a poor response to chemotherapy and a poor prognosis for patients treated with neoadjuvant chemotherapy for esophageal squamous cell carcinoma. *Ann. Surg. Oncol.* 24, 4025–4032. doi: 10.1245/s10434-017-6096-8

Yan, C., Luo, L., Guo, C.-Y., Goto, S., Urata, Y., Shao, J.-H., et al. (2017). Doxorubicin-induced mitophagy contributes to drug resistance in cancer stem

cells from HCT8 human colorectal cancer cells. *Cancer Lett.* 388, 34–42. doi: 10.1016/j.canlet.2016.11.018

Yang, Z., Feng, Z., Gu, J., Li, X., Dong, Q., Liu, K., et al. (2017). microRNA-488 inhibits chemoresistance of ovarian cancer cells by targeting Six1 and mitochondrial function. *Oncotarget* 8, 80981–80993. doi: 10.18632/oncotarget.20941

Yao, N., Wang, C., Hu, N., Li, Y., Liu, M., Lei, Y., et al. (2019). Inhibition of PINK1/Parkin-dependent mitophagy sensitizes multidrug-resistant cancer cells to B5G1, a new betulinic acid analog. *Cell Death Dis.* 10:232. doi: 10.1038/s41419-019-1470-z

Youle, R. J., and Narendra, D. P. (2011). Mechanisms of mitophagy. *Nat. Rev. Mol. Cell Biol.* 12, 9–14. doi: 10.1038/nrm3028

Zhang, C., Lin, M., Wu, R., Wang, X., Yang, B., Levine, A. J., et al. (2011). Parkin, a p53 target gene, mediates the role of p53 in glucose metabolism and the Warburg effect. *Proc. Natl. Acad. Sci. U.S.A.* 108, 16259–16264. doi: 10.1073/pnas.1113884108

Zhang, X., Wang, X., Wu, T., Li, B., Liu, T., Wang, R., et al. (2015). Isoliensinine induces apoptosis in triple-negative human breast cancer cells through ROS generation and p38 MAPK/JNK activation. *Sci. Rep.* 5:12579. doi: 10.1038/srep12579

Zhang, Y., Yao, Y., Qiu, X., Wang, G., Hu, Z., Chen, S., et al. (2019). Listeria hijacks host mitophagy through a novel mitophagy receptor to evade killing. *Nat. Immunol.* 20, 433–446. doi: 10.1038/s41590-019-0324-2

Zhao, J., Zhang, J., Yu, M., Xie, Y., Huang, Y., Wolff, D. W., et al. (2013). Mitochondrial dynamics regulates migration and invasion of breast cancer cells. *Oncogene* 32, 4814–4824. doi: 10.1038/onc.2012.494

Zhou, J., Li, G., Zheng, Y., Shen, H.-M., Hu, X., Ming, Q.-L., et al. (2015). A novel autophagy/mitophagy inhibitor liensinine sensitizes breast cancer cells to chemotherapy through DNM1L-mediated mitochondrial fission. *Autophagy* 11, 1259–1279. doi: 10.1080/15548627.2015.1056970

Zhu, Y., Massen, S., Terenzio, M., Lang, V., Chen-Lindner, S., Eils, R., et al. (2013). Modulation of serines 17 and 24 in the LC3-interacting region of Bnip3 determines pro-survival mitophagy versus apoptosis. *J. Biol. Chem.* 288, 1099–1113. doi: 10.1074/jbc.M112.399345

Zhu, Y.-X., Jia, H.-R., Gao, G., Pan, G.-Y., Jiang, Y.-W., Li, P., et al. (2020). Mitochondria-acting nanomicelles for destruction of cancer cells via excessive mitophagy/autophagy-driven lethal energy depletion and phototherapy. *Biomaterials* 232:119668. doi: 10.1016/j.biomaterials.2019.119668

Conflict of Interest: The authors declare that the research was conducted in the absence of any commercial or financial relationships that could be construed as a potential conflict of interest.

frontiers in Cell and Developmental Biology

REVIEW
published: 18 June 2020
doi: 10.3389/fcell.2020.00428

Endoplasmic Reticulum–Mitochondria Contact Sites and Neurodegeneration

*Lingna Xu[1,2], Xi Wang[1,2] and Chao Tong[1,2]**

[1] *Ministry of Education Key Laboratory of Biosystems Homeostasis and Protection and Innovation Center for Cell Signaling Network, Life Sciences Institute, Zhejiang University, Hangzhou, Zhejiang, China,* [2] *The Second Affiliated Hospital, School of Medicine, Zhejiang University, Hangzhou, Zhejiang, China*

Endoplasmic reticulum–mitochondria contact sites (ERMCSs) are dynamic contact regions with a distance of 10–30 nm between the endoplasmic reticulum and mitochondria. Endoplasmic reticulum–mitochondria contact sites regulate various biological processes, including lipid transfer, calcium homeostasis, autophagy, and mitochondrial dynamics. The dysfunction of ERMCS is closely associated with various neurodegenerative diseases, including Parkinson's disease, Alzheimer's disease, and amyotrophic lateral sclerosis. In this review, we will summarize the current knowledge of the components and organization of ERMCSs, the methods for monitoring ERMCSs, and the physiological functions of ERMCSs in different model systems. Additionally, we will emphasize the current understanding of the malfunction of ERMCSs and their potential roles in neurodegenerative diseases.

Keywords: endoplasmic reticulum, mitochdonrion, contact sites, neurodegeneration, autophagy

OPEN ACCESS

Edited by:
Laura Lackner,
Northwestern University,
United States

Reviewed by:
Guangpu Li,
The University of Oklahoma Health Sciences Center, United States
Fengguang Guo,
Texas A&M University, United States

****Correspondence:***
Chao Tong
ctong@zju.edu.cn

Specialty section:
This article was submitted to Membrane Traffic, a section of the journal Frontiers in Cell and Developmental Biology

Received: *14 February 2020*
Accepted: *07 May 2020*
Published: *18 June 2020*

Citation:
Xu L, Wang X and Tong C (2020) Endoplasmic Reticulum–Mitochondria Contact Sites and Neurodegeneration. Front. Cell Dev. Biol. 8:428. doi: 10.3389/fcell.2020.00428

INTRODUCTION

Endoplasmic reticulum (ER) forms interconnected networks of membrane tubules and sacs that play a major role in the synthesis, modification, and transport of proteins and lipids in the eukaryotic cells (Schwarz and Blower, 2016). Mitochondrion serves as a powerhouse and metabolic center for the production of ATP and precursors of macromolecules, such as proteins, lipids, DNA, and RNA (Devine and Kittler, 2018). The contact sites between ER and mitochondria are not only critical for the communications between these two important organelles but also serve as a platform to regulate other cellular events (Cohen et al., 2018). Since the early 1970s, ER–mitochondria contact sites (ERMCSs) have been observed through ultrastructural electron microscopy. The subcellular fractionation studies also indicated a close association between the membranes of ER and mitochondria. Although ERMCSs are conserved structures in all eukaryotic cells, the tethering molecules are diverse across species. Recent studies have developed many methods to monitor ERMCS and identified multiple tethering complexes that mediate ERMCS formation. Previous studies have extensively investigated the functions of ERMCS at the cellular levels. Several diseases, including neurogenerative disorders, are associated with abnormal ERMCSs (Paillusson et al., 2016). Since there are many high-quality reviews published recently, we will briefly give an

introduction to the organization and functions of ERMCSs in this review (Phillips and Voeltz, 2016; Lackner, 2019; Moltedo et al., 2019).

THE ORGANIZATION OF ERMCSs

In the last few decades, several pairs of protein complexes have been identified that bridge the ER and mitochondria. The mitochondria and ER membrane components mediate the formation of ERMCSs with the help of some cytosolic proteins to promote the exchange of cellular components and signals between the ER and mitochondria (**Figure 1**).

The Tethering Molecules in Yeast

ER–mitochondria encounter structure (ERMCS), a protein complex in yeast, was reported to mediate the contacts between ER and mitochondria. The mitochondrial outer membrane proteins (Mdm10 and Mdm34), cytosolic protein (Mdm12), and integral ER protein (Mmm1) mediate the tethering between mitochondria and ER to form ERMES. Gem1, the yeast ortholog of Miro, is enriched in the contact sites and regulates ERMES (Kornmann et al., 2011). Additionally, the ER membrane protein complex (EMC) interacts with the mitochondrial translocase of outer membrane (TOM) complex to tether ER to the mitochondria (Lahiri et al., 2014). In contrast to ERMES, EMC is conserved in higher organisms. The role of mammalian EMC in tethering ER to the mitochondria is not known. Ltc1/Lam6 is also reported to regulate the contact between the ER and mitochondria in yeast (Elbaz-Alon et al., 2015; Murley et al., 2015). Ltc1/Lam6 is conserved among the mammalian cells. However, the role of mammalian orthologs of Ltc1/Lam6 in ERMCSs is not known.

The Tethering Molecules in Mammals

Mitofusin 2

In mammals, several tether molecules are reported to mediate the formation of ERMCSs. Mitofusin 2 (MFN2) is a dynamin-like GTPase that is located not only on the mitochondrial outer membrane but also is enriched in the interface between ER and mitochondria. MFN2 can form a homotypic dimer and a heterotypic dimer with its paralog MFN1, which plays a major role in the mitochondrial outer membrane fusion. In 2008, MFN2 was reported to tether ER to the mitochondria and to regulate mitochondrial calcium uptake from ER. *Mfn2* ablation in the mouse embryonic fibroblasts (MEFs) and HeLa cells increases the distance between ER and mitochondria and decreases the calcium transfer from ER to the mitochondria (De Brito and Scorrano, 2008). Several groups have reported new components that regulate ER–mitochondrial tethering via MFN2 (Cerqua et al., 2010; Sugiura et al., 2013; Daniele et al., 2014; Morales et al., 2014). However, later studies have challenged the role of MFN2 in mediating the formation of ERMCS. The loss of *Mfn2* does not decrease the formation of ERMCS but increases both ERMCS formation and calcium trafficking between the ER and mitochondria (Cosson et al., 2012; Filadi et al., 2016; Leal et al., 2016). This indicated that MFN2 serves as an antagonist to ERMCS formation. Further studies are needed to elucidate the role of MFN2 in tethering ER to the mitochondria.

VAPB and PTPIP51

Vesicle-associated membrane protein (VAMP)-associated proteins (VAPs) are integral ER membrane proteins that contain an N-terminal major sperm protein (MSP) domain, a central coiled-coil region, and a C-terminal transmembrane domain. The vertebrates have two VAPs (VAPA and VAPB). Mutations in VAPB cause rare forms of spinal muscular atrophy (SMA) and amyotrophic lateral sclerosis 8 (ALS8) in patients. VAPs play an important role in membrane trafficking, lipid transfer and metabolism, unfolded protein response (UPR), and autophagy (Kaiser et al., 2005; Lev et al., 2008; Zhao et al., 2018). VAPs interact with various proteins containing the FFAT-motif, which comprises consensus EFFDAXE amino acid sequence and serves as a versatile access point for the ER (Murphy and Levine, 2016). Several FFAT-motif-containing proteins mediate the contact between ER and other organelles. Protein tyrosine phosphatase-interacting protein-51 (PTPIP51) is a mitochondrial outer membrane protein containing an FFAT-motif that binds to VAPB (De Vos et al., 2012). Overexpression of either VAPB or PTPIP51 increases the ERMCS formation and calcium transfer from ER to mitochondria. The RNA interference (RNAi)-mediated silencing of VAPB or PTPIP51 or overexpression of ALS mutant form of VAPB (VAPBP56S) decreases the ERMCS formation and disturbs the calcium exchange between these two organelles (Stoica et al., 2014). TDP-43 and FUS are two proteins that are pathologically linked to ALS and frontotemporal dementia (FTD). TDP-34 and FUS modulate the interaction between VAPB and PTPIP51 via the activation of GSK-3β protein kinase and therefore perturbs ERMCS (Stoica et al., 2014; Stoica et al., 2016). The Parkinson's disease (PD)-related protein, α-synuclein, binds to VAPB and disrupts the interaction between VAPB and PTPIP51, which leads to the loss of contact between ER and mitochondria (Paillusson et al., 2017).

B-Cell Receptor-Associated Protein 31 and Its Binding Partners

B-cell receptor-associated protein 31 (Bap31) is an integral ER membrane protein containing an N-terminal membrane-bound region with three predicted transmembrane helices and a cytosolic C-terminal domain with one or two predicted coiled coils (Iwasawa et al., 2011). During apoptosis, the mitochondrial fission protein, fission 1 homolog (Fis1) interacts with Bap31 to bridge the ER and mitochondria and promotes the caspase-8-mediated cleavage of Bap31 into the pro-apoptotic p20Bap31 (Chandra et al., 2004). The ablation of phosphofurin acidic cluster sorting protein 2 (PACS-2), a multifunctional ER-associated vesicular sorting protein, leads to Bap31-dependent mitochondrial fragmentation and uncoupling of the ER from the mitochondria (Simmen et al., 2005). However, further studies are needed to confirm whether PACS-2 functions as a component of the Fis1–Bap31 complex or as a regulator of Fis1–Bap31 interaction.

Bap31 also interacts with Bcl-2, which is localized in the mitochondria. The interaction between Bap31 and Bcl-2 is

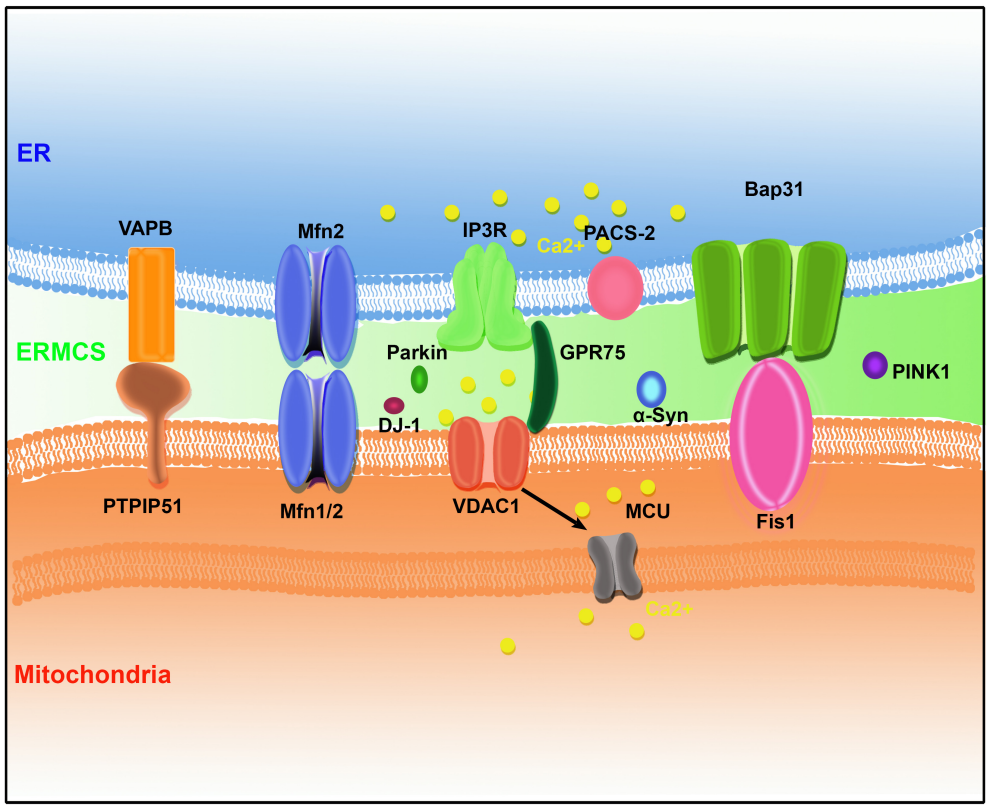

FIGURE 1 | The protein organization at ER–mitochondria contact sites (ERMCSs) in mammalian systems. Several pairs of proteins located on mitochondria and ER surface to form tethers, including vesicle-associated membrane protein (VAMP)-associated protein (VAP) B (VAPB)–protein tyrosine phosphatase-interacting protein-51 (PTPIP51), Mfn1/2, inositol 1,4,5-trisphosphate receptor (IP3R)–glucose-regulated protein 75 (GPR75)–voltage-dependent anion channel (VDAC1) complex, and B-cell receptor-associated protein 31 (Bap31) (Bap31)–fission 1 homolog (Fis1). Neurodegenerative disease-related proteins such as α-synuclein (α-Syn), DJ-1, PINK1, and Parkin were concentrated at ERMCSs.

facilitated by the interaction between CDIP1 and Bap31 in the ER during ER-stress (Namba et al., 2013).

A recent study reported that Bap31 could also form an ER–mitochondrial bridging complex by interacting with translocase of the outer mitochondrial membrane 40 (Tom40). The Bap31–Tom40 complex facilitates nuclear-encoded mitochondrial protein translocation and mitochondrial homeostasis (Namba, 2019).

VDAC1–Grp75–IP3R

The voltage-dependent anion channel (VDAC), which is located at the mitochondrial outer membrane, is a key component that mediates calcium transport to the mitochondria (Rapizzi et al., 2002). Voltage-dependent anion channel physically interacts with inositol 1,4,5-trisphosphate receptor (IP3R), the ER calcium release channel, through the molecular chaperone glucose-regulated protein 75 (Grp75). These tripartite complexes colocalize on the mitochondrial-associated membranes (MAMs) and directly enhance the mitochondrial calcium uptake (Szabadkai et al., 2006). This suggested that the VDAC1–Grp75–IP3R complex may serve as an ER–mitochondria tether. The silencing of Grp75 abolishes the mitochondrial calcium uptake. Transglutaminase type 2 (TG2) interacts with Grp75 in the MAMs. Disrupting the TG2–Grp75 interaction decreases the number of ER–mitochondria contact sites (D'eletto et al., 2018). Sigma-1 receptor (Sig-1R) binds to IP3R at MAM to regulate ER–mitochondrial interorganellar calcium signaling (Hayashi and Su, 2007). Other modulators, such as mitochondrial calcium uniporter (MCU; Xu et al., 2018) and etoposide-induced protein 2.4 (EI24; Yuan et al., 2019), were also reported to regulate the VDAC1–Grp75–IP3R scaffolds. However, IP3R ablation does not affect ER–mitochondria contacts, which indicates that VDAC1–Grp75–IP3R scaffold is not involved in physical tethering (Csordas et al., 2006).

THE FUNCTIONS OF ERMCSs

Endoplasmic reticulum–mitochondria contact sites regulate a variety of biological processes, including calcium homeostasis, lipid transfer, autophagy, and mitochondrial dynamics (**Figure 2**).

Regulation of Mitochondrial Dynamics

Mitochondria are highly dynamic organelles that undergo fusion and fission to maintain their healthy state. Interestingly, the

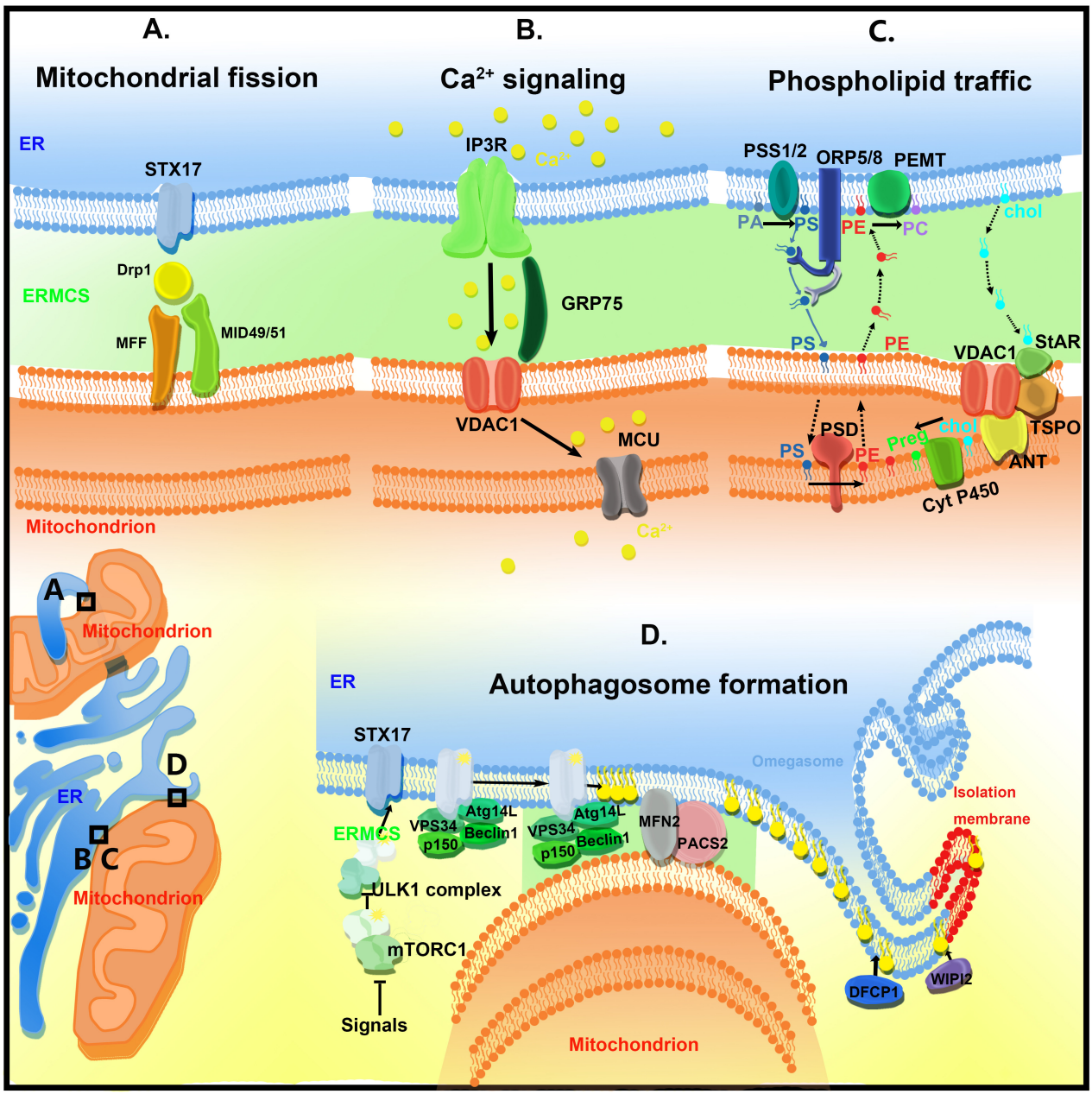

FIGURE 2 | The functions of ER–mitochondria contact sites (ERMCSs). The typical ERMCSs are illustrated at the bottom left corner. The boxed regions are enlarged to show the detailed cellular events and molecular organizations. **(A)** Mitochondria fission occurs at the ERMCSs. ER-located protein Syntaxin 17 (STX17) presents at ERMCS and mediates mitochondrial division by determining the localization and activity of Drp1. **(B)** The VDAC1–Grp75–IP3R tripartite complex serves as the major platform that coordinates calcium transfer between ER and mitochondria. Mitochondrial inner membrane located mitochondrial calcium uniporter (MCU) takes up the calcium transported from VDAC1. **(C)** The ERMCSs form the platform for phospholipid traffic between ER and mitochondria. **(D)** The pre-autophagosome/autophagosome proteins re-localize to the ERMCS to promote the initiation of autophagosome formation.

ER tubules define the position of mitochondrial fission sites (Friedman et al., 2011). In both yeast and mammalian cells, mitochondrial division initially occurs at the ER-mitochondrial contact sites, and the ER–mitochondrial contacts are formed before the recruitment of fission machinery proteins, such as Drp1 and Mff (Friedman et al., 2011). Inverted formin 2 (INF2), an ER-located protein, regulates actin polymerization and drives the mitochondrial constriction and division in the mammalian cells (Korobova et al., 2013). Syntaxin 17 is located on the tubular, smooth ER membranes. Syntaxin 17 is involved in the ER–Golgi intracellular trafficking and autophagy. Recently, Syntaxin 17 was reported to be present at the ER–mitochondrial contact sites and to mediate mitochondrial division by determining the localization and activity of Drp1

(Arasaki et al., 2015). Sept2, a subset of proteins localized to the mitochondrial constrictions, was reported to physically bind to Drp1 and to mediate Drp1-dependent mitochondrial division in the mammalian cells (Pagliuso et al., 2016). The contact sites not only mark the mitochondrial fission sites but also mark the replication sites of mtDNA (Lewis et al., 2016). The mtDNA is localized in the matrix. Thus, it would be interesting to determine the communication between ERMCS and mtDNA replication machinery in the mitochondrial matrix. The results of high-resolution microscopy imaging analysis indicated that some mitochondrial fusion events also occur at the ERMCSs (Guo et al., 2018). However, the molecular mechanisms underlying this process are still elusive.

Calcium Transfer

ER lumen is the major calcium store in the mammalian cells. The ER calcium level is determined by sarco-ER Ca^{2+} transport ATPases (SERCAs), intraluminal calcium-binding proteins, such as calreticulin, calnexin (CNX), and BiP/GRP78. SERCA2b is a ubiquitously expressed isoform of SERCAs that is critical for ER calcium uptake. Calnexin and thioredoxin-related transmembrane protein 1 (TMX1) regulate SERCA2b activity. Calnexin is enriched at the ER luminal side of the ERMCSs through palmitoylation and interaction with PACS-2. Transmembrane protein 1 belongs to the family of protein disulfide isomerases. Transmembrane protein 1 has a single transmembrane domain and is palmitoylated at the cytosolic stretch, which is required for its targeting to the ERMCS (Lynes et al., 2012). Transmembrane protein 1 inhibits the activity of SERCA2b, which can be antagonized by CNX, the positive regulator of SERCA2b. The loss of TMX1 increases the ER calcium store.

Upon stimulation, calcium is released to the cytosol through IP3R on the ER membrane. The external signals stimulate the production of Ins(1,4,5)P3 that binds and activates IP3R and triggers the calcium release from ER to the cytosol and enhances the local calcium concentration. The calcium flux from ER to mitochondria is critical for multiple mitochondrial functions. Basal calcium oscillation in mitochondria is required for multiple metabolic processes (Gellerich et al., 2010). The calcium overload in the mitochondria leads to the opening of the mitochondrial permeability transition pore and subsequentially results in cell death (Baumgartner et al., 2009). As the MCU complex has low calcium affinity, ER and mitochondria must be in close proximity for producing high local calcium concentration. Thus, ERMCS is a hot spot for calcium transfer between the ER and mitochondria.

IP3R, which is enriched in the ERMCS, interacts with VDAC1 located at the mitochondrial outer membrane via a chaperone, Grp75. The resulting VDAC1–Grp75–IP3R complex serves as the major platform and chaperone complexes that coordinate calcium transfer between ER and mitochondria (Bononi et al., 2012). MCU localized at the mitochondrial inner membrane takes up the calcium transported from VDAC1. When ER calcium level is low, Sig-1R is released from BIP/GPR78 to stabilize IP3R3 at ERMCSs and promote prolonged ER calcium release (Hayashi and Su, 2007; **Figure 2B**).

Lipid Synthesis and Exchange

The cellular transport and homeostasis are dependent on the extensive transport of lipids and their precursors between ER and mitochondria (Osman et al., 2011; **Figure 2C**). Endoplasmic reticulum is a major membrane lipid synthesis center in the cells. The mitochondrial membrane has high levels of phospholipid and low levels of sterols and sphingolipids. Sphingolipids and phospholipids, such as phosphatidic acid (PA), phosphatidylserine (PS), phosphotidylcholine (PC), and phosphatidylinositol (PI), are synthesized in the ER. Cardiolipin (CL), a diglycerophospholipid, is a mitochondrial-specific phospholipid enriched in the inner mitochondrial membrane. Cardiolipin is synthesized in the mitochondria at the matrix side of the inner membrane using PA transported from the ER (Tatsuta et al., 2014). Phosphatidylserine is converted to phosphatidylethanolamine (PE) by PS decarboxylase (PSD) on the inner mitochondrial membrane. The mitochondrion-derived PE is transferred back to the ER, where it serves as a precursor for synthesizing PC. As mitochondria are not integrated into the classical vesicular trafficking routes, non-vesicular mediated transports that occur at the contact sites of membranes play major roles in the lipid transport between the ER and mitochondria. Several key enzymes mediate phospholipid synthesis, such as phosphatidylserine synthase-1/2 (PSS1/2) and phosphatidylethanolamine N-methyltransferase 2 (PEMT2), an enzyme implicated in PC synthesis. These enzymes are localized to the ERMCSs (Cui et al., 1993). In yeast, ERMES-deficient mitochondria exhibit an altered membrane lipid composition and an impaired conversion of PS to PC (Kornmann et al., 2009). However, there is no direct evidence to show that ERMES participates in the lipid transfer directly. The EMC complex in yeast is also involved in PS shuttling from ER to mitochondria (Lahiri et al., 2014). However, the EMC proteins do not have a lipid-binding domain and, therefore, may regulate lipid transfer indirectly. In mammals, further studies are needed to elucidate the mechanism underlying lipid transfer at ERMESs. Oxysterol-binding protein (OSBP)-related protein 5 and 8 (ORP5/ORP8) were recently reported to be localized at the ERMCSs and to potentially mediate the transport of phospholipid (probably PS) between two organelles (Galmes et al., 2016).

In addition to phospholipid, key regulators of triacylglycerol synthesis and steroidogenesis, such as acyl-CoA/diacylglycerol acyltransferase 2 (DGAT2; Stone et al., 2009) and steroidogenic acute regulatory protein (StAR; Prasad et al., 2015) are enriched in the ERMCSs. Long-chain-fatty-acid-CoA ligase 4 (FACL4; Lewin et al., 2001), an enzyme that mediates the ligation of fatty acids to coenzyme A (CoA), and acyl-coenzyme A:cholesterol acyltransferase-1 (ACAT1/SOAT1), an enzyme that catalyzes the generation of cholesterol esters, is also enriched in ERMCSs (Lewin et al., 2002). These findings indicate that the ERMCSs are closely related to lipid exchange between the ER and mitochondria, and lipid metabolism.

Regulation of Autophagy Process

Autophagy is an intracellular bulk degradation process, which is tightly regulated. Autophagy dysfunction is closely

associated with numerous human diseases (Mizushima and Komatsu, 2011). The initiation of autophagy involves the formation of isolation membranes, which engulf some cytosolic components and damaged organelles. The isolation membranes are sealed to form double-membraned autophagosomes, which fuse with the lysosomes where the contents are degraded. Although the ER, mitochondria, and plasma membrane are reported to contribute to the original autophagosome membrane, the origin of the autophagosomal membranes is still controversial. In 2013, Hamasaki et al. (2013) demonstrated that ERMCSs mediate autophagosome formation. Upon starvation, the pre-autophagosome/autophagosome markers, ATG14 and ATG6, re-localize to the ERMCS to initiate autophagosome formation. The disruption of the ERMCSs decreases the number of ATG14-positive autophagosomes. Meanwhile, Syntaxin 17 is redistributed to ERMCSs to mediate PI3–kinase complex recruitment by physically binding to ATG14. PTPIP51 is also reported to bind to VAPB and to regulate autophagy (Gomez-Suaga et al., 2017). Increasing ERMCS formation by overexpressing VAPB or PTPIP51 impairs autophagosome formation. Conversely, decreasing the expression of VAPB or PTPIP51 stimulates autophagy. These data indicate that ERMCS is a hot spot to regulate the autophagy process (**Figure 2D**).

ERMCSs AND NEURODEGENERATION

ERMCSs have attracted widespread attention in neurodegenerative diseases, mainly because they are widely involved in processes closely related to mitochondrial function and cell survival. Several neurodegenerative disease-associated proteins are enriched in the ER–mitochondrial interface. Several studies have demonstrated that ERMCSs, which are the key regulators of lipid metabolism, Ca^{2+} homeostasis, and autophagosome formation, are affected by pathogenic mutations (**Figure 3**).

Alzheimer's Disease

Familial cases of Alzheimer's disease (AD) are rare and are caused due to the mutations in the amyloid precursor protein (APP) or presenilins (PS1 and PS2). The APP Swe/Lon mouse model exhibit enhanced ER–mitochondria connection and enhanced mitochondrial calcium concentrations without marked changes in the lipid composition (Hedskog et al., 2013).

PS1 and PS2 are components of the γ-secretase complex, which is involved in APPβ processing (Naj and Schellenberg, 2017). Both PS1 and PS2 are enriched in the mitochondria-associated ER membranes (Area-Gomez et al., 2009). The mutations in PS2 increase ERMCS formation and enhance cholesteryl ester and phospholipid synthesis in the cellular models (Zampese et al., 2011; Area-Gomez et al., 2012). Additionally, PS2 mutations increase the ER–mitochondria connection in the fibroblasts of patients with sporadic AD (Area-Gomez et al., 2012). Although mutations in PS1 and PS2 can enhance cholesteryl ester and phospholipid synthesis, only PS2 can modulate the Ca^{2+} shuttling between ER and mitochondria (Zampese et al., 2011).

Sig-1R forms a Ca^{2+}-sensitive chaperone complex with Bip/GRP78 and promotes Ca^{2+} release from the ER by stabilizing IP3R3. It has been proposed that Sig-1R forms part of the endogenous defense system against AD (Maurice and Goguadze, 2017). Reportedly, compounds with Sig-1R agonist activity possess neuroprotective abilities. These findings indicate that the activity of Sig-1R may prevent AD pathology, therefore, presenting a promising therapeutic target for AD (Jia et al., 2019).

Individuals carrying the ε4 allele of apolipoprotein E (ApoE4) have increased risk for developing AD compared to the ones carrying ApoE3, the most common isoform. Cells treated with ApoE4 containing astrocyte conditioned media (ACM) have increased synthesis of phospholipids and of cholesteryl esters compared to those treated with ApoE3 containing ACM, suggesting an upregulated ERMCS functions in the cells treated with ApoE4 containing ACM (Tambini et al., 2016).

Although most evidence illustrates that enhanced ERMCS activity is associated with AD, conflicting results have been suggested in other studies. It has been demonstrated that expressing a linker that can force contacts between mitochondria and the ER suppressed motor impairment and extended the lifespan in a *Drosophila* model of AD (Garrido-Maraver et al., 2020).

Parkinson's Disease

Parkinson's disease is a progressive movement disorder with selective loss of dopaminergic (DA) neurons in the substantia nigra and accumulation of Lewy bodies consisting of α-synuclein aggregates in the patient's brains. Most PD cases are sporadic, and less than 10% are familial cases caused by genetic mutations in genes, such as *SNCA*, *LRRK2*, *VPS35*, *PINK1*, *PARK2*, and *PARK7* (Liu et al., 2019).

α-Synuclein, a presynaptic protein encoded by *SNCA*, is detected in the ERMCSs. In HeLa cells, PD-associated synuclein mutations decreased ER–mitochondria connections, as well as phospholipid synthesis (Guardia-Laguarta et al., 2014). α-Synuclein binds to the ERMCS tether protein VAPB. The VAPB–PTPIP51 tethers were disrupted when either the wild type or the PD-associated mutant forms of α-synuclein were overexpressed. A similar disruption of the VAPB–PTPIP51 interaction was also observed in neurons derived from induced pluripotent stem cells from familial PD patients with an affected *SNCA* gene. Hence, the contacts between the ER and mitochondria were loosened, and Ca^{2+} signaling at neuronal ERMCSs was affected (Paillusson et al., 2017).

DJ-1 is a conserved multifunctional protein encoded by *PARK7*. Loss of DJ-1 leads to early-onset recessive familial PD. DJ-1 is enriched in ERMCSs and interacts with the VDAC1–Grp75–IP3R complex (Liu et al., 2019). In HeLa cells, overexpression of DJ-1 enhanced ER–mitochondrial calcium transfer and marginally increased ERMCSs (Ottolini et al., 2013). DJ-1 ablation disrupted the formation of the VDAC1–Grp75–IP3R complex, causing IP3R accumulation at ERMCSs. Furthermore, similar ERMCS defects were observed in the

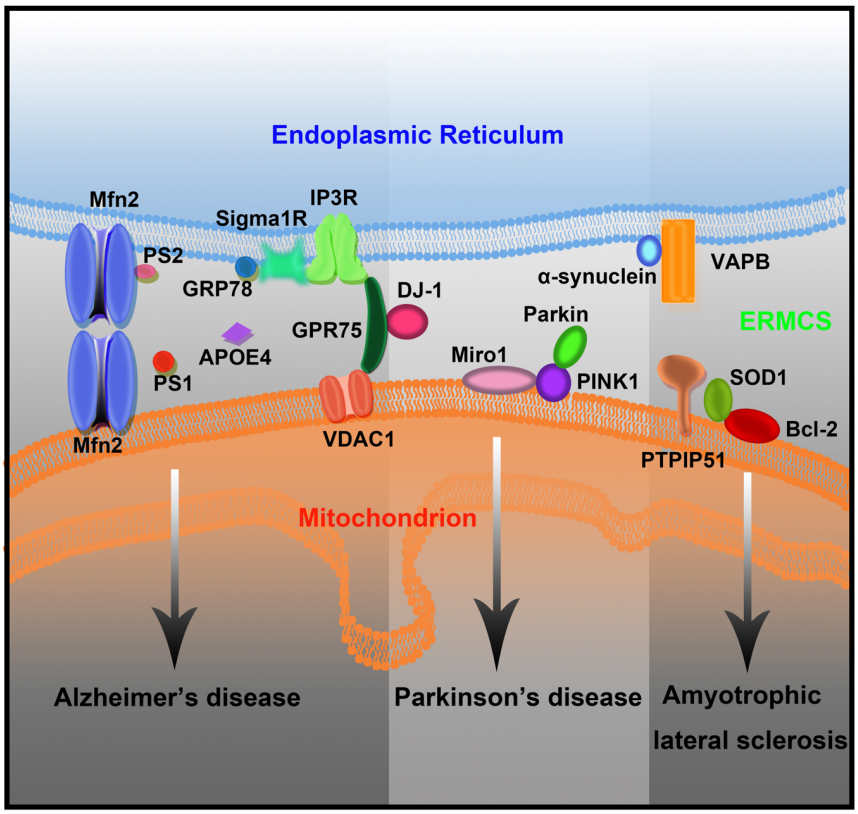

FIGURE 3 | The mutant forms of neurodegenerative disease-associated protein lead to ERMCS defects and finally neuronal death.

brain of DJ-1 knockout mice and sporadic PD patients. In *DJ-1* knockout M17 cell lines, the length of ERMCSs was greatly reduced, and the ER–mitochondria calcium transfer was significantly decreased (Liu et al., 2019).

PARK2 is an important gene whose mutation is responsible for 50% of familial autosomal recessive PD cases and probably some sporadic PD cases (Wang et al., 2010). *PARK2* encodes an E3 ligase Parkin that play critical roles in mitophagy. Calì et al. demonstrated that the upregulation of *PARK2* can enhance the mitochondrial Ca^{2+} uptake from ER (Cali et al., 2013). Consistent with this study, Basso et al. observed that the tether between the ER and mitochondria decreased in *PARK2* mutant human fibroblasts. Furthermore, the locomotor deficit in the *Drosophila* model of PD can be rescued by expressing an ER–mitochondria synthetic linker to increase ER–mitochondria tethering (Basso et al., 2018). However, Gautier et al. revealed that the ER and mitochondria are closely associated and the ER–mitochondria Ca^{2+} transfer was enhanced in the primary cells from patients with PD presenting *PARK2* mutations (Gautier et al., 2016). The rationale underlying the differences in these findings remain unclear.

PINK1 is a protein kinase necessary for the recruitment of Parkin to the damaged mitochondria during mitophagy. In DA neurons with *PINK1* mutations, ERMCSs were strengthened, and the mitochondrial Ca^{2+} level was increased. Miro, a protein well known for axonal transport of mitochondria, mediated the effects of PINK1 on mitochondrial calcium and morphology. Miro overexpression mimicked *PINK1* mutant-induced mitochondrial Ca^{2+} elevation, which could be rescued by inhibiting the genes involved in calcium transfer in ERMCSs. Inhibition of Miro or components of ERMCSs rescued the defects induced by the *PINK1* mutation. Surprisingly, the Miro-mediated calcium transfer was independent of its mitochondrial transport activity (Lee et al., 2018). Recently, *RHOT1*, the gene coding for Miro1, was found to carry mutations in patients with PD. The structure and number of ERMCSs were altered, and Ca^{2+} homeostasis was impaired in patient-derived fibroblasts carrying *RHOT1* mutants (Berenguer-Escuder et al., 2019).

Amyotrophic Lateral Sclerosis

Amyotrophic lateral sclerosis is a fatal late-stage neurodegenerative disorder, characterized by progressive loss of motor neurons, muscle weakness, spasms, and death within a few years of diagnosis. Over 90% of ALS cases occur sporadically, and familial cases of ALS are rare. Furthermore, approximately 15% of ALS present with frontotemporal lobar dementia (ALS/FTD). Familial ALS is caused due to mutations in the genes encoding for the antioxidant protein superoxide dismutase 1 (SOD1), the TAR-DNA binding protein 43 (TDP43), ubiquilin 2 (Ubqln2), and VAPB (De Mario et al., 2017; Perrone et al., 2020).

Dominant mutations in the gene encoding SOD1 leads to familial ALS and accumulation of SOD1 mutant proteins in

the ERMCSs (Bruijn et al., 2004). Reportedly, the mutant SOD1 interacts with Bcl-2, affecting calcium homeostasis (Eckenrode et al., 2010).

Accumulation of TDP-43 is a hallmark of ALS/FTD pathology. Overexpression of wild type, as well as mutant TDP-43, leads to reduced ER–mitochondria association, decreased VAPB–PTPIP51 interaction, and affects Ca^{2+} homeostasis (Stoica et al., 2014).

In the spinal cord of patients with ALS, VAPB mRNA levels were decreased when compared to control subjects (Anagnostou et al., 2010). The P56S mutant form of VAPB has been associated with ALS type 8 (Perrone et al., 2020). VAPB–P56S has demonstrated altered affinity to PTPIP51 and increased Ca^{2+} release from ER stores, consequently elevating Ca^{2+} uptake by the mitochondria (De Vos et al., 2012).

TOOLS FOR STUDYING ERMCSs

Since Copeland and Dalton first discovered ERMCSs in the pseudobranch glands of *Fundulus heteroclitus* by electron microscopy, various methods have been used to study the structure and function of ERMCSs. The function and structure of ERMCSs were gradually revealed after the establishment of protocols for isolating membrane contacts and high-resolution microscopy (**Table 1**).

Study of ERMCS Morphology and Structure

Electron Microscopy

Transmission electron microscopy (TEM) is still considered as the gold standard to study the structure of ERMCS. TEM analysis provides static, high-resolution, and ultrastructure information about the contact sites. Transmission electron microscopy is particularly suitable for samples with a large number of contact sites or those with resident proteins that can be analyzed by immune electron microscopy analysis (Honscher et al., 2014).

Electron tomography (ET) provides a three-dimensional view of the subcellular structures. In ET, a micrograph of a sample is recorded by tilting the sample in different directions and then merged into a three-dimensional structure. Electron tomography often requires serial sectioning, which could be laborious and technically challenging. Additionally, the incomplete 3D reconstructions with regions lacking information often leads to "missing wedge" artifacts (Fernández-Busnadiego, 2016).

Volume EM techniques based on scanning electron microscopy (SEM) not only provide high-resolution 3D images of large specimen volumes but also overcome the "missing wedge" artifacts (Peddie and Collinson, 2014). However, volume EM needs a powerful computer to process large datasets.

Epifluorescence and Confocal Microscopy

The most common technique to visualize the contacts is to express fluorescent proteins that label mitochondria and ER in the cells and observe the overlapping signals. This simple application is suitable for both static and live-cell imaging and is a readily available tool to study ERMCSs. However, this technique is associated with some inherent limitations because of its optical diffraction limit and some artifacts introduced by fixation (Scorrano et al., 2019). The development of super-resolution microscopy has enabled the high-resolution observation of ERMC dynamics (Guo et al., 2018). However, super-resolution microscopy does not conclusively provide information on the formation of contacts between two spatially close organelles.

A drug-inducible Forster resonance energy transfer (FRET)-based reporter was developed to visualize ERMCSs (Csordás et al., 2010). This technique involves introducing a rapamycin-induced dimerization domain, which can provide temporal quantitative measurements of contact distance. However, prolonged drug treatments can introduce artifacts. Several groups have reported the use of ERMCS reporters using split green fluorescent protein (GFP; Cieri et al., 2018; Yang et al., 2018). One half of the split GFP protein labels the ER surface, while the other labels the mitochondrial surface. The fluorescence of GFP is detected if the ER and mitochondria are spatially close enough to form contacts. The narrow (8–10 nm) probe and wide probe (10–50 nm) with short or long linker could be used to examine the narrow and wide contacts, respectively. These reporters do not artificially increase tethering between ER and mitochondria. Additionally, a light-inducible ER–mitochondria tethering (LIT) system was developed to temporally regulate the tethering between ER and mitochondria (Shi et al., 2018). This will be useful for studies that require multiple switching on–off steps and for avoiding side effects caused by continuous ER–mitochondria tethering.

Split Rluc8

Renilla luciferase (Rluc) is a bioluminescent enzyme. The reconstitution of split fragments of RLuc enables the detection of two closely associated proteins. Lim et al. (2015) developed a tool with Mito–RLuc8N and RLuc8C–ER to label the mitochondria and ER, respectively. When the ER and mitochondria are far apart, the activity of RLuc8 cannot be reconstructed. When the ER and mitochondria form contacts, Mito–RLuc8N will be close to RLuc8C-ER, and the total enzyme activity of RLuc8 is detected through the luminescence conversion of substrates (Lim et al., 2015).

Proximity Ligation Assay

Proximity ligation assay (PLA) is an antibody-based method for detecting biomolecules and their physical proximity at a single molecule level resolution. Typically, two unique proteins are recognized by primary antibodies raised in different species. The secondary antibodies conjugated with a pair of oligonucleotides (PLA probes) bind to the primary antibody. The PLA probes will hybridize with the connector oligos only if they are in close proximity to each other. The ligase forms a closed, circle DNA template, and the PLA probe acts as a primer to generate concatemeric sequences, which amplify the signals that are still tethered to the PLA probe by 1000-fold. The labeled oligos hybridize to the complementary sequences within the amplicon, which could then be analyzed by microscopy analysis. This technique was first introduced in 2002 to detect Zeptomoles (10 or 21 mol) of platelet-derived growth factor

TABLE 1 | Advantages and disadvantages of the various experimental approaches to study endoplasmic reticulum–mitochondria contact sites (ERMCSs).

Approaches		Advantages	Disadvantages
Study of ERMCS morphology and structure			
Electron microscopy	Transmission electron microscopy (TEM)	• Golden standard • Provides static, high-resolution ultrastructure information	• Suitable for samples with a large amount of contact sites • Fixation may introduce artifacts
	Electron tomography (ET)	• Three-dimensional view of the subcellular structures	• Technically challenging • "missing wedge" artifacts
	Scanning electron microscopy (SEM)	• Provides high-resolution 3D image • Overcome the "missing wedge" artifacts	• Needs powerful computer to process large datasets
Epifluorescence and confocal microscopy	Super-resolution microscopy	• Suitable for both static and live-cell imaging • Enable the high-resolution observation of ERMCS dynamics	• Optical diffraction limit • Fixation may introduce artifacts
	FRET-based reporter	• Provides temporal quantitative measurements of contact distance	• Prolonged drug treatments can introduce artifacts
	Split green fluorescent protein (GFP)	• Different probes could be used to examine the narrow and wide contacts	• Less responsive to the subtle changes in the contacts
	Light-inducible ER–mitochondria tethering (LIT) system	• Temporally regulate the contacts • Avoid side effects caused by continuous ER–mitochondria tethering	• Needs careful control
Split Rluc8		• Easy technique	• Needs careful control
Proximity ligation assay (PLA)		• Mainly used to detect the proximity between the two proteins	• Requires antibodies to the proteins of interest
Detection of resident proteins in ERMCSs			
Cell fractionation		• Major technique to isolate the fraction of ERMCS and identify its protein components	• Purity is hard to guarantee
Ascorbate peroxidase (APEX) Tagging		• Identify new contact-site proteins • Combining it with biochemical cell fractionation will reach a better purity	• Technically challenging • Needs careful control

(PDGF) in the solution phase (Fredriksson et al., 2002). Currently, this assay is mainly used to detect the proximity between the two proteins (Bagchi et al., 2015). In PLA, two contact specific proteins on the ER side and mitochondria side are recognized by their antibodies, and the signals could quantitatively indicate the distance or contact range between the two membranes.

Detection of Resident Proteins in ERMCSs

Cell Fractionation

Cell fractionation mainly refers to the separation of organelles by sucrose gradient. In 1957, Lever (1958) demonstrated that the mitochondria separated by sucrose gradient were always mixed with ER, which indicated the association between ER and mitochondria. Currently, cell fractionation is still a major technique to isolate the fraction of ERMCSs and identify its protein components. The purity of the fraction obtained remains a concern.

Ascorbate Peroxidase Tagging

In situ proximity labeling method uses an engineered ascorbate peroxidase (APEX) to tag a protein of interest and evaluate its expression. The cells are then treated with hydrogen peroxide (H_2O_2) in the presence of biotin–phenol. The proteins proximal to the APEX fusion protein will be covalently labeled with biotin, which could then be purified and detected via mass spectrometry. Using this APEX tagging technique, the ERMCS-specific protein could be tagged with APEX, and the other proteins located at the ERMCSs could be identified (Cho et al., 2017).

In conclusion, ERMCSs are hot spots for multiple cellular events and are critical for neuronal homeostasis. Although there is no direct evidence to indicate that changes in the ERMCSs can cause neurodegeneration, further studies on ERMCs will provide valuable insights into neurodegeneration and potentially a novel therapeutic target. As mentioned earlier, there are inconsistencies regarding some findings related to the roles of ERMCSs in neurodegenerative diseases. The rationales underlying these remain elusive. Developing a standardized approach to analyze and quantify ERMCSs might be the key to resolve the inconsistencies.

AUTHOR CONTRIBUTIONS

CT obtained financial support. All authors wrote and approved the final version of the manuscript.

FUNDING

CT is supported by the National Natural Science Foundation of China (91754103, 31622034, and 31571383), National Key Research and Developmental Program of China (2017YFC1001100 and 2017YFC1001500), Natural Science Foundation of Zhejiang Province, China (LR16C070001), and Fundamental research funds for the central universities. CT is a Qianjiang Scholar.

REFERENCES

Anagnostou, G., Akbar, M. T., Paul, P., Angelinetta, C., Steiner, T. J., and De Belleroche, J. (2010). Vesicle associated membrane protein B (VAPB) is decreased in ALS spinal cord. *Neurobiol Aging* 31, 969–985. doi: 10.1016/j.neurobiolaging.2008.07.005

Arasaki, K., Shimizu, H., Mogari, H., Nishida, N., Hirota, N., Furuno, A., et al. (2015). A role for the ancient SNARE syntaxin 17 in regulating mitochondrial division. *Dev. Cell* 32, 304–317. doi: 10.1016/j.devcel.2014.12.011

Area-Gomez, E., De Groof, A. J., Boldogh, I., Bird, T. D., Gibson, G. E., Koehler, C. M., et al. (2009). Presenilins are enriched in endoplasmic reticulum membranes associated with mitochondria. *Am. J. Pathol.* 175, 1810–1816. doi: 10.2353/ajpath.2009.090219

Area-Gomez, E., Del Carmen, Lara Castillo, M., Tambini, M. D., Guardia-Laguarta, C., De Groof, A. J., et al. (2012). Upregulated function of mitochondria-associated ER membranes in Alzheimer disease. *EMBO J.* 31, 4106–4123. doi: 10.1038/emboj.2012.202

Bagchi, S., Fredriksson, R., and Wallen-Mackenzie, A. (2015). In situ proximity ligation assay (PLA). *Methods Mol. Biol.* 1318, 149–159. doi: 10.1007/978-1-4939-2742-5_15

Basso, V., Marchesan, E., Peggion, C., Chakraborty, J., Von Stockum, S., Giacomello, M., et al. (2018). Regulation of ER-mitochondria contacts by Parkin via Mfn2. *Pharmacol. Res.* 138, 43–56. doi: 10.1016/j.phrs.2018.09.006

Baumgartner, H. K., Gerasimenko, J. V., Thorne, C., Ferdek, P., Pozzan, T., Tepikin, A. V., et al. (2009). Calcium elevation in mitochondria is the main Ca2+ requirement for mitochondrial permeability transition pore (mPTP) opening. *J. Biol. Chem.* 284, 20796–20803. doi: 10.1074/jbc.m109.025353

Berenguer-Escuder, C., Grossmann, D., Massart, F., Antony, P., Burbulla, L. F., Glaab, E., et al. (2019). Variants in miro1 cause alterations of ER-mitochondria contact sites in fibroblasts from Parkinson's Disease Patients. *J. Clin. Med.* 8:2226. doi: 10.3390/jcm8122226

Bononi, A., Missiroli, S., Poletti, F., Suski, J. M., Agnoletto, C., Bonora, M., et al. (2012). Mitochondria-associated membranes (MAMs) as hotspot Ca(2+) signaling units. *Adv. Exp. Med. Biol.* 740, 411–437. doi: 10.1007/978-94-007-2888-2_17

Bruijn, L. I., Miller, T. M., and Cleveland, D. W. (2004). Unraveling the mechanisms involved in motor neuron degeneration in ALS. *Annu. Rev. Neurosci.* 27, 723–749. doi: 10.1146/annurev.neuro.27.070203.144244

Cali, T., Ottolini, D., Negro, A., and Brini, M. (2013). Enhanced parkin levels favor ER-mitochondria crosstalk and guarantee Ca(2+) transfer to sustain cell bioenergetics. *Biochim. Biophys. Acta* 1832, 495–508. doi: 10.1016/j.bbadis.2013.01.004

Cerqua, C., Anesti, V., Pyakurel, A., Liu, D., Naon, D., Wiche, G., et al. (2010). Trichoplein/mitostatin regulates endoplasmic reticulum-mitochondria juxtaposition. *EMBO Rep.* 11, 854–860. doi: 10.1038/embor.2010.151

Chandra, D., Choy, G., Deng, X., Bhatia, B., Daniel, P., and Tang, D. G. (2004). Association of active caspase 8 with the mitochondrial membrane during apoptosis: potential roles in cleaving BAP31 and caspase 3 and mediating mitochondrion-endoplasmic reticulum cross talk in etoposide-induced cell death. *Mol. Cell Biol.* 24, 6592–6607. doi: 10.1128/mcb.24.15.6592-6607.2004

Cho, I.-T., Adelmant, G., Lim, Y., Marto, J. A., Cho, G., and Golden, J. A. (2017). Ascorbate peroxidase proximity labeling coupled with biochemical fractionation identifies promoters of endoplasmic reticulum–mitochondrial contacts. *J. Biol.Chem.* 292, 16382–16392. doi: 10.1074/jbc.m117.795286

Cieri, D., Vicario, M., Giacomello, M., Vallese, F., Filadi, R., Wagner, T., et al. (2018). SPLICS: a split green fluorescent protein-based contact site sensor for narrow and wide heterotypic organelle juxtaposition. *Cell Death Differ.* 25, 1131–1145. doi: 10.1038/s41418-017-0033-z

Cohen, S., Valm, A. M., and Lippincott-Schwartz, J. (2018). Interacting organelles. *Curr. Opin. Cell Biol.* 53, 84–91. doi: 10.1016/j.ceb.2018.06.003

Cosson, P., Marchetti, A., Ravazzola, M., and Orci, L. (2012). Mitofusin-2 independent juxtaposition of endoplasmic reticulum and mitochondria: an ultrastructural study. *PLoS One* 7:e46293. doi: 10.1371/journal.pone.0046293

Csordas, G., Renken, C., Varnai, P., Walter, L., Weaver, D., Buttle, K. F., et al. (2006). Structural and functional features and significance of the physical linkage between ER and mitochondria. *J. Cell Biol.* 174, 915–921. doi: 10.1083/jcb.200604016

Csordás, G., Várnai, P., Golenár, T., Roy, S., Purkins, G., Schneider, T. G., et al. (2010). Imaging interorganelle contacts and local calcium dynamics at the er-mitochondrial interface. *Mol. Cell* 39, 121–132. doi: 10.1016/j.molcel.2010.06.029

Cui, Z., Vance, J. E., Chen, M. H., Voelker, D. R., and Vance, D. E. (1993). Cloning and expression of a novel phosphatidylethanolamine N-methyltransferase. A specific biochemical and cytological marker for a unique membrane fraction in rat liver. *J. Biol. Chem.* 268, 16655–16663.

Daniele, T., Hurbain, I., Vago, R., Casari, G., Raposo, G., Tacchetti, C., et al. (2014). Mitochondria and melanosomes establish physical contacts modulated by Mfn2 and involved in organelle biogenesis. *Curr. Biol.* 24, 393–403. doi: 10.1016/j.cub.2014.01.007

De Brito, O. M., and Scorrano, L. (2008). Mitofusin 2 tethers endoplasmic reticulum to mitochondria. *Nature* 456, 605–610. doi: 10.1038/nature07534

De Mario, A., Quintana-Cabrera, R., Martinvalet, D., and Giacomello, M. (2017). (Neuro)degenerated mitochondria-ER contacts. *Biochem. Biophys. Res. Commun.* 483, 1096–1109. doi: 10.1016/j.bbrc.2016.07.056

De Vos, K. J., Morotz, G. M., Stoica, R., Tudor, E. L., Lau, K. F., Ackerley, S., et al. (2012). VAPB interacts with the mitochondrial protein PTPIP51 to regulate calcium homeostasis. *Hum. Mol. Genet.* 21, 1299–1311. doi: 10.1093/hmg/ddr559

D'eletto, M., Rossin, F., Occhigrossi, L., Farrace, M. G., Faccenda, D., Desai, R., et al. (2018). Transglutaminase Type 2 Regulates ER-Mitochondria Contact Sites by Interacting with GRP75. *Cell Rep.* 25, 3573.e4–3581.e4.

Devine, M. J., and Kittler, J. T. (2018). Mitochondria at the neuronal presynapse in health and disease. *Nat. Rev. Neurosci.* 19, 63–80. doi: 10.1038/nrn.2017.170

Eckenrode, E. F., Yang, J., Velmurugan, G. V., Foskett, J. K., and White, C. (2010). Apoptosis protection by Mcl-1 and Bcl-2 modulation of inositol 1,4,5-trisphosphate receptor-dependent Ca2+ signaling. *J. Biol. Chem.* 285, 13678–13684. doi: 10.1074/jbc.m109.096040

Elbaz-Alon, Y., Eisenberg-Bord, M., Shinder, V., Stiller, S. B., Shimoni, E., Wiedemann, N., et al. (2015). Lam6 regulates the extent of contacts between organelles. *Cell Rep.* 12, 7–14. doi: 10.1016/j.celrep.2015.06.022

Fernández-Busnadiego, R. (2016). Supramolecular architecture of endoplasmic reticulum–plasma membrane contact sites. *Biochem. Soc.Trans.* 44, 534–540. doi: 10.1042/bst20150279

Filadi, R., Greotti, E., Turacchio, G., Luini, A., Pozzan, T., and Pizzo, P. (2016). Presenilin 2 modulates endoplasmic reticulum-mitochondria coupling by tuning the antagonistic effect of mitofusin 2. *Cell Rep.* 15, 2226–2238. doi: 10.1016/j.celrep.2016.05.013

Fredriksson, S., Gullberg, M., Jarvius, J., Olsson, C., Pietras, K., Gustafsdottir, S. M., et al. (2002). Protein detection using proximity-dependent DNA ligation assays. *Nat. Biotechnol.* 20, 473–477. doi: 10.1038/nbt0502-473

Friedman, J. R., Lackner, L. L., West, M., Dibenedetto, J. R., Nunnari, J., and Voeltz, G. K. (2011). ER tubules mark sites of mitochondrial division. *Science* 334, 358–362. doi: 10.1126/science.1207385

Galmes, R., Houcine, A., Van Vliet, A. R., Agostinis, P., Jackson, C. L., and Giordano, F. (2016). ORP5/ORP8 localize to endoplasmic reticulum-mitochondria contacts and are involved in mitochondrial function. *EMBO Rep.* 17, 800–810. doi: 10.15252/embr.201541108

Garrido-Maraver, J., Loh, S. H. Y., and Martins, L. M. (2020). Forcing contacts between mitochondria and the endoplasmic reticulum extends lifespan in a *Drosophila* model of Alzheimer's disease. *Biol. Open* 9:bio047530. doi: 10.1242/bio.047530

Gautier, C. A., Erpapazoglou, Z., Mouton-Liger, F., Muriel, M. P., Cormier, F., Bigou, S., et al. (2016). The endoplasmic reticulum-mitochondria interface is perturbed in PARK2 knockout mice and patients with PARK2 mutations. *Hum. Mol. Genet.* 25, 2972–2984.

Gellerich, F. N., Gizatullina, Z., Trumbeckaite, S., Nguyen, H. P., Pallas, T., Arandarcikaite, O., et al. (2010). The regulation of OXPHOS by extramitochondrial calcium. *Biochim. Biophys. Acta* 1797, 1018–1027. doi: 10.1016/j.bbabio.2010.02.005

Gomez-Suaga, P., Paillusson, S., Stoica, R., Noble, W., Hanger, D. P., and Miller, C. C. J. (2017). The ER-Mitochondria tethering complex VAPB-PTPIP51 regulates autophagy. *Curr. Biol.* 27, 371–385. doi: 10.1016/j.cub.2016.12.038

Guardia-Laguarta, C., Area-Gomez, E., Rub, C., Liu, Y., Magrane, J., Becker, D., et al. (2014). alpha-Synuclein is localized to mitochondria-associated ER membranes. *J. Neurosci.* 34, 249–259. doi: 10.1523/jneurosci.2507-13.2014

Guo, Y., Li, D., Zhang, S., Yang, Y., Liu, J. J., Wang, X., et al. (2018). Visualizing intracellular organelle and cytoskeletal interactions at nanoscale resolution on millisecond timescales. *Cell* 175, 1430.e17–1442.e17.

Hamasaki, M., Furuta, N., Matsuda, A., Nezu, A., Yamamoto, A., Fujita, N., et al. (2013). Autophagosomes form at ER-mitochondria contact sites. *Nature* 495, 389–393. doi: 10.1038/nature11910

Hayashi, T., and Su, T. P. (2007). Sigma-1 receptor chaperones at the ER-mitochondrion interface regulate Ca(2+) signaling and cell survival. *Cell* 131, 596–610. doi: 10.1016/j.cell.2007.08.036

Hedskog, L., Pinho, C. M., Filadi, R., Ronnback, A., Hertwig, L., Wiehager, B., et al. (2013). Modulation of the endoplasmic reticulum-mitochondria interface in Alzheimer's disease and related models. *Proc. Natl. Acad. Sci. U.S.A.* 110, 7916–7921. doi: 10.1073/pnas.1300677110

Honscher, C., Mari, M., Auffarth, K., Bohnert, M., Griffith, J., Geerts, W., et al. (2014). Cellular metabolism regulates contact sites between vacuoles and mitochondria. *Dev. Cell* 30, 86–94. doi: 10.1016/j.devcel.2014.06.006

Iwasawa, R., Mahul-Mellier, A. L., Datler, C., Pazarentzos, E., and Grimm, S. (2011). Fis1 and Bap31 bridge the mitochondria-ER interface to establish a platform for apoptosis induction. *EMBO J.* 30, 556–568. doi: 10.1038/emboj.2010.346

Jia, H., Zhang, Y., and Huang, Y. (2019). Imaging sigma receptors in the brain: New opportunities for diagnosis of Alzheimer's disease and therapeutic development. *Neurosci. Lett.* 691, 3–10. doi: 10.1016/j.neulet.2018.07.033

Kaiser, S. E., Brickner, J. H., Reilein, A. R., Fenn, T. D., Walter, P., and Brunger, A. T. (2005). Structural basis of FFAT motif-mediated ER targeting. *Structure* 13, 1035–1045. doi: 10.1016/j.str.2005.04.010

Kornmann, B., Currie, E., Collins, S. R., Schuldiner, M., Nunnari, J., Weissman, J. S., et al. (2009). An ER-mitochondria tethering complex revealed by a synthetic biology screen. *Science* 325, 477–481. doi: 10.1126/science.1175088

Kornmann, B., Osman, C., and Walter, P. (2011). The conserved GTPase Gem1 regulates endoplasmic reticulum-mitochondria connections. *Proc. Natl. Acad. Sci. U.S.A.* 108, 14151–14156. doi: 10.1073/pnas.1111314108

Korobova, F., Ramabhadran, V., and Higgs, H. N. (2013). An actin-dependent step in mitochondrial fission mediated by the ER-associated formin INF2. *Science* 339, 464–467. doi: 10.1126/science.1228360

Lackner, L. L. (2019). The expanding and unexpected functions of mitochondria contact sites. *Trends Cell Biol.* 29, 580–590. doi: 10.1016/j.tcb.2019.02.009

Lahiri, S., Chao, J. T., Tavassoli, S., Wong, A. K., Choudhary, V., Young, B. P., et al. (2014). A conserved endoplasmic reticulum membrane protein complex (EMC) facilitates phospholipid transfer from the ER to mitochondria. *PLoS Biol.* 12:e1001969. doi: 10.1371/journal.pbio.1001969

Leal, N. S., Schreiner, B., Pinho, C. M., Filadi, R., Wiehager, B., Karlstrom, H., et al. (2016). Mitofusin-2 knockdown increases ER-mitochondria contact and decreases amyloid beta-peptide production. *J. Cell Mol. Med.* 20, 1686–1695. doi: 10.1111/jcmm.12863

Lee, K. S., Huh, S., Lee, S., Wu, Z., Kim, A. K., Kang, H. Y., et al. (2018). Altered ER-mitochondria contact impacts mitochondria calcium homeostasis and contributes to neurodegeneration in vivo in disease models. *Proc. Natl. Acad. Sci. U.S.A.* 115, E8844–E8853.

Lev, S., Ben Halevy, D., Peretti, D., and Dahan, N. (2008). The VAP protein family: from cellular functions to motor neuron disease. *Trends Cell Biol.* 18, 282–290. doi: 10.1016/j.tcb.2008.03.006

Lever, J. D. (1958). Mitochondria Isolated from rat brown adipose tissue and liver. *J. Cell Bio.* 4, 287–290. doi: 10.1083/jcb.4.3.287

Lewin, T. M., Kim, J. H., Granger, D. A., Vance, J. E., and Coleman, R. A. (2001). Acyl-CoA synthetase isoforms 1, 4, and 5 are present in different subcellular membranes in rat liver and can be inhibited independently. *J. Biol. Chem.* 276, 24674–24679. doi: 10.1074/jbc.m102036200

Lewin, T. M., Van Horn, C. G., Krisans, S. K., and Coleman, R. A. (2002). Rat liver acyl-CoA synthetase 4 is a peripheral-membrane protein located in two distinct subcellular organelles, peroxisomes, and mitochondrial-associated membrane. *Arch. Biochem. Biophys.* 404, 263–270. doi: 10.1016/s0003-9861(02)00247-3

Lewis, S. C., Uchiyama, L. F., and Nunnari, J. (2016). ER-mitochondria contacts couple mtDNA synthesis with mitochondrial division in human cells. *Science* 353, aaf5549. doi: 10.1126/science.aaf5549

Lim, Y., Cho, I. T., Schoel, L. J., Cho, G., and Golden, J. A. (2015). Hereditary spastic paraplegia-linked REEP1 modulates endoplasmic reticulum/mitochondria contacts. *Ann. Neurol.* 78, 679–696. doi: 10.1002/ana.24488

Liu, Y., Ma, X., Fujioka, H., Liu, J., Chen, S., and Zhu, X. (2019). DJ-1 regulates the integrity and function of ER-mitochondria association through interaction with IP3R3-Grp75-VDAC1. *Proc. Natl. Acad. Sci. U.S.A.* 116, 25322–25328. doi: 10.1073/pnas.1906565116

Lynes, E. M., Bui, M., Yap, M. C., Benson, M. D., Schneider, B., Ellgaard, L., et al. (2012). Palmitoylated TMX and calnexin target to the mitochondria-associated membrane. *EMBO J.* 31, 457–470. doi: 10.1038/emboj.2011.384

Maurice, T., and Goguadze, N. (2017). "Role of σ1 receptors in learning and memory and Alzheimer's disease-type dementia," in *Sigma Receptors: Their Role in Disease and as Therapeutic Targets*, eds S. B. Smith, and T.-P. Su (Cham: Springer International Publishing), 213–233. doi: 10.1007/978-3-319-50174-1_15

Mizushima, N., and Komatsu, M. (2011). Autophagy: renovation of cells and tissues. *Cell* 147, 728–741. doi: 10.1016/j.cell.2011.10.026

Moltedo, O., Remondelli, P., and Amodio, G. (2019). The mitochondria-endoplasmic reticulum contacts and their critical role in aging and age-associated diseases. *Front. Cell Dev. Biol.* 7:172. doi: 10.3389/fcell.2019.00017

Morales, P. E., Torres, G., Sotomayor-Flores, C., Pena-Oyarzun, D., Rivera-Mejias, P., Paredes, F., et al. (2014). GLP-1 promotes mitochondrial metabolism in vascular smooth muscle cells by enhancing endoplasmic reticulum-mitochondria coupling. *Biochem. Biophys. Res. Commun.* 446, 410–416. doi: 10.1016/j.bbrc.2014.03.004

Murley, A., Sarsam, R. D., Toulmay, A., Yamada, J., Prinz, W. A., and Nunnari, J. (2015). Ltc1 is an ER-localized sterol transporter and a component of ER-mitochondria and ER-vacuole contacts. *J. Cell Biol.* 209, 539–548. doi: 10.1083/jcb.201502033

Murphy, S. E., and Levine, T. P. (2016). VAP, a versatile access point for the endoplasmic reticulum: review and analysis of FFAT-like motifs in the VAPome. *Biochim. Biophys. Acta* 1861, 952–961. doi: 10.1016/j.bbalip.2016.02.009

Naj, A. C., and Schellenberg, G. D. (2017). Genomic variants, genes, and pathways of Alzheimer's disease: An overview. *Am. J. Med. Genet. Part BNeuropsychiatr. Genet.* 174, 5–26. doi: 10.1002/ajmg.b.32499

Namba, T. (2019). BAP31 regulates mitochondrial function via interaction with Tom40 within ER-mitochondria contact sites. *Sci. Adv.* 5:eaaw1386. doi: 10.1126/sciadv.aaw1386

Namba, T., Tian, F., Chu, K., Hwang, S. Y., Yoon, K. W., Byun, S., et al. (2013). CDIP1-BAP31 complex transduces apoptotic signals from endoplasmic reticulum to mitochondria under endoplasmic reticulum stress. *Cell Rep.* 5, 331–339. doi: 10.1016/j.celrep.2013.09.020

Osman, C., Voelker, D. R., and Langer, T. (2011). Making heads or tails of phospholipids in mitochondria. *J. Cell Biol.* 192, 7–16. doi: 10.1083/jcb.201006159

Ottolini, D., Cali, T., Negro, A., and Brini, M. (2013). The Parkinson disease-related protein DJ-1 counteracts mitochondrial impairment induced by the tumour suppressor protein p53 by enhancing endoplasmic reticulum-mitochondria tethering. *Hum. Mol. Genet.* 22, 2152–2168. doi: 10.1093/hmg/ddt068

Pagliuso, A., Tham, T. N., Stevens, J. K., Lagache, T., Persson, R., Salles, A., et al. (2016). A role for septin 2 in Drp1-mediated mitochondrial fission. *EMBO Rep.* 17, 858–873. doi: 10.15252/embr.201541612

Paillusson, S., Gomez-Suaga, P., Stoica, R., Little, D., Gissen, P., Devine, M. J., et al. (2017). alpha-Synuclein binds to the ER-mitochondria tethering protein VAPB to disrupt Ca(2+) homeostasis and mitochondrial ATP production. *Acta Neuropathol.* 134, 129–149. doi: 10.1007/s00401-017-1704-z

Paillusson, S., Stoica, R., Gomez-Suaga, P., Lau, D. H. W., Mueller, S., Miller, T., et al. (2016). There's something wrong with my MAM; the ER-mitochondria axis and Neurodegenerative Diseases. *Trends Neurosci.* 39, 146–157. doi: 10.1016/j.tins.2016.01.008

Peddie, C. J., and Collinson, L. M. (2014). Exploring the third dimension: volume electron microscopy comes of age. *Micron* 61, 9–19. doi: 10.1016/j.micron.2014.01.009

Perrone, M., Caroccia, N., Genovese, I., Missiroli, S., Modesti, L., Pedriali, G., et al. (2020). The role of mitochondria-associated membranes in cellular homeostasis and diseases. *Int. Rev. Cell Mol. Biol.* 350, 119–196. doi: 10.1016/bs.ircmb.2019.11.002

Phillips, M. J., and Voeltz, G. K. (2016). Structure and function of ER membrane contact sites with other organelles. *Nat. Rev. Mol. Cell Biol.* 17, 69–82.

Prasad, M., Kaur, J., Pawlak, K. J., Bose, M., Whittal, R. M., and Bose, H. S. (2015). Mitochondria-associated endoplasmic reticulum membrane (MAM)

regulates steroidogenic activity via steroidogenic acute regulatory protein (StAR)-voltage-dependent anion channel 2 (VDAC2) interaction. *J. Biol. Chem.* 290, 2604–2616. doi: 10.1074/jbc.m114.605808

Rapizzi, E., Pinton, P., Szabadkai, G., Wieckowski, M. R., Vandecasteele, G., Baird, G., et al. (2002). Recombinant expression of the voltage-dependent anion channel enhances the transfer of Ca2+ microdomains to mitochondria. *J. Cell Biol.* 159, 613–624. doi: 10.1083/jcb.200205091

Schwarz, D. S., and Blower, M. D. (2016). The endoplasmic reticulum: structure, function and response to cellular signaling. *Cell Mol. Life Sci.* 73, 79–94. doi: 10.1007/s00018-015-2052-6

Scorrano, L., De Matteis, M. A., Emr, S., Giordano, F., Hajnoczky, G., Kornmann, B., et al. (2019). Coming together to define membrane contact sites. *Nat. Commun.* 10, 1287.

Shi, F., Kawano, F., Park, S. E., Komazaki, S., Hirabayashi, Y., Polleux, F., et al. (2018). Optogenetic control of endoplasmic reticulum-mitochondria tethering. *ACS Synth. Biol.* 7, 2–9. doi: 10.1021/acssynbio.7b00248

Simmen, T., Aslan, J. E., Blagoveshchenskaya, A. D., Thomas, L., Wan, L., Xiang, Y., et al. (2005). PACS-2 controls endoplasmic reticulum-mitochondria communication and Bid-mediated apoptosis. *EMBO J.* 24, 717–729. doi: 10.1038/sj.emboj.7600559

Stoica, R., De Vos, K. J., Paillusson, S., Mueller, S., Sancho, R. M., Lau, K. F., et al. (2014). ER-mitochondria associations are regulated by the VAPB-PTPIP51 interaction and are disrupted by ALS/FTD-associated TDP-43. *Nat. Commun.* 5:3996.

Stoica, R., Paillusson, S., Gomez-Suaga, P., Mitchell, J. C., Lau, D. H., Gray, E. H., et al. (2016). ALS/FTD-associated FUS activates GSK-3beta to disrupt the VAPB-PTPIP51 interaction and ER-mitochondria associations. *EMBO Rep.* 17, 1326–1342. doi: 10.15252/embr.201541726

Stone, S. J., Levin, M. C., Zhou, P., Han, J., Walther, T. C., and Farese, R. V. Jr. (2009). The endoplasmic reticulum enzyme DGAT2 is found in mitochondria-associated membranes and has a mitochondrial targeting signal that promotes its association with mitochondria. *J. Biol. Chem.* 284, 5352–5361. doi: 10.1074/jbc.m805768200

Sugiura, A., Nagashima, S., Tokuyama, T., Amo, T., Matsuki, Y., Ishido, S., et al. (2013). MITOL regulates endoplasmic reticulum-mitochondria contacts via Mitofusin2. *Mol. Cell* 51, 20–34. doi: 10.1016/j.molcel.2013.04.023

Szabadkai, G., Bianchi, K., Varnai, P., De Stefani, D., Wieckowski, M. R., Cavagna, D., et al. (2006). Chaperone-mediated coupling of endoplasmic reticulum and mitochondrial Ca2+ channels. *J. Cell Biol.* 175, 901–911. doi: 10.1083/jcb.200608073

Tambini, M. D., Pera, M., Kanter, E., Yang, H., Guardia-Laguarta, C., Holtzman, D., et al. (2016). ApoE4 upregulates the activity of mitochondria-associated ER membranes. *EMBO Rep.* 17, 27–36. doi: 10.15252/embr.201540614

Tatsuta, T., Scharwey, M., and Langer, T. (2014). Mitochondrial lipid trafficking. *Trends Cell Biol.* 24, 44–52. doi: 10.1016/j.tcb.2013.07.011

Wang, C., Ma, H., Feng, X., Xie, S., and Chan, P. (2010). Parkin dosage mutations in patients with early-onset sporadic and familial Parkinson's disease in Chinese: an independent pathogenic role. *Brain Res.* 1358, 30–38. doi: 10.1016/j.brainres.2010.08.060

Xu, H., Guan, N., Ren, Y. L., Wei, Q. J., Tao, Y. H., Yang, G. S., et al. (2018). IP3R-Grp75-VDAC1-MCU calcium regulation axis antagonists protect podocytes from apoptosis and decrease proteinuria in an Adriamycin nephropathy rat model. *BMC Nephrol.* 19:140. doi: 10.1186/s12882-018-0940-3

Yang, Z., Zhao, X., Xu, J., Shang, W., and Tong, C. (2018). A novel fluorescent reporter detects plastic remodeling of mitochondria-ER contact sites. *J. Cell Sci.* 131:jcs208686. doi: 10.1242/jcs.208686

Yuan, L., Liu, Q., Wang, Z., Hou, J., and Xu, P. (2019). EI24 tethers endoplasmic reticulum and mitochondria to regulate autophagy flux. *Cell Mol. Life Sci.* 77, 1591–1606. doi: 10.1007/s00018-019-03236-9

Zampese, E., Fasolato, C., Kipanyula, M. J., Bortolozzi, M., Pozzan, T., and Pizzo, P. (2011). Presenilin 2 modulates endoplasmic reticulum (ER)-mitochondria interactions and Ca2+ cross-talk. *Proc. Natl. Acad. Sci. U.S.A.* 108, 2777–2782. doi: 10.1073/pnas.1100735108

Zhao, Y. G., Liu, N., Miao, G., Chen, Y., Zhao, H., and Zhang, H. (2018). The ER contact proteins VAPA/B interact with multiple autophagy proteins to modulate autophagosome biogenesis. *Curr. Biol.* 28, 1234.e4–1245.e4.

Conflict of Interest: The authors declare that the research was conducted in the absence of any commercial or financial relationships that could be construed as a potential conflict of interest.

frontiers in Cell and Developmental Biology

REVIEW
published: 23 June 2020
doi: 10.3389/fcell.2020.00512

Peroxisomal Membrane Contact Sites in Mammalian Cells

Chao Chen[1†], Jing Li[2†], Xuhui Qin[3†] and Wei Wang[3]*

[1] Department of Orthopaedics, Union Hospital, Tongji Medical College, Huazhong University of Science and Technology, Wuhan, China, [2] Department of Integrated Traditional Chinese and Western Medicine, Tongji Hospital, Tongji Medical College, Huazhong University of Science and Technology, Wuhan, China, [3] Department of Human Anatomy, School of Basic Medicine, Tongji Medical College, Huazhong University of Science and Technology, Wuhan, China

Peroxisomes participate in essential cellular metabolic processes, such as oxidation of fatty acids (FAs) and maintenance of reactive oxygen species (ROS) homeostasis. Peroxisomes must communicate with surrounding organelles to exchange information and metabolites. The formation of membrane contact sites (MCSs), where protein-protein or protein-lipid complexes tether the opposing membranes of two organelles, represents an essential means of organelle crosstalk. Peroxisomal MCS (PO-MCS) studies are emerging but are still in the early stages. In this review, we summarize the identified PO-MCSs with the ER, mitochondria, lipid droplets, and lysosomes in mammalian cells and discuss their tethering mechanisms and physiological roles. We also highlight several features of PO-MCSs that may help future studies.

Keywords: peroxisomes, membrane contact sites, tethering complexes, metabolism, organelle crosstalk

OPEN ACCESS

Edited by:
Laura Lackner, Northwestern University, United States

Reviewed by:
Michael Schrader, University of Exeter, United Kingdom
Markus Islinger, Heidelberg University, Germany
Marc Fransen, KU Leuven, Belgium

***Correspondence:**
Wei Wang
wekle@hust.edu.cn

[†] These authors have contributed equally to this work

Specialty section:
This article was submitted to Molecular Medicine, a section of the journal Frontiers in Cell and Developmental Biology

Received: *26 January 2020*
Accepted: *28 May 2020*
Published: *23 June 2020*

Citation:
Chen C, Li J, Qin X and Wang W (2020) Peroxisomal Membrane Contact Sites in Mammalian Cells. Front. Cell Dev. Biol. 8:512. doi: 10.3389/fcell.2020.00512

Peroxisomes are essential single-membrane-bound organelles present in virtually all eukaryotic cells (Smith and Aitchison, 2013). Peroxisomes play indispensable roles in both catabolic (degradative) and anabolic (biosynthetic) metabolism through the enzymes located in the peroxisomal matrix (Waterham et al., 2016). The primary catabolic pathways include the oxidation of fatty acids (FAs) and the detoxification of glyoxylates. The main anabolic pathways include the biosynthesis of bile acids, ether phospholipids, and docosahexaenoic acids. In addition, peroxisomes are involved in the production and decomposition of reactive oxygen species (ROS), which is partly coupled to the above peroxisomal metabolic pathways. Peroxisomes can serve as signaling platforms for antiviral innate immunity (Cook et al., 2019), and ROS modulated mTORC1 activity (Zhang et al., 2013, 2015).

Peroxisome deficiency causes severe human diseases, emphasizing the crucial role of peroxisomes. The diseases fall into two main categories: single peroxisomal enzyme deficiencies and peroxisome biogenesis disorders (PBDs) (Waterham et al., 2016). PBDs are inherited in an autosomal recessive manner and affect the overall assembly and function of peroxisomes. Patients with Zellweger syndrome (ZS), the most severe form of PBDs, fail to make any developmental progress and die at an early age (Suzuki et al., 2001). Depending on the organism, tissue, cell type, and environmental factors, the functions of peroxisomes can change to meet the metabolic needs of cells (Mast et al., 2020).

Organelles are cellular compartments that perform specific enzymatic reactions. However, organelles cannot exert their activities alone and must exchange information and metabolites with others to coordinate cellular functions. Several mechanisms have been proposed for this crosstalk, including vesicular trafficking and signal transduction pathways (Shai et al., 2016). Accumulating studies now show that membrane contact sites (MCSs) represent a fast and efficient way to

communicate between organelles (Prinz et al., 2020). A bona fide MCS is defined as follows: (1) close apposition (10∼30 nm) of the membranes from two tethered organelles; (2) lack of membrane fusion or transient hemifusion may occur; (3) enrichment of specific proteins and/or lipids at the MCS; and (4) regulation of the composition and/or function of one or two of the organelles (Prinz, 2014).

For many years, electron microscopy (EM) studies in fungi, plants, and mammals revealed that peroxisomal membranes are juxtaposed to many other organelles, such as the ER, lipid droplets (LDs), plasma membrane (PM), mitochondria, and chloroplasts (Schrader et al., 2013). The simultaneous fluorescent labeling of six organelles in COS-7 cells reveals that peroxisomes associate with the ER, mitochondria, LDs, the Golgi, and lysosomes (Valm et al., 2017). To date, the tethering complexes and physiological roles of peroxisomal MCSs (PO-MCSs) with the ER, mitochondria, LDs, and lysosomes have been investigated in mammalian cells (Castro et al., 2018; Sargsyan and Thoms, 2020; Schrader et al., 2020). In this review, we focus on these identified PO-MCSs in mammalian cells and discuss several features of PO-MCSs.

PEROXISOME-ER-MCSs

In human cells, the biosynthesis of unsaturated FAs, sterols, ether phospholipids, and bile acids involves both the ER and peroxisomes and requires intimate crosstalk. Metabolic defects in these organelles lead to severe human diseases (Schrader et al., 2013). The ER represents the largest membrane-bound organelle in eukaryotic cells and forms MCSs with many other organelles, including peroxisomes. Although peroxisome-ER (PO-ER) associations were identified by EM in mammalian cells nearly 50 years ago (Novikoff and Novikoff, 1972), the MCSs mediating their crosstalk remained elusive.

Acyl-CoA binding domain containing 5 (ACBD5) is a peroxisomal tail-anchored membrane protein, and its deficiency can cause a defect in peroxisomal very-long-chain FA metabolism (Ferdinandusse et al., 2017). ACBD5 and its fungal ortholog, ATG37, have been suggested to play critical roles in phagophore formation during pexophagy (Nazarko et al., 2014). VAPA and VAPB (VAPA/B) are tail-anchored and ER vesicle-associated membrane proteins. These proteins can act as the MCS tether through the major sperm protein (MSP) domain that interacts with the two phenylalanines in an acidic tract (FFAT) motif of client proteins localized in the opposing organelles (Lev et al., 2008). Two independent studies showed that the tether ACBD5-VAPA/B mediates the formation of PO-ER-MCS (Costello et al., 2017a; Hua et al., 2017; **Figure 1A**).

In these studies, super-resolution microscopy and EM visualization revealed that the two organelles were in proximity to each other. Cooverexpression of ACBD5 and VAPA/B or their knockdowns increases and decreases MCS formation, respectively, suggesting that tethering relies on the ACBD5-VAPA/B interaction. As shown for other VAPA/B interacting proteins, ACBD5 interacts with the MSP domain of VAPA/B through the FFAT motif. ACBD4, a second ACBD family protein, also interacts with VAPB for PO-ER associations (Costello et al., 2017b; **Figure 1A**).

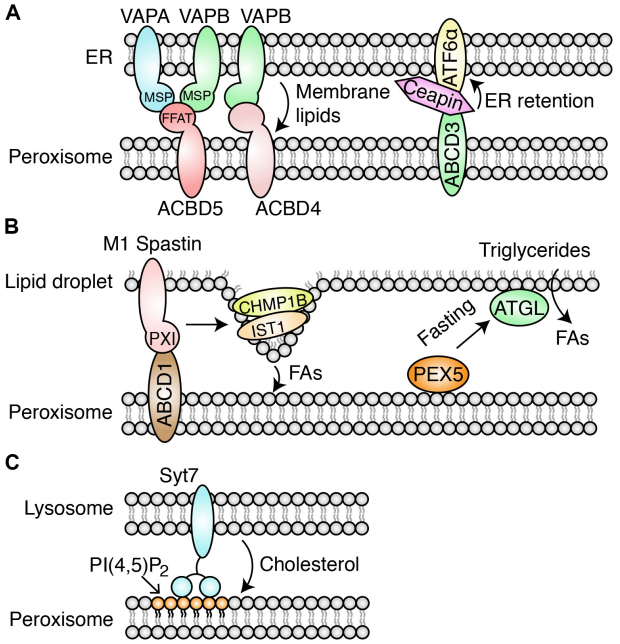

FIGURE 1 | Identified PO-MCSs in mammalian cells. **(A)** PO-ER-MCS. At the MCS, the FFAT motif in ACBD5 interacts with the MSP domain in VAPA/B. The ACBD4/5-VAPA/B-tethered MCS facilitates lipid transfer from the ER to peroxisomes and promotes the expansion of peroxisomal membranes. Ceapin sequesters ATF6α at the ER by tethering ATF6α to peroxisomal ABCD3. **(B)** PO-LD-MCS. M1 Spastin interacts with ABCD1 through the peroxisome-interacting (PXI) region. M1 Spastin recruits the ESCRT-III subunits IST1 and CHMP1B to the surface of LDs to promote FA trafficking through the MCS. ATGL is recruited to the MCS by PEX5 in response to fasting stress, promoting lipolysis of triglycerides stored in LDs. **(C)** PO-Lyso-MCS mediated by $PI(4,5)P_2$ and Syt7. This MCS facilitates cholesterol trafficking from lysosomes to peroxisomes.

Peroxisomes can proliferate through the growth and division model, which involves membrane elongation, constriction, and fission (Schrader et al., 2012). Since peroxisomes share division proteins with mitochondria (e.g., DRP1, MFF, and FIS1) (Smith and Aitchison, 2013) and ER-MCSs have been shown to mark mitochondrial or endosomal fission sites and modulate their division (Friedman et al., 2011; Rowland et al., 2014), it is reasonable to hypothesize that PO-ER-MCSs play a role in peroxisome division. However, peroxisome biogenesis is unaffected in ACBD5-deficient cells (Ferdinandusse et al., 2017; Yagita et al., 2017), and peroxisome morphology is normal in cells with reduced PO-ER-MCSs due to ACBD5/VAP silencing (Costello et al., 2017a; Hua et al., 2017). These results suggest that the ACBD5-VAPA/B tethered MCSs may not play a role in peroxisome division.

The phospholipid contents of peroxisome membranes are rich in phosphatidylcholine (PC) and phosphatidylethanolamine (PE), similar to the contents of the ER (Hardeman et al., 1990). The peroxisome is unable to generate membrane lipids locally because it does not contain biosynthesis enzymes. MFF

and DRP1 are two crucial molecules involved in peroxisome and mitochondrion fission, and their deficiencies result in pronounced elongation of the two organelles, likely through a constant transfer of lipids from the ER to peroxisomes (Schrader et al., 2012). It has been found that disrupting the ACBD5-VAPA/B tethered MCS in MFF- or DRP1-deficient cells significantly inhibited the elongation of peroxisomes but not of mitochondria, suggesting that the MCS may supply the lipids required for peroxisome membrane expansion.

Both groups found that disrupting the ACBD5-VAPA/B tethered MCS increases the movement of peroxisomes, suggesting that the MCS negatively regulates peroxisome motility through ER anchoring. A motility-restricting role is also indicated for the yeast PO-ER-MCS, which can retain a fraction of peroxisomes by anchoring with the ER in mother cells when peroxisomes passage into the daughter cells (Knoblach et al., 2013). In addition, Hua et al. (2017) found a potential role of PO-ER-MCSs in the synthesis of plasmalogen phospholipids and the maintenance of cellular cholesterol levels. VAP proteins also play roles in lipid transfer at ER-MCSs with other organelles, such as the Golgi, mitochondria, and LDs (Kamemura and Chihara, 2019). Expression of an artificial PO-ER tether without any functional domain partially restored peroxisomal membrane expansion after ACBD5 silencing (Costello et al., 2017a), suggesting that VAPA/B and ACBD5 do not play an active lipid-transferring role in PO-ER-MCSs. Deficiency in both the ACBD5 and VAPB genes has been implicated in human disorders, emphasizing the significance of the identified PO-ER-MCSs (Kim et al., 2010; Abu-Safieh et al., 2013; Ferdinandusse et al., 2017; Yagita et al., 2017).

Other PO-ER-MCSs have also been identified. The MCS tethered by the peroxisomal PI(4,5)P2 and ER-resident extended synaptotagmins (E-Syts) may facilitate the transport of cholesterol from the peroxisome to the downstream ER organelle (Xiao et al., 2019). ATF6α is an unfolded protein response (UPR) sensor, which traffics to the Golgi apparatus for proteolysis and its subsequent movement to the nucleus for transcriptional activation during ER stress (Haze et al., 1999). A genome-wide CRISPR interference screening revealed that the drug Ceapin induces PO-ER-MCS formation by forcing the interaction between ATF6α and the peroxisomal transmembrane protein ABCD3 (Torres et al., 2019). The ATF6α-ABCD3 interaction sequesters ATF6α at the ER and inhibits its activity as the UPR sensor (**Figure 1A**). Notably, the MCS does not require the known ACBD4/5-VAPA/B tether. The study suggests that Ceapin may be used for the treatment of cancer, since cancer development relies on active ATF6α signaling; this finding presents a novel drug-development strategy for targeting the MCS.

PEROXISOME-MITOCHONDRION-MCSs

Peroxisomes and mitochondria must communicate with each other to meet the metabolic needs of cells. The best examples are illustrated by the β-oxidation of FAs and metabolism of ROS (discussed below). These processes share some crucial division proteins (Delille et al., 2009), de novo biogenesis of peroxisomes relies on mitochondrion-derived vesicles (Sugiura et al., 2017), and these organelles function cooperatively in antiviral signaling and defense (Kagan, 2012). In addition, defective mitochondria are observed in several peroxisomal disorders (Baumgart et al., 2001; Lopez-Erauskin et al., 2013).

In the 1970s, a close spatial peroxisome-mitochondrion (PO-Mito) association was observed in the myocardium of rodents and primates by a peroxidative catalase activity-based alkaline DAB staining method (Hicks and Fahimi, 1977). Overexpression of PEX11β, a critical peroxisome division factor, induces the formation of mitochondrion-interacting membrane protrusions (Kustatscher et al., 2019). The PO-Mito interaction increases when cells are infected with an RNA virus, suggesting a critical role of PO-Mito-MCSs in RNA virus infections (Horner et al., 2011). The role of PO-Mito-MCSs has been implicated in the transfer of metabolites involved in steroid biosynthesis in mouse Leydig tumor cells (Fan et al., 2016). This study suggests that the tethering complex consists of a splice isoform of an acyl-CoA binding domain-containing protein, enoyl-CoA δ isomerase 2 (ACBD2/ECI2). However, as ACBD2/ECI2 proteins are transported into the matrix of both mitochondria and peroxisomes, their tethering role needs further investigation.

Both peroxisomes and mitochondria possess separate β-oxidation pathways in mammalian cells, which are different from those in yeast and plants, whose peroxisomes are the sole organelles for β-oxidation of FAs. The enzymatic steps of β-oxidation of FAs in these two organelles are similar but differ in the catalyzed substrates. For example, peroxisomes preferentially catalyze the β-oxidation of very-long-chain FAs, while the mitochondrial β-oxidation system catalyzes medium and long-chain FAs. The chain-shortened FAs, as well as the acetyl-CoA generated through peroxisomal β-oxidation, need to be directed to mitochondria for further oxidation and ATP production. Different mechanisms have been proposed for the transfer of these metabolites, including the carnitine system, membrane pores, and vesicular transport (Antonenkov and Hiltunen, 2012; Sugiura et al., 2014). A high content screening approach for PO-MCSs in yeast suggests that the tethering complex (Pex11, Fzo1, and Pex34) contributes to PO-Mito-MCS formation, which facilitates the transfer of β-oxidation products (Shai et al., 2018). The conserved function of mammalian PO-Mito-MCS remains to be determined.

In addition, both organelles contain pro-oxidant and antioxidant systems. Increasing evidence demonstrates that these organelles undergo intimate crosstalk during cellular redox metabolism (Fransen and Lismont, 2018). For example, inhibition of the peroxisomal antioxidant enzyme catalase or excess ROS generation in peroxisomes disrupts mitochondrial redox (Walton and Pizzitelli, 2012; Wang et al., 2013). Expression of peroxisome-targeted PRDX5 (Peroxiredoxin-5) protects cells from the oxidative insults generated from mitochondria (Walbrecq et al., 2015). The ER-Mito-MCS has been shown to transfer ER-derived ROS to mitochondria, causing the cell to be sensitive to mitochondrial apoptosis (Verfaillie et al., 2012). ER-Mito-MCS-mediated Ca^{2+} transfer stimulates ROS translocation from mitochondria to the MCS. The local H_2O_2

enrichment at the MCS further augments the ER-Mito $Ca2^+$ flux, likely through H_2O_2-mediated oxidation of specific thiol groups of the pump receptor IP3 (Booth et al., 2016). To date, no studies have shown the role of PO-Mito-MCS in redox crosstalk. It is tempting to speculate that such a PO-Mito-MCS exists for maintaining cellular redox balance.

The above results suggest that MCSs play critical roles in PO-Mito crosstalk. However, the mechanism of PO-Mito-MCSs remains elusive. Future studies identifying the tethering components would increase our understanding of PO-Mito crosstalk.

PEROXISOME-LIPID DROPLET-MCSs

Lipid droplets are essential and significant lipid storage organelles for neutral lipids, such as triacylglycerol and cholesterol ester. The lipids must be imported into oxidative organelles, such as mitochondria and peroxisomes, for β-oxidation to enable cellular homeostasis (Thiam and Dugail, 2019). Indeed, aberrant FA metabolism in LDs is implicated in severe physiological disorders, including lipodystrophy and neurological diseases (Welte, 2015). Defective FA metabolism in peroxisomes causes an accumulation of LDs, as found in patients with peroxisomal disorders (Schaumburg et al., 1972; Engelen et al., 2012). Changes in the number and size of LDs are observed in peroxisome-deficient mice (Baes et al., 1997; Dirkx et al., 2005). These results suggest that the two organelles need to cooperate to maintain cellular homeostasis. Two recent studies find that they communicate through the peroxisome-lipid droplet (PO-LD)-MCSs as follows (Chang et al., 2019; Kong et al., 2020).

Spastin is a microtubule-severing protein that belongs to the AAA (ATPases Associated with various cellular Activities) family. The longer M1 variant (M1 Spastin) encodes an N-terminal hydrophobic hairpin motif, which targets M1 Spastin to LDs (Errico et al., 2002). Chang et al. (2019) demonstrated that M1 Spastin forms a tethering complex with the peroxisome membrane protein ABCD1 to maintain the PO-LD MCS for FA trafficking from LDs to peroxisomes. M1 Spastin also recruits the curvature-generating ESCRT III subunits IST1 and CHMP1B to the surface of LDs to promote FA trafficking (**Figure 1B**). The trafficking of FAs through the MCS prevents the accumulation of peroxidated lipids following oxidative stress (Chang et al., 2019). Spastin gene mutations are the most common cause of hereditary spastic paraplegias (HSPs), a group of inherited neurological disorders (Blackstone, 2018). The results suggest that failure to induce LD-PO-MCS formation and subsequent FA transport by the M1 Spastin mutation (K388R) may contribute to HSP (Chang et al., 2019), highlighting the critical role of PO-LD-MCS in HSP pathogenesis.

Another study revealed the role of PO-LD-MCS in regulating lipolysis, the hydrolysis of lipid metabolites stored in LDs (Kong et al., 2020). During fasting, the increase in PO-LD-MCSs facilitates the spatial translocation of adipose triglyceride lipase (ATGL) onto LDs for lipolysis. PEX5 recruits ATGL to the MCS, independent of its role as the receptor for the import of peroxisomal matrix proteins (**Figure 1B**). It would be interesting to investigate whether the M1 Spastin-ABCD1 complex tethers this MCS for lipolysis. Importantly, these results are verified by studies in multiple models, such as mammalian adipocytes, *Caenorhabditis elegans*, and mice. The study reveals the physiological significance of the PO-LD-MCS in maintaining energy homeostasis in response to nutritional status. As aberrant lipolysis is associated with severe metabolic diseases, such as obesity and diabetes, this study suggests PO-LD-MCSs as a potential therapeutic target for these diseases.

As discussed above, the MCS can facilitate the transport of lipids from LDs to peroxisomes for their breakdown or function as a station enriched with lipases to hydrolyze the lipids in LDs. Detection of peroxisome-derived metabolites (e.g., ether-linked lipids) in LDs suggests that they may be transferred from peroxisomes to LDs through the MCS (Bartz et al., 2007). The bidirectional transfer at the PO-LD-MCS awaits discovery.

PEROXISOME-LYSOSOME-MCSs

Lysosomes are degradative and metabolic organelles. Many essential metabolic processes, such as those for cholesterol, occur in this organelle. Cholesterol is a crucial component for maintaining the fluidity, permeability, and organization of mammalian membranes. Cholesterol is unevenly distributed in cellular membrane structures, with the highest contents (60∼80% of total cellular cholesterol) in the PM (Lange et al., 1989). The low-density lipoprotein-derived cholesteryl ester is internalized through endocytosis, hydrolyzed to unesterified cholesterol in lysosomes and further delivered to downstream organelles (Chang et al., 2006).

A genome-wide pooled shRNA screen identified a list of peroxisome genes required for cholesterol trafficking (Chu et al., 2015). These genes are either essential for peroxisome biogenesis or involved in its metabolism. These authors observed a dramatic accumulation of cholesterol in lysosomes and a significant reduction of peroxisome-lysosome (PO-Lyso)-MCS formation in cells deficient in these peroxisome genes. These authors further revealed that peroxisomal $PI(4,5)P_2$ lipid and lysosomal synaptotagmin VII (Syt7) protein tether the MCS for cholesterol trafficking from lysosome to peroxisome (Chu et al., 2015; **Figure 1C**). Time-lapse visualization reveals that the PO-Lyso-MCS is transient. Depletion and repletion of cholesterol inhibit and recover the MCS, respectively, indicating that MCS formation depends on the presence of cholesterol. The follow-up study found that PIP4K2A, a PI(5)P-kinase, contributes to the generation of peroxisomal PI(4,5)P2, enhances PO-Lyso-MCS formation, and promotes cholesterol trafficking (Hu et al., 2018).

Drastic amounts of cholesterol accumulate in the mouse model and the patient fibroblasts with peroxisomal disorders, as these authors have examined. This study suggests that part of the pathological mechanisms of peroxisomal disorders may be attributed to the blockage of cholesterol trafficking caused by defective PO-Lyso-MCS formation and may provide novel strategies for their diagnoses and treatments (Chu et al., 2015). However, as the experimental method for peroxisome purification in this study is under debate (Schrader et al., 2020)

and the study does not examine the loss of PO-Lyso-MCS in these patient fibroblasts, other mechanisms may contribute to abnormal cholesterol accumulation. Studies have shown that the initial step of plasmalogen synthesis occurs in peroxisomes and that its deficiency interferes with the transport of cholesterol from the PM or endocytic compartments to the ER (Thai et al., 2001; Munn et al., 2003). The accumulation of lysosomal cholesterol in peroxisome-deficient cells could result from insufficient plasmalogen synthesis due to loss of peroxisome functions.

In addition, lysosomes can serve as the signaling hub for the vital growth regulator mTOR. When there are sufficient nutrients, mTOR is recruited to lysosomes and activated by lysosomal Rheb proteins to promote downstream anabolism for cellular growth (Saxton and Sabatini, 2017). Interestingly, a study showed that peroxisome-localized TSC1/2 proteins function as Rheb GTPase-activating proteins to repress mTOR signaling in response to the ROS generated within peroxisomes (Zhang et al., 2013). It is unknown how mTOR signaling is coordinated in response to nutrients and oxidative stresses. The PO-Lyso-MCS enriched with Rheb proteins may fulfill such a role, similar to that proposed for the lysosome-Golgi-MCS in the activation of mTOR signaling (Hao et al., 2018). However, TSC1/2 proteins were not detected in several proteomic studies of purified peroxisomes (Yifrach et al., 2018), and they dissociate from the lysosomes to the cytosol upon insulin stimulation, resulting in Rheb-mediated mTORC1 activation at lysosomes (Menon et al., 2014). These findings do not support the role of PO-Lyso-MCS in modulating mTORC1 signaling, as hypothesized above.

PO-MCSs WITH OTHER ORGANELLES

In addition, PO-MCSs with other organelles have been indicated. Peroxisomes move to the cell periphery near the PM by ACBD5 overexpression in neurons. This peroxisome redistribution does not depend on the interaction of ACBD5 with VAPs, suggesting that other ACBD5 interacting proteins may tether peroxisomes to PM (Wang et al., 2018). Live imaging of fusion cells expressing peroxisomal proteins fused to different fluorescence tags reveals that peroxisomes can interact with each other in a transient and long-term manner. The contact does not promote the exchange of matrix and membrane proteins, FAs, and H_2O_2 (Bonekamp et al., 2012). Global analysis of the organelle interactome reveals that peroxisomes contact the Golgi, in addition to the ER, mitochondria, LDs, and lysosomes (Valm et al., 2017). With more PO-contacting organelles being identified, their tethering components and functions remain to be characterized.

DISCUSSION

The MCSs open an avenue for peroxisomes to communicate with other organelles for diverse purposes, including organelle positioning, lipid supply for membrane elongation, and metabolism coordination, as discussed above. However, MCSs are much more complicated than initially thought. We highlight and discuss several features of PO-MCSs that may help future studies.

Heterogeneity of Peroxisomes

Peroxisomes are heterogeneous in terms of their number, morphology, distribution, and composition in different cells or environmental settings (Mast et al., 2020). For example, the number of peroxisomes increases when rodents are administered fibrate derivatives but decreases rapidly upon withdrawal of the drugs (Fahimi et al., 1982; Yokota, 1986; Yokota, 1993). Enveloped virus infection induces significant peroxisome biogenesis, promoting phospholipid plasmalogen synthesis for virus production (Jean Beltran et al., 2018). Peroxisomes also display heterogeneity in the same cell. An example is that two populations of peroxisomes that contain different ratios of lipid β-oxidation enzymes to catalase are isolated in HepG2 cells (Schrader et al., 1994). The population containing higher contents of β-oxidation enzymes may favor PO-MCSs for FA metabolism. In contrast, those with higher catalases may prefer MCSs for ROS crosstalk. Hence, PO-MCSs may differ in terms of their tethering mechanisms and functions under these varying conditions, and selecting an appropriate cell or animal model would facilitate PO-MCS studies.

Unconventional PO-MCSs

The identified PO-MCSs are tethered through different protein-protein or protein-lipid complexes and manifest a variety of physiological roles. In addition, as each cellular organelle has a unique structure, the mode of PO-MCS formation may be organelle-specific, as discussed below.

Mitochondria are surrounded by double membranes, which separate the organelle into two compartments, the intermembrane space and the matrix. Peroxisomes may contact the outer membranes, as shown for the ER-Mito MCS (Murley and Nunnari, 2016). This MCS may indirectly facilitate metabolic exchange with the matrix through transporters located at the inner membranes. Alternatively, it is tempting to speculate that the PO-tethering complexes may extend into the inner membranes to facilitate the exchange of metabolites.

Compared to bilayer-bound organelles, LDs have phospholipid monolayer membranes that surround the lipid core. This unique monolayer of LDs may be continuous with the outer leaflet of the bilayer of apposing organelles, as has been shown for ER-LD-MCS (Wang et al., 2016). This MCS does not exist between bilayer membranes and is distinct from the traditional MCS. In yeast, PO-LD-MCS formation increases in peroxisome-inducing conditions. The MCSs are enriched in β-oxidation enzymes, suggesting their roles in FA transfer from LDs to peroxisomes. At these MCSs, peroxisomal protrusions extend into the core of LDs, likely representing the "bridging contact" (Binns et al., 2006). It remains to be investigated whether peroxisomes form such a "bridging contact" with LDs in mammalian cells.

The Components at the PO-MCSs

The identified PO-MCSs are tethered through the protein-protein or protein-lipid complexes present on the opposing membranes of the organelles. The tethering complexes may play additional roles in the MCSs. For example, the tether M1

Spastin also recruits membrane curvature-shaping proteins to promote lipid transfer at the PO-LD-MCS (Chang et al., 2019). The identified peroxisomal tethers play MCS-independent roles, such as in metabolic/enzymatic activities. Hence, to elucidate whether the phenotype is solely caused by defective PO-MCS formation, it is necessary to test if a mutant defective in its tethering activity but maintaining other activities inhibits PO-MCS functions. Multiple tethering pairs may also exist for the PO-MCS, as shown for the PO-ER-MCSs as discussed above and for other organelle MCS (Scorrano et al., 2019). In this scenario, loss of the identified PO-MCS tether does not necessarily reduce their contacts and/or functions because of the redundancy of the tethering complexes. In addition, other effector proteins may be enriched at the MCSs to regulate MCS formation or facilitate the exchange of metabolites (Scorrano et al., 2019). As discussed above, ATGL can be grouped as the effector protein that promotes lipolysis at the PO-LD-MCS during fasting (Kong et al., 2020).

Although some components of the PO-MCS have been elucidated as discussed above, many questions remain to be answered. Elucidating components, such as tethering complexes and effector proteins, at PO-MCSs is a major challenge but will profoundly increase our understanding of PO-MCSs.

Coordination of PO-MCSs With Multiple Organelles

Membrane contact sites do not function alone. MCSs must be integrated and coordinated in response to the changing cellular environment. Peroxisomes can contact multiple organelles simultaneously, as shown for the PO-interacting network in COS-7 cells (Valm et al., 2017). The peroxisome-contacting organelles can be shifted to other organelles in varying conditions. An example is that PO-Mito contact increases when MAM (mitochondrial associated membrane, a specialized ER subdomain)-mitochondria contacts are disrupted, resulting in a concomitant increase in IFN-β signaling during virus infection (Horner et al., 2011). We discuss three potential mechanisms for coordinating PO-MCSs with multiple organelles as follows.

A study investigated the assembly of ER-MCSs with a variety of organelles through lipid-based phase separation (King et al., 2020). By employing hypotonic cell swelling, the ER and other membrane-bound organelles can be converted into micrometer-scale large intracellular vesicles (LICVs). Upon cooling, the ER-derived LICVs phase-partition into the ER ordered (ER_o) and disordered (ER_d) lipid domains. Interestingly, they find that the PO-ER-MCS is located at the ER_o/ER_d interphase, involving association with a mitochondrion. A yeast study also found that peroxisomes contact the ER and mitochondria at the three-way junction through Pex11 interacting with Mdm34, a component of ERMES (ER-mitochondria encounter structure) (Mattiazzi Usaj et al., 2015). As the three organelles are crucial for lipid and redox metabolism, the MCS at the tri-junction interface may allow efficient transfer of these metabolites among them. Hence, establishing PO-MCSs at the junction interface may coordinate peroxisome crosstalk with multiple organelles to meet metabolic needs.

Membrane contact site coordination can be achieved through the regulation of common tethering molecules (Harper et al., 2020). For example, in yeast, the tethering proteins Lam6 and Vps13 proteins are present at multiple contact sites, and they shift from one MCS to the other in response to changing carbon sources (Elbaz-Alon et al., 2015; Lang et al., 2015). As discussed above, The ER-localized VAPA/B proteins act as tethers with many other organelles, including peroxisomes (Eisenberg-Bord et al., 2016) and the $PI(4,5)P_2$ lipid at peroxisomal membranes tethers peroxisomes to both lysosomes and the ER. Regulation of these common PO tethers, such as VAPA/B and $PI(4,5)P_2$, may provide mechanistic hints for PO-MCS coordination.

The movement of peroxisomes in mammalian cells preferentially depends on the microtubular network and allows peroxisomes to be uniformly dispersed for metabolism (Neuhaus et al., 2016). PO-LD-MCS depends on the motility of peroxisomes along microtubules through the kinesin-like motor KifC3 to promote lipolysis under fasting stress conditions (Kong et al., 2020). Microtubule disruption by nocodazole treatment in COS-7 cells decreases peroxisome contacts with all the examined organelles (the ER, mitochondria, LDs, Golgi, and lysosomes) (Valm et al., 2017). These studies suggest that organelle motility is critical for PO-MCS formation. In turn, the MCSs regulate the movement and position of peroxisomes, exemplified by the role of PO-ER-MCS in restricting peroxisome motility, as discussed above. Peroxisomes can hitchhike on the microtubule-based motor machinery of endosomes for long-range movements through PO-endosome-MCSs in the filamentous fungus *Aspergillus nidulans*. Given the crucial role of microtubules in organizing a variety of organelle contacts and the reciprocal relationships between organelle motility and contact (de Forges et al., 2012; Valm et al., 2017), it is tempting to speculate that modulating the microtubular network can serve as another strategy for PO-MCS coordination.

CONCLUDING REMARKS

In summary, the vital importance of peroxisomes is underscored not only by the essential metabolism within this organelle but also by the intimate crosstalk with other organelles. MCS formation is an efficient means by which peroxisomes communicate with other organelles. Some of the tethering mechanisms and physiological functions have been elucidated or suggested. These studies have increased our understanding of not only peroxisomes but also other organelles, including their biogenesis/turnover and metabolic functions. However, these studies are still in the early phase, and much that is unknown remains to be addressed. Future PO-MCS studies would shed novel insights into human diseases and determine their therapeutic targets.

AUTHOR CONTRIBUTIONS

CC, JL, and XQ wrote the draft of the manuscript. WW drew the figure and organized and proofread the manuscript. All authors contributed to the article and approved the submitted version.

FUNDING

This work was supported by the National Natural Science Foundation of China (Nos. 81903016 and 81904024).

ACKNOWLEDGMENTS

The authors apologize for any citations absent due to space constraints.

REFERENCES

Abu-Safieh, L., Alrashed, M., Anazi, S., Alkuraya, H., Khan, A. O., Hashem, M., et al. (2013). Autozygome-guided exome sequencing in retinal dystrophy patients reveals pathogenetic mutations and novel candidate disease genes. *Genome Res.* 23, 236–247. doi: 10.1101/gr.144105.112

Antonenkov, V. D., and Hiltunen, J. K. (2012). Transfer of metabolites across the peroxisomal membrane. *Biochim. Biophys. Acta* 1822, 1374–1386. doi: 10.1016/j.bbadis.2011.12.011

Baes, M., Gressens, P., Baumgart, E., Carmeliet, P., Casteels, M., Fransen, M., et al. (1997). A mouse model for Zellweger syndrome. *Nat. Genet.* 17, 49–57.

Bartz, R., Li, W. H., Venables, B., Zehmer, J. K., Roth, M. R., Welti, R., et al. (2007). Lipidomics reveals that adiposomes store ether lipids and mediate phospholipid traffic. *J. Lipid Res.* 48, 837–847. doi: 10.1194/jlr.m600413-jlr200

Baumgart, E., Vanhorebeek, I., Grabenbauer, M., Borgers, M., Declercq, P. E., Fahimi, H. D., et al. (2001). Mitochondrial alterations caused by defective peroxisomal biogenesis in a mouse model for Zellweger syndrome (PEX5 knockout mouse). *Am. J. Pathol.* 159, 1477–1494. doi: 10.1016/s0002-9440(10)62534-5

Binns, D., Januszewski, T., Chen, Y., Hill, J., Markin, V. S., and Zhao, Y. (2006). An intimate collaboration between peroxisomes and lipid bodies. *J. Cell Biol.* 173, 719–731. doi: 10.1083/jcb.200511125

Blackstone, C. (2018). Converging cellular themes for the hereditary spastic paraplegias. *Curr. Opin. Neurobiol.* 51, 139–146. doi: 10.1016/j.conb.2018.04.025

Bonekamp, N. A., Sampaio, P., Luers, G. H., and Schrader, M. (2012). Transient complex interactions of mammalian peroxisomes without exchange of matrix or membrane marker proteins. *Traffic* 13, 960–978. doi: 10.1111/j.1600-0854.2012.01356.x

Booth, D. M., Enyedi, B., Geiszt, M., Varnai, P., and Hajnoczky, G. (2016). Redox nanodomains are induced by and control calcium signaling at the ER-mitochondrial interface. *Mol. Cell* 63, 240–248. doi: 10.1016/j.molcel.2016.05.040

Castro, I. G., Schuldiner, M., and Zalckvar, E. (2018). Mind the organelle gap - peroxisome contact sites in disease. *Trends Biochem. Sci.* 43, 199–210. doi: 10.1016/j.tibs.2018.01.001

Chang, C. L., Weigel, A. V., Ioannou, M. S., Pasolli, H. A., Xu, C. S., and Peale, D. R. (2019). Spastin tethers lipid droplets to peroxisomes and directs fatty acid trafficking through ESCRT-III. *J. Cell Biol.* 218, 2583–2599. doi: 10.1083/jcb.201902061

Chang, T. Y., Chang, C. C., Ohgami, N., and Yamauchi, Y. (2006). Cholesterol sensing, trafficking, and esterification. *Annu. Rev. Cell Dev. Biol.* 22, 129–157. doi: 10.1146/annurev.cellbio.22.010305.104656

Chu, B. B., Liao, Y. C., Qi, W., Xie, C., Du, X., Wang, J., et al. (2015). Cholesterol transport through lysosome-peroxisome membrane contacts. *Cell* 161, 291–306. doi: 10.1016/j.cell.2015.02.019

Cook, K. C., Moreno, J. A., Jean Beltran, P. M., and Cristea, I. M. (2019). Peroxisome plasticity at the virus-host interface. *Trends Microbiol.* 27, 906–914. doi: 10.1016/j.tim.2019.06.006

Costello, J. L., Castro, I. G., Hacker, C., Schrader, T. A., Metz, J., Zeuschner, D., et al. (2017a). ACBD5 and VAPB mediate membrane associations between peroxisomes and the ER. *J. Cell Biol.* 216, 331–342. doi: 10.1083/jcb.201607055

Costello, J. L., Castro, I. G., Schrader, T. A., Islinger, M., and Schrader, M. (2017b). Peroxisomal ACBD4 interacts with VAPB and promotes ER-peroxisome associations. *Cell Cycle* 16, 1039–1045. doi: 10.1080/15384101.2017.1314422

de Forges, H., Bouissou, A., and Perez, F. (2012). Interplay between microtubule dynamics and intracellular organization. *Int. J. Biochem. Cell Biol.* 44, 266–274. doi: 10.1016/j.biocel.2011.11.009

Delille, H. K., Alves, R., and Schrader, M. (2009). Biogenesis of peroxisomes and mitochondria: linked by division. *Histochem. Cell Biol.* 131, 441–446. doi: 10.1007/s00418-009-0561-9

Dirkx, R., Vanhorebeek, I., Martens, K., Schad, A., Grabenbauer, M., Fahimi, D., et al. (2005). Absence of peroxisomes in mouse hepatocytes causes mitochondrial and ER abnormalities. *Hepatology* 41, 868–878. doi: 10.1002/hep.20628

Eisenberg-Bord, M., Shai, N., Schuldiner, M., and Bohnert, M. (2016). A tether is a tether is a tether: tethering at membrane contact sites. *Dev. Cell* 39, 395–409. doi: 10.1016/j.devcel.2016.10.022

Elbaz-Alon, Y., Eisenberg-Bord, M., Shinder, V., Stiller, S. B., Shimoni, E., Wiedemann, N., et al. (2015). Lam6 regulates the extent of contacts between organelles. *Cell Rep.* 12, 7–14. doi: 10.1016/j.celrep.2015.06.022

Engelen, M., Kemp, S., de Visser, M., van Geel, B. M., Wanders, R. J., and Aubourg, P. (2012). X-linked adrenoleukodystrophy (X-ALD): clinical presentation and guidelines for diagnosis, follow-up and management. *Orphanet J. Rare Dis.* 7:51. doi: 10.1186/1750-1172-7-51

Errico, A., Ballabio, A., and Rugarli, E. I. (2002). Spastin, the protein mutated in autosomal dominant hereditary spastic paraplegia, is involved in microtubule dynamics. *Hum. Mol. Genet.* 11, 153–163. doi: 10.1093/hmg/11.2.153

Fahimi, H. D., Reinicke, A., Sujatta, M., Yokota, S., Ozel, M., Hartig, F., et al. (1982). The short- and long-term effects of bezafibrate in the rat. *Ann. N. Y. Acad. Sci.* 386, 111–135. doi: 10.1111/j.1749-6632.1982.tb21410.x

Fan, J., Li, X., Issop, L., Culty, M., and Papadopoulos, V. (2016). ACBD2/ECI2-mediated peroxisome-mitochondria interactions in leydig cell steroid biosynthesis. *Mol. Endocrinol.* 30, 763–782. doi: 10.1210/me.2016-1008

Ferdinandusse, S., Falkenberg, K. D., Koster, J., Mooyer, P. A., Jones, R., and Waterham, H. R. (2017). ACBD5 deficiency causes a defect in peroxisomal very long-chain fatty acid metabolism. *J. Med. Genet.* 54, 330–337. doi: 10.1136/jmedgenet-2016-104132

Fransen, M., and Lismont, C. (2018). Peroxisomes and cellular oxidant/antioxidant balance: protein redox modifications and impact on inter-organelle communication. *Subcell. Biochem.* 89, 435–461. doi: 10.1007/978-981-13-2233-4_19

Friedman, J. R., Lackner, L. L., West, M., DiBenedetto, J. R., Nunnari, J., and Voeltz, G. K. (2011). ER tubules mark sites of mitochondrial division. *Science* 334, 358–362. doi: 10.1126/science.1207385

Hao, F., Kondo, K., Itoh, T., Ikari, S., Nada, S., Okada, M., et al. (2018). Rheb localized on the Golgi membrane activates lysosome-localized mTORC1 at the Golgi-lysosome contact site. *J. Cell Sci.* 131:jcs208017.

Hardeman, D., Zomer, H. W., Schutgens, R. B., Tager, J. M., and van den Bosch, H. (1990). Effect of peroxisome proliferation on ether phospholipid biosynthesizing enzymes in rat liver. *Int. J. Biochem.* 22, 1413–1418. doi: 10.1016/0020-711x(90)90231-q

Harper, C. S., White, A. J., and Lackner, L. L. (2020). The multifunctional nature of mitochondrial contact site proteins. *Curr. Opin. Cell Biol.* 65, 58–65. doi: 10.1016/j.ceb.2020.02.010

Haze, K., Yoshida, H., Yanagi, H., Yura, T., and Mori, K. (1999). Mammalian transcription factor ATF6 is synthesized as a transmembrane protein and activated by proteolysis in response to endoplasmic reticulum stress. *Mol. Biol. Cell* 10, 3787–3799. doi: 10.1091/mbc.10.11.3787

Hicks, L., and Fahimi, H. D. (1977). Peroxisomes (microbodies) in the myocardium of rodents and primates. A comparative Ultrastructural cytochemical study. *Cell Tissue Res.* 175, 467–481.

Horner, S. M., Liu, H. M., Park, H. S., Briley, J., and Gale, M. Jr. (2011). Mitochondrial-associated endoplasmic reticulum membranes (MAM) form innate immune synapses and are targeted by hepatitis C virus. *Proc. Natl. Acad. Sci. U.S.A.* 108, 14590–14595. doi: 10.1073/pnas.1110133108

Hu, A., Zhao, X. T., Tu, H., Xiao, T., Fu, T., Wang, Y., et al. (2018). PIP4K2A regulates intracellular cholesterol transport through modulating PI(4,5)P2 homeostasis. *J. Lipid Res.* 59, 507–514. doi: 10.1194/jlr.m082149

Hua, R., Cheng, D., Coyaud, E., Freeman, S., Wang, Y., Vissa, A., et al. (2017). VAPs and ACBD5 tether peroxisomes to the ER for peroxisome maintenance and lipid homeostasis. *J. Cell Biol.* 216, 367–377. doi: 10.1083/jcb.201608128

Jean Beltran, P. M., Cook, K. C., Hashimoto, Y., Galitzine, C., Murray, L. A., Vitek, O., et al. (2018). Infection-induced peroxisome biogenesis is a metabolic strategy for Herpesvirus replication. *Cell Host Microbe* 24, 526–541.e7. doi: 10.1016/j.chom.2018.09.002

Kagan, J. C. (2012). Signaling organelles of the innate immune system. *Cell* 151, 1168–1178. doi: 10.1016/j.cell.2012.11.011

Kamemura, K., and Chihara, T. (2019). Multiple functions of the ER-resident VAP and its extracellular role in neural development and disease. *J. Biochem.* 165, 391–400. doi: 10.1093/jb/mvz011

Kim, S., Leal, S. S., Ben Halevy, D., Gomes, C. M., and Lev, S. (2010). Structural requirements for VAP-B oligomerization and their implication in amyotrophic lateral sclerosis-associated VAP-B(P56S) neurotoxicity. *J. Biol. Chem.* 285, 13839–13849. doi: 10.1074/jbc.m109.097345

King, C., Sengupta, P., Seo, A. Y., and Lippincott-Schwartz, J. (2020). ER membranes exhibit phase behavior at sites of organelle contact. *Proc. Natl. Acad. Sci. U.S.A.* 117, 7225–7235. doi: 10.1073/pnas.1910854117

Knoblach, B., Sun, X., Coquelle, N., Fagarasanu, A., Poirier, R. L., and Rachubinski, R. A. (2013). An ER-peroxisome tether exerts peroxisome population control in yeast. *EMBO J.* 32, 2439–2453. doi: 10.1038/emboj.2013.170

Kong, J., Ji, Y., Jeon, Y. G., Han, J. S., Han, K. H., Lee, J. H., et al. (2020). Spatiotemporal contact between peroxisomes and lipid droplets regulates fasting-induced lipolysis via PEX5. *Nat. Commun.* 11:578.

Kustatscher, G., Grabowski, P., Schrader, T. A., Passmore, J. B., Schrader, M., and Rappsilber, J. (2019). Co-regulation map of the human proteome enables identification of protein functions. *Nat. Biotechnol.* 37, 1361–1371. doi: 10.1038/s41587-019-0298-5

Lang, A. B., John Peter, A. T., Walter, P., and Kornmann, B. (2015). ER-mitochondrial junctions can be bypassed by dominant mutations in the endosomal protein Vps13. *J. Cell Biol.* 210, 883–890. doi: 10.1083/jcb.201502105

Lange, Y., Swaisgood, M. H., Ramos, B. V., and Steck, T. L. (1989). Plasma membranes contain half the phospholipid and 90% of the cholesterol and sphingomyelin in cultured human fibroblasts. *J. Biol. Chem.* 264, 3786–3793.

Lev, S., Ben Halevy, D., Peretti, D., and Dahan, N. (2008). The VAP protein family: from cellular functions to motor neuron disease. *Trends Cell Biol.* 18, 282–290. doi: 10.1016/j.tcb.2008.03.006

Lopez-Erauskin, J., Galino, J., Ruiz, M., Cuezva, J. M., Fabregat, I., Cacabelos, D., et al. (2013). Impaired mitochondrial oxidative phosphorylation in the peroxisomal disease X-linked adrenoleukodystrophy. *Hum. Mol. Genet.* 22, 3296–3305. doi: 10.1093/hmg/ddt186

Mast, F. D., Rachubinski, R. A., and Aitchison, J. D. (2020). Peroxisome prognostications: exploring the birth, life, and death of an organelle. *J. Cell Biol.* 219:e201912100.

Mattiazzi Usaj, M., Brloznik, M., Kaferle, P., Zitnik, M., Wolinski, H., Leitner, F., et al. (2015). Genome-wide localization study of yeast Pex11 identifies peroxisome-mitochondria interactions through the ERMES complex. *J. Mol. Biol.* 427, 2072–2087. doi: 10.1016/j.jmb.2015.03.004

Menon, S., Dibble, C. C., Talbott, G., Hoxhaj, G., Valvezan, A. J., Takahashi, H., et al. (2014). Spatial control of the TSC complex integrates insulin and nutrient regulation of mTORC1 at the lysosome. *Cell* 156, 771–785. doi: 10.1016/j.cell.2013.11.049

Munn, N. J., Arnio, E., Liu, D., Zoeller, R. A., and Liscum, L. (2003). Deficiency in ethanolamine plasmalogen leads to altered cholesterol transport. *J. Lipid Res.* 44, 182–192. doi: 10.1194/jlr.m200363-jlr200

Murley, A., and Nunnari, J. (2016). The emerging network of mitochondria-organelle contacts. *Mol. Cell* 61, 648–653. doi: 10.1016/j.molcel.2016.01.031

Nazarko, T. Y., Ozeki, K., Till, A., Ramakrishnan, G., Lotfi, P., Yan, M., et al. (2014). Peroxisomal Atg37 binds Atg30 or palmitoyl-CoA to regulate phagophore formation during pexophagy. *J. Cell Biol.* 204, 541–557. doi: 10.1083/jcb.201307050

Neuhaus, A., Eggeling, C., Erdmann, R., and Schliebs, W. (2016). Why do peroxisomes associate with the cytoskeleton? *Biochim. Biophys. Acta* 1863, 1019–1026. doi: 10.1016/j.bbamcr.2015.11.022

Novikoff, P. M., and Novikoff, A. B. (1972). Peroxisomes in absorptive cells of mammalian small intestine. *J. Cell Biol.* 53, 532–560. doi: 10.1083/jcb.53.2.532

Prinz, W. A. (2014). Bridging the gap: membrane contact sites in signaling, metabolism, and organelle dynamics. *J. Cell Biol.* 205, 759–769. doi: 10.1083/jcb.201401126

Prinz, W. A., Toulmay, A., and Balla, T. (2020). The functional universe of membrane contact sites. *Nat. Rev. Mol. Cell Biol.* 21, 7–24. doi: 10.1038/s41580-019-0180-9

Rowland, A. A., Chitwood, P. J., Phillips, M. J., and Voeltz, G. K. (2014). ER contact sites define the position and timing of endosome fission. *Cell* 159, 1027–1041. doi: 10.1016/j.cell.2014.10.023

Sargsyan, Y., and Thoms, S. (2020). Staying in healthy contact: how peroxisomes interact with other cell organelles. *Trends Mol. Med.* 26, 201–214. doi: 10.1016/j.molmed.2019.09.012

Saxton, R. A., and Sabatini, D. M. (2017). mTOR signaling in growth. *Metab. Dis. Cell* 169, 361–371.

Schaumburg, H. H., Richardson, E. P., Johnson, P. C., Cohen, R. B., Powers, J. M., and Raine, C. S. (1972). Schilder's disease. Sex-linked recessive transmission with specific adrenal changes. *Arch. Neurol.* 27, 458–460.

Schrader, M., Baumgart, E., Volkl, A., and Fahimi, H. D. (1994). Heterogeneity of peroxisomes in human hepatoblastoma cell line HepG2. Evidence of distinct subpopulations. *Eur. J. Cell Biol.* 64, 281–294.

Schrader, M., Bonekamp, N. A., and Islinger, M. (2012). Fission and proliferation of peroxisomes. *Biochim. Biophys. Acta* 1822, 1343–1357. doi: 10.1016/j.bbadis.2011.12.014

Schrader, M., Grille, S., Fahimi, H. D., and Islinger, M. (2013). Peroxisome interactions and cross-talk with other subcellular compartments in animal cells. *Subcell. Biochem.* 69, 1–22. doi: 10.1007/978-94-007-6889-5_1

Schrader, M., Kamoshita, M., and Islinger, M. (2020). Organelle interplay-peroxisome interactions in health and disease. *J. Inherit. Metab. Dis.* 43, 71–89. doi: 10.1002/jimd.12083

Scorrano, L., Emr, S., Giordano, F., Hajnoczky, G., Kornmann, B., and Lackner, L. L. (2019). Coming together to define membrane contact sites. *Nat. Commun.* 10:1287.

Shai, N., Schuldiner, M., and Zalckvar, E. (2016). No peroxisome is an island - Peroxisome contact sites. *Biochim. Biophys. Acta* 1863, 1061–1069. doi: 10.1016/j.bbamcr.2015.09.016

Shai, N., Yifrach, E., Cohen, N., Bibi, C., Meurisse, J., Schuster, R., et al. (2018). Systematic mapping of contact sites reveals tethers and a function for the peroxisome-mitochondria contact. *Nat. Commun.* 9:1761.

Smith, J. J., and Aitchison, J. D. (2013). Peroxisomes take shape. *Nat. Rev. Mol. Cell Biol.* 14, 803–817. doi: 10.1038/nrm3700

Sugiura, A., Mattie, S., Prudent, J., and McBride, H. M. (2017). Newly born peroxisomes are a hybrid of mitochondrial and ER-derived pre-peroxisomes. *Nature* 542, 251–254. doi: 10.1038/nature21375

Sugiura, A., McLelland, G. L., Fon, E. A., and McBride, H. M. (2014). A new pathway for mitochondrial quality control: mitochondrial-derived vesicles. *EMBO J.* 33, 2142–2156. doi: 10.15252/embj.201488104

Suzuki, Y., Shimozawa, N., Orii, T., Tsukamoto, T., Osumi, T., Fujiki, Y., et al. (2001). Genetic and molecular bases of peroxisome biogenesis disorders. *Genet. Med.* 3, 372–376. doi: 10.1097/00125817-200109000-00007

Thai, T. P., Rodemer, C., Jauch, A., Hunziker, A., Moser, A., Gorgas, K., et al. (2001). Impaired membrane traffic in defective ether lipid biosynthesis. *Hum. Mol. Genet.* 10, 127–136. doi: 10.1093/hmg/10.2.127

Thiam, A. R., and Dugail, I. (2019). Lipid droplet-membrane contact sites - from protein binding to function. *J. Cell Sci.* 132:jcs230169. doi: 10.1242/jcs.230169

Torres, S. E., Gallagher, C. M., Plate, L., Gupta, M., Liem, C. R., Guo, X., et al. (2019). Ceapins block the unfolded protein response sensor ATF6alpha by inducing a neomorphic inter-organelle tether. *eLife* 8:e46595.

Valm, A. M., Cohen, S., Legant, W. R., Melunis, J., Hershberg, U., Wait, E., et al. (2017). Applying systems-level spectral imaging and analysis to reveal the organelle interactome. *Nature* 546, 162–167. doi: 10.1038/nature22369

Verfaillie, T., Rubio, N., Garg, A. D., Bultynck, G., Rizzuto, R., Decuypere, J. P., et al. (2012). PERK is required at the ER-mitochondrial contact sites to convey apoptosis after ROS-based ER stress. *Cell Death Differ.* 19, 1880–1891. doi: 10.1038/cdd.2012.74

Walbrecq, G., Wang, B., Becker, S., Hannotiau, A., Fransen, M., and Knoops, B. (2015). Antioxidant cytoprotection by peroxisomal peroxiredoxin-5. *Free Radic. Biol. Med.* 84, 215–226. doi: 10.1016/j.freeradbiomed.2015.02.032

Walton, P. A., and Pizzitelli, M. (2012). Effects of peroxisomal catalase inhibition on mitochondrial function. *Front. Physiol.* 3:108. doi: 10.3389/fphys.2012.00108

Wang, B., Brees, C., Rubio, N., Nordgren, M., Apanasets, O., Kunze, M., et al. (2013). Mitochondria are targets for peroxisome-derived oxidative stress in cultured mammalian cells. *Free Radic. Biol. Med.* 65, 882–894. doi: 10.1016/j.freeradbiomed.2013.08.173

Wang, H., Becuwe, M., Housden, B. E., Chitraju, C., Porras, A. J., and Graham, M. M. (2016). Seipin is required for converting nascent to mature lipid droplets. *eLife* 5:e16582.

Wang, Y., Metz, J., Costello, J. L., Passmore, J., Schrader, M., Schultz, C., et al. (2018). Intracellular redistribution of neuronal peroxisomes in response to ACBD5 expression. *PLoS One* 13:e0209507. doi: 10.1371/journal.pone.0209507

Waterham, H. R., Ferdinandusse, S., and Wanders, R. J. (2016). Human disorders of peroxisome metabolism and biogenesis. *Biochim. Biophys. Acta* 1863, 922–933. doi: 10.1016/j.bbamcr.2015.11.015

Welte, M. A. (2015). Expanding roles for lipid droplets. *Curr. Biol.* 25, R470–R481.

Xiao, J., Luo, J., Hu, A., Xiao, T., Li, M., Kong, Z., et al. (2019). Cholesterol transport through the peroxisome-ER membrane contacts tethered by PI(4,5)P2 and extended synaptotagmins. *Sci. China Life Sci.* 62, 1117–1135. doi: 10.1007/s11427-019-9569-9

Yagita, Y., Shinohara, K., Abe, Y., Nakagawa, K., Alkuraya, F. S., and Fujiki, Y. (2017). Deficiency of a retinal dystrophy protein, Acyl-CoA binding domain-containing 5 (ACBD5), impairs peroxisomal beta-oxidation of very-long-chain fatty acids. *J. Biol. Chem.* 292, 691–705. doi: 10.1074/jbc.m116.760090

Yifrach, E., Fischer, S., Oeljeklaus, S., Schuldiner, M., Zalckvar, E., and Warscheid, B. (2018). Defining the mammalian peroxisomal proteome. *Subcell. Biochem.* 89, 47–66. doi: 10.1007/978-981-13-2233-4_2

Yokota, S. (1986). Quantitative immunocytochemical studies on differential induction of serine:pyruvate aminotransferase in mitochondria and peroxisomes of rat liver cells by administration of glucagon or di-(2-ethylhexyl)phthalate. *Histochemistry* 85, 145–155. doi: 10.1007/bf00491762

Yokota, S. (1993). Formation of autophagosomes during degradation of excess peroxisomes induced by administration of dioctyl phthalate. *Eur. J. Cell Biol.* 61, 67–80.

Zhang, J., Kim, J., Alexander, A., Cai, S., Tripathi, D. N., and Dere, R. (2013). A tuberous sclerosis complex signalling node at the peroxisome regulates mTORC1 and autophagy in response to ROS. *Nat. Cell Biol.* 15, 1186–1196. doi: 10.1038/ncb2822

Zhang, J., Tripathi, D. N., Jing, J., Alexander, A., Kim, J., and Powell, R. T. (2015). ATM functions at the peroxisome to induce pexophagy in response to ROS. *Nat. Cell Biol.* 17, 1259–1269. doi: 10.1038/ncb3230

Conflict of Interest: The authors declare that the research was conducted in the absence of any commercial or financial relationships that could be construed as a potential conflict of interest.

frontiers in Cell and Developmental Biology

BRIEF RESEARCH REPORT
published: 30 June 2020
doi: 10.3389/fcell.2020.00545

The Autophagy Machinery Contributes to E-cadherin Turnover in Breast Cancer

Valentina Damiano[1], Paola Spessotto[2], Giulia Vanin[1], Tiziana Perin[3], Roberta Maestro[1] and Manuela Santarosa[1]**

[1] Unit of Oncogenetics and Functional Oncogenomics, Centro di Riferimento Oncologico di Aviano (CRO) IRCCS, Aviano, Italy, [2] Unit of Molecular Oncology, Centro di Riferimento Oncologico di Aviano (CRO) IRCCS, Aviano, Italy, [3] Pathology Unit, Centro di Riferimento Oncologico di Aviano (CRO) IRCCS, Aviano, Italy

Autophagy is an intracellular catabolic process that is increasingly being recognized as a crucial factor in several human diseases including cancers. Mounting evidence suggests that autophagy allows tumor cells to overcome otherwise fatal stresses and to increase dissemination. Nevertheless, how autophagy controls these processes and in particular how it impinges on cell-cell adhesion is still poorly understood. Here, we investigate the role of autophagy in the turnover of the epithelial adhesion molecule E-cadherin in the context of breast cancer. We demonstrated in breast cancer cell lines that autophagy impinges on E-cadherin expression and in the configuration of adherens junctions. Besides, we showed that E-cadherin colocalizes with LC3B and SQSTM1/p62, two components of the autophagosome machinery. Pull down and immunoprecipitation analyses provided evidence that E-cadherin and SQSTM1/p62 physically interact. Moreover, the physical closeness of E-cadherin and SQSTM1/p62 was demonstrated by proximity ligation assays in breast cancer cell lines and primary tumors. Finally, we proved that the silencing of SQSTM1/p62 diminished the E-cadherin/LC3B colocalization, further supporting the role of SQSTM1/p62 in E-cadherin delivery to autophagosomes. These findings suggest that the activation of autophagy, reported in breast cancers with poor prognosis and in dormant breast cancer cells, may contribute to the control of tumor progression via downmodulation of E-cadherin protein levels.

Keywords: autophagy, E-cadherin, breast cancer, SQSTM1, adherens junctions

OPEN ACCESS

Edited by:
Du Feng,
Guangzhou Medical University, China

Reviewed by:
Eva Sjottem,
Arctic University of Norway, Norway
Sol Sotillos,
Andalusian Center for Development Biology (CABD), Spain

****Correspondence:***
Roberta Maestro
rmaestro@cro.it
Manuela Santarosa
msantarosa@cro.it

Specialty section:
This article was submitted to Molecular Medicine, a section of the journal Frontiers in Cell and Developmental Biology

Received: *27 February 2020*
Accepted: *09 June 2020*
Published: *30 June 2020*

Citation:
Damiano V, Spessotto P, Vanin G, Perin T, Maestro R and Santarosa M (2020) The Autophagy Machinery Contributes to E-cadherin Turnover in Breast Cancer. Front. Cell Dev. Biol. 8:545. doi: 10.3389/fcell.2020.00545

INTRODUCTION

Autophagy is an evolutionarily conserved catabolic process whereby a double membrane compartment, named autophagosome, sequesters cytoplasmic cargo and delivers it to lysosomes for degradation (Mizushima and Komatsu, 2011). Dysfunction of autophagy is involved in multiple human diseases (Levine and Kroemer, 2008; Liang, 2010), including cancer where autophagy plays a double role: in oncogenically challenged cells autophagy may prevent tumor progression by removing ROS and damaged mitochondria (White, 2012; Amaravadi and Debnath, 2014);

Abbreviations: AJ, Adherens-junctions; BAF, Bafilomycin A1; BC, Breast cancer; CQ, Chloroquine Diphosphate Salt; IP, immunoprecipitation; LC3B, MAP1LC3B; PD, pull-down; PLA, Proximity ligation assay; Rapa, Rapamycin; shRNA, short hairpin RNA; Starv, starvation.

on the other hand, in overt tumors, autophagy seems to contribute to tumor cell survival by promoting nutrient recycling and sustaining anti-apoptotic pathways (Levy et al., 2017; Mowers et al., 2017). Along with this line, increased autophagic flux has been reported for various types of tumors, including breast cancer (BC) (Lazova et al., 2012; Mikhaylova et al., 2012; Giatromanolaki et al., 2018).

Mounting evidence suggests that autophagy endows tumor cells with the capability to survive anoikis, hypoxia and chemotherapy treatments (Levine and Kroemer, 2008; Levy et al., 2014; Daskalaki et al., 2018). Besides, in certain contexts, autophagy has been shown to trigger an epithelial to mesenchymal transition-like program that accounts for the downregulation of cell-cell and cell-basal membrane interactions and an increase in migratory capability (Nieto et al., 2016; Mowers et al., 2017; Alizadeh et al., 2018). These phenomena contribute to cancer stem-like cell maintenance and high metastatic potential of BC, in particular of triple negative BC (ER, PGR, and HER2 receptor negative tumors) (Vera-Ramirez, 2019).

E-cadherin is a major component of the adherens junctions that maintain cell-cell adhesion, basal-apical polarity, and epithelial tissue homeostasis, thus restraining cell motility and cancer progression (Perl et al., 1998; Izaguirre and Casco, 2016; Kourtidis et al., 2017; Carneiro et al., 2019). E-cadherin interacts with p120 catenin and beta-catenin through its cytoplasmic domain forming a core complex that connects the adherens junctions to the actin cytoskeleton and preserves junctional maintenance and dynamics (Ireton et al., 2002; Brüser and Bogdan, 2017).

Several mechanisms have been described that contribute to the downregulation of E-cadherin in cancer. Loss of function mutations of the CDH1 gene, which result in impaired E-cadherin protein expression, are commonly detected in lobular breast carcinomas and diffuse gastric cancers (Graziano et al., 2003; Ciriello et al., 2015). In other tumors, the CDH1 gene is transcriptionally repressed (Nieto et al., 2016; Kourtidis et al., 2017). Augmented endocytosis of E-cadherin has also been reported (Jones et al., 2006; Kourtidis et al., 2017) and autophagy-induced degradation, due to overexpression of SIRT1, SPHK1, or PHF8 have been described in melanoma and hepatocarcinoma (Liu et al., 2017; Sun et al., 2018; Zhou et al., 2018). Yet, the mechanisms whereby autophagy impacts on E-cadherin expression in the setting of BC are not fully elucidated.

Here we demonstrate that the autophagy machinery impinges upon E-cadherin protein levels by chaperoning it to autophagosome via interaction with the autophagic cargo adaptor SQSTM1/p62.

MATERIALS AND METHODS

Cell Models and Treatments

The human breast cancer cell lines MDA-MB-231 (here referred to as MDA231), HCC1937, and MCF7 were obtained from the ATCC (LGC Standards). All cell lines were periodically authenticated by short tandem repeat profiling and tested mycoplasma-negative. They were cultured as previously described (Santarosa et al., 2009; Borgna et al., 2012) or, also, in Hanks' Balanced Salt Solution (HBSS; Sigma-Aldrich) for achieving nutrient starvation; in medium containing either 50 μM Chloroquine Diphosphate Salt (CQ; Sigma-Aldrich) or 40 nM Bafilomycin A1 (BAF; Bioviotica Naturstoffe) to block autophagy by preventing autophagosome acidification and degradation; in medium containing 5 μM Rapamycin (Rapa; LC Laboratories), an inhibitor of mTOR, which activates autophagy or in the presence of 5 mM 3-Methyladenine (3MA; Selleckchem) to inhibit autophagosome formation.

Stably ATG7 (shATG7) and SQSTM1/p62 (shp62-1, shp62-2) silenced cell lines, as well as control (shCTR) cells were generated by using lentiviral plasmids obtained from a modified version of pRSI9 DECIPHER vector (Cellecta) as previously described (di Gennaro et al., 2018). Individual short hairpin RNA (shRNA) sequences are reported in **Supplementary Table 1**.

To generate MDA231-GFP-LC3B and HCC1937-GFP-LC3B cell lines, the GFP-LC3B sequence was amplified form pEX-GFP-hLC3WT (Addgene #24987; Tanida et al., 2008) with the following primers: F 5′-AAAAAACCGGTATGGTGAGCA AGGGGGAGG and R 5′-AAAAAGAATTCCACCTGAGGAGT GAATTGAGC. The GFP-LC3B PCR was cloned, as an AgeI-EcoRI fragment, into a pLJM-based vector (Addgene #19319; Sancak et al., 2008) and MDA231 and HCC1937 cells were then lentivirally infected. pLJM-EGFP was used as a negative control.

MDA231-E-cad-Strep-Tag and MDA231-p62-Strep-Tag cells were generated by transduction with either pLJM-Ecad-Strep-Tag or pLJM-p62-Strep-Tag lentiviral vectors. To generate vectors, we used the Strep-tag sequence, which exhibits intrinsic affinity toward Strep-Tactin and is codified by the pPSG-IBA105 vector (IBA LifeSciences), and firstly cloned in the pCS2-myc vector (a gift from Dave L Turner). The engineered vector was used as a template for the Strep-tag amplification by using the following primers F 5′-AAAACCGGTACCATGGGTTAACGTTAGCGC ATGGAGTCATCC and R 5′-AAAAGAATTCCTCGAGTTAA TTCAAGTCCTCTTCAG designed to keep out the Strep-tag ATG site, to insert a TAA stop codon at the 3′ terminus, to insert restriction sites AgeI at 5′ site and EcoRI at 3′ site and an in-frame HpaI site in the 5′ side of Strep-tag. After AgeI/EcoRI digestion the amplified sequence was cloned in the pLJM-EGFP vector (Addgene #19319; Sancak et al., 2008). The generated pLJM-Strep-Tag vector was then used as a backbone to clone E-cadherin (at N terminus of Strep-tag). This was achieved by amplifying the gene from the E-cadherin-GFP plasmid (Addgene #28009; Miranda et al., 2001) with oligos allowing for NheI/HpaI digestion (F-5′ AAAAAgctagcTATCGAATTCCGGAAAGCAC and R 5′ AAAAAGTTAACGCTCCGCGGGTCGTCCTC). To generate the pLJM-p62-Strep-Tag vector, p62 was first obtained by HindIII and NotI digestion from HA-p62 plasmid (Addgene #28027; Fan et al., 2010) and cloned in pcDNA 3.1. The cloned fragment was then digested with ApaI, blunted by incubating with DNA Polymerase I Klenow Fragment (New England Biolabs), digested with NheI and cloned in the pLJM-Strep-Tag.

MDA231 cells were engineered to ectopically express E-cadherin (MDA231-E-cad) by transduction of the pLJM-E-cad lentiviral vector. This vector was obtained from

pLJM-Ecad-Strep-Tag by removing the Strep-Tag sequence. pLJM-EGFP vector was used as a negative control.

All the generated vectors were verified by Sanger sequencing. Lentiviral particles were generated as previously described (Damiano et al., 2017). Puromycin treatment selected the efficiently transduced cells.

Western Blot Analyses

Protein extraction and western blot were performed as previously described (Santarosa et al., 2010). **Supplementary Table 2** reported the primary antibodies used. Immunoreactivity was detected with anti-mouse or anti-rabbit secondary antibodies HRP-labeled (Perkin Elmer) and Western Lightning Chemiluminescence Reagent Plus (Perkin Elmer). Chemidoc XRS+ system (Bio-Rad) and ImageLab imaging software (Bio-Rad) were used to capture and analyze images, respectively. Immunoreactivity to E-cadherin and relative loading control, in HCC1937 and MCF7 cell lines, was measured by using Alexa Fluor-680 conjugated secondary antibodies and the Odyssey infrared imaging system (LI-COR, Biosciences) for blot visualization and quantization. Results were confirmed in at least 3 independent experiments.

Immunofluorescence

For immunofluorescence analyses, cells were cultured on coverslips in the medium described in the text. After treatment, cells were fixed in 4% paraformaldehyde/PBS for 15 min, permeabilized with 0.4% Triton X-100/PBS for 10 min, and incubated for 1 h with 0.04% Triton X-100/PBS containing 3% of BSA to block non-specific antigens. In the case of antibody-mediated LC3B labeling, cells were permeabilized with ice-cold 100% methanol. Cells were stained with the appropriate antibody (reported in **Supplementary Table 2**) at 4°C overnight. Primary antibodies were visualized with goat anti-mouse Alexa Fluor 594 or 633 (Thermo Fisher Scientific), or with goat anti-rabbit Alexa Fluor 594 or 633 (Thermo Fisher Scientific). TO-PRO-3 (Thermo Fisher Scientific) was used for nuclear labeling. Cells were then analyzed by using the TCS-SP8 Confocal System (Leica Microsystems) interfaced with the Leica Application Suite (LAS) software. When all three fluorochromes were used, individual cells were identified by capturing transmitted light images. Total and colocalized dots were quantified by using the Fiji/ImageJ software (Schneider et al., 2012) and the ComDet v.0.5.1 plugin[1].

Analyses of Adherens Junctions

Cells were seeded on coverslips and grown to confluence, then cells were either treated with standard medium, starved for 8 h, or treated with 5 μM Rapamacyn for 24 h or 10 mM 4-dithiothreitol (DTT; Sigma-Aldrich) for 3 h. Immunofluorescence staining was then carried out as above described. Alexa Fluor 488 or 594 Phalloidin (Thermo Fisher Scientific) was used to probe F-actin. Images were captured with TCS-SP8 Confocal System (Leica Microsystems) and analyzed with Fiji/ImageJ software (Schneider et al., 2012), similarly, to what previously described (Di Russo et al., 2017). Briefly, adherens junctions, considered as the E-cadherin/beta-catenin positive cell-cell border fragment, were measured on the focal plane corresponding to the maximum intensity of the E-cadherin signal. Adherens junctions ratio was calculated as the length of adherens-junctions over the length of the perimeter of the cell that was manually measured by using the border of phalloidin maximum intensity projections. Experiments were performed in triplicate and, overall, at least 100 cells per sample were measured.

Time-lapse images of cells were captured every 20 min for 20 h by AF6000 microscope system and LASX software (Leica Microsystems).

Patients

Formalin-fixed, paraffin-embedded specimens of 18 consecutively E-cadherin expressing BC were prospectively collected at the CRO Aviano National Cancer Institute. E-cadherin expression was routinely assessed at the Pathology Unit of the Institute. Informed consent was obtained and the use of patient samples was approved by the Institutional Review Board. Clinicopathological data were retrieved from clinical records.

Proximity Ligation Assay (PLA)

For *in vitro* PLA experiments, cells were cultured on coverslips, treated as indicated in the text and fixed and permeabilized as reported in the immunofluorescence section.

For *ex vivo* analyses, 5 μm breast cancer tissue sections were deparaffinized by incubation in xylene (soaking twice for 10 min each), and rehydrated with ethanol solutions (twice in 100, 90, 70, and 50% ethanol solutions for 3 min each) and water (twice for 5 min). Heat-induced antigen retrieval was performed in citrate buffer (10 mM, pH 6) for 10 min in the microwave. Permeabilization was carried out as reported above. Tissues were treated for 10 min with 0.1M Glycine to reduce background fluorescence. Slides were checked for the emission of autofluorescence. Indeed, four breast cancer tissues showed red- and green-emitting dots in the cytoplasm of tumor cells that might reflect the presence of lipofuscins, fluorescent components that accumulate in the lysosomal compartment of many cell types (Moreno-García et al., 2018; **Supplementary Figure 1A**). These samples were excluded from further investigations.

Then, the analysis was performed by using the DuoLink PLA kit (Sigma-Aldrich) with Detection Reagents Red and following the manufacturer's protocol. **Supplementary Table 2** displayed the antibodies used in the analyses. Coverslips/slides were incubated overnight at 4°C with primary antibodies and 1 h and 30 min at 37°C with secondary antibodies-PLA probes. After that, ligation and amplification steps were performed as the producer instructions. Finally, coverslips or slides were mounted with DuoLink *in situ* mounting medium containing DAPI. Images were captured with the Nikon Eclipse-Ti fluorescence microscope equipped with Plan Fluor 40x objective and with TRITC and UV2A filter cubes (EX-filter 540/25, barrier-filter 590LP; EX-filter 355/50, barrier-filter 410, respectively).

For dot quantification, we analyzed the captured images with Fiji/ImageJ software (Schneider et al., 2012) and ComDet v.0.3.7

[1]https://github.com/ekatrukha/ComDet

plugin for FIJI with a particle size of 4 pixels and signal-to-noise ratio 4. At least 50 cells per sample were analyzed.

Strep-Tag Pull-Down and Immunoprecipitation Assays

MDA231-E-cad-Strep-Tag and MDA231-p62-Strep-Tag cells were lysed with Pierce Lysis Buffer. Lysates were incubated with Strep-Tactin Sepharose 50% suspension (IBA Lifesciences) and, after washing, bound proteins were retrieved with Laemmli buffer and analyzed in western blot.

Immunoprecipitation (IP) of endogenous proteins was performed by lysing cells in PLB buffer (20 mM Tris pH 7.5, 200 mM NaCl, 1 mM EDTA, 0.5% Igepal) supplemented with Complete Protease Inhibitor Cocktail (Sigma-Aldrich) and PMSF. Protein lysates (0.5 mg) were immunoprecipitated overnight with the mouse anti-SQSTM1/p62 antibody (Santa Cruz Biotechnology) and then conjugated to Protein G Sepharose 4 Fast Flow beads (Sigma-Aldrich) for 2 h. Immunocomplexes were washed five times with PLB buffer, resuspended in Laemmli buffer containing β-mercaptoethanol and heated at 100°C for 10 min prior gel loading. Proteins were resolved by SDS–PAGE (4–15% gradient). E-cadherin and SQSTM1/p62 were immunodetected with the mouse anti-E-cadherin (BD Biosciences) and the rabbit anti-SQSTM1/p62 (Thermo Fisher Scientific) antibodies, respectively.

Statistical Analyses

Statistical differences between groups were evaluated using a one-way analysis of variance (ANOVA) followed by a test for linear trend or by unpaired *t*-test, taking advantage of GraphPad PRISM8 software (GraphPad Software). Differences in the PLA puncta per cell between samples were appraised by using the Mann–Whitney Rank Sum Test.

RESULTS

Autophagy Modulation Affects E-cadherin Expression in Breast Cancer

To shed light on the relationship between autophagy and E-cadherin expression in the setting of BC, we inhibited autophagosome acidification and digestion by chloroquine (CQ) in MDA231, a breast cancer cell line that expresses a very low level of E-cadherin (Borgna et al., 2012). CQ treatment produced a significant time-dependent augment of E-cadherin within 24 h, corroborating the hypothesis of a role for autophagy in E-cadherin regulation in these cells (**Figure 1A** and **Supplementary Figure 2A**). To further explore this hypothesis, autophagy was induced by starvation and/or inhibited with either CQ or Bafilomycin A1 (BAF, which prevents autophagosome acidification) in MDA231 as well as in HCC1937 and MCF7 E-cadherin expressing BC cell lines. The efficacy of treatments was monitored by assessing the expression of the un-conjugated and the phosphatidylethanolamine (PE) conjugated forms of MAP1LC3B (LC3B), LC3B-I, and LC3B-II, respectively (**Supplementary Figures 2B–D**). In fact, short after synthesis LC3B is cleaved to generate LC3B-I that, upon autophagy activation, is PE-conjugated to form LC3B-II. This, in turn, is recruited onto the growing phagophore and therein degraded (Klionsky et al., 2016). As expected, the ratio between LC3B-II and LC3B-I augmented in starved samples and in cells in which autophagosome degradation was blocked. SQSTM1/p62, an autophagy receptor that interacts with autophagic substrates and LC3B and that is itself an autophagic target (Johansen and Lamark, 2011), diminished upon starvation and accumulated when autophagy was blocked (**Supplementary Figures 2B–D**). The magnitude of autophagy modulation varied in the different cell models, a finding that is keeping with the reported differences in the response to autophagy of breast cancer cell lines (Maycotte et al., 2014; Zhu et al., 2017).

Notably, in MDA231, HCC1937, and MCF7 the inhibition of autophagy induced by CQ and BAF was paralleled by an augment of E-cadherin protein levels; vice versa, starvation reduced E-cadherin levels in HCC1937 and counteracted the effect of autophagy inhibitors (**Figures 1B–D**). In HCC1937 and MCF7 cell lines, the increased levels of E-cadherin associated to the inhibition of autophagosome lysis rendered more visible the anti-E-cadherin reactive band of higher molecular weight. This extra band might represent uncleaved pro-E-cadherin or post-translationally modified (e.g., glycosylation, ubiquitination) E-cadherin forms (Geng et al., 2012; Carvalho et al., 2016).

On the other hand, treatment of MDA231 with 3-Methyladenine, an inhibitor of autophagosome formation, produced an increment of E-cadherin at the membrane levels (**Supplementary Figures 3A,B**).

Thus, these data support a role for autophagy in the control of E-cadherin expression.

Autophagy Induction Disrupts Cell-Cell Adhesion

Since E-cadherin is pivotal in maintaining epithelial features, we then explored whether autophagy modulation, by affecting E-cadherin levels, impinges on cell morphology and cell-cell junctions.

Indeed, treatments with either CQ or BAF promoted a cobblestone-like morphology in the spindle-like MDA231 cells whereas the starvation-mediated induction of autophagy increased the spindle-like features of both MDA231 and HCC1937 models (**Figure 2A**). Notably, the block of autophagy by silencing of ATG7, a key component of the autophagic machinery, neutralized the effects on cell morphology induced by starvation, a phenomenon particularly evident in HCC1937 cells which, compared to MDA231, display higher levels of E-cadherin and cell-to-cell adhesion (**Figure 2B** and **Supplementary Figures 4A,B**). In these same cells, the induction of autophagy by starvation or Rapamycin treatment (**Supplementary Figure 4C**) resulted in a decrease of E-cadherin and beta-catenin staining at cell-cell borders, associated with a significant drop in the cell-to-cell adhesion (**Figures 2C,D**). As a positive control, we used cells treated with 1,4-dithiothreitol (DTT), a reagent known for reducing the disulfide bridges that sustained the E-cadherin connection between neighboring cells (Brückner and Janshoff, 2018; **Supplementary Figure 4D**). Moreover, starvation, similar

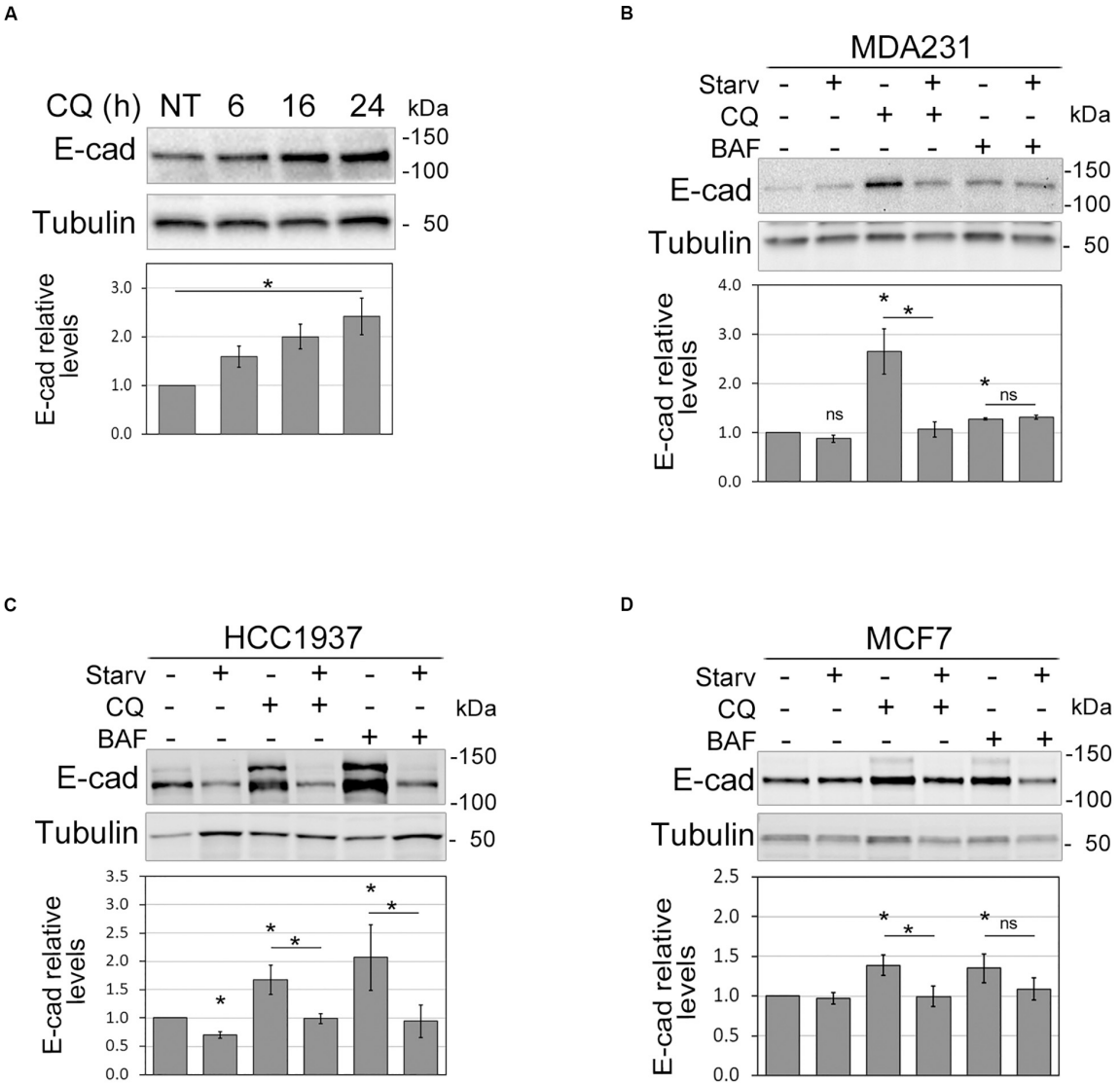

FIGURE 1 | Autophagy modulation affects E-cadherin levels. **(A)** Immunoblot showing the increment of E-cadherin (E-cad) levels in MDA231 cells treated with CQ for 6, 16, and 24 h. NT represents the untreated cells. γ-tubulin (Tubulin) was used as a loading control. *Statistical significance ($p < 0.01$) in the ANOVA test followed by a test for linear trend. **(B–D)** Representative immunoblots displaying the levels of E-cadherin (E-cad) in MDA231 **(B)**, HCC1937 **(C)**, and MCF7 **(D)** cell lines either treated with CQ or BAF (for 8 h), in standard medium or upon nutrient starvation (Starv). Graphs below blots report the mean of E-cadherin relative levels of three experiments with SEM as error bars. E-cadherin relative levels were obtained by normalization over γ-tubulin (Tubulin, loading control) and rescaling to the untreated sample. The asterisks above the histograms and lines mean statistical significance ($p < 0.05$) in the unpaired *t*-test comparisons to the untreated sample or between indicated samples, respectively. ns, not statistically significant.

to DTT, produced a remarkable disruption of cell monolayer (Supplementary time-lapse videos).

Again, the silencing of ATG7 abated the starvation-mediated decrement of adherens-junctions length ratio (**Figures 2E,F**) supporting the role of autophagy in these phenomena.

E-cadherin Localizes in Autophagosomes

Because autophagy is known to deliver protein aggregates to lysosomes for degradation, we investigated whether E-cadherin was a target of such a metabolic mechanism. To this end, we measured the colocalization of E-cadherin with LC3B dots, as previously described (Birgisdottir et al., 2019). E-cadherin and LC3B colocalization was detected in both HCC1937 (endogenous LC3B) as well as in MDA231-GFP-LC3B engineered to express ectopic LC3B (**Figures 3A–D**). Endogenous and GFP-LC3B dots were barely detectable in untreated (NT) cells because of their rapid turnover. Instead, upon starvation-induced autophagy and CQ-mediated block of the autophagosome lysis (Starv+CQ), LC3B dots became readily detectable as puncta (**Figures 3A–D** and **Supplementary Figures 5A,B**). Interestingly, in MDA231

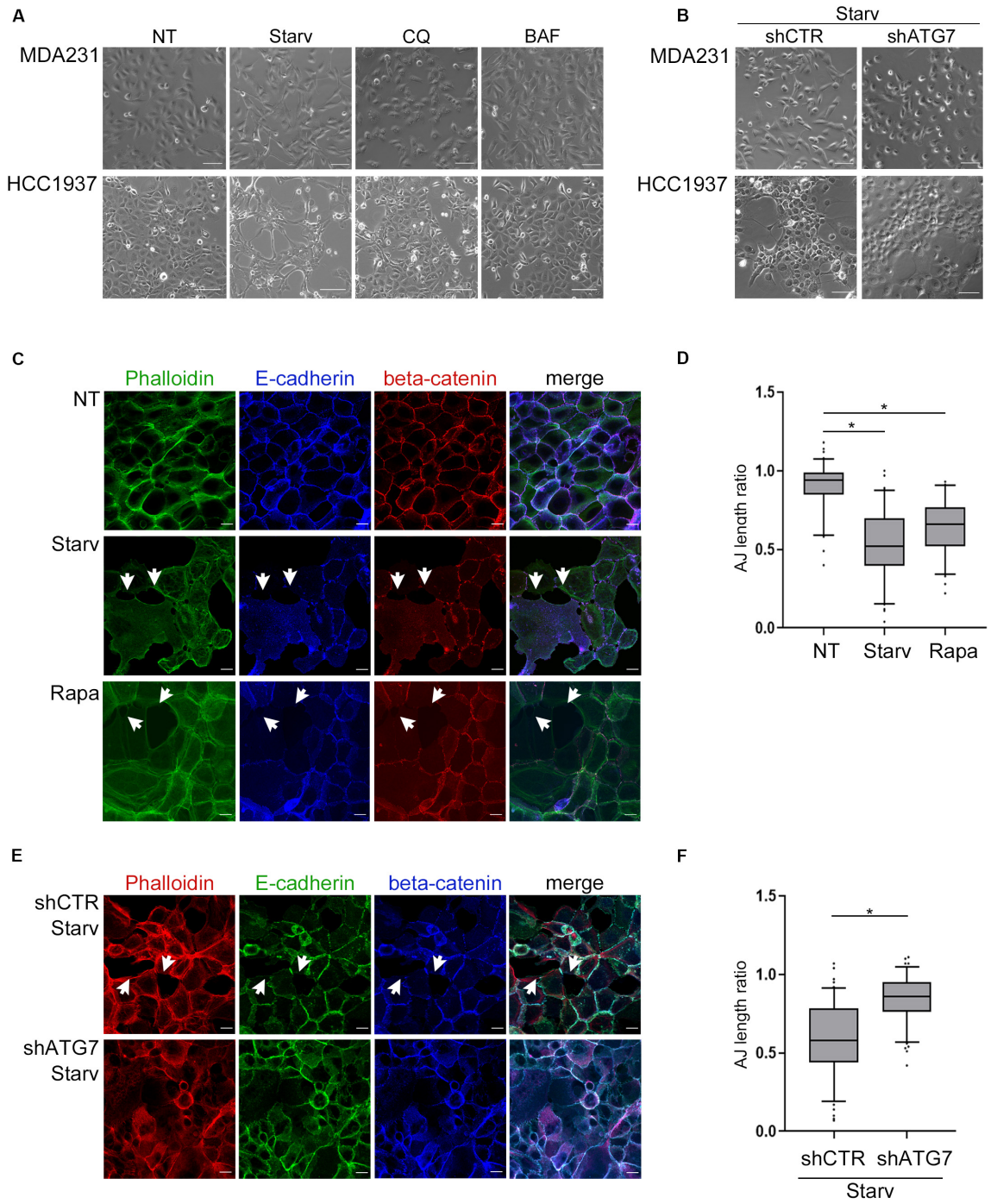

FIGURE 2 | Autophagy induction impinges upon cell morphology and cell-cell adhesion. **(A)** Depicting images (bright field) of MDA231 and HCC1937 untreated (NT), starved (Starv; 8 h) or treated with either CQ or BAF (8 h). Scale bar, 50 μm. **(B)** Representative images of MDA231 and HCC1937 cell models silenced for ATG7 (shATG7) and the respective controls (shCTR). Cells were starved for 8 h. Scale bar, 50 μm. **(C)** Confocal fluorescence images of HCC1937 untreated (NT), starved (Starv) or treated with 5 μM Rapamycin (Rapa) for 24 h and immunostained with Alexa Fluor 488 Phaolloidin, E-cadherin/Alexa Fluor 633 (E-cad) and beta-catenin/Alexa Fluor 594. White arrowheads indicate representative loss of cell-to-cell cohesion. Scale bar, 20 μm. **(D)** Quantification of adherens junctions (AJ length ratio; measured as described in section "Materials and Methods") of the HCC1937 cells treated as described in **(C)**. **(E)** Confocal fluorescence images of HCC1937 cells silenced for ATG7 (shATG7) and the related control (shCTR) starved for 8 h. Cells were immunostained with E-cadherin/Alexa Fluor 488 (E-cad), beta-catenin/Alexa Fluor 633 and Alexa Fluor 594 Phaolloidin to probe F-actin. White arrowheads indicate representative lack of cell-to-cell cohesion regions. Scale bar, 20 μm. **(F)** Quantification of AJ length ratio of the cells described in **(E)**. **(D,F)** At least 100 cells per sample were measured in three independent experiments. Lines within the boxes mark the median, boundaries represent the 25th and the 75th percentiles, whiskers below and above the boxes indicate the 5th and 95th percentiles, respectively, and dots the outliers. An unpaired *t*-test was used to assess statistical significance. *$p < 0.001$.

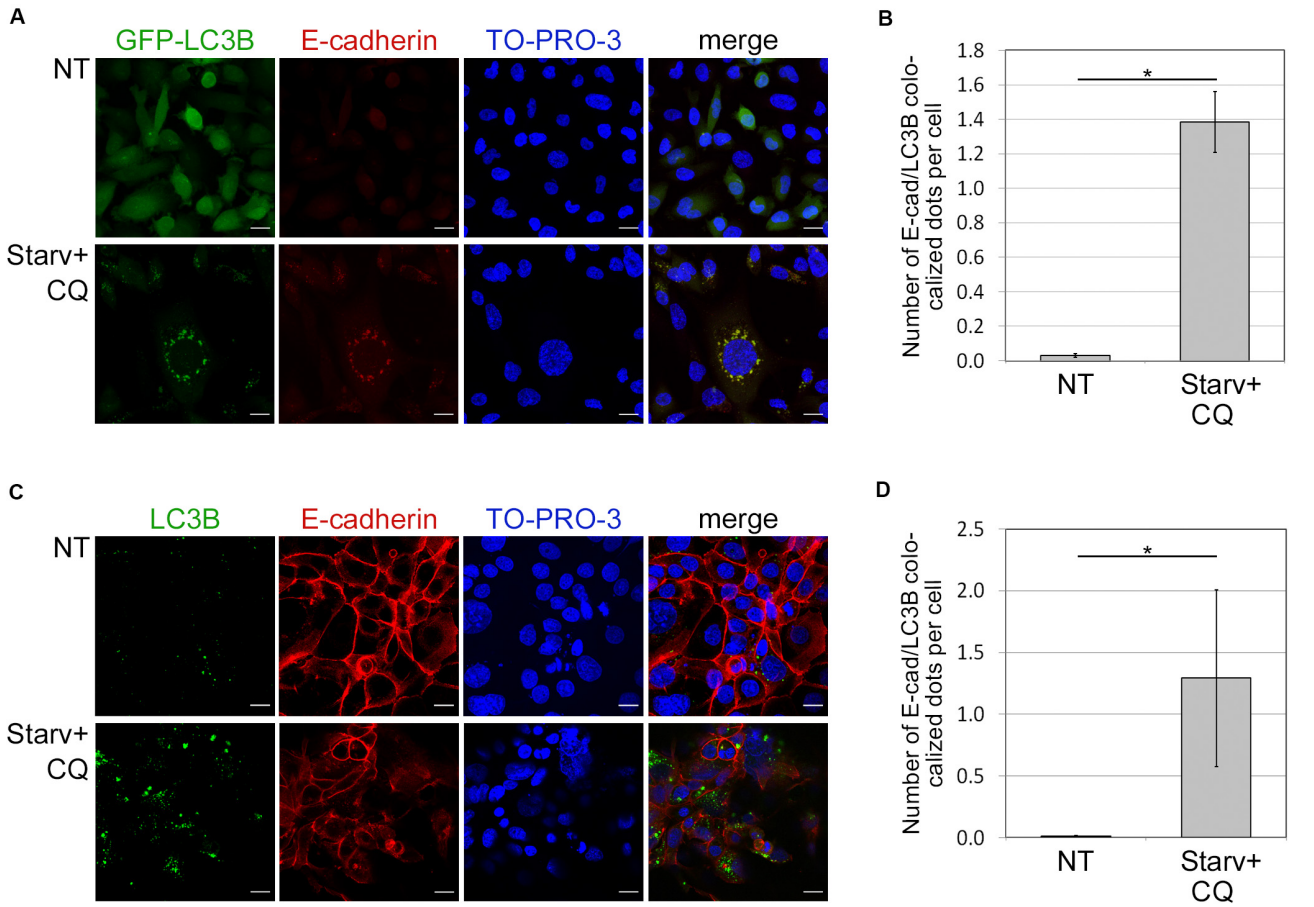

FIGURE 3 | Colocalization of E-cadherin and the autophagosomal LC3B. **(A)** MDA231 cells expressing GFP tagged form of LC3B (GFP-LC3B) were either grown in standard conditions (NT) or starved in the presence of CQ (Starv+CQ) for 8 h. Cells were stained with anti-E-cadherin/Alexa594 antibodies and analyzed by confocal microscopy. Nuclei were labeled with TO-PRO-3. Representative merge images are reported. **(B)** Quantification of GFP-LC3B and E-cadherin colocalized dots per cell measured in the experiments as in **(A)**. The analysis was performed as described in section "Materials and Methods." **(C)** HCC1937 cells treated as in **(A)** and stained with anti-LC3B/Alexa488, anti-E-cadherin/Alexa549 antibodies, and TO-PRO-3. **(D)** Graph reported the quantification of the experiments carried out as in **(C)**. **(B,D)** At least 100 cells per sample were measured in three independent experiments. Graphs report the mean number of E-cadherin and LC3B colocalized dots per cell of at least 100 cells per sample measured in three independent experiments. Bars represent SEM; $^{*}p < 0.01$ in unpaired *t*-test.

and HCC1937 cell lines, treatments caused an increment of E-cadherin/LC3B colocalized dots (**Figures 3A–D**).

In both treated and untreated MDA231-EGFP negative control, EGFP appeared diffuse (**Supplementary Figure 5C**) discarding the possibility that puncta observed in treated cell models were the result of unspecific aggregates. Besides, GFP-LC3B and endogenous LC3B yielded similar levels of dots in the MDA231 cell line (**Supplementary Figures 5A,B**).

SQSTM1/p62 Interacts With E-cadherin

SQSTM1/p62 is a multidomain protein whose UBA (Ubiquitin associated) and LIR (LC3 interacting region) domains, by interacting with ubiquitinated autophagic substrates and LC3, respectively, are crucial in targeting ubiquitinated proteins or aggregates to autophagosomes (Taniguchi et al., 2016).

Having demonstrated that E-cadherin was delivered to autophagosomes, we then investigated whether SQSTM1/p62 was the cargo adaptor for this process. To this end we took advantage of cells models engineered to express GFP-LC3B (MDA231-GFP-LC3B and HCC1937-GFP-LC3B). E-cadherin, LC3B, and SQSTM1/p62 colocalized in the typical puncta of autophagosomes (**Figures 4A,B**, arrowheads; **Supplementary Figure 6**), particularly under Starv+CQ condition. Moreover, under Starv+CQ, both E-cadherin/GFP-LC3B and E-cadherin/SQSTM1/p62 colocalized dots were significantly augmented (**Figures 4A,B**, right graphs). GPF-positive dots were absent/negligible detected in cells expressing EGFP (**Supplementary Figures 5C,D**) ruling out that GFP-LC3B puncta were a side-effect of EGFP overexpression.

The interaction between E-cadherin and SQSTM1/p62 was further revealed by proximity ligation assay (PLA) (Weibrecht et al., 2010). The number of PLA puncta were significantly higher in MDA231 cells ectopically expressing E-cadherin (MDA231-E-cad) compared to MDA231-EGFP control cells (**Figure 4C**). A similar PLA pattern was demonstrated in HCC1937 cells on endogenous E-cadherin (**Figure 4D**). Interestingly, the amount

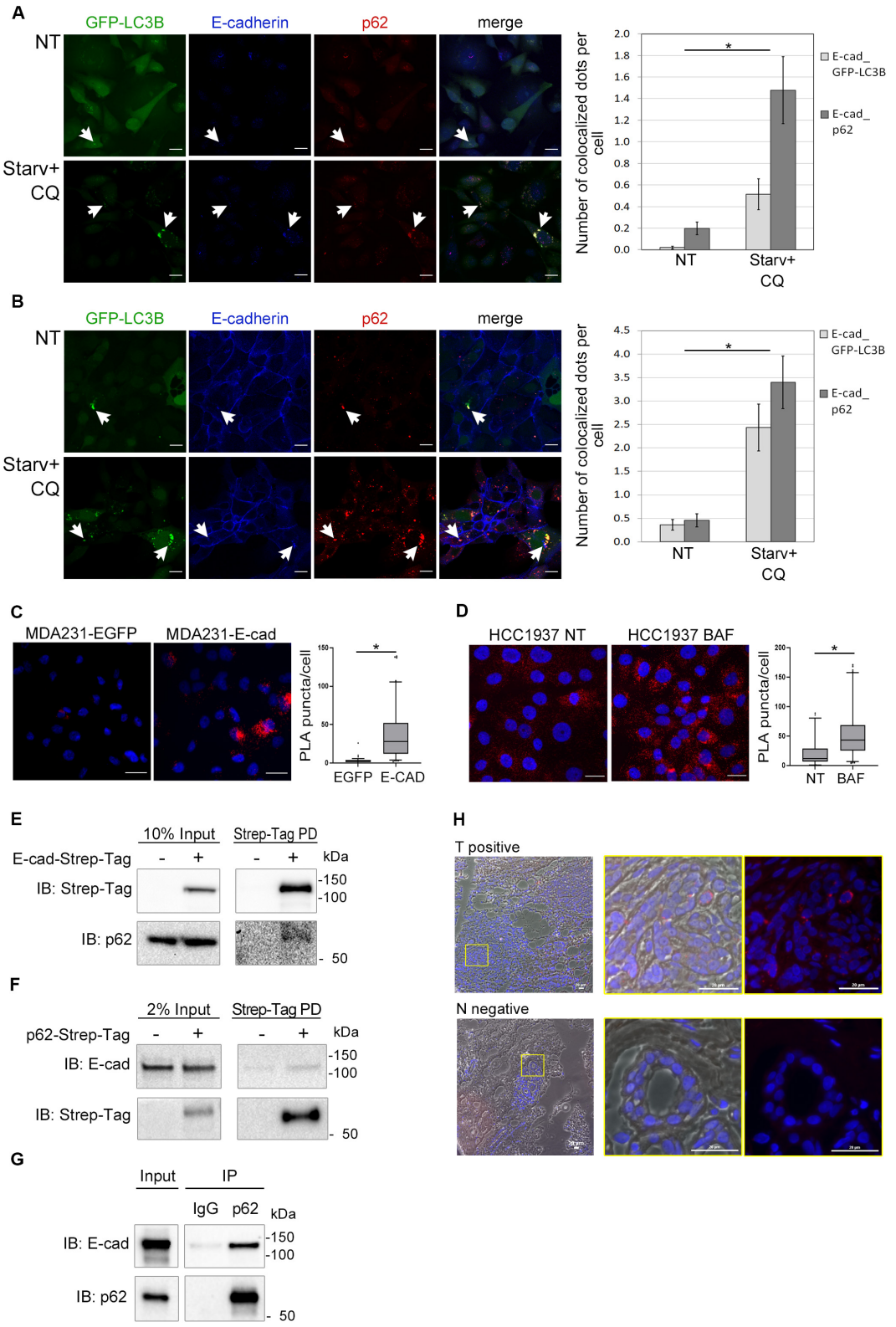

FIGURE 4 | E-cadherin and SQSTM1/p62 interaction. **(A,B)** Representative confocal images of MDA231-GFP-LC3B **(A)** and HCC1937-GFP-LC3B **(B)** cell lines untreated (NT) or starved in the presence of CQ (Starv+CQ) for 8 h. Cells were stained with rabbit anti-E-cadherin/AlexaFluor 633 (E-cadherin) and anti-SQSTM1/p62/AlexaFluor 594 (p62) antibodies. Individual and merged fluorescence images are reported on the left. Arrowheads indicate representative spots of

(Continued)

FIGURE 4 | Continued
co-occurrence of GFP-LC3B, E-cadherin and SQSTM1/p62 (p62) signals. On the right, the graphs showed the mean number of dots per cell in which E-cadherin and GFP-LC3B (E-cad_GFP-LC3B) or E-cadherin and SQSTM1/p62 (E-cad_p62) colocalized. Data are the result of the quantification of at least 100 cells per sample measured in three independent experiments. Bars represent SEM; $^*p < 0.01$ in unpaired *t*-test. **(C)** In situ proximity ligation assay (PLA) in MDA231 cells ectopically expressing E-cadherin (MDA231-E-cad) or EGFP (MDA231-EGFP as a control). Cells were stained with rabbit anti-E-cadherin and mouse anti SQSTM1/p62 antibodies. Nuclei were stained with DAPI (blue); PLA positive signals appear as red puncta. Scale bar, 20 μm. Quantification of PLA puncta/cell in at least 50 cells per sample was shown in the box plots on the right. **(D)** *In situ* PLA, carried out as in **(C)**, in HCC1937 cells treated with either BAF or DMSO (NT, as a control) for 8 h. Scale bar, 20 μm. Quantification of PLA red puncta per cell in at least 50 cells per sample is reported in the box plots on the right. **(C,D)** Lines within the boxes mark the median, boundaries represent the 25th and the 75th percentiles, whiskers below and above the boxes indicate the 5th and 95th percentiles, respectively, and dots the outliers. $^*p < 0.001$ evaluated by using the Mann-Whitney Rank Sum Test. **(E)** Strep-Tag-mediated pull-down (PD) assay shows that a fraction of SQSTM1/p62 (p62) is collected through Strep-Tactin binding of E-cadherin Strep-Tag (Strep-Tag PD, on the right) expressed in MDA231. E-cadherin-Strep-Tag (Strep-Tag) and SQSTM1/p62 (p62) levels in the input samples are reported on the left. **(F)** Immunoblots representing the PD of p62-Strep-Tag in MDA231 cells. p62-Strep-Tag (p62) and E-cadherin (E-cad) proteins were analyzed by western blot (on the right). Input levels of the proteins are reported on the left. In **(E,F)**, cellular extracts from cells ectopically expressing Strep-Tag-only vector (left lines) were used as a negative controls. **(G)** Immunoblots representing the immunoprecipitation (IP) of endogenous E-cadherin (E-cad) from HCC1937 cell extract using the antibodies anti- SQSTM1/p62 (p62) or anti-immunoglobulin G1 (IgG), used as a negative control. Anti- E-cadherin (E-cad) and anti- SQSTM1/p62 (p62) antibodies are used for immunoblotting. Input levels of the proteins are reported on the left. **(H)** Representative images of a PLA positive BC sample (T positive) and its normal counterpart that scored negative in PLA (N negative). Merge of bright field, Red fluorescence and DAPI is reported. Images on the right are the magnification of regions delimited by a yellow square. Scale bar, 20 μm.

of PLA puncta per cell significantly increased in HCC1937 cells treated with BAF compared to untreated control consistent with the increment of both E-cadherin and SQSTM1/p62 in these cells ($p < 0.01$, **Figure 4D** and **Supplementary Figure 2C**). Samples stained with either anti-SQSTM1/p62 or anti-E-cadherin single antibody and samples incubated with both anti-E-cadherin and anti-GAPDH antibodies, as a negative control, scored essentially negative by PLA whereas in both MDA231-E-cad and HCC1937 cells the assay with anti-E-cadherin and anti-beta-catenin antibodies yielded positive results, as expected (**Supplementary Figures 7A,B**).

Next, we further sought to validate the SQSTM1/p62-E-cadherin physical interaction by pull-down experiments. To this end, we generated MDA231 cells expressing either E-cadherin or SQSTM1/p62 fused with Strep-Tag and tested these cells in Strep-tactin pull-down experiments. The pull-down of E-cadherin-Strep-Tag allowed the recovery of SQSTM1/p62 (**Figure 4E**) whereas the reciprocal experiment with SQSTM1/p62-Strep-Tag yielded the recovery of E-cadherin (**Figure 4F**). Importantly, SQSTM1/p62-E-cadherin binding was confirmed on endogenous proteins by co-immunoprecipitation (IP) in HCC1937 cells (**Figure 4G**).

Additionally, E-cadherin-SQSTM1/p62 interaction was validated on human primary tumors by performing PLA on a series of E-cadherin positive breast cancers. Colocalization of the two proteins was detected in 20% of tumor samples suitable for the PLA assay (**Figure 4H** and **Supplementary Figure 1B**). In tumor sections scoring positive in the PLA assay, normal ducts were PLA negative, hinting that the SQSTM1/p62-E-cadherin colocalization may be a cancer specific phenomenon (**Figure 4H**).

SQSTM1/p62 Downregulation Impacts on E-cadherin and LC3B Colocalization

To further validate the role of SQSTM1/p62 in E-cadherin delivery into autophagosomes, we assessed whether E-cadherin and LC3B colocalized dots decreased by SQSTM1/p62 knock-down. To this end, two different shRNA sequences (shp62-1, shp62-2; **Figure 5A**) targeting SQSTM1/p62 were transduced by lentiviral infection into HCC1937 and the autophagic process was triggered by Starv+CQ treatment. Knock-down of SQSTM1/p62 expression was associated with a reduction in colocalized E-Cadherin and LC3B dots in the Starv+CQ condition (**Figures 5B,C**).

DISCUSSION

Mounting evidence suggests that autophagy modifies the expression of epithelial molecules, affects the integrity of epithelium and impacts on tumor cell motility, invasion, and metastasis (Sharifi et al., 2016).

Here we show that autophagy modulation impinges upon E-cadherin levels and is instrumental in disrupting adherens junctions. Thus, our results broaden the spectrum of cell-to-cell adhesion molecules whose expression is affected by autophagy activation (Fong et al., 2012).

The fact that E-cadherin may be downregulated through the activation of autophagy has been already demonstrated on melanoma and hepatoma cells in which SIRT1 and SPHK1, respectively, regulate this process (Liu et al., 2017; Sun et al., 2018; Zhou et al., 2018). Here we went further by demonstrating that in breast cancer E-cadherin is delivered to autophagosomes. This phenomenon contributes to regulating E-cadherin levels in addition to the previously reported proteasomal and endo/lysosomal degradation pathways (Palacios et al., 2005; Cadwell et al., 2016) and reducing E-cadherin availability at the cell-cell junctions. Notably, the trafficking of E-cadherin to lysosomes has been shown to impinge on the stability of the epithelium and is considered an early event that precedes transcriptional inhibition of CDH1 during epithelial to mesenchymal transition (Palacios et al., 2005).

In addition, we demonstrated that the delivery of E-cadherin to autophagosomes is mediated by the autophagy adaptor SQSTM1/p62. Intriguingly, SQSTM1/p62 was one of the molecules isolated as part of E-cadherin-and F-actin-mediated adherens plaques (Guo et al., 2014).

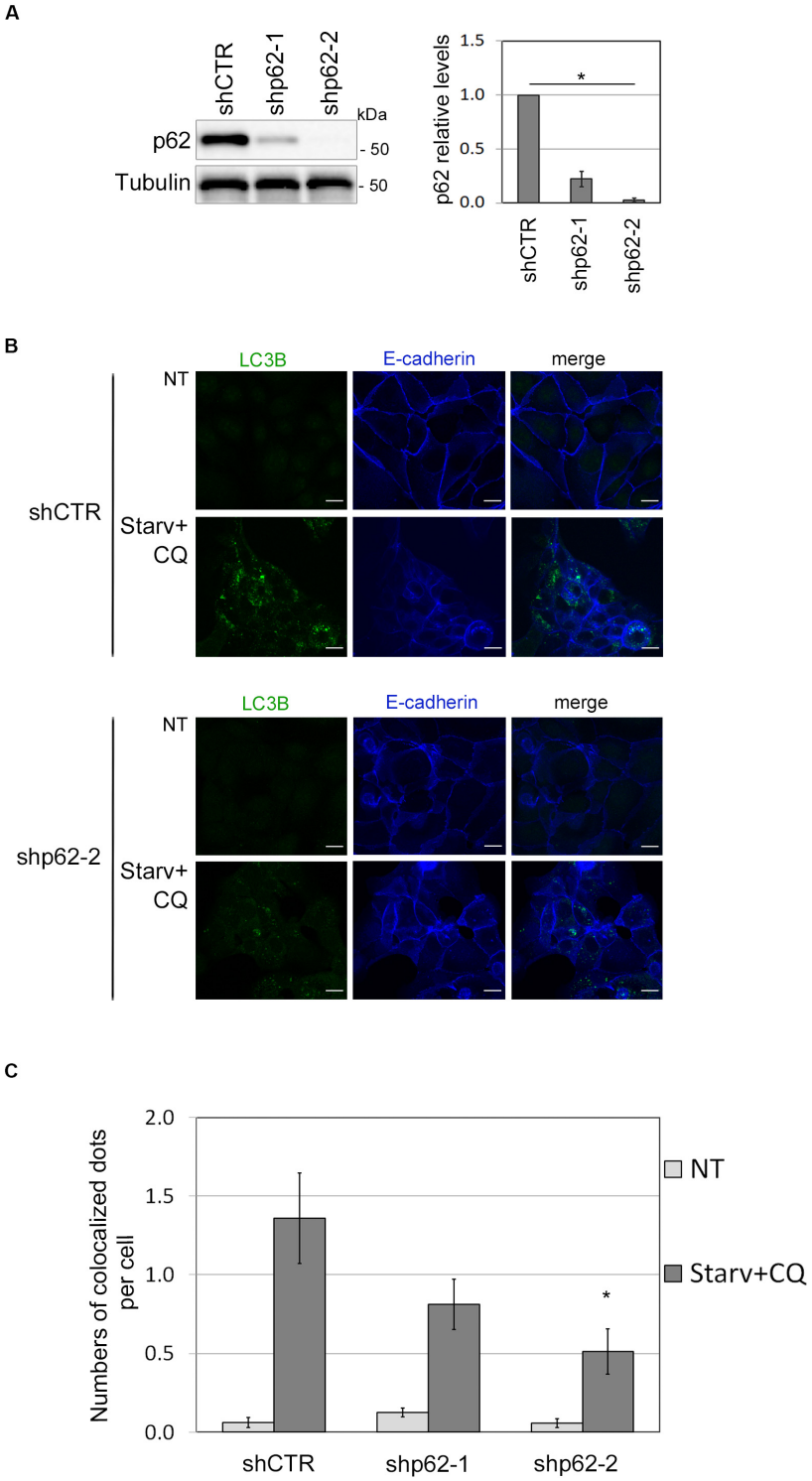

FIGURE 5 | SQSTM1/p62 knock-down restrains the E-cadherin delivery into autophagosomes. **(A)** Immunoblot showing the expression of SQSTM1/p62 in silenced (shp62-1, shp62-2) and in control (shCTR) HCC1937 cell line. The graph on the right reports the mean of SQSTM1/p62 relative levels of three experiments with SEM as error bars. SQSTM1/p62 relative levels were obtained by normalization over γ-tubulin (Tubulin, loading control) and rescaling to the control sample. The asterisk means statistical significance ($p < 0.001$) in the ANOVA test. **(B)** Representative images of shp62-2 and shCTR HCC1937 cell models untreated (NT) or starved and treated with CQ (Starv+CQ) for 8 h showing the E-cadherin and LC3B molecules stained with anti-E-cadherin/Alexa Fluor 633 and anti-LC3B/Alexa Fluor 488 antibodies, respectively. Merge images are reported. Scale bar, 20 μm. **(C)** Graph reported the quantification of LC3B and E-cadherin colocalized dots per cell in the experiments carried out as in **(B)**. At least 100 cells per sample were measured in three independent experiments. Bars show SEM. *$p < 0.05$.

SQSTM1/p62 has been found to be overexpressed in several cancer types where it induces the expression of inflammatory genes and triggers epithelial to mesenchymal transition, cell proliferation and metastasis (Qiang et al., 2014; Moscat et al., 2016; Puvirajesinghe et al., 2016; Taniguchi et al., 2016). Our data on the role of SQSTM1/p62 in the E-cadherin turnover add a piece of evidence in support of the role of this molecule in these tumor phenotypes.

Further investigations on a larger series of breast cancer might determine the prognostic role of E-cadherin and SQSTM1/p62 interaction and might shed light on the lack of consensus regarding the prognostic value of the sole E-cadherin (Horne et al., 2018).

Interestingly, a recent report involves another autophagy cargo protein, namely NBR1, in breast cancer metastatic dissemination (Marsh et al., 2020). By using different mammary cancer mouse models, the authors show that although genetic ablation of autophagy attenuates primary tumor growth, eventually fuels metastatic outgrowth and that NBR1 plays a key role in this context. These results suggest that the autophagic machinery may participate to tumor inception and progression by relying on different actors.

In conclusion, these findings suggest a model in which autophagy controls E-cadherin turnover through SQSTM1-mediated autophagosome delivery. Thus, the activation of autophagy, which is reported in breast cancers with poor prognosis and in dormant breast cancer cells (Lazova et al., 2012; Vera-Ramirez, 2019), might participate in the control of tumor cells spreading via modulation of E-cadherin.

DATA AVAILABILITY STATEMENT

The datasets generated for this study are available on request to the corresponding author.

ETHICS STATEMENT

The studies involving human participants were reviewed and approved by the Institutional Review Board of CRO Aviano National Cancer Institute. The patients/participants provided their written informed consent to participate in this study.

AUTHOR CONTRIBUTIONS

VD performed the western blots and IP, PD and time-lapse experiments as well as participated in the design of the study and in writing the manuscript. PS gave key ideas for the experiments with confocal laser scanning microscopy and participated in those analyses. GV performed the western blots analyses. TP assessed and selected E-cadherin positive breast tumors. RM discussed the interpretation of data and participated in writing the manuscript. MS designed experiments, did immunofluorescence and PLA studies, analyzed the data, and wrote the manuscript. All authors contributed to the article and approved the submitted version.

FUNDING

This study was supported by the Italian Ministry of Health and by CRO Intramural Research Grants (CUP J32F16001240001). VD was supported by an AIRC fellowship.

SUPPLEMENTARY MATERIAL

The Supplementary Material for this article can be found online at: https://www.frontiersin.org/articles/10.3389/fcell.2020.00545/full#supplementary-material

REFERENCES

Alizadeh, J., Glogowska, A., Thliveris, J., Kalantari, F., Shojaei, S., Hombach-Klonisch, S., et al. (2018). Autophagy modulates transforming growth factor beta 1 induced epithelial to mesenchymal transition in non-small cell lung cancer cells. *Biochim. Biophys. Acta* 1865, 749–768. doi: 10.1016/j.bbamcr.2018.02.007

Amaravadi, R., and Debnath, J. (2014). Mouse models address key concerns regarding autophagy inhibition in cancer therapy. *Cancer Discov.* 4, 873–875. doi: 10.1158/2159-8290.CD-14-0618

Birgisdottir, ÅB., Mouilleron, S., Bhujabal, Z., Wirth, M., Sjøttem, E., Evjen, G., et al. (2019). Members of the autophagy class III phosphatidylinositol 3-kinase complex I interact with GABARAP and GABARAPL1 via LIR motifs. *Autophagy* 15, 1333–1355. doi: 10.1080/15548627.2019.1581009

Borgna, S., Armellin, M., di Gennaro, A., Maestro, R., and Santarosa, M. (2012). Mesenchymal traits are selected along with stem features in breast cancer cells grown as mammospheres. *Cell Cycle* 11, 4242–4251. doi: 10.4161/cc.22543

Brückner, B. R., and Janshoff, A. (2018). Importance of integrity of cell-cell junctions for the mechanics of confluent MDCK II cells. *Sci. Rep.* 8:14117. doi: 10.1038/s41598-018-32421-2

Brüser, L., and Bogdan, S. (2017). Adherens junctions on the move-membrane trafficking of E-cadherin. *Cold Spring Harb. Perspect. Biol.* 9:a029140. doi: 10.1101/cshperspect.a029140

Cadwell, C. M., Su, W., and Kowalczyk, A. P. (2016). Cadherin tales: regulation of cadherin function by endocytic membrane trafficking. *Traffic* 17, 1262–1271. doi: 10.1111/tra.12448

Carneiro, P., Moreira, A. M., Figueiredo, J., Barros, R., Oliveira, P., Fernandes, M. S., et al. (2019). S100P is a molecular determinant of E-cadherin function in gastric cancer. *Cell Commun. Signal.* 17:155. doi: 10.1186/s12964-019-0465-9

Carvalho, S., Catarino, T. A., Dias, A. M., Kato, M., Almeida, A., Hessling, B., et al. (2016). Preventing E-cadherin aberrant N-glycosylation at Asn-554 improves its critical function in gastric cancer. *Oncogene* 35, 1619–1631. doi: 10.1038/onc.2015.225

Ciriello, G., Gatza, M. L., Beck, A. H., Wilkerson, M. D., Rhie, S. K., Pastore, A., et al. (2015). Comprehensive molecular portraits of invasive lobular breast cancer. *Cell* 163, 506–519. doi: 10.1016/j.cell.2015.09.033

Damiano, V., Brisotto, G., Borgna, S., di Gennaro, A., Armellin, M., Perin, T., et al. (2017). Epigenetic silencing of miR-200c in breast cancer is associated with aggressiveness and is modulated by ZEB1. *Genes Chromosomes Cancer* 56, 147–158. doi: 10.1002/gcc.22422

Daskalaki, I., Gkikas, I., and Tavernarakis, N. (2018). Hypoxia and selective autophagy in cancer development and therapy. *Front. Cell Dev. Biol.* 6:104. doi: 10.3389/fcell.2018.00104

di Gennaro, A., Damiano, V., Brisotto, G., Armellin, M., Perin, T., Zucchetto, A., et al. (2018). A p53/miR-30a/ZEB2 axis controls triple negative breast cancer aggressiveness. *Cell Death Differ.* 25, 2165–2180. doi: 10.1038/s41418-018-0103-x

Di Russo, J., Luik, A.-L., Yousif, L., Budny, S., Oberleithner, H., Hofschröer, V., et al. (2017). Endothelial basement membrane laminin 511 is essential for shear stress response. *EMBO J.* 36, 183–201. doi: 10.15252/embj.201694756

Fan, W., Tang, Z., Chen, D., Moughon, D., Ding, X., Chen, S., et al. (2010). Keap1 facilitates p62-mediated ubiquitin aggregate clearance via autophagy. *Autophagy* 6, 614–621. doi: 10.4161/auto.6.5.12189

Fong, J. T., Kells, R. M., Gumpert, A. M., Marzillier, J. Y., Davidson, M. W., and Falk, M. M. (2012). Internalized gap junctions are degraded by autophagy. *Autophagy* 8, 794–811. doi: 10.4161/auto.19390

Geng, F., Zhu, W., Anderson, R. A., Leber, B., and Andrews, D. W. (2012). Multiple post-translational modifications regulate E-cadherin transport during apoptosis. *J. Cell Sci.* 125, 2615–2625. doi: 10.1242/jcs.096735

Giatromanolaki, A., Koukourakis, M. I., Georgiou, I., Kouroupi, M., and Sivridis, E. (2018). LC3A, LC3B and Beclin-1 expression in gastric cancer. *Anticancer Res.* 38, 6827–6833. doi: 10.21873/anticanres.13056

Graziano, F., Humar, B., and Guilford, P. (2003). The role of the E-cadherin gene (CDH1) in diffuse gastric cancer susceptibility: from the laboratory to clinical practice. *Ann. Oncol.* 14, 1705–1713. doi: 10.1093/annonc/mdg486

Guo, Z., Neilson, L. J., Zhong, H., Murray, P. S., Zanivan, S., and Zaidel-Bar, R. (2014). E-cadherin interactome complexity and robustness resolved by quantitative proteomics. *Sci. Signal.* 7:rs7. doi: 10.1126/scisignal.2005473

Horne, H. N., Oh, H., Sherman, M. E., Palakal, M., Hewitt, S. M., Schmidt, M. K., et al. (2018). E-cadherin breast tumor expression, risk factors and survival: pooled analysis of 5,933 cases from 12 studies in the breast cancer association consortium. *Sci. Rep.* 8:6574. doi: 10.1038/s41598-018-23733-4

Ireton, R. C., Davis, M. A., van Hengel, J., Mariner, D. J., Barnes, K., Thoreson, M. A., et al. (2002). A novel role for p120 catenin in E-cadherin function. *J. Cell Biol.* 159, 465–476. doi: 10.1083/jcb.200205115

Izaguirre, M. F., and Casco, V. H. (2016). E-cadherin roles in animal biology: a perspective on thyroid hormone-influence. *Cell Commun. Signal.* 14:27. doi: 10.1186/s12964-016-0150-1

Johansen, T., and Lamark, T. (2011). Selective autophagy mediated by autophagic adapter proteins. *Autophagy* 7, 279–296. doi: 10.4161/auto.7.3.14487

Jones, M. C., Caswell, P. T., and Norman, J. C. (2006). Endocytic recycling pathways: emerging regulators of cell migration. *Curr. Opin. Cell Biol.* 18, 549–557. doi: 10.1016/j.ceb.2006.08.003

Klionsky, D. J., Abdelmohsen, K., Abe, A., Abedin, M. J., Abeliovich, H., Acevedo Arozena, A., et al. (2016). Guidelines for the use and interpretation of assays for monitoring autophagy (3rd edition). *Autophagy* 12, 1–222. doi: 10.1080/15548627.2015.1100356

Kourtidis, A., Lu, R., Pence, L. J., and Anastasiadis, P. Z. (2017). A central role for cadherin signaling in cancer. *Exp. Cell Res.* 358, 78–85. doi: 10.1016/j.yexcr.2017.04.006

Lazova, R., Camp, R. L., Klump, V., Siddiqui, S. F., Amaravadi, R. K., and Pawelek, J. M. (2012). Punctate LC3B expression is a common feature of solid tumors and associated with proliferation, metastasis, and poor outcome. *Clin. Cancer Res.* 18, 370–379. doi: 10.1158/1078-0432.CCR-11-1282

Levine, B., and Kroemer, G. (2008). Autophagy in the pathogenesis of disease. *Cell* 132, 27–42. doi: 10.1016/j.cell.2007.12.018

Levy, J. M. M., Thompson, J. C., Griesinger, A. M., Amani, V., Donson, A. M., Birks, D. K., et al. (2014). Autophagy inhibition improves chemosensitivity in BRAF(V600E) brain tumors. *Cancer Discov.* 4, 773–780. doi: 10.1158/2159-8290.CD-14-0049

Levy, J. M. M., Towers, C. G., and Thorburn, A. (2017). Targeting autophagy in cancer. *Nat. Rev. Cancer* 17, 528–542. doi: 10.1038/nrc.2017.53

Liang, C. (2010). Negative regulation of autophagy. *Cell Death Differ.* 17, 1807–1815. doi: 10.1038/cdd.2010.115

Liu, H., Ma, Y., He, H.-W., Zhao, W.-L., and Shao, R.-G. (2017). SPHK1 (sphingosine kinase 1) induces epithelial-mesenchymal transition by promoting the autophagy-linked lysosomal degradation of CDH1/E-cadherin in hepatoma cells. *Autophagy* 13, 900–913. doi: 10.1080/15548627.2017.1291479

Marsh, T., Kenific, C. M., Suresh, D., Gonzalez, H., Shamir, E. R., Mei, W., et al. (2020). Autophagic Degradation of NBR1 restricts metastatic outgrowth during mammary tumor progression. *Dev. Cell* 52, 591–604.e6. doi: 10.1016/j.devcel.2020.01.025

Maycotte, P., Gearheart, C. M., Barnard, R., Aryal, S., Mulcahy Levy, J. M., Fosmire, S. P., et al. (2014). STAT3-mediated autophagy dependence identifies subtypes of breast cancer where autophagy inhibition can be efficacious. *Cancer Res.* 74, 2579–2590. doi: 10.1158/0008-5472.CAN-13-3470

Mikhaylova, O., Stratton, Y., Hall, D., Kellner, E., Ehmer, B., Drew, A. F., et al. (2012). VHL-regulated MiR-204 suppresses tumor growth through inhibition of LC3B-mediated autophagy in renal clear cell carcinoma. *Cancer Cell* 21, 532–546. doi: 10.1016/j.ccr.2012.02.019

Miranda, K. C., Khromykh, T., Christy, P., Le, T. L., Gottardi, C. J., Yap, A. S., et al. (2001). A dileucine motif targets E-cadherin to the basolateral cell surface in Madin-Darby canine kidney and LLC-PK1 epithelial cells. *J. Biol. Chem.* 276, 22565–22572. doi: 10.1074/jbc.M101907200

Mizushima, N., and Komatsu, M. (2011). Autophagy: renovation of cells and tissues. *Cell* 147, 728–741. doi: 10.1016/j.cell.2011.10.026

Moreno-García, A., Kun, A., Calero, O., Medina, M., and Calero, M. (2018). An overview of the role of lipofuscin in age-related neurodegeneration. *Front. Neurosci.* 12:464. doi: 10.3389/fnins.2018.00464

Moscat, J., Karin, M., and Diaz-Meco, M. T. (2016). p62 in cancer: signaling adaptor beyond autophagy. *Cell* 167, 606–609. doi: 10.1016/j.cell.2016.09.030

Mowers, E. E., Sharifi, M. N., and Macleod, K. F. (2017). Autophagy in cancer metastasis. *Oncogene* 36, 1619–1630. doi: 10.1038/onc.2016.333

Nieto, M. A., Huang, R. Y.-J., Jackson, R. A., and Thiery, J. P. (2016). EMT: 2016. *Cell* 166, 21–45. doi: 10.1016/j.cell.2016.06.028

Palacios, F., Tushir, J. S., Fujita, Y., and D'Souza-Schorey, C. (2005). Lysosomal targeting of E-cadherin: a unique mechanism for the down-regulation of cell-cell adhesion during epithelial to mesenchymal transitions. *Mol. Cell. Biol.* 25, 389–402. doi: 10.1128/MCB.25.1.389-402.2005

Perl, A. K., Wilgenbus, P., Dahl, U., Semb, H., and Christofori, G. (1998). A causal role for E-cadherin in the transition from adenoma to carcinoma. *Nature* 392, 190–193. doi: 10.1038/32433

Puvirajesinghe, T. M., Bertucci, F., Jain, A., Scerbo, P., Belotti, E., Audebert, S., et al. (2016). Identification of p62/SQSTM1 as a component of non-canonical Wnt VANGL2-JNK signalling in breast cancer. *Nat. Commun.* 7:10318. doi: 10.1038/ncomms10318

Qiang, L., Zhao, B., Ming, M., Wang, N., He, T.-C., Hwang, S., et al. (2014). Regulation of cell proliferation and migration by p62 through stabilization of Twist1. *Proc. Natl. Acad. Sci. U.S.A.* 111, 9241–9246. doi: 10.1073/pnas.1322913111

Sancak, Y., Peterson, T. R., Shaul, Y. D., Lindquist, R. A., Thoreen, C. C., Bar-Peled, L., et al. (2008). The Rag GTPases bind raptor and mediate amino acid signaling to mTORC1. *Science* 320, 1496–1501. doi: 10.1126/science.1157535

Santarosa, M., Del Col, L., Tonin, E., Caragnano, A., Viel, A., and Maestro, R. (2009). Premature senescence is a major response to DNA cross-linking agents in BRCA1-defective cells: implication for tailored treatments of BRCA1 mutation carriers. *Mol. Cancer Ther.* 8, 844–854. doi: 10.1158/1535-7163.MCT-08-0951

Santarosa, M., Del Col, L., Viel, A., Bivi, N., D'Ambrosio, C., Scaloni, A., et al. (2010). BRCA1 modulates the expression of hnRNPA2B1 and KHSRP. *Cell Cycle* 9, 4666–4673. doi: 10.4161/cc.9.23.14022

Schneider, C. A., Rasband, W. S., and Eliceiri, K. W. (2012). NIH Image to ImageJ: 25 years of image analysis. *Nat. Methods* 9, 671–675. doi: 10.1038/nmeth.2089

Sharifi, M. N., Mowers, E. E., Drake, L. E., Collier, C., Chen, H., Zamora, M., et al. (2016). Autophagy promotes focal adhesion disassembly and cell motility of metastatic tumor cells through the direct interaction of paxillin with LC3. *Cell Rep.* 15, 1660–1672. doi: 10.1016/j.celrep.2016.04.065

Sun, T., Jiao, L., Wang, Y., Yu, Y., and Ming, L. (2018). SIRT1 induces epithelial-mesenchymal transition by promoting autophagic degradation of E-cadherin in melanoma cells. *Cell Death Dis.* 9:136. doi: 10.1038/s41419-017-0167-4

Tanida, I., Yamaji, T., Ueno, T., Ishiura, S., Kominami, E., and Hanada, K. (2008). Consideration about negative controls for LC3 and expression vectors for four colored fluorescent protein-LC3 negative controls. *Autophagy* 4, 131–134. doi: 10.4161/auto.5233

Taniguchi, K., Yamachika, S., He, F., and Karin, M. (2016). p62/SQSTM1-Dr. Jekyll and Mr. Hyde that prevents oxidative stress but promotes liver cancer. *FEBS Lett.* 590, 2375–2397. doi: 10.1002/1873-3468.12301

Vera-Ramirez, L. (2019). Cell-intrinsic survival signals. The role of autophagy in metastatic dissemination and tumor cell dormancy. *Semin. Cancer Biol.* 60, 28–40. doi: 10.1016/j.semcancer.2019.07.027

Weibrecht, I., Leuchowius, K.-J., Clausson, C.-M., Conze, T., Jarvius, M., Howell, M. W., et al. (2010). Proximity ligation assays: a recent addition to the proteomics toolbox. *Expert Rev. Proteomics* 7, 401–409. doi: 10.1586/epr.10.10

White, E. (2012). Deconvoluting the context-dependent role for autophagy in cancer. *Nat. Rev. Cancer* 12, 401–410. doi: 10.1038/nrc3262

Zhou, W., Gong, L., Wu, Q., Xing, C., Wei, B., Chen, T., et al. (2018). PHF8 upregulation contributes to autophagic degradation of E-cadherin, epithelial-mesenchymal transition and metastasis in hepatocellular carcinoma. *J. Exp. Clin. Cancer Res.* 37, 215. doi: 10.1186/s13046-018-0890-4

Zhu, W., Qu, H., Xu, K., Jia, B., Li, H., Du, Y., et al. (2017). Differences in the starvation-induced autophagy response in MDA-MB-231 and MCF-7 breast cancer cells. *Anim. Cells Syst.* 21, 190–198. doi: 10.1080/19768354.2017.1330763

Conflict of Interest: The authors declare that the research was conducted in the absence of any commercial or financial relationships that could be construed as a potential conflict of interest.

frontiers in Cell and Developmental Biology

BRIEF RESEARCH REPORT
published: 07 July 2020
doi: 10.3389/fcell.2020.00460

Casein Kinase 1 Family Member CK1δ/Hrr25 Is Required for Autophagosome Completion

*Yuting Li[1], Xuechai Chen[1], Qianqian Xiong[1], Yong Chen[2], Hongyu Zhao[2], Muhammad Tahir[1], Jingdong Song[3], Bing Zhou[4] and Juan Wang[1]**

[1] College of Life Science and Bioengineering, Beijing University of Technology, Beijing, China, [2] National Laboratory of Biomacromolecules, CAS Center for Excellence in Biomacromolecules, Institute of Biophysics, Chinese Academy of Sciences, Beijing, China, [3] National Institute for Viral Disease Control and Prevention, Chinese Center for Disease Control and Prevention, Beijing, China, [4] State Key Laboratory of Membrane Biology, School of Life Sciences, Tsinghua University, Beijing, China

Autophagy starts with the initiation and nucleation of isolation membranes, which further expand and seal to form autophagosomes. The regulation of isolation membrane closure remains poorly understood. CK1δ is a member of the casein kinase I family of serine/threonine specific kinases. Although CK1δ is reported to be involved in various cellular processes, its role in autophagy is unknown. Here, we show that CK1δ regulates the progression of autophagy from the formation of isolation membranes to autophagosome closure, and is essential for macroautophagy. CK1δ depletion results in impaired autophagy flux and the accumulation of unsealed isolation membranes. The association of LC3 with ATG9A, ATG14L, and ATG16L1 was found to be increased in CK1δ-depleted cells. The role of CK1δ in autophagosome completion appears to be conserved between yeasts and humans. Our data reveal a key role for CK1δ/Hrr25 in autophagosome completion.

Keywords: autophagy, CK1δ, Hrr25, isolation membrane, autophagosome closure

OPEN ACCESS

Edited by:
Du Feng,
Guangzhou Medical University, China

Reviewed by:
Mario Mauthe,
University Medical Center Groningen, Netherlands
Maurizio Renna,
University of Cambridge, United Kingdom

****Correspondence:***
Juan Wang
juanwang@bjut.edu.cn

Specialty section:
This article was submitted to Membrane Traffic, a section of the journal Frontiers in Cell and Developmental Biology

Received: *31 January 2020*
Accepted: *18 May 2020*
Published: *07 July 2020*

Citation:
Li Y, Chen X, Xiong Q, Chen Y, Zhao H, Tahir M, Song J, Zhou B and Wang J (2020) Casein Kinase 1 Family Member CK1δ/Hrr25 Is Required for Autophagosome Completion. Front. Cell Dev. Biol. 8:460. doi: 10.3389/fcell.2020.00460

INTRODUCTION

Autophagy is an evolutionarily conserved pathway in which cytoplasmic components are sequestered within double-membrane vesicles called autophagosomes, and then transported into lysosomes or vacuoles for degradation (Nakatogawa et al., 2009; Lamb et al., 2013; Feng et al., 2014). Autophagy is essential for cellular homeostasis and the cellular response to stress conditions such as nutrient starvation. Defects in autophagy pathways have been associated with numerous human pathologies including infectious diseases, neurodegenerative disorders, and cancer (Yang and Klionsky, 2010; Dikic and Elazar, 2018). Starvation-induced macroautophagy is non-selective; by contrast, selective autophagy involves the recognition of cellular cargoes by specific receptors and their subsequent engulfment by autophagosomes (Nakatogawa et al., 2009; Lamb et al., 2013; Feng et al., 2014).

Autophagy is initiated with the *de novo* formation of a cup-shaped membrane, known as the isolation membrane or phagophore, which expands and seals to form the autophagosome (Nakatogawa et al., 2009; Lamb et al., 2013; Feng et al., 2014). In mammalian cells, this is followed by the fusion of autophagosomes with endosomes and lysosomes to form degradative autolysosomes. Autophagy is regulated by autophagy-related (ATG) proteins, which are recruited to the site of

autophagosome formation, in a hierarchical order, upon autophagy induction (Nakatogawa et al., 2009; Lamb et al., 2013; Feng et al., 2014). Autophagy-related proteins include the ULK1/Atg1 complex, which is required for the initiation of autophagy; the PI3K complex, which is essential for nucleation of the isolation membrane; Atg9, the only transmembrane core ATG protein, which is required during the early stages of autophagy; and the Atg12 and Atg8 conjugation systems, which have roles in vesicle expansion. Although most ATG proteins disassociate from the autophagic membrane structures during autophagosome closure, the lipidated form of LC3/Atg8 associates with autophagic structures at all stages; therefore, LC3/Atg8 represents a useful marker of isolation membranes and autophagosomes (Lamb et al., 2013; Klionsky et al., 2016).

CK1δ (casein kinase I δ), a member of the CK1 family of serine/threonine specific kinases, is involved in the regulation of various cellular processes including circadian rhythms, Wnt signaling, cytoskeleton maintenance, the cell cycle, and DNA damage repair (Xu et al., 2019). Hrr25, the yeast homolog of CK1δ, has been reported to activate multiple selective autophagy pathways by phosphorylating cargo receptors and promoting the interactions of these receptors with the scaffold protein Atg11 (Mochida et al., 2014; Pfaffenwimmer et al., 2014; Tanaka et al., 2014). We previously reported that Hrr25 is also required for macroautophagy (Wang et al., 2015). However the role of CK1δ in macroautophagy in mammalian cells remains unclear.

In this study, we show that CK1δ is essential for macroautophagy in mammalian cells, and that CK1δ depletion or Hrr25 mutation results in blockade of the progression of isolation membranes to autophagosomes, thus revealing a key role of CK1δ/Hrr25 in autophagosome completion.

TABLE 1 | List of antibodies used in this study.

Antibodies	Source	Identifier	Dilution
Rabbit poly clonal anti-p62	MBL	Cat#PM045	1:1000 (WB), 1:500 (IF)
Rabbit poly clonal anti-LC3B	Cell Signaling Technology	Cat#2775	1:1000 (WB)
Rabbit poly clonal anti-P-Actin	Solarbio	Cat#K101527P	1:1000 (WB)
Rabbit poly clonal anti-GFP	Abeam	Cat#ab290	1:2000 (WB)
Rabbit Poly clonal anti-Casein Kinase 1 delta	Proteintech	Cat# 14388-1-AP	1:600 (WB)
Goat Anti-Rabbit IgG-HRP	Solarbio	Cat#SE134	1:5000 (WB)
Rabbit poly clonal anti-ATG14	Cell Signaling Technology	Cat#5504	1:100 (IF)
Rabbit monoclonal anti-ATG16LI	Cell Signaling Technology	Cat#8089	1:80 (IF)
Rabbit poly clonal anti-ATG9A	MBL	Cat#PD042	1:200 (IF)
Mouse monoclonal anti-LC3B	MBL	Cat#M152-3	1:100 (IF)
Fluorescein(FITC)-conjugated AffiniPure Goat Anti-Rabbit IgG(H+L)	Jackson Immuno Research	Cat# 111-095-003	1:100 (IF)
Flu ores cein(FITC)-conjugated AffiniPure Goat Anti -Mouse IgG(H+L)	Jackson Immuno Research	Cat# 115-095-003	1:100 (IF)
Rhodamine(TRITC)-conjugated AffiniPure Goat Anti-Mouse IgG(H+L)	Jackson Immuno Research	Cat# 115-025-003	1:100 (IF)

WB, Western Blot; IF, Immunofluorescence.

MATERIALS AND METHODS

Cell Culture and Transfection

HeLa cells were cultured in DMEM (Hyclone) and 10% fetal bovine serum (FBS, Gibco) supplemented with 1% penicillin-streptomycin (Gibco) at 37°C and 5% CO_2. For starvation, cells were washed with PBS three times and incubated with Earle's balanced salt solution (EBSS, Gibco) for 2–h at 37°C. Transfection of plasmids was carried out with Lipofectamine 3000 (Invitrogen) according to the manufacturer's protocols. Transfection of small interfering RNAs (siRNAs) was carried out with Lipofectamine RNAi MAX (Invitrogen). To knockdown CK1δ, double-stranded siRNAs were purchased from GenePharma. The following sequences were used: human CK1δ siRNA 5′-CGACCUCACAGGCCGACAATT-3′ and control siRNA 5′-UUCUCCGAACGUGUCACGUTT-3′.

Yeast Media

Yeast cells were grown at 25°C in yeast extract peptone dextrose media (YPD; 1% yeast extract, 2% peptone, and 2% dextrose) or synthetic minimal media (SMD; 0.67% yeast nitrogen base, 2% dextrose, and auxotrophic amino acids, as needed). To induce starvation, yeast cells were transferred to SD(–N) medium (0.17% yeast nitrogen base without amino acids and 2% dextrose) or treated with 400 ng/ml rapamycin.

Quantitative RT-PCR

Total RNA was extracted from CK1δ-knockdown HeLa cells using the Cultured CellTotal RNA Extraction Kit (TIANGEN), and cDNA was reverse-transcribed using the FastQuant RT Kit(TIANGEN). Quantitative PCR was carried out on a Step One PlusTM RealTime PCR system using SuperReal PreMix Plus (TIANGEN). Data were normalized to the expression level of β-actin. Results are representative of at least three experiments. The following primers were used: F-CK1 Delta, 5′-CTCCGTGTTCCGTTTC-3′; R-CK1 Delta, 5′-TGCTACTCGCCATCCT-3′; F-GAPDH, 5′-GGCATCCTGGGCTACACTGA-3′; R-GAPDH, 5′-GTGGTC GTTGAGGGCAATG-3′.

Immunoblotting

Total proteins were extracted from HeLa cells with RIPA Lysis Buffer (Solarbio) supplemented with 1 mM PMSF, and incubated for 30 min on 4°C. Cell lysates were centrifuged at 12000 *g* for 30 min at 4°C. Supernatants were separated by SDS-PAGE and transferred onto a PVDF membrane, followed by incubation with

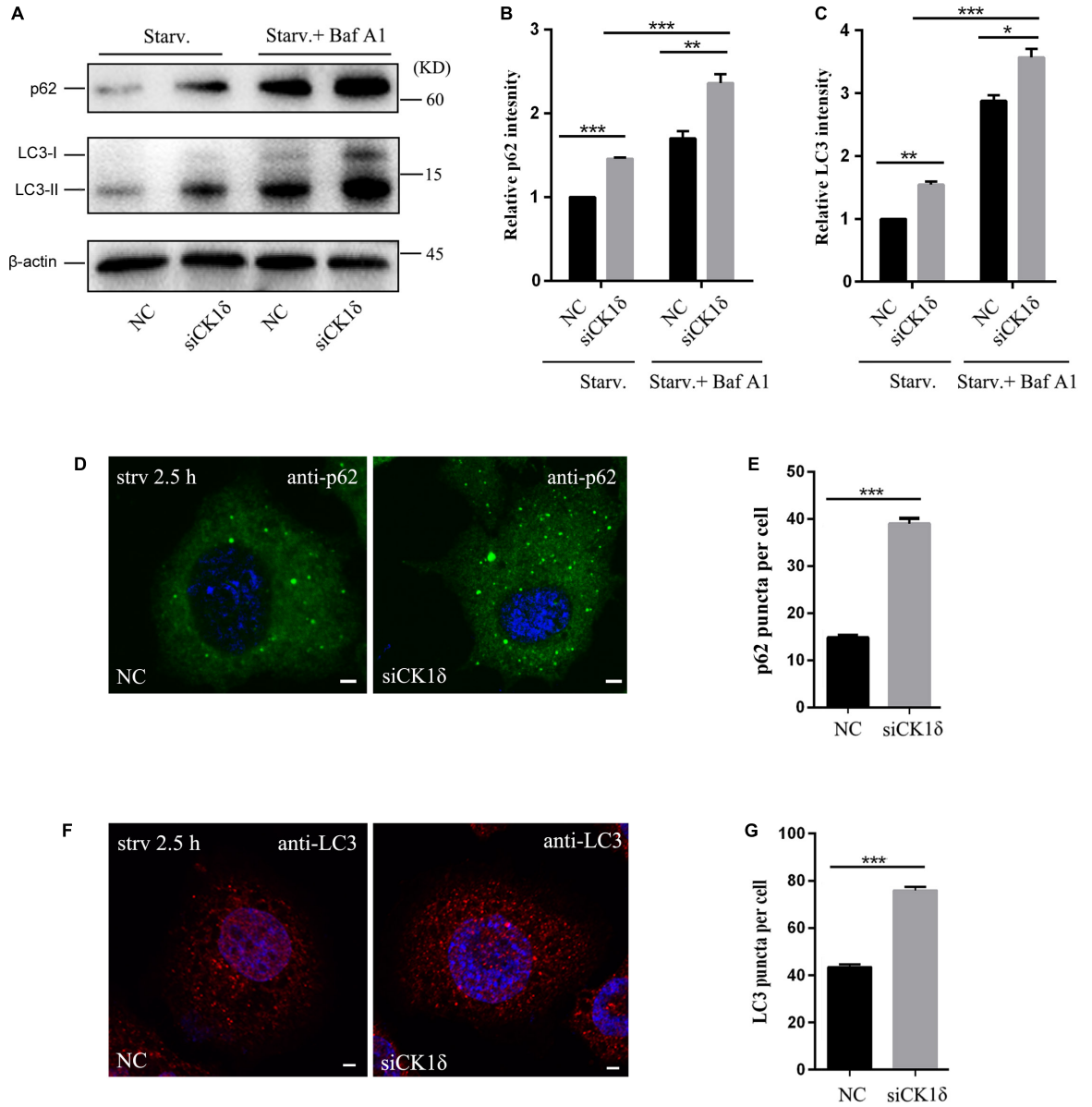

FIGURE 1 | CK1δ depletion impairs autophagic flux. **(A–C)** Immunoblotting of LC3 and p62 in negative control (NC) and CK1δ-depleted HeLa cells. Cells were starved were starved in EBSS for 2.5 h with or without bafilomycin A1 (100 nM, 6 h). The relative levels of p62 and LC3-II were normalized to β-actin levels as shown in panels **(B)** and **(C)**, respectively. NC under starvation condition was normalized to be 1. Error bars represent SEM; $n = 3$; $^{*}p < 0.05$, $^{**}p < 0.01$, $^{***}p < 0.001$, Student's *t* test. **(D,E)** Immunostaining of p62 using endogenous antibody. CK1δ-depleted HeLa cells and control cells were starved in EBSS for 2.5 h. Scale bars, 5 μm. Quantification of p62 puncta number is shown in panel **(E)**. Cells from three separate experiments (200 in total) were examined to calculate the numbers of p62 puncta. Error bars represent SEM; $^{***}p < 0.001$, Student's *t* test. **(F,G)** Immunostaining of LC3 using endogenous antibody. CK1δ-depleted HeLa cells and control cells were starved in EBSS for 2.5 h. Scale bars, 5 μm. Quantification of p62 puncta number is shown in panel **(G)**. Cells from three separate experiments (200 in total) were examined to calculate the numbers of LC3 puncta. Error bars represent SEM; $^{***}p < 0.001$, Student's *t* test.

primary and secondary antibodies (**Table 1**); then, the PVDF membrane was visualized using an ECL kit (Millipore). Results are representative of at least three experiments. The relative levels of p62 and LC3-II were normalized to β -actin levels.

Immunofluorescence

HeLa cells grown on cover slips were fixed with 4% paraformaldehyde for 20 min. Cells were permeabilized in 10 μg/mL digitonin (Sigma) for 15 min at 25°C. After blocking with 5% goat serum for 60 min at 25°C, cells were incubated with the indicated primary antibodies overnight at 4°C. After three washes with PBS, cells were stained with FITC or Rhodamine-labeled secondary antibodies for 1 h at room temperature. Nuclei were stained with 0.2% Hoechst 33258 for 30 min. Images were acquired using a FV3000 confocal microscope (Olympus). The colocalization was measured using the ImageJ software.

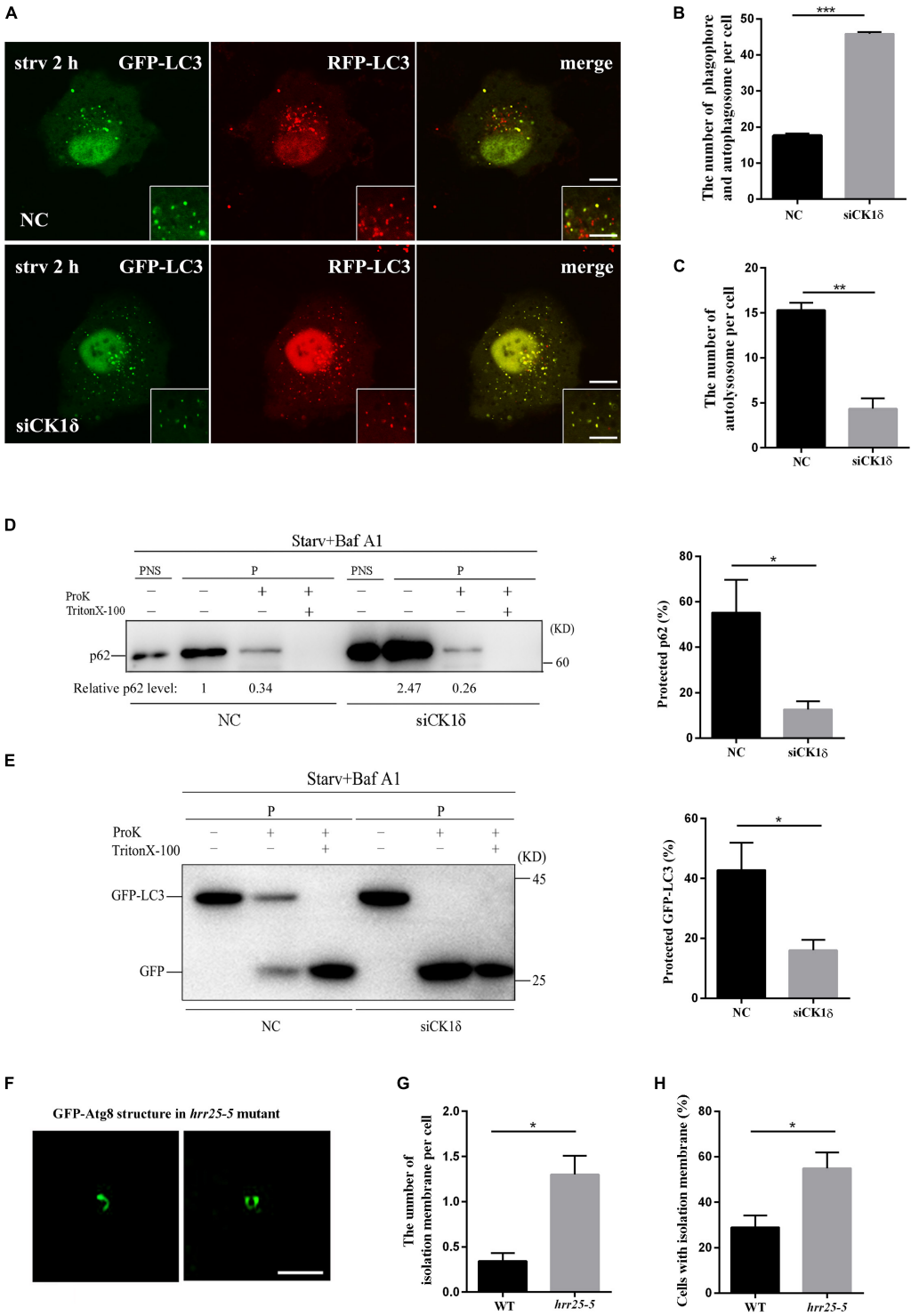

FIGURE 2 | Unsealed isolation membranes accumulate in CK1δ-depleted cells and the *hrr25-5* mutant. **(A–C)** CK1δ-depleted HeLa cells and control cells transfected with RFP-GFP-LC3 reporter plasmid were starved for 2 h. Scale bars in panel **(A)**, 5 μm; Scale bars in insets, 2 μm. Quantification of the number of yellow puncta (autophagosome and isolation membranes) is shown in panel **(B)**. Quantification of the number of red puncta (autolysosome) is shown in panel **(C)**. Cells from three separate experiments (200 in total) were examined to calculate the numbers of LC3 puncta. Error bars represent SEM; $^{**}p < 0.01$. $^{***}p < 0.001$, Student's *t* test. **(D)** CK1δ-depleted HeLa cells and control cells were starved starved in EBSS for 2 h and treated with 100 nM bafilomycin A1 for 6 h. The post-nuclear supernatant (PNS) and high-speed pellet (P) fractions were analyzed by immunoblotting using anti-p62 antibody. The subfractions were incubated in the presence or absence of proteinase K (Pro K) and Triton X-100. The percentage of protected p62 were calculated from four separate experiments and shown

(Continued)

FIGURE 2 | Continued
in the right. Error bars represent SEM; *$p < 0.05$, Student's *t* test. **(E)** GFP-LC3 expressing CK1δ-depleted HeLa cells and control cells were starved in EBSS for 2 h and treated with 100 nM bafilomycin A1 for 6 h. The high-speed pellet (P) fractions were analyzed by immunoblotting using anti-GFP antibody. The subfractions were incubated in the presence or absence of proteinase K (Pro K) and Triton X-100. The percentage of protected GFP-LC3 were calculated from four separate experiments and shown in the right. Error bars represent SEM; *$p < 0.05$, Student's *t* test. **(F–H)** Wild-type yeast cells and *hrr25-5* mutant cells expressing GFP-Atg8 were grown to log phase and treated with 400 ng/ml rapamycin for 1 h at 37°C. Deconvolved images of isolation membranes in the *hrr25-5* mutant are shown in panel **(F)**. Scale bars, 1 μm. Numbers of isolation membranes were calculated in 100 cells from three separate experiments and shown in panel **(G)**. Percentage of cells with isolation membrane was calculated in 100 cells from three separate experiments and shown in panel **(H)**. Error bars represent SEM; *$p < 0.05$, Student's *t* test.

Protease Protection Assay

HeLa cells were starved in EBSS for 2 h, treated with 100 nM bafilomycin A1 for 6 h, and suspended in ice-cold homogenization buffer (composed of 20 mM HEPES, 0.22 M mannitol, 0.07 M sucrose, and protease inhibitors; pH 7.4). Cells were then passed 10 times through a 27-gauge needle using a 1 ml injection syringe, and the post-nuclear supernatant (PNS) was recovered by centrifugation at 4500 *g* and at 4°C, for 10 min. The supernatant was then centrifuged again at 100,000 *g* for 30 min to acquire the pellet fraction. The pellet was resuspended in homogenization buffer and then treated with 100 μg/ml proteinase K (ProK) with or without 0.5% Triton X-100. After incubation for 20 min on ice, 10% Trichloroacetic acid (TCA) was added, and the samples were centrifuged at 15,000 *g* for 10 min. The pellet was washed with ice-cold acetone, resuspended in SDS-PAGE sample buffer, and boiled at 100°C for 10 min. Proteinase K digestion products were detected by immunoblotting.

Super-Resolution Structured Illumination Microscopy

To analyze phagophore formation, yeast cells were fixed with 3.7% formaldehyde at 25°C for 30 min, and then visualized by super-resolution structured illumination microscopy (SIM), at 25°C, on an Applied Precision DeltaVision OMX Super Resolution System using an Olympus UPlanSApo 100 × 1.4 NA oil objective. The data were acquired and processed using Delta Vision OMX Master Control software and SoftWoRx reconstruction and analysis software.

Statistical Analysis

The significance of differences was evaluated by an unpaired two-tailed *t* test. Data were analyzed for statistical significance after at least three repeated experiments. Threshold for statistical significance for each test was set at 95% confidence ($p < 0.05$). Error bars represent SEM. *$p < 0.05$, **$p < 0.01$. ***$p < 0.001$.

RESULTS

Depletion of CK1δ Impairs Autophagic Flux

To determine whether CK1δ is essential for autophagy, we used siRNAs to deplete HeLa cells of CK1δ, and examined the autophagic flux by monitoring the level of p62, an autophagy substrate (Klionsky et al., 2016). As shown in **Supplementary Figure S1**, CK1δ was efficiently depleted. CK1δ depletion resulted in increased levels of p62 (**Figures 1A,B**). Immunostaining of p62 also showed that, the number of p62 puncta was higher in CK1δ-depleted cells than that in control cells under starvation conditions (**Figures 1D,E**), suggesting the blockade of autophagic flux.

Following the induction of autophagy, the non-lipidated form of LC3 (LC3-I) is conjugated to PE to form the lipidated LC3-II form, which associates with autophagic membrane structures and forms punctate structures. Analysis of LC3-II levels serves as a useful assay to determine which step of autophagy is affected (Klionsky et al., 2016). We examined the levels of LC3 II in CK1δ-depleted cells under starvation conditions with or without bafilomycin A1, an autophagosome-lysosome fusion inhibitor. As shown in **Figures 1A,C**, CK1δ depletion resulted in increased levels of LC3-II, indicating that the defect in autophagic flux occurs after LC3 lipidation. The addition of bafilomycin A1 significantly increased the LC3-II levels in CK1δ-depleted cells, suggesting that autophagosome-lysosome fusion is not blocked by CK1δ depletion. LC3 immunostaining revealed that the number of LC3 puncta was increased in CK1δ-depleted cells (**Figures 1F,G**). The non-lipidated form of LC3-I is diffuse, and only the lipidated LC3-II form associates with autophagic membrane structures; therefore, these data indicate that LC3-II-positive structures accumulate in CK1δ-depleted cells. These data are consistent with results in temperature-sensitive yeast *hrr25-5* mutant cells; in a previous study, we observed numerous punctate GFP-Atg8 structures in the *hrr25-5* mutant, despite the decreased autophagic activity in these cells (Wang et al., 2015).

Collectively, these results indicate that CK1δ depletion impairs autophagic flux downstream of LC3 lipidation and leads to the accumulation of LC3-II-positive structures.

Unsealed Autophagosomes Accumulate in CK1δ-Depleted Cells and the *hrr25-5* Mutant

To determine which step of the autophagy pathway is affected by CK1δ depletion, we examined the stage of the autophagic structures observed in CK1δ-depleted cells and *hrr25-5* mutant cells. The tandem red fluorescent protein (RFP)-green fluorescent protein (GFP)-LC3 reporter was transfected into CK1δ-depleted cells and control cells as previously described. The GFP fluorescence signal is quenched in

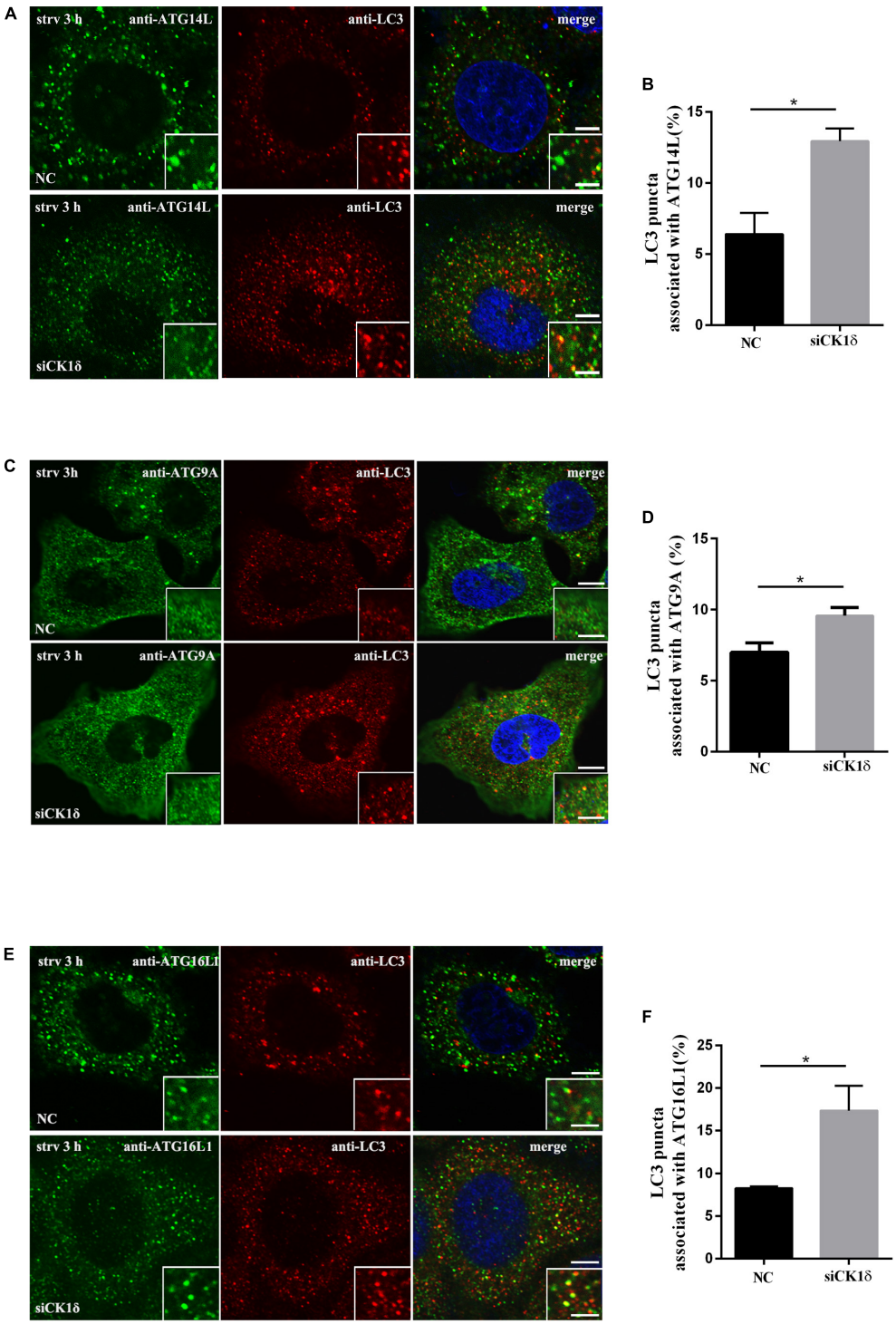

FIGURE 3 | Depletion of CK1δ results in increased association of LC3 and multiple ATG proteins. **(A,B)** Immunostaining of LC3 and ATG14L using endogenous antibodies. HeLa cells depleted of CK1δ and control HeLa cells were starved for 3 h. Scale bars, 5 μm. Scale bars in insets, 2 μm. Quantification of the percentage of LC3 puncta that associate with ATG14L puncta is shown in panel **(B)**. Cells from three separate experiments (150 in total) were examined. Error bars represent SEM; *$p < 0.05$, Student's *t* test. **(C,D)** Immunostaining of LC3 and ATG9A using endogenous antibodies. HeLa cells depleted of CK1δ and control HeLa cells were starved for 3 h. Scale bars, 5 μm. Scale bars in insets, 2 μm. Quantification of the percentage of LC3 puncta that associate with ATG9A puncta is shown in panel **(D)**. Cells from three separate experiments (150 in total) were examined. Error bars represent SEM; *$p < 0.05$. Student's *t* test. **(E,F)** Immunostaining of LC3 and ATG16L1 using endogenous antibodies. HeLa cells depleted of CK1δ and control HeLa cells were starved for 3 h. Scale bars, 5 μm. Scale bars in insets, 2 μm. Quantification of the percentage of LC3 puncta that associate with ATG16L1 puncta is shown in panel **(D)**. Cells from three separate experiments (150 in total) were examined. Error bars represent SEM; *$p < 0.05$. Student's *t* test.

acidified compartments; accordingly, prior to fusion with the lysosome, the isolation membranes and immature autophagosomes decorated with RFP-GFP-LC3 are visible as yellow puncta, whereas red puncta represent acidified autolysosomes (Kimura et al., 2007). We found that after 2 h of starvation, larger numbers of yellow puncta had accumulated and very few red puncta had formed in CK1δ-depleted cells (**Figures 2A–C**). These results indicate that CK1δ depletion causes a defect in the progression of isolation membranes to autolysosomes, and that accumulated LC3 puncta in CK1δ-depleted cells represent isolation membranes or autophagosomes, not autolysosomes.

To verify that the LC3-positive structures in CK1δ-depleted cells represented isolation membranes or autophagosomes, we performed a protease protection assay, which is based on the accessibility of GFP-LC3 or p62, sequestered in autophagosomes or not, to protease (Klionsky et al., 2016): when GFP-LC3 and p62 are sequestered by sealed autophagosomes, they are inaccessible to the protease; by contrast, GFP-LC3 and p62 in isolation membranes are accessible to the enzyme. We found that the sensitivity of GFP-LC3 and p62 to ProK was enhanced in CK1δ-depleted cells (**Figures 2D,E**). These results confirm that the LC3-positive structures in CK1δ-depleted cells are isolation membranes, revealing a role for CK1δ in autophagosome completion.

Consistent with the results in CK1δ-depleted cells, SIM revealed that elongated isolation membranes were accumulated in the temperature-sensitive *hrr25-5* mutant at 37°C, a non-permissive temperature. As shown in **Figures 2F,G**, the number of isolation membranes was significantly increased in the *hrr25-5* mutant compared with that in the wild type. The percentage of cells with isolation membrane was also significantly higher in the *hrr25-5* mutant (**Figure 2H**). Together, these findings show that CK1δ depletion or the *hrr25* mutation results in a defect in the progression of the autophagy pathway from the formation of isolation membranes to sealed autophagosomes.

Depletion of CK1δ Results in Increased Association of LC3 With Multiple ATG Proteins

Upon autophagy induction, ATG proteins are recruited to the autophagosome formation site in a hierarchical order. Most ATG proteins disassociate from the autophagic membrane structures as autophagosomes close, whereas the lipidated form of LC3/Atg8 associates with autophagic structures at all stages (Itakura and Mizushima, 2010; Lamb et al., 2013). Failure of isolation membranes to seal and form closed autophagosomes results in ATG proteins, which act during the early stages of autophagy, becoming trapped in the isolation membranes along with LC3. Accordingly, we examined the colocalization or association of LC3 puncta with multiple ATG proteins, including ATG9A, ATG14L, and ATG16L1, by immunofluorescence. As shown in **Figure 3**, the association of LC3 with all three ATG proteins increased in CK1δ-depleted cells although the numbers of ATG9A, ATG14L, and ATG16L1 puncta in CK1δ-depleted cells were comparable to those in control cells (**Supplementary Figure S2**). These data are consistent with the hypothesis that CK1δ regulates autophagosome completion.

DISCUSSION

We showed that CK1δ regulates autophagosome completion, and is required for autophagy in mammalian cells. CK1δ depletion was found to result in the accumulation of isolation membranes and increased association of LC3 with ATG9A, ATG14L, and ATG16L1. To the best of our knowledge, this is the first report of the essential role of CK1δ in macroautophagy. The role of CK1δ/Hrr25 in autophagosome completion appears to be conserved between yeasts and humans.

Although the regulation of autophagosome completion is not fully understood, several proteins have been reported to regulate autophagosome completion. In mammalian cells, depletion of CHMP2A, a component of ESCRT (endosomal sorting complex required for transport), a dominant-negative $VPS4A^{E228Q}$ mutant, overexpression of $Atg4B^{C74A}$ mutant, and knockdown of ATG2A and ATG2B cause defects in autophagosome closure (Fujita et al., 2008; Velikkakath et al., 2012; Takahashi et al., 2018). In yeast, the Vps21 module, ESCRT components are considered to play roles in autophagosome closure and PI3P phosphatase Ymr1 is essential for the clearance of PI3P and release of Atg proteins from the closed autophagosome (Cebollero et al., 2012; Zhou et al., 2017, 2019a,b). At present, the relationship between CK1δ and other regulators remains unknown, as do the substrates that CK1δ phosphorylates during autophagosome completion. Elucidation of these aspects should further advance the understanding of the mechanisms involved in autophagosome completion. Furthermore, the dysregulation of CK1δ and mutations in this kinase are linked to various diseases, including cancer, neurodegenerative disorders, and metabolic diseases (Xu et al., 2019); therefore, future studies should aim to determine whether CK1δ contributes to the development of these diseases through its role in autophagy.

DATA AVAILABILITY STATEMENT

All datasets generated for this study are included in the article/**Supplementary Material**.

AUTHOR CONTRIBUTIONS

JW designed the research. YL, QX, XC, YC, HZ, and JS performed the experiments. JW, YL, BZ,

and QX analyzed the data. JW and MT wrote the manuscript. All authors contributed to the article and approved the submitted version.

FUNDING

This work was supported by the National Natural Science Foundation of China (Nos. 91854115, 31771571, and 31970044 to JW) and the State Key Laboratory of Membrane Biology, Beijing, China.

ACKNOWLEDGMENTS

We thank Dr. Susan Ferro-Novick for providing the *hrr25-5* mutant strain.

SUPPLEMENTARY MATERIAL

The Supplementary Material for this article can be found online at: https://www.frontiersin.org/articles/10.3389/fcell.2020.00460/full#supplementary-material

REFERENCES

Cebollero, E., van der Vaart, A., Zhao, M., Rieter, E., Klionsky, D. J., Helms, J. B., et al. (2012). Phosphatidylinositol-3-phosphate clearance plays a key role in autophagosome completion. *Curr. Biol.* 22, 1545–1553. doi: 10.1016/j.cub.2012.06.029

Dikic, I., and Elazar, Z. (2018). Mechanism and medical implications of mammalian autophagy. *Nat. Rev. Mol. Cell Biol.* 19, 349–364. doi: 10.1038/s41580-018-0003-4

Feng, Y., He, D., Yao, Z., and Klionsky, D. J. (2014). The machinery of macroautophagy. *Cell Res.* 24, 24–41. doi: 10.1038/cr.2013.168

Fujita, N., Hayashi-Nishino, M., Fukumoto, H., Omori, H., Yamamoto, A., Noda, T., et al. (2008). An Atg4B mutant hampers the lipidation of LC3 paralogues and causes defects in autophagosome closure. *Mol. Biol. Cell* 19, 4651–4659. doi: 10.1091/mbc.E08-03-0312

Itakura, E., and Mizushima, N. (2010). Characterization of autophagosome formation site by a hierarchical analysis of mammalian Atg proteins. *Autophagy* 6, 764–776. doi: 10.4161/auto.6.6.12709

Kimura, S., Noda, T., and Yoshimori, T. (2007). Dissection of the autophagosome maturation process by a novel reporter protein, tandem fluorescent-tagged LC3. *Autophagy* 3, 452–460. doi: 10.4161/auto.4451

Klionsky, D. J., Abdelmohsen, K., Abe, A., Abedin, M. J., Abeliovich, H., Acevedo Arozena, A., et al. (2016). Guidelines for the use and interpretation of assays for monitoring autophagy (3rd edition). *Autophagy* 12, 1–222. doi: 10.1080/15548627.2015.1100356

Lamb, C. A., Yoshimori, T., and Tooze, S. A. (2013). The autophagosome: origins unknown, biogenesis complex. *Nat. Rev. Mol. Cell Biol.* 14, 759–774. doi: 10.1038/nrm3696

Mochida, K., Ohsumi, Y., and Nakatogawa, H. (2014). Hrr25 phosphorylates the autophagic receptor Atg34 to promote vacuolar transport of alpha-mannosidase under nitrogen starvation conditions. *FEBS Lett.* 588, 3862–3869. doi: 10.1016/j.febslet.2014.09.032

Nakatogawa, H., Suzuki, K., Kamada, Y., and Ohsumi, Y. (2009). Dynamics and diversity in autophagy mechanisms: lessons from yeast. *Nat. Rev. Mol. Cell Biol.* 10, 458–467. doi: 10.1038/nrm2708

Pfaffenwimmer, T., Reiter, W., Brach, T., Nogellova, V., Papinski, D., Schuschnig, M., et al. (2014). Hrr25 kinase promotes selective autophagy by phosphorylating the cargo receptor Atg19. *EMBO Rep.* 15, 862–870. doi: 10.15252/embr.201438932

Takahashi, Y., He, H., Tang, Z., Hattori, T., Liu, Y., Young, M. M., et al. (2018). An autophagy assay reveals the ESCRT-III component CHMP2A as a regulator of phagophore closure. *Nat. Commun.* 9:2855. doi: 10.1038/s41467-018-05254-w

Tanaka, C., Tan, L. J., Mochida, K., Kirisako, H., Koizumi, M., Asai, E., et al. (2014). Hrr25 triggers selective autophagy-related pathways by phosphorylating receptor proteins. *J. Cell Biol.* 207, 91–105. doi: 10.1083/jcb.201402128

Velikkakath, A. K., Nishimura, T., Oita, E., Ishihara, N., and Mizushima, N. (2012). Mammalian Atg2 proteins are essential for autophagosome formation and important for regulation of size and distribution of lipid droplets. *Mol. Biol. Cell* 23, 896–909. doi: 10.1091/mbc.E11-09-0785

Wang, J., Davis, S., Menon, S., Zhang, J., Ding, J., Cervantes, S., et al. (2015). Ypt1/Rab1 regulates Hrr25/CK1delta kinase activity in ER-Golgi traffic and macroautophagy. *J. Cell Biol.* 210, 273–285. doi: 10.1083/jcb.201408075

Xu, P., Ianes, C., Gartner, F., Liu, C., Burster, T., Bakulev, V., et al. (2019). Structure, regulation, and (patho-)physiological functions of the stress-induced protein kinase CK1 delta (CSNK1D). *Gene* 715:144005. doi: 10.1016/j.gene.2019.144005

Yang, Z., and Klionsky, D. J. (2010). Eaten alive: a history of macroautophagy. *Nat. Cell Biol.* 12, 814–822. doi: 10.1038/ncb0910-814

Zhou, F., Wu, Z., Zhao, M., Murtazina, R., Cai, J., Zhang, A., et al. (2019a). Rab5-dependent autophagosome closure by ESCRT. *J. Cell Biol.* 218, 1908–1927. doi: 10.1083/jcb.201811173

Zhou, F., Wu, Z., Zhao, M., Segev, N., and Liang, Y. (2019b). Autophagosome closure by ESCRT: Vps21/RAB5-regulated ESCRT recruitment via an Atg17-Snf7 interaction. *Autophagy* 15, 1653–1654. doi: 10.1080/15548627.2019.1628547

Zhou, F., Zou, S., Chen, Y., Lipatova, Z., Sun, D., Zhu, X., et al. (2017). A Rab5 GTPase module is important for autophagosome closure. *PLoS Genet.* 13:e1007020. doi: 10.1371/journal.pgen.1007020

Conflict of Interest: The authors declare that the research was conducted in the absence of any commercial or financial relationships that could be construed as a potential conflict of interest.

frontiers in Cellular Neuroscience

REVIEW
published: 07 August 2020
doi: 10.3389/fncel.2020.00194

The Molecular Determinants of Mitochondrial Membrane Contact With ER, Lysosomes and Peroxisomes in Neuronal Physiology and Pathology

Yajin Liao[1†], *Yuan Dong*[2†] *and Jinbo Cheng*[1*]

[1]*Center on Translational Neuroscience, College of Life & Environmental Science, Minzu University of China, Beijing, China,*
[2]*Department of Biochemistry, Medical College, Qingdao University, Qingdao, China*

Membrane tethering is an important communication method for membrane-packaged organelles. Mitochondria are organelles with a bilayer membrane, and the membrane contact between mitochondria and other organelles is indispensable for maintaining cellular homeostasis. Increased levels of molecular determinants that mediate the membrane contact between mitochondria and other organelles, and their functions, have been revealed in recent years. In this review article, we aim to summarize the findings on the tethering between mitochondria and other organelles in physiological or pathological conditions, and discuss their roles in cellular homeostasis, neural activity, and neurodegenerative diseases.

Keywords: mitochondria, membrane contact, determinant, physiological condition, pathological condition, neurological diseases

OPEN ACCESS

Edited by:
Marta Giacomello,
University of Padua, Italy

Reviewed by:
Tito Cali',
University of Padua, Italy
Sonia Missiroli,
University of Ferrara, Italy

****Correspondence:***
Jinbo Cheng
cheng_jinbo@126.com

†These authors share first authorship

Specialty section:
This article was submitted to Cellular Neuropathology, a section of the journal Frontiers in Cellular Neuroscience

Received: *15 February 2020*
Accepted: *05 June 2020*
Published: *07 August 2020*

Citation:
Liao Y, Dong Y and Cheng J (2020) The Molecular Determinants of Mitochondrial Membrane Contact With ER, Lysosomes and Peroxisomes in Neuronal Physiology and Pathology. Front. Cell. Neurosci. 14:194. doi: 10.3389/fncel.2020.00194

INTRODUCTION

Most of the organelles within cells are membrane-bound. Membrane tethering is one of the communication methods for signal/material exchanges between organelles. Membrane contact was first observed 60 years ago (Bernhard and Rouiller, 1956; Dalen et al., 1983; Grönblad and Akerman, 1984), however, the roles and molecular determinants of organelle juxtaposition

Abbreviations: MFN1/2, mitofusin-1/2; ER, endoplasmic reticulum; AD, Alzheimer's disease; PD, Parkinson's disease; ALS, amyotrophic lateral sclerosis; ERMES, ER-mitochondria encounter structure; Mdm10/12/34, mitochondrial distribution and morphology protein 10/12/34; Mmm1, maintenance of mitochondrial morphology protein 1; Gem1, mitochondrial Rho GTPase 1; SMP, mitochondrial lipid-binding protein; EMC, ER membrane protein complex; TOM5, translocase of outer membrane 5 kDa subunit; MAM, mitochondria-associated ER membrane; PACS2, phosphofurin acidic cluster sorting protein 2; GRP75, 75 kDa glucose-regulated protein; VDAC1/2, voltage-dependent anion-selective channel protein 1/2; IP3R3, inositol 1,4,5-trisphosphate receptor type 3; FBXL2, F-box protein FBXL2; MITOL, mitochondrial ubiquitin ligase; PINK1, PTEN-induced putative kinase protein 1; TG2, transglutaminase type 2; PDK4, pyruvate dehydrogenase kinase 4; Miro, mitochondrial Rho; PIGBOS, PIGB opposite strand; MICOS, mitochondrial contact site and cristae organizing system; ERMCS, ER-mitochondria contact sites; CLCC1, chloride channel CLIC-like protein 1; ORP5/8, oxysterol-binding protein (OSBP)-related proteins 5/8; PTPIP51, protein tyrosine phosphatase interacting protein-51; VAPB, vesicle-associated membrane protein-associated protein B; Rmdn3, regulator of microtubule dynamics protein 3; PDZD8, PDZ domain-containing protein 8; APP, amyloid-beta precursor protein; SNCA, synuclein-α; Sig-1R, sigma-1 receptor; FTD, frontotemporal dementia; TDP43, TAR DNA-binding protein 43; RAB7, Ras-related protein Rab 7; TBC1D15, TBC1 domain family member 15; FIS1, fission 1 protein; MDVs, mitochondria-derived vesicles; Pex11, Peroxisomal membrane protein 11; ACBD2/ECI2, Acyl-coenzyme A-binding domain 2/ECI2 isoform A.

were discovered only recently. The contact between two organelles is achieved by means of proteins that tether them directly. Mitochondria are vital ATP-generating organelles, and play a critical role in synapse activity, neurite outgrowth, neurogenesis, and neuronal cell death (Sun et al., 2013; Liao et al., 2015; Khacho et al., 2016; Norkett et al., 2016; Vaccaro et al., 2017). The dysfunction of mitochondria, including Ca^{2+} overload, excessive fission, disrupted distribution, and clearance of damaged mitochondria has been observed in multiple disorders of the nervous system (Calkins et al., 2011; Guardia-Laguarta et al., 2014; Lee et al., 2018; Berenguer-Escuder et al., 2020; Tsai et al., 2020). In previous studies, many advances have been made in the identification of the contacts among various organelles and on their structural determinants. These studies have proved that membrane contacts regulate several aspects of the biology and the behavior of mitochondria (Filadi et al., 2018; McLelland et al., 2018; Grossmann et al., 2019). Considering the example of mitofusin-1/2 (MFN1/2), their ability to control the endoplasmic reticulum (ER)-mitochondria tethering is associated with the activity of regulating the balance between mitochondrial fusion and fission (de Brito and Scorrano, 2008; Li et al., 2015; Qi et al., 2016). Either a decrease or an increase in the interaction levels between mitochondria and other organelles have been proved to induce mitochondrial dysfunction, in turn effecting energy metabolism, respiration, apoptosis, oxidative stress, and inflammation (De Vos et al., 2012; Lee et al., 2016). In addition, a growing amount of evidence indicates that the dysfunction of membrane contacts between mitochondria and other organelles is involved in the development of neural stem cell-related and neurodegenerative diseases, including Alzheimer's disease (AD), Parkinson's disease (PD), and amyotrophic lateral sclerosis (ALS; Area-Gomez et al., 2012; Lee et al., 2016, 2018; Stoica et al., 2016). In this review, we mainly aim to summarize the determinants of mitochondria contacts with other organelles under different physiological or pathological conditions.

THE DETERMINANTS OF ER-MITOCHONDRIA MEMBRANE CONTACT

General Characteristics and Functions of ER-Mitochondria Membrane Contact

One of the most well-studied membrane contacts is ER-mitochondrial tethering. The interplay between these two organelles is necessary for the proper functioning of the cell, by maintaining Ca^{2+} homeostasis, lipid metabolism, and autophagy (Voss et al., 2012; Wideman et al., 2013; Gomez-Suaga et al., 2017b; Hirabayashi et al., 2017; Eisenberg-Bord et al., 2019).

The ER-mitochondria encounter structure (ERMES) is the first identified complex that was found to mediate the structural interaction between the ER and mitochondria. In yeast, the ERMES is composed of mitochondrial distribution and morphology protein 10/12/34 (Mdm10/12/34), maintenance of mitochondrial morphology protein 1 (Mmm1), and mitochondrial Rho GTPase 1 (Gem1; **Figure 1**; Kornmann et al., 2011; Jeong et al., 2016). Among these proteins, Mdm12, Mmm1, and Mdm34 contain a conserved synaptotagmin-like mitochondrial lipid-binding protein (SMP) domain that is important for the formation of the ERMES complex and to facilitate the contacts between the ER and mitochondria (AhYoung et al., 2015). Another conserved complex, the ER membrane protein complex (EMC), also plays an important role in tethering the ER to mitochondria (Lahiri et al., 2014). By interacting with the translocase of outer membrane 5 kDa subunit (TOM5) on the outer membrane of mitochondria, EMC1-6 of the EMC complex mediates the ER-mitochondria contact necessary for phosphatidylserine transfer in yeast (**Figure 1**; Lahiri et al., 2014). Importantly, both ERMES- and EMC-mediated tethering is essential for cell growth.

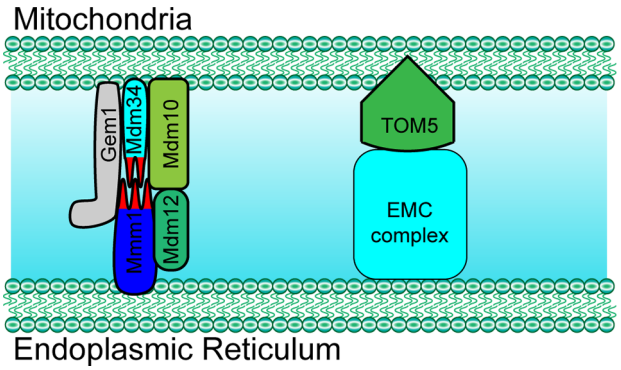

FIGURE 1 | Paradigm of molecular determinants in endoplasmic reticulum (ER)-mitochondria tethering in yeast. Mdm10, Mdm34 and Gem1 located at the outer mitochondrial membrane (OMM) mediate ER-mitochondria tethering by forming a complex with ER membrane located proteins Mmm1 and cytosol Mdm12 in yeast. ER membrane protein complex (EMC) mediates ER-mitochondria contact by interacting with TOM5 at the mitochondrial OMM in yeast. Mdm10/34, mitochondrial distribution and morphology protein 10/34; Gem1, mitochondrial Rho GTPase 1; TOM5, translocase of outer membrane 5 kDa subunit.

In mammal cells, some proteins also localize into a subcompartment on the membrane of the ER, which makes contact with mitochondria and is referred to as the mitochondria-associated ER membrane (MAM; Vance, 1990; Rusinol et al., 1994; Csordás et al., 2006; Area-Gomez et al., 2012). MAM molecular determinants are dynamic and shape ER-mitochondria function (Poston et al., 2013; Gelmetti et al., 2017; Ma et al., 2017; Pera et al., 2017). The classic molecules that are involved in ER-mitochondria tethering include MFN1/2, phosphofurin acidic cluster sorting protein 2 (PACS2), sigma-1 receptor (Sig-1R), F-box protein FBXL2 (FBXL2), 75 kDa glucose-regulated protein (GRP75), voltage-dependent anion-selective channel protein 1/2 (VDAC1/2), and inositol 1,4,5-trisphosphate receptor type 3 (IP_3R3; **Figure 2** and **Table 1**; Simmen et al., 2005; Szabadkai et al., 2006; Hayashi and Su, 2007; de Brito and Scorrano, 2008; Mori et al., 2013; Naon et al., 2016; Kuchay et al., 2017; Veeresh et al., 2019). Both the formation of the MFN2 dimer and IP_3R3-VDAC-GRP75 complex in the MAM could mediate the physical linkage between the ER and

mitochondria (Csordás et al., 2006; Szabadkai et al., 2006; de Brito and Scorrano, 2008; McLelland et al., 2018). In addition, some molecules have been proven to enhance ER-mitochondria contacts in a dose-dependent manner, which promote the transfer of Ca^{2+} and other chemicals between the ER and mitochondria (Chen et al., 2012; Mori et al., 2013; McLelland et al., 2018; Yu et al., 2019). Furthermore, accumulative evidence suggests that the post-translational modification of these proteins is also essential for the tethering activity and dynamic balance of ER-mitochondria contacts involving the aforementioned determinants (McLelland et al., 2018). Considering the example of MFN2, a mitochondrial outer membrane protein that mediates fusion, mitophagy regulates ER-mitochondria contacts (de Brito and Scorrano, 2008; Chen et al., 2012; Naon et al., 2016). MFN2 ablation or silencing enhances ER-mitochondria close contacts and leads cells more sensitive for mitochondrial calcium overload-dependent cell death (Filadi et al., 2015). Moreover, MFN2-mediated ER-mitochondria tethering is regulated by ubiquitination. Mitochondrial ubiquitin ligase (MITOL)-mediated ubiquitination, PTEN-induced putative kinase protein 1 (PINK1) and Parkin-mediated mono-ubiquitination of MFN2 promote its tethering activity, while PINK1 and Parkin-mediated poly-ubiquitination of MFN2 result in MFN2 retrotranslocation and disrupt ER-mitochondria contacts to drive mitophagy (**Figure 2**; Sugiura et al., 2013; Basso et al., 2018; McLelland et al., 2018). These post-translational modifications likely explain the different findings on the role of MFN2 in keeping mitochondria and ER together (Naon et al., 2016; Filadi et al., 2017). Besides PINK1 and Parkin, other mitophagy-associated proteins, such as Beclin-1, have been found to relocalize in the MAMs during mitophagy (Gelmetti et al., 2017; McLelland et al., 2018). The relocalization of these proteins in the MAMs promotes ER-mitochondrial tethering and autophagosome formation (Gelmetti et al., 2017). Apart from post-translational modification, the interaction between the MAM components and other proteins also affects the ER-mitochondria contacts. Considering the example of IP_3R3-GRP75-VDAC complex, the IP_3R3-PTEN interaction and IP_3R3-Sig-1R interaction promote the stability of IP_3R3 and maintain the complex, while the IP_3R3-BiP interaction and IP_3R3-FBXL2 interaction induce the degradation of IP_3R3 and disruption of the complex (Hayashi and Su, 2007; Kuchay et al., 2017). The Transglutaminase type 2 (TG2) was found to interact with GRP75 and to subsequently decrease the interaction level between GRP75 and IP_3R3, thereby maintaining mitochondrial Ca^{2+} homeostasis. The loss of TG2 was found to increase GRP75-IP_3R3 interaction levels and to decrease ER-mitochondria contact levels as well as mitochondrial Ca^{2+} levels (D'Eletto et al., 2018). Pyruvate dehydrogenase kinase 4 (PDK4) is another GRP75-interacting protein, and the upregulated expression of PDK4 could promote the formation of the VDAC1-GRP75-IP_3R3 complex, which results in increased ER-mitochondria contact levels (Thoudam et al., 2019).

Besides these canonical molecular determinants that mediate ER-mitochondria tethering, in the last few years, several other proteins that translocate to the MAM and that mediate ER-mitochondria tethering have been identified [i.e., Mitochondrial Rho (Miro) and PIGB opposite strand 1 (PIGBOS); Chu et al., 2019; Modi et al., 2019]. In 2016, Miro1 and Miro2, two mitochondrial Rho GTPases, were discovered to mediate ER-mitochondria tethering (Lee et al., 2016). Recent studies have revealed that Miro1 and Miro2 form nanometer-sized clusters along the outer membrane of the mitochondria and are components of the mitochondrial contact site and cristae organizing system (MICOS) and ER-mitochondria contact sites (ERMCS; **Figure 2**; Lee et al., 2016; Modi et al., 2019). The loss of Miro1/2 results in decreased ER-mitochondria contact sites and mitochondrial Ca^{2+} uptake (**Figure 1**; Modi et al., 2019). Another study has indicated that Miro can be phosphorylated by polo-like kinase 1, leading to the activation of Miro (Lee et al., 2016). In neural stem cells, the inactivation of Miro leads to the depletion of mitochondrial Ca^{2+} levels resulting in a metabolic impairment, and the overexpression of Miro1/2 results in Ca^{2+} overload and cell death (Lee et al., 2016). PIGBOS, a novel microprotein that localizes on the outer membrane of the mitochondria (Chu et al., 2019), is found to mediate ER-mitochondria contact. The loss of PIGBOS elevates unfolded protein response (UPR) and increases cell death under stress conditions. The results of further investigation indicate that PIGBOS is able to interact with chloride channel CLIC-like protein 1 (CLCC1) on the membrane of the ER, and this interaction is essential for the function of PIGBOS (**Figure 2**; Chu et al., 2019). However, the interaction between PIGBOS and CLCC1 does not act as a tether between the ER and mitochondria (Chu et al., 2019). The oxysterol-binding protein (OSBP)-related proteins 5/8 (ORP5/8) mediate ER-mitochondria tethering by interacting with protein tyrosine phosphatase interacting protein-51 (PTPIP51; **Figure 2**). The depletion of ORP5/8 results in changes in the mitochondrial morphology and respiratory functions (Galmes et al., 2016). As the most extensively studied type of membrane contact, an increasing number of determinants that are involved in ER-mitochondria tethering is being discovered (**Table 1**), which promotes the understanding of the functions and regulatory mechanisms of ER-mitochondria contacts.

THE FUNCTIONS OF ER-MITOCHONDRIA MEMBRANE CONTACT IN THE NERVOUS SYSTEM

In neuronal cells, some molecules that mediate the local ER-mitochondria contacts regulate dendritic Ca^{2+} homeostasis in order to facilitate the adaptation to synapse stimulation, thereby playing a critical role in synaptic integration properties and plasticity. For example, vesicle-associated membrane protein-associated protein B (VAPB) and PTPIP51 form a complex at the synapses and mediate ER-mitochondria tethering (**Figure 3**; Gómez-Suaga et al., 2019). The interaction between VAPB (localization in the ER) and PTPIP51 (localization in the mitochondria) is critical for mitochondrial Ca^{2+} homeostasis (De Vos et al., 2012). The loss of VAPB or PTPIP51 results in higher cytosolic Ca^{2+} levels in the case of dendrite postsynaptic stimulation. In addition, the number of dendritic spines is reduced in VAPB- or PTPIP51-silenced neurons (Gómez-Suaga et al., 2019). Recently, on performing cell-type-specific profiling

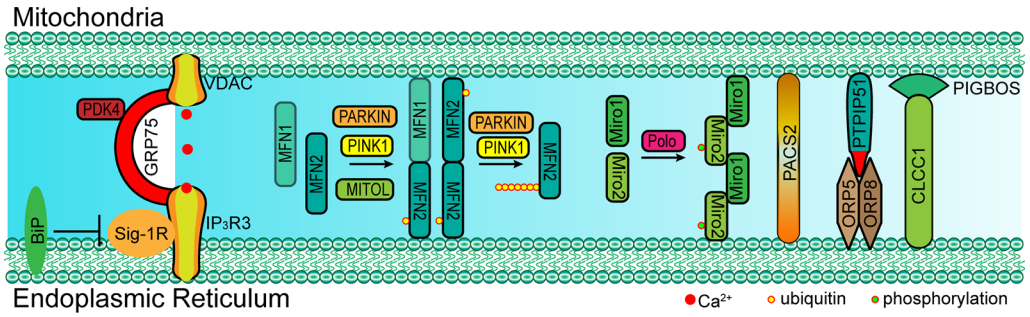

FIGURE 2 | Paradigm of molecular determinants in ER-mitochondria tethering in mammal. Left: GRP75 interacts with both VDAC (located at OMM) and IP_3R3 (located at MAM) to form a complex that mediates the ER-mitochondria contact. The interaction between Sig-1R and IP_3R3 promotes the stability of IP_3R3, which is essential for the IP_3R3-GRP75-VDAC complex, while BiP inhibits this interaction by competitive binding to Sig-1R. Middle: MFN1/2 form a dimer at MAM and mediate ER-mitochondria tethering. PARKIN, PINK1 and MITOL mediate the mono-ubiquitination of MFN2 and promote MFN2 translocation to MAM. However, the poly-ubiquitination of MFN2 mediated *via* PARKIN and PINK1 leads to the tethering disruption. Right: Miro1/2 form a cluster at MAM and mediate ER-mitochondria tethering, and the phosphorylation of Miro2 by polo kinase is essential for the formation of the Miro cluster. Cytosolic PACS2 recruits to the MAMs and OMM to mediate ER-mitochondria membrane contact. The OMM-resident PTPIP51 interacts with ORP5/8 at MAM to maintain mitochondrial morphology and respiratory functions. The OMM-resident PIGBOS interacts with the ER membrane protein CLCC1 to maintain ER–mitochondrial contact. GRP75, 75 kDa glucose-regulated protein; VDAC1/2, voltage-dependent anion-selective channel protein; IP_3R3, inositol 1,4,5-trisphosphate receptor type 3; MFN1/2, mitofusin-1/2; Sig-1R, sigma-1 receptor; ORP5/8, oxysterol-binding protein (OSBP)-related proteins 5/8; PTPIP51, protein tyrosine phosphatase interacting protein-51; CLCC1, chloride channel CLIC-like protein 1; PIGBOS, PIGB opposite strand 1; PACS2, phosphofurin acidic cluster sorting protein 2; Miro1/2, mitochondrial Rho 1/2; MITOL: mitochondrial ubiquitin ligase; PINK1, PTEN-induced putative kinase protein 1.

of the brain mitochondria, a regulator of microtubule dynamics protein 3 (Rmdn3) was found to predominantly mediate ER-mitochondria tethering in the Purkinje cells (**Figure 3**), rather than in the astrocyte and granule cells (Fecher et al., 2019). Even if a previous study suggests that Rmdn3 mediates the ER-mitochondria tethering by interacting with VAPB, the mechanism of Rmdn3-mediated ER-mitochondria tethering in neurons is unknown (Gomez-Suaga et al., 2017a). Recently, PDZ domain-containing protein 8 (PDZD8), a SMP domain-containing protein localized in the ER membrane, has been proven to mediate ER-mitochondria tethering in the neurons (**Figure 3**), which is critical for dendrites activity (Hirabayashi et al., 2017). Usually, Ca^{2+} released from the ER can induce the subsequent mitochondrial Ca^{2+} uptake (Hirabayashi et al., 2017). However, the mitochondrial Ca^{2+} import is significantly reduced in PDZD8-deficient neurons, resulting in higher Ca^{2+} levels in the dendrites (Hirabayashi et al., 2017). These results suggest that particular determinants mediate the ER-mitochondria membrane contacts in the neurons, especially in the neural dendrites, and that the absence of these proteins could result in decreased synaptic plasticity and activity.

Besides the molecules that are present within the EMRES or MAM under normal physiological conditions, some molecules (i.e., APP-C99 and Tau) are found to localize within the ERMES or MAM under pathological conditions, resulting in excessive ER-mitochondria contacts, and mitochondrial Ca^{2+} overload, and cell death (Guardia-Laguarta et al., 2014; Pera et al., 2017; Cieri et al., 2018). Furthermore, excessive ER-mitochondria contacts have been recently found to be involved in neurodegenerative diseases. Based on the findings through biopsies of AD patients, the number of ER-mitochondria contact sites is positively correlated with elevated ventricular cerebrospinal fluid β-amyloid (Aβ) levels (Leal et al., 2018). A nanomolar concentration of Aβ is sufficient to increase the expression of VDAC1 and IP_3R3, resulting in elevated ER-mitochondria contact levels and mitochondrial Ca^{2+} overload (**Figure 4**; Hedskog et al., 2013; Schreiner et al., 2015). The amyloid-beta precursor protein (APP)-C99, the C-terminal fragment of APP, is also found to localize in the MAM (Pera et al., 2017). The accumulation of C99 in the MAM region induces sphingolipid turnover (thereby leading to altered lipid composition in both the MAM and mitochondrial membrane), increased ER–mitochondria contacts and mitochondrial dysfunction (**Figure 4**; Pera et al., 2017), indicating that C99 may act as a risk factor for AD. Tau, another risk factor for AD and other types of dementia, is found to be present in the outer membrane of mitochondria and in the mitochondrial intermembrane space. Tau localization at mitochondria affects their distribution and enhances Ca^{2+} transfer from the ER to mitochondria (Cieri et al., 2018). Moreover, dysregulated ER-mitochondria contacts have also been observed in PD models. Synuclein-α (SNCA), a critical protein for the development of PD, has been proven to enhance the ER-mitochondria contacts, resulting in mitochondrial Ca^{2+} overload (Guardia-Laguarta et al., 2014; Calì et al., 2019). In neurons that were differentiated from PD-patient derived induced pluripotent stem cells (iPSC) with mutations in Parkin and PINK1, the ER-mitochondria contacts were found to be increased, resulting in elevated ER to mitochondrial lipid trafficking and the disrupted production of neuropeptide-containing vesicles (Valadas et al., 2018). Increased ER-mitochondria contacts and mitochondrial Ca^{2+} levels induced by PINK1 mutations lead to mitochondrial enlargement and neuronal cell death. These phenotypes could be

TABLE 1 | The molecular determinant for endoplasmic reticulum (ER)-mitochondria tethering in mammal cell.

Tethering complex	Localization	Function	Pathogenicity
IP_3R3-GRP75-VDAC, Sig-1R, BiP, TOM70, TG2, PDK4, FBXL2, Aβ	ER membrane and MAMs: IP_3R3, Sig-1R, BiP (Hayashi and Su, 2007) Mitochondrial OMM: VDAC, TOM70 (Shoshan-Barmatz et al., 2008; Filadi et al., 2018) Cytosol: TG2, PDK4, FBXL2, GRP75 (D'Eletto et al., 2018; Thoudam et al., 2019)	1. IP_3R3-GRP75-VDAC complex mediates ER-mitochondria Ca^{2+} transfer and homeostasis (Szabadkai et al., 2006). 2. Sig-1R, PDK4, TOM70 and Aβ promote the formation of IP_3R3-GRP75-VDAC complex (Filadi et al., 2018; Thoudam et al., 2019). 3. TG2, BiP and FBXL2 inhibit the complex formation (Hayashi and Su, 2007; D'Eletto et al., 2018).	1. Upregulated IP3R3-GRP75-VDAC complex is associated with mitochondrial Ca^{2+} overload (Kuchay et al., 2017). 2. Mutations in Sig-1R are associated with ALS and neuropathy (Al-Saif et al., 2011; Gregianin et al., 2016). 3. Aβ-induced upregulation of IP_3R3 and VDAC are associated with AD (Hedskog et al., 2013).
MFN1/2 dimer, PINK1, PARKIN, BECN1, MITOL	Mitochondrial OMM and MAMs: MFN1/2 Cytosol: PINK1, PARKIN, BECN1, MITOL (Sugiura et al., 2013; Basso et al., 2018; McLelland et al., 2018)	1. MFN1/2 dimer mediates ER-mitochondria Ca^{2+} transfer and mitophagy (de Brito and Scorrano, 2008; Chen et al., 2012; Qi et al., 2016). 2. PINK1, PARKIN and BECN1 mediated ubiquitination of MFN2 is essential for MFN2 translocation.	Cells lacking MFN1/2 are associated with mitochondrial fragmentation (Chen et al., 2003).
PIGBOS-CLCC1	ER membrane: CLCC1 Mitochondrial OMM: PIGBOS (Chu et al., 2019)	PIGBOS mediates the ER-mitochondrial tethering by interacting with an identified protein (Chu et al., 2019).	Loss of PIGBOS elevated unfolded protein response (UPR) and increased cell death under stress conditions (Chu et al., 2019).
Miro1/2 cluster, Polo	Mitochondrial OMM and MAMs (Lee et al., 2016; Modi et al., 2019)	1. Miro1/2 cluster mediates Mitochondrial Ca^{2+} uptake (Modi et al., 2019). 2. Polo mediated phosphorylation of Miro promotes the activation of Miro (Lee et al., 2016).	Cells lacking Miro leads to decreased mitochondrial Ca^{2+} uptake, while overexpression of Miro1/2 result in Ca^{2+} overload and cell death (Lee et al., 2016; Modi et al., 2019).
VAPB-PTPIP51, FUS, TDP43	ER membrane and MAMs: VAPB Mitochondrial OMM: PTPIP51 (De Vos et al., 2012) Cytosol: FUS, TDP43 (Stoica et al., 2014, 2016)	VAPB-PTPIP51 interaction mediates ER-mitochondria tethering, which is essential for mitochondrial Ca^{2+} homeostasis, mitophagy and neural activity (De Vos et al., 2012; Gomez-Suaga et al., 2017b; Gómez-Suaga et al., 2019).	1. Loss of VAPB or PTPIP51 results in decreased synaptic activity (Gómez-Suaga et al., 2019). 2. Disrupted VAPB-PTPIP51 interaction and loss of function of the complex is associated with ALS (Stoica et al., 2014, 2016).
ORP5/8-PTPIP51	ER membrane and MAMs: ORP5/8 (Galmes et al., 2016) Mitochondrial OMM: PTPIP51	ORP5/8-PTPIP51 interaction mediated ER-mitochondria tethering is associated with mitochondrial morphology and respiratory function (Galmes et al., 2016).	Cells lacking ORP5 display low respiratory function (Galmes et al., 2016).
PACS2	mitochondria and MAMs (Yu et al., 2019)	ER-mitochondrial Ca^{2+} transfer and apoptosis (Yu et al., 2019).	Downregulation of PACS2 leads to decreased ER-mitochondria tethering and cells become more sensitivity to ox-LDL-induced cell death (Yu et al., 2019).
Rmdn3	Mitochondrial OMM (Fecher et al., 2019)	Rmdn3 mediates the ER-mitochondria tethering in Purkinje cells (Fecher et al., 2019).	Cells lacking Rmdn3 leads to decreased autophagosome formation (Gomez-Suaga et al., 2017a).
PDZD8	ER membrane (Hirabayashi et al., 2017)	PDZD8 mediates the dendritic ER-mitochondria Ca^{2+} transfer in neuron upon stimulation (Hirabayashi et al., 2017).	PDZD8-deficiency leads to decreased ER-mitochondrial Ca^{2+} release-uptake coupling (Hirabayashi et al., 2017).

rescued by the inhibition of Miro or components of the ERMES (Valadas et al., 2018).

In conclusion, these results suggest that some molecules could enhance ER-mitochondria tethering by acting as membrane contact determinants or enhancers under pathological conditions, which leads to mitochondrial Ca^{2+} overload, oxidative stress, neuroinflammation, or apoptosis.

Apart from excessive ER-mitochondria contacts being associated with the development of diseases, decreased ER-mitochondria contacts are also found to induce the

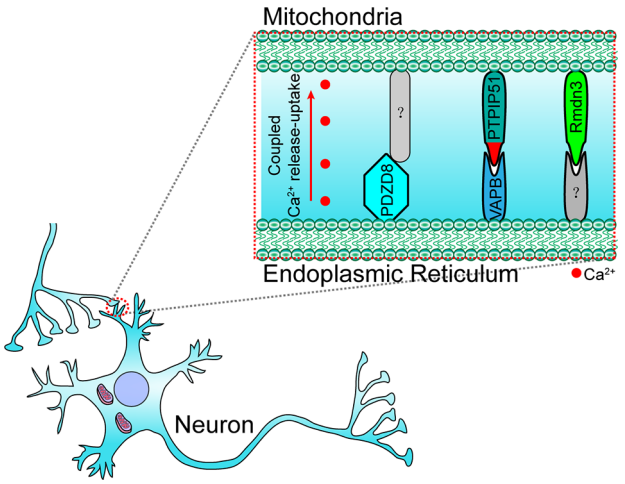

FIGURE 3 | Paradigm of molecular determinants in ER-mitochondria tethering in the dendrite of neurons. In the dendrite, VAPB (located at ER) interacts with PTPIP51 (located at OMM) to maintain ER–mitochondria tethering and synaptic activity-coupled Ca^{2+} release-uptake. PDZD8 (located at ER) and Rmdn3 (located at OMM) are also involved in synaptic activity-coupled Ca^{2+} release-uptake and ER-mitochondria membrane contact. However, their interacting partners have still not been identified. VAPB, vesicle-associated membrane protein-associated protein B; PDZD8, PDZ domain-containing protein 8; Rmdn3, regulator of microtubule dynamics protein 3.

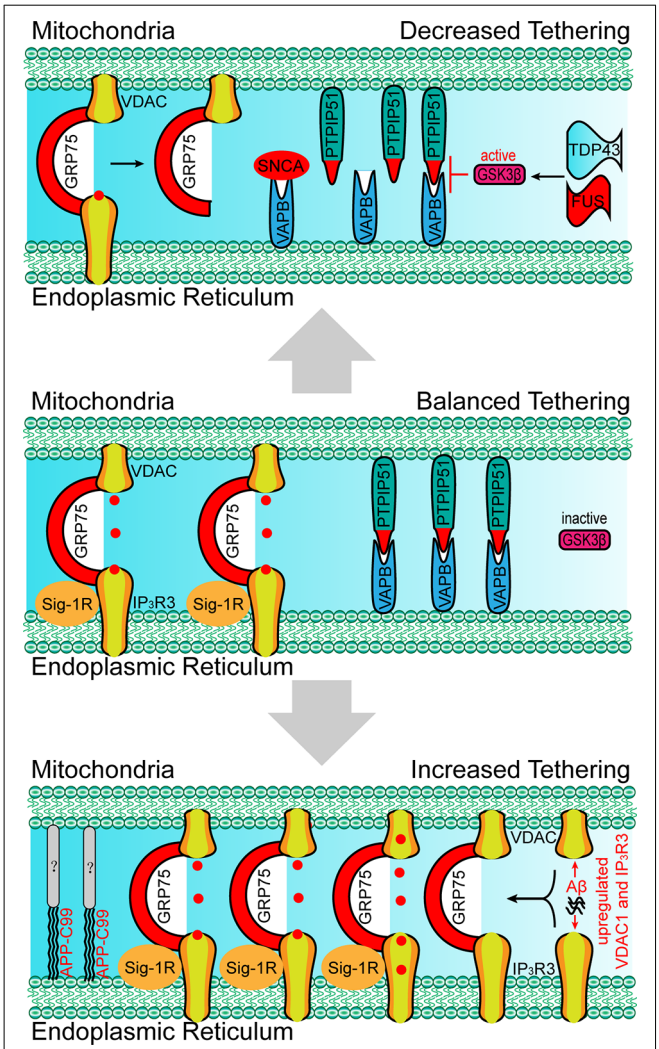

FIGURE 4 | Paradigm of changes in molecular determinants and ER-mitochondria tethering in neurodegenerative disorders. Upper: the absence of Sig-1R at MAM leads to the de-stabilization of IP_3R3, resulting in the decreased IP_3R3-GRP75-VDAC complex and ER-mitochondria tethering, which is associated with the development of amyotrophic lateral sclerosis (ALS). SNCA, FUS and TDP43 disrupt the VAPB-PIPTP51 interaction and ER–mitochondria contact, which is associated with the development of Parkinson's disease (PD) and ALS. Bottom: the accumulation of Aβ at MAM promotes the expression of VDAC and IP_3R3, which leads to the increased formation of the IP_3R3-GRP75-VDAC complex, ER-mitochondria tethering, and mitochondrial Ca^{2+} overload. APP-C99 is also observed at MAMs, which enhances the ER-mitochondrial contact. The presence of Aβ and APP-C99 at MAMs are associated with the development of Alzheimer's disease (AD). SNCA, synuclein-α; TDP43, TAR DNA-binding protein 43; FUS, RNA-binding protein FUS; Aβ, β amyloid.

onset of abnormalities in cellular metabolism, especially in the neurons. For example, MITOL-mediated ubiquitination of MFN2 is critical for the formation of the MFN2 dimers and in facilitating the tethering of ER-mitochondria (Sugiura et al., 2013). The loss of MITOL leads to a reduction in ER-mitochondria contact sites and an increase in oxidative stress in the neurons (Nagashima et al., 2019), which also render cells more vulnerable to ER-stress induced apoptosis (Takeda et al., 2019). The mutation of Miro1 in PD patients leads to decreased ER-mitochondria contacts and low basal mitochondrial Ca^{2+} levels, thereby impairing energy metabolism and mitophagy (Grossmann et al., 2019). In VAPB-, PTPIP51-, or PDZD8-deficient neurons the lack of ER-mitochondria tethering at the synapses lead to decreased synaptic activities (Hirabayashi et al., 2017; Gómez-Suaga et al., 2019). Moreover, the loss of VAPB/PTPIP51-mediated ER-mitochondria contact causes a reduced number of dendritic spines in the neurons (Gómez-Suaga et al., 2019). In familial PD involving mutations in SNCA, mutated SNCA interacts with VAPB and decreases the VAPB-PTPIP51 interaction, leading to decreased dendritic ER-mitochondria contact and low synaptic activity levels (**Figure 4**; Paillusson et al., 2017). In addition, shrunken mitochondria were observed in neurons with mutated SNCA neurons, indicating morphological changes in the mitochondria (Little et al., 2018). Apart from SNCA mutants, the RNA-binding protein FUS can also disrupt the VAPB-PIPTP51 interaction (**Figure 4**). A reduction in mitochondrial adenosine triphosphate (ATP) production and Ca^{2+} concentration is observed in FUS-upregulated neurons, which may be associated with the development of ALS and frontotemporal dementia (FTD; Stoica et al., 2016). TAR DNA-binding protein 43 (TDP43), another ALS-associated protein, can also inhibit the VAPB-PIPTP51 interaction (**Figure 4**). Cells with high expression levels of TDP43 were found to exhibit the same characteristics as those of FUS-upregulated cells, including increased cytosolic Ca^{2+} levels and decreased mitochondrial Ca^{2+} levels (**Figure 3**; Stoica et al., 2014). In addition, the inhibition of the VAPB-PTPIP51 interaction mediated by

FUS and TDP43 is associated with the activation of glycogen synthase kinase-3 beta (Stoica et al., 2014, 2016). Decreased ER-mitochondria tethering is also found in Sig-1R- and SOD1-linked ALS (Watanabe et al., 2016). Sig-1R locates in the MAM and promotes ER-mitochondria tethering by stabilizing IP3R3 (Hayashi and Su, 2007). Aberrant subcellular distribution of Sig-1R mutations is associated with ALS and distal hereditary motor neuropathy (Al-Saif et al., 2011; Almendra et al., 2018). Further studies reveal that aberrant subcellular distribution of Sig-1R results in the decrease of ER-mitochondria tethering and mitochondrial Ca^{2+} levels (**Figure 4**; Al-Saif et al., 2011; Gregianin et al., 2016). In addition, increasing ER-mitochondria tethering by activation of Sig-1R is proven to be beneficial for SOD1-linked ALS. Considered together, the above studies indicate that decreased ER-mitochondria contacts or protein interaction changes are also harmful and result in alterations in cell fate, neural activity, and synaptic plasticity in the neurons.

In summary, apart from the classic membrane contact determinants that mediate the ER-mitochondria communication and metabolism, some disease-associated abnormal proteins or peptides could also play critical roles as determinants or regulators that disrupt the contact balance between the ER and mitochondria. Enhanced ER-mitochondria contact levels in the soma of neurons induce mitochondria Ca^{2+} overload and neuronal cell death, while decreased ER-mitochondria contact levels in the dendrites of neurons lead to reduced synaptic activity and spine density, suggesting that dysregulated ER-mitochondria interaction are involved in the development of some neurodegenerative disorders, such as AD, PD and ALS.

THE DETERMINANTS OF MITOCHONDRIA-LYSOSOME MEMBRANE CONTACT AND MITOCHONDRIA-PEROXISOME MEMBRANE CONTACT

Mitochondria-Lysosomes Membrane Contacts

Besides mitochondria-ER contacts, determinants of mitochondria-lysosomes and of mitochondria-peroxisomes contacts have been recently discovered, further enhancing the understanding of the communication between these organelles in the cells. Here, we have mainly summarized the determinants between these organs in the neuronal system.

A lysosome is a highly dynamic organelle that mediates the degradation of unfolded proteins, damaged organelles, and pathogen-derived components. Under stress conditions or during the process of aging, the lysosome-mediated clearance of damaged mitochondria is crucial for maintaining mitochondrial homeostasis (Wang and Klionsky, 2011). The accumulation of damaged mitochondria is observed in multiple cells with dysfunction in lysosome performance, which is also involved in development neurodegenerative diseases. However, because the lysosome-mediated clearance of damaged mitochondria is believed to be autophagy-dependent, the mitochondrial-lysosome interaction has been considered indirect membrane contact.

Recently, direct mitochondria-lysosome contacts have been discovered through multiple super-resolution imaging modalities. Ras-related protein Rab-7 (RAB7) was the first identified mitochondrial-lysosome membrane contact determinant (Wong et al., 2018). The presence of RAB7 is sufficient to mediate mitochondrial-lysosome tethering. The recruitment of TBC1 domain family member 15 (TBC1D15) by mitochondrial fission 1 protein (FIS1) at the membrane of mitochondria, enhances RAB7 activity (GTP hydrolysis), which results in mitochondrial-lysosome untethering (Wong et al., 2018). The GTP- guanosine diphosphate (GDP) cycling dynamic regulates the mitochondrial-lysosome contact and fission of the mitochondria. Moreover, a deficiency in *RAB7* levels in the neurons causes axonal degeneration and the development of Charcot-Marie-Tooth neuropathy type 2B (Ponomareva et al., 2016). With developments in imaging technology, apart from RAB7, we believe that other molecules mediating and controlling mitochondrial-lysosome tethering will be identified and characterized in the future.

Mitochondria-Peroxisomes Membrane Contacts

Peroxisomes are membrane-bound oxidative organelles that play an indispensable role in the metabolism of fatty acids, glyoxylate, amino acids, and reactive oxygen species (ROS; Schrader et al., 2015). The evidence generated by studies on yeast demonstrate that peroxisomes are localized to mitochondria-ER junctions and sites of acetyl-CoA synthesis (Cohen et al., 2014). This finding suggests that the mitochondria-peroxisome contacts may be important for the β-oxidation of fatty acids in the peroxisomes or mitochondria. In mammal cells, mitochondria-derived vesicles (MDVs) are considered as one of the origins of peroxisomes, as some of the components of mitochondria are selectively integrated into peroxisomes (Sugiura et al., 2017). Peroxisomal membrane protein 11 (Pex11), a peroxin that is localized within the peroxisomes, is found to interact with Mdm34 (localized in the membrane of the ER and one of the components of the ERMES) in yeast (Mattiazzi Ušaj et al., 2015). In addition, the initiation of membrane contact between peroxisomes and mitochondria mediated by Pex11 and Mdm34 is ER-dependent (Mattiazzi Ušaj et al., 2015). On systematically mapping the contact sites, Pex34 and Fzo1 were discovered to localize at the membrane of peroxisomes, which can facilitate their tethering to mitochondria. The loss of Pex34 results in reduced β-oxidation of fatty acids (Shai et al., 2018). Acyl-coenzyme A-binding domain 2 (ACBD2)/ECI2 isoform A is another newly identified protein, with a C-terminal peroxisome targeting signal-1, which aids in the localization of ACBD2/ECI2 in peroxisomes. Further, by interacting with TOM20, ACBD2/ECI2 can mediate membrane contact between peroxisomes and mitochondria (Fan et al., 2016). A functional study revealed that ACB2/ECI2-TOM20 mediated peroxisome-mitochondria tethering is essential for the biosynthesis of steroids in Leydig Cells (Fan et al., 2016). Considered together, these studies suggest that proteins localized at the membrane

of mitochondria and peroxisomes regulate the mitochondria-peroxisome membrane contacts and affect the lipid metabolism in peroxisomes.

In the nervous system, although the mitochondria-lysosome membrane contact and mitochondria-peroxisome membrane contact have not been studied as much as the mitochondria-ER contact, we believe that more and more contact determinants will be discovered and characterized in the near future.

CONCLUDING REMARKS

Mitochondria exchange signals and materials with other organelles through membrane contacts. During this process, molecular determinants dynamically regulate the tethering and untethering between mitochondria and other organelles. However, in pathological conditions, some disease-associated molecules have been retrieved at MAM, where they act as membrane contact determinants (such as Aβ), disrupt physiological interactions *via* post-translational modification (such as PINK1), and participate in competitive interactions (such as FUS; **Figure 1**). These abnormal proteins present in the MAM cause dysfunctions in the tethering between mitochondria and other organelles, and thus leads to subsequent mitochondrial Ca^{2+} overload, lower synaptic activity levels, metabolic disorders, and finally neural cell death. An increasing amount of evidence shows that the dysregulation of mitochondria membrane contacts with other organelles cause mitochondrial dysfunctions underlying neurodegenerative diseases. However, extensive investigations are still needed to fully characterize the regulatory mechanism involved. Accordingly, in clinical practice, pharmacological modulation of contacts still has a long way to go.

AUTHOR CONTRIBUTIONS

YL conceived the review topic, reviewed the literature, wrote the manuscript, and prepared the figure. YD and JC reviewed the manuscript. YL and JC performed a comprehensive review of the literature.

FUNDING

This work was supported by grants from the National Nature Science Foundation of China (81870839 and 81701187).

REFERENCES

AhYoung, A. P., Jiang, J., Zhang, J., Khoi Dang, X., Loo, J. A., Zhou, Z. H., et al. (2015). Conserved SMP domains of the ERMES complex bind phospholipids and mediate tether assembly. *Proc. Natl. Acad. Sci. U S A* 112, E3179–E3188. doi: 10.1073/pnas.1422363112

Almendra, L., Laranjeira, F., Fernandez-Marmiesse, A., and Negrao, L. (2018). *SIGMAR1* gene mutation causing distal hereditary motor neuropathy in a portuguese family. *Acta Myol.* 37, 2–4.

Al-Saif, A., Al-Mohanna, F., and Bohlega, S. (2011). A mutation in sigma-1 receptor causes juvenile amyotrophic lateral sclerosis. *Ann. Neurol.* 70, 913–919. doi: 10.1002/ana.22534

Area-Gomez, E., Del Carmen Lara Castillo, M., Tambini, M. D., Guardia-Laguarta, C., de Groof, A. J., Madra, M., et al. (2012). Upregulated function of mitochondria-associated ER membranes in Alzheimer disease. *EMBO J.* 31, 4106–4123. doi: 10.1038/emboj.2012.202

Basso, V., Marchesan, E., Peggion, C., Chakraborty, J., von Stockum, S., Giacomello, M., et al. (2018). Regulation of ER-mitochondria contacts by Parkin *via* Mfn2. *Pharmacol. Res.* 138, 43–56. doi: 10.1016/j.phrs.2018.09.006

Berenguer-Escuder, C., Grossmann, D., Antony, P., Arena, G., Wasner, K., Massart, F., et al. (2020). Impaired mitochondrial-endoplasmic reticulum interaction and mitophagy in miro1-mutant neurons in Parkinson's disease. *Hum. Mol.genetics* 29, 1353–1364. doi: 10.1093/hmg/ddaa066

Bernhard, W., and Rouiller, C. (1956). Close topographical relationship between mitochondria and ergastoplasm of liver cells in a definite phase of cellular activity. *J. Biophys. Biochem. Cytol.* 2, 73–78. doi: 10.1083/jcb.2.4.73

Calì, T., Ottolini, D., Vicario, M., Catoni, C., Vallese, F., Cieri, D., et al. (2019). splitGFP technology reveals dose-dependent ER-mitochondria interface modulation by alpha-synuclein A53T and A30P mutants. *Cells* 8:1072. doi: 10.3390/cells8091072

Calkins, M. J., Manczak, M., Mao, P., Shirendeb, U., and Reddy, P. H. (2011). Impaired mitochondrial biogenesis, defective axonal transport of mitochondria, abnormal mitochondrial dynamics and synaptic degeneration in a mouse model of Alzheimer's disease. *Hum. Mol. Genet.* 20, 4515–4529. doi: 10.1093/hmg/ddr381

Chen, Y., Csordás, G., Jowdy, C., Schneider, T. G., Csordás, N., Wang, W., et al. (2012). Mitofusin 2-containing mitochondrial-reticular microdomains direct rapid cardiomyocyte bioenergetic responses *via* interorganelle Ca^{2+} crosstalk. *Circ. Res.* 111, 863–875. doi: 10.1161/circresaha.112.266585

Chen, H., Detmer, S. A., Ewald, A. J., Griffin, E. E., Fraser, S. E., and Chan, D. C. (2003). Mitofusins Mfn1 and Mfn2 coordinately regulate mitochondrial fusion and are essential for embryonic development. *J. Cell Biol.* 160, 189–200. doi: 10.1083/jcb.200211046

Chu, Q., Martinez, T. F., Novak, S. W., Donaldson, C. J., Tan, D., Vaughan, J. M., et al. (2019). Regulation of the ER stress response by a mitochondrial microprotein. *Nat. Commun.* 10:4883. doi: 10.1038/s41467-019-12816-z

Cieri, D., Vicario, M., Vallese, F., D'Orsi, B., Berto, P., Grinzato, A., et al. (2018). Tau localises within mitochondrial sub-compartments and its caspase cleavage affects ER-mitochondria interactions and cellular Ca^{2+} handling. *Biochim. Biophys. Acta Mol. Basis Dis.* 1864, 3247–3256. doi: 10.1016/j.bbadis.2018.07.011

Cohen, Y., Klug, Y. A., Dimitrov, L., Erez, Z., Chuartzman, S. G., Elinger, D., et al. (2014). Peroxisomes are juxtaposed to strategic sites on mitochondria. *Mol. Biosyst.* 10, 1742–1748. doi: 10.1039/c4mb00001c

Csordás, G., Renken, C., Várnai, P., Walter, L., Weaver, D., Buttle, K. F., et al. (2006). Structural and functional features and significance of the physical linkage between ER and mitochondria. *J. Cell Biol.* 174, 915–921. doi: 10.1083/jcb.200604016

Dalen, H., Scheie, P., Myklebust, R., and Saetersdal, T. (1983). An ultrastructural study of cryofractured myocardial cells with special attention to the relationship between mitochondria and sarcoplasmic reticulum. *J. Microsc.* 131, 35–46. doi: 10.1111/j.1365-2818.1983.tb04228.x

de Brito, O. M., and Scorrano, L. (2008). Mitofusin 2 tethers endoplasmic reticulum to mitochondria. *Nature* 456, 605–610. doi: 10.1038/nature07534

D'Eletto, M., Rossin, F., Occhigrossi, L., Farrace, M. G., Faccenda, D., Desai, R., et al. (2018). Transglutaminase type 2 regulates ER-mitochondria contact sites by interacting with GRP75. *Cell Rep.* 25, 3573.e4–3581.e4. doi: 10.1016/j.celrep.2018.11.094

De Vos, K. J., Mórotz, G. M., Stoica, R., Tudor, E. L., Lau, K. F., Ackerley, S., et al. (2012). VAPB interacts with the mitochondrial protein PTPIP51 to regulate calcium homeostasis. *Hum. Mol. Genet.* 21, 1299–1311. doi: 10.1093/hmg/ddr559

Eisenberg-Bord, M., Tsui, H. S., Antunes, D., Fernandez-Del-Rio, L., Bradley, M. C., Dunn, C. D., et al. (2019). The endoplasmic reticulum-mitochondria encounter structure complex coordinates coenzyme Q biosynthesis. *Contact* 2:2515256418825409. doi: 10.1177/2515256418825409

Fan, J., Li, X., Issop, L., Culty, M., and Papadopoulos, V. (2016). ACBD2/ECI2-mediated peroxisome-mitochondria interactions in leydig cell steroid biosynthesis. *Mol. Endocrinol.* 30, 763–782. doi: 10.1210/me.2016-1008

Fecher, C., Trovò, L., Müller, S. A., Snaidero, N., Wettmarshausen, J., Heink, S., et al. (2019). Cell-type-specific profiling of brain mitochondria reveals functional and molecular diversity. *Nat. Neurosci.* 22, 1731–1742. doi: 10.1038/s41593-019-0479-z

Filadi, R., Greotti, E., Turacchio, G., Luini, A., Pozzan, T., and Pizzo, P. (2015). Mitofusin 2 ablation increases endoplasmic reticulum-mitochondria coupling. *Proc. Natl. Acad. Sci. U S A* 112, E2174–2181. doi: 10.1073/pnas.1504880112

Filadi, R., Greotti, E., Turacchio, G., Luini, A., Pozzan, T., and Pizzo, P. (2017). On the role of mitofusin 2 in endoplasmic reticulum-mitochondria tethering. *Proc. Natl. Acad. Sci. U S A* 114, E2266–E2267. doi: 10.1073/pnas.1616040114

Filadi, R., Leal, N. S., Schreiner, B., Rossi, A., Dentoni, G., Pinho, C. M., et al. (2018). TOM70 sustains cell bioenergetics by promoting IP3R3-mediated ER to mitochondria Ca^{2+} transfer. *Curr. Biol.* 28, 369.e6–382.e6. doi: 10.1016/j.cub.2017.12.047

Galmes, R., Houcine, A., van Vliet, A. R., Agostinis, P., Jackson, C. L., and Giordano, F. (2016). ORP5/ORP8 localize to endoplasmic reticulum-mitochondria contacts and are involved in mitochondrial function. *EMBO Rep.* 17, 800–810. doi: 10.15252/embr.201541108

Gelmetti, V., De Rosa, P., Torosantucci, L., Marini, E. S., Romagnoli, A., Di Rienzo, M., et al. (2017). PINK1 and BECN1 relocalize at mitochondria-associated membranes during mitophagy and promote ER-mitochondria tethering and autophagosome formation. *Autophagy* 13, 654–669. doi: 10.1080/15548627.2016.1277309

Gomez-Suaga, P., Paillusson, S., and Miller, C. C. J. (2017a). ER-mitochondria signaling regulates autophagy. *Autophagy* 13, 1250–1251. doi: 10.1080/15548627.2017.1317913

Gomez-Suaga, P., Paillusson, S., Stoica, R., Noble, W., Hanger, D. P., and Miller, C. C. J. (2017b). The ER-mitochondria tethering complex VAPB-PTPIP51 regulates autophagy. *Curr. Biol.* 27, 371–385. doi: 10.1016/j.cub.2016.12.038

Gómez-Suaga, P., Pérez-Nievas, B. G., Glennon, E. B., Lau, D. H. W., Paillusson, S., Mórotz, G. M., et al. (2019). The VAPB-PTPIP51 endoplasmic reticulum-mitochondria tethering proteins are present in neuronal synapses and regulate synaptic activity. *Acta Neuropathol. Commun.* 7:35. doi: 10.1186/s40478-019-0688-4

Gregianin, E., Pallafacchina, G., Zanin, S., Crippa, V., Rusmini, P., Poletti, A., et al. (2016). Loss-of-function mutations in the SIGMAR1 gene cause distal hereditary motor neuropathy by impairing ER-mitochondria tethering and Ca^{2+} signalling. *Hum. Mol. Genet.* 25, 3741–3753. doi: 10.1093/hmg/ddw220

Grönblad, M., and Akerman, K. E. (1984). Electron-dense endoplasmic reticulum-like profiles closely associated with mitochondria in glomus cells of the carotid body after fixation with oxalate. *Exp. Cell Res.* 152, 161–168. doi: 10.1016/0014-4827(84)90240-4

Grossmann, D., Berenguer-Escuder, C., Bellet, M. E., Scheibner, D., Bohler, J., Massart, F., et al. (2019). Mutations in *RHOT1* disrupt endoplasmic reticulum-mitochondria contact sites interfering with calcium homeostasis and mitochondrial dynamics in Parkinson's disease. *Antioxid. Redox Signal.* 31, 1213–1234. doi: 10.1089/ars.2018.7718

Guardia-Laguarta, C., Area-Gomez, E., Rüb, C., Liu, Y., Magrané, J., Becker, D., et al. (2014). α-synuclein is localized to mitochondria-associated ER membranes. *J. Neurosci.* 34, 249–259. doi: 10.1523/JNEUROSCI.2507-13.2014

Hayashi, T., and Su, T. P. (2007). Sigma-1 receptor chaperones at the ER-mitochondrion interface regulate Ca^{2+} signaling and cell survival. *Cell* 131, 596–610. doi: 10.1016/j.cell.2007.08.036

Hedskog, L., Pinho, C. M., Filadi, R., Ronnback, A., Hertwig, L., Wiehager, B., et al. (2013). Modulation of the endoplasmic reticulum-mitochondria interface in Alzheimer's disease and related models. *Proc. Natl. Acad. Sci. U S A* 110, 7916–7921. doi: 10.1073/pnas.1300677110

Hirabayashi, Y., Kwon, S. K., Paek, H., Pernice, W. M., Paul, M. A., Lee, J., et al. (2017). ER-mitochondria tethering by PDZD8 regulates Ca^{2+} dynamics in mammalian neurons. *Science* 358, 623–630. doi: 10.1126/science.aan6009

Jeong, H., Park, J., and Lee, C. (2016). Crystal structure of Mdm12 reveals the architecture and dynamic organization of the ERMES complex. *EMBO Rep.* 17, 1857–1871. doi: 10.15252/embr.201642706

Khacho, M., Clark, A., Svoboda, D. S., Azzi, J., MacLaurin, J. G., Meghaizel, C., et al. (2016). Mitochondrial dynamics impacts stem cell identity and fate decisions by regulating a nuclear transcriptional program. *Cell Stem Cell* 19, 232–247. doi: 10.1016/j.stem.2016.04.015

Kornmann, B., Osman, C., and Walter, P. (2011). The conserved GTPase Gem1 regulates endoplasmic reticulum-mitochondria connections. *Proc. Natl. Acad. Sci. U S A* 108, 14151–14156. doi: 10.1073/pnas.1111314108

Kuchay, S., Giorgi, C., Simoneschi, D., Pagan, J., Missiroli, S., Saraf, A., et al. (2017). PTEN counteracts FBXL2 to promote IP3R3- and Ca^{2+}-mediated apoptosis limiting tumour growth. *Nature* 546, 554–558. doi: 10.1038/nature22965

Lahiri, S., Chao, J. T., Tavassoli, S., Wong, A. K., Choudhary, V., Young, B. P., et al. (2014). A conserved endoplasmic reticulum membrane protein complex (EMC) facilitates phospholipid transfer from the ER to mitochondria. *PLoS Biol.* 12:e1001969. doi: 10.1371/journal.pbio.1001969

Leal, N. S., Dentoni, G., Schreiner, B., Kämäräinen, O. P., Partanen, N., Herukka, S. K., et al. (2018). Alterations in mitochondria-endoplasmic reticulum connectivity in human brain biopsies from idiopathic normal pressure hydrocephalus patients. *Acta Neuropathol. Commun.* 6:102. doi: 10.1186/s40478-018-0605-2

Lee, K. S., Huh, S., Lee, S., Wu, Z., Kim, A. K., Kang, H. Y., et al. (2018). Altered ER-mitochondria contact impacts mitochondria calcium homeostasis and contributes to neurodegeneration in vivo in disease models. *Proc. Natl. Acad. Sci. U S A* 115, E8844–E8853. doi: 10.1073/pnas.1721136115

Lee, S., Lee, K. S., Huh, S., Liu, S., Lee, D. Y., Hong, S. H., et al. (2016). Polo kinase phosphorylates miro to control ER-mitochondria contact sites and mitochondrial Ca^{2+} homeostasis in neural stem cell development. *Dev. Cell* 37, 174–189. doi: 10.1016/j.devcel.2016.03.023

Li, D., Li, X., Guan, Y., and Guo, X. (2015). Mitofusin-2-mediated tethering of mitochondria and endoplasmic reticulum promotes cell cycle arrest of vascular smooth muscle cells in G0/G1 phase. *Acta Biochim. Biophys. Sin.* 47, 441–450. doi: 10.1093/abbs/gmv035

Liao, Y., Hao, Y., Chen, H., He, Q., Yuan, Z., and Cheng, J. (2015). Mitochondrial calcium uniporter protein MCU is involved in oxidative stress-induced cell death. *Protein Cell* 6, 434–442. doi: 10.1007/s13238-015-0144-6

Little, D., Luft, C., Mosaku, O., Lorvellec, M., Yao, Z., Paillusson, S., et al. (2018). A single cell high content assay detects mitochondrial dysfunction in iPSC-derived neurons with mutations in SNCA. *Sci. Rep.* 8:9033. doi: 10.1038/s41598-018-27058-0

Ma, J. H., Shen, S., Wang, J. J., He, Z., Poon, A., Li, J., et al. (2017). Comparative proteomic analysis of the mitochondria-associated ER membrane (MAM) in a long-term type 2 diabetic rodent model. *Sci. Rep.* 7:2062. doi: 10.1038/s41598-017-02213-1

Mattiazzi Ušaj, M., Brložnik, M., Kaferle, P., Žitnik, M., Wolinski, H., Leitner, F., et al. (2015). Genome-wide localization study of yeast Pex11 identifies peroxisome-mitochondria interactions through the ERMES complex. *J. Mol. Biol.* 427, 2072–2087. doi: 10.1016/j.jmb.2015.03.004

McLelland, G. L., Goiran, T., Yi, W., Dorval, G., Chen, C. X., Lauinger, N. D., et al. (2018). Mfn2 ubiquitination by PINK1/parkin gates the p97-dependent release of ER from mitochondria to drive mitophagy. *eLife* 7:e32866. doi: 10.7554/eLife.32866

Modi, S., López-Doménech, G., Halff, E. F., Covill-Cooke, C., Ivankovic, D., Melandri, D., et al. (2019). Miro clusters regulate ER-mitochondria contact sites and link cristae organization to the mitochondrial transport machinery. *Nat. Commun.* 10:4399. doi: 10.1038/s41467-019-12382-4

Mori, T., Hayashi, T., Hayashi, E., and Su, T. P. (2013). Sigma-1 receptor chaperone at the ER-mitochondrion interface mediates the mitochondrion-ER-nucleus signaling for cellular survival. *PLoS One* 8:e76941. doi: 10.1371/journal.pone.0076941

Nagashima, S., Takeda, K., Ohno, N., Ishido, S., Aoki, M., Saitoh, Y., et al. (2019). MITOL deletion in the brain impairs mitochondrial structure and ER tethering leading to oxidative stress. *Life Sci. Alliance* 2:e201900308. doi: 10.26508/lsa.201900308

Naon, D., Zaninello, M., Giacomello, M., Varanita, T., Grespi, F., Lakshminaranayan, S., et al. (2016). Critical reappraisal confirms that mitofusin 2 is an endoplasmic reticulum-mitochondria tether. *Proc. Natl. Acad. Sci. U S A* 113, 11249–11254. doi: 10.1073/pnas.1606786113

Norkett, R., Modi, S., Birsa, N., Atkin, T. A., Ivankovic, D., Pathania, M., et al. (2016). DISC1-dependent regulation of mitochondrial dynamics controls the morphogenesis of complex neuronal dendrites. *J. Biol. Chem.* 291, 613–629. doi: 10.1074/jbc.m115.699447

Paillusson, S., Gomez-Suaga, P., Stoica, R., Little, D., Gissen, P., Devine, M. J., et al. (2017). α-synuclein binds to the ER-mitochondria tethering protein VAPB to disrupt Ca^{2+} homeostasis and mitochondrial ATP production. *Acta Neuropathol.* 134, 129–149. doi: 10.1007/s00401-017-1704-z

Pera, M., Larrea, D., Guardia-Laguarta, C., Montesinos, J., Velasco, K. R., Agrawal, R. R., et al. (2017). Increased localization of APP-C99 in mitochondria-associated ER membranes causes mitochondrial dysfunction in Alzheimer disease. *EMBO J.* 36, 3356–3371. doi: 10.15252/embj.201796797

Ponomareva, O. Y., Eliceiri, K. W., and Halloran, M. C. (2016). Charcot-Marie-Tooth 2b associated Rab7 mutations cause axon growth and guidance defects during vertebrate sensory neuron development. *Neural Dev.* 11:2. doi: 10.1186/s13064-016-0058-x

Poston, C. N., Krishnan, S. C., and Bazemore-Walker, C. R. (2013). In-depth proteomic analysis of mammalian mitochondria-associated membranes (MAM). *J. Proteomics* 79, 219–230. doi: 10.1016/j.jprot.2012.12.018

Qi, Y., Yan, L., Yu, C., Guo, X., Zhou, X., Hu, X., et al. (2016). Structures of human mitofusin 1 provide insight into mitochondrial tethering. *J. Cell Biol.* 215, 621–629. doi: 10.1083/jcb.201609019

Rusinol, A. E., Cui, Z., Chen, M. H., and Vance, J. E. (1994). A unique mitochondria-associated membrane fraction from rat liver has a high capacity for lipid synthesis and contains pre-Golgi secretory proteins including nascent lipoproteins. *J. Biol. Chem.* 269, 27494–27502.

Schrader, M., Costello, J., Godinho, L. F., and Islinger, M. (2015). Peroxisome-mitochondria interplay and disease. *J. Inherit. Metab. Dis.* 38, 681–702. doi: 10.1007/s10545-015-9819-7

Schreiner, B., Hedskog, L., Wiehager, B., and Ankarcrona, M. (2015). Amyloid-beta peptides are generated in mitochondria-associated endoplasmic reticulum membranes. *J. Alzheimers Dis.* 43, 369–374. doi: 10.3233/jad-132543

Shai, N., Yifrach, E., van Roermund, C. W. T., Cohen, N., Bibi, C., Lodewijk, I., et al. (2018). Systematic mapping of contact sites reveals tethers and a function for the peroxisome-mitochondria contact. *Nat. Commun.* 9:1761. doi: 10.1038/s41467-018-03957-8

Shoshan-Barmatz, V., Keinan, N., and Zaid, H. (2008). Uncovering the role of VDAC in the regulation of cell life and death. *J. Bioenerg. Biomembr.* 40, 183–191. doi: 10.1007/s10863-008-9147-9

Simmen, T., Aslan, J. E., Blagoveshchenskaya, A. D., Thomas, L., Wan, L., Xiang, Y., et al. (2005). PACS-2 controls endoplasmic reticulum-mitochondria communication and Bid-mediated apoptosis. *EMBO J.* 24, 717–729. doi: 10.1038/sj.emboj.7600559

Stoica, R., De Vos, K. J., Paillusson, S., Mueller, S., Sancho, R. M., Lau, K. F., et al. (2014). ER-mitochondria associations are regulated by the VAPB-PTPIP51 interaction and are disrupted by ALS/FTD-associated TDP-43. *Nat. Commun.* 5:3996. doi: 10.1038/ncomms4996

Stoica, R., Paillusson, S., Gomez-Suaga, P., Mitchell, J. C., Lau, D. H., Gray, E. H., et al. (2016). ALS/FTD-associated FUS activates GSK-3beta to disrupt the VAPB-PTPIP51 interaction and ER-mitochondria associations. *EMBO Rep.* 17, 1326–1342. doi: 10.15252/embr.201541726

Sugiura, A., Mattie, S., Prudent, J., and McBride, H. M. (2017). Newly born peroxisomes are a hybrid of mitochondrial and ER-derived pre-peroxisomes. *Nature* 542, 251–254. doi: 10.1038/nature21375

Sugiura, A., Nagashima, S., Tokuyama, T., Amo, T., Matsuki, Y., Ishido, S., et al. (2013). MITOL regulates endoplasmic reticulum-mitochondria contacts *via* Mitofusin2. *Mol. Cell* 51, 20–34. doi: 10.1016/j.molcel.2013.04.023

Sun, T., Qiao, H., Pan, P. Y., Chen, Y., and Sheng, Z. H. (2013). Motile axonal mitochondria contribute to the variability of presynaptic strength. *Cell Rep.* 4, 413–419. doi: 10.1016/j.celrep.2013.06.040

Szabadkai, G., Bianchi, K., Varnai, P., De Stefani, D., Wieckowski, M. R., Cavagna, D., et al. (2006). Chaperone-mediated coupling of endoplasmic reticulum and mitochondrial Ca^{2+} channels. *J. Cell. Biol.* 175, 901–911. doi: 10.1083/jcb.200608073

Takeda, K., Nagashima, S., Shiiba, I., Uda, A., Tokuyama, T., Ito, N., et al. (2019). MITOL prevents ER stress-induced apoptosis by IRE1alpha ubiquitylation at ER-mitochondria contact sites. *EMBO J.* 38:e100999. doi: 10.15252/embj.2018100999

Thoudam, T., Ha, C. M., Leem, J., Chanda, D., Park, J. S., Kim, H. J., et al. (2019). PDK4 augments ER-mitochondria contact to dampen skeletal muscle insulin signaling during obesity. *Diabetes* 68, 571–586. doi: 10.2337/db18-0363

Tsai, Y. L., Coady, T. H., Lu, L., Zheng, D., Alland, I., Tian, B., et al. (2020). ALS/FTD-associated protein FUS induces mitochondrial dysfunction by preferentially sequestering respiratory chain complex mRNAs. *Genes Dev.* 34, 785–805. doi: 10.1101/gad.335836.119

Vaccaro, V., Devine, M. J., Higgs, N. F., and Kittler, J. T. (2017). Miro1-dependent mitochondrial positioning drives the rescaling of presynaptic Ca^{2+} signals during homeostatic plasticity. *EMBO Re.* 18, 231–240. doi: 10.15252/embr.201642710

Valadas, J. S., Esposito, G., Vandekerkhove, D., Miskiewicz, K., Deaulmerie, L., Raitano, S., et al. (2018). ER lipid defects in neuropeptidergic neurons impair sleep patterns in Parkinson's disease. *Neuron* 98, 1155.e6–1169.e6. doi: 10.1016/j.neuron.2018.05.022

Vance, J. E. (1990). Phospholipid synthesis in a membrane fraction associated with mitochondria. *J. Biol. Chem.* 265, 7248–7256.

Veeresh, P., Kaur, H., Sarmah, D., Mounica, L., Verma, G., Kotian, V., et al. (2019). Endoplasmic reticulum-mitochondria crosstalk: from junction to function across neurological disorders. *Ann. N Y Acad. Sci.* 1457, 41–60. doi: 10.1111/nyas.14212

Voss, C., Lahiri, S., Young, B. P., Loewen, C. J., and Prinz, W. A. (2012). ER-shaping proteins facilitate lipid exchange between the ER and mitochondria in S. cerevisiae. *J. Cell Sci.* 125, 4791–4799. doi: 10.1242/jcs.105635

Wang, K., and Klionsky, D. J. (2011). Mitochondria removal by autophagy. *Autophagy* 7, 297–300. doi: 10.4161/auto.7.3.14502

Watanabe, S., Ilieva, H., Tamada, H., Nomura, H., Komine, O., Endo, F., et al. (2016). Mitochondria-associated membrane collapse is a common pathomechanism in SIGMAR1- and SOD1-linked ALS. *EMBO Mol. Med.* 8, 1421–1437. doi: 10.15252/emmm.201606403

Wideman, J. G., Gawryluk, R. M., Gray, M. W., and Dacks, J. B. (2013). The ancient and widespread nature of the ER-mitochondria encounter structure. *Mol. Biol. Evol.* 30, 2044–2049. doi: 10.1093/molbev/mst120

Wong, Y. C., Ysselstein, D., and Krainc, D. (2018). Mitochondria-lysosome contacts regulate mitochondrial fission *via* RAB7 GTP hydrolysis. *Nature* 554, 382–386. doi: 10.1038/nature25486

Yu, S., Zhang, L., Liu, C., Yang, J., Zhang, J., and Huang, L. (2019). PACS2 is required for ox-LDL-induced endothelial cell apoptosis by regulating mitochondria-associated ER membrane formation and mitochondrial Ca^{2+} elevation. *Exp. Cell Res.* 379, 191–202. doi: 10.1016/j.yexcr.2019.04.002

Conflict of Interest: The authors declare that the research was conducted in the absence of any commercial or financial relationships that could be construed as a potential conflict of interest.

frontiers in Cell and Developmental Biology

PERSPECTIVE
published: 23 October 2020
doi: 10.3389/fcell.2020.592651

Reweaving the Fabric of Mitochondrial Contact Sites in Astrocytes

Matteo Bergami[1,2,3]* *and Elisa Motori*[1,4]*

[1] Cologne Excellence Cluster on Cellular Stress Responses in Aging-Associated Diseases (CECAD), University Hospital Cologne, Cologne, Germany, [2] Institute of Genetics, University of Cologne, Cologne, Germany, [3] Center for Molecular Medicine Cologne, University of Cologne, Cologne, Germany, [4] Max Planck Institute for Biology of Ageing, Cologne, Germany

The endoplasmic reticulum (ER) and mitochondria are classically regarded as very dynamic organelles in cell lines. Their frequent morphological changes and repositioning underlie the transient generation of physical contact sites (so-called mitochondria-ER contacts, or MERCs) which are believed to support metabolic processes central for cellular signaling and function. The extent of regulation over these organelle dynamics has likely further achieved a higher level of complexity in polarized cells like neurons and astrocytes to match their elaborated geometries and specialized functions, thus ensuring the maintenance of MERCs at metabolically demanding locations far from the soma. Yet, live imaging of adult brain tissue has recently revealed that the true extent of mitochondrial dynamics in astrocytes is significantly lower than in cell culture settings. On one hand, this suggests that organelle dynamics in mature astroglia *in vivo* may be highly regulated and perhaps triggered only by defined physiological stimuli. On the other hand, this extent of control may greatly facilitate the stabilization of those MERCs required to maintain regionalized metabolic domains underlying key astrocytic functions. In this perspective, we review recent evidence suggesting that the resulting spatial distribution of mitochondria and ER in astrocytes *in vivo* may create the conditions for maintaining extensive MERCs within specialized territories – like perivascular endfeet – and discuss the possibility that their enrichment at these distal locations may facilitate specific forms of cellular plasticity relevant for physiology and disease.

Keywords: mitochondrial dynamics, endoplasmic reticulum, astrocytes, calcium, endfoot, Mfn2, mitochondria, MERCs

OPEN ACCESS

Edited by:
Laura Lackner,
Northwestern University,
United States

Reviewed by:
Thomas Simmen,
University of Alberta, Canada
Benoît Kornmann,
University of Oxford, United Kingdom

***Correspondence:**
Matteo Bergami
matteo.bergami@uk-koeln.de
Elisa Motori
elisa.motori@uk-koeln.de

Specialty section:
This article was submitted to Molecular Medicine, a section of the journal Frontiers in Cell and Developmental Biology

Received: *07 August 2020*
Accepted: *06 October 2020*
Published: *23 October 2020*

Citation:
Bergami M and Motori E (2020) Reweaving the Fabric of Mitochondrial Contact Sites in Astrocytes. Front. Cell Dev. Biol. 8:592651. doi: 10.3389/fcell.2020.592651

INTRODUCTION

Substantial effort is being made in understanding the mechanisms that regulate tethering between mitochondria and other organelles, particularly the endoplasmic reticulum (ER), given that important functions have been ascribed to these mitochondria-ER contacts (MERCs) (Csordas et al., 2018). In particular, evidence exists for specific portions of the mitochondrial outer membrane being opposed by ER tubules within a distance of 15–30 nm. A growing number of tethering and regulatory proteins has been identified or proposed for maintaining in place these MERCs (Csordas et al., 2018). So far, these specialized domains have been implicated

in the regulation of key cellular processes such as phospholipid metabolism (Vance, 2015; Dimmer and Rapaport, 2017), autophagosome formation (Hamasaki et al., 2013), and the transfer of Ca^{2+} between the two organelles (Csordas and Hajnoczky, 2009; Raffaello et al., 2016). Furthermore, MERCs also serve as sub-cellular signaling platforms, particularly in coordinating reactive oxygen species (ROS) signaling nanodomains (Booth et al., 2016). Finally, studies in cell lines have shown that the transient formation of MERCs is linked to membrane and organelle remodeling (Friedman et al., 2011; Lewis et al., 2016). While emerging evidence has begun disclosing the physiological and pathological relevance of MERCs in some peripheral tissues, our understanding of the principles regulating their formation and maintenance in the central nervous system, as well as their role for cellular function, is very limited. In part, this is likely due to the marked heterogeneity of cell sub-types characterizing brain tissue, which poses significant challenges in properly examining with sufficient spatial resolution the extent of MERCs and their dynamics *in situ* via imaging approaches. Electron microscopy is the method of choice for studying organelle contact sites and reconstructing organelle networks in whole cells, however, in brain tissue this approach may still be very time consuming on account of the geometric complexity of most cells contained within (e.g., neurons, astrocytes, and oligodendrocytes) and the intrinsic variability in cell sub-types across brain regions. As a result, these studies generally lead to the reconstruction of only few selected cells or even just part of them. Likewise, a systematic analysis of the signaling functions of MERCs in brain cells *in situ* may prove challenging to achieve. Yet, in parallel to recent studies that have begun addressing the extent of MERCs and potential regulatory tethering proteins in neurons (Hirabayashi et al., 2017; Wu et al., 2017), some of the implications of MERC dysfunction in neurodegeneration are also emerging (Area-Gomez and Schon, 2017; De Mario et al., 2017). Significant efforts are being also made to investigate organelle morphology, dynamics, and MERCs on at least one other type of brain cell, namely the astrocyte. Astrocytes exerts essential metabolic functions in the adult brain owing to their unique cellular architecture and positioning within the neurovascular unit (**Figure 1**), and recent studies have revealed an unexpected complexity of their mitochondrial and ER networks *in vivo*. Intriguingly, alongside with their elaborated morphologies, these two organelles were also found to be differentially distributed across cellular territories (Mathiisen et al., 2010; Cali et al., 2019; Göbel et al., 2020) and to give rise to a significant extent of MERCs in remote regions of the astrocyte – like the perivascular endfeet – where their specialized functions are most likely sustaining important roles in physiological and disease settings.

UNEXPECTED COMPLEXITY OF MITOCHONDRIAL AND ER NETWORKS IN ASTROCYTES

While the ER has been under intense investigation for its recognized role in Ca^{2+} handling in astrocytes (Bazargani and Attwell, 2016), the structure and function of astrocytic mitochondria have received much less attention. This underestimation of astrocytic mitochondrial metabolism has been, at least in part, a direct consequence of the generally accepted notion that astrocytes – in contrast to neurons – are mostly glycolytic in nature (Hertz et al., 2007; Supplie et al., 2017), and so this bias has for long time diverted the attention away from mitochondria, in which oxidative phosphorylation (OXPHOS) takes place. However, the recent employment of mitochondrial-targeted fluorescent indicators to investigate astrocytes *ex vivo* and *in vivo* disclosed a convoluted mitochondrial network, which is indicative of astrocytes relying substantially on this organelle for energy metabolism. In particular, the use of mito-YFP (and similar) reporters in astrocytes combined with high-resolution optic and electron microscopy recently allowed to fully appreciate the extent of mitochondrial mass and heterogeneity of mitochondrial morphologies displayed by astrocytes across their territories (Motori et al., 2013; Stephen et al., 2015; Agarwal et al., 2017; Gobel et al., 2018; Jackson and Robinson, 2018; Henneberger et al., 2019). While the exact morphological transformation of the mitochondrial network throughout astrocyte development still remains to be investigated, it is now clear that mature astrocytes possess a robust mitochondrial network, with large bundles of mitochondria that coalesce within main branches originating from the soma and invade the cell's periphery (**Figure 2A**; Motori et al., 2013; Cali et al., 2019). Interestingly, the larger the distance from the soma, the smaller mitochondria appear with respect to their size, particularly within the numerous fine branches and branchlets that surround neuronal synapses (**Figures 2B,C**). This seemingly recapitulates what has been described in neurons, where active mechanisms sculpt mitochondrial morphology in distal dendrites and axons to achieve proper mitochondrial distribution at synapses (Li et al., 2004; Lewis et al., 2018). However, in contrast to fine astrocytic perisynaptic processes, which can at best accommodate the smallest mitochondria (Lovatt et al., 2007; Agarwal et al., 2017), perivascular endfeet (i.e., processes unsheathing most of the brain microvasculature and ensuring transfer of ions, water, and key metabolic substrates from/to the blood-brain-barrier) make a unique exception being capable to host quite elaborated morphologies, including long and branched mitochondria (**Figure 2C**; Mathiisen et al., 2010). Specifically, ultrastructural studies of the endfoot showed that the astrocytic terminals wrapping around microvessels are often packed with large mitochondria and, interestingly, ER tubules (Mathiisen et al., 2010; Göbel et al., 2020). Intriguingly, in contrast to the ER in perisynaptic processes which presents itself as short smooth tubules, the endfeet are characterized by a rather peculiar distribution of the ER. In these processes long bundles of both smooth and rough ER surround the basal lamina facing the endothelial side, thus generating a layer of ER membranes that virtually shield mitochondria from directly contacting the basal lamina (Göbel et al., 2020). While ER tubules are also found distributed across the entirety of the endfoot, the unique layered disposition of ER and mitochondria in the region adjacent the endothelium suggests that this arrangement of organelles may serve specific perivascular functions.

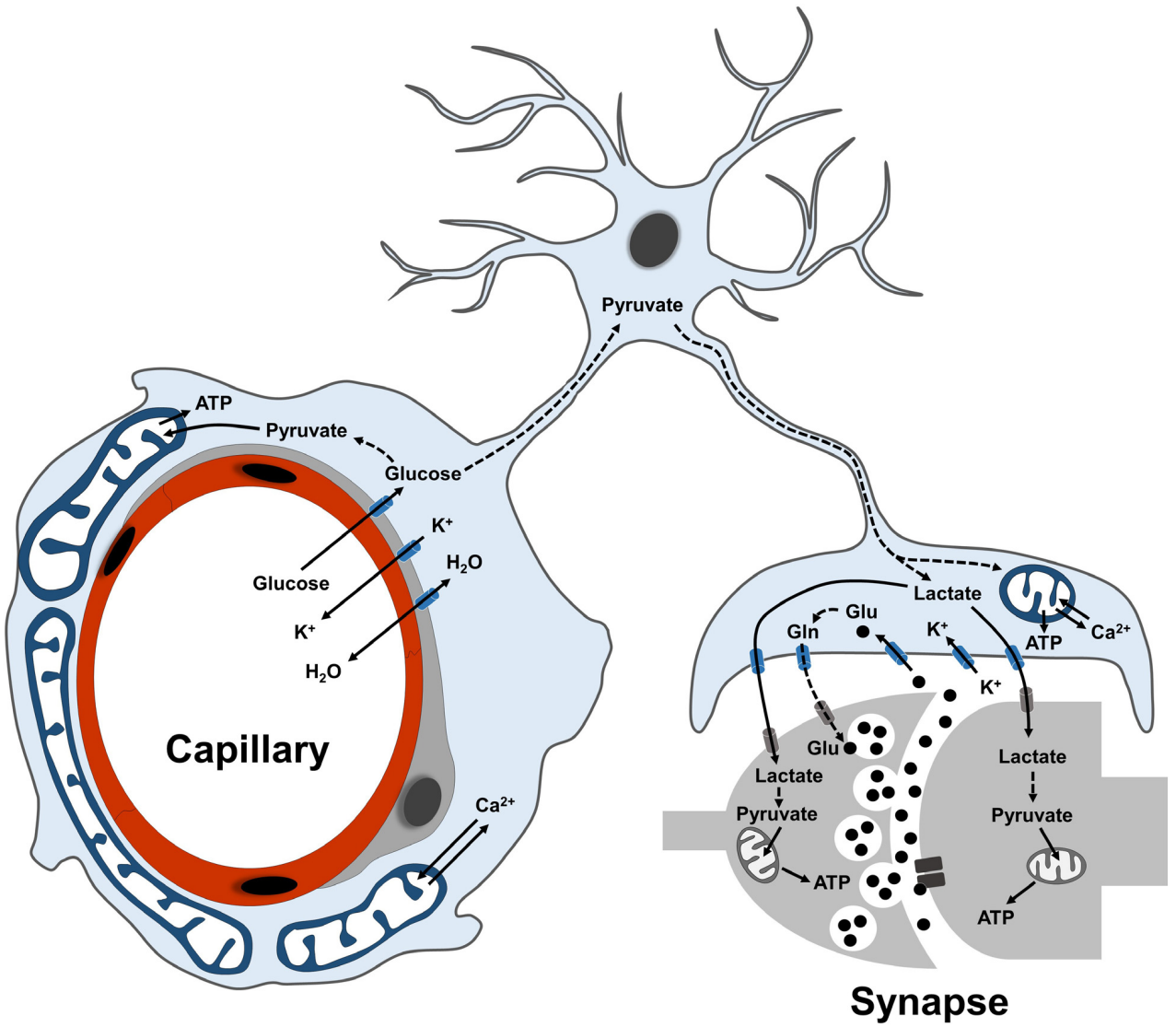

FIGURE 1 | Overview of astrocyte functions in the neurovascular unit. Scheme illustrating the main metabolic functions of astrocytes at their perivascular (endfeet) and perisynaptic processes. Glucose is mostly taken up via the endfeet, where also ions and water molecules can be actively exchanged with the blood-brain barrier. Following glycolytic conversion to pyruvate, glucose can be utilized as energy substrate by astrocytic mitochondria or further converted into lactate to fuel synaptic transmission. At perisynaptic processes, astrocytes contribute to replenish the glutamate pool of neurotransmitters via the glutamate-glutamine cycle. Dashed lines between metabolites indicate a metabolic conversion. Plasma membrane transporters and ionic pumps are indicated with blue (for astrocytes) or gray (for neurons) symbols.

LOCALIZED ENRICHMENT OF MERCs AND ITS CONSEQUENCE IN ASTROCYTES

One of the best-studied aspects of astrocyte physiology is the remarkable extent and diversity of cytosolic Ca^{2+} transients displayed by the processes of these cells (Shigetomi et al., 2016). Thus, it is not surprising that these cells are differentially enriched in size and density of mitochondria as well as ER membranes across their territories, as both these two organelles play important roles in Ca^{2+} buffering and regulation. However, it is noteworthy that out of the vast number of mitochondria contained in all distal astrocytic processes, those confined within the ∼3 (in average) perivascular endfeet per astrocyte contain almost twice the extent of MERCs as compared to those in perisynaptic processes (Göbel et al., 2020). In part, this is facilitated by the natural enrichment in mitochondria and ER membranes within the endfoot. However, this asymmetry in the distribution of MERCs suggests that the perivascular region may be characterized by particularly elevated rates of lipid homeostasis, Ca^{2+} signaling and membrane dynamics, which so far represent the main functions ascribed to these contact sites (Csordas et al., 2018). Similar to other differentiated cell

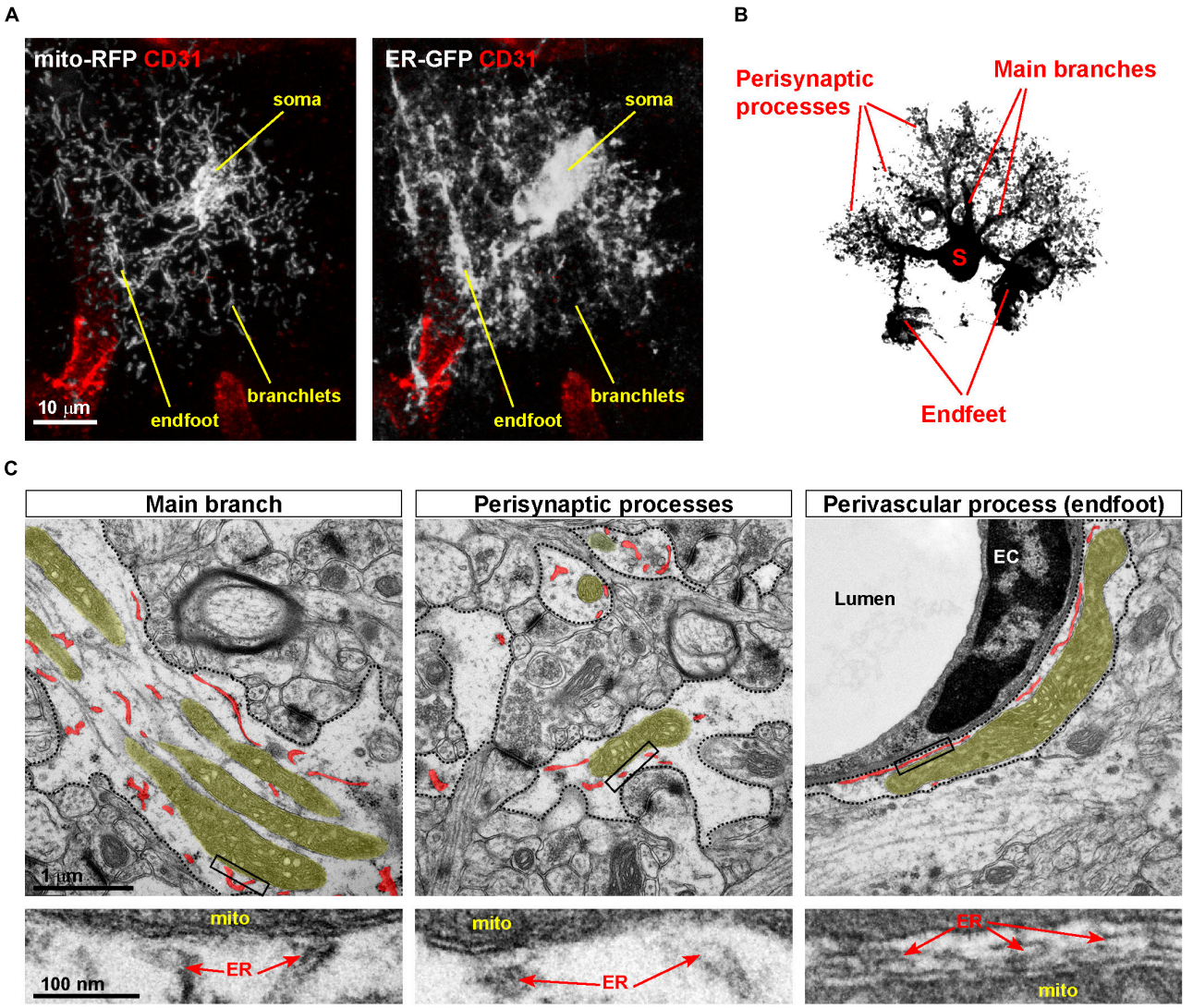

FIGURE 2 | Asymmetric distribution of MERCs in astrocytic processes. **(A)** Example of a cortical astrocyte co-transduced with ER-GFP and mito-RFP viruses, showing the distribution of both organelles *in vivo* across astrocytic territories, particularly perivascular endfeet and fine branchlets. Immunostaining against the endothelial marker CD31, labeling the vasculature, is shown. **(B)** Scheme of an astrocyte showing the location of somas, main branches, perisynaptic, and perivascular processes (the latter ones visible as tube-like structures). **(C)** Electron microscopic pictures of distinct portions of the astrocyte (dashed areas correspond to astrocytic processes). While in main branches and endfeet large mitochondria are often visible, in processes surrounding synapses mitochondria display a smaller size. In each panel, mitochondria and ER are highlighted in different colors (yellow, mitochondria; red, ER). Lower panels depict zooms of the boxed areas, pointing to putative MERCs. EC, endothelial cell.

types, it is still unclear which exact proteins regulate the extent of MERCs in astrocytes out of the many possible proposed candidates (Csordas et al., 2018). While it is tempting to assume that many of the proposed natural tethers may share similar functions also in astrocytes, cell-type specificity within brain tissue may bring about additional layers of complexity, with certain tethers having for example a more prominent role in neurons than in astrocytes (Hirabayashi et al., 2017; Fecher et al., 2019). Furthermore, the intrinsic structural heterogeneity of MERCs among distinct astrocytic territories likely reflects a sub-specialization in ER-mitochondria tether proteins. If this is the case, one may expect an asymmetric enrichment in certain tether proteins among astrocytic territories, mirroring intracellular differences in organelle morphology and possibly function. Despite lack of clear evidence in astrocytes for the regulatory role of many previously proposed MERC-associated proteins (Csordas et al., 2018), recent work has begun to shed some light on the relevance of local MERC enrichment in astrocyte processes. For example, conditional deletion of the GTPase Mitofusin 2 (Mfn2), which resides at the ER-mitochondria interface (Hung et al., 2017) and has been proposed to regulate contact sites in cell lines (de Brito and Scorrano, 2008; Filadi et al., 2015; Naon et al., 2016), was indeed sufficient to alter the extent of MERCs *in vivo* and as a result interfere

with the Ca^{2+} uptake capacity of astrocytic mitochondria (Göbel et al., 2020). In turn, the impaired mitochondrial Ca^{2+} buffering had direct consequences for local cytosolic transients, however, this effect appeared to be most prominent within the endfeet. Importantly, these functional alterations at the mitochondrial level were almost completely restored following expression of an artificial ER-mitochondria tether (Csordas et al., 2006; Göbel et al., 2020). This example demonstrates the functional relevance of an asymmetric distribution of MERCs in astrocytes, and provides a first evidence that a regionalized signaling in glial cells can be facilitated by local enrichments in mitochondrial and ER organelles. Yet, to which extent astrocytic MERCs can be considered as dynamic domains, especially in an *in vivo* situation, remains unclear. In cells *in vitro*, including astrocytes, these two organelles display a very active behavior, with mitochondria undergoing frequent fusion and fission events and ER tubules forming both stable and transient contacts at locations of future mitochondrial division (Friedman et al., 2011; Motori et al., 2013; Lewis et al., 2016). However, despite evidence for mitochondrial trafficking and fusion/fission dynamics in both acute and organotypic brain slice preparations (Motori et al., 2013; Jackson and Robinson, 2015; Stephen et al., 2015), distinct astrocytic territories appear to be independently regulated, with perivascular endfeet displaying much less dynamics as compared for instance to other branches and terminals (Göbel et al., 2020). However, it is unclear to what extent mitochondrial dynamics reflect actual changes in MERCs in astrocytes *in situ*. Given the spatial heterogeneity of some of the physiological functions to which MERCs may contribute (e.g., local Ca^{2+} dynamics) (Shigetomi et al., 2013; Agarwal et al., 2017; Bindocci et al., 2017), it is tempting to speculate that certain regions of the astrocyte might be subjected to a higher level of MERC regulation compared to other territories. For instance, bursts of dynamic changes in mitochondrial morphology and MERCs at perisynaptic processes may take place only in response to specific stimuli, as in the case of neurotransmitter spillover (Jackson et al., 2014; Stephen et al., 2015) or following induction of synaptic plasticity (i.e., potentiation) (Henneberger et al., 2019). Likely, the optimization of existing genetically encoded molecular sensors (Csordas et al., 2010) and the further development of *in situ* super-resolution approaches (Jakobs et al., 2020) may ultimately provide better access to live-cell organelle contact dynamics with minimal interference and possibly link these to specific astrocytic cellular functions (Iliff et al., 2012; Mishra et al., 2016).

RELEVANCE OF MERCs FOR ASTROCYTIC REACTIVITY STATES

In response to brain injury and inflammation, astrocytes are well known for their capability to acquire a so-called "reactivity state," which is known to influence the progression of the initial insult (Khakh and Sofroniew, 2015). Indeed, reactive astrocytes – classically recognizable for their hypertrophic aspect and increased expression of markers such as glial fibrillary acidic protein (GFAP) (an intermediate filament marker) – have been identified in most neurological diseases (Sofroniew, 2014). Several studies, however, pointed out that this seemingly unique cellular state is rather characterized by a spectrum of heterogeneous changes, including profound alterations in gene and protein expression, thus suggesting the existence of multiple reactive states depending on type, severity, location and context of the triggering insult (Sofroniew, 2014; Liddelow and Barres, 2017). Further evidence now disclosed that reactive astrocytes may undergo significant metabolic rewiring when facing challenging conditions, as in the case of antiviral signaling response or in mouse models of Huntington disease (Chao et al., 2019; Polyzos et al., 2019). Yet, whether this rewiring under these conditions also involves changes in the metabolic functions of MERCs remains to be investigated. Metabolic flexibility in brain cells *in vivo* has been known for quite some time to be a fundamental feature of glial cells (Hertz et al., 2007; Weber and Barros, 2015), and while only recent work has begun to reveal neuron-specific forms of metabolic rewiring (Motori et al., 2020), the fact that astrocytes can efficiently reprogram their energy metabolism may explain their almost unique resilience to brain damage. In this respect, it is becoming clear that while reactive astrocytes can increase their glycolytic and glycogenolytic rates (Brown et al., 1995; Almeida et al., 2004; Motori et al., 2013), mitochondrial metabolism also plays a fundamental role in sustaining astrocyte functions following brain insult (Ignatenko et al., 2018; Fiebig et al., 2019). This reactivity state is indeed accompanied by a time-dependent transformation of the mitochondrial network in astrocytes directly exposed to acute injury and inflammation, which encompasses a general fragmentation shortly after injury followed by network re-tubulation during the next few weeks (Motori et al., 2013). Furthermore, simultaneous investigation of ER and mitochondrial network dynamics in injury-induced reactive astrocytes disclosed the marked accumulation of both these organelles in perivascular endfeet during an early phase after the initial insult, thus facilitating the formation of MERCs in these perivascular processes (Göbel et al., 2020). Preventing or enhancing this accumulation had effects not only on the magnitude and duration of local cytosolic Ca^{2+} transients of the astrocyte, but also influenced the extent of neo-angiogenesis in a model of penetrating brain injury (Göbel et al., 2020). While the precise mechanisms underlying this non-cell-autonomous effect on endothelial cells can only be speculated, these findings suggest that a dynamic reorganization of MERCs at precise locations of the astrocyte may serve to generate local metabolic domains important for tissue healing. Further studies are thus needed to investigate whether similar changes may also take place at perisynaptic processes. Likewise, additional work is necessary to establish the role of other tethers as well as putative regulatory MERC proteins other than Mfn2, and ascertain whether they might influence MERCs in astrocytes as well as astrocyte function. Still, these findings obviously raise the intriguing possibility that regulating the extent of MERCs in astrocytes (or other brain cells) may play a role in expressing distinct reactivity states, with direct

consequences for neuronal viability (Anderson et al., 2016; Liddelow et al., 2017).

CONCLUSION

Recent progress in microscopy and genetic techniques began unveiling an important role played by mitochondria and ER networks in regulating astrocytic functions, yet our understanding of organelle physiology and "contact-ology" in astrocytes is still rudimentary. For instance, we do not fully understand how much dynamic or static these contact sites are between ER and mitochondria. We also likely underestimate the extent to which MERCs differentially contribute to specific metabolic or signaling functions in distinct territories of the astrocyte. Likewise, very little is known about the role of astrocytic mitochondrial contacts with other organelles, for instance during postnatal astrocytic development, or following the acquisition of reactive states. In light of the recent suggestion that mitochondria may be transferred from/to astrocytes and other brain cells in settings of disease (Davis et al., 2014; Joshi et al., 2019), and that this transfer may even possibly compensate for certain metabolic deficits (Hayakawa et al., 2016), understanding the mechanisms regulating mitochondrial function at sites of contact with other organelles may lay the ground for targeted therapeutic approaches to improve brain repair during acute trauma and chronic neurodegeneration.

DATA AVAILABILITY STATEMENT

All datasets presented in this study are included in the article/supplementary material.

ETHICS STATEMENT

The animal study was reviewed and approved by Landesamt für Natur, Umwelt und Verbraucherschutz Nordrhein-Westfalen.

AUTHOR CONTRIBUTIONS

All authors listed have made a substantial, direct and intellectual contribution to the work, and approved it for publication.

FUNDING

This work was supported by the Deutsche Forschungsgemeinschaft (SFB1218 – 269925409 and CECAD EXC 2030 – 390661388) and European Research Council (ERC-StG-2015, grant number 67844) to MB. EM was supported by an Advanced Postdoc Grant (Deutsche Forschungsgemeinschaft, SFB1218 – 269925409).

REFERENCES

Agarwal, A., Wu, P. H., Hughes, E. G., Fukaya, M., Tischfield, M. A., Langseth, A. J., et al. (2017). Transient opening of the mitochondrial permeability transition pore induces microdomain calcium transients in astrocyte processes. *Neuron* 93, 587–605e587. doi: 10.1016/j.neuron.2016.12.034

Almeida, A., Moncada, S., and Bolanos, J. P. (2004). Nitric oxide switches on glycolysis through the AMP protein kinase and 6-phosphofructo-2-kinase pathway. *Nat. Cell Biol.* 6, 45–51. doi: 10.1038/ncb1080

Anderson, M. A., Burda, J. E., Ren, Y., Ao, Y., O'shea, T. M., Kawaguchi, R., et al. (2016). Astrocyte scar formation aids central nervous system axon regeneration. *Nature* 532, 195–200. doi: 10.1038/nature17623

Area-Gomez, E., and Schon, E. A. (2017). On the pathogenesis of alzheimer's disease: the MAM hypothesis. *FASEB J.* 31, 864–867. doi: 10.1096/fj.201601309

Bazargani, N., and Attwell, D. (2016). Astrocyte calcium signaling: the third wave. *Nat. Neurosci.* 19, 182–189. doi: 10.1038/nn.4201

Bindocci, E., Savtchouk, I., Liaudet, N., Becker, D., Carriero, G., and Volterra, A. (2017). Three-dimensional Ca2+ imaging advances understanding of astrocyte biology. *Science* 356:eaai8185. doi: 10.1126/science.aai8185

Booth, D. M., Enyedi, B., Geiszt, M., Varnai, P., and Hajnoczky, G. (2016). Redox nanodomains are induced by and control calcium signaling at the ER-Mitochondrial interface. *Mol. Cell* 63, 240–248. doi: 10.1016/j.molcel.2016.05.040

Brown, G. C., Bolanos, J. P., Heales, S. J., and Clark, J. B. (1995). Nitric oxide produced by activated astrocytes rapidly and reversibly inhibits cellular respiration. *Neurosci. Lett.* 193, 201–204. doi: 10.1016/0304-3940(95)11703-Y

Cali, C., Agus, M., Kare, K., Boges, D. J., Lehvaslaiho, H., Hadwiger, M., et al. (2019). 3D cellular reconstruction of cortical glia and parenchymal morphometric analysis from serial block-face electron microscopy of juvenile rat. *Prog. Neurobiol.* 183:101696. doi: 10.1016/j.pneurobio.2019.101696

Chao, C. C., Gutierrez-Vazquez, C., Rothhammer, V., Mayo, L., Wheeler, M. A., Tjon, E. C., et al. (2019). Metabolic control of astrocyte pathogenic activity via cPLA2-MAVS. *Cell* 179, 1483–1498. doi: 10.1016/j.cell.2019.11.016

Csordas, G., and Hajnoczky, G. (2009). SR/ER-mitochondrial local communication: calcium and ROS. *Biochim. Biophys. Acta* 1787, 1352–1362. doi: 10.1016/j.bbabio.2009.06.004

Csordas, G., Renken, C., Varnai, P., Walter, L., Weaver, D., Buttle, K. F., et al. (2006). Structural and functional features and significance of the physical linkage between ER and mitochondria. *J. Cell. Biol.* 174, 915–921. doi: 10.1083/jcb.200604016

Csordas, G., Varnai, P., Golenar, T., Roy, S., Purkins, G., Schneider, T. G., et al. (2010). Imaging interorganelle contacts and local calcium dynamics at the ER-mitochondrial interface. *Mol. Cell* 39, 121–132. doi: 10.1016/j.molcel.2010.06.029

Csordas, G., Weaver, D., and Hajnoczky, G. (2018). Endoplasmic reticulum-mitochondrial contactology: structure and signaling functions. *Trends Cell Biol.* 28, 523–540. doi: 10.1016/j.tcb.2018.02.009

Davis, C. H., Kim, K. Y., Bushong, E. A., Mills, E. A., Boassa, D., Shih, T., et al. (2014). Transcellular degradation of axonal mitochondria. *Proc. Natl. Acad. Sci. U S A* 111, 9633–9638. doi: 10.1073/pnas.1404651111

de Brito, O. M., and Scorrano, L. (2008). Mitofusin 2 tethers endoplasmic reticulum to mitochondria. *Nature* 456, 605–610. doi: 10.1038/nature07534

De Mario, A., Quintana-Cabrera, R., Martinvalet, D., and Giacomello, M. (2017). (Neuro)degenerated mitochondria-ER contacts. *Biochem. Biophys. Res. Commun.* 483, 1096–1109. doi: 10.1016/j.bbrc.2016.07.056

Dimmer, K. S., and Rapaport, D. (2017). Mitochondrial contact sites as platforms for phospholipid exchange. *Biochim. Biophys. Acta. Mol. Cell Biol. Lipids* 1862, 69–80. doi: /10.1016/j.bbalip.2016.07.010

Fecher, C., Trovo, L., Muller, S. A., Snaidero, N., Wettmarshausen, J., Heink, S., et al. (2019). Cell-type-specific profiling of brain mitochondria reveals

functional and molecular diversity. *Nat. Neurosci.* 22, 1731–1742. doi: 10.1038/s41593-019-0479-z

Fiebig, C., Keiner, S., Ebert, B., Schaffner, I., Jagasia, R., Lie, D. C., et al. (2019). Mitochondrial dysfunction in astrocytes impairs the generation of reactive astrocytes and enhances neuronal cell death in the cortex upon photothrombotic lesion. *Front. Mol. Neurosci.* 12:40. doi: 10.3389/fnmol.2019.00040

Filadi, R., Greotti, E., Turacchio, G., Luini, A., Pozzan, T., and Pizzo, P. (2015). Mitofusin 2 ablation increases endoplasmic reticulum-mitochondria coupling. *Proc. Natl. Acad. Sci. U S A* 112, E2174–E2181. doi: 10.1073/pnas.1504880112

Friedman, J. R., Lackner, L. L., West, M., Dibenedetto, J. R., Nunnari, J., and Voeltz, G. K. (2011). ER tubules mark sites of mitochondrial division. *Science* 334, 358–362. doi: 10.1126/science.1207385

Göbel, J., Engelhardt, E., Pelzer, P., Sakthivelu, V., Jahn, H. M., Jevtic, M., et al. (2020). Mitochondria-endoplasmic reticulum contacts in reactive astrocytes promote vascular remodeling. *Cell Metab.* 31, 791–808. doi: 10.1016/j.cmet.2020.03.005

Gobel, J., Motori, E., and Bergami, M. (2018). Spatiotemporal control of mitochondrial network dynamics in astroglial cells. *Biochem. Biophys. Res. Commun.* 500, 17–25. doi: 10.1016/j.bbrc.2017.06.191

Hamasaki, M., Furuta, N., Matsuda, A., Nezu, A., Yamamoto, A., Fujita, N., et al. (2013). Autophagosomes form at ER-mitochondria contact sites. *Nature* 495, 389–393. doi: 10.1038/nature11910

Hayakawa, K., Esposito, E., Wang, X., Terasaki, Y., Liu, Y., Xing, C., et al. (2016). Transfer of mitochondria from astrocytes to neurons after stroke. *Nature* 535, 551–555. doi: 10.1038/nature18928

Henneberger, C., Bard, L., Panatier, A., Reynolds, J. P., Medvedev, N. I, Minge, D., et al. (2019). LTP induction drives remodeling of astroglia to boost glutamate escape from synapses. *bioRxiv*

Hertz, L., Peng, L., and Dienel, G. A. (2007). Energy metabolism in astrocytes: high rate of oxidative metabolism and spatiotemporal dependence on glycolysis/glycogenolysis. *J. Cereb. Blood Flow Metab.* 27, 219–249. doi: 10.1038/sj.jcbfm.9600343

Hirabayashi, Y., Kwon, S. K., Paek, H., Pernice, W. M., Paul, M. A., Lee, J., et al. (2017). ER-mitochondria tethering by PDZD8 regulates Ca(2+) dynamics in mammalian neurons. *Science* 358, 623–630. doi: 10.1126/science.aan6009

Hung, V., Lam, S. S., Udeshi, N. D., Svinkina, T., Guzman, G., Mootha, V. K., et al. (2017). Proteomic mapping of cytosol-facing outer mitochondrial and ER membranes in living human cells by proximity biotinylation. *Elife* 6:e24463. doi: 10.7554/eLife.24463.020

Ignatenko, O., Chilov, D., Paetau, I., De Miguel, E., Jackson, C. B., Capin, G., et al. (2018). Loss of mtDNA activates astrocytes and leads to spongiotic encephalopathy. *Nat. Commun.* 9:70. doi: 10.1038/s41467-017-01859-9

Iliff, J. J., Wang, M., Liao, Y., Plogg, B. A., Peng, W., Gundersen, G. A., et al. (2012). A paravascular pathway facilitates CSF flow through the brain parenchyma and the clearance of interstitial solutes, including amyloid beta. *Sci. Transl. Med.* 4:147ra111. doi: 10.1126/scitranslmed.3003748

Jackson, J. G., O'donnell, J. C., Takano, H., Coulter, D. A., and Robinson, M. B. (2014). Neuronal activity and glutamate uptake decrease mitochondrial mobility in astrocytes and position mitochondria near glutamate transporters. *J. Neurosci.* 34, 1613–1624. doi: 10.1523/JNEUROSCI.3510-13.2014

Jackson, J. G., and Robinson, M. B. (2015). Reciprocal regulation of mitochondrial dynamics and calcium signaling in astrocyte processes. *J. Neurosci.* 35, 15199–15213. doi: 10.1523/JNEUROSCI.2049-15.2015

Jackson, J. G., and Robinson, M. B. (2018). Regulation of mitochondrial dynamics in astrocytes: mechanisms, consequences, and unknowns. *Glia* 66, 1213–1234. doi: 10.1002/glia.23252

Jakobs, S., Stephan, T., Ilgen, P., and Bruser, C. (2020). Light microscopy of mitochondria at the nanoscale. *Annu. Rev. Biophys.* 49, 289–308. doi: 10.1146/annurev-biophys-121219-081550

Joshi, A. U., Minhas, P. S., Liddelow, S. A., Haileselassie, B., Andreasson, K. I., Dorn, G. W. II, et al. (2019). Fragmented mitochondria released from microglia trigger A1 astrocytic response and propagate inflammatory neurodegeneration. *Nat. Neurosci.* 22, 1635–1648. doi: 10.1038/s41593-019-0486-0

Khakh, B. S., and Sofroniew, M. V. (2015). Diversity of astrocyte functions and phenotypes in neural circuits. *Nat. Neurosci.* 18, 942–952. doi: 10.1038/nn.4043

Lewis, S. C., Uchiyama, L. F., and Nunnari, J. (2016). ER-mitochondria contacts couple mtDNA synthesis with mitochondrial division in human cells. *Science* 353:aaf5549. doi: 10.1126/science.aaf5549

Lewis, T. L. Jr., Kwon, S. K., Lee, A., Shaw, R., and Polleux, F. (2018). MFF-dependent mitochondrial fission regulates presynaptic release and axon branching by limiting axonal mitochondria size. *Nat. Commun.* 9:5008. doi: 10.1038/s41467-018-07416-2

Li, Z., Okamoto, K., Hayashi, Y., and Sheng, M. (2004). The importance of dendritic mitochondria in the morphogenesis and plasticity of spines and synapses. *Cell* 119, 873–887. doi: 10.1016/j.cell.2004.11.003

Liddelow, S. A., and Barres, B. A. (2017). Reactive Astrocytes: Production, Function, and Therapeutic Potential. *Immunity* 46, 957–967. doi: 10.1016/j.immuni.2017.06.006

Liddelow, S. A., Guttenplan, K. A., Clarke, L. E., Bennett, F. C., Bohlen, C. J., Schirmer, L., et al. (2017). Neurotoxic reactive astrocytes are induced by activated microglia. *Nature* 541, 481–487. doi: 10.1038/nature21029

Lovatt, D., Sonnewald, U., Waagepetersen, H. S., Schousboe, A., He, W., Lin, J. H., et al. (2007). The transcriptome and metabolic gene signature of protoplasmic astrocytes in the adult murine cortex. *J. Neurosci.* 27, 12255–12266. doi: 10.1523/JNEUROSCI.3404-07.2007

Mathiisen, T. M., Lehre, K. P., Danbolt, N. C., and Ottersen, O. P. (2010). The perivascular astroglial sheath provides a complete covering of the brain microvessels: an electron microscopic 3D reconstruction. *Glia* 58, 1094–1103. doi: 10.1002/glia.20990

Mishra, A., Reynolds, J. P., Chen, Y., Gourine, A. V., Rusakov, D. A., and Attwell, D. (2016). Astrocytes mediate neurovascular signaling to capillary pericytes but not to arterioles. *Nat. Neurosci.* 19, 1619–1627. doi: 10.1038/nn.4428

Motori, E., Atanassov, I., Kochan, S. M. V., Folz-Donahue, K., Sakthivelu, V., Giavalisco, P., et al. (2020). Neuronal metabolic rewiring promotes resilience to neurodegeneration caused by mitochondrial dysfunction. *Sci. Adv.* 6:eaba8271. doi: 10.1126/sciadv.aba8271

Motori, E., Puyal, J., Toni, N., Ghanem, A., Angeloni, C., Malaguti, M., et al. (2013). Inflammation-induced alteration of astrocyte mitochondrial dynamics requires autophagy for mitochondrial network maintenance. *Cell Metab.* 18, 844–859. doi: 10.1016/j.cmet.2013.11.005

Naon, D., Zaninello, M., Giacomello, M., Varanita, T., Grespi, F., Lakshminaranayan, S., et al. (2016). Critical reappraisal confirms that Mitofusin 2 is an endoplasmic reticulum-mitochondria tether. *Proc. Natl. Acad. Sci. U S A* 113, 11249–11254. doi: 10.1073/pnas.1606786113

Polyzos, A. A., Lee, D. Y., Datta, R., Hauser, M., Budworth, H., Holt, A., et al. (2019). Metabolic reprogramming in astrocytes distinguishes region-specific neuronal susceptibility in huntington mice. *Cell. Metab.* 29, 1258.e–1273.e. doi: 10.1016/j.cmet.2019.03.004

Raffaello, A., Mammucari, C., Gherardi, G., and Rizzuto, R. (2016). Calcium at the center of cell signaling: interplay between endoplasmic reticulum, mitochondria, and lysosomes. *Trends Biochem. Sci.* 41, 1035–1049. doi: 10.1016/j.tibs.2016.09.001

Shigetomi, E., Bushong, E. A., Haustein, M. D., Tong, X., Jackson-Weaver, O., Kracun, S., et al. (2013). Imaging calcium microdomains within entire astrocyte territories and endfeet with GCaMPs expressed using adeno-associated viruses. *J. Gen. Physiol.* 141, 633–647. doi: 10.1085/jgp.201210949

Shigetomi, E., Patel, S., and Khakh, B. S. (2016). Probing the complexities of astrocyte calcium signaling. *Trends Cell Biol.* 26, 300–312. doi: 10.1016/j.tcb.2016.01.003

Sofroniew, M. V. (2014). Astrogliosis. *Cold Spring Harb. Perspect. Biol.* 7:a020420. doi: 10.1101/cshperspect.a020420

Stephen, T. L., Higgs, N. F., Sheehan, D. F., Al Awabdh, S., Lopez-Domenech, G., Arancibia-Carcamo, I. L., et al. (2015). Miro1 regulates activity-driven positioning of mitochondria within astrocytic processes apposed to synapses

to regulate intracellular calcium signaling. *J. Neurosci.* 35, 15996–16011. doi: 10.1523/JNEUROSCI.2068-15.2015

Supplie, L. M., Duking, T., Campbell, G., Diaz, F., Moraes, C. T., Gotz, M., et al. (2017). Respiration-deficient astrocytes survive as glycolytic cells in vivo. *J. Neurosci.* 37, 4231–4242. doi: 10.1523/JNEUROSCI.0756-16.2017

Vance, J. E. (2015). Phospholipid synthesis and transport in mammalian cells. *Traffic* 16, 1–18. doi: 10.1111/tra.12230

Weber, B., and Barros, L. F. (2015). The astrocyte: powerhouse and recycling center. *Cold Spring Harb. Perspect. Biol.* 7:a020396. doi: 10.1101/cshperspect.a020396

Wu, Y. M., Whiteus, C., Xu, C. S., Hayworth, K. J., Weinberg, R. J., Hess, H. F., et al. (2017). Contacts between the endoplasmic reticulum and other membranes in neurons. *Proc. Nat. Acad. Sci. U S A* 114, E4859–E4867. doi: 0.1073/pnas.1701078114

Conflict of Interest: The authors declare that the research was conducted in the absence of any commercial or financial relationships that could be construed as a potential conflict of interest.

frontiers in Cell and Developmental Biology

REVIEW
published: 30 April 2021
doi: 10.3389/fcell.2021.642717

Effects of Hyperoxia on Mitochondrial Homeostasis: Are Mitochondria the Hub for Bronchopulmonary Dysplasia?

*Yu Xuefei, Zhao Xinyi, Cai Qing, Zhang Dan, Liu Ziyun, Zheng Hejuan, Xue Xindong and Fu Jianhua**

Department of Pediatrics, Shengjing Hospital of China Medical University, Shenyang City, China

OPEN ACCESS

Edited by:
Du Feng,
Guangzhou Medical University, China

Reviewed by:
Lynette Kay Rogers,
The Research Institute at Nationwide Children's Hospital, United States
Michael Adam O'Reilly,
University of Rochester, United States
Ana Hou,
ShengJing Hospital of China Medical University, China

***Correspondence:**
Fu Jianhua
fujh@sj-hospital.org

Specialty section:
This article was submitted to Molecular Medicine, a section of the journal Frontiers in Cell and Developmental Biology

Received: *16 December 2020*
Accepted: *12 April 2021*
Published: *30 April 2021*

Citation:
Xuefei Y, Xinyi Z, Qing C, Dan Z, Ziyun L, Hejuan Z, Xindong X and Jianhua F (2021) Effects of Hyperoxia on Mitochondrial Homeostasis: Are Mitochondria the Hub for Bronchopulmonary Dysplasia? Front. Cell Dev. Biol. 9:642717. doi: 10.3389/fcell.2021.642717

Mitochondria are involved in energy metabolism and redox reactions in the cell. Emerging data indicate that mitochondria play an essential role in physiological and pathological processes of neonatal lung development. Mitochondrial damage due to exposure to high concentrations of oxygen is an indeed important factor for simplification of lung structure and development of bronchopulmonary dysplasia (BPD), as reported in humans and rodent models. Here, we comprehensively review research that have determined the effects of oxygen environment on alveolar development and morphology, summarize changes in mitochondria under high oxygen concentrations, and discuss several mitochondrial mechanisms that may affect cell plasticity and their effects on BPD. Thus, the pathophysiological effects of mitochondria may provide insights into targeted mitochondrial and BPD therapy.

Keywords: mitochondria, hyperoxia, lung development, bronchopulmonary dysplasia, alveolarisation

INTRODUCTION

Morphological findings have shown that preterm infants are born with immature lungs in the saccular stage or even the canalicular stage (Joshi and Kotecha, 2007; Rodriguez-Castillo et al., 2018). Similarly, postpartum lung tissues in rodent models are far from mature and require postpartum differentiation and alveolar regeneration (Silva et al., 2015). Immature alveolar epithelium becomes the first line of exposure to the external environment, and if exposed to oxygen over the long term, lung development is simplified that ultimately leads to bronchopulmonary dysplasia (BPD) (Massaro et al., 1975; Dasgupta et al., 2020). A series of adverse factors, such as long-term postpartum period or inappropriate hyperoxic treatment, mechanical ventilation, infections, and chemical stimulations, can cause an imbalance between alveolar damage and pre and postnatal repair and damage to the immature lungs, resulting in developmental arrest of the alveoli and pulmonary blood vessels (Jensen et al., 2019; Bonadies et al., 2020).

The pathological changes associated with BPD present a simplified model of alveolar and pulmonary vascular structure that is now referred to as "new BPD" (Collins et al., 2017; Jensen et al., 2019). Studies have confirmed that exposure to high oxygen concentrations can cause

mitochondrial damage, simplify the lung structure, and ultimately lead to BPD (Ratner et al., 2009; Narala et al., 2018). Effective oxidative metabolism and low reactive oxygen species (ROS) levels are essential for stem cell self-renewal and preserving homeostasis. During embryonic development, mitochondria regulate organ differentiation and development (Lima et al., 2018), cellular energy production, redox reactions, aerobic glycolysis, calcium signaling, ROS generation, macromolecule synthesis, and other biological activities (Smith and Gallo, 2018).

The process of lung development begins at the embryonic stage. Lung buds from the ventral endoderm of the foregut continuously branch along the proximal–distal axis through ordered tissue events (Joshi and Kotecha, 2007; Metzger et al., 2008). Development gradually progresses through epithelial–mesenchymal interactions with the subsequent involvement of several transcription and growth factors, such as the epidermal (EGF), vascular endothelial (VEGF), and fibroblast (FGF) growth factors, and bone morphogenetic protein (BMP), resulting in alveolarization and lung development (Demayo et al., 2002; Serls et al., 2005; Lignelli et al., 2019). The lung tissue of premature infants is relatively hypoxic in the fetal environment for two major reasons: (1) the amniotic fluid contains <1% oxygen (Sjostedt et al., 1958), and (2) fetal blood is ∼40% normative because of pulmonary and cardiac shunts. This seems to favor differentiation and development of the lung at a later stage as a part of preparing the organ for the postnatal demands of gas exchange. The premature lung under hyperoxic conditions is prone to high oxidative stress that can lead to mitochondrial damage owing to the less developed antioxidant capacity of the lung. This review primarily focuses on the pathological processes of late stage lung development under exposure to hyperoxia, discusses the role of mitochondria in alveolar dysplasia, and describes the effects of mitochondrial function on potential pathophysiological effects during epithelial cell development. In addition, we have updated the current understanding of the application of preclinical and clinical mitochondria-targeted therapies for BPD.

MORPHOLOGICAL ABNORMALITIES IN MITOCHONDRIA

Mitochondria are organelles with an outer (OMM) and an inner (IMM) membrane, an intermembrane space (IMS), a matrix, and they have their own DNA and protein structures (Gail and Lenfant, 1983). The OMM is primarily associated with protein exchange; folded cristae of the IMM have proteins associated with oxidative phosphorylation (OXPHOS), including the mitochondrial electron transport chain (ETC) proteins and ATP synthase, distributed over them (Aravamudan et al., 2013; Prakash et al., 2017; Zhang et al., 2017). More than 40 cell types with different mitochondrial densities exist in the lung tissue; for example, the numbers of mitochondria can be up to 31-fold higher in alveolar type 2 (AT2) than in type 1 (AT1) cells (Massaro et al., 1975). Mitochondria can participate in alveolar epithelial cell activities through complex functions and mechanisms. The number and function of mitochondria continue to increase during postnatal growth and development (El-Merhie et al., 2017). Postnatal mitochondrial changes in AT2, ciliated, and club cells at different stages have been assessed by transmission electron microscopy (TEM) in neonatal mice. Starting on day 15, the mitochondrial structure of AT2 gradually expands and elongates, and the cristae gradually become denser. As glycogen deposits in the cells decrease, the number of lamellar bodies also gradually increases. The mitochondrial fragmentation index of pulmonary vascular endothelial cells increases from 6 h of hyperoxia, and during this time, pulmonary vascular endothelial cells separate from the basement membrane (while the basement membrane remains intact). The ultrastructure of endothelial cell mitochondria is destroyed, and TEM has revealed mitochondrial swelling, vacuolization, disrupted mitochondrial structure, matrix shrinkage, wider and fewer cristae, and disorganization (Ma et al., 2018). The endoplasmic reticulum of endothelial cells is swollen with wider gaps (Teng et al., 2017). However, after 72 h of hyperoxic exposure, the phospholipid content in mouse lung epithelial cells significantly increases (Lee et al., 2013). These results suggest that exposing premature infants to oxygen can disrupt the structure of mitochondria and other organelles in lung cells, and the level of damage gradually increases with prolonged exposure.

CELL AND MITOCHONDRIAL PLASTICITY

The basis of alveolus formation is in the immature inter-airspace wall, which consists of two capillary layers and a central sheet of connective tissue (Burri, 2006). The number of alveoli increased significantly increases after delivery, and with the continuous progression of alveoli, the number of alveoli increased by 17.1 times (Burri, 2006). It is worth noting that mitochondria are highly plastic organelles (Bahat and Gross, 2019) and play crucial role in stem cell biology through ROS generation, TCA cycle metabolite production, NAD^+/NADH ratio regulation, pyruvate metabolism and mitochondrial dynamics (Tan and Suda, 2018). Transcription factors (Nkx2.1, SOX2, Nrf2) and signaling pathways (Wnt pathway, Notch pathway and Shh pathway) related to lung development can be regulated by mitochondrial plasticity (Khacho et al., 2016). AT2 cells are strictly regulated to inhibit the amount of proliferation under baseline conditions and to rapidly and restore barrier integrity after acute injury. Yee et al. (2016) detected alveolar epithelial cell-specific markers during postpartum exposure to different concentrations of oxygen (12, 17, 21, 40, 60, or 100%) and found that the AT2-specific markers pulmonary surfactant-associated protein C (Sftpc) and ATP-binding cassette sub-family A member 3 (Abca3) had a nonlinear response to oxygen during the postpartum expansion of the alveolar epithelium, however, EGFP labeled AT2 don't produce labeled AT1 cells in neonatal mice. These findings suggest that oxygen in the environment increases AT2 self-renewal ability. $Scgb1a1^+$ cuboidal cells in the terminal bronchi are reprogrammed and differentiated under the

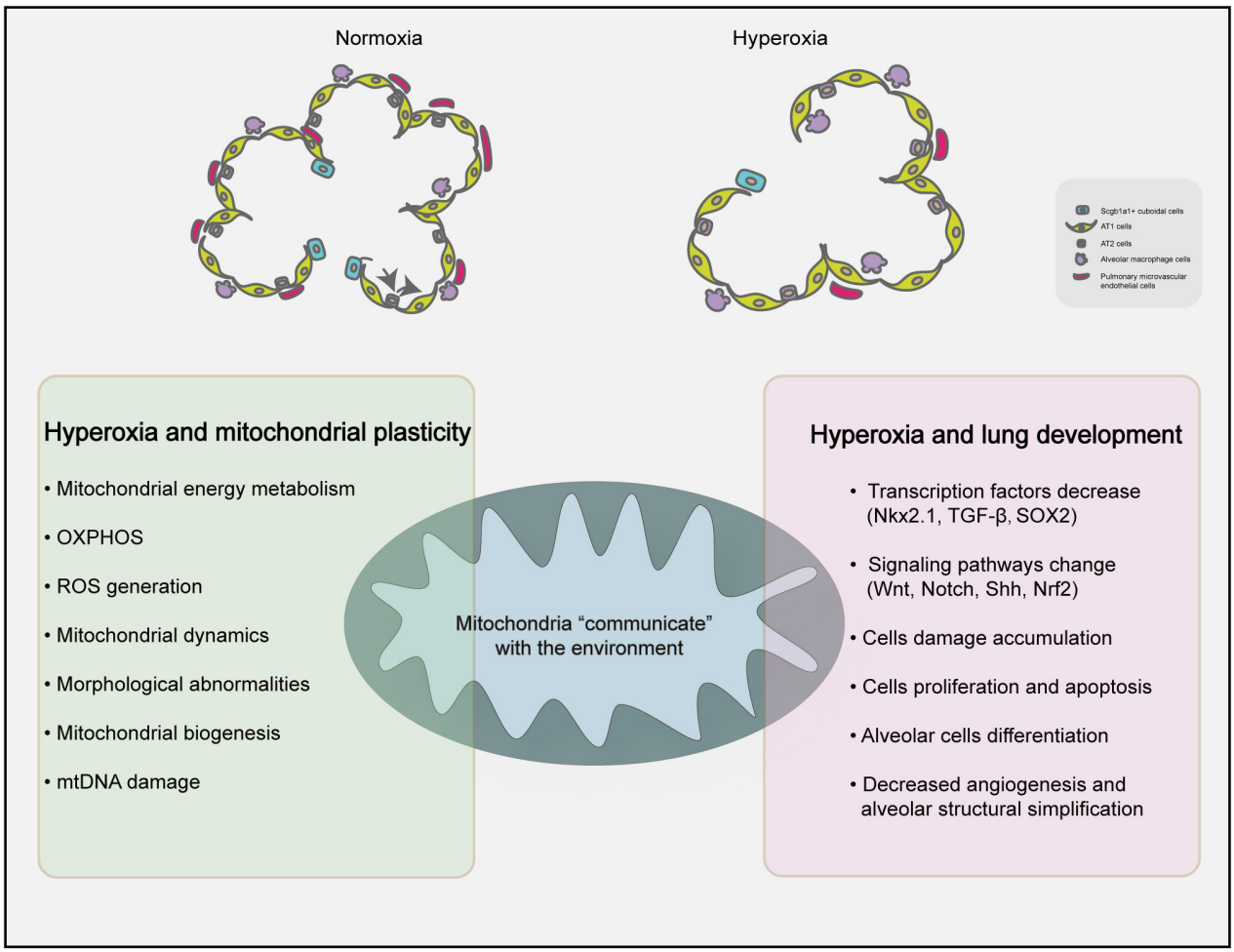

FIGURE 1 | Proposed mechanisms of mitochondrial homeostasis and lung development under hyperxia. Hyperoxia exposure can simplify the lung structure of premature infants, reduce the number of alveoli and reduce the number of microvascular in the lungs compared with the normal group. High oxygen can affect the plasticity of mitochondria and influence BPD.

influence of niches formed in the surrounding environment and dynamic changes in intracellular signals (Parekh et al., 2020). **Figure 1** summarizes the contents of this paragraph, changes in the environment affect the oxygen dialogue mitochondria and the environment, which may affect the process of lung development. The plasticity and adaptability of alveolar epithelial cells under changing conditions enables lung epithelial cells to maintain the homeostasis and equilibrium of self-renewal through signal circuits (Demayo et al., 2002). Imbalanced mitochondrial plasticity, however, may be responsible for stunted lung development.

OXYGEN SENSING BY MITOCHONDRIA

Although the mechanism by which mitochondria use oxygen sensing is of pivotal significance, theories on postpartum alveolar oxygen sensing are scant. The human body contains chemoreceptors such as the carotid sinus and the aortic body that monitor the internal oxygen concentration by sensing changes in the vicinity. However, the molecular responses of living cells to altered gas conditions have been difficult to determine. Nevertheless, the continuous emergence of new techniques and technologies has facilitated more investigative options (Tretter et al., 2020). At the cellular level, 80 and 20% of available oxygen is utilized by mitochondria and other organelles, respectively. As the main oxygen consumer and metabolizer, mitochondria normally function under a partial pressure of oxygen of only 1–3 mmHg (Loenarz, 2020). According to Henry's law, the oxygen exchange capacity of lung epithelial cells is associated with the intracellular partial pressure of oxygen, the thickness of the cell membrane, and the density of erythrocytes (Weibel, 2017). At high oxygen concentrations, proteins other than hemoglobin gain oxygen-carrying capacity, which increases the ability of oxygen to diffuse from plasma into the mitochondria of various cells (Echevarria et al., 2007).

The way by which cells sense and respond to changes in oxygen levels through hypoxia-inducible factor-1 (HIF-1) has

been determined (Wang and Semenza, 1993). When the oxygen supply is sufficient for a cell to meet its energy demand, HIF hydroxylase inhibits HIF through the ubiquitin–proteosome degradation pathway. Conversely, HIF is induced under hypoxia and can activate subsequent target genes, including those that regulate angiogenesis, metabolism, and erythropoiesis, leading to increased blood and oxygen supply to hypoxic tissues (Webb et al., 2009). Current studies have focused more on mitochondrial oxygen sensing and signal transduction under hypoxia, rather than hyperoxia. However, fluctuations in oxygen levels caused by intermittent positive pressure ventilation triggers cells to exit a hyperoxic non-hypoxic state that produces a reaction similar to hypoxia, called the "hyperoxia–hypoxia paradox" (Hadanny and Efrati, 2020). Therefore, the primary mechanism mediating changes in the alveolar epithelium under hyperoxia conditions is believed to increase AT2 oxygen-uptake capacity. Based on this theory, hyperoxia exposed-premature infants and animal models might be exposed to fluctuating, and relatively low oxygen levels (Wohlrab et al., 2021). Another classical theory describes that increased O_2 content triggers an imbalance of ROS production by intracellular oxidase/antioxidant enzymes, increasing ROS production, and unbalancing the ETC, which leads to the conversion of mitochondrial energy and regeneration of tissue adaptation. Excessive ROS levels are not direct agents of damage but serve as signaling molecules that affect normal cellular function and cause damage to mitochondrial DNA (mtDNA) (Schumacker et al., 2014).

OXIDATIVE STRESS IN MITOCHONDRIA

Several studies have investigated mitochondrial damage caused by cellular ROS that comprise a primary cause of BPD in pediatric patients (Valencia et al., 2018; Wang and Dong, 2018). Mitochondria are important sites where cells produce ROS (Collins et al., 2017). Compared to those in adult lung, neonatal lung mitochondria produce higher amounts of ROS, whereas cytoplasmic ROS levels are relatively low (Berkelhamer et al., 2013). Neonatal animals can also tolerate hyperoxia better than adults (Koo et al., 2005). However, preterm human infants with non-fatal oxidative stress damage after delivery can develop impaired mitochondrial function, which in turn affects cell maturation and tissue development, ultimately leading to brain damage and BPD (Ten, 2017). The effects of hyperoxia on immature lungs are regulated by development, and the duration of hyperoxic exposure is associated with ROS levels and the degree of pulmonary vascular dysplasia. Neonatal mice exposed to 75% oxygen for 72 h had reduced alveoli and septa, increased vascularization of resistant pulmonary arteries, and right ventricular hypertrophy (RVH) compared with normoxic controls at early, but not later stages (Datta et al., 2015).

Endogenous oxygen free radicals are produced primarily by the mitochondrial respiratory chain, NADPH oxidase (NOX), xanthine oxidase (XO), and other oxidative enzymatic pathways. Hyperoxic conditions can damage alveolar epithelial cells through NOX, and increase elastin deposition in the alveolar septum (Auten et al., 2009). The expression of NOX2 and NOX4 in vascular endothelial cells increases under hyperoxia (Pendyala et al., 2009) and can activate two antioxidant response elements (ARE) on the NOX4 promoter in pulmonary vascular endothelial cells. Loss or mutation of nuclear factor erythroid 2-related factor 2 (*Nrf2*) can cause mitochondrial dysfunction and metabolic disorders induced by ROS (Cho and Kleeberger, 2020). The transcription level of NOX4 can also promote angiogenesis and migration through Nrf2-ARE (Pendyala et al., 2011).

Innovative mitochondrially targeyed triphenylphosphonium antioxidants, such as mitoTEMPO and MitoQ, can scavenge ROS (Oyewole and Birch-Machin, 2015). Specifically, mitoTEMPO targets mitochondria and can prevent hyperoxia-induced lung injury by reducing NOX1 levels, suggesting that the NOX1 production is ROS-dependent (Datta et al., 2015). Classical antioxidants, such as Cu-ZnSOD, MnSOD, and GSH, have been used clinically, but their application as therapeutics has been limited by biochemical and physiological issues (Asikainen and White, 2004). Other antioxidants such as cationic plastoquinone derivatives (SkQ), carotenoids (especially astaxanthin), vitamin E, coenzyme Q10, and resveratrol can also reduce oxidative damage in the mitochondria, but further corroborating studies are required (Teixeira et al., 2018). Further investigation of mitochondrial targeted antioxidants can provide insights into treatment of oxidative stress injury in premature infants.

MITOCHONDRIAL ENERGY METABOLISM

The principal biological function of mitochondria is to produce ATP and deliver energy to cells. Mitochondrial oxidation includes the nicotinamide adenine dinucleotide (NAD)-mediated complex I pathway and the flavin adenine dinucleotide (FAD)-mediated complex II pathway. Reduced NAD (NADH) and reduced FAD (FADH2) are the principal substrates for the redox reactions that facilitate electron transfer and OXPHOS through enzyme complexes I and II (Guo et al., 2018). A comparison of the respiratory chain complex I–IV in AT2 and club cells between 15-day-old and adult mice using PCR and western blotting showed that except for succinate dehydrogenase (SDH) complex II, all other complexes increased gradually over time, suggesting that changes in the morphology and number of mitochondria throughout postnatal development are associated with a higher cellular metabolic demand (El-Merhie et al., 2017).

Regarding the strategy of enhancing oxidative metabolism in lung epithelial and endothelial cells, reactivating metabolic enzymes that protect the integrity of the mitochondrial respiratory chain and matrix membrane during mechanical ventilation and hyperoxia might protect against vascular remodeling (Ten and Ratner, 2020). The tricarboxylic acid cycle is inhibited under hyperoxia, and activities of the key enzyme, that is aconitase (Aco), are decreased (Gardner et al., 1994). In mice, mitochondrial oxygen consumption and ATP production rates are decreased, the surface area of alveoli is reduced, and the numbers of alveoli are significantly reduced under hyperoxia, suggesting that inhibited mitochondrial OXPHOS is associated

with bronchoalveolar growth arrest (Ratner et al., 2009). A549 lung epithelial cells decrease mitochondrial spare respiratory capacity at 12 h under hyperoxia and basal respiratory capacity in 48 h. Damage to the mitochondrial respiratory chain under hyperoxic conditions has been analyzed using specific inhibitors of respiratory chain complexes I–V. This is accompanied by an increase in the conversion of glucose to nucleic acid ribose *via* the pentose phosphate pathway (Tetri et al., 2018).

Notably, AT2 cells can secrete special lung surfactants to stabilize the breathing process of the alveoli. Lipid synthesis at the lung surface requires the participation of mitochondria. Hyperoxia affects the fatty acid oxidase, long-chain acyl-CoA dehydrogenase (LCAD), by regulating the mitochondrial lipid synthesis and metabolism pathway, which in turn affects lung surface tension and compliance (Otsubo et al., 2015). This shows that enhanced fatty acid usage helps endothelial cells to maintain their proliferation and alveolarization (Dennery et al., 2018; Yao et al., 2019). The carnitine palmitoyltransferase 1a gene (*Cpt1a*) plays an important role in BPD and fatty acid oxidation prevents hyperoxia-induced endothelial cell damage in neonatal mouse models (Fanos et al., 2014). Adipose fibroblasts in the lung interstitium provide neutral lipids to type II lung cells for the synthesis of phospholipids, which are surfactants in the lungs of immature fetuses. However, hyperoxia can cause the transdifferentiation of adipose fibroblasts into myofibroblasts, accompanied by increased conversion of glucose to the nucleic acid ribose *via* the pentose phosphate pathway. Hyperoxia decreases lipid synthesis *de novo*, which might explain fibroblast formation and the decrease in alveolar type II cell surfactants (Boros et al., 2002; Zhao et al., 2018).

MITOCHONDRIAL DNA DAMAGE

Hyperoxia damages mtDNA in many types of lung cells (Roper et al., 2004; Kandasamy et al., 2019), and such damage can repeatedly increase cellular OS, senescence, and apoptosis (Dobson et al., 2002; Ruchko et al., 2005; Chan, 2006). Human mtDNA is a double-stranded closed loop (16.5 kb) that encodes 13 proteins associated with mitochondrial function, as well as 22 tRNAs and two rRNAs that play significant roles in cells. Unlike nuclear DNA, mtDNA lacks damage repair enzymes and are closer to the source of ROS production, rendering it vulnerable to structural and functional damages (Aravamudan et al., 2013). The mtDNA of alveolar epithelial cells serves as a type of danger-associated molecular pattern (DAMP), as it is released by damaged cells under mechanical stress and activates local fibroblasts (Yang et al., 2020). In addition to responding to mechanical stress, mtDNA produces signaling molecules that communicate with the neighboring cells to promote fibrosis. Damaged mtDNA can be released through mitochondrial permeability transition pores (mPTP) that induce inflammatory and immune responses (Schumacker et al., 2014). For example, ATP released by damaged alveolar epithelial cells under mechanical pressure activates NLRP3 in the endothelial cells to promote endothelial–mesenchymal transition, interacts with P2X7R in macrophages to induce IL-1B production, and locally activates fibroblasts (Yang et al., 2020).

A study of the mechanism of hyperoxia-induced mtDNA damage found that mtDNA repair mediated by the targeted DNA repair enzyme endonuclease III (EndoIII) decreases ROS production and returns branching morphology and levels of surfactant protein C (SFPTC) mRNA to normal in the lungs of neonatal rats (Gebb et al., 2013). The mitochondrial targeted DNA repair enzymes 8-oxoguanine DNA glycosylase (mt-OGG1) and Aco-2 reduce hyperoxia-induced mtDNA damage, thus reducing the apoptosis of alveolar epithelial cells (Kim et al., 2014).

The targeted repair of mtDNA of pulmonary artery endothelial cells with oxidative damage using OGG1 inhibits apoptosis caused by the activation of caspase-3 *via* the xanthine oxidase pathway (Ruchko et al., 2005). Exposing neonatal C57BL/6 mice to 75% oxygen for 14 days causes increased peroxide production and alveolar simplification, and poorer lung function (increased resistance, decreased compliance) compared with normoxic mice (Dylag et al., 2019; Kandasamy et al., 2019). This is important because it shows that mitochondrially encoded genes confer sensitivity or tolerance to oxygen-induced neonatal respiratory diseases. The above-mentioned studies show that targeted repair of mtDNA can reduce hyperoxia-related damage to lung cells. Survivors of preterm birth have increased risk of neurologic and cardiopulmonary disease as they age (Hwang and Rehan, 2018). Hyperoxia has been used to model the oxidative effects of aging. There are many examples of how mitochondria accumulate DNA damage as people age. The question is whether disorders in survivors of preterm infants are related to mitochondrial damage at birth. Perhaps, the threshold of damage is high in them that eventually leads to development of such metabolic diseases later in life.

MITOCHONDRIAL BIOGENESIS

Mitochondria are central hubs of catabolic and anabolic reactions that ensure sufficient cellular metabolic adaptation during development and differentiation. At the transcriptional level, mitochondrial biogenesis is regulated by the mitochondrial and nuclear genes (Jornayvaz and Shulman, 2010). Peroxisome proliferator-activated receptor γ coactivator α (PGC-1α) is a master regulator of mitochondrial biogenesis, belonging to a family of transcriptional coactivators that also includes PGC-1β and the peroxisome proliferator-activated receptor gamma, coactivator-related 1 (PPRC1). PGC-1α activates various proteins, including nuclear respiratory factors 1 and 2 (NRF1 and NRF2) and mitochondrial transcription factors A and B (TFAM and TFBM), and regulates the transcription and translation of mtDNA (Jornayvaz and Shulman, 2010). TFAM is critical for the development of the lung. Notably, fetuses harboring a TFAM mutant exhibit branching defects during embryonic development and incomplete peripheral airways; thus, they cannot survive after birth (Srivillibhuthur et al., 2018). Mitochondrial biogenesis can be regulated *via* the AMPK–PGC-1a and SIRT1–PGC-1a axes, which play a central role in promoting mitochondrial energy

metabolism and biogenesis (Lehman et al., 2000; Liang and Ward, 2006). Tracking the relationship between mitochondrial biogenesis and acute lung injury, inflammation, and pulmonary fibrosis using mitochondria-specific green fluorescent protein, has revealed that mitochondrial biogenesis is most prominent in pulmonary vascular endothelial cells during hyperoxia-induced lung damage (Carraway et al., 2008).

Under various stimulated environmental factors, hormones, secondary messengers (calcium, endothelial nitric oxide synthase eNOS, cAMP), and kinase pathways (PKA, MAPK, PRKAA2) can regulate the expression and post-translational modification of PGC-1α *via* regulation of protein localization and function. Regulating PGC-1α can affect the transcription of a variety of steroid receptors and nuclear receptors, and mediate the transcriptional activity of PPAR-γ and thyroid hormone receptor on the uncoupling protein promoter (Zhu et al., 2013). It can also regulate the key mitochondrial genes involved in adaptive thermogenesis by coordinating the expression of a large number of genes involved in glucose and fatty acid metabolism. Studies have shown that the clinical drugs used to improve breathing, such as aminophylline and montelukast, can promote the biogenesis of human alveolar epithelium mitochondria through cAMP responsive element binding protein (CREB)/PGC-1α (Wang et al., 2019; Wei et al., 2019). The use of the mitochondrial antioxidant resveratrol can protect mtDNA and reduce apoptosis through SIRT1–PGC-1a (Wang et al., 2020; Zhu et al., 2021). These findings suggest that the biogenesis of mitochondria plays an important role in protecting against hyperoxic lung injuries.

MITOCHONDRIAL DYNAMICS

Mitochondria are in a dynamic equilibrium of continuous fusion and fission, which plays an important role in energy metabolism and maintaining stability of the intracellular environment, as well as the differentiation and development of cells. Mitochondrial division is mainly mediated by dynamin-related protein 1 (Drp1) and mitochondrial fission protein 1 (Fis1); mitochondrial fusion is mediated by the IMM fusion optic atrophy 1 (OPA1) and mitochondrial fusion by the fusion proteins (mitofusin1 and 2, Mfn1, and Mfn2). The level of oxidative stress can cause imbalance in the levels of the above-mentioned proteins, and thereby resulting in mitochondrial fragmentation (Wu et al., 2011). Some researchers suggest that mitochondrial fusion and fission are unbalanced in lungs damaged by hyperoxia, which directly inhibits their function (Ten and Ratner, 2020; Lee et al., 2020). Reportedly, mitochondrial fragmentation of lung endothelial cells increased, p-Drp1 increased, Mfn1 decreased, OPA1 increased, and the autophagy-related proteins P62, PINK-1, and LC3B increased compared with the control group after 48 h of hyperoxia. However, exposing the cells to air for 24 h could reverse the trend (Ma et al., 2018). Recently, Teng et al. (2017) found that caffeine used to stimulate the respiratory center of premature infants can also improve the endoplasmic reticulum stress caused by hyperoxia, and that the endoplasmic reticulum and mitochondria can interact with each other through the participation of MFN2 and DRP1, inducing mitochondrial division.

Mitochondrial dynamics are also regulated by epigenetics. Sirtuins (SIRT) comprise a family of highly conserved NAD^+ dependent histone deacetylases that are distributed in different parts of the cell (Ma et al., 2018). Reportedly, their expression is decreased under hyperoxic conditions. SIRT3 can deacetylate OPA1, thus increasing the efficiency of mitochondrial fission (Samant et al., 2014) and SIRT1 can regulate SUMOylation, affect mitochondrial dynamics, and reduce damage (Tan et al., 2018). Mitophagy and mitochondrial synthesis and division jointly participate in the quality control of intracellular mitochondria, which is conducive to mitochondrial homeostasis (Pickles et al., 2018). Mitophagy is mainly mediated by the PINK1/Parkin pathway. In addition, other mitochondrial proteins, such as NIX (also known as BNIPL), BNIP3, and FUNDC1, also mediate mitochondrial autophagy (Wei et al., 2015). We have previously shown that oxygen exposure can affect the expression of mitochondrial autophagy (Yu et al., 2020). In conclusion, mitochondrial fusion and fission are unbalanced in the lungs injured by hyperoxia, which directly affects the quality control of mitochondria.

CLINICAL APPLICATION OF MITOCHONDRIAL THERAPY

Clinical studies have suggested that the maximum mitochondrial oxygen consumption of umbilical vein endothelial cells can serve as an important predictor of BPD, and that mitochondrial function serves as a predictor of the long-term prognosis and mortality rates of preterm infants with BPD (Kandasamy et al., 2017). The quality of placental mitochondria can be used to assess sensitivity to ROS, but its application to determining pathological processes and prognostic relationships with chronic lung disease requires further investigation (Papa Gobbi et al., 2018).

Glucocorticoids play a major role in the regulation of fetal and postnatal lung development, and changes in glucocorticoids can significantly affect the mitochondrial dynamic regulation in lung development (Du et al., 2009); in ways that can persist into adulthood. Changes in glucocorticoid sensitivity and mitochondrial protein abundance can be used to identify those at the highest risk of developing advanced lung diseases (Gnanalingham et al., 2006). Xanthines (theophylline and caffeine) have been widely applied in neonatology for treating apnea in premature infants. Their mechanism of action is primarily by inhibiting adenosine receptor stimulation in the respiratory center, whereas phosphodiesterase inhibition affects bronchodilation (Reyburn et al., 2012). Caffeine attenuates cyclooxygenase-2 activation induced by hyperoxia and protects mitochondria, thus reducing lung damage due to hyperoxia (Teng et al., 2017).

Mitochondrial replacement therapy is proposed to improve pathological outcomes and resolve pulmonary stagnation. Exogenous supplementation with healthy mitochondria is emerging as a potential therapeutic approach that should be

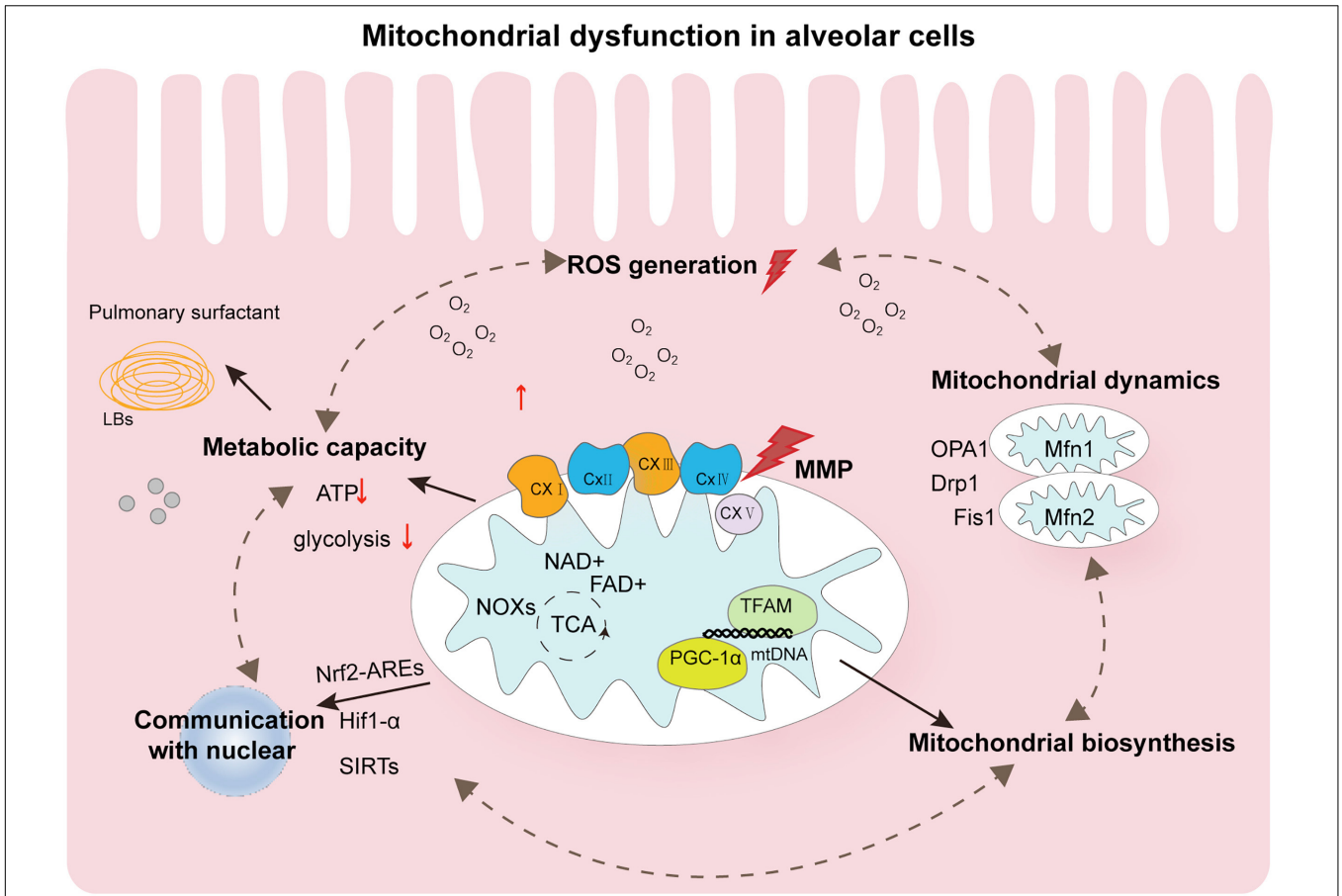

FIGURE 2 | Summary of the major pathophysiological events contributing to mitochondrial dysfunction in hyperoxia-exposed neonatal lung. Oxygen affects the mechanism of alveolar morphology mainly through mitochondrial dysfunction. Altered ROS levels and mitochondrial metabolism in alveolar cells and mitochondrial homeostasis disorders are involved in the occurrence of BPD. These states of dysfunction are interdependent and can further form loops that influence each other. They can also be simultaneously affected by controlling the quality of mitochondria. In addition, mitochondria in alveolar cells communicate with the nucleus by regulating several transcription factors, such as Nrf2-AREs, HIF-1α, and SIRTs, and undergo epigenetic modifications. All these aspects provide possible evidence for the important role of mitochondria in BPD. ROS, reactive oxygen species; AT2, alveolar type 2; BPD, bronchopulmonary dysplasia; LBs, Lamellar corpuscle; ATP, adenosine triphosphate; OPA1, optic atrophy 1; Drp1, dynamin-related protein 1; Fis1, mitochondrial fission protein 1; Mfn1, mitofusins protein 1; NOX, NADPH oxidase; TFAM, mitochondrial transcription factor A; TFBM, mitochondrial transcription factor B; PGC-1α, peroxisome proliferator-activated receptor γ coactivator 1-α.

investigated in detail, as it improves the status of mitochondrial damage *via* the endocytosis by damaged cells to offset diseases (Agrawal and Mabalirajan, 2016). The delivery of mitochondria through blood vessels of the pulmonary artery or through the trachea (nebulization) could improve lung ischemia-reperfusion damage in C57 mice (Moskowitzova et al., 2020). The transplanted mitochondria initially increase the amount of intracellular ATP and activate ATP synthesis, they then migrate to the target cells through actin-dependent endocytosis, and release protective cytokines that promote cell growth and proliferation. In addition, normal mtDNA of transplanted mitochondria can also replace damaged mtDNA (Eyre-Walker, 2017). The first clinical study of mitochondrial transplantation therapy at Boston Children's Hospital had a great impact in the field of medicine. They performed autologous mitochondrial transplantation for myocardial ischemia–reperfusion injury in pediatric patients who required extracorporeal membrane oxygenation (ECMO). Following transplantation, most of the dysregulated cardiac functions were recovered in the patients and they were successfully freed from ECMO support (Emani et al., 2017). However, there are several issues that need to be overcome for improving the efficiency and success of mitochondrial transplantation therapy. For example, a single administration of mitochondria does not result in the maintenance of long-term therapeutic efficacy. In the above-mentioned case, the method of mitochondrial isolation, mitochondrial source, route of administration, and number of doses were dependent on the ease of performing mitochondrial transplantation. Therefore, optimal standard protocols for targeted mitochondrial transplantation therapy need to be developed (Yamada et al., 2020). Since mitochondria in the extracellular space can also serve as DAMP that activate inflammation and exacerbate damage, clinical mitochondrial transplantation requires considerable caution that cannot be overlooked (Zhang et al., 2010).

DISCUSSION

The role of mitochondria in postnatal lung development remains poorly understood with respect to the mechanisms that cause alveolar cavity enlargement and structural simplification during oxygen therapy for lung damage caused by lack of oxygen. The pathophysiological mechanism of mitochondrial damage in BPD is extremely complex. In this article, we summarize that hyperoxia will affect the homeostasis of mitochondria. These dysfunction states are interdependent and will affect each other and thus affect developmental results, as shown in **Figure 2**. As a consensus view of neonatologists, hyperoxia inhibits angiogenesis, stimulate expansion of alveolar epithelial cells, and promotes recruitment of inflammatory cells into the lung. However, each cell type responds differently to hyperoxia. Despite extensive research, the way by which different cell types respond to hyperoxia remains poorly understood that warrants further investigation. Mitochondrial damage in BPD is associated with changes in signal transduction and energy metabolism. How the quantity and function of mitochondria affect hyperoxia-exposed lungs at the tissue and cellular levels is one of the keys to further understanding the pathogenesis of hyperoxia-induced mitochondrial damage. Further, in-depth studies are required to elucidate how the dynamic changes in mitochondrial functions affect the outcomes of lung development in preterm infants during the repair of reversible damage caused by hyperoxic lung injury. A clearer understanding of the mechanisms of mitochondrial damage and its associated upstream and downstream regulatory pathways will deepen our understanding of the pathological processes of BPD, which holds major implications in appropriate oxygen therapy as well as the diagnosis and treatment of preterm infants with BPD.

AUTHOR CONTRIBUTIONS

YX wrote the manuscript and designed the figures. ZX, CQ, ZD, LZY, ZH, XX, and FJ wrote specific parts of the manuscript and reviewed the final draft of the manuscript. All authors contributed to the article and approved the submitted version.

FUNDING

This study was supported by Grants from the National Natural Science Foundation of China (No. 81571479), the National Natural Science Foundation of China (No. 82071688), the 345 Talent Project of the Shengjing Hospital (No. M0428), National Natural Science Foundation Youth Project of China (No. 81901520), General Program of China Postdoctoral Science Foundation (No. 2019M661164), and Key R&D Guidance Plan Projects In Liaoning Province (2020JH1/10300001).

ACKNOWLEDGMENTS

We thank Drs. Wen Shuyan, Liu Di, and Li Yinai for their insightful discussions and unreserved support.

REFERENCES

Agrawal, A., and Mabalirajan, U. (2016). Rejuvenating cellular respiration for optimizing respiratory function: targeting mitochondria. *Am. J. Physiol. Lung. Cell. Mol. Physiol.* 310, L103–L113. doi: 10.1152/ajplung.00320.2015

Aravamudan, B., Thompson, M. A., Pabelick, C. M., and Prakash, Y. S. (2013). Mitochondria in lung diseases. *Expert Rev. Respir. Med.* 7, 631–646. doi: 10.1586/17476348.2013.834252

Asikainen, T. M., and White, C. W. (2004). Pulmonary antioxidant defenses in the preterm newborn with respiratory distress and bronchopulmonary dysplasia in evolution: implications for antioxidant therapy. *Antioxid. Redox. Signal* 6, 155–167. doi: 10.1089/152308604771978462

Auten, R. L., Mason, S. N., Auten, K. M., and Brahmajothi, M. (2009). Hyperoxia impairs postnatal alveolar epithelial development via NADPH oxidase in newborn mice. *Am. J. Physiol. Lung. Cell. Mol. Physiol.* 297, L134–L142. doi: 10.1152/ajplung.00112.2009

Bahat, A., and Gross, A. (2019). Mitochondrial plasticity in cell fate regulation. *J. Biol. Chem.* 294, 13852–13863. doi: 10.1074/jbc.rev118.000828

Berkelhamer, S. K., Kim, G. A., Radder, J. E., Wedgwood, S., Czech, L., Steinhorn, R. H., et al. (2013). Developmental differences in hyperoxia-induced oxidative stress and cellular responses in the murine lung. *Free Radic. Biol. Med.* 61, 51–60. doi: 10.1016/j.freeradbiomed.2013.03.003

Bonadies, L., Zaramella, P., Porzionato, A., Perilongo, G., Muraca, M., and Baraldi, E. (2020). Present and future of bronchopulmonary dysplasia. *J. Clin. Med.* 9:1539. doi: 10.3390/jcm9051539

Boros, L. G., Torday, J. S., Paul Lee, W. N., and Rehan, V. K. (2002). Oxygen-induced metabolic changes and transdifferentiation in immature fetal rat lung lipofibroblasts. *Mol. Genet. Metab.* 77, 230–236. doi: 10.1016/s1096-7192(02)00140-3

Burri, P. H. (2006). Structural aspects of postnatal lung development - alveolar formation and growth. *Biol. Neonate* 89, 313–322. doi: 10.1159/000092868

Carraway, M. S., Suliman, H. B., Kliment, C., Welty-Wolf, K. E., Oury, T. D., and Piantadosi, C. A. (2008). Mitochondrial biogenesis in the pulmonary vasculature during inhalational lung injury and fibrosis. *Antioxid. Redox. Signal* 10, 269–275. doi: 10.1089/ars.2007.1910

Chan, D. C. (2006). Mitochondria: dynamic organelles in disease, aging, and development. *Cell* 125, 1241–1252. doi: 10.1016/j.cell.2006.06.010

Cho, H. Y., and Kleeberger, S. R. (2020). Mitochondrial biology in airway pathogenesis and the role of NRF2. *Arch. Pharm. Res.* 43, 297–320. doi: 10.1007/s12272-019-01182-5

Collins, J. J. P., Tibboel, D., de Kleer, I. M., Reiss, K. M., and Rottier, R. J. (2017). The future of bronchopulmonary dysplasia: emerging pathophysiological concepts and potential new avenues of treatment. *Front. Med.* 4:61. doi: 10.3389/fmed.2017.00061

Dasgupta, A., Wu, D., Tian, L., Xiong, P. Y., Dunham-Snary, K. J., Chen, K. H., et al. (2020). Mitochondria in the pulmonary vasculature in health and disease: oxygen-sensing, metabolism, and dynamics. *Compr. Physiol.* 10, 713–765. doi: 10.1002/cphy.c190027

Datta, A., Kim, G. A., Taylor, J. M., Gugino, S. F., Farrow, K. N., Schumacker, P. T., et al. (2015). Mouse lung development and NOX1 induction during hyperoxia are developmentally regulated and mitochondrial ROS dependent. *Am. J. Physiol. Lung. Cell. Mol. Physiol.* 309, L369–L377. doi: 10.1152/ajplung.00176.2014

Demayo, F., Minoo, P., Plopper, C. G., Schuger, L., Shannon, J., and Torday, J. S. (2002). Mesenchymal-epithelial interactions in lung development and repair: are modeling and remodeling the same process? *Am. J. Physiol. Lung. Cell. Mol. Physiol.* 283, L510–L517. doi: 10.1152/ajplung.00144.2002

Dennery, P. A., Carr, J., Peterson, A., and Yao, H. (2018). The role of mitochondrial fatty acid use in neonatal lung injury and repair. *Trans. Am. Clin. Climatol. Assoc.* 129, 195–201.

Dobson, A. W., Grishko, V., LeDoux, S. P., Kelley, M. R., Wilson, G. L., and Gillespie, M. N. (2002). Enhanced mtDNA repair capacity protects pulmonary

artery endothelial cells from oxidant-mediated death. *Am J Physiol Lung Cell Mol Physiol.* 283, L205–L210. doi: 10.1152/ajplung.00443.2001

Du, J., Wang, Y., Hunter, R., Wei, Y., Blumenthal, R., Falke, C., et al. (2009). Dynamic regulation of mitochondrial function by glucocorticoids. *Proc. Natl. Acad. Sci. U S A.* 106, 3543–3548. doi: 10.1073/pnas.0812671106

Dylag, A. M., Brookes, P. S., and O'Reilly, M. A. (2019). Swapping mitochondria: a key to understanding susceptibility to neonatal chronic lung disease. *Am. J. Physiol. Lung. Cell. Mol. Physiol.* 317, L737–L739. doi: 10.1152/ajplung.00395.2019

Echevarria, M., Munoz-Cabello, A. M., Sanchez-Silva, R., Toledo-Aral, J. J., and Lopez-Barneo, J. (2007). Development of cytosolic hypoxia and hypoxia-inducible factor stabilization are facilitated by aquaporin-1 expression. *J. Biol. Chem.* 282, 30207–30215. doi: 10.1074/jbc.m702639200

El-Merhie, N., Baumgart-Vogt, E., Pilatz, A., Pfreimer, S., Pfeiffer, B., Pak, O., et al. (2017). Differential alterations of the mitochondrial morphology and respiratory chain complexes during postnatal development of the mouse lung. *Oxid. Med. Cell. Longev.* 2017:9169146. doi: 10.1155/2017/9169146

Emani, S. M., Piekarski, B. L., Harrild, D., Del Nido, P. J., and McCully, J. D. (2017). Autologous mitochondrial transplantation for dysfunction after ischemia-reperfusion injury. *J. Thorac. Cardiovasc. Surg.* 154, 286–289. doi: 10.1016/j.jtcvs.2017.02.018

Eyre-Walker, A. (2017). Mitochondrial replacement therapy: are mito-nuclear interactions likely to be a problem? *Genetics* 205, 1365–1372. doi: 10.1534/genetics.116.196436

Fanos, V., Pintus, M. C., Lussu, M., Atzori, L., Noto, A., Stronati, M., et al. (2014). Urinary metabolomics of bronchopulmonary dysplasia (BPD): preliminary data at birth suggest it is a congenital disease. *J. Matern. Fetal. Neonatal. Med.* 27, 39–45. doi: 10.3109/14767058.2014.955966

Gail, D. B., and Lenfant, C. J. (1983). Cells of the lung: biology and clinical implications. *Am. Rev. Respir. Dis.* 127, 366–387.

Gardner, P. R., Nguyen, D. D., and White, C. W. (1994). Aconitase is a sensitive and critical target of oxygen poisoning in cultured mammalian cells and in rat lungs. *Proc. Natl. Acad. Sci. U S A.* 91, 12248–12252. doi: 10.1073/pnas.91.25.12248

Gebb, S. A., Decoux, A., Waggoner, A., Wilson, G. L., and Gillespie, M. N. (2013). Mitochondrial DNA damage mediates hyperoxic dysmorphogenesis in rat fetal lung explants. *Neonatology* 103, 91–97. doi: 10.1159/000342632

Gnanalingham, M. G., Mostyn, A., Gardner, D. S., Stephenson, T., and Symonds, M. E. (2006). Developmental regulation of the lung in preparation for life after birth: hormonal and nutritional manipulation of local glucocorticoid action and uncoupling protein-2. *J. Endocrinol.* 188, 375–386. doi: 10.1677/joe.1.06530

Guo, R., Gu, J., Zong, S., Wu, M., and Yang, M. (2018). Structure and mechanism of mitochondrial electron transport chain. *Biomed. J.* 41, 9–20. doi: 10.1016/j.bj.2017.12.001

Hadanny, A., and Efrati, S. (2020). The hyperoxic-hypoxic paradox. *Biomolecules* 10:958. doi: 10.3390/biom10060958

Hwang, J. S., and Rehan, V. K. (2018). Recent advances in bronchopulmonary dysplasia: pathophysiology, prevention, and treatment. *Lung* 196, 129–138. doi: 10.1007/s00408-018-0084-z

Jensen, E. A., Dysart, K., Gantz, M. G., McDonald, S., Bamat, N. A., Keszler, M., et al. (2019). The diagnosis of bronchopulmonary dysplasia in very preterm infants. an evidence-based approach. *Am. J. Respir. Crit. Care Med.* 200, 751–759. doi: 10.1164/rccm.201812-2348OC

Jornayvaz, F. R., and Shulman, G. I. (2010). Regulation of mitochondrial biogenesis. *Essays Biochem.* 47, 69–84. doi: 10.1042/bse0470069

Joshi, S., and Kotecha, S. (2007). Lung growth and development. *Early Hum. Dev.* 83, 789–794. doi: 10.1016/j.earlhumdev.2007.09.007

Kandasamy, J., Olave, N., Ballinger, S. W., and Ambalavanan, N. (2017). Vascular endothelial mitochondrial function predicts death or pulmonary outcomes in preterm infants. *Am. J. Respir. Crit. Care Med.* 196, 1040–1049. doi: 10.1164/rccm.201702-0353oc

Kandasamy, J., Rezonzew, G., Jilling, T., Ballinger, S., and Ambalavanan, N. (2019). Mitochondrial DNA variation modulates alveolar development in newborn mice exposed to hyperoxia. *Am. J. Physiol. Lung. Cell. Mol. Physiol.* 317, L740–L747. doi: 10.1152/ajplung.00220.2019

Khacho, M., Clark, A., Svoboda, D. S., Azzi, J., MacLaurin, J. G., Meghaizel, C., et al. (2016). Mitochondrial dynamics impacts stem cell identity and fate decisions by regulating a nuclear transcriptional program. *Cell. Stem Cell* 19, 232–247. doi: 10.1016/j.stem.2016.04.015

Kim, S. J., Cheresh, P., Williams, D., Cheng, Y., Ridge, K., Schumacker, P. T., et al. (2014). Mitochondria-targeted Ogg1 and aconitase-2 prevent oxidant-induced mitochondrial DNA damage in alveolar epithelial cells. *J. Biol. Chem.* 289, 6165–6176. doi: 10.1074/jbc.m113.515130

Koo, H. C., Davis, J. M., Li, Y., Hatzis, D., Opsimos, H., Pollack, S., et al. (2005). Effects of transgene expression of superoxide dismutase and glutathione peroxidase on pulmonary epithelial cell growth in hyperoxia. *Am. J. Physiol. Lung. Cell. Mol. Physiol.* 288, L718–L726. doi: 10.1152/ajplung.00456.2003

Lee, J. E., Seo, B. J., Han, M. J., Hong, Y. J., Hong, K., Song, H., et al. (2020). Changes in the expression of mitochondrial morphology-related genes during the differentiation of murine embryonic stem cells. *Stem Cells Int.* 2020:9369268. doi: 10.1155/2020/9369268

Lee, S. J., Zhang, J. L., Choi, A. M. K., and Kim, H. P. (2013). Mitochondrial dysfunction induces formation of lipid droplets as a generalized response to stress. *Oxid. Med. Cell. Longev.* 2013:327167. doi: 10.1155/2013/327167

Lehman, J. J., Barger, P. M., Kovacs, A., Saffitz, J. E., Medeiros, D. M., and Kelly, D. P. (2000). Peroxisome proliferator-activated receptor gamma coactivator-1 promotes cardiac mitochondrial biogenesis. *J. Clin. Invest.* 106, 847–856. doi: 10.1172/jci10268

Liang, H., and Ward, W. F. (2006). PGC-1alpha: a key regulator of energy metabolism. *Adv. Physiol. Educ.* 30, 145–151. doi: 10.1152/advan.00052.2006

Lignelli, E., Palumbo, F., Myti, D., and Morty, R. E. (2019). Recent advances in our understanding of the mechanisms of lung alveolarization and bronchopulmonary dysplasia. *Am. J. Physiol. Lung. Cell. Mol. Physiol.* 317, L832–L887. doi: 10.1152/ajplung.00369.2019

Lima, A., Burgstaller, J., Sanchez-Nieto, J. M., and Rodriguez, T. A. (2018). The mitochondria and the regulation of cell fitness during early mammalian development. *Curr. Top Dev. Biol.* 128, 339–363. doi: 10.1016/bs.ctdb.2017.10.012

Loenarz, C. (2020). An oxygen sensation: progress in macromolecule hydroxylation triggered by the elucidation of cellular oxygen sensing. *Angew. Chem. Int. Ed. Engl.* 59, 3776–3780. doi: 10.1002/anie.201913263

Ma, C., Beyer, A. M., Durand, M., Clough, A. V., Zhu, D., Norwood Toro, L., et al. (2018). Hyperoxia causes mitochondrial fragmentation in pulmonary endothelial cells by increasing expression of pro-fission proteins. *Arterioscler. Thromb. Vasc. Biol.* 38, 622–635. doi: 10.1161/atvbaha.117.310605

Massaro, G. D., Gail, D. B., and Massaro, D. (1975). Lung oxygen consumption and mitochondria of alveolar epithelial and endothelial cells. *J. Appl. Physiol.* 38, 588–592. doi: 10.1152/jappl.1975.38.4.588

Metzger, R. J., Klein, O. D., Martin, G. R., and Krasnow, M. A. (2008). The branching programme of mouse lung development. *Nature* 453, 745–750. doi: 10.1038/nature07005

Moskowitzova, K., Orfany, A., Liu, K., Ramirez-Barbieri, G., Thedsanamoorthy, J. K., Yao, R., et al. (2020). Mitochondrial transplantation enhances murine lung viability and recovery after ischemia-reperfusion injury. *Am. J. Physiol. Lung. Cell. Mol. Physiol.* 318, L78–L88. doi: 10.1152/ajplung.00221.2019

Narala, V. R., Fukumoto, J., Hernandez-Cuervo, H., Patil, S. S., Krishnamurthy, S., Breitzig, M., et al. (2018). Akap1 genetic deletion increases the severity of hyperoxia-induced acute lung injury in mice. *Am. J. Physiol. Lung. Cell. Mol. Physiol.* 314, L860–L870. doi: 10.1152/ajplung.00365.2017

Otsubo, C., Bharathi, S., Uppala, R., Ilkayeva, O. R., Wang, D., McHugh, K., et al. (2015). Long-chain acylcarnitines reduce lung function by inhibiting pulmonary surfactant. *J. Biol. Chem.* 290, 23897–23904. doi: 10.1074/jbc.m115.655837

Oyewole, A. O., and Birch-Machin, M. A. (2015). Mitochondria-targeted antioxidants. *FASEB J.* 29, 4766–4771. doi: 10.1096/fj.15-275404

Papa Gobbi, R., Magnarelli, G., and Rovedatti, M. G. (2018). Susceptibility of placental mitochondria to oxidative stress. *Birth Defects Res.* 110, 1228–1232. doi: 10.1002/bdr2.1377

Parekh, K. R., Nawroth, J., Pai, A., Busch, S. M., Senger, C. N., and Ryan, A. L. (2020). Stem cells and lung regeneration. *Am. J. Physiol. Cell. Physiol.* 319, C675–C693. doi: 10.1152/ajpcell.00036.2020

Pendyala, S. I, Gorshkova, A., Usatyuk, P. V., He, D., Pennathur, A., Lambeth, J. D., et al. (2009). Role of Nox4 and Nox2 in hyperoxia-induced reactive oxygen species generation and migration of human lung endothelial cells. *Antioxid. Redox. Signal.* 11, 747–764. doi: 10.1089/ars.2008.2203

Pendyala, S., Moitra, J., Kalari, S., Kleeberger, S. R., Zhao, Y., Reddy, S. P., et al. (2011). Nrf2 regulates hyperoxia-induced Nox4 expression in human lung endothelium: identification of functional antioxidant response elements on the Nox4 promoter. *Free Radic. Biol. Med.* 50, 1749–1759. doi: 10.1016/j.freeradbiomed.2011.03.022

Pickles, S., Vigie, P., and Youle, R. J. (2018). Mitophagy and quality control mechanisms in mitochondrial maintenance. *Curr. Biol.* 28, R170–R185. doi: 10.1016/j.cub.2018.01.004

Prakash, Y. S., Pabelick, C. M., and Sieck, G. C. (2017). Mitochondrial dysfunction in airway disease. *Chest* 152, 618–626. doi: 10.1016/j.chest.2017.03.020

Ratner, V., Starkov, A., Matsiukevich, D., Polin, R. A., and Ten, V. S. (2009). Mitochondrial dysfunction contributes to alveolar developmental arrest in hyperoxia-exposed mice. *Am. J. Respir. Cell. Mol. Biol.* 40, 511–518. doi: 10.1165/rcmb.2008-0341rc

Reyburn, B., Martin, R. J., Prakash, Y. S., and MacFarlane, P. M. (2012). Mechanisms of injury to the preterm lung and airway: implications for long-term pulmonary outcome. *Neonatology* 101, 345–352. doi: 10.1159/000337355

Rodriguez-Castillo, J. A., Perez, D. B., Ntokou, A., Seeger, W., Morty, R. E., and Ahlbrecht, K. (2018). Understanding alveolarization to induce lung regeneration. *Respir. Res.* 19:148. doi: 10.1186/s12931-018-0837-5

Roper, J. M., Mazzatti, D. J., Watkins, R. H., Maniscalco, W. M., Keng, P. C., and O'Reilly, M. A. (2004). In vivo exposure to hyperoxia induces DNA damage in a population of alveolar type II epithelial cells. *Am. J. Physiol. Lung. Cell. Mol. Physiol.* 286, L1045–L1054. doi: 10.1152/ajplung.00376.2003

Ruchko, M., Gorodnya, O., LeDoux, S. P., Alexeyev, M. F., Al-Mehdi, A. B., and Gillespie, M. N. (2005). Mitochondrial DNA damage triggers mitochondrial dysfunction and apoptosis in oxidant-challenged lung endothelial cells. *Am. J. Physiol. Lung. Cell. Mol. Physiol.* 288, L530–L535. doi: 10.1152/ajplung.00255.2004

Samant, S. A., Zhang, H. J., Hong, Z., Pillai, V. B., Sundaresan, N. R., Wolfgeher, D., et al. (2014). SIRT3 deacetylates and activates OPA1 to regulate mitochondrial dynamics during stress. *Mol. Cell. Biol.* 34, 807–819. doi: 10.1128/mcb.01483-13

Schumacker, P. T., Gillespie, M. N., Nakahira, K., Choi, A. M., Crouser, E. D., Piantadosi, C. A., et al. (2014). Mitochondria in lung biology and pathology: more than just a powerhouse. *Am. J. Physiol. Lung. Cell. Mol. Physiol.* 306, L962–L974. doi: 10.1152/ajplung.00073.2014

Serls, A. E., Doherty, S., Parvatiyar, P., Wells, J. M., and Deutsch, G. H. (2005). Different thresholds of fibroblast growth factors pattern the ventral foregut into liver and lung. *Development* 132, 35–47. doi: 10.1242/dev.01570

Silva, D. M., Nardiello, C., Pozarska, A., and Morty, R. E. (2015). Recent advances in the mechanisms of lung alveolarization and the pathogenesis of bronchopulmonary dysplasia. *Am. J. Physiol. Lung. Cell. Mol. Physiol.* 309, L1239–L1272. doi: 10.1152/ajplung.00268.2015

Sjostedt, S., Rooth, G., and Caligara, F. (1958). The oxygen tension of the amniotic fluid. *Am. J. Obstet. Gynecol.* 76, 1226–1230. doi: 10.1016/S0002-9378(16)36937-X

Smith, G. M., and Gallo, G. (2018). The role of mitochondria in axon development and regeneration. *Dev. Neurobiol.* 78, 221–237. doi: 10.1002/dneu.22546

Srivillibhuthur, M., Warder, B. N., Toke, N. H., Shah, P. P., Feng, Q., Gao, N., et al. (2018). TFAM is required for maturation of the fetal and adult intestinal epithelium. *Dev. Biol.* 439, 92–101. doi: 10.1016/j.ydbio.2018.04.015

Tan, D. Q., and Suda, T. (2018). Reactive oxygen species and mitochondrial homeostasis as regulators of stem cell fate and function. *Antioxid. Redox. Signal.* 29, 149–168. doi: 10.1089/ars.2017.7273

Tan, F., Dong, W., Lei, X., Liu, X., Li, Q., Kang, L., et al. (2018). Attenuated SUMOylation of sirtuin 1 in premature neonates with bronchopulmonary dysplasia. *Mol. Med. Rep.* 17, 1283–1288. doi: 10.3892/mmr.2017.8012

Teixeira, J., Deus, C. M., Borges, F., and Oliveira, P. J. (2018). Mitochondria: targeting mitochondrial reactive oxygen species with mitochondriotropic polyphenolic-based antioxidants. *Int. J. Biochem. Cell. Biol.* 97, 98–103. doi: 10.1016/j.biocel.2018.02.007

Ten, V. S. (2017). Mitochondrial dysfunction in alveolar and white matter developmental failure in premature infants. *Pediatr. Res.* 81, 286–292. doi: 10.1038/pr.2016.216

Ten, V. S., and Ratner, V. (2020). Mitochondrial bioenergetics and pulmonary dysfunction: current progress and future directions. *Paediatr. Respir. Rev.* 34, 37–45. doi: 10.1016/j.prrv.2019.04.001

Teng, R. J., Jing, X., Michalkiewicz, T., Afolayan, A. J., Wu, T. J., and Konduri, G. G. (2017). Attenuation of endoplasmic reticulum stress by caffeine ameliorates hyperoxia-induced lung injury. *Am J Physiol Lung Cell Mol Physiol.* 312, L586–L598. doi: 10.1152/ajplung.00405.2016

Tetri, L. H., Diffee, G. M., Barton, G. P., Braun, R. K., Yoder, H. E., Haraldsdottir, K., et al. (2018). Sex-specific skeletal muscle fatigability and decreased mitochondrial oxidative capacity in adult rats exposed to postnatal hyperoxia. *Front. Physiol.* 9:326. doi: 10.3389/fphys.2018.00326

Tretter, V., Zach, M. L., Bohme, S., Ullrich, R., Markstaller, K., and Klein, K. U. (2020). Investigating disturbances of oxygen homeostasis: from cellular mechanisms to the clinical practice. *Front. Physiol.* 11:947. doi: 10.3389/fphys.2020.00947

Valencia, A. M., Abrantes, M. A., Hasan, J., Aranda, J. V., and Beharry, K. D. (2018). Reactive oxygen species, biomarkers of microvascular maturation and alveolarization, and antioxidants in oxidative lung injury. *React. Oxyg. Spec.* 6, 373–388. doi: 10.20455/ros.2018.867

Wang, F., Lei, X., Kang, L., Zhu, X., Ruan, Y., and Dong, W. (2020). [Down-regulation of SIRT1 and PGC-1alpha expression caused by hyperoxia induces mitochondrial dysfunction in human alveolar epithelial cells]. *Xi Bao Yu Fen Zi Mian Yi Xue Za Zhi* 36, 788–793.

Wang, G. L., and Semenza, G. L. (1993). General involvement of hypoxia-inducible factor 1 in transcriptional response to hypoxia. *Proc. Natl. Acad. Sci. U S A* 90, 4304–4308. doi: 10.1073/pnas.90.9.4304

Wang, H., Cheng, Y., Liu, Y., Shi, J., and Cheng, Z. (2019). Montelukast promotes mitochondrial biogenesis via CREB/PGC-1alpha in human bronchial epithelial cells. *Artif. Cells Nanomed. Biotechnol.* 47, 4234–4239. doi: 10.1080/21691401.2019.1687502

Wang, J., and Dong, W. (2018). Oxidative stress and bronchopulmonary dysplasia. *Gene* 678, 177–183. doi: 10.1016/j.gene.2018.08.031

Webb, J. D., Coleman, M. L., and Pugh, C. W. (2009). Hypoxia, hypoxia-inducible factors (HIF), HIF hydroxylases and oxygen sensing. *Cell Mol. Life Sci.* 66, 3539–3554. doi: 10.1007/s00018-009-0147-7

Wei, G., Sun, R., Xu, T., Kong, S., and Zhang, S. (2019). Aminophylline promotes mitochondrial biogenesis in human pulmonary bronchial epithelial cells. *Biochem. Biophys. Res. Commun.* 515, 31–36. doi: 10.1016/j.bbrc.2019.05.013

Wei, H., Liu, L., and Chen, Q. (2015). Selective removal of mitochondria via mitophagy: distinct pathways for different mitochondrial stresses. *Biochim. Biophys. Acta* 1853, 2784–2790. doi: 10.1016/j.bbamcr.2015.03.013

Weibel, E. R. (2017). Lung morphometry: the link between structure and function. *Cell Tissue Res.* 367, 413–426. doi: 10.1007/s00441-016-2541-4

Wohlrab, P., Johann Danhofer, M., Schaubmayr, W., Tiboldi, A., Krenn, K., Markstaller, K., et al. (2021). Oxygen conditions oscillating between hypoxia and hyperoxia induce different effects in the pulmonary endothelium compared to constant oxygen conditions. *Physiol. Rep.* 9:e14590. doi: 10.14814/phy2.14590

Wu, S., Zhou, F., Zhang, Z., and Xing, D. (2011). Mitochondrial oxidative stress causes mitochondrial fragmentation via differential modulation of mitochondrial fission-fusion proteins. *FEBS J.* 278, 941–954. doi: 10.1111/j.1742-4658.2011.08010.x

Yamada, Y., Ito, M., Arai, M., Hibino, M., Tsujioka, T., and Harashima, H. (2020). Challenges in promoting mitochondrial transplantation therapy. *Int. J. Mol. Sci.* 21:6365. doi: 10.3390/ijms21176365

Yang, J., Pan, X., Wang, L., and Yu, G. (2020). Alveolar cells under mechanical stressed niche: critical contributors to pulmonary fibrosis. *Mol. Med.* 26:95. doi: 10.1186/s10020-020-00223-w

Yao, H., Gong, J., Peterson, A. L., Lu, X., Zhang, P., and Dennery, P. A. (2019). Fatty acid oxidation protects against hyperoxia-induced endothelial cell apoptosis and lung injury in neonatal mice. *Am. J. Respir. Cell. Mol. Biol.* 60, 667–677. doi: 10.1165/rcmb.2018-0335oc

Yee, M., Gelein, R., Mariani, T. J., Lawrence, B. P., and O'Reilly, M. A. (2016). The oxygen environment at birth specifies the population of alveolar epithelial stem cells in the adult lung. *Stem Cells* 34, 1396–1406. doi: 10.1002/stem.2330

Yee, M., Vitiello, P. F., Roper, J. M., Staversky, R. J., Wright, T. W., McGrath-Morrow, S. A., et al. (2006). Type II epithelial cells are critical target for hyperoxia-mediated impairment of postnatal lung development. *Am. J. Physiol. Lung. Cell. Mol. Physiol.* 291, L1101–L1111. doi: 10.1152/ajplung.00126.2006

Yu, X., Sun, Y., Cai, Q., Zhao, X., Liu, Z., Xue, X., et al. (2020). Hyperoxia exposure arrests alveolarization in neonatal rats via PTENinduced putative kinase 1Parkin and Nip3like protein Xmediated mitophagy disorders. *Int. J. Mol. Med.* 46, 2126–2136. doi: 10.3892/ijmm.2020.4766

Zhang, L., Wang, W., Zhu, B., and Wang, X. (2017). Epithelial mitochondrial dysfunction in lung disease. *Adv. Exp. Med. Biol.* 1038, 201–217. doi: 10.1007/978-981-10-6674-0_14

Zhang, Q., Raoof, M., Chen, Y., Sumi, Y., Sursal, T., Junger, W., et al. (2010). Circulating mitochondrial DAMPs cause inflammatory responses to injury. *Nature* 464, 104–107. doi: 10.1038/nature08780

Zhao, H., Dennery, P. A., and Yao, H. (2018). Metabolic reprogramming in the pathogenesis of chronic lung diseases, including BPD, COPD, and pulmonary fibrosis. *Am. J. Physiol. Lung. Cell. Mol. Physiol.* 314, L544–L554. doi: 10.1152/ajplung.00521.2017

Zhu, J., Wang, K. Z., and Chu, C. T. (2013). After the banquet: mitochondrial biogenesis, mitophagy, and cell survival. *Autophagy* 9, 1663–1676. doi: 10.4161/auto.24135

Zhu, X., Wang, F., Lei, X., and Dong, W. (2021). Resveratrol alleviates alveolar epithelial cell injury induced by hyperoxia by reducing apoptosis and mitochondrial dysfunction. *Exp. Biol. Med.* 246, 596–606. doi: 10.1177/1535370220975106

Conflict of Interest: The authors declare that the research was conducted in the absence of any commercial or financial relationships that could be construed as a potential conflict of interest.

Advantages of publishing in Frontiers

OPEN ACCESS
Articles are free to read for greatest visibility and readership

FAST PUBLICATION
Around 90 days from submission to decision

HIGH QUALITY PEER-REVIEW
Rigorous, collaborative, and constructive peer-review

TRANSPARENT PEER-REVIEW
Editors and reviewers acknowledged by name on published articles

Frontiers
Avenue du Tribunal-Fédéral 34
1005 Lausanne | Switzerland

Visit us: www.frontiersin.org
Contact us: frontiersin.org/about/contact

REPRODUCIBILITY OF RESEARCH
Support open data and methods to enhance research reproducibility

DIGITAL PUBLISHING
Articles designed for optimal readership across devices

FOLLOW US
@frontiersin

IMPACT METRICS
Advanced article metrics track visibility across digital media

EXTENSIVE PROMOTION
Marketing and promotion of impactful research

LOOP RESEARCH NETWORK
Our network increases your article's readership